September, 1959
Vol. 47 No. 9

Proceedings of the IRE

Poles and Zeros

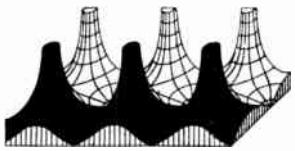

IRE and IRIS. We have always been privately pleased that no one seems able to propose a generally acceptable definition of scope for the field of electronics. The very process of defining an area seems to imply bounding or circumscribing—placing certain subject matter properly inside, setting other areas outside the purview—the result seeming to limit growth and development to areas and subjects in view at the time of definition. Where would we be professionally today if a defined bound of 1920 had limited us to radio and the vacuum tube?

One may suspect that the defining operation is a luxury which only mature fields should undertake—and only as an exercise in geriatrics even then. Certainly electronics derives much virility from its immaturity, and its willingness and ability to follow new paths wherever scientific curiosity leads.

This special issue of the PROCEEDINGS is a result of this freedom to invade new areas, which is characteristic of electronics. Infrared radiation, discovered and explored by the great classical physicists of an earlier century, remained only an obscure portion of the electromagnetic spectrum until a succession of recent engineering and scientific developments, particularly in the solid-state field, led us to the state of the art detailed in this publication. In the process we have once more gone full circle—from the incoherent radiation of the early sparks, to the highly sophisticated coherent radiation forms of our tube transmitters, and now back to the incoherent molecular radiation of the infrared!

The infrared spectrum, usually thought of as valuable only before the fireplace on winter evenings, is already one of our most complex areas, calling for application of a great variety of optical and electronic methods. Since all objects are emitters of infrared energy, then any signal will likely be received with a high-noise level, and filtering techniques are of value. Frequency translation, as illustrated by the methods required to produce our first-of-its-kind cover illustration, is another adaptation of standard concepts in a totally new frame. As electronic science grows the problems get no easier.

This gives us also another opportunity to reiterate our philosophy that a major reason-to-be of a professional organization should be the education of its members in those things to be needed in the profession of the future—and that the society's publications should consistently carry their readers to the brink of the precipice of knowledge. Of especial importance in this particular illustration of this philosophy is the opportunity to take you to the brink in a region all too long enshrouded in a fog of official secrecy and classification.

Infrared, more optical than electronic in its genesis, now represents possible tools and potential products for many facets of the electronic industry. We believe this issue, virtually a textbook on infrared, should stand well as an example of the policy of seeking out and developing the background of new scientific areas, and is well worthy of inclusion on our growing shelf of IRE PROCEEDINGS' Special Issues.

We wish to record here that the idea for this issue developed from a casual luncheon on October 24, 1957, with Harry Dauber, of the Department of Defense, as a guest of E. K. Gannett, our Managing Editor. As first discussed the subject was thought appropriate for a single paper, but it was soon seen that part of an issue would be needed, and finally it developed that nothing less than a complete issue could do justice to the available material. It was felt that the government-industry group known as IRIS (InfraRed Information Symposia) could be of great help in planning for the issue, and this aid brought with it the support of the IRIS chairman, Dr. Arthur R. Laufer, of the Office of Naval Research. The major effort in organizing the issue and coordinating the 70 contributions into a logical whole was made by Dr. Stanley S. Ballard, of the University of Florida. We also wish to recognize the section editors, Warren N. Arnquist, Lewis Larmore, Sidney Passman, Paul J. Ovrebo, and William Wolfe, as well as Harry Dauber, who generated the spark and fanned it into a roaring fire—of course he had a warm subject.

Saddle Points. Soon to be available is the index of IRE publications—yes, ALL of them, for the years 1953–1958. By use of a simple code you will find all the papers by prolific Jonathan Gloop properly listed, be they in PROCEEDINGS, TRANSACTIONS of the 28 Groups, or THE STUDENT QUARTERLY. Also in planning is a complete fifty-year index, again including all publications of the IRE, to be issued after the celebration of our Golden Anniversary in 1962.

As another improvement in service, we hope, your next PG assessment billing will include the assessments for all Professional Groups of which you are a member. As a result you may find a few fractional year amounts on the bill for some of your PG memberships, to adjust all to a common date, but we are sure you will understand the arithmetic when the bill arrives. Now you will know all at once to which PG's you belong, and more importantly—the ones to which you do not and should.—J.D.R.

A. P. H. Barclay

Director, 1959-1960

Alexander P. H. Barclay (SM'46) was born in Glasgow, Scotland in 1913, but has lived in Canada since 1926. He was graduated in 1935 from the McMaster University, in Hamilton, Ontario, where he studied chemistry and physics. The following year he received the M.S. degree in physics and communications from Cornell University, Ithaca, N. Y.

He then joined Canadian Westinghouse Co. where he designed radio receivers. Two years later he transferred to Northern Electric Co. to work on broadcast transmitters and audio equipment. During World War II, as a member of Research Enterprises, a Crown company, he coordinated most of the Canadian activity connected with the design and manufacture of magnetrons, klystrons, and VHF tubes for the company-produced radars.

Since the war he has served with Philips Electronics Industries of Toronto, successively as chief engineer of the electron tube division, government projects officer, director of engineering of the professional equipment division, and general manager of engineering and manufacturing of the same division, a post he currently occupies.

He is a registered professional engineer and has at various times been chairman of the Toronto Section of the IRE, a member of the Canadian Convention Committee and chairman of its Papers Committee. He is chairman of the Microwave Committee of the Canadian Radio Technical Planning Committee and also takes an active part in the Electronics Industries Association.

PREFACE*

ARTHUR R. LAUFER†, CHAIRMAN, NATIONAL EXECUTIVE COMMITTEE OF IRIS, AND EDITOR-IN-CHIEF, *Proceedings of IRIS*

ONE hundred and fifty-nine years ago, while moving a thermometer through the sun's spectrum, the astronomer Sir William Herschel found that the temperature recorded by the thermometer increased from violet to red and then continued to increase, reaching a maximum in the dark region beyond the red end of the visible spectrum. Thus was discovered the "infra"-red region of the electromagnetic spectrum. For more than one hundred years little use was made of infrared energy, largely because of the lack of a suitable detector. The detection problem can be understood from the fact that a modern wide-range infrared detector, the thermocouple, must often detect radiation which causes a temperature rise of only one-millionth of a degree with a resulting electrical signal of less than one billionth of a volt; the infrared radiation, being incoherent in nature, cannot be amplified through the use of resonant circuits such as are commonly employed with the coherent radiation in the radio portion of the electromagnetic spectrum.

Despite the discovery in 1917 by T. W. Case that thallous sulfide is photosensitive in the infrared, little practical use was found for this radiation outside the laboratory. Then, early in World War II, captured equipment revealed that the Germans were using infrared for secret signalling between infantry groups, for the surveillance of Russian tanks supposedly secure in the darkness, and for the detection of Allied night bombers which confused radars by the use of chaff. This was the turning point in the practical application of infrared to military problems. At about the same time, the American synthetic rubber program required rapid analysis of the C_4 fraction in butadiene production; since this could best be achieved through infrared spectroscopy, commercial infrared spectrophotometers for chemical analysis began to appear in 1943. This was the turning point for the commercial application of infrared. Also at this time, Dr. Robert J. Cashman of Northwestern University developed a design and a sensitizing treatment for thallous sulfide that resulted in a detector which was both simpler and more rugged than previous cells. The practical application of infrared radiation was now assured.

The physical basis for the military interest in infrared is simply that any object at a temperature above absolute zero (and every object is), having an emissivity greater than zero (and every object has), radiates electromagnetic energy, much of which is in the infrared. Thus all objects, ranging from heavenly bodies to jet aircraft to human beings, are natural radiators of invisible infrared energy, and can thereby be detected by means of passive instrumentation which does not reveal the presence of the observer. Add to this the facts that infrared detection is virtually jamproof, as contrasted with radio and radar, that many military targets are copious emitters of infrared, that infrared systems are far smaller, lighter, less complex and less expensive than comparable radar systems, and that the shortness of infrared wavelengths permits resolution far higher than that attainable even with our highest-resolution radars —and the military interest becomes obvious. An example often quoted is that whereas an X-band (3-cm) radar, with a 12-inch-diameter antenna and at a range of 5 miles, can resolve two twin-engine aircraft as separate targets if they are laterally separated by at least 1 mile, at the same range an infrared system working at 2 microns (0.002 mm) and using a 3-inch-diameter scanner can resolve individual engines on each aircraft.

Commercial interest in infrared stems not only from this natural emission, but also from the fact that the spectral absorption bands of most molecules lie in the infrared. Thus the selective absorption of infrared radiation by molecules reveals their presence and structure.

The development in production quantities during the past decade of new photoconductive detectors such as lead sulfide and lead selenide, which are both highly sensitive and fast in response, and of suitable optical materials, has led to an enormous growth in the commercial and military applications of infrared. Several hundred industrial and military organizations now include infrared research, development, and production in their programs. In industry, several thousand infrared spectrophotometers are being employed for the nondestructive and quantitative identification of chemical and biological unknowns, and this application is only in its infancy. Infrared is also being used in the automatic monitoring of chemical and biological processing, in temperature measurement and control in the manufacture of textiles, plastics, and metals, in fire and incipient-explosion detection, and in weather research. Future civilian applications are being developed in navigation, altitude determination, collision-avoidance systems, ground-speed indication, automatic landing systems, and in astronomy and various outer-space projects.

Ever-increasing military use for infrared is being found in surveillance, early warning and detection, photography and aerial mapping, search, acquisition and track, secure communications, missile guidance, fire control, fuzing, decoying, and countermeasures.

* Original manuscript received by the IRE, February 25, 1959.
† Office of Naval Research, Branch Office, Pasadena, Calif.

Despite the major current and anticipated activity in the infrared field, there is at present no unclassified American publication which brings together in one place the bulk of the basic information on infrared physics and technology. The PROCEEDINGS OF THE IRE appears to be a highly appropriate journal in which to publish a review of the infrared field, inasmuch as the field is substantially a marriage of optical physics and electronics. An attempt has been made to present here as comprehensive a review of the subject as security restrictions will allow. The material has been prepared under the auspices of the Infrared Information Symposia (IRIS), an organization sponsored by the Office of Naval Research and under joint-service direction. The IRIS organization sponsors a continuing series of classified symposia devoted to the military applications of infrared. The symposia are designed to facilitate the exchange of technical information, on a "need to know" basis, among the many government laboratories and industrial contractors engaged in infrared research, development, and production. The papers presented at the symposia are published in the classified journal entitled *Proceedings of IRIS*, which is distributed to all members of IRIS and to such others as establish the required need to know.

It may be of interest to mention here, as being representative of the difficulties encountered in fields other than infrared, the factors which led to the creation of IRIS. In the years immediately following World War II, the military infrared program was severely handicapped by the inadequate facilities for the exchange of information, such exchange being effected at best only with delay and through the exercise of considerable persistence and inquisitiveness. The flow of information was restricted to such an extent that certain contractors were not even aware of the existence of almost identical efforts being conducted by certain other contractors. These difficulties were not occasioned primarily by the need for military security, but stemmed rather from the lack of rapport between the different cognizant branches of the armed services, institutional rivalries, the desire of commercial concerns to keep secret their own technical procedures, and the absence of unifying meetings and reports. Such needless barriers were a real impediment to the military program, resulting in the duplication of effort from ignorance of parallel efforts, and slowing the advance of science and technology which thrive on the cross-fertilization of ideas.

In an effort to alleviate this situation, the Office of Naval Research, which has the responsibility for the coordination of research and development within the Naval establishment, in 1949 undertook the creation and sponsorship of the IRIS organization. IRIS meetings, now held bimonthly on alternate coasts, are attended by hundreds of scientists and engineers who gather together to discuss freely their problems and achievements in the classified areas of infrared. By publishing in the *Proceedings of IRIS*, these men have the opportunity of presenting their results to a relatively wide audience and of benefiting from the constructive criticism which such publication engenders. In substance, the IRIS organization affords those employed in this classified area the opportunity for discussion and publication which is afforded in unclassified areas by organizations such as the Institute of Radio Engineers and the American Physical Society. As a result, these scientists and engineers, though engaged in classified work which formerly entailed confining procedures and oppressive secrecy, now may again enjoy the feeling of "belonging" to the scientific community, with many of the benefits that society membership provides. The consequent improvement in the attitudes of these scientists and engineers and in the quality of their efforts cannot help being reflected in achievements beneficial to the missions of the military services.

Holding membership in IRIS are all the leading investigators in the field of military infrared; it is for this reason that the material in the following pages, prepared by these men, can be regarded as current and authentic. The difficult task of procuring, reviewing, and coordinating the material submitted by the many authors has been handled with high competence by the various section editors, whose efforts are gratefully acknowledged. Special acknowledgment must be made of the contribution of Dr. Stanley S. Ballard, whose responsibility it was to coordinate the over-all effort.

It is hoped that this presentation of the physics and technology of infrared radiation will furnish engineers with the necessary background for understanding the field, and will provide them with a foundation for further study of this rapidly growing science, which appears to be only on the threshold of its full realization.

SECTION 1. INFRARED, A NEW FRONTIER OF PHYSICS AND TECHNOLOGY*

STANLEY S. BALLARD†, GUEST EDITOR

INFRARED techniques have already proved their worth in academic and industrial applications and are now considered to be indispensable to the organic chemist and to many others. The acceptance of infrared as a basic technique in military applications has lagged behind its acceptance in the laboratory by 15 or 20 years, however, and is only now becoming generally acknowledged. Thus in semitechnical magazines and the press one sees infrared referred to as "the frontier frequency" and sees reference to "the infrared challenge of radar." It does appear that infrared is supplanting or at least supplementing radar as a basic detection, tracking, and reconnaissance technique, very much as radar partially replaced visual-optical methods during the course of World War II. The reasons for this emergence of infrared techniques after such a long period of borderline acceptance (or often downright rejection on the grounds of ineffectiveness) are now clearly seen: The greatest factor has been the development of more sensitive, faster, more reliable receivers of infrared radiation, usually called "detectors." Another important fact bearing on the favor now being found for infrared military applications is that military targets, for example jet engines and rocket motors, radiate much more power in the infrared portion of the spectrum than was previously the case. The fact that infrared is a passive technique in most applications is also strongly in its favor in the military theater, as is its admitted difficulty of being countermeasured and jammed. Finally, much more is now known about atmospheric absorption processes, but many military operations are now taking place at such high altitudes that atmospheric attenuation is no longer a serious factor. These various facts are well known by persons involved in military technology, but they bear repeating since they account, in a very real sense, for the present high level of interest in infrared.

The final user of an infrared equipment is not likely to be interested in the individual components, but rather in the device, machine, or over-all system. It is informative to compare the various elements of a laboratory infrared instrument such as a spectrophotometer with the elements in an infrared detection and tracking system such as an air-to-air homing missile. At first glance one sees very little similarity between these two major applications of infrared. On closer examination, however, one sees that in every case there are five basic units: the source of radiant energy, an absorbing medium, an optical system, a detector of radiant energy, and finally a presentation or output by which the data are made available to the operator or observer. In a spectrophotometer, which is of such great value to chemists and others in analyzing the molecular constituents of gases, liquids, and solids, the elements are as follows: The radiant source is fixed and is controlled so as to be as constant and steady in output as possible; the absorbing medium is usually of the greatest interest since it is the "unknown"—the sample being analyzed chemically or whose composition is used to control a chemical manufacturing process. The optical system of the spectrophotometer performs two functions: the first is to bring to a focus on the detector the energy from the radiant source, often providing a parallel beam in which the sample can be placed; the second is to vary the wavelength at which the absorption measurement is being made. This variation is carried out by rotating prisms or gratings and is usually programmed so as to sweep through a predetermined part of the spectrum. The detector in a spectrophotometer should be a very stable element. Sensitivity is important, but a short time constant is not nearly as critical as in "field" applications. The presentation means is usually simple and straightforward, such as a pen-chart recording in which transmission or absorption of the sample is plotted against wavelength. For some special spectroscopic instruments such as those used in studying flame and explosion spectra, faster operation is required and the spectrum is scanned at a much more rapid rate of several times per second; cathode-ray-oscilloscope presentation is ordinarily employed.

In what might be called a field equipment and is most often a military infrared device, the same five elements are present but the requirements placed on them differ considerably. For instance, the source is usually not controllable but is in fact the item which is being detected, tracked, or mapped—the "target," in military parlance. The target is always seen against some sort of background: the cold blue sky, a cloudy sky, the horizon thermal discontinuity, or perhaps ground clutter. Therefore considerations of source or target radiation end up as considerations of target signal vs background signal. The absorbing unit in this second example is the earth's

* Original manuscript received by the IRE, July 22, 1959.
† University of Florida, Gainesville, Fla., and Consultant to The RAND Corp., Santa Monica, Calif.

atmosphere. At the lower altitudes, say 30,000 feet and below, and particularly in times of inclement weather, the infrared absorption of the atmosphere may be the limiting factor in the operation of the system. For very-high-altitude observations, however, one is above most of the water vapor and carbon dioxide absorption and is in an environment where the weather is always clear and the deleterious effects of atmospheric absorption need hardly be considered. A critical case is in reconnaissance or mapping the surface of the earth from a high altitude, when the incidence of cloud cover may interfere entirely with obtaining the desired results.

The optical system of a military infrared device is ordinarily rather simple and comprises chiefly a means of intercepting radiation from the target or source and bringing it to focus on the sensitive area of the detector. Sometimes scanning motions are incorporated for the search phase, and usually the beam is chopped just in front of the detector in order to provide an ac signal and also to permit spatial filtering techniques to be used. Very rarely is the wavelength band passed by the system varied during operation—it is usually predetermined by the transmitting optical elements and optical filters in the system as well as by the sensitivity limits of the detector. The special requirements placed on the detector usually emphasize high sensitivity, short time constant, and low noise. The presentation features of modern infrared systems may incorporate the various sophisticated techniques that are now used in radar and sonar systems. The signal may be stored on a magnetic tape for playing back at leisure and through appropriate filter circuits to bring out the desired frequency components and enhance contrast, or it may be presented for visual observation in real time on a cathode-ray-tube face, where it can be photographed for later study.

A final general consideration which should be mentioned is that of noise, in its broadest sense. In each unit of an over-all system, noise must be considered and its suppression or control must be properly effected. Background noise may limit target detection, detector noise has been a limiting factor in many systems until relatively recently, and amplifier and circuit noise are subjects well known to the readers of this journal.

The major sections of this issue are devoted to detailed and critical treatments of the various components, factors, systems, and applications involved in present-day infrared instrumentation. Many if not all of the items mentioned in the above comparison of the spectrophotometer with a military system are treated in considerable detail, as the reader will discover. Additionally, some less technical, qualitative material has been included both because of its possible interest to the reader and because it serves to complete the picture of "infrared today." Section 5 on applications is a rather lengthy but probably not exhaustive listing and brief discussion of the many places, both military and nonmilitary, where infrared is being used with success—some of the items included therein may be surprising even to those who have worked in the field for many years. Section 2 is a survey of early infrared developments, and it effectively traces the history of the field from the time of World War I up to practically the present day. The more academically minded reader will realize that the infrared art is an older one and that whereas great advances have been made during the last decade or two, there must have been significant discoveries made in the early days. An excellent discussion and historical survey of the very early development of the infrared spectral region, commencing of course with Sir William Herschel's discovery in 1800 and carrying through to the end of the 19th century, has been prepared by Professor E. Scott Barr of the University of Alabama and Redstone Arsenal and will be published in an early issue of the *American Journal of Physics*.

A 100-item bibliography is given in Section 6 to supplement the specific literature references quoted in the several papers of this issue.

There are references, especially in Section 2, to the fact that infrared developments have been pursued also in England and in Germany during this same time period. The French have been active in cell development work and are now producing satisfactory photoconductive detectors. Some indication as to the Russian interest in infrared matters is given in paper 5.1.10.

Section 3, "Infrared Physics," lays the scientific groundwork for discussing the subsequent technological applications by treating sources, atmospheric properties, detectors, and finally the basic range equation which is the theoretical and predictive heart of any detection system. Section 4, "Infrared System Considerations," is the largest of all, including some 27 papers as compared to 15 in Section 3. Tables of contents of each of the larger sections are given in the introductory paragraphs for the convenience of the reader, and a master Table of Contents is of course to be found in the front of the issue.

It will be understood that the several sections cannot be written at the same technical level, because of the differing nature of their subject matter. Therefore Sections 1, 2, 5, and, of course, 6 are necessarily of a qualitative nature whereas some of the papers in Sections 3 and 4 should be sufficiently highly technical and mathematical to satisfy the most demanding reader.

It might be thought that a collection of papers such as this, with over fifty individual contributors, would provide what might be called a "Who's Who" of infrared physics and technology, and this possibility is alluded to at the end of the Preface. This is partially true, to be sure, but several individuals who were invited to prepare papers for this issue were unable to do so because of the urgency of their professional duties. Also, there are those who were active in infrared during World War II but have gone into other fields and would no longer consider themselves to be contemporary workers in infrared physics and technology. I am glad that Dr. Arnquist has listed, throughout Section 2, so many

of the individuals who have been active in infrared research and development during recent years. The combination of his extensive listing of persons with the authors of articles in this issue does in fact comprise a fairly complete list of the acknowledged contributors to the advance of contemporary infrared. There are a few names missing that come to my mind immediately, such as those of A. H. Canada and E. R. Ricker, who were active during the war in infrared developments at the U. S. Army Engineer Board, now called the Engineer Research and Development Laboratories; and J. M. Fluke and F. B. Isakson, then in the Navy's Bureau of Ships, who were vigorous exponents of applications of near-infrared, active systems. There were a number of persons who worked on infrared projects of the National Defense Research Committee but who are no longer as active in this field; the names of E. H. Land and D. S. Grey of Polaroid Corporation should be mentioned, as well as J. S. Owens and G. A. Van Lear, formerly of the University of Michigan, and A. C. Bemis and R. C. Lord of M.I.T. H. H. Nielsen carried out the first comparison of the new infrared detectors at the Ohio State University. N. F. Beardsley was active in optical projects in those days, and since the war has played a major part in the sponsoring of infrared developments by the Wright Air Development Center, where his place has recently been taken by L. H. Meuser. L. M. Biberman, T. R. Whitney, and R. S. Estey worked in infrared at the Naval Ordnance Test Station, as did a number of others whose names are not listed on these pages.

Finally, the name of Harry Dauber must be mentioned. It is he who originally conceived the idea of having a special issue of this journal devoted to infrared technology, and he was active in planning the contents of the issue. It is regretted that the pressure of his professional duties, plus the fact that he has recently set up his own business, with offices in New Jersey and in Germany, prevented him from continuing to work with us in the preparation of this issue. We have known Mr. Dauber as a vigorous worker in electronics, and his many ingenious and far-looking projects in infrared instrumentation are well recognized. It is particularly appropriate that the cover photograph illustrates one of his favorite developments namely the use of color translation to aid in the presentation and interpretation of infrared reconnaissance pictures.

SECTION 2. SURVEY OF EARLY INFRARED DEVELOPMENTS*

W. N. ARNQUIST†

INFRARED energy and its interaction with matter represent at the same time a branch of physics dating from the pioneering discoveries of Sir William Herschel in 1800, and a rapidly expanding area for applications to industrial and military problems today. After more than a century of basic research, practical problems are utilizing infrared techniques more and more and we are witnessing the birth of a new technology. That the current applications are but a beginning may be confidently anticipated. Man is moving rapidly in the direction of "seeing" his environment by making full use of the thermal radiations characteristic of all bodies in many octaves of the electromagnetic spectrum instead of just the one octave of the visible region.

The word "infrared" recalls different things to different individuals. It reminds the physicist of a comparatively small part of the electromagnetic spectrum, and of numerous characteristic interactions between the radiation in this region and various forms of matter. To the chemist and chemical engineer, it recalls that tremendously useful area known as molecular spectroscopy and all of the analytic and control processes that make use of these techniques. The industrial design engineer and the space technologist think of radiative heat-transfer processes and various specialized devices. Finally, the man on the street remembers heat lamps, infrared photography, infrared cooking, Sniperscopes, Sidewinders, and various other wonders which he hears about from time to time.

The present survey of early infrared developments was prepared to serve as background material for the technical articles on current infrared physics and its applications found in this issue. As such, it is restricted largely to those developments leading to the current emphasis on photodetectors. The first phase is the World War I period and the decade following this in which the Case Thalofide cell appeared. The second period carries through World War II, when infrared photoemissive and phosphor devices appeared and many improvements were made on photoconductive receivers. The more recent period has been characterized by rather sophisticated developments with photoconductive and photovoltaic receivers, making use of the tremendous current advances in solid-state physics and electronics. A section entitled "Other Applications" is included to give some idea of the breadth of the infrared field today and of the possibilities for tomorrow.

Besides being appropriate for the present purpose, the emphasis outlined above results in very little duplication with other surveys in the open literature. This is largely because the early infrared developments, outside the field of infrared spectroscopy and related areas, were for military devices and only scattered accounts are available. Even today the influence of military interest in the field of photodetectors is the dominant one. It is interesting to note the recent words of the Director of the National Physical Laboratory of England, a leading physicist in that country and for a number of years Professor of Physics at the University of Michigan. On the occasion of the Forty-Eighth Kelvin Lecture delivered before the Institution of Electrical Engineers in 1957, Sutherland[1] said, "There is little doubt that the problem of detecting a military target by the 'passive' method of observing the heat radiated from it was primarily responsible for the recent remarkable advances in the techniques of photodetection of infra-red radiation. Yet the applications of these new photodetectors have been of far greater importance in pure and industrial science than in the military field." It is well to remember that knowledge and techniques developed for military applications reach their greatest importance when introduced into scientific and industrial fields.

Because of the restrictions of time and space, the present survey is not as complete as it might be. The available sources have been limited, particularly with regard to pertinent military developments. It is well-known that the policies of sovereign states are far from uniform in the release of military information. For the present purpose, it is particularly fortunate that volumes 3 and 4 of the Summary Technical Report of Division 16, National Defense Research Committee, have been declassified recently. If the account of German military infrared seems proportionately large, it is because this information was carefully collected by the occupying powers at the end of the war and much of it has been released in the United States.

Infrared systems are classified ordinarily as image-forming or non-image-forming. Also, one distinguishes "active" systems, where the target must be illuminated appropriately, from "passive" systems, where the nat-

* Original manuscript received by the IRE, July 17, 1959.
† System Development Corp., Santa Monica, Calif.

[1] G. B. B. M. Sutherland, "Infra-red radiation," *Proc. IEE*, vol. 105, pt. B, pp. 306–316; 1958.

ural radiations of the target are utilized. Systems are sometimes identified according to the detecting element used as "thermal," where the change in temperature of the receiving element is important, or "photo," where a specific effect results from the absorption of a photon. Furthermore, the region of the spectrum is often used to distinguish near- (NIR), intermediate- (IIR), or far- (FIR) infrared types. For an introduction and general reference to modern infrared instrumentation and techniques, the reader is referred to the recent book by Smith, Jones, and Chasmar[2] to which a number of subsequent particular references will be made.

Early Applications

It is not generally known that the United States, the British, and the German military organizations had active interests in infrared systems nearly half a century ago. In World War I, each country produced devices which were promising, and in some cases these were used in an experimental fashion. In the second World War, the corresponding programs were much larger, so that certain devices went into limited production and were used with some success; also other countries became interested.

It is easy to see the origin of this interest. The infrared part of the spectrum represents that invisible radiation which makes possible secure signaling and communication with light-weight equipment and the detection of military targets by means of their natural radiations. "Seeing in the dark" is facilitated, and thus nocturnal military operations can be conducted, often to better advantage than in the daytime. The hopes of military planners frequently outdistanced the technological development of the time and so, in the words of a military observer a few years ago, infrared has been until recently, "always a bridesmaid, never a bride." Basically, this has been because the military needs have been, almost exclusively, for information-gathering systems, and so success has depended on the development of both high-speed receivers of sufficient sensitivity and high-speed information-handling equipments; that is, on photodetectors and electronic systems. Thus, the history of military infrared follows very closely the development of fast receivers whose output is electrical, and the successful devices make full use of the available electronic development at the time.

Although optical photoconductivity was discovered in selenium in 1873 by Smith[3] and a similar photovoltaic effect had been noted as far back as 1839 by Becquerel,[4] the phenomena attracted little interest. Apparently nothing was done with infrared in this connection until 1904 when Bose[5] announced the discovery of an infrared photovoltaic effect in naturally-occurring lead sulfide or galena. This too was seemingly ignored until the World War I period, at which time Case[6] reported the "change of resistance" of a number of natural minerals besides galena in the visible and near infrared, and Pfund[7] studied this photoconductivity in cuprous oxide. However, because of the relatively advanced state of thermocouples and bolometers, most workers tried to use these receivers in military devices in this country and also in England and Germany, but with little success. Hoffman[8] has described one of the earliest passive systems, utilizing a thermopile and galvanometer, with which a man could be detected at 600 feet and an airplane at nearly a mile.

The principal historical development of this period was the Case "Thalofide" cell. This was invented during the war years, and some of its properties were described by Coblentz.[9] Although some infrared photoconductivity was found in pure thallous sulfide, the big discovery of Case[10] was that appropriate heat treatments with the addition of oxygen increased the sensitivity considerably. Furthermore, the cells were fast in their response compared to thermocouples and bolometers. This work represents the first attempt to enhance the natural photoconductivity of a material by the addition of small amounts of another substance; it made possible the first military use of infrared.

Late in 1917,[11] the Case Research Laboratory at Auburn, N. Y., demonstrated to the U. S. Army and Navy an active system composed of a filtered searchlight source, a 24-inch collector, and a Thalofide cell. The device transmitted and received blinker signals over an 18-mile range in "average" weather. Smaller versions usable to about 4 miles were built by the end of the war. Voice systems were also developed using modulated acetylene flame sources with some success. Thalofide blinker systems actually saw field use with the military forces during the latter part of the war in guiding airplanes to landing fields and in keeping convoys together.[11] Some of this early work has been described by Case.[12]

[2] R. A. Smith, F. E. Jones, and R. P. Chasmar, "The Detection and Measurement of Infra-Red Radiation," Oxford University Press, New York, N. Y.; 1957.

[3] W. Smith, "Effect of light on selenium during the passage of an electric current," *Nature*, vol. 7, p. 303; 1873.

[4] A. E. Becquerel, "On electric effects under the influence of solar radiation," *Compt. rend. Acad. Sci.*, vol. 9, pp. 711–714; 1839.

[5] J. C. Bose, U. S. Patent No. 755,840; 1904.

[6] T. W. Case, "Notes on the change of resistance of certain substances in light," *Phys. Rev.*, vol. 9, pp. 305–310; 1917.

[7] A. H. Pfund, "The light sensitiveness of copper oxide," *Phys. Rev.*, vol. 7, pp. 289–301; 1916.

[8] S. O. Hoffman, "The detection of invisible objects by heat radiation," *Phys. Rev.*, vol. 14, pp. 163–166; 1919.

[9] W. W. Coblentz, "The spectro-photo-electric sensitivity of thalofide," *Phys. Rev.*, vol. 15, pp. 139–140; 1920.

[10] T. W. Case, " 'Thalofide cell'—a new photo-electric substance," *Phys. Rev.*, vol. 15, pp. 289–292; 1920.

[11] "Summary Technical Report of Division 16, National Defense Research Committee," vol. 3, chs. 1, 6 by W. L. Hole, pp. 18–26 (microflash lamps), pp. 38–43 (cesium vapor lamps), pp. 200–214 (IRRAD); vol. 3, chs. 4, 5 by J. R. Platt, pp. 108, 109, 111, 146 (military communication systems), pp. 170–189 (Type D system); vol. 4, ch. 2, by C. A. Federer, Jr., pp. 28–30 (night driving); 1946.

[12] T. W. Case, "Infrared telegraphy and telephony," *J. Opt. Soc. Am.*, vol. 6, pp. 398–406; 1922.

The Thalofide cell was marketed for a few years after the war and, partly because it was incompletely described in the literature, it did much to stimulate interest in infrared in other countries. Thallous sulfide cells were made in Italy by Majorana and Todesco[13] and in Germany by Sewig.[14] Similar cells of the photovoltaic type were developed in the U.S.S.R. and have been described by Kolomiez.[15] An excellent review of this field, which includes an account of the comparable cells made for the British Admiralty, has been published by Sutherland and Lee.[16]

The military developments for signaling purposes in Germany during the first World War were largely confined to narrow-beam optical systems in the visible range using a selenium photoconductive receiver. These forerunners of the "Lichtsprechers" of the next war period have been described by Thirring,[17] including a device which went into production but did not see field use. As selenium is sensitive in the near infrared, this could have been an early infrared system. However, no infrared filter is mentioned in this account. Work on similar communication systems was done in England at this time and has been described by Rankine.[18]

World War II Applications

After a decade of essentially no infrared activity, interest in improved detectors began in Germany around 1930 when Lange[19,20] described a galena photovoltaic cell for detecting infrared radiation. In about 1932, the German military infrared program was resumed. The initial work was with galena using "cat-whisker" contacts. It was found that some natural crystals were much better than others, that the contacts were unreliable and, in general, that the detectors were far from satisfactory. Two approaches were used in developing sensitive layers with dependable electrode contacts. In time, not only lead sulfide but also lead selenide and lead telluride detectors were made by several organizations, and many of the properties of the cells were measured, including the increase in sensitivity due to cooling. This feature was incorporated into a few practical devices using solid carbon dioxide as the coolant in most cases and liquid nitrogen in a few instances. The two approaches were differentiated by the method used in forming the layers. Professor B. Gudden of the University of Prague used the vacuum evaporation or "dry" technique and made excellent receivers. Uncooled lead sulfide cells of this type that were used mainly in signaling and communication equipment were produced at Zeiss-Ikon, Dresden, by a group under P. Goerlich. At the University of Berlin, a group under E. W. Kutzscher became interested in chemical deposition, or "wet" techniques, and ultimately made the most sensitive of the German cells. These detectors were known as Elac cells and were produced mainly at the Electroacustic Gesellschaft in the city of Kiel by an infrared research and development group under Kutzscher. Laboratory-type lead selenide cells were made by this group also. These detectors have been described by Oxley[21] and others.[16] At the Research Institute of the Siemens-Halske A.G. in Berlin, some investigations on lead telluride cells were conducted, and in the field of thermal detectors, bolometers were developed at the Physical Institute of the University of Frankfurt by Professor M. Czerny and his collaborators and at the Carl Zeiss Company in Jena.

The availability of photoconductive and thermal detectors made possible the development of a number of infrared detection systems. These included a ground-based device for directing searchlights and anti-aircraft fire against airplanes, a ground-based device for detecting ships from the shore, a fixed-base triangulation-type rangefinder for night use, a Snorkel installation for detecting ships and airplanes, airborne detection devices for airplanes and hot targets, both air-to-air and air-to-ground homing controls for missiles, and an infrared proximity fuze. Work on these systems was performed by a number of governmental and industrial organizations. Most of the devices became available for tests in the laboratory and some were produced on a limited scale. Among the latter were two types of a ship detector and tracker; one of these, using photoconductive detectors, was developed by Kutzscher's group at Kiel while the other, using a bolometric detector, was developed by a group under W. K. Weihe at the Carl Zeiss Company in Jena. Both devices were used against shipping on the English Channel. The devices for the detection of bombers from night fighters were known as Keil systems, and one of these, which became known as the Kiel IV, was planned for substantial production when the war ended; it was developed by Weihe and his group. Other devices were in a partially developed state at the end of the war, and since most of the research and development centers were by that time located in the eastern and central parts of Germany, much of the equipment, engineering data, and reports were acquired by the U.S.S.R.

[13] Q. Majorana and G. Todesco, "Thallium photo-conducting cells," *Atti accad. nazl. Lincei*, vol. 8, pp. 9–14; 1928.
[14] R. Sewig, "Thallofide and selenium cells," *Z. tech. Physik*, vol. 11, pp. 269–273; 1930.
[15] B. Kolomiez, "New positive barrier plane photoelectric effect and the new barrier plane photo-cell," *Compt. rend. Acad. Sci., U.R.S.S.*, vol. 19, p. 5; 1938.
[16] G. B. B. M. Sutherland and E. Lee, "Developments in the infra-red region of the spectrum," *Repts. Prog. Phys.*, vol. 11, pp. 144–177; 1946–1947; published by The Physical Soc., 1948.
[17] H. Thirring, "Neue Apparate für Lichttelephonie," *Physik Z.*, vol. 21, pp. 67–73; 1920.
[18] A. O. Rankine, "On the transmission of speech by light," *Proc. Phys. Soc. London*, vol. 31, pp. 242–268; 1919.
[19] B. Lange, "Über eine neue Art von Photozellen," *Physik Z.*, vol. 31, pp. 964–969; 1930.
[20] B. Lange, "Über die spektrale Empfindlichkeit von Sperrschicht-Photozellen," *Naturwiss.*, vol. 19, pp. 525–530; 1931.
[21] C. L. Oxley, "Characteristics of cooled lead sulfide photoconductive cells," *J. Opt. Soc.*, vol. 36, p. 365; 1946.

Considerable effort was directed toward the development of the voice communication devices known as "Lichtsprechers."[22,23] They employed thallous sulfide and later lead sulfide receivers and were of ingenious design using a variable total-reflection-type modulation system with precision optics. The performance was nearly as good in the daytime as at night up to ranges of about 10 miles. Although they were used in the African campaign, their narrow beams resulted in alignment problems which limited their military importance. Infrared image converters of the focused-electron-beam type were developed by two groups in Germany under W. Schaeffernicht and W. Heimann, respectively. These saw limited applications in communication devices, in detecting infrared identification signals, and in night driving with infrared headlights, but apparently they were not made in sufficient quantity to be of real value. Some imaging work was done with phosphors, but this was started too late to result in usable devices.

As a matter of history, the first working infrared image device, based on a technique called "evaporography," should be mentioned here; it is due to Czerny[24] in 1929 and dates from the original work of Sir John Herschel.[25] The operation depends on the differential evaporation of a volatile liquid sprayed on a thin membrane, when an infrared image is formed on the membrane. As a detector, it is relatively slow and fragile; therefore, there was little military interest in it. Further work since the war has been done in Germany by Gobrecht and Weiss.[26] B. H. Billings and co-workers, with Air Force and Signal Corps support at Baird Associates (now Baird-Atomic, Inc.), have developed an advanced design which is quite successful and which has been declassified; it is described elsewhere in this issue.

Besides the Kiel IV, there were other noteworthy developments from the research laboratories of the Zeiss company. About 1940, G. Hass found that silicon monoxide could be used as a protective layer on front-surface mirrors. This was of special importance for the German optical and infrared equipment, as the protected surfaces could be cleaned repeatedly in the field with ordinary care, without destroying the optical properties. Since the war, SiO layers have been used by many workers in providing protective or antireflection coatings on various optical materials, and Hass and co-workers[27,28] have described these developments for infrared applications. Another important discovery from the same laboratories, due to A. Smakula and R. Koops about 1943, was KRS-5 and the other mixed crystals of this kind. KRS, incidentally, stands for "Kristalle aus dem Schmelzflus"—crystals from the melting-pot. These crystals are remarkably transparent at the longer wavelengths. For example, KRS-5, which is given by Koops[29] as being 44 per cent thallium bromide and 56 per cent thallium iodide, is transparent to about 40 μ. Further references to these interesting materials may be found in the volume by Smith and co-authors,[2] and in this issue.[30]

Shortly after the National Defense Research Committee and the Office of Scientific Research and Development were established in the United States, in 1940–1941, Division 16 Optics and Camouflage, was organized to deal with the fields of light and infrared, under the direction of Dean George R. Harrison of the Massachusetts Institute of Technology. Two volumes of the NDRC Summary Technical Report are devoted to Non-Image-Forming Infrared and Image-Forming Infrared, respectively. The work on components, communication by voice and code, recognition and identification, ranging and direction of targets, and development of detectors and of receiving equipments for a variety of purposes was carried out by Section 16.4 under O. S. Duffendack. Section 16.5, under W. E. Forsythe and H. E. Ives, was concerned with imaging devices and their applications. A list of the major organizations in this OSRD program together with a description of some of the components developed has been given by Fluke and Porter.[31]

Probably the most significant infrared development in the United States during the 1930's was the RCA infrared image tube. Using the silver-cesium-oxide photoemissive surface, due mainly to the work of Koller,[32] and the developments in electron optics of Morton and Ramberg,[33] Zworykin and Morton at the Radio Corporation of America constructed a device which accepted an infrared image at one end and delivered a corresponding visible image at the other. With

[22] A. Elliott, "Recent advances in photo-cells for the infrared, in "Electronics and their Application in Industry and Research, Pilot Press, London, Eng.; 1947.

[23] W. S. Huxford and J. R. Platt, "Survey of near infrared communication systems," *J. Opt. Soc. Am.*, vol. 38, pp. 253–268; 1948.

[24] M. Czerny, "Über Photographie im Ultraroten," *Z. Physik.*, vol. 53, pp. 1–12; 1929.

[25] J. F. W. Herschel, "Account of a process for rendering visible the calorific spectrum by its effect on paper properly prepared and some further results obtained respecting the distributions of heat therein," *Trans. Roy. Soc., London*, vol. 131, pt. I, pp. 52–59; 1840.

[26] H. Gobrecht and W. Weiss, "Zur photographischen Aufname im Ultrarot nach der Methode von Czerny (Evaporographie)," *Z. angew. Physik.*, vol. 5, pp. 207–211; 1953.

[27] G. Hass, H. H. Schroeder, and A. F. Turner, "Mirror coatings for low visible and high infrared reflectance," *J. Opt. Soc. Amer.*, vol. 46, pp. 31–35; 1956.

[28] J. T. Cox and G. Hass, "Antireflection coatings for germanium and silicon in the infrared," *J. Opt. Soc. Am.*, vol. 48, pp. 677–680; 1958.

[29] R. Kopps, "Optische baustoffe aus binären Mischkristallen," *Optik*, vol. 3, pp. 298–304; 1948.

[30] W. L. Wolfe and S. S. Ballard, "Optical materials, films, and filters for infrared instrumentation," paper 4.2.3, this issue.

[31] J. M. Fluke and N. E. Porter, "Some developments in infrared communications components," PROC. IRE, vol. 34, pp. 876–883; November, 1946.

[32] L. R. Koller, "Some characteristics of photoelectric tubes," *J. Opt. Soc. Am.*, vol. 19, pp. 135–145; 1929.

[33] G. A. Morton and E. G. Ramberg, "Electron optics of an image tube," *J. Appl. Phys.*, vol. 7, pp. 451–459; 1936.

this "image-converter" tube, both an infrared telescope and a microscope were built and described by these workers[34] in 1936. Improvements were added at RCA until, in 1939, the sensitivity was adequate for a night-driving demonstration for the military. With the establishment of the National Defense Research Committee, the development of the tube was accelerated and work was started on a number of active systems built around it. In 1942, the tube went into production as the RCA 1P25 shown in Fig. 1, and several thousand were manufactured. The chief uses in the Army were in the Snooperscope and the Sniperscope, which were employed to a considerable extent, especially in the Pacific. Fig. 2 shows modern Sniperscopes mounted on carbines ready for use. Truck- and tank-driving equipments, including a binocular electronic telescope with which a driver could operate a vehicle at about 25 miles per hour,[11] were developed for the Army. This binocular instrument made possible airplane landings on a dark runway marked out with infrared sources. Devices using the image-converter tube were shown to be useful in launching and landing boats at night, in driving locomotives, and for night communication between ships. Morton and Flory[35–37] have described this modern focusing-type image converter and some of its military uses.

Infrared detection devices of quite another type resulted from the development of phosphors, principally by B. O'Brien and his group at the University of Rochester. Following earlier work in Vienna just before the war broke out, F. Urbach with others[38] continued the development of phosphors at Rochester and introduced the concept of double activation. Further refinements were added by Ward[39] at the Brooklyn Polytechnic Institute, where production of the phosphor surfaces took place. The detection devices, called "metascopes," depended on the stimulated emission of visible light from previously-excited phosphor layers by focused infrared radiation on these surfaces. Excitation by ultraviolet or visible light or by the use of radium radiations was employed. These devices were lighter, cheaper, less fragile and simpler, but inferior in sensitivity and resolution as compared to the image tube. The metascopes went into production and were used by the Army and the Navy in both the European and the Pacific Theaters. A number of types were developed, together with appropriate infrared sources, for special applications including paratroop reconnoitering operations. Much of this work has been described by O'Brien.[40]

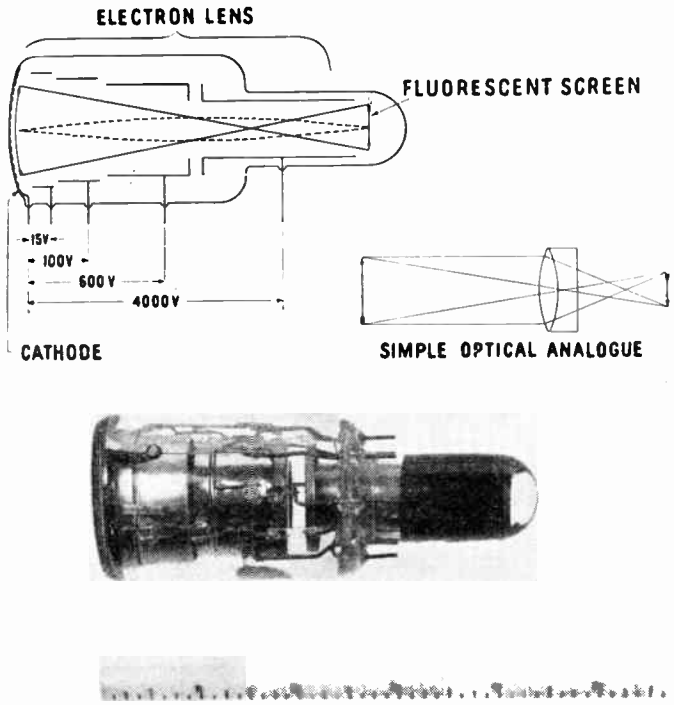

Fig. 1—The original 1P25 image converter tube developed by the Radio Corporation of America. Its operation is indicated by the schematic drawing.

Fig. 2—Sniperscopes mounted on carbines for use by foot soldiers.

The "icaroscope," or sun telescope, is of interest as a novel application of the phosphor research at the University of Rochester, although not as an infrared device. With it one could look directly at the sun and spot airplanes at more than 25,000-foot altitude with ordinary sky conditions. Operation depended on the saturation effect in the afterglow of a specially-developed phosphor. With a suitable arrangement of rotating shutters, the phosphor surface first received the focused incoming light and was stimulated by it. Then the light was cut

[34] V. K. Zworykin and G. A. Morton, "Applied electron optics," *J. Opt. Soc. Am.*, vol. 26, pp. 181–189; 1936.
[35] G. A. Morton and L. E. Flory, "Infrared image tube," *Electronics*, vol. 19, pp. 112–114; 1946.
[36] G. A. Morton and L. E. Flory, "Night vision with electronic infrared equipment," *Electronics*, vol. 19, pp. 192–204; 1946.
[37] G. A. Morton and L. E. Flory, "An infrared image tube and its military applications," *RCA Rev.*, vol. 7, pp. 385–413; 1946.
[38] F. Urbach, D. Pearlman, and H. Hemmendinger, "On infra-red sensitive phosphors," *J. Opt. Soc. Am.*, vol. 36, pp. 372–381; 1946.
[39] R. Ward, "Preparation and properties of infra-red sensitive strontium selenide and sulfide-selenide phosphors," *J. Opt. Soc. Am.*, vol. 36, pp. 351–352; 1946.
[40] B. O'Brien, "Development of infra-red sensitive phosphors," *J. Opt. Soc. Am.*, vol. 36, pp. 369–371; 1946.

off and the eye viewed only the afterglow in which the sun's brightness was reduced to some 20 to 50 times that of the surrounding sky.

Considerable effort was expended in the NDRC program on sources and filters, especially for the active infrared systems. High-power sources were desired, with all visible light filtered out for security purposes. The most practical of the known intense sources were the heated filament, the carbon arc, and the high-current gas or vapor lamps. All were strong radiators in the visible so that the rather severe filtering problem was to develop sharp long-wave-pass materials which would be rugged and stand relatively high temperatures. Two groups in the United States undertook this problem, each producing filters with excellent spectral characteristics but with less heat stability than desired. At the Ohio State University, Shenk and co-workers[41] developed a series of modified formaldehyde plastics using commercially-available dyes. These were mounted on glass plates and had sharp cutoffs from 0.5 to 1.0 μ. Similar filters were made at the Polaroid Corporation by finding dyes appropriate for treating cellophane, nylon, and polyvinyl alcohol films on glass. These developments have been described by Blout and coworkers;[42] they included a band-pass filter that uses the cutoff of glass for the long-wave limit.[30] In general, these filters were very successful and were used for the Snooperscope and Sniperscope, and for most of the signaling or communication devices. In some of the night-driving systems it was necessary to fall back on glass filters, which were supplied by the Corning Glass Works in laminated sheets, and in other cases these were used as a matter of convenience.

Many of the sources used in the active systems were tungsten-filament lamps. These were dependable, simple, rugged, and inexpensive. They were used, for example, in the Snooperscope and Sniperscope, and in the night-driving illuminators. General Eletric constructed special lamps of this type which could be modulated up to about 90 cps and thus could be used in code-signaling systems. In voice communication, low-pressure cesium-vapor lamps of high modulation efficiency were developed by Westinghouse. These were very efficient from the standpoint of energy concentration in the infrared, with some 20 per cent of the input power appearing in the two resonance lines at 0.85 and 0.89 μ. Microflash lamps were developed by General Electric using moderate pressures of an argon-hydrogen mixture, for example. They were made in three types, with flash durations of 30, 3, and 1 μsec, and were used in an infrared "radar" device known as IRRAD (Infrared Range and Direction). When triple-mirror reflectors

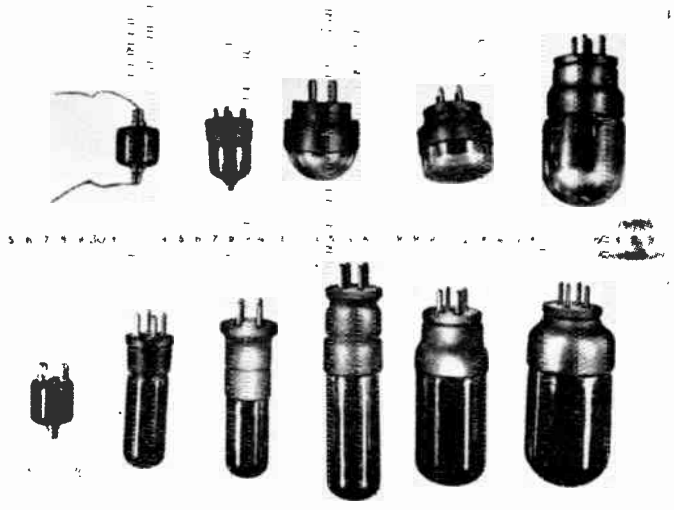

Fig. 3—Cashman thallous sulfide cells of about 1944.

were used to return the beam, this device operated reasonably well at ranges of the order of a mile or two. Diffusely reflecting targets such as a man or a ship offshore were tried, and it was found that the physical size of the target tended to compensate for the low reflectivity, so that the best ranges again turned out to be of the order of a mile. Although these devices were not produced, they are of interest as the first application of pulsing infrared for range determinations.

In that part of the NDRC infrared work which had to do with non-image-forming devices, there were broad programs for active systems in the near infrared and for passive applications in the far infrared. Each required detector development. Professor R. J. Cashman and his group at Northwestern University made the most useful NIR detectors. Beginning in 1941, the Case Thalofide cells, which had always been relatively unstable and thus undependable, were highly developed and made equal to or better than cesium phototubes in both sensitivity and stability.[43,44] A number of these early units are shown in Fig. 3 to indicate something of the state of the art at that time. The General Electric Company produced them in considerable quantity. In 1944, Cashman turned his attention to lead sulfide and developed this detector also for production. He discovered the large improvement due to cooling, and both the room-temperature cells and those cooled with solid CO_2 were in considerable demand for a number of years after the war.

The Cashman detectors were used in most of the active systems. These included an airborne glider position indicator, a life-raft search equipment, an enemy infrared installation locator, a detection and range-measuring device, and various code- and voice-communication

[41] J. H. Shenk, E. D. Hodge, R. J. Morris, E. E. Pickett, and W. R. Brode, "Plastic filters for the visible and near infra-red regions," *J. Opt. Soc. Am.*, vol. 36, pp. 569–575; 1946.

[42] E. R. Blount, W. F. Amon, R. G. Shepherd, A. Thomas, C. D. West, and E. H. Land, "Near infra-red transmitting filters," *J. Opt. Soc. Am.*, vol. 36, pp. 460–464; 1946.

[43] R. J. Cashman, "New photo-conductive cells," *J. Opt. Soc. Am.*, vol. 36, p. 356; 1946.

[44] R. J. Cashman, "Photodetectors for ultraviolet, visible and infrared radiation," *Proc. Natl. Electronics Conf.*, vol. 2, pp. 171–180; 1946.

systems for convoy station-keeping, plane-to-plane and plane-to-ground identification. Of these, only the thallous sulfide code communication equipment, known as type D, was in quantity production by the end of the war. Fig. 4 shows the type D-2 receiver equipment. A good account of much of the communications developments and an excellent history of infrared signaling has been given by Huxford and Platt.[23]

The far-infrared program included several detector projects. Thermopiles were developed by a number of groups, especially by L. Harris at the Massachusetts Institute of Technology, and metal-strip bolometers were improved by various individuals including J. Strong working at Harvard University. However, the semiconductor bolometer or "thermistor," developed by Becker and Brattain[45] at the Bell Telephone Laboratories, was by all odds the most successful detector. Thermistors were used in all the FIR equipments which were made either at the Bell Laboratories or at Harvard University. They included a portable ship detector, a stabilized ship detector, a rangefinder, a portable and later scanning detector for personnel, tanks, vehicles, ships, etc., a thermal map recorder, and a bombsight with angular rate release. None of these devices was developed in time to go into production. The thermistor found an important use in a drift-free, non-microphonic detector for recording spectrometers which was used by the chemical industry in the production of aviation gasoline and synthetic rubber.

Two particularly novel thermal detectors appeared during the war. The first of these was the ingenious modification of the simple gas thermometer due to Golay.[46] In this device, infrared radiation is absorbed by a small gas volume. The resulting gas expansion distorts a diaphragm and modifies the reflection of visible light from the diaphragm through a grid to a photocell. In a more advanced design, chopped radiation is used and the detector is rendered insensitive to lower frequencies by incorporating a suitable pneumatic by-pass compensator into the system. During the war, several Golay cells were made by the Signal Corps Laboratories at Eatontown, N. J., and by Don Lee, Inc., in Los Angeles, and these were used in experimental devices. The cells did not lend themselves to use in field equipment, although their sensitivity and speed were excellent for uncooled detectors. The cells are now manufactured by Eppley Laboratories. The other novel detector was the superconducting bolometer, first announced in 1942 by Andrews and co-workers;[47] it used tantalum at liquid-helium temperature.

Subsequently, the device was improved by using niobium (columbium) nitride[48] as the sensitive element. This detector depends for its very high sensitivity on the extremely rapid change in electrical conductivity at the superconducting transition of the material. With niobium nitride, this transition takes place between about 14.34° and 14.38°K so that liquid hydrogen is convenient as the coolant. Because of the relatively high degree of temperature stability required, this detector, although the most sensitive known for modulation frequencies up to about 1000 cps, remains a special research instrument for the laboratory.

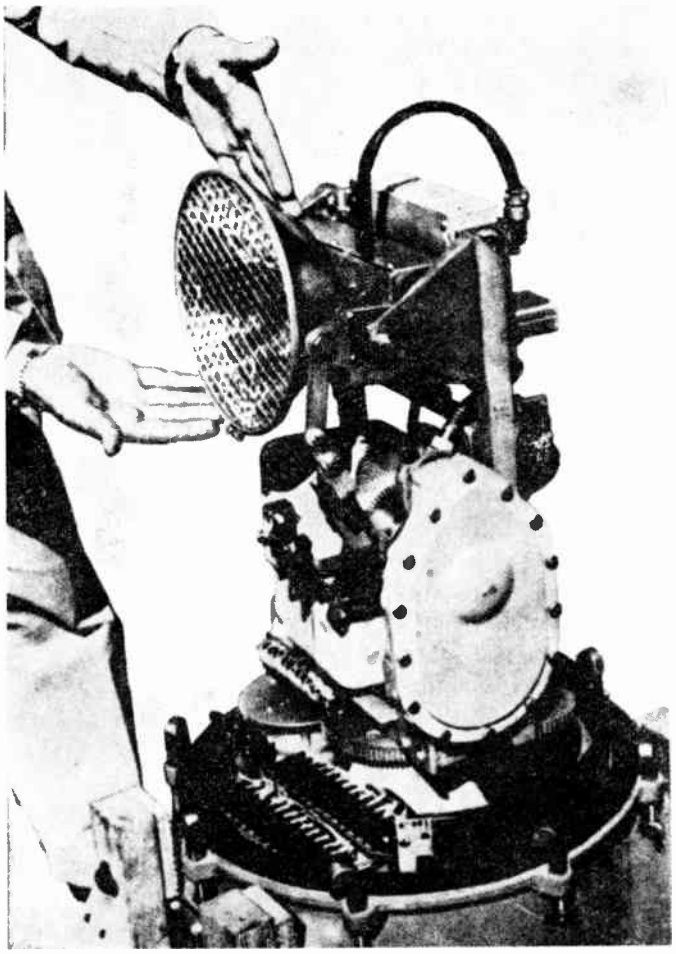

Fig. 4—Type D-2 code communication receiver with cover removed.

The information available on foreign infrared systems developed during the World War II period is limited, as pointed out above. In England, the infrared program was carried out principally at the Admiralty Signals Establishment and the Admiralty Research Laboratory, and accounts of this work have been given by Elliott[22] and by Pratt.[49] Most of the detector development was done at ARL with good technical liaison through the London OSRD office with the corresponding work in

[45] J. A. Becker and W. H. Brattain, "Thermistor bolometers," *J. Opt. Soc. Am.*, vol. 36, p. 354; 1946.
[46] M. J. E. Golay, "A pneumatic infra-red detector," *Rev. Sci. Instr.*, vol. 18, pp. 357–359; 1947.
[47] D. H. Andrews, W. F. Brucksch, W. T. Zeigler, and E. R. Blanchard, "Attenuated superconductors," *Rev. Sci. Instr.*, vol. 13, pp. 281–292; 1942.
[48] D. H. Andrews, R. M. Milton, and D. De Sorbo, "A fast superconducting bolometer," *J. Opt. Soc. Am.*, vol. 36, pp. 518–524; 1946.
[49] T. H. Pratt, "An infra-red image-converter tube," *J. Sci. Instr.*, vol. 24, pp. 312–314; 1947.

this country. Good thallous sulfide cells were made which were used in communication devices, both code and voice, and in monitoring operations such as guarding harbor entrances. As in the U. S., cell development turned to lead sulfide during the last year of the war, using both the "wet" method (chemical precipitation) and the "dry" process (vacuum evaporation). A narrow-beam infrared telephone was developed with a cesium photocell as detector. Also, a wide-angle communication system of limited range up to two hundred yards was made for infantry use at night using the thallous sulfide cell. In image tubes, efforts were concentrated on the "uniform-field image converter," first made by Holst and co-workers[50] in 1934. Although these devices used cesium-silver-oxygen photoemissive surfaces and the photoelectrons were accelerated sufficiently to excite a phosphor screen, electron focusing was not employed since the screen was mounted very close to the emitting surface. In other words, the device operated much as contact prints are made. The work was done by J. D. McGee and his group at Electrical and Musical Industries, Ltd., where a simplified design was completed in 1940 which was put into limited production at Gramophone Ltd.[49] and used in night driving and other equipment to some extent.

There are brief references[11] to infrared devices that were developed and used in the war by the French, the Italians, the Russians, and the Japanese. Undoubtedly, a number of individuals deserve recognition for these accomplishments, but the information is not available to the writer. It is known that the Japanese made considerable use of a light-beam telephone employing a vibrating mirror—double-grid-modulation scheme and a phototube. The corresponding device developed in Italy was called a photophone. It employed a directly modulated tungsten lamp as a source, a very narrow beamwidth of about 0.5°, and concave mirrors instead of lenses. The French had an advanced communication system under development as early as 1939 which used a gas-discharge source modulated at 120 kc and a phototube as a receiver. It was reported that six channels could be used simultaneously, but details are lacking.

Recent Developments

Following the end of the war, the infrared programs both in the U. S. and in England were continued with emphasis on receivers. Cashman, with Navy support, developed PbS cells further and extended his work to PbSe and PbTe using the evaporation process for depositing the layers. An extensive program, principally on chemically-deposited lead sulfide cells, has been under way at the Eastman Kodak Company, also with Navy support. This work was begun and conducted until his death by the late Dr. Gustav W. Hammar. The Air Force has supported a program on lead sulfide cells and mosaics at the Electronics Corporation of America (formerly Photoswitch, Inc.) under R. H. McFee (now at Aerojet-General Corporation), and on lead telluride cells at both Syracuse University under H. Levinstein and Farnsworth Radio and Television Company under J. Kaspar. All these organizations have made excellent receivers. Other organizations have entered the field until now lead-salt receivers can be obtained in an assortment of sizes and shapes for general and special applications from a number of other companies such as the Santa Barbara Research Center, Infrared Industries, and others. The cell work in England, at both the Admiralty Research Laboratory and the Telecommunications Research Establishment, made more rapid progress for several years than that in the U. S. Moss[51] has given an excellent review of the lead-salt photoconductors which includes a bibliography of 130 references. Shortly after 1950, the Admiralty work was shifted to the Services Electronics Research Laboratory, and the Ministry of Supply development from TRE to Mullard, Ltd. Now Mullard produces good-quality lead-salt receivers for the open market. Much of the early British work of this period has been described by Elliott[22] and by Sutherland and Lee.[16] A review of all infrared detectors has been made very recently by Moss.[52] In France, excellent lead sulfide cells were made by a group under A. Lallemand at the Observatory of Paris for astrophysical research. The Etablissement Jean Turck in Paris has continued the development of these receivers and has produced them for the open market. They also have made lead selenide and lead telluride cells.

With the disestablishment of the National Defense Research Committee and the Office of Scientific Research and Development at the end of the war, the military infrared program in the United States was taken over by the respective military services and coordinated by the Research and Development Board, Panel on Infrared. Several of the agencies became interested in the further development and application of the lead-salt photodetectors. Infrared activity began in the rapidly-developing Southern California area. To assist in the coordination of this effort, and especially to aid in the dissemination of the increasing volume of detector knowledge, the Office of Naval Research, Pasadena Branch, organized a continuing Conference on Infrared Instrumentation in 1949. This activity has grown steadily since that time until the national Infrared Information Symposia (IRIS) were organized in 1957. The Physics Branch of the Office of Naval Research under F. B. Isakson continues to sponsor this organization as a Defense Department effort. Policy is determined by an Executive Committee which includes equal representa-

[50] G. Holst, J. H. DeBoer, M. C. Teresa, and C. F. Veenemans, "An apparatus for the transformation of light of long wavelength into light of short wavelength," *Physica*, vol. 1, pp. 297–305; 1934

[51] T. S. Moss, "Lead salt photoconductors," Proc. IRE, vol. 43, pp. 1869–1881; December, 1955.

[52] T. S. Moss, "Advances in Spectroscopy," Interscience Publishers, New York, N. Y., vol. 1, 1959.

tion from the three military departments and a number of defense contractor representatives. The list of Program Chairmen includes several of the authors of this issue, namely, and in chronological order, W. N. Arnquist, S. S. Ballard, L. Larmore, and S. Passman for the West Coast Section, and T. B. Dowd for the more recently organized East Coast Section. A. R. Laufer of ONR, Pasadena, is chairman of the National IRIS Executive Committee and editor of the *Proceedings of IRIS*, a classified publication.

No mention of ONR's national role in infrared would be complete without referring to the liaison work which has been conducted by the ONR London Branch office, the "successor" to the OSRD liaison office in London. Numerous classified and unclassified reports have been prepared and distributed by the following succession of individuals: K. R. Eldredge, L. W. Hyde, W. N. Arnquist, and D. R. Gates; now D. Z. Robinson is continuing this work.[53] Another achievement indicating the extent of infrared activity over the past two decades is the infrared bibliography prepared by the Library of Congress at the request of ONR. As originally issued in 1954, it covered all of the available references to published literature from 1935 through 1951, some 5500 reports or publications. A second part of about 1600 references was prepared in 1957 to include the many government reports which had been declassified by that time. There is a classified bibliography also.

In the years since the Korean War, technical progress has been very rapid and it is difficult to view it from a historical standpoint as yet. Great advances have been made in detectors, in understanding the fundamental properties of materials, and in a variety of applications especially in military systems. Besides the lead-salt detectors and thermistors that have been developed further by a number of groups, a great deal of work has been done with "doped" germanium and silicon, especially by G. A. Morton and E. Burstein in the United States and B. V. Rollin in England. A very recent announcement[54] describes the ZIP (Zinc-Impurity Photodetector) Model 536-1 made by Perkin-Elmer Corporation and originally developed at the Naval Research Laboratory by Burstein and his group. This remarkable receiver has a reasonably flat maximum in sensitivity from 20 to 40 μ with a response time of less than 0.01 μsec. It must be cooled to the temperature of liquid helium. Indium antimonide has appeared as an excellent receiver for the 3- to 7-μ range; its photovoltaic properties have been utilized as well as its photoconductivity. In many applications now, the limiting sensitivity is no longer determined by detector noise but by other considerations. Solid-state physics has given an adequate quantitative theory for the interpretation of many of the physical phenomena in photon detectors, and the tremendous advances in this field have stimulated much of the almost fantastic progress with detectors. An interesting development is the photo-electromagnetic effect, originally discovered by Kikoin and Noskov.[55] Aigrain and Bulliard[56] in France, and Moss, Pincherle and Woodward [57] in England, have studied this effect in geranium. Hilsum and Ross[58] have described an infrared detector based on the photo-electromagnetic effect in indium antimonide. In the articles to follow, these and other current applications are reviewed more completely.

Other Applications

It is not possible to discuss here the history of other infrared developments, but mention will be made of many of the directions in which applications have been made, with reference to published material for further information. The known interactions with matter involve a number of fundamentally different phenomena ranging from atomic and molecular resonances and scattering in the gaseous state to much more complicated interactions in the condensed phases. Many properties utilizing the emission, absorption, reflection, refraction, polarization, and scattering of infrared radiation have been employed for particular purposes and essentially all of the applications have utilized only energy in the first of the three decades comprising the infrared spectrum, *i.e.*, 1 to 30 μ.

Although by far the most extensive applications of infrared have been in the field of infrared spectroscopy, no attempt will be made to say anything of this enormous field in a few words. A good historical account of infrared atomic spectroscopy and current work has been given by Humphreys,[59] who points out that this field began before molecular spectroscopy. There are many references that could be cited regarding the development of infrared molecular spectroscopy. Coblentz,[60] Barnes and Bonner,[61] Williams,[62] and Strong,[63] have

[53] The work of D. S. Lowe as the liaison representative of the Naval Ordnance Laboratory, White Oak, Md., should be mentioned also as an important contribution to this infrared liaison during the period 1955–1956.

[54] See *Aviation Week*, vol. 70, p. 82; April 13, 1959.

[55] I. K. Kikoin and M. M. Noskov, "New photoelectric effect in cuprous oxide," *Phys. Z. Sowjetunion*, vol. 5.4, pp. 586–596; 1934.

[56] P. Aigrain and H. Bulliard, "Resultats expérimentaux de l'effet photomagnétoélectrique," *Compt. rend. Acad. Sci.*, vol. 236, pp. 672–674; February, 1953.

[57] T. S. Moss, L. Pincherle, and A. M. Woodward, "Photoelectromagnetic and photodiffusion effects in germanium," *Proc. Phys. (London) B*, vol. 66, pp. 743–752; September, 1953.

[58] C. Hilsum and I. M. Ross, "An infra-red photocell based on the photo-electromagnetic effect in indium antimonide," *Nature*, vol. 179, p. 146; 1957.

[59] C. J. Humphreys, "Infrared Atomic Spectroscopy, Based on Use of Photoconductive Detectors," Naval Ord. Lab., Corona, Calif., Rept. No. 146; May, 1954. Also presented at the Rydberg Centennial Conf., University of Lund, Sweden; 1954.

[60] W. W. Coblentz, "Early history of infrared spectroradiometry," *Sci. Monthly*, vol. 68, pp. 102–107; February, 1949.

[61] R. B. Barnes and L. G. Bonner, "The early history and the methods of infrared spectroscopy," *Amer. Phys. Teacher*, vol. 4, no. 4, pp. 181–189; 1936.

[62] V. Z. Williams, "Infra-red instrumentation and techniques," *Rev. Sci. Instr.*, vol. 19, pp. 135–178; 1948.

[63] J. Strong, "Experimental infrared spectroscopy," *Physics Today*, vol. 4, pp. 14–21; April, 1951.

contributed to the literature. A review of the industrial field including some 360 absorption spectra and over 2700 references by Barnes and co-authors,[64] is a standard reference.

Throughout the history of infrared applications, radiation sources of various kinds have been required for research, testing, and calibration purposes. The most useful have been those that closely approximate blackbody radiations, at least over limited spectral ranges, such as the Nernst glower, the carbon arc, the Welsbach mantle, the "Globar" source, and the tungsten filament. A number of gas or vapor discharge lamps have appeared in recent years and the intensive development of luminescent materials as visible sources is being extended into the infrared. Similarly, optical materials have had a long period of development and many substances are now available for prisms, lenses, windows, and filters.[30] An outline of the historical developments is outside the scope of the present article. The reader is referred to Ballard and McCarthy[65] for a fairly recent treatment, to Sutherland and Lee[16] for developments to about 1947, and to Smith and co-authors,[2] with their many references to both the early work and modern developments. Report number 2389-11-S, from the Infrared Information and Analysis Center at the University of Michigan, describes the status of this subject as of the summer of 1958.[66]

Modern infrared photography has been made possible by the development of numerous sensitizing dyes. Although a number of early workers had made spectrographic records with photographic plates sensitized in various ways, no really useful sensitizers for infrared were available until the period just before the first World War. This war stimulated the chemical dye industry outside of Germany and resulted in important developmental investigations in England, France, Canada, and this country. The discovery of neocyanine at the Kodak Research Laboratories enabled H. D. Babcock in 1930 to photograph the solar spectrum to about 11,600 Å at the Mt. Wilson Observatory, and to make the first published all-infrared photograph in complete darkness using a 48-hour exposure. The period 1931–1935 saw the development of other dyes at Eastman Kodak, which extended the wavelength range to the present limit, about 13,500 Å, and put infrared photography within reach of amateur photographers. An excellent summary of this field has been prepared by Clark.[67]

Infrared measurements have been used by astrophysicists for many years. An enormous amount of information has been obtained about the sun, the planets, and the stars with infrared spectrographs and spectrometers. New stars have been found. The transmission of the earth's atmosphere, always a problem to the astronomer, has been studied extensively and this information now is of great importance to the missile and satellite programs. The atmospheres of the planets are being investigated. Thus we know of the large amounts of CO_2 on Venus and of methane on Jupiter, Saturn, Uranus, and Neptune. The polar caps on Mars are probably ice and Saturn's rings may be ice also. In this field, the publication of Kuiper[68] should be read by anyone interested.

There are, of course, many applications of infrared in space heating, in cooking, in therapeutic medical treatments and the like, where the heating effects alone due to the absorption of the radiant energy are important. Paint drying is a good example; in 1938, the Ford Motor Company first publicized the use of infrared tunnels for drying automobile finishes. Hall[69] has described this and many other applications of this type.

In biology and medicine, infrared techniques have been applied with many interesting results.[67] An infrared pupillometer has been devised to study the dark-adapted eye. Other studies of the eye have been possible with infrared because of the smaller scattering of infrared as compared to visible light in such conditions as scratched corneas or turbid conditions of the eye. In dermatology, the better penetration of infrared radiation through the skin has been utilized in the study of lesions, of healing under scabs, and of the subcutaneous circulation system. In hematology, the composition of the blood has been studied and poisoning by carbon monoxide is easily detected. More than a beginning has been made in such directions as the study of plant diseases and the characterization and identification of fossils. Infrared photography has been used in the study of textile fabrics where dyes are more readily evaluated in many cases with infrared than with visible light. The broad field of camouflage is important especially for the military. In graphic arts, it has been found that many visually similar pigments can be easily differentiated with infrared. Thus, paintings have been examined to find that the original scene had been covered with another. Original documents, precious stones, and the like have been distinguished from imitations. In criminology, erasures and forgeries have been detected, charred remains of documents examined for their information content, sealed envelopes inspected, and clandestine photographs of operations in the dark taken to trap criminals or expose frauds. Aerial photographs have assisted in geological surveys and the Forestry Service

[64] R. B. Barnes, R. C. Gore, U. Liddel, and V. Z. Williams, "Infrared Spectroscopy—Industrial Applications and Bibliography," Reinhold Publishing Corp., New York, N. Y.; 1944.

[65] S. S. Ballard and K. A. McCarthy, "Optical materials for infrared instrumentation," *Nuevo cimento*, suppl. 3 to vol. 2, ser. 10, pp. 648–652; 1955.

[66] The availability of copies of this report can be determined by writing William Wolfe, Willow Run Labs., University of Michigan, P.O. Box 2008, Ann Arbor, Mich.

[67] W. Clark, "Photography by Infrared," John Wiley and Sons, Inc., New York, N. Y.; 1946.

[68] G. P. Kuiper, "The Atmospheres of the Earth and Planets," University of Chicago Press, Chicago, Ill.; 1949.

[69] J. D. Hall, "Industrial Applications of Infrared," McGraw-Hill Book Co., Inc., New York, N. Y.; 1947.

has used such photographs to evaluate forests. In short, infrared radiation is all about us, techniques are available, and the possibilities of applications seem limited only by our imaginations.

It is a source of considerable regret that it has not been possible in this survey to include something of the history of the developments in such important directions as atmospheric attenuation, infrared instrumentation, infrared optical materials, infrared emission, and the like. This is particularly unfortunate since the field of infrared applications has developed so extensively over the past decade that the contributions of a number of individuals who are active today represent pioneering work which should be better known than it is. The reader will realize that any attempt to remedy this situation will necessarily be incomplete and even misleading in some respects. Nevertheless it is felt that this survey would be unfinished without at least a passing reference to a few individuals, as for example, A. Adel, W. M. Elsasser, L. Goldberg, and J. Strong in atmospheric absorption work in this country. Important basic work on infrared atmospheric scattering was done by J. A. Sanderson and his group at the Naval Research Laboratory and by H. A. Gebbie and co-workers in England. M. Migeotte and others have been active in this field on the Continent. In the infrared instrumentation and materials field, many individuals such as R. Bowling Barnes, Van Zandt Williams, P. Nolan, E. D. McAlister, S. S. Ballard, B. H. Billings, and S. Silverman did important pioneering work. The fundamental contributions from the U. S. Bureau of Standards in infrared, connected with such names as W. W. Coblentz, W. F. Meggers, E. K. Plyler, and C. J. Humphreys, are well-known.

Similarly, the infrared laboratories at the University of Michigan, directed for so many years by H. M. Randall, and those at The Johns Hopkins University under A. H. Pfund and J. Strong, have produced important work and have served to train scores of physicists who have been responsible for expanding the field in many directions.

Acknowledgment

Many individuals have cooperated in supplying information and otherwise assisting in the preparation of this survey. It is a pleasure to recognize especially E. W. Kutzscher of the Lockheed Aircraft Company and W. K. Weihe of the U. S. Army Engineer Research and Development Laboratories for their assistance regarding German infrared developments. G. A. Morton of the Radio Corporation of America, R. J. Cashman of Northwestern University and T. S. Moss of the Royal Aircraft Establishment were particularly helpful with information and suggestions. E. Scott Barr of the University of Alabama has been generous with his time in discussions and correspondence. F. B. Isakson of the Office of Naval Research has supplied a large number of useful documents. In addition, helpful correspondence has been had with R. B. Barnes of Barnes Engineering Company, H. Levinstein of Syracuse University, J. A. Sanderson of the Naval Research Laboratory, R. A. Smith of the Royal Radar Establishment, England, and J. Strong of Johns Hopkins University. Discussions with many other individuals too numerous to mention have been of aid in selecting material and forming opinions. To each of these, and to the Systems Development Corporation for logistic support, the writer wishes to express his appreciation.

SECTION 3. INFRARED PHYSICS

Paper 3.0 Introduction*

LEWIS LARMORE†, EDITOR

THE infrared region of the electromagnetic spectrum extends between the long wavelength cutoff of the human eye sensitivity (about 0.72 micron) and the short wavelengths produced by microwave radiation (about 1000 microns). This region is frequently further divided into the near-infrared, intermediate-infrared, and far-infrared regions because of the methods used for detecting the radiation. Thus, the instrumentation used most frequently for the near-infrared region closely parallels that used for the visible region of the spectrum, and we find photography, infrared-vidicons, and photomultipliers as typical detectors. The intermediate region of the infrared spectrum requires the use of photoconductors for most efficient detection, while the far-infrared region can be detected only with a device which absorbs the radiation and changes one or more of its physical properties as a result of the increase in temperature.

A large portion of the technical progress in recent years has been due to developments in the field of detectors. Thus, a good portion of this section on "Infrared Physics" is devoted to the physics of infrared detectors. Much of the progress in this field has resulted from work in the area of solid-state physics, and, while the reader is assumed to be partially familiar with the basic concepts, considerable emphasis has been placed on applying solid-state principles to infrared-detection problems. Also, the limiting noise of any system frequently depends on the noise inherent in a detector. These concepts are given as they apply to the detection problem in general.

Properties of the source of radiation form an important part of the discussion of infrared radiation. Blackbody radiation characteristics and selective radiators are both discussed from the standpoint of the physics involved. Atmospheric properties play a dominant role in the transmission of infrared radiation. Selective absorption due to the molecular vibrations of the atmospheric constituents allows certain useful windows, while other regions are rendered almost completely useless. The physics behind the atmospheric transmission is treated, as well as the infrared emission of the atmosphere itself.

Finally, the basic range equations are derived for an infrared-detection system. These equations form the basis for discussion in later sections concerned with infrared systems and applications.

The following outline gives the headings of the major divisions of this section.

3.1 *Radiators*

- 3.1.1 Radiometric Quantities, Symbols, and Units
- 3.1.2 Blackbody Radiation
- 3.1.3 Selective Radiators

3.2 *Atmospheric Properties*

- 3.2.1 The Infrared Radiation Flux in the Atmosphere
- 3.2.2 The Transmission of the Atmosphere in the Infrared

3.3 *Detectors*

- 3.3.1 Fundamentals of Infrared Detectors
- 3.3.2 Infrared Photoemission
- 3.3.3 Thermal Radiation Detectors
- 3.3.4 Film-Type Infrared Photoconductors
- 3.3.5 Single-Crystal Infrared Detectors Based Upon Intrinsic Absorption
- 3.3.6 Impurity Photoconductivity in Germanium
- 3.3.7 Noise in Radiation Detectors
- 3.3.8 Infrared Photography

3.4 *Basic Range Equations*

- 3.4.1 Range Equation for Passive-Infrared Devices
- 3.4.2 Range Equation for Active Devices

It is a pleasure to acknowledge the cooperation of the various authors who contributed to this section on Infrared Physics. In addition, Dr. Lloyd Mundie edited most of the part on infrared detectors, and it is largely through his efforts that complete coverage is given in so many areas of interest.

* Original manuscript received by the IRE, June 26, 1959.
† Lockheed Aircraft Corp., Burbank, Calif.

Paper 3.1.1

Radiometric Quantities, Symbols, and Units*

ELY E. BELL†

Introduction

THE nomenclature, units, and descriptions of the primary physical quantities considered most important to infrared technology are given so that workers in this field may communicate in a common language. The group prefers the names, symbols, and units, which follow. These are taken, in the most part, from the American Standards Association Standard Z 58.1.1-1953.

General Description of Radiometric Quantities

The concepts of radiant emittance, radiant intensity, and radiance are usually considered in reference to a radiating source and are measures of the properties of a source. These properties can be determined by measurements made at a distance from the source if the intervening space contains a nonattenuating medium. Let us consider, first, for the following discussion, that the measurements are made in a nonabsorbing and nonscattering medium and leave the difficulties which arise because of the medium for later discussion.

Radiometric Quantities Referred to a Source in Vacuum

The average emittance of a source is the ratio of the total power radiated away from the source to the total area of the source. The average radiant emittance of a small portion of a source is the ratio of the total power radiated from that small portion of the source to the area of that small portion. The limiting value of the average radiant emittance of a small portion of a source as the area is reduced in size about a point is the radiant emittance of the source at that point. The total radiation from the elemental area is to include all that which is radiated into the hemisphere (2π steradians). Radiant emittance measures the power radiated into the hemisphere per unit area of the source and is, then, $W=\delta P/\delta A$, where A is a measure of area, with W usually given in watts·cm^{-2}.

The average radiant intensity of a source is the total power radiated by the source divided by the total solid angle about the source (4π steradians). The average radiant intensity within a given solid angle of direction is the ratio of the power radiated within the given solid angle to the size of the solid angle. The limiting value of the average radiant intensity in a solid angle as the solid angle is reduced in extent about a particular direction is the radiant intensity J in that direction. Radiant intensity measures the power radiated per unit solid angle in a particular direction, and it is $J=\delta P/\delta\Omega$, where Ω is the measure of the solid angle, and J is given as watts·steradian^{-1}.

The average radiance of an area of a source in a given solid angle is the total amount of power radiated from that area into that solid angle divided by the product of the area and the solid angle. The limiting value of the average radiance as both the area and the solid angle are reduced in extent is the radiance at a point in a direction. The radiance measures the radiant power per unit area per unit solid angle in a particular direction, and it is $N=\delta^2P/\delta A\delta\Omega$. From this definition it follows that $J=\int N dA$, where the integral is over the source area, and also that $W=\int N d\Omega$, where the integral is over 2π steradians.

A determination of a value of the radiance at a point on a source necessitates a determination of the size of a small, elemental area of the source. Since the measurement is made from a distance, as it always must be, sometimes there can be a lack of knowledge of the orientation of the elemental area with respect to the line of observation, and, therefore, the area may be undetermined. The projection of the area onto a plane perpendicular to the direction of the measurement can usually be determined, however. If the projected area rather than the true area is used in the definition of radiance, then the orientation of the source need not be known for the radiance to be determined. The use of the projected area leads to the useful radiance concept that sources which obey Lambert's Cosine Law have a radiance which is independent of the direction of measurement. It also allows a sensible measure for the area of a rough or tortuous surface. In the measurements and considerations of background radiances, it is this projected area of the background that is usually assumed. The sky, for example, does not have a uniquely associated true area —the sky does not even have a distance away from the observer—yet there is a good measure for the radiance of such a background. It should be made clear in any work which of these area concepts is being used.

Irradiance, H, is a measure of the radiant power per unit area received by an elemental surface area. It has the same units as radiant emittance but refers to the radiation incident upon a receiving surface rather than that leaving an emitting surface. Both emittance and irradiance are measures of the areal density of radiant power (often called flux density). The radiation incident upon the receiving surface may be limited, in a particular situation, to that which originates from a given source or which arrives within a given solid angle. When so restricted, the receiver surface irradiance is the areal density of the power from the source under consideration, and this power need not arrive from a full 2π

* Original manuscript received by the IRE, June 26, 1959.
† Dept. of Physics, The Ohio State University, Columbus, Ohio.

steradians of solid angle. It is sufficient, then, to speak of the irradiance of a radiometer collecting mirror produced by a particular source under measurement simply as the irradiance of the collecting mirror if the source and its extent have been implied by previous remarks.

Radiometric Quantities as Field Concepts

As has been indicated, the concepts of emittance and radiance are normally thought of as referring to a source of radiation and the irradiance concept, in reference to a sink, or receiver, of radiation. These radiometric concepts can also be applied to the radiation in a radiation field away from sources and sinks, however, and it is often convenient to do so. One could place in the radiant field a barrier surface containing an aperture. This aperture has the essential radiant properties of a source for the radiation leaving the aperture and the essential properties of a sink for the radiation incident on the aperture. At this point in the radiation field defined by reducing the size of the aperture, there is a sensible measure of the emittance, irradiance, and radiance of the "aperture" and thus of the radiation field. These radiometric quantities will be dependent upon the orientation of the aperture in the radiation field. For the usual consideration of the radiation field produced by a single, distant, small source, it is natural to specify the radiometric quantities only along the direction of rays from the source.

It can be seen that these radiometric field quantities can be measured, ideally, at a point in a radiation field by a properly calibrated radiometer placed at that point.

The extension of the definitions of these radiometric quantities to measure the properties of a radiant field, as well as the properties of a source, is of great utility. These field quantities can be evaluated, for example, as lenses, mirrors, apertures, entrance pupils, exit pupils, real images, or virtual images in a variety of ways to make calculations simpler or more understandable. Of special importance, in this regard, is the fact that the radiance from a source measured at any point along a ray in an image-forming system is a constant. (To be correct for radiation passing through several media without loss, the constant quantity is N/n^2, where n is the index of refraction of the medium at the point of evaluation of N.) It is because these radiometric quantities have meaning in the radiation field away from the source that it is necessary to modify carefully the names of the quantities when they are used away from the true source. Without such modification, it would normally be assumed that the values were those as measured neighboring the actual source of the radiation.

The measurement of the radiometric properties of a source by a radiometer at a distance from the source is equivalent, in practice, to the measurement of some radiant field quantity together with certain geometrical factors, such as the field of view, entrance pupil area or distance from the radiometer to the source. For example, in the case of a small source at a large distance s from the radiometer, the radiant intensity of the source is related to the entrance pupil irradiance by $J = s^2H$. Thus the determination of H at the radiometer and the distance s allows one to calculate J at the source. Such determinations of the source properties will be valid only to the approximation that the intervening medium is transparent and nonscattering. For attenuating media, the calculation of the source quantities from the distant field quantities is difficult—in detail, usually impossible.

Radiometric Quantities Referred to a Source in an Attenuating Medium

The calculation of radiometric characteristics of a source in an attenuating medium from measurements made at a distance always involves some assumptions about the nature of the attenuation, emission, and scattering of the intervening medium. Thus, the calculated source characteristics may be in error by an unknown amount. If no attempt is made in the calculation of the source characteristics to include the effects of the intervening medium, then the calculated quantities are "apparent" quantities. The radiant intensity of a target calculated from measurements made one mile away with no correction for atmospheric attenuation would be the "apparent radiant intensity" of the target. If, on the other hand, the calculation corrects for the attenuation and other effects of the atmosphere to the satisfaction of the data reporter, then it may be called the "radiant intensity" of the target. Likewise, without consideration of the intervening medium, one can calculate the apparent emittance or the apparent radiance of a target. The calculation of the emittance or the radiance would include some consideration of the intervening medium.

An infrared background is defined to include the emission, absorption, and scattering of the atmosphere. An infrared background, therefore, extends from the measuring radiometer outward. Thus for backgrounds, unlike targets, a properly calibrated radiometer measures radiance rather than apparent radiance.

The irradiance of a radiometer, likewise, is measured by the radiometer rather than an "apparent" irradiance. The concept of irradiance is that of the power density at the receiver and, as such, is not referred to the source position.

Spectral Radiometric Quantities

The radiometric quantities of radiant emittance, irradiance, radiant intensity, and radiance are used to help specify a particular portion—that within a particular solid angle, or passing through a particular area—of all the radiation which is under consideration. These are quantities differential with respect to solid angle and area and they must be integrated over the appropriate variable in order to obtain the radiant power.

There are also quantities differential with respect to wavelength. One of these is the spectral radiant power, which is the radiant power per unit wavelength interval

or $\delta P/d\lambda = P_\lambda$. The value of P_λ will ordinarily vary with λ, and the radiant power with λ_1 and λ_2 is given by $\int_{\lambda_1}^{\lambda_2} P_\lambda d\lambda$.

Other spectral quantities of use are: spectral emittance $\delta W/\delta\lambda = W_\lambda$; spectral irradiance, $\delta H/\delta\lambda = H_\lambda$; spectral intensity, $\delta J/\delta\lambda = J_\lambda$; and spectral radiance $\delta N/\delta\lambda = N_\lambda$. It is to be noted that the subscript notation for the partial derivative with respect to wavelength for these particular quantities has had almost universal acceptance, and therefore the subscript λ should not be used on these particular quantities in any other context.

These spectral quantities are measured by spectroradiometers, but may be crudely measured by radiometers equipped with filters.

Other Radiometric Quantities

The absorption α of a system measures the fraction of the incident radiation which is absorbed by the system. The absorption must be distinguished from an "absorption constant" which measures the fraction absorbed per unit path or the fraction absorbed per unit concentration.

The meaning of a value of the reflectance ρ for a single, specularly-reflecting surface is well understood. The meaning of a value of ρ for a diffusely-reflecting surface or for a partially transparent body with internal scattering is not easily specified. This difficulty arises from the complicated angular dependence of the "reflected" radiation and from the inability to separate, in a general definition, the transmitted, scattered, and reflected portions of the radiation. In the situation in which the reflection is nonspecular or from more than one surface, the reporter should carefully specify what he means by "reflectance."

The meaning of a value of the transmittance τ of a nonscattering homogeneous medium is well understood. As in the case of reflectance, however, some systems have irregular reflectance, scattering, etc., so that the reporter may need to specify carefully what he means by "transmittance."

The absorption of a system is usually calculated from measurements on the reflectance and transmittance by the relation $\alpha = 1 - \rho - \tau$. When there is no scattering and when the reflection is specular, calculation is simple. If there are diffuse reflections and scattering, then the calculations will be complex, necessarily including all of the incident radiation which escapes, without absorption, from the system.

The emissivity of a body at some temperature is the ratio of the emittance of the body to the emittance of a blackbody having the same temperature. If a body does not have a single, recognizable, temperature, then its "emissivity" will be meaningless.

Physical systems have values of α, ρ, τ, and ϵ which are dependent upon the spectral distribution of the radiation used in the measurement of these quantities. If the radiation used for the measurement is confined to an infinitesimally small wavelength range about wavelength λ, then the particular values $\alpha(\lambda)$, $\rho(\lambda)$, $\tau(\lambda)$, and $\epsilon(\lambda)$ are determined. The subscript notation α_λ, ρ_λ, ϵ_λ, τ_λ etc., is likely to be confused with the differential notation W_λ, H_λ, P_λ, J_λ. Hence, the parenthetic notation is preferred.

Units

The following list of units in Table I gives those described in the previous section along with symbols which have been recommended by the Working Group on Infrared Backgrounds. Units differing from the given units by factors which are an integral power of ten are desirable where the size of the measured quantity makes such a change convenient.

TABLE I

Preferred Symbols, Names, and Units

Symbol	Name	Description	Unit
U	Radiant energy		Joule
u	Radiant energy density		Joule cm^{-3}
P	Radiant power	Rate of transfer of radiant energy	Watt
W	Radiant emittance	Radiant power per unit area emittd from a surface	Watt cm^{-2}
H	Irradiance	Radiant power per unit area incident upon a surface	Watt cm^{-2}
J	Radiant intensity	Radiant power per unit solid angle from a source	Watt $ster^{-1}$
N	Radiance	Radiant power per unit solid angle per unit area from a source	Watt $ster^{-1}$ cm^{-2}
P_λ	Spectral radiant power	Radiant power per unit wavelength interval	Watt $micron^{-1}$
W_λ	Spectral radiant emittance	Radiant emittance per unit wavelength interval	Watt cm^{-2} $micron^{-1}$
H_λ	Spectral irradiance	Irradiance per unit wavelength interval	Watt cm^{-2} $micron^{-1}$
J_λ	Spectral radiant intensity	Radiant intensity per unit wavelength interval	Watt $ster^{-1}$ $micron^{-1}$
N_λ	Spectral radiance	Radiance per unit wavelength interval	Watt $ster^{-1}$ cm^{-2} $micron^{-1}$
ϵ	Radiant emissivity	Ratio of "emitted" radiant power to the radiant power from a black body at the same temperature	
α	Radiant absorption	Ratio of "absorbed" radiant power to incident radiant power	
ρ	Radiant reflectance	Ratio of "reflected" radiant power to incident radiant power	
τ	Radiant transmittance	Ratio of "transmitted" radiant power to incident radiant power	
λ	Wavelength		micron

Paper 3.1.2

Blackbody Radiation*

T. P. MERRITT† AND F. F. HALL, JR.‡

ALL objects in the physical universe which are not at absolute zero radiate energy in the form of electromagnetic waves. This fact is not surprising when it is understood that matter is composed of electrically-charged particles which are constantly undergoing energy changes because of thermal agitation. Furthermore, a body upon which electromagnetic radiation is incident may transmit, reflect or absorb certain portions of this radiation, or combinations of these phenomena may occur simultaneously.

In 1860 G. R. Kirchhoff [1] demonstrated that a good absorber is also a good radiator, and that consequently, a complete absorber is also a perfect radiator. An object which absorbs all of the radiation incident upon it is commonly known as a *blackbody;* hence, when reference is made to this type of radiator or absorber, it may be assumed that we mean a "perfect" blackbody. When reference is made to a radiator less than "perfect," the term graybody will be used.

Results of observations on the nature of the spectral distribution of the radiation from a blackbody are shown in Fig. 1. The ordinate is given in arbitrary units,

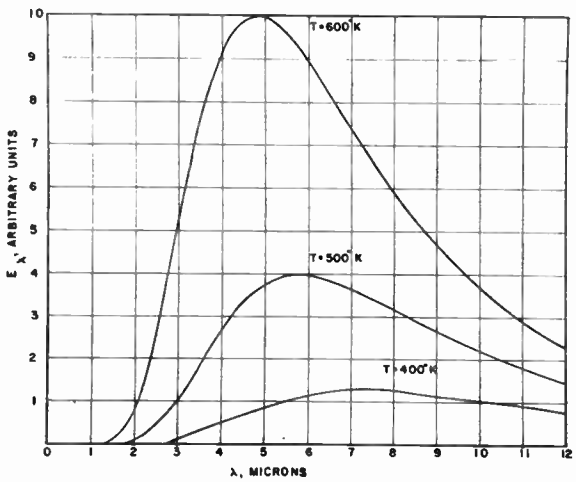

Fig. 1—Relative spectral energy distributions for blackbodies at temperatures indicated.

but it may have dimensions of power per unit area per unit wavelength or frequency interval, in which case it is called the spectral emissive power, or spectral radiant emittance. Radiation curves representing emission from blackbodies of higher temperatures lie completely above those for lower temperatures, and in the longer wavelength regions, the radiated power is directly proportional to the temperature. It is also to be noted that the peak of the radiation curve moves toward the shorter wavelengths as the temperature is increased.

The role of physics in connection with blackbody radiation becomes that of describing mathematically what is observed experimentally. Prior to 1900, the mathematical tools available were in the realm of classical physics, and it was on this basis that attempts were first made to explain this type of radiation. Following the turn of the century, however, quantum theory was introduced to account for the discrepancies arising from the inability of classical methods to account for the experimental data.

The Stefan-Boltzmann Law

It is observed that a solid body heated to a temperature T above absolute zero will radiate energy in the form of electromagnetic waves at a rate proportional to the fourth power of the temperature. This fact may be expressed in equation form as

$$E = \sigma T^4 \tag{1}$$

where σ is the proportionality constant. E is usually expressed in dimensions of power per unit area, and as such is called the total emissive power, or radiant emittance. The energy may be radiated into a sphere as from a spherical surface or a point source, or into a hemisphere as from a flat surface, but in either case the radiating region should be specified. An enclosure in isothermal equilibrium, called an isothermal enclosure, will contain radiant energy, the density of which is proportional to the emissive power of the inner surface, and may be expressed as energy per unit volume. The proportionality constant obviously involves the velocity of the radiation, c, and, for a complete enclosure, it can be shown [1] that the radiation density, ρ, is related to E by $\rho = 4E/c$. We can then write

$$\rho = 4\sigma T^4/c. \tag{2}$$

The fourth-power relationship was originally stated by Josef Stefan in 1879, and was later verified theoretically from thermodynamic considerations by Ludwig Boltzmann in 1884.

The line of argument followed by Boltzmann consisted in the application of radiation as a working substance in a Carnot engine. It is shown, classically, that the average pressure on the walls of an isothermal enclosure is equal to one-third of the energy density within the enclosure. Utilizing two isothermal enclosures at temperatures T_1 and T_2 as heat source and receiver, respectively, one can readily compute the heat ex-

* Original manuscript received by the IRE, June 26, 1959.
† Lockheed Aircraft Corp., Burbank, Calif. Formerly with ITT Labs., San Fernando, Calif.
‡ ITT Labs., San Fernando, Calif.

changes taking place as a Carnot engine executes a complete cycle.

If the work done on the piston while producing an increase, Δv, in the volume of the cylinder is given by $(1/3)\rho_1\Delta v$, the energy supplied to the engine can be shown to be

$$H_1 = (4/3)\rho_1\Delta v \tag{3}$$

where ρ_1 is the radiation density (constant if T_1 remains constant) within the heat source.

For small pressure changes

$$\Delta p = (1/3)\Delta\rho \tag{4}$$

and the adiabatic changes taking place can be considered negligible. Thus ρ_1 of the source and ρ_2 of the receiver remain unchanged. The net energy expended on the system by the working substance becomes

$$\Delta W = \Delta v\Delta_p = (1/3)\Delta v\Delta\rho. \tag{5}$$

The fundamental relationship for the Carnot cycle is

$$\Delta W/H_1 = \Delta T/T_1 \tag{6}$$

giving

$$(1/3)\Delta v\Delta\rho/(4/3)\Delta v\rho_1 = \Delta T/T_1 \tag{7}$$

and for any temperature, T, associated with a radiation density ρ we have

$$\Delta\rho/\rho = 4\Delta T/T. \tag{8}$$

Integration gives

$$\rho = bT^4 \tag{9}$$

where b is the constant of integration. Since $\rho = 4E/c$

$$E = cbT^4/4 = \sigma T^4 \tag{10}$$

where $\sigma = cb/4$, and is called the Stefan-Boltzmann constant. It will be shown later how the Stefan-Boltzmann Law can be obtained directly by integration of the Planck radiation equation. A body which radiates according to this law is known as a blackbody, and the radiation is called blackbody radiation. The magnitude of σ is given as 5.668×10^{-8} watt·m^{-2}·°K^{-4} and is calculated from atomic constants appearing in the integration of the Planck radiation equation which will be derived subsequently. Thus σ itself becomes one of the well-known atomic constants.

The Wien Displacement Law

Classical thinking was brought into play in an attempt to explain the wavelength distribution of the energy as shown in Fig. 1. From purely thermodynamic considerations, and application of the theory of Doppler shift, W. Wien [1] in 1898 showed that the effect of an adiabatic expansion on blackbody radiation is to change the wavelength of any spectral component in such a manner that at any moment the wavelength of this component is inversely proportional to the absolute temperature of the enclosure. This relationship may be stated as

$$\lambda_1 T_1 = \lambda_2 T_2 \tag{11}$$

and is known as the Wien Displacement Law. A special condition of this law occurs for the wavelength of the maximum of the energy curve, in which case we write

$$\lambda_{1m} T_1 = \lambda_{2m} T_2 = \text{a constant}. \tag{12}$$

Eq. (12) indicates that the peak of the radiation curve is shifted toward shorter wavelengths as the temperature is increased, and accounts for the red glow of a solid object which has been raised to a temperature so that it just begins to emit radiation in the visible portion of the spectrum. Electric heaters, for example, have this red glow. Objects at higher temperatures such as the carbon particles in a candle flame emit a yellow-orange light, indicative of the shift of the radiation peak to shorter wavelengths, while tungsten filaments in evacuated envelopes can be raised to a temperature permitting radiation of sufficient intensity at all wavelengths in the visible region that they appear white in color.

With a knowledge of the general shape of the blackbody radiation curve, together with the Stefan-Boltzmann and Wien displacement laws, attempts were made to fit equations to this curve. Considerations leading to the Wien law indicated that the spectral emissive power should be of the form

$$E_\lambda = \lambda^{-5} f(\lambda T). \tag{13}$$

On assumptions of emission and absorption processes Wien developed a formula of the form

$$E_\lambda = c_1\lambda^{-5}e^{-c_2/\lambda T}. \tag{14}$$

For especially selected values of c_1 and c_2, this equation will fit the experimental curve near and at wavelengths less than that for the peak, and for temperatures below 4000°K. For this reason, this equation has been found to be satisfactory in optical pyrometry applications.

The Rayleigh-Jeans Law

It can be shown, by a consideration of the number of modes of vibration, or degrees of freedom, per unit volume for electromagnetic waves in a rectangular enclosure with reflecting walls, that this number, within a wavelength range λ to $\lambda+d\lambda$, is

$$dn = 8\pi d\lambda/\lambda^4. \tag{15}$$

Since, by the principle of the equipartition of energy, each degree of freedom has associated with it an average energy, kT, the radiant energy per unit volume, or energy density, becomes

$$\rho_\lambda d\lambda = 8\pi kT\lambda^{-4}d\lambda \tag{16}$$

where k is the Boltzmann constant having the magnitude 1.38×10^{-23} Joules °K^{-1}. This equation reduces to

$$\rho_\nu d\nu = (8\pi\nu^2 kT/c^3)d\nu \tag{17}$$

since $\lambda = c/\nu$, and $d\lambda = -cd\nu/\nu^2$. Eq. (17) is a form of the Rayleigh-Jeans (Lord Rayleigh and Sir James Jeans, 1900) law of radiation, giving the energy density as a direct function of the absolute temperature and the square of the frequency. The latter produces what was called the "ultraviolet catastrophe," in which the energy density increases without limit with increased frequency, and was in direct discord with the experimental facts. The equation fits the experimental curves well at longer wavelengths or higher temperatures, where a direct dependence on temperature is observed.

The Planck Radiation Equation

The quantum theory approach to the Planck radiation equation is long and tedious [1], [2]. However, certain approaches with particular assumptions can simplify the calculations.

We shall begin with the consideration of a group of simple harmonic oscillators in thermal equilibrium, each possessing a frequency of vibration ν. The total energy of a single oscillator written in terms of momentum (p) and displacement (q) is given by

$$\begin{aligned} U &= \text{kinetic energy} + \text{potential energy} \\ &= p^2/2m + 2\pi^2 m\nu^2 q^2. \end{aligned} \tag{18}$$

This is the equation of an ellipse in p and q coordinates, such a system of coordinates being commonly known as phase space, and shown diagrammatically in Fig. 2. The

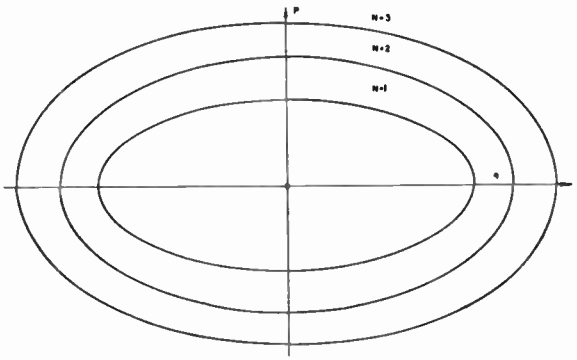

Fig. 2—Phase space for harmonic oscillator.

semi-major and -minor axes and area of the ellipse specified by a particular energy U are, respectively,

$$a = \sqrt{2mU} \tag{19}$$

$$b = \sqrt{U/2\pi^2 m\nu^2} \tag{20}$$

$$A = \pi ab = U/\nu. \tag{21}$$

The quantum theory now states that an oscillator cannot have any value for the total energy, but only discrete values, the oscillator changing energy by discontinuous jumps. Let us then write (21) as $U = A\nu$, and assume that the ellipses in phase space have areas which increase sequentially by an amount h. When U increases by the smallest allowable amount, the energy for the nth ellipse is given by

$$U_n = nh\nu. \tag{22}$$

The factor h has come to be universally known as Planck's constant, and has the magnitude of 6.624×10^{-34} Joule·sec.

Now, the average energy for N oscillators is obtained by weighting the values shown in (22) in accordance with the Boltzmann factor, giving

$$\overline{U} = h\nu \frac{\sum_{n=0}^{\infty} ne^{-nh\nu/kT}}{\sum_{n=0}^{\infty} e^{-nh\nu/kT}}. \tag{23}$$

Carrying out the summations indicated, we can write

$$\overline{U} = h\nu[e^{h\nu/kT} - 1]^{-1}. \tag{24}$$

It is possible to show that, within a parallelepiped of volume V, which is large compared with the wavelength, the number of vibrations possible within the frequency range ν to $\nu + d\nu$ is given by

$$dn = (8\pi\nu^2 V/c^2)d\nu \tag{25}$$

where c is the velocity of light. If the average energy of an oscillator is given by $\overline{U}$, the density of radiant energy in an isothermal enclosure within the above frequency range is $\rho_\nu d\nu$, and

$$\rho_\nu = \overline{U}(8\pi\nu^2/c^3). \tag{26}$$

Substitution from (24) gives

$$\rho_\nu = (8\pi h\nu^3/c^3)/(e^{h\nu/kT} - 1) \tag{27}$$

which is Planck's radiation equation, giving the radiation density per unit frequency interval in an isothermal enclosure. To place (27) in terms of unit wavelength interval corresponding to the equivalent frequency interval, we recall that $\rho_\lambda d\lambda = -\rho_\nu d\nu$, $\nu = c/\lambda$ and $d\nu = -cd\lambda/\lambda^2$, giving

$$\rho_\lambda = \frac{8\pi ch}{\lambda^5}[e^{ch/\lambda kT} - 1]^{-1}. \tag{28}$$

Since the spectral emissive power E_λ is related to spectral energy density by $E_\lambda = c\rho_\lambda/4$, we have

$$E_\lambda = c_1\lambda^{-5}[e^{c_2/\lambda T} - 1]^{-1} \tag{29}$$

where

$$c_1 = 2\pi c^2 h = 3.74 \times 10^8 \text{ watts} \cdot \text{micron}^4 \cdot \text{m}^{-2} \tag{30}$$

and

$$c_2 = ch/k = 1.4388 \times 10^4 \text{ micron} \cdot {}^\circ\text{K} \tag{31}$$

and are known as the first and second radiation constants. It should be pointed out that $8\pi ch$ in (28) is often indicated as c_1, and to avoid errors in using any particular value from a reference, one should be certain as to how it is defined. Furthermore, the spectral emissive power is sometimes defined as that radiated into unit solid angle normal to a Lambert radiating surface.

In this instance, c_1 is given by $2c^2h$. Table I shows the different values of c_1 for the different conditions indicated. If the wavelength is given in microns, the three quantities defined in Table I take on, respectively, the following dimensions: Joules·m^{-3}·micron^{-1}, watts·m^{-2}·micron^{-1}, and watts·m^{-2}·steradian^{-1}·micron^{-1}.

TABLE I
VALUES OF c_1 FOR DIFFERENT QUANTITIES DEFINED BY PLANCK'S EQUATION

Quantity Defined	Expression for c_1	Magnitude of c_1
Spectral Radiant Density in Isothermal Enclosure	$8\pi ch$	4.99 Joule·micron^4·m^{-3}
Spectral Emissive Power into a Hemisphere	$2\pi c^2h$	3.74×10^8 watt·micron^4·m^{-2}
Spectral Emissive Power into Unit Solid Angle Normal to Radiating Surface, or Spectral Radiance	$2c^2h$	1.19×10^8 watt·micron^4·m^{-2} steradian^{-1}

Integration of the Planck equation over all wavelengths results in the Stefan-Boltzmann Law. Substituting $u=c_2/\lambda T$ in (29) gives

$$\int_0^\infty E_\lambda d\lambda = E = (c_1T^4/c_2^4)\int_\infty^0 u^3(e^u - 1)^{-1}du. \quad (32)$$

The value of the integral can be shown to be $6\pi^4/90$, so that

$$E = (c_1/c_2^4)(6\pi^4/90)T^4 = \sigma T^4 \quad (33)$$

where σ is the Stefan-Boltzmann constant referred to earlier.

By differentiating the Planck equation with respect to wavelength and setting the result equal to zero, the condition for the maximum of the radiation curve will be obtained. Performing this operation on (29), we have

$$dE_\lambda/d\lambda = -5/\lambda + (c_2/\lambda^2T)e^{c_2/\lambda T}(e^{c_2/\lambda T} - 1)^{-1} = 0. \quad (34)$$

Simplification will give

$$(1 - c_2/5\lambda T)e^{c_2/\lambda T} = 1. \quad (35)$$

It can be shown that to satisfy this equation, $c_2/\lambda T$ must be either zero or 4.965. The first root is of no interest. Using the second root, and setting $\lambda=\lambda_m$ we have the Wien Displacement Law for the maxima,

$$\lambda_m T = c_2/4.965. \quad (36)$$

Substitution for c_2 gives

$$\lambda_m T = 2891 \text{ micron}\cdot^\circ\text{K}. \quad (37)$$

Planck's radiation equation should also reduce to Wien's equation for small values of λT, and to the Rayleigh-Jeans equation for large values of this quantity. If λT is sufficiently small, $e^{c_2/\lambda T}$ is substantially greater than unity, and (29) may be written

$$E_\lambda = c_1\lambda^{-5}e^{-c_2/\lambda T} \quad (38)$$

which is the Wien expression.

For large values of λT we may obtain an expression by expanding the reciprocal factor in brackets, giving

$$E_\lambda = c_1\lambda^{-5}[c_2/\lambda T + (1/2)(c_2^2/\lambda^2T^2) + \cdots]^{-1}. \quad (39)$$

Using the first term, (39) becomes

$$E_\lambda = (c_1/c_2)\lambda^{-4}T \quad (40)$$

which is the Rayleigh-Jeans equation.

The deviations of both the Wien and Rayleigh-Jeans equations from the Planck equation are shown in Fig. 3, where these deviations are plotted as functions of λT.

It is also of interest to note that a single blackbody-radiation curve may be drawn which can be used for determining spectral emissive power at any wavelength and temperature if this quantity is known for $\lambda_m T$.

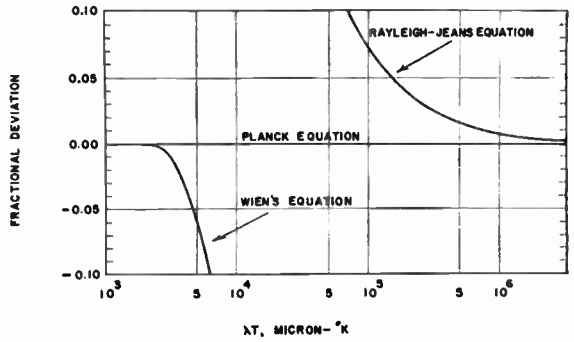

Fig. 3—Fractional deviation of classical radiation equations from the Planck equation.

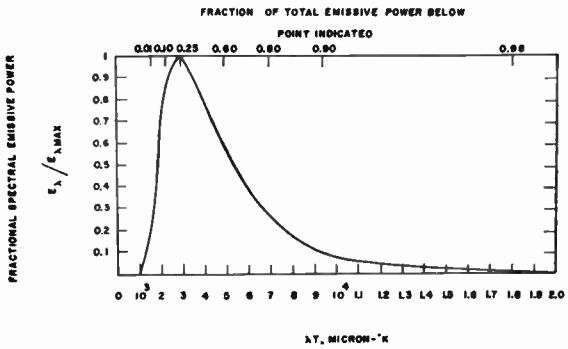

Fig. 4—General blackbody radiation curve useful for any combination of λ and T.

This curve is shown in Fig. 4, where the fractional emissive power relative to that at the peak is plotted as a function of λT. The fraction of the total energy lying below any given value of λT is also shown. It is of further interest to note that one-fourth of the total power radiated always lies on the shorter wavelength side of the peak of the radiation curve.

Another method of representing the radiation curves is to plot both the spectral emissive power and the wavelength logarithmically, as shown in Fig. 5. When this is done, it becomes obvious that all curves have the same shape, and are simply shifted to their proper positions, the peaks falling on a line representing the Wien

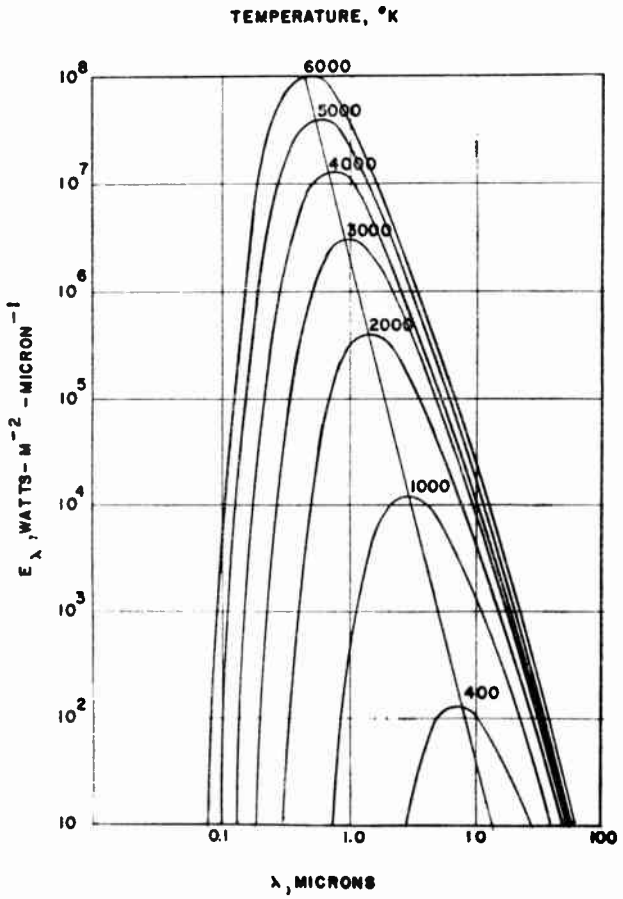

Fig. 5—Absolute spectral emissive powers for blackbody at temperatures indicated.

Displacement Law. An additional advantage of this method of plotting is that absolute values of emissive power can be shown over a considerably large temperature variation.

Practical Considerations

Up to this point, we have considered thermal radiation only when it is contained within an isothermal enclosure. Such conditions are practically realized, for instance, in a well-insulated furnace which has reached a stable temperature. Under such conditions, the interior of the furnace is traversed uniformly in all directions by thermal radiation, as has been assumed to be the case in the theoretical derivation given previously. In many cases, however, the conditions of the isothermal enclosure are not experimentally realizable, and it becomes necessary to study the physics of more general situations.

The rate at which a body emits radiation depends not only upon its temperature, as given by Planck's radiation law, but also upon the physical characteristics of its surface. The total emissive power E of a body has already been defined as the total radiant energy emitted in unit time per unit area of the surface of the body. If the total emissive power is multiplied by the area of the body, the product is termed the radiant flux. Since the physical dimensions of radiant flux are energy per unit time, this quantity is, in fact, power in the form of radiation, and may be called radiant power. The total emissive power of tungsten frequently used in heaters and filaments was investigated at an early date [3], and by studying such data, one notes a rapid increase of E with increasing temperature.

Lambert's Cosine Law

A knowledge of total emissive power of a body does not allow one to calculate the radiation field surrounding that body, unless additional information is given on the directional distribution of emission. Simple experiments may be conducted to measure the radiation from a heated surface, and such an experiment is suggested in Fig. 6. The area dS is a small surface element of a

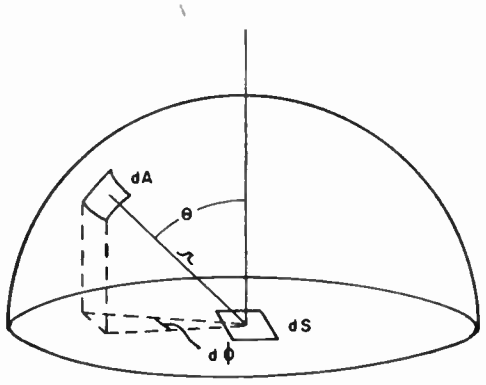

Fig. 6—Geometry for experimental investigation of Lambert's cosine law.

radiating body, and the radiation detector, which might be a thermocouple, is of area dA, located on a hemisphere of radius r surrounding dS. The radius vector from dS to dA makes an angle θ with the normal to the surface element. Many experimental studies have shown [4] that the radiant energy intercepted by dA from the area dS is proportional to the cosine of the angle θ. This effect, known as Lambert's cosine law, is not unexpected, since the solid angle subtended by dS as seen from dA is also proportional to cosine θ. A radiating surface which obeys this cosine law exactly is an ideal, diffuse radiator, and is known as a Lambert surface. It should be noted that, although surfaces which are good diffuse reflectors [5] are also good diffuse radiators, specular metal surfaces may also act as good diffuse radiators. This explains why objects which have been brought to incandescence in furnaces seem to appear flat and somewhat transparent, since all sides look equally bright from all directions. In addition to its dependence upon the cosine law, the power, dp, intercepted by the area, dA, also depends upon the familiar inverse square law, the area dS, and the area dA. Since dA divided by r^2 is simply the solid angle $d\omega$ which the detector subtends at dS, the above relationships may be stated more simply in the equation:

$$dp = BdSd\omega \cos\theta = Bc'S\left[\cos\theta \sin\theta d\theta d\phi\right]. \quad (41)$$

The proportionality constant B is defined as the steradiance of the surface, and has the dimensions power ·area^{-1}·steradian^{-1}. It is measured in a direction normal to the surface or to a projected area of the surface. This quantity is sometimes called the radiance [26], but since radiant intensity is then used to denote power per steradian, and these terms are confusingly similar, steradiance is preferred by many authors. There is, unfortunately, no internationally accepted terminology in the field of radiometry at the present time, although many systems have been proposed [27].[1]

For extended surfaces which obey Lambert's law, B will be the same in all directions provided a unit area on the projected radiating area is considered. Integrating the factor shown in brackets over the hemisphere, the power radiated by dS is

$$dP = \pi BdS, \quad (42)$$

but dP/dS is the total emissive power, E, of the surface, and we may write

$$E = \pi B. \quad (43)$$

Since this relationship obviously holds for any given spectral region, the monochromatic emissive power may be expressed in terms of the monochromatic steradiance as $E_\lambda = \pi B_\lambda$.

The discussion thus far has dealt only with surfaces which radiate into a hemisphere, and we note that the effect of Lambert's law is to yield only one-half the emissive power which might be expected for a surface radiating into 2π steradians. Occasionally, one finds the total radiant flux defined for a body which is free to radiate in all directions. If care is not taken, it is easy to see how an error by the factor 4 may occur, since the cross-sectional area of a radiating sphere is only one-fourth of the surface area.

Emissivity

Another important characteristic of surface radiators is the manner in which they react with radiant energy. Electromagnetic radiation incident upon a surface may be either reflected from the surface or transmitted through the surface. Of the transmitted component, some may be absorbed and converted into heat, while the remaining fraction may pass on through the body and escape. For simplicity, we may confine our discussion to objects which are either so thick or so highly absorbing that the sum of the fraction reflected and the fraction absorbed is unity. The reflectance r will, in general, be a function of the angle of incidence, so that, precisely, r is defined as that fraction of the energy at normal incidence which is reflected by the surface. Similarly, the absorptance a is the fraction which is absorbed. Both r and a are numerical ratios, and are less than unity for any realizable objects. Both are functions of wavelength of the incident radiation, and it is this effect in the visual region of the spectrum which produces the sensation of color. A perfectly black surface would be one for which $r=0$ and $a=1$, while a perfectly white surface would be described by $r=1$ and $a=0$. Additionally, such perfect surfaces should obey Lambert's cosine law.

Suppose that a body with a perfectly black surface is placed within an isothermal enclosure. Eventually, the body will come to an equilibrium temperature with the enclosure, and, since it is perfectly black, it would reflect none of the radiation incident upon it. All radiation leaving the surface of the body would be thermally emitted by the black surface. If the enclosure were suddenly removed, the radiation leaving the surface of the blackbody would be identical with that moving in any one direction within an isothermal enclosure at the same temperature as the body. Thus, blackbody radiation and radiation within an isothermal enclosure are mathematically identical and may be treated as such. Experimentally, a black surface is closely approximated by coatings of metallic blacks [6]–[8], [25], or by openings into spheres, cones, or grooves where incident radiation is permitted to leave the aperture only after many low-order internal reflections [9], [10]. Carbon or graphite surfaces are only fair approximations to black surfaces [11], [25].

Since a perfectly black surface has the highest possible emissive power E_b, any real surface will be characterized by a smaller emissive power E. The ratio E/E_b is termed the total radiant emissivity of the surface and is indicated by ϵ.

If a body has reached an equilibrium temperature, it is necessarily emitting the same amount of radiation as it absorbs from its surroundings, or otherwise its temperature would change. Thus, the absorptance equals the emissivity under such conditions. This fact, which may be proven more rigorously if desired [12], is known as Kirchhoff's law.

Monochromatic radiant emissivity is defined similarly, in terms of monochromatic emissive power, as $\epsilon_\lambda = E_\lambda/E_{b\lambda}$. For most surfaces the monochromatic radiant emissivity is a function of wavelength and, to a lesser extent, of the temperature of the body. A good example of the wide variation of ϵ_λ over the spectrum is given by white paint which reflects a large fraction of visual wavelength energy, but emits well at wavelengths beyond three microns [13]. This explains why white, painted surfaces have temperatures only slightly above ambient in direct sunlight. Much of the solar energy is concentrated in the visible spectrum, and any energy which is not reflected is efficiently radiated in the infrared, with the maximum spectral emissive power occurring near 10μ for surfaces at or near room temperatures. Tests made at Naval Ordnance Test Station, China Lake, Calif. [14], showed that white, painted surfaces were up to 19°C cooler in direct sunlight than an aluminum plate, for, although visual region reflectivities are similar, the metal has a low emissivity in the infrared and thus cannot radiate away its excess heat at the same temperature. Airline operators have recently rec-

[1] See E. E. Bell, "Radiometric quantities, symbols, and units," paper 3.1.1, this issue, p. 1432.

ognized this fact and many are painting fuselage tops white, to relieve air-conditioning requirements during airport based operations.

The emissive power for a blackbody over a finite spectral region is given by

$$E_{b(\lambda_2-\lambda_1)} = \int_{\lambda_2}^{\lambda_1} E_{b\lambda} d\lambda \tag{44}$$

as discussed earlier. For real surfaces, the emissivity would enter into such an expression, so that

$$E_{(\lambda_2-\lambda_1)} = \int_{\lambda_2}^{\lambda_1} \epsilon_\lambda E_{b\lambda} d\lambda. \tag{45}$$

It is usually not possible to express ϵ_λ in functional form. Consequently such integrations are performed using numerical methods.

A surface for which the monochromatic emissivity is less than unity and does not vary rapidly with wavelength may be descriptively termed a graybody. Such a body will have a spectral distribution of energy very similar to that of a blackbody, as given by Planck's radiation law, except that the monochromatic emissive power will always be less than that of a perfectly black surface. A blackbody and a graybody at the same temperature, therefore, will appear to be the same color by virtue of their thermal radiation, the blackbody being somewhat brighter. The so-called color temperature of the body [15], [16] relates the dominant wavelength as seen by the human observer to the corresponding blackbody temperature, and this relationship is made use of in the design of optical pyrometers [17] used to measure temperatures of glowing objects at a convenient distance. The device is merely a telescope which serves to superimpose the optical image of the body to be measured upon that of a glowing filament whose temperature may be controlled by the observer. The voltage across the filament is equivalent to a given temperature when the colors are matched, and once the device is properly calibrated it will serve to measure temperatures of bodies whose monochromatic emissivities are not too different from those of the comparison filament.

Calculations Involving Blackbody Radiation

Due to the complicated mathematical nature of Planck's equation, it is not a convenient tool to use directly in solving problems dealing with blackbody radiation. Fortunately, many graphs and tables are available [18]–[20], [24] from which numerical values of the function may be obtained. The explanations given with these tables are usually such that little previous experience is required, but care must be taken, as has been pointed out earlier, in the choice of the proper value for the constant c_1. Special slide rules [21], [22] are also available which enable one to determine simply and accurately such quantities as total emissive power, emissive power in a given spectral region, the wavelength where maximum monochromatic emissive power is located, the numbers of quanta in blackbody radiation, and many combinations of these quantities. Although not as accurate as the radiation tables, the slide rules are fast and convenient to use. Values of emissivities of many surfaces are also available over various temperature ranges [18], enabling one to calculate graybody radiation from such sources, and a bibliography consisting of 127 entries has been prepared by the Atomic Energy Commission [23].

References

[1] F. K. Richtmyer and E. H. Kennard, "Introduction to Modern Physics," McGraw-Hill Book Co. Inc., New York, N. Y.; 1947.
[2] L. Page, "Introduction to Theoretical Physics," D. Van Nostrand Inc., New York, N. Y., pp. 326–330, 554–549; 1935.
[3] W. E. Forsythe and A. G. Worthing, *Astrophys. J.*, vol. 61, p. 146; 1925.
[4] A. G. Worthing and W. E. Forsythe, "Deviation from Lambert's law and polarization of light emitted by incandescent tungsten, tantalum, and molybdenum and changes in the optical constants of tungsten with temperature," *J. Opt. Soc. Am.*, vol. 13, p. 635; 1926.
[5] J. T. Agnew and R. B. McQuistan, "Experiments concerning infrared diffuse reflectance standards in the range 0.8 to 20.0 microns," *J. Opt. Soc. Am.*, vol. 43, pp. 999–1007; November, 1953.
[6] L. Harris, R. T. McGinnies, and B. M. Siegel, "Preparation and optical properties of gold blacks," *J. Opt. Soc. Am.*, vol. 38, pp. 582–589; July, 1948.
[7] A. H. Pfund, "The optical properties of metallix and crystalline powders," *J. Opt. Soc. Amer.*, vol. 23, pp. 375–378; October, 1933.
[8] A. H. Pfund, "Bismuth black and its applications," *Rev. Sci. Instr.*, vol. 1, pp. 397–399; July, 1930.
[9] L. F. Daws, "The emissivity of a groove," *Brit. J. Appl. Phys.*, vol. 5, pp. 182–187; May, 1954.
[10] M. Michaud, "The emissivity of cavities of simple geometric shapes," *Compt. Rend. Acad. Sci. (Paris)*, vol. 226, pp. 999–1000; March 22, 1948.
[11] R. J. Thorn and O. C. Simpson, "Spectral emissivities of graphite and carbon," *J. Appl. Phys.*, vol. 24, pp. 633–639; May, 1953.
[12] L. D. Weld, "A Textbook of Heat," Macmillan Co., New York, N. Y., pp. 353–359; 1948.
[13] C. D. Reid and E. D. McAlister, "Measurement of spectral emissivity from 2 μ to 15 μ," *J. Opt. Soc. Am.*, vol. 49, pp. 78–82; January, 1959.
[14] C. M. Arney and C. L. Evans, Jr., "Effect of Solar Radiation on the Temperatures in Metal Plates with Various Surface Finishes," NAVORD Rept. 6401 (NOTS 2097); May, 1953.
[15] H. G. W. Harding, "The colour temperature of light sources," *Proc. Phys. Soc. (London)B*, vol. 63, pp. 685–698; September, 1950.
[16] F. Hoffman, "The optical temperature scale and the radiation constants," *Z. angew Phys.*, vol. 2, no. 2, pp. 88–95; 1950.
[17] W. E. Forsythe, "Measurement of Radiant Energy," McGraw-Hill Book Co., Inc., New York, N. Y., pp. 355–407; 1937.
[18] M. M. Fulk, M. M. Reynolds, and R. M. Burley, "American Institute of Physics Handbook," McGraw-Hill Book Co., Inc., New York, N. Y., pp. 6-64–6-67; 1957.
[19] F. E. Foule, "International Critical Tables," vol. 5, McGraw-Hill Book Co., Inc., New York, N. Y., pp. 238–242; 1929.
[20] W. H. McAdams, "Heat Transmission," McGraw-Hill Book Co., Inc., New York, N. Y., p. 60; 1954.
[21] A. H. Canada, "Simplified calculation of black-body radiation," *G. E. Rev.*, vol. 51, pp. 50–54; December, 1948.
[22] R. S. Knox, "Direct reading Planck distribution slide rule," *J. Opt. Soc. Am.*, vol. 46, pp. 879–881; October, 1956.
[23] M. P. Bauleke, "Spectral and Total Emissivity, A Guide to the Literature (1910–1951)," ISC-364, USAEC; June 1, 1953; (Available through U. S. Dept. Commerce.)
[24] R. L. LaFara, E. L. Miller, W. E. Pearson, and J. F. Peoples, "Tables of Black Body Radiation and the Transmission Factor for Radiation Through Water Vapor," NAVORD Rept. 3171, U. S. Naval Ordnance Plant; November 15, 1955.
[25] E. K. Plyler and J. J. Ball, "Infrared absorption of deposited blacks," *J. Opt. Soc. Am.*, vol. 38, p. 988; November, 1948.
[26] Technical Note, "American Standards Association Nomenclature for Radiometry and Photometry Z 58.1.1—1953," *J. Opt. Soc. Am.*, vol. 43, p. 809; September, 1953.
[27] P. Moon and D. E. Spencer, "Study of photometric nomenclature," *J. Opt. Soc. Am.*, vol. 36, pp. 666–675; November, 1946.

Paper 3.1.3

Selective Radiators*

GILBERT N. PLASS†

Introduction

THE absorption coefficient for radiation is nearly constant over wide frequency intervals for many solids and liquids. In this case, the intensity of a beam of radiation decreases exponentially with the amount of absorbing material traversed (Beer's law). Unfortunately Beer's law is not valid for gaseous substances, except at very high pressures. Absorption by gaseous molecules can occur only at certain frequencies corresponding to allowed quantum transitions. A number of different processes cause the absorption to take place over a small range of frequencies around each transition frequency. For infrared applications, the perturbation from the collisions between gas molecules is usually the most important such process. The spread in frequencies is specified by the half-width of the resulting spectral lines. This Lorentz or pressure-broadened half-width is nearly proportional to the total pressure in the gas.

A typical molecule that absorbs in the infrared has a large number of spectral lines arranged in bands which occur in certain definite frequency intervals. The half-width of these spectral lines at atmospheric pressure is usually somewhat smaller than the average spacing between the lines. There are usually a number of spectral lines in any frequency interval of practical interest. The absorption coefficient oscillates rapidly between large and small values in such an interval. After integration over frequency, it is found that the absorption depends on the shape of the spectral lines and their particular arrangement into a band. The dependence on pressure and the amount of absorbing gas is in general quite different from Beer's law. Kirchhoff's law of radiation states that the emission and absorption coefficients of a given substance are proportional to each other at a particular frequency. Thus, the same results apply to both the absorption and emission from a band. In the following sections, the most convenient process is chosen for discussion.

The physical processes and mathematical equations which describe the absorption and emission of radiation by gaseous substances are presented. The emission from a single spectral line is discussed first. Then the influence on the emission of various arrangements of spectral lines into bands is considered. Finally, several examples of emission from flames are given.

Emission From a Single Spectral Line

The emission from a single spectral line is discussed in this section. The total emission from a band of spectral lines can be obtained by merely multiplying the emission from a single line by the number of lines, provided that the lines do not overlap appreciably. As the amount of radiating gas increases, the spectral lines begin to overlap at a point determined by their intensity and half-width and the amount of radiating gas. When overlapping occurs, the particular arrangement of the spectral lines in the band influences the emission, and must be taken into account. The effects due to overlapping are considered in the following section.

For most problems of practical interest in the infrared, the shape of an individual spectral line can be taken to be the Lorentz pressure-broadened line shape. Only at pressures equivalent to those encountered at 50 km or higher in the atmosphere is it sometimes necessary to include the Doppler line shape in the calculations.[1] The Lorentz line shape is given by the expression

$$k_\nu = (S/\pi)[\alpha/((\nu - \nu_0)^2 + \alpha^2)], \tag{1}$$

where k_ν is the absorption coefficient at the frequency ν, S and α are the total intensity and half-width of the spectral line, and ν_0 is the frequency of the line center. The half-width is nearly proportional to the total pressure in the gas.

The emission from a gas at the frequency ν is obtained by considering the change in the radiation intensity I in passing through an infinitesimal slice of the material. The change in the intensity is

$$dI_\nu = k_\nu I_{b\nu} du - k_\nu I_\nu du, \tag{2}$$

where dI_ν is the change in the intensity I_ν in a layer du, k_ν is the absorption coefficient at the frequency ν, $I_{b\nu}$ is the blackbody intensity, and $u = \rho l$ is the mass of radiating gas per unit area. The first term on the right-hand side of (2) represents the radiation emitted by the thickness du of the gas and added to the original beam, while the second term represents the absorption in this same thickness.

When the pressure and temperature are constant along the path, the solution of (2) is

$$I_\nu = I_{b\nu}(1 - e^{-k_\nu u}). \tag{3}$$

Thus, at a particular frequency, the exponential dependence of Beer's law is obtained. When the temperature and pressure vary along the path, more general solutions are available.[2]

For most applications, the emitted flux over a frequency interval $\Delta\nu$ is desired, where $\Delta\nu$ is large com-

* Original manuscript received by the IRE, June 26, 1959.
† Aeronutronic Systems, Inc., Glendale, Calif.

[1] G. N. Plass, "Influence of Doppler effect and damping on line-absorption coefficient and atmospheric radiation transfer," *Astrophys. J.*, vol. 117, pp. 225–233; January, 1953.

[2] G. N. Plass, "Infrared radiation in the atmosphere," *Am. J. Phys.*, vol. 24, pp. 303–321; May, 1956.

pared to the half-width of a spectral line. At the same time, the interval $\Delta\nu$ must be sufficiently small so that there is only a small change in the blackbody flux over the entire interval. Then, from the integral of (3) over the interval $\Delta\nu$, the emitted flux is found to be

$$I = I_b \int_{\Delta\nu} (1 - e^{-k\nu u}) d\nu, \tag{4}$$

where I_b is the average value of the blackbody intensity over $\Delta\nu$.

If there is only a single spectral line in the interval $\Delta\nu$, then the result of the substitution of (1) in (4) is that

$$I = I_b \alpha \int_{-\infty}^{\infty} \{1 - \exp[-2x/(1 + \nu'^2)]\} d\nu', \tag{5}$$

where

$$x = Su/2\pi\alpha, \tag{6}$$

and

$$\nu' = (\nu - \nu_0)/\alpha. \tag{7}$$

The limits of integration have been extended to infinity since it is assumed that the frequency interval $\Delta\nu$ is very large compared to the half-width of the spectral lines. Since there is a negligible contribution from the ends of the interval, the absorption from a single line is the same over the interval $\Delta\nu$ or over an infinite interval.

Two limiting results for the absorption can readily be derived from (5): 1) the linear region; 2) the square-root region. First, if x is sufficiently small, the exponential in (5) can be replaced by the first two terms in its series expansion around the origin. After an elementary integration, it is found that

$$I = I_b 2\pi\alpha x = I_b d\beta x, \qquad x < 0.2, \tag{8}$$

where

$$\beta = 2\pi\alpha/d. \tag{9}$$

It has been shown[3] that this equation is accurate within 10 per cent when $x<0.2$. Thus, when the emission is small even at the center of the spectral line, the emission increases linearly with the amount of radiating gas. It is also directly proportional to the intensity of the spectral line and is independent of pressure. Each spectral line is emitting as much radiation as possible for its strength and the amount of radiating gas present. There is negligible absorption by the gas of the emitted radiation.

It is instructive to compare this result with a substance that has an average absorption coefficient k and obeys Beer's law over a spectral interval $\Delta\nu$. For such a substance, the emitted flux is

$$I = I_b \Delta\nu (1 - e^{-ku}). \tag{10}$$

If ku is sufficiently small so that the exponential can be replaced by its series expansion, then

$$I = I_b \Delta\nu k u. \tag{11}$$

Thus the emission from a substance that follows Beer's law also increases linearly with the amount of radiating gas, when the emission is a small fraction of the blackbody intensity. In fact, (8) and (11) are formally identical if $k\Delta\nu = S$. However, as the amount of radiating gas increases, the emission from a band of spectral lines at moderate pressures is quite different from that predicted by Beer's law.

The square-root region occurs for larger values of x. In this case, the emission can be calculated approximately by neglecting the factor unity compared to ν'^2 in the denominator of the exponential of (5). When $\nu' \gg 1$, this factor is always negligible. On the other hand, when ν' is of the order of unity or smaller, the exponential is nearly zero for large values of x and need not be evaluated accurately. After the introduction of a new variable $v = 2x/\nu'^2$, it is found that

$$I = I_b (2\beta^2 x/\pi)^{1/2}, \qquad x > 1.63. \tag{12}$$

This equation is accurate within 10 per cent for a single spectral line when $x > 1.63$.[3,4] In this region the emission increases as the square root of both the pressure and amount of radiating gas. In this square-root region, the full blackbody radiation is emitted over a frequency interval of at least several half-widths around the center of the spectral line. The emission falls off from the blackbody value only at frequencies that are many half-widths from the line center. Thus, as the amount of emitting gas increases, additional emission can only come from the wings of the spectral lines. In this case, there is appreciable absorption by the gas of its own emitted radiation at frequencies near the line center. This process limits the total radiation to the blackbody intensity at any particular frequency.

An exact expression for the emission from a single spectral line can be written in terms of the Bessel functions of imaginary argument.[3,5] However, it is only necessary to use this more complicated expression when $0.2 < x < 1.63$. For larger and smaller values of x, the limiting forms given by (9) and (12) may be used.

Band Emission

The emission from a band can be obtained by multiplying the number of spectral lines by the emission from a single line, (9) and (12), as long as the lines do not overlap appreciably. However, when the lines do overlap, the emission depends on whether the lines are regularly arranged in the band or occur virtually at random throughout the frequency interval. It also depends, to a lesser extent, on the distribution of line intensity throughout the band.

Because of the large number of spectral lines that

[3] G. N. Plass, "Models for spectral band absorption," *J. Opt. Soc. Am.*, vol. 48, pp. 690–703; October, 1958.

[4] G. N. Plass, "Useful representations for measurements of spectral band absorption," *J. Opt. Soc. Am.*; 1959. (In press.)

[5] W. M. Elsasser, "Heat Transfer by Infrared Radiation in the Atmosphere," Harvard Meteor. Studies No. 6, Harvard University Press, Cambridge, Mass.; 1942.

occur in many bands and because of the extremely rapid fluctuations of the absorption coefficient as a function of frequency, a numerical integration over frequency of the emission is a formidable task even with a large electronic computer. Fortunately, three models have been developed which accurately represent the absorption for the various possible arrangements of spectral lines in a band. Relatively simple mathematical expressions can be obtained in each case for the band emission. Thus, once an appropriate model is chosen, the emission can be calculated easily and accurately.

The three models are: 1) Elsasser model;[6] 2) statistical model;[7,8] and 3) random Elsasser model.[3,9] The arrangement of the spectral lines in the band for each of these models is illustrated in Fig. 1. The Elsasser model is applicable to a band of equally-spaced and equally-intense spectral lines. Portions of the CO_2 spectrum can be accurately represented by this model. The statistical model represents a band where the spacing between adjacent spectral lines varies in an essentially random fashion. The intensity of the spectral lines may also vary in any manner whatsoever, as long as it can be represented by some distribution function. The statistical model accurately represents portions of the H_2O spectrum.

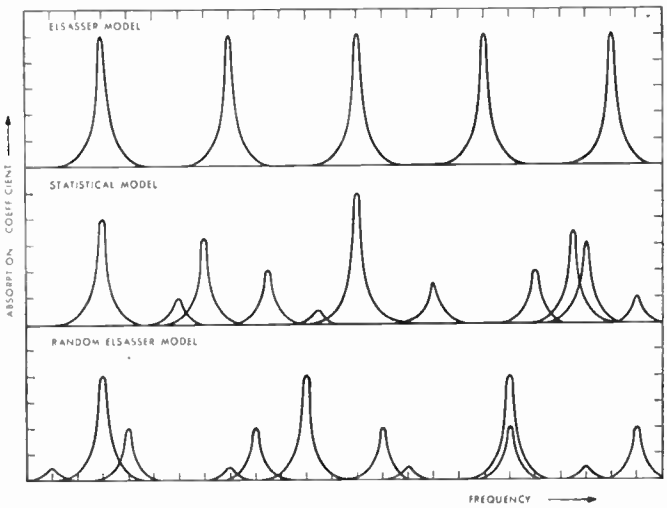

Fig. 1—Typical arrangement of spectral lines in a band for the Elsasser model, the statistical model, and the random Elsasser model.

An actual band is formed by the superposition of a number of fairly evenly-spaced transitions from different groups of quantum transitions and possibly from different isotopic forms of the molecule. If only a single one of these quantum transitions has an appreciable intensity, then the Elsasser model is applicable. If many different groups of transitions are superposed, then the resulting arrangement of spectral lines is nearly random and the statistical model applied. However, in many cases, a small number of groups of spectral lines are superposed. Then the random Elsasser model applies. It assumes that the band is composed of a random superposition of a small number of Elsasser bands, each of which may have a different line spacing and line intensity. In Fig. 1, the random superposition of three Elsasser bands of different spacing and intensity is shown. Portions of the HCl spectrum can be represented accurately by the random Elsasser model.

A detailed study has been made by Plass[3,4] of the conditions under which these models are applicable and when various simple mathematical expressions may be used for the calculation of the emission. It is found that the region of validity of the single line, (8) and (12), depends on the arrangement of the lines in the band. For example, when $\beta=0.1$ and the Elsasser model is valid, the overlapping can be neglected when $x<60$. On the other hand, it can be neglected for the statistical model when $x<6.3$. The physical reason for these different regions of validity is that some of the spectral lines always occur by chance very close to each other in the statistical model. Thus the effects due to overlapping occur with less emitting material in this case than for the Elsasser model.

For larger values of x, the single-line equations for the emission must be generalized to include the effects of overlapping. For large values of β, effects due to overlapping may occur for quite small values of x. The emission for small values of x is found to be[3,4]

$$I = I_b(1 - e^{-\beta x}). \tag{13}$$

This expression is accurate within 10 per cent when $x=S\mu/2/2\pi\alpha<0.2$. Since the half-width of the spectral lines is directly proportional to the total pressure of the gas, it follows that (13) is valid, either for small amounts of radiating gases or at large pressures. This equation has the same exponential dependence as appears in Beer's law. The physical reason for this is that the emission from a single spectral line is small even at its center under these conditions. Thus, either the lines act individually giving a contribution to the emission proportional to their intensity or, when they overlap, the spectral lines are so broadened that the emission is nearly constant as a function of frequency, instead of being a rapidly-varying function.

On the other hand, when $x>1.63$, the emission for each of the three models can be written as:

Elsasser model:

$$I = I_b\phi\left[(\tfrac{1}{2}\beta^2 x)^{1/2}\right], \tag{14}$$

statistical model:

$$I = I_b\left\{1 - \exp\left[-(2\beta^2 x/\pi)^{1/2}\right]\right\}, \tag{15}$$

random Elsasser model:

[6] W. M. Elsasser, "Mean absorption and equivalent absorption coefficient of a band spectrum," *Phys. Rev.*, vol. 54, pp. 126–127; 1938.
[7] H. Mayer, "Methods of Opacity Calculations" Los Alamos, LA-647; October 31, 1947.
[8] R. M. Goody, "A statistical model for water-vapour absorption," *Quart. J. Roy. Meteor. Soc.*, vol. 78, pp. 165–169; April, 1952.
[9] L. D. Kaplan, "A quasi-statistical approach to the calculation of atmospheric transmission," *Proc. 1953 Toronto Meteor. Conf.*, pp. 43–48; 1954.

$$I = I_b\left\{1 - \prod_{i=1}^{N}\left(1 - \phi[(\tfrac{1}{2}\beta_i^2 x_i)^{1/2}]\right)\right\}, \qquad (16)$$

where ϕ is the error function integral, and the summation in (16) is over the N superposed Elsasser bands each with a half-width α_i and line intensity S_i, so that $\beta_i = 2\pi\alpha_i/d$ and $x_i = S_i u/2\pi\alpha_i$. In (15), an average value of S over the intensity distribution is used. Plass[3,4] describes the correct method for the computation of the average value of the intensity, and also gives more complicated equations for intermediate values of x. Eqs. (14), (15), and (16) are valid when the emission is nearly equal to the blackbody intensity for at least several half-widths away from the centers of the strongest lines in the band. Thus, the dependence of the emission on the amount of radiating gas depends both on the line shape far from the line center and on the manner in which neighboring spectral lines overlap. When there is no appreciable overlapping of the spectral lines, (14)–(16) reduce to (12).

Some typical absorption curves for the Elsasser model are shown in Fig. 2. The absorption is plotted against

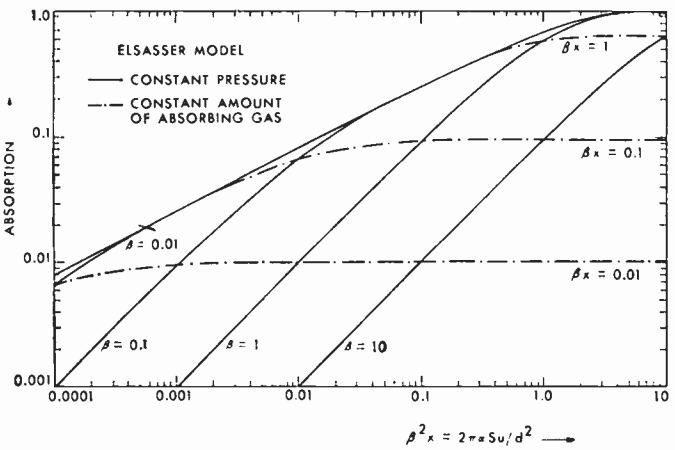

Fig. 2—Absorption by the Elsasser model as a function of $\beta^2 x = 2\pi\alpha Su/d^2$. Absorption curves are shown for constant pressure (β = const.) and constant amount of absorbing gas (βx = const.).

$\beta^2 x = 2\pi\alpha Su/d^2$ on a log-log scale. Of course, the same curves are valid in emission by Kirchhoff's law. The absorption curves are shown both at constant pressure (β = constant) and at constant amount of absorbing gas (βx = constant). The absorption curves for the other models are qualitatively similar to those for the Elsasser model.[3,4]

First, let us consider an absorption curve at constant pressure; for example, $\beta = 0.1$. As the amount of absorbing gas, u, slowly increases from a very small value, the absorption at first is directly proportional to u. The absorption curve has a slope of unity on a log-log plot. The linear approximation for the absorption, (8), is valid when $x < 0.2$. As u further increases, the slope of the absorption curve decreases to a value of one-half, as a region several half-widths wide around the line center becomes completely absorbing. When $1.63 < x < 60$ (the particular value, $\beta = 0.1$, is assumed in this paragraph), the absorption increases as $u^{1/2}$. The square-root approximation, (12), is valid until $x = 60$, where the effect of the overlapping of the spectral lines begins to become appreciable. As u increases further, the slope of the absorption curve decreases slowly from a value of one-half to zero. For a sufficiently large value of u, all of the incident radiation is absorbed. The slope of the absorption curve on a log-log plot indicates immediately whether the absorption is from the centers or the wings of the spectral lines, and the extent of the overlapping of the neighboring lines.

When $\beta = 10$ (which for most gases corresponds to a pressure considerably above atmospheric pressure), the absorption curve is the same as described above, except that there is no square-root region. For this particular value of β, the absorption increases linearly with u until $x = 0.02$. For larger values of x, overlapping must be taken into account. In this case, the slope of the absorption curve continuously changes from unity to zero as u increases.

Absorption curves at constant u where the pressure, p, varies are also shown in Fig. 2. Since x varies inversely with p, small values of p correspond to large values of x. Thus, for a given value of u ($\beta x = 1$, for example), the absorption increases as $p^{1/2}$ for small values of p. This occurs because the half-width decreases with the pressure and, for sufficiently small values of p, the spectral line becomes completely absorbing near its center. As p increases at constant u, the absorption increases as p^1, as long as $x > 1.63$. For still larger values of p and smaller values of x, the absorption increases less rapidly, and approaches a limiting value which depends on the amount of absorbing gas present and on the extent of the overlapping of the spectral lines.

The slope of the absorption curves on a log-log plot varies from unity to zero at constant p and from one-half to zero at constant u. Thus in a series of experiments which cover a wide range of values of u and p, the absorption is always found to depend more strongly on u than on p.

It is often useful to know that the absorption can never be greater than the uppermost curve in Fig. 2. The mathematical expression for this limiting curve for each model is given by either (14), (15), or (16). This limiting result is called the strong line approximation.[4] Other useful limiting curves which can be drawn are the weak line and nonoverlapping line approximations.[4]

A series of laboratory absorption measurements may be analyzed from graphs of this type. The resulting curves may then be used directly for the calculation of the emissivity or the atmospheric absorption of the gas. As an example of this method, the absorption measurements of Walshaw[10] for the 9.6-μ band of ozone are

[10] C. D. Walshaw, "Integrated absorption by the 9.6μ band of ozone," *Quart. J. Roy. Meteor. Soc.*, vol. 83, pp. 315–321; 1957.

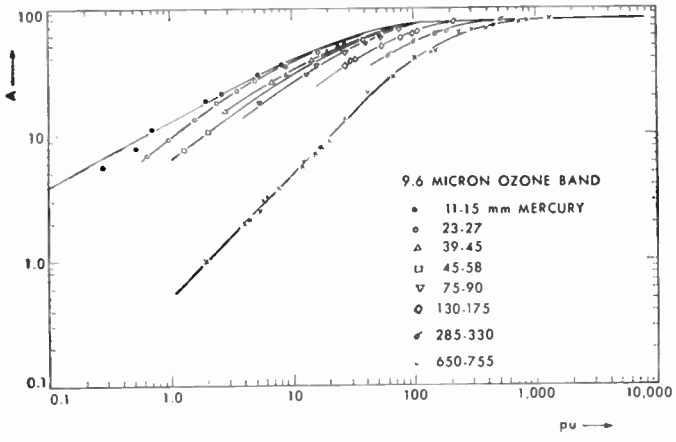

Fig. 3—Absorption of the 9.6-μ band of ozone as a function of pu as measured by Walshaw.[10]

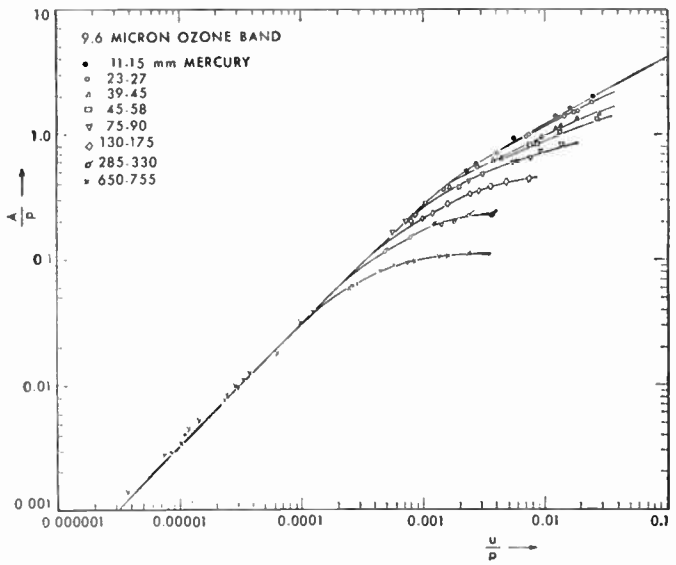

Fig. 4—Absorption divided by pressure as a function of u/p for the 9.6-μ band of ozone as measured by Walshaw.[10]

shown in Fig. 3 and Fig. 4. All of the measurements for the indicated pressure ranges have been included. The curves in these figures were calculated from the appropriate theoretical equations discussed here.

The absorption is plotted against pu in Fig. 3. The strong line approximation is clearly shown with the square-root region, together with the region where the spectral lines overlap. The absorption divided by p is plotted againts u/p in Fig. 4. The uppermost limiting curve in this case can be shown to represent the absorption when there is no overlapping.[4] The linear and square-root regions are clearly shown in Fig. 4, together with the transition region in between.

Emission from Flames

The general features of band emission have been discussed in the preceding section. In order to apply these theoretical results to the various infrared bands of practical interest, the theoretical parameters which appear in (13)–(16) must be evaluated. This can be done either by comparing experimental measurements with the theoretical results as discussed above, or by actually calculating the intensity and position of the spectral lines by the rules of quantum mechanics. In atmospheric problems it is necessary to take into account the variation of the intensity with the temperature and the variation of the half-width with temperature and pressure.

The emissivity of a flame depends on the temperature and pressure in the various regions of the flame as well as on the composition of the fuel. However, it is found experimentally that the spectral emissivities of many different types of flames are remarkably similar. An emissivity curve of a white gasoline and air flame as measured by Bell, *et al.*,[11] is shown in Fig. 5. It is typical of many flames. Large corrections had to be made to the experimental values in regions of large atmospheric absorption. Although the curve is somewhat uncertain in these regions, the general features of the emission are clearly determined.

Most of the emission occurs in the band from 4 to 5μ, with most of the remaining radiation emitted at wavelengths just below 3μ. The majority of the radiation from 4 to 5μ is emitted by the 4.3-μ band of CO_2; the radiation just below 3μ is from the 2.8-μ bands of CO_2 and H_2O.

Both CO_2 and H_2O are abundantly present among the combustion products of most flames. This is the reason that there is strong emission from these in the same spectral region. If other molecules are present which emit strongly in the infrared, their emission is added to that of CO_2 and H_2O. Two other molecules commonly present in flames are CO and OH. However, they do not increase the emissivity greatly, since their bands happen to occur at nearly the same wavelengths where there is already appreciable emission from CO_2 and H_2O. On the other hand, if a molecule such as HCl is present, the emission may be greatly increased, since its bands occur in the spectral region from 3 to 4μ where there is little emission from CO_2 and H_2O.

Extensive calculations of the total emissivity of numerous gases have been made by Penner[12] and his students together with important contributions to the theory of these processes. The only calculations of the spectral emissivities of gases which have been reported to date are for CO_2[13] and HCl.[14]

The spectral emissivities of these gases have been cal-

[11] E. E. Bell, C. F. Dam, F. P. Dickey, S. L. Kopczynski, E. D. Palik, and R. F. Rowntree, "Study of Infrared Emission From Flames," The Ohio State University, Columbus, Ohio, Final Rept., Contract AF 30(602)-1047; January, 1956.

[12] S. S. Penner, "Infrared Emissivity of Diatomic Gases," NBS Circular No. 523 on "Energy Transfer in Hot Gases," U. S. Gov. Printing Office, Washington, D. C.; 1954.

[13] G. N. Plass, "Spectral emissivity of carbon dioxide from 1800–2500 cm^{-1}," *J. Opt. Soc. Am.*, vol. 49; August, 1959. Similar calculations have been reported in the classified literature by R. O'B Carpenter.

[14] V. R. Stull and G. N. Plass, "Spectral emissivity of hydrogen chloride from 1000–3400 cm^{-1}," *J. Opt. Soc. Am.*: 1959. (In press.)

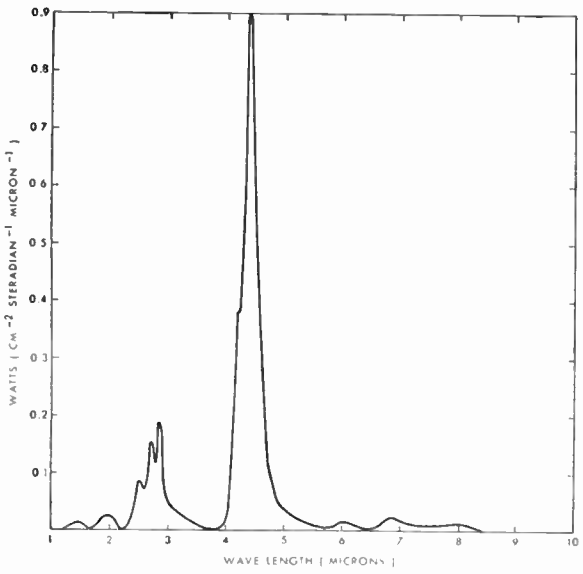

Fig. 5—Spectral radiance of a white gasoline-air flame as measured by Bell, Dam, Dickey, Kopczynski, Palik, and Rowntree.[11] This is typical of the emission of many flames.

culated for a range of temperatures from 300 to 2400°K. From these results the emission may readily be obtained for any amount of emitting gas at any pressure that may occur in practice. As an example, the emissivity of CO_2 at 1800 and 2400°K is given in Fig. 6 and Fig. 7. The curves show the emissivity for various values of p^2X, where p is the pressure in atmospheres and X is the thickness in centimeters of CO_2 at one atmosphere pressure. For a given amount of emitting gas, the emissivity decreases with increasing temperature near the center of the band, while it increases at longer wavelengths far from the band center. Thus, the emission appears to shift to longer wavelengths as the temperature increases. The sharp drop in the emissivity near 2400 cm^{-1} is due to the formation of a band head.

Conclusion

Emission of radiation from gaseous substances occurs through bands of spectral lines. The dependence of this emission on the amount of radiating material is, in general, quite different from the case of a solid or liquid substance where the absorption coefficient is usually a slowly-varying function of frequency. The general features of band emission have been discussed. The application of these results to the determination of the emissivity of flames has been considered.

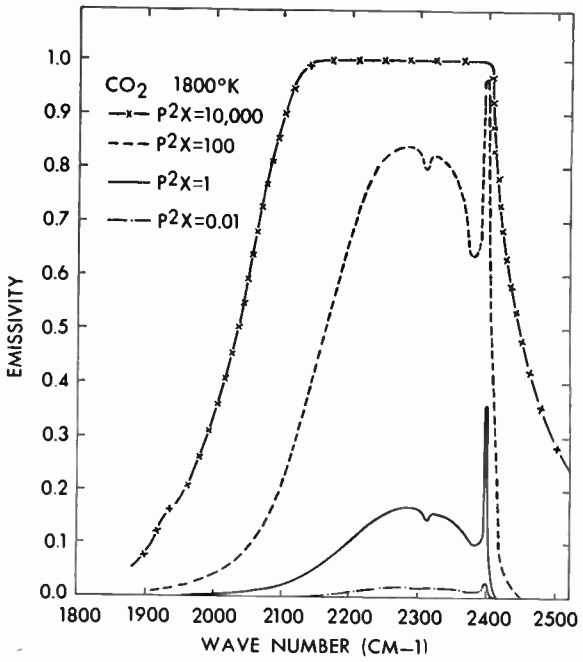

Fig. 6—Emissivity of carbon dioxide as a function of wave number at 1800°K for various values of p^2X, where p is the pressure in atmospheres and X is the thickness in centimeters of CO_2 at one atmosphere pressure.

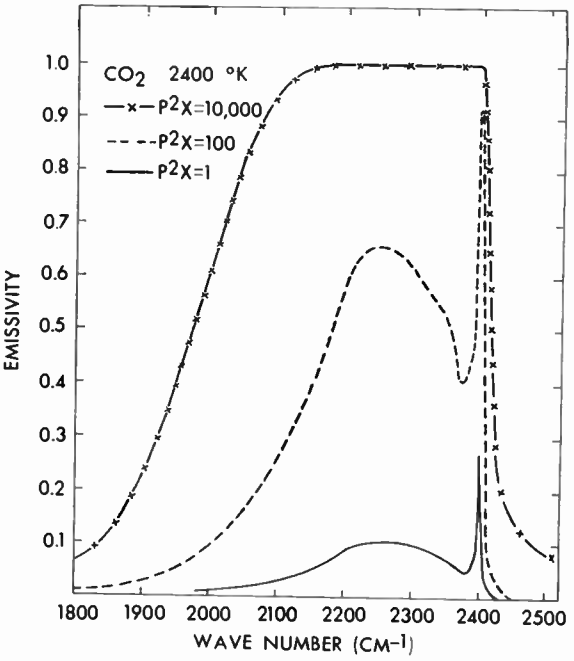

Fig. 7—Emissivity of carbon dioxide as a function of wave number at 2400°K for various values of p^2X, where p is the pressure in atmospheres and X is the thickness in centimeters of CO_2 at one atmosphere pressure.

Paper 3.2.1

The Infrared Radiation Flux in the Atmosphere*

GILBERT N. PLASS†

I. Introduction

THE background of natural infrared radiation emitted by the ground and atmosphere is determined by the absorption bands of the atmospheric molecules and by the emission characteristics of emitting surfaces such as the ground, ocean, and clouds. The same absorption bands, discussed in the article by Howard,[1] determine the radiative flux in the atmosphere and its variation with altitude. In the frequency region near the center of a strong absorption band, the infrared flux is nearly equal to the blackbody intensity appropriate to the local atmospheric temperature. This relation is valid from the ground up to a considerable altitude where, finally, the few remaining atmospheric molecules are no longer able to interact appreciably with the radiation. On the other hand, in a frequency region of weak absorption, the flux is determined largely by the emission of the ground, ocean, or clouds, rather than by the atmospheric molecules. Our present knowledge of the atmospheric infrared flux is reviewed in the following sections. The relevant atmospheric parameters which determine this flux and the heat budget of the earth are also discussed.

II. Atmospheric Properties

In order to determine the atmospheric infrared flux, the temperature, pressure, and composition of the atmosphere must be known as a function of height. In addition, the relevant parameters which determine the absorption by a given infrared band and its variation with path length, pressure, and temperature must be available in a form which can be used for the variable conditions along a path in the atmosphere.

The three most abundant gases in the earth's atmosphere, nitrogen, oxygen, and argon, have no absorption bands in the infrared. The atmospheric gases that have important infrared absorption bands are H_2O, CO_2, and O_3. The amount of water vapor in the atmosphere is highly variable and may range from 1 per cent to 0.001 per cent by volume. The average relative humidity over an entire latitude zone is usually between 70 and 80 per cent. The relative humidity is a minimum at altitudes of 5 to 10 km where it usually has a value from 30 to 55 per cent. It rises again at higher altitudes to a value of 50 to 90 per cent at the tropopause. However, the amount of water vapor that can be held in a given volume of air decreases very rapidly with temperature. Thus, because of the decrease of temperature with height, most of the water vapor is near the surface of the earth and only very small amounts can be present in the stratosphere. In the troposphere, the average water vapor concentration relative to the major atmospheric constituents varies approximately with altitude as the cube of the pressure.

Carbon dioxide is more uniformly distributed throughout the atmosphere. The average amount present in the atmosphere today is 0.033 per cent. The amount present in a given air mass depends somewhat on its past history. Such factors as whether the air mass has recently been over the ocean or a land mass, or whether it has been over a large forest or over a city, can change the carbon dioxide amount by as much as 50 per cent. However, these fluctuations should be a maximum near the ground and should be much smaller at higher altitudes. There is now rather convincing evidence that the average amount of CO_2 in the atmosphere has increased by 10 per cent in the past fifty years, due to the burning of fossil fuels.

The ozone concentration is also highly variable. The amount of ozone in the air increases with altitude to a maximum of about 0.001 per cent at around 30 km and decreases rapidly at greater heights. Minor constituents of the atmosphere that can absorb over long path lengths are CO (2×10^{-5} per cent), CH_4 (1.6×10^{-4} per cent), and N_2O (3.5×10^{-5} per cent).

The temperature of the atmosphere influences infrared radiation in three different ways: 1) the blackbody intensity changes with temperature; 2) the population of the energy levels of the atoms changes with temperature so that the absorption at a particular frequency may be a rapidly-varying function of temperature; 3) the half-width of the spectral lines varies with temperature. The atmospheric temperature decreases to a minimum of about 210°K in the lower stratosphere, rises to a maximum between 270 and 330°K at 50 km, falls to another minimum of about 190°K at 75 km, and then increases to very large values as the altitude further increases. A recent survey has been given by Goody.[2]

At standard temperature and pressure the half-width of the spectral lines that are of interest generally is in the range from 0.1 to 0.2 cm^{-1}. This Lorentz half-width decreases linearly with the pressure, and this variation must be taken into account in atmospheric work. As the pressure decreases, the Doppler half-width, due to the thermal motion of the molecules, becomes equal to the Lorentz half-width at some height. This usually occurs at altitudes from 20 to 35 km.

* Original manuscript received by the IRE, June 26, 1959.
† Aeronutronic Systems, Inc., Glendale, Calif.
[1] J. N. Howard, "The transmission of the atmosphere in the infrared," paper 3.2.2, this issue, p. 1451.

[2] R. M. Goody, "The Physics of the Stratosphere," Cambridge University Press, Cambridge, Eng.; 1954.

III. Atmospheric Emission

Since a strong absorber of radiation is also a good emitter, the H_2O, CO_2, and O_3 molecules in the atmosphere emit strongly in the frequency regions where they have infrared absorption bands. However, the background radiation in the atmosphere arises not only from the emission of these atmospheric molecules, but also from other sources, such as the ground and clouds. Fortunately, at least to a first approximation, most types of ground cover and sufficiently thick clouds radiate as a blackbody in the infrared. Thus the initial flux of radiation entering the atmosphere from such surfaces is known.

This radiation, however, is greatly modified in many frequency bands as it passes through the atmosphere. This can be calculated from the differential equation which describes the change in the flux as it passes through an atmospheric layer of thickness, dz:

$$dI^{\uparrow} = -kI^{\uparrow} \sec\theta \rho_r dz + kI_b \sec\theta \rho_r dz, \qquad (1)$$

where $I^{\uparrow}$ is the upward component of the radiative flux which makes an angle θ with the verticle, k is the absorption coefficient, I_b is the blackbody radiation flux determined from the Planck radiation law, ρ_r is the density of the radiating gas, and z is the height above the surface of the earth. The first term on the right of (1) represents the energy absorbed from the incoming beam by the absorbing gas in the infinitesimal layer; the second term represents the energy that is emitted by this same layer of gas and thus is added to the original beam.

In order to solve (1), it is convenient to introduce two quantities: 1) the mass of radiating gas per unit area from the top of the atmosphere down to the height z,

$$u = \int_z^{\infty} \rho_r dz; \qquad (2)$$

and 2), the transmission function between the two heights, z_0 and z_1, where u takes on the values u_0 and u_1, and makes an angle along the slant path with the verticle,

$$\tau(u_0, u_1) = \exp\left[-\sec\theta \int_{u_0}^{u_1} k du\right], \qquad u_0 < u_1. \qquad (3)$$

It can be verified by direct substitution that the general solution of (1) is

$$I^{\uparrow}(u) = I^{\uparrow}(u_1)\tau(u, u_1) + \sec\theta \int_u^{u_1} k(v) I_b(v) \tau(u, v) dv, \qquad (4)$$

where u_1 is the value of u at the lower boundary (usually the surface of the earth or the upper surface of a cloud). The physical meaning of (4) is that the total upward flux at a given height, u, is equal to the sum of two terms: 1) the upward flux that enters the atmosphere at the lower boundary, u_1, multiplied by the transmission between u and u_1; and 2) the blackbody flux emitted by each layer of the atmosphere between u and u_1, multiplied by the transmission along the path between u and the emitting layer.

In a similar manner, it is found that the downward flux is given by

$$I^{\downarrow}(u) = I^{\downarrow}(u_0)\tau(u_0, u) + \sec\theta \int_{u_0}^{u} k(v) I_b(v) \tau(v, u) dv, \qquad (5)$$

where u_0 is the value of u at the upper boundary.

As an example, let us consider a particularly simple solution of (4) and (5). If the atmospheric temperature is a constant independent of height, and if the ground has this same temperature, then

$$I^{\uparrow}(u) = I_b$$
$$I^{\downarrow}(u) = I_b[1 - \tau(0, u)]. \qquad (6)$$

Thus, the upward flux has the same value at all heights. The downward flux is zero at the top of the atmosphere (it is assumed that there is no incident flux from outside the atmosphere) and increases as the height decreases. If the transmission becomes nearly zero between the top of the atmosphere and some altitude, then the downward flux has nearly the limiting blackbody intensity below this altitude.

This simple example illustrates qualitatively how the downward flux in the atmosphere arises from molecular emission. In the actual atmosphere, the upward and downward fluxes are also modified by the atmosphere because the temperature varies with height. Molecular absorption and emission act to bring the radiative flux more closely into agreement with the blackbody intensity appropriate to the temperature at a particular altitude.

Because of the many spectral lines that comprise a molecular absorption band, the absorption coefficient, k, is a rapidly varying function of frequency. Eqs. (1) through (6) are valid only at a particular frequency. For a band of frequencies, it is usually difficult to decide on the appropriate average values to be used in these equations. Some of the complications are: 1) the half-width of a pressure-broadened line varies linearly with the pressure and approximately inversely as the square root of the absolute temperature; 2) the intensity of an individual spectral line is usually a rapidly-varying function of temperature; 3) the absorption from a pressure-broadened line increases linearly as the amount of absorber for small values of the absorption, and then increases as the square root of the amount of absorber as the absorption increases; 4) for larger absorption, the spectral lines overlap, causing the absorption to depend on the particular arrangement of the lines in the band; 5) in the stratosphere above a certain height, the Doppler line shape must be taken into account. A number of papers have been written on this subject which cannot be discussed further in this brief review.

A recent summary of some of this work has been published.[3]

Although an order of magnitude estimate of the radiative flux can often be made quite easily, an accurate calculation which takes into account all of the above factors requires an elaborate calculation using an electronic computer. The only such calculations that have been published are for the 15-μ band of CO_2[4] and the 9.6-μ band of O_3.[5] The results for the upward and downward radiation flux in the atmosphere for the 12- to 18-μ region are shown in Fig. 1. The solid curves refer to the present average CO_2 concentration. The other two curves give the flux if this concentration were to be doubled or halved.

Since the absorption is nearly symmetrical around the center of the band at 15μ, the results for similar wavelength intervals (for example, 12–13 and 17–18μ) have been combined.

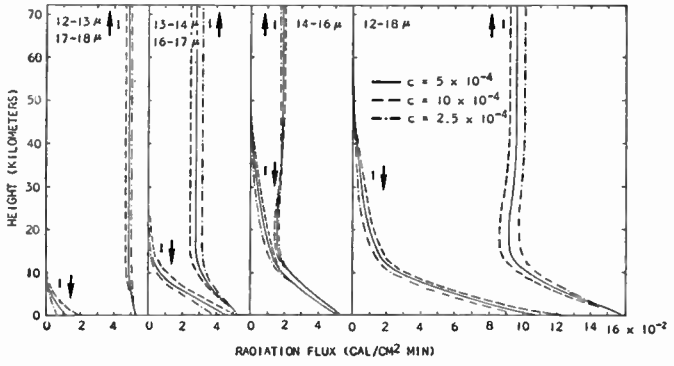

Fig. 1—The upward and downward radiation flux in the atmosphere as a function of height for the combined frequency intervals from 12–13 and 17–18 μ; from 13–14 and 16–17 μ; from 14–16 μ; and for the entire interval from 12–18 μ. The results are given for the following CO_2 concentrations: $c=5\times10^{-4}$(0.033 per cent by volume); $c=10\times10^{-4}$(0.066 per cent by volume); $c=2.5\times10^{-4}$ (0.0165 per cent by volume).

The typical behavior of the flux in regions of weak, intermediate and strong absorption is illustrated by the results shown in Fig. 1. If the absorption is strong, the upward flux nearly follows the blackbody curve appropriate to the atmospheric temperature at each height. The curves for the 14–16-μ interval do this up to 22 km and clearly show the temperature minimum in the atmosphere. The flux further increases a small amount at higher altitudes because of a weak interaction with the warm atmosphere at these heights. When the absorption is weak, (12–13 and 17–18μ), the upward flux is nearly constant, since the atmosphere has only a small interaction with the radiation stream. Similar considerations show that the downward flux is small when the absorption is weak. It has an appreciable value only at altitudes of less than 10 km for the 12–13- and 17–18-μ intervals. However, in the interval 14–16μ, the downward flux is appreciable at much greater altitudes and approaches the backbody curve below 13 km.

Experimental measurements of the infrared emission of the atmosphere as observed on the ground have shown[6] that for a clear sky, the downward radiation flux is strong near the 6.3-μ band of H_2O and the 4.3-μ and 15-μ bands of CO_2. In addition, a weak emission is observable near the 9.6-μ band of O_3. The emission varies greatly with the humidity. On an overcast day, the downward flux is nearly equal to the blackbody radiation appropriate to the temperature of the lower surface of the cloud.

IV. Heat Budget of the Earth

The heat budget of the earth's atmosphere is determined by the absorption, reflection, and reradiation of the solar and terrestrial radiation, and by the transport of latent and sensible heat from the surface of the earth. The interaction of the infrared flux with the atmosphere has been discussed in Section III above.

The absorption of solar radiation by the atmosphere has been studied extensively. Howard[1] reviews this work and gives the solar spectrum as observed at ground level. It is interesting to compare the heating caused by solar energy absorption at high altitudes with the cooling from infrared radiation. The result is usually expressed as the temperature change in degrees Kelvin per day caused by the process in question. Theoretical calculations[7,8] of the ultraviolet ozone absorption of solar radiation show that it is the main radiative heat source of the atmosphere from 30 to 70 km. The heating rates vary with latitude and season, but are usually in the range of 1–10°K/day. The maximum heating is usually at about 45 km. Below 30 km, the near infrared bands of water vapor absorb solar radiation. The heating rates vary with the amount of water vapor, but may be as large as 4°K/day in the lower stratosphere.

The stratosphere is cooled by the infrared bands of CO_2 and O_3. The 15-μ CO_2 band has a maximum cooling rate of 5°K/day at 45 km for typical conditions.[4] Similarly, the 9.6-μ O_3 band has a maximum cooling rate of about 2°K/day at 45 km.[5] It is interesting that the sum of these cooling rates nearly balances the heating rates from solar radiation. This indicates that the stratosphere is, at least approximately, in radiative equilibrium.

The most extensive recent study of the heat balance of the entire earth has been made by London.[9] He has calculated the various terms in the heat budget for each of the four seasons and for 10° latitude belts in the Northern Hemisphere. For the entire year and the Northern Hemisphere, the main items in the heat budget

[3] G. N. Plass, *Am. J. Phys.*, vol. 24, pp. 303; 1956.
[4] G. N. Plass, *Quart. J. Roy. Meteor. Soc.*, vol. 82, p. 310; 1956.
[5] G. N. Plass, *Quart. J. Roy. Meteor. Soc.*, vol. 82, p. 30; 1956.
[6] R. Sloan, J. H. Shaw, and D. Williams, *J. Opt. Soc. Am.*, vol. 45, p. 455; 1955.
[7] F. S. Johnson, *Bull. Am. Meteor. Soc.*, vol. 34, p. 106; 1953.
[8] J. Pressman, *J. Meteor.*, vol. 12, p. 87; 1955.
[9] J. London, "A Study of the Atmospheric Heat Balance," New York University, New York, N. Y., Final Rept. Contract No. AF 19(122)-165; 1957.

are given below expressed as a per cent of the average incoming solar energy received outside of the earth's atmosphere.

The albedo of the earth is estimated at 35 per cent. The solar energy is reflected from clouds (24 per cent), from the molecules and dust particles in the atmosphere (7 per cent), and directly from the ground (4 per cent). In addition, an observer outside the earth's atmosphere receives infrared radiation emitted directly by the ground (5.5 per cent), emitted by the molecules in the troposphere (56.5 per cent), and emitted in the stratosphere (3 per cent). The total of the above figures is 100 per cent, which equals the incoming solar radiation. Approximately 3 per cent of the average incoming solar radiation is absorbed in the stratosphere and this energy is re-emitted in the infrared.

The energy balance in the troposphere is more complicated. Energy is gained from direct absorption of the solar radiation (13 per cent), absorption by clouds (1.5 per cent), absorption of terrestrial infrared radiation (109 per cent), release of the latent heat of water vapor (18.5 per cent), and the transport of sensible heat from the ground to the atmosphere (11 per cent). This is balanced by the energy loss from infrared radiation to space (56.5 per cent) and to the ground (96.5 per cent).

The ground and ocean surfaces gain energy by the direct absorption of solar radiation (22.5 per cent), absorption of solar radiation transmitted through clouds (14.5 per cent), absorption of solar radiation scattered by the molecules and dust particles in the atmosphere (10.5 per cent), and absorption of infrared radiation emitted by the atmosphere (96.5 per cent). This is balanced by the emission of infrared radiation (114.5 per cent), loss of latent heat by evaporation of water (18.5 per cent), and of sensible heat (11 per cent).

Variations in the average amount of absorbing atmospheric gases can change the heat balance sufficiently to cause important climatic changes. For example, an increase in the amount of carbon dioxide in the atmosphere prevents the infrared radiation from escaping to space and thus raises the surface temperature. Many complex factors influence the climate; all past climatic changes certainly cannot be explained by variations of a single factor. Yet it is interesting that the carbon dioxide theory[10] can explain in simple terms many of the known facts about past climates: during a single glacial epoch, the continual oscillations of the climate between a glacial and an interglacial stage with a period of tens of thousands of years; the increased precipitation at the beginning of a glacial period; the time lag between a period of mountain building and the onset of glaciation; the simultaneous occurrence of glacial periods in both hemispheres; the general warming of the climate during the last fifty years.

[10] G. N. Plass, *Tellus*, vol. 8, p. 140; 1956

Paper 3.2.2

The Transmission of the Atmosphere in the Infrared*

J. N. HOWARD†

Introduction

THIS article is intended as a short review of our present knowledge about atmospheric transmission of infrared radiation. Several excellent detailed studies devoted to this same topic already exist, so that we should first review the reviews. There are several different types of researchers who are all interested in atmospheric transmission. Much of the original work was done by astronomers, whose principal interest was in seeing through the atmosphere to measure the spectrum of the sun. This spectrum was called a "solar spectrum" and the published spectrum called a "solar map," or a "solar atlas," a rather unfortunate nomenclature, as most of the structure observed in the infrared is due to absorption of the solar radiation by the molecules of the atmosphere. Goldberg has written an excellent review on the absorption spectrum of the earth's atmosphere from this point of view [1].

Meteorologists and geophysicists are mostly interested in the physics of the atmosphere itself for understanding such problems as the temperature profile of the atmosphere, or the heat balance (heat budget) of the earth. Articles on various phases of meteorological infrared problems can be found in the "Compendium of Meteorology" [2], or in the book by Goody [3]. For the geophysicist there are several review articles in the book by Beer [4] and excellent articles by Moller and by

* Original manuscript received by the IRE, June 26, 1959.
† U. S. Air Force Cambridge Res. Center, Bedford, Mass.

Paetzold in one volume of the new "Handbook of Physics" [5]. The pure physicist working in the fields of infrared optics or molecular spectroscopy has also made major contributions to our knowledge of the mechanism of infrared atmospheric transmission. For example, if one measures the transmission of the atmosphere when the sun is directly overhead, one would have to have an absorption path of eight kilometers at one atmosphere pressure (ground level) in order to have the same number of molecules in the path. (This number of molecules is called one "air mass.")

When the sun is near the horizon, the absorption path can be of the order of ten air masses. Under these conditions, very weak absorption bands can be detected and measured. These weak bands may be due to very minor constituents of the atmosphere, or to isotopic variants of the common constituents, or may originate from energy transitions that are less populated or of less probability. Measurements on such weak bands can be very useful in testing and extending the basic theoretical treatment of molecular spectroscopy. A very fine review of infrared spectroscopy from this point of view was recently written by Lecomte [6]. Finally, since World War II, infrared has found a large number of military applications, in detection of targets, guidance, reconnaissance, surveillance, and so on. Almost all of these applications have an intervening atmosphere between the infrared source and the infrared detector. An excellent review of atmospheric transmission from this point of view is the chapter by Sanderson in the book by Locke [7].

So much for our review of reviews. It ought to be observed at this point that the authors of these various reviews may consider themselves astronomers, astrophysicists, meteorologists, geophysicists, molecular spectroscopists, or even physical chemists, but called by whatever name, they are all capable practitioners of infrared physics. The military applications of infrared have brought into the field a vast influx of military men, engineers, businessmen, salesmen, and politicians who have acquired the jargon of infrared without always understanding the physics of it, resulting in a considerable amount of practicing medicine without a license. In the remaining part of this article, we will endeavor to point out a few of the pitfalls and peculiarities of the study of infrared transmission.

Fig. 1 presents a so-called solar spectrum for the region 1 to 15 microns [8]. The other curves of Fig. 1 show the positions and approximate relative intensities of absorption bands of the molecules known to occur in the atmosphere. It is a fortunate circumstance of nature that the molecules N_2 and O_2, being homonuclear diatomic molecules, have neither a permanent nor an oscillating electric dipole moment, so that they have no infrared rotation-vibration bands. They do exhibit some very weak electronic bands [1] which we need not consider here. Collisions of these "transparent" molecules with the molecules that do have absorption bands in the infrared can have a considerable influence on the intensities of the observed absorption bands. This is due to a phenomenon called pressure or collision-broadening (also Lorentz broadening), which will be discussed. In the lower atmosphere, the principal absorbers are H_2O and CO_2. Ozone is not distributed uniformly through the atmosphere, but is mostly concentrated between 10 and 40 km above the earth's surface, with a fairly sharp peak in the distribution at about 20–30 km. The other minor constituents, CH_4, N_2O and CO, appear to be, like CO_2, uniformly distributed through the atmosphere. Water vapor is highly variable in its concentration in the atmosphere because the humidity of air fluctuates widely and most of the water vapor concentration is near ground level. For example, the H_2O absorption bands near 1.38, 1.87, and 2.7 microns, which are very strong at ground level, can scarcely be detected in measurements of the solar spectrum taken at 50,000 feet [9].

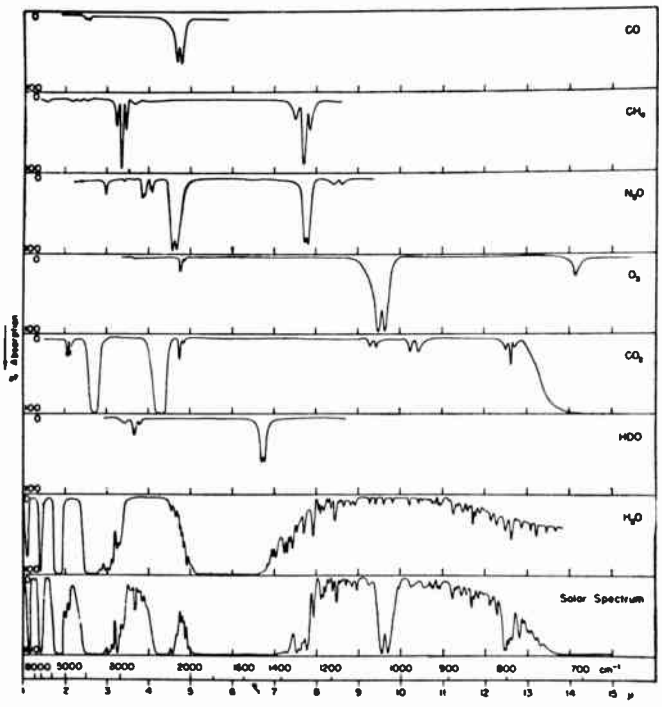

Fig. 1—The near-infrared solar spectrum (bottom curve). Other curves are laboratory spectra of the molecules indicated.

Low Resolution Studies

It is customary, for most problems of atmospheric transmission in the lower atmosphere, to neglect the absorption bands of the minor constituents and of ozone, and to consider the regions of absorption as being due entirely to H_2O and CO_2. Accordingly, in 1948, a laboratory study was begun at The Ohio State University on the absorption bands of H_2O at 1.38, 1.87, 2.7, 3.2 and 6.2 microns and those of CO_2 at 2.7 and 4.3 microns, in order to determine the total absorption of each band as

a function of absorber concentration, path length, and total pressure. The results of this study have been published [10], [11]. However, absorption path lengths of only about 60 meters could be achieved, limiting the range of concentrations that could be studied to less than approximately 50 atm·cm, of CO_2 and less than 0.2 cm of precipitable water.

It is customary to express the water vapor concentration in cm of precipitable water; that is, if the absorption path is replaced by a tube of length equal to the path length and of uniform cross section, and then all the water contained in the tube is condensed as a liquid at one end of the tube, the depth of this liquid in cm is a measure of the amount of water in the absorption path. For long absorption paths at ground level in the open air, this quantity is readily calculable if the temperature and humidity are known. The carbon dioxide concentration is expressed in atm·cm; that is, the centimeters of path length of the carbon dioxide in the path if it were present alone at one atmosphere pressure.

At about the same time as the Ohio State Studies, a group at the British Admiralty Establishment at Teddington was working on infrared atmospheric transmission of long path lengths in the open air. In the published description of this work [12], a spectrum is presented of a 2000-yard open-air path containing 1.7 cm of precipitable water. Yates [13] has prepared from the Ohio State absorption data and from the Admiralty scattering data a set of tables and curves from which one can obtain the total transmission of the atmosphere at ground level for radiation from sources at temperatures from 373°K to 6000°K, for path lengths up to 20,000 yards, and for various conditions of atmospheric haze.

In 1953, Elder and Strong [14] reviewed all the available laboratory and long-path open-air infrared transmission data for the 0.7- to 15-micron region. In addition to the Ohio State and British Admiralty data, they included early data by Fowle and wartime data by John Strong and Heinz Fischer. Elder and Strong divided the spectrum into eight "windows"; that is, the spectral regions located between the principal absorption bands. They found that, to a good approximation, the window transmission data could be fitted to equations of the form

$$T' = -k \log w + T_0 \qquad (1)$$

where T' is the average transmission of a window, w is the water vapor concentration of the absorption path, and k and T_0 are empirical constants for each window. These values are presented in Table I.

Although very useful for many calculations, the Elder and Strong summary of earlier data served equally well to point out areas in need of additional research. High-resolution data were needed to determine the effects of minor constituents; no data existed for paths longer than three miles, and data were needed for horizontal paths at high altitudes, as well as for vertical or slant paths through the atmosphere.

TABLE I
WINDOW REGIONS IN THE INFRARED*

Window Wavelength Interval (microns)	K	T_0
0.72–0.92	15.1	106.3
0.92–1.1	16.5	106.3
1.1–1.4	17.1	96.3
1.4–1.9	13.1	81.0
1.9–2.7	13.1	72.5
2.7–4.3	12.5	72.3
4.3–5.9	21.2	51.2
5.9–14	†	†

* Elder and Strong [14].
† Lauger [32].

SOLAR MAPS

In 1950, the group at the University of Michigan published [15] a high-resolution atlas of the solar spectrum from 0.8 to 2.6 microns. A volume of identifications of the structure of this atlas was published in 1955 [16]. In 1951, the Ohio State group published [17] an atlas of the region 3.0 to 5.2 microns, and later an atlas of the region 7 to 13 microns [18]. The data presented in The Ohio State Atlas were measured at Columbus, Ohio, at about 800 feet above sea level. Over 1600 absorption lines were resolved in the region from 3 to 13 microns, and more than 70 per cent were identified as belonging to bands of gases occurring in the earth's atmosphere.

The solar spectrum from 2.8 to 23.7 microns has been mapped by Migeotte, Neven, and Swensson of the University of Liege [19]. These measurements will be discussed further. A second volume by the same group [20] consists of a table of identifications of the more than 3600 absorption lines observed in this region. Also included in this second volume are comments by W. S. Benedict on the spectra of H_2O and CO_2. Recently, measurements were made of the solar spectrum under lower resolution than that of Migeotte, but at the 17,000-foot altitude of Mt. Chacaltaya, Bolivia, by the group at the Naval Ordnance Laboratory, White Oak, Md., [21].

LONG PATH OPEN-AIR STUDIES

Several groups have made useful studies on the transmission of infrared through long paths in the open air. In France, a group working under Arnulf [22] is studying infrared transmission over land areas under conditions of incipient fog. Studies are being made at the Chicago Midway Laboratories over long air paths under various haze conditions [23]. At the Naval Research Laboratory, Taylor and Yates [24] have made a very valuable study of the near-infrared atmospheric transmission over paths as long as 10.1 miles across Chesapeake Bay.

TOTAL ABSORPTION

Another approach to atmospheric transmission studies, which differs in several ways from the measurement

of solar spectra or open-air studies, is the measurement of the individual atmospheric gases under controlled conditions in the laboratory. The chief difficulty is that very long absorption path lengths are required in order to simulate atmospheric conditions. The usual solution to this problem is to use a multiple-traversal cell, in which the radiation is reflected back and forth many times inside the absorption cell in order to achieve a long total path length. Such a cell is described in the literature [25]. Cells of this sort generally have only a small aperture, however, and some radiation is also lost at each reflection, so that it is necessary to use a fast spectrometer and to open wide the spectrometer slits in order to increase the radiation received. This smooths out the finer details of the spectrum and decreases the resolution. The "true" spectrum has been modified by the slit function of the spectrometer. Such smoothed spectra can still be useful for coarse measurements. Alternatively, one can determine the "total absorption" of the infrared band being studied. This quantity is the area under the curve of fractional absorption against wavenumber. This quantity is measured because, under a wide variety of conditions, it is independent of the width of the slit of the spectrometer or of other characteristics of the instrumentation, and depends only on the amount of absorber present, its partial pressure, the total pressure, and other parameters of the sample. The multiple-traversal cell at The Ohio State University is capable of total paths in excess of 2000 meters, and the cell at The Johns Hopkins University, although only about 200 meters in path, is capable of much higher resolution [26]. The chief advantage of such a multiple-traversal study is that altitude conditions can be simulated.

Fig. 2 shows the near-infrared spectrum of CO_2 and

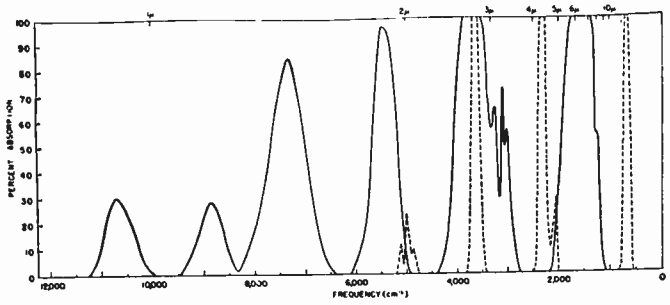

Fig. 2—The near-infrared spectrum of CO_2 and H_2O. Broken curve represents the absorption of 46 atm-cm of CO_2; solid curve represents the absorption by 0.7 pr. cm of H_2O.

H_2O. This is a composite low-resolution spectrum as obtained with a multiple-traversal cell. Let us forget pressure variation for the moment and assume that the H_2O and CO_2 absorption bands are all broadened to a total pressure of one atmosphere with dry, CO_2-free air (or nitrogen, which has practically the same effect). If we increase the amount of the absorber, say by increasing the path, then we increase the absorption at each and every wavelength (except, of course, where the absorption is already 100 per cent). We also increase the "total absorption" of each band, which is the area under the band. (The band "grows" or follows a "curve of growth.") Alternatively, to use the language of Elder and Strong [14], we decrease the transmission of the "window" between the bands. Table I lists the empirically determined coefficients k and T_0 for (1), for window transmission as determined by Elder and Strong (the H_2O content is here expressed as precipitable millimeters of H_2O). Melnick [27] has written an interesting report giving a physical interpretation to the empirically-postulated type of equation of Elder and Strong. Burch and Howard [28] treated their total absorption data somewhat differently. First of all, they measured the total absorption of each band, rather than the window transmission between bands. This avoids the troublesome treatment of a window bounded on one side by a band of H_2O and on the other by a band of CO_2, when both bands are growing at different rates. They also collected a large body of data, and found that the curve of growth of each absorption band did not follow the Elder and Strong logarithmic form for all concentrations, but that the curve of growth could be separated into two regions; one for very small concentrations, where the band is weak, and in which the total absorption increased proportionally to the square root of the amount of absorbing gas, and a "strong band" region, in which the total absorption increased proportionally to the logarithm of the amount of absorber. The chief contribution of their study, however, was that they were able also to vary the total pressure of the sample, and to determine that for a fixed absorber concentration, the total absorption increased approximately proportionally to the square root of the total pressure in the "weak band" region, and to the logarithm of the total pressure in the "strong band" region. When both concentration and pressure are varied, one has the following relationships for the total absorption of each band:

$$\text{(weak band)} \quad \int_{\nu_1}^{\nu_2} A_\nu d\nu = cw^{1/2}P^k \tag{2}$$

$$\text{(strong band)} \quad \int_{\nu_1}^{\nu_2} A_\nu d\nu = C + D\log w + K\log P. \tag{3}$$

Here ν_1 and ν_2 are the limits of each absorption band, that is, frequencies outside of which the absorption by a given band can be considered negligible, c, C, D, k, and K, are empirically determined constants for each band, w is the concentration of the absorber, and P the total pressure. In addition, one must more or less arbitrarily determine values of total absorption for each band below which one uses the weak form of the curve of growth. For many low-resolution problems, particularly radiometric studies, knowledge of the total absorption of the atmospheric H_2O and CO_2 bands is all that is required. For those interested in this, the values of these constants are given in [25], [28], and also in [29] for all

of the near-infrared bands of H_2O and CO_2. A wide variety of the spectral curves used in obtaining the total absorption, in a form similar to Fig. 2 has been presented [25]. Larmore and Passman have constructed from minute measurements on the contours of the curves in [25] a set of very useful tables for the spectral transmission at sea level in 0.1-micron intervals from 0.3 to 7.0 microns for H_2O concentrations between 0.01 cm and 100 cm of precipitable H_2O and for dry air paths (containing 0.03 per cent CO_2) between 0.1 and 1000 km. In addition, they include a table of correction factors for altitudes of 1000 to 100,000 feet. This set of tables has been published [30] and is also reproduced in the "Handbook of Geophysics" [29]. Plass is presently extending this set of tables to longer wavelengths [31].

Langer [32] has recently published two reports that should be very useful for ground-level transmission calculations, particularly for radiometry and low-resolution (broad-band) applications. Langer measured the laboratory absorption curves of [25] in order to determine the window transmission between bands, but with a much more detailed and elaborate treatment than that of Elder and Strong. He also presents a compact chart showing, for blackbody sources of temperature 250, 293, 500, 1000, 2000, 3000, 4000, 6000, and 8000°K, the absolute value of the energy transmitted through the eight major infrared atmospheric windows (the wavelength intervals of Table I) for paths of up to 100 cm of precipitable H_2O.

Pressure Broadening

The multiple-traversal cell described in the preceding section has been used to study the effects of pressure on infrared absorption bands of atmospheric molecules. One can put a gaseous sample into such a cell with a known absorption path length, measure the absorption as a function of wavelength (or frequency) and then, without changing the path length or the sample pressure, add an optically transparent gas such as nitrogen or oxygen to increase the total pressure. If the spectrum is again measured, it is found that there is more absorption than before, even though the added gas has no absorption of its own in the spectral region studied. This phenomenon was experimentally observed by Angstrom in 1892 [33] and was explained theoretically by Lorentz in 1906 [34] as being caused by the collisions between the molecules of the absorbing molecule and those of the added gas. There are also other effects which cause broadening of spectral lines. Most of the common types of line broadening are described in detail and derived by Born [35]. It has been pointed out, particularly by Hettner [36], that the Lorentz collision broadening predominates over other causes of line broadening for infrared absorption by molecules of the air under conditions in the lower atmosphere. The quantum transitions giving rise to each individual absorption line are not strictly monoenergetic, and the resulting absorption line is therefore not monochromatic. Rather, one has an absorption coefficient for each pressure-broadened absorption line given by

$$k_\nu = \frac{S}{\pi} \frac{\alpha}{(\nu - \nu_0)^2 + \alpha^2} \tag{4}$$

where S is an intensity factor (the line "strength"), ν_0 is the frequency of the line center, and α is called the half-width at half-maximum k_ν, or simply the half-width of the line. α is a function of the total pressure (and, to a lesser extent, a function of the temperature) of the absorbing gas. This is usually called a Lorentzian line shape.

An actual spectrometer cannot see this "true" contour of a spectral line, however, and if an absorption band is being examined, one may be measuring simultaneously several different overlapped lines with the resultant spectral blend also modified by the spectral slit function of the apparatus. Under such circumstances, one cannot expect such simple formulations for absorption as the Beer-Lambert law to hold. It is therefore difficult to predict in terms of simple absorption coefficients the absorption to be expected for path lengths that are greatly extrapolated from laboratory data. Furthermore, since the half-width of each line is a function of total pressure, it becomes almost impossible to predict the absorption through a vertical or oblique path through the atmosphere, in which the total pressure is changing with altitude. The only practical way to treat situations of this sort is to postulate certain mathematical functions for the shape of each line (such as the Lorentz shape given above), make certain assumptions about line intensities and half-widths, and assume certain models which describe how groups of these lines are arranged into bands. This is decidedly beyond the scope of this article, and for detailed discussions concerning band models, one should consult the literature [37] or [38].

Minor Constituents

Prof. M. V. Migeotte of the University of Liege has recently published an atlas of the solar spectrum as measured under high resolution from the Jungfraujoch, Switzerland [19]. The observing station was at an altitude of about 12,000 feet, and the amount of H_2O in the air path was substantially lower than at ground level. This permitted the detection of weaker absorption bands of the minor constituents CO_2, CO, N_2O, and CH_4. All these constituents are uniformly distributed in the atmosphere, and, at higher altitudes, where the water content becomes vanishingly small, these absorption bands will become comparatively more important. As an example, for such military applications as the detection of an aircraft by its exhaust radiation, the CO_2 emission observed is mostly from excited transitions (the so-called "hot" bands) which occur generally just on the long wavelength side of the CO_2 atmospheric absorption bands. The N_2O molecule is similar in many ways to the CO_2 molecule (it has the same molecular

weight, and comparable force constants, for example) and it so happens that for almost every CO_2 absorption band, there is a band of N_2O lying just to the long wavelength side of the CO_2. Therefore, this minor constituent of the atmosphere, N_2O (forming about one-half part per million in the atmosphere), must be considered in problems concerned with CO_2 emission. A detailed description of the spectra of these minor constituents as measured by Migeotte and others has been given for the 3- to 5-micron spectral region [39] and also for the 8- to 13-micron spectral region [40].

High-Altitude and Slant Path Studies

Only very limited data presently exist for infrared transmission at altitude or for vertical or oblique absorption paths in the atmosphere. The Jungfraujoch data of Migeotte [19], taken at 12,000 feet, are the most detailed altitude data. A group from the Naval Ordnance Laboratory, White Oak, Md. [21], have taken solar spectra from a mountain in Bolivia at an altitude of 17,000 feet. Yates [41] has reported a study of the infrared transmission between two Hawaiian peaks, 20 miles apart, both of which are more than 10,000 feet high. In 1953, a group at the Radar Research Establishment at Malvern instrumented a Lincoln aircraft with an infrared spectrometer [42], [43] and took solar data in the spectral region 2–5 microns from altitudes of 30,000 feet. At ground level, the absorption between 2.5 and 3.5 microns is dominated by the ν_1 and ν_3 bands of H_2O at 2.7 microns, and the weaker $2\nu_2$ band of H_2O at 3.2 microns. At 30,000 feet, the H_2O absorption has nearly vanished (the absorption at 2.7 microns is probably due to CO_2), and the ν_3 fundamental band of CH_4 at 3.3 microns is clearly visible. In the 4.2–4.7 micron region, the P branch of the ν_3 fundamental of N_2O is already visible at 12,000 feet, and at 30,000 feet, both branches of the band can be seen. In 1954 Hampson [44] obtained data in the PbTe region up to 47,000 feet. At the Royal Aircraft Establishment at Farnborough, Houghton [45] has equipped a Canberra aircraft to obtain high-resolution spectra at altitudes higher than 50,000 feet. Some of these data have been published [46]. There are groups at the University of Denver and at The Johns Hopkins University performing balloon-borne spectral studies of solar spectra and earth albedo from altitudes of up to 100,000 feet [47]. Other groups (Suomi at Wisconsin, Stroud at Ft. Monmouth, the University of Colorado, and others) are designing filter radiometers and simple spectrometers for similar studies to be made from satellites.

The problem of transmission along vertical or slant paths in the atmosphere is particularly complex. Not only is the pressure varying along the path, but so is the temperature, and H_2O, which is one of the chief infrared absorbers, does not have a uniform distribution in the atmosphere (even apart from its variable day-to-day concentration). Except for some of the multiple-traversal cell studies there is almost no laboratory or field data applicable to reduced pressure conditions. There have been studies, however, which give procedures for predicting slant path transmission in the atmosphere. These usually postulate a mathematical model for the absorption band, assume that each individual line has an absorption coefficient of Lorentzian shape, and present the results in a series of charts. In general, one can observe that such procedures are only as valid as the validity of the mathematical model or line shape chosen. Altschuler [48] describes such a procedure for the spectral region 1 to 15 microns, assuming an Elsasser model [37] for the absorption bands. Subsequently, he revised his procedure [49] to the more recent King model of an absorption band [50]. Carpenter has written [51] a detailed treatment of this topic. His calculations are all based on the ARDC model Atmosphere 1956, and simple procedures for correcting to existing weather conditions are given. Only CO_2 and H_2O are treated in detail. The suggested procedure gives tables and graphs for the determination of an "equivalent optical path length" for comparison with laboratory measurements. He prefers the direct use of multiple-traversal cell data, rather than recourse to any theoretical formula for the variation of transmission with equivalent path.

It ought to be pointed out that there are certain crude approximations to slant path transmission which, however, may be completely adequate for many purposes. For example, if one desires to know the transmission in a certain spectral region through a long slant path from an altitude of 30,000 feet to an altitude of 100,000 feet, and meteorological data indicate that this long path contains, say, 1 cm of precipitable H_2O, one could determine for the desired spectral region from the Larmore and Passman tables the transmission of 1 cm of precipitable H_2O at a horizontal path at 30,000 feet altitude and also the comparable transmission for a horizontal path at 100,000 feet altitude. Then the slant path transmission could be assumed to be intermediate to these extreme values. Such a procedure, of course, assumes the validity of the Elsasser absorption model used by Larmore and Passman in computing their correction factors for altitude.

Attenuation Due to Scattering

In addition to the absorption of infrared radiation by atmospheric molecules, there is a further attenuation due to scattering of radiation out of the light path by the molecules of the air itself and also by particles in the atmosphere (aerosols) such as smoke, haze, and gog. The scattering by the molecules of the air itself is called Rayleigh scattering, and is responsible for such phenomena as the blue of the sky and the red of the sunset. Although this sort of scattering is very important in the ultraviolet and blue end of the visible, it falls off in intensity inversely as the fourth power of the wavelength and for all practical purposes can be ignored in the infrared beyond about 2 microns. When the diameter of

the aerosol particles of the atmosphere becomes comparable with the wavelength of the incident radiation, another type of scattering, called Mie scattering, takes place. The mathematical treatment of Mie scattering is very complex, and is discussed in several excellent articles by Middleton, Sekera, Bricard, and Ludlam in [5]. In principle, if the aerosol particles are of uniform composition and diameter and if they are uniformly distributed in a homogeneous atmosphere, one can compute an attenuation coefficient for Mie scattering. Actually, none of these conditions obtains even approximately, but one can still define an approximate attenuation coefficient for scattering, which one applies as a correction factor to the transmission. Sanderson [7] gives a discussion of such factors, as do Taylor and Yates [24], and Churchill [52].

References

[1] L. Goldberg, ch. 9, "The Earth as a Planet," ed. G. P. Kuiper, University of Chicago Press, Chicago, Ill.; 1954.
[2] T. F. Malone, "Compendium of Meteorology," American Meteorological Society, Boston, Mass.; 1951.
[3] R. M. Goody, "The Physics of the Stratosphere," Cambridge University Press, Cambridge, Eng.; 1954.
[4] A. Beer, "Vistas in Astronomy," Pergamon Press, London, Eng., vol. 2; 1956.
[5] S. Fluegge, "Handbuch der Physik," Springer Verlag, Berlin, Ger., vol. 48, pt. 2; 1957.
[6] S. Fluegge, "Handbuch der Physik," Springer Verlag, Berlin, Ger., vol. 26, pt. 2; 1958.
[7] A. S. Locke, "Guidance," D. Van Nostrand and Co., Inc., New York, N. Y.; 1955.
[8] J. H. Shaw, "The Ohio State University, Columbus, Ohio, Final Rept. Contract No. AF19(122)-65; 1954.
[9] D. Murcray, J. Brooks, F. Murcray, and C. S. Shaw, "High altitude infrared studies of the atmosphere," *J. Geophys. Res.;* June, 1958.
[10] J. N. Howard and R. M. Chapman, *J. Opt. Soc. Am.*, vol. 42, pp. 423 and 856; 1952.
[11] J. N. Howard, The Ohio State University, Columbus, Ohio, Rept. No. 1, Contract DA 44-099-eng-12; March, 1950.
[12] H. A. Gebbie, W. R. Harding, C. Hilsum, A. W. Pryce, and V. Roberts, "Atmospheric transmission in the 1 to 14 micron region," *Proc. Roy. Soc. (A) (London)*, vol. 206, p. 87; 1951.
[13] H. Yates, NRL Rept. 3858, Washington, D. C.; September, 1951.
[14] T. Elder and J. Strong, *J. Franklin Inst.*, vol. 255, p. 189; 1953.
[15] O. C. Mohler, A. K. Pierce, R. R. McMath, and L. Goldberg, "Atlas of the Solar Spectrum from 0.84 to 2.52 Microns," University of Michigan Press, Ann Arbor, Mich.; 1950.
[16] O. C. Mohler, "Table of Solar Spectrum Wavelengths, 1.20–2.55 Microns," University of Michigan Press, Ann Arbor, Mich.; 1955.
[17] J. H. Shaw, R. M. Chapman, J. N. Howard, and M. L. Oxholm, *Astrophys. J.*, vol. 113, p. 268; 1951.
[18] J. H. Shaw, M. L. Oxholm, and H. H. Claaseen, *Astrophys. J.*, vol. 116, p. 554; 1952.
[19] M. Migeotte, L. Neven, and J. Swenson, "The Solar Spectrum from 2.8 to 23.7 Microns," Univ. of Liege, Final Rept., Contract AF61(514) 432, Phase A, Part I; 1956.
[20] M. Migeotte, L. Neven, and J. Swensson, "The Solar Spectrum from 2.8 to 23.7 Microns," Univ. of Liege, Final Rept., Contract AF61(514)-432, Phase A, Part 2; 1957. (Including also an Introduction by S. W. Benedict.)
[21] W. W. Talbert, H. A. Templin, and R. E. Morrison, presented at East Coast IRIS, Washington, D. C.; February 3, 1958. See also *J. Opt. Soc. Am.*, vol. 47, p. 1056; 1957.
[22] A. Arnulf, "Transmission by haze and fog, 0.35 to 10 microns," presented at 4th Congress International Commission of Optics, Mass. Inst. Tech., Cambridge, Mass.; April 2, 1956. Also *J. Opt. Soc. Am.*, vol. 47, p. 491; 1957.
[23] L. Biberman (private communication). (To be presented in Scientific Rept., Contract AF19(604)-3909.
[24] J. H. Taylor and H. W. Yates, NRL Rept. 4759, Washington, D. C.; July 2, 1956. Also *J. Opt. Soc. Am.*, vol. 47, p. 223; 1957.
[25] J. N. Howard, D. E. Burch, and D. Williams, "Near-infrared transmission through synthetic atmospheres," Geophys. Res. Paper No. 40, AFCRC; November, 1955. Also *J. Opt. Soc. Am.*, vol. 46, pp. 186, 237, 243, 334, 452; 1956.
[26] H. Palmer, *J. Opt. Soc. Am.*, vol. 47, p. 367; 1957.
[27] D. A. Melnick, "Operations Research Inc., Silver Spring, Md., Scientific Rept. 5, Contract AF19(694)-1422; May 10, 1958. Also *J. Opt. Soc. Am.*, vol. 47, p. 1055; 1957.
[28] D. H. Burch and J. N. Howard, The Ohio State University, Columbus, Ohio, Scientific Rept. 2, Contract AF19(604)-516; 1955.
[29] "Handbook of Geophysics for Air Force Designers," Geophys. Res. Directorate, Boston, Mass.; 1957. This volume is being commercially published by The Macmillan Co., New York, N. Y.
[30] L. Larmore and S. Passman, *Proc. IRIS*, vol. 1, no. 1, p. 1, vol. 1, no. 2, p. 15; 1956.
[31] G. N. Plass (private communication).
[32] R. M. Langer, Final Rept., Part 1, Contract DA-36-039 Sc-72351; November, 1958. Also *ibid.*, Part 2; July, 1958.
[33] K. Angstrom, *Phys. Rev.*, vol. 1, p. 597; 1892.
[34] H. A. Lorentz, *Proc. Amst. Acad. Soc.*, vol. 8, p. 591; 1906.
[35] M. Born, "Optik," Edwards Brothers, Ann Arbor, Mich.; 1943.
[36] G. Hettner, *Physik. Z.*, vol. 27, p. 787; 1926.
[37] J. N. Howard, D. E. Burch, and D. Williams, *J. Opt. Soc. Am.*, vol. 46, p. 334; 1956.
[38] G. N. Plass, *J. Opt. Soc. Am.*, vol. 48, p. 690; 1958.
[39] J. N. Howard, *Proc. IRIS*, vol. 2, pp. 59–75; 1957.
[40] J. N. Howard, (in press).
[41] H. W. Yetes, *J. Opt. Soc. Am.*, vol. 47, p. 1054; 1957.
[42] A. H. Brown and V. Roberts, *J. Sci. Instr.*, vol. 30, p. 5; 1953.
[43] F. H. Jones, and V. Roberts, *Proc. Roy. Soc. A (London)*, vol. 236, p. 171; 1956.
[44] J. Hampson (private communication).
[45] J. T. Houghton, T. S. Moss, J. S. Seeley, and T. D. F. Hawkins, *Nature*, vol. 180, p. 1187; 1957.
[46] J. T. Houghton, T. S. Moss, and J. P. Chamberlain, *J. Sci. Instr.*, vol. 35, p. 329; 1958.
[47] D. M. Gates, D. G. Murcray, C. C. Shaw, and R. J. Herbold, *J. Opt. Soc. Am.*, vol. 48, p. 1010; 1958.
[48] T. L. Altschuler, General Electric Co., Schenectady, N. Y., Rept. TIS-R57 ELC 15; 1956.
[49] T. L. Altschuler, *J. Opt. Soc. Am.*, vol. 47, p. 1055; 1957.
[50] J. I. F. King, *J. Opt. Soc. Am.*, vol. 47, p. 1054; 1957.
[51] R. O'B. Carpenter, Baird-Atomic, Inc., Cambridge, Mass., Scientific Rept. 1, Contract AF19(604) 2405; November, 1957. Also *J. Opt. Soc. Am.*, vol. 48, p. 285; 1958.
[52] S. Churchill, "The Transmission of Radiation through Real Atmospheres," AFSWP Rept., University of Michigan, Ann Arbor, Mich.; 1956.

Paper 3.3.1

Fundamentals of Infrared Detectors*

RICHARD L. PETRITZ†, MEMBER, IRE

Introduction

TWO fundamental types of infrared detectors are thermal detectors and photodetectors. Incident radiation changes the electrical properties in each of the detectors. Both thermal and photodetectors are quantum detectors, since radiation is quantized; however, a distinction can be made if the nature of the solid is considered.

The modern description of the solid divides it into two thermodynamic systems—lattice and electronic. The electronic system is characterized by a system of energy levels: the conduction band, forbidden band impurity levels, and the valence band (see Fig. 1). The lattice is composed of atoms or molecules which constitute the solid and can be characterized by lattice vibrations which have mathematical properties analogous to radiation (lattice *phonons* are analogous to *photons*).

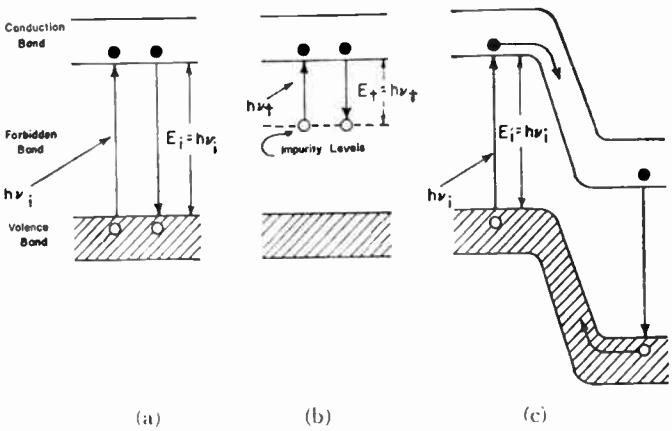

Fig. 1—Generation of carriers in photoconductive detectors (a) Intrinsic absorption. (b) Impurity absorption. (c) *P-n* junction.

The fundamental difference between photo- and thermal-type detectors can now be stated precisely. In thermal detectors, the radiation is absorbed by the lattice, causing heating of the lattice. The change in the temperature of the lattice causes a change in the electronic system. Two of the most common thermal detectors are thermocouples which develop a thermal voltage, and bolometers which change electrical resistance as a result of lattice heating. In photodetectors, the radiation is absorbed directly by the electronic system to cause changes in the electrical properties. Photodetectors include photoconductive, photovoltaic, and photoelectromagnetic detectors.

* Original manuscript received by the IRE, June 26, 1959.
† Texas Instruments Inc., Dallas, Texas.

Photodetectors

Contemporary infrared photodetectors [1] with response beyond 1.5 microns are semiconductors with energy level systems similar to those shown in Fig. 1. For the visible and near infrared, photoemissive tubes are ordinarily used. These tubes are discussed by Morton and Forque [1a].

After the radiation flux is converted to an electrical signal, the electrical signal can be amplified to the level desired. Detection systems generally have sufficient amplification to cause the system to be limited by noise; therefore, the signal-to-noise ratio is of basic interest in the physics of detectors.

Signal Properties

In a photodetector, the infrared radiation which is usefully absorbed excites electrons (and/or holes) to the conducting state. The generation of carriers per unit volume is given by

$$\text{generation rate} = \alpha J_s, \tag{1}$$

where J_s is the number of incident photons/cm² sec and α is that part of the absorption coefficient relating to carrier excitation. The excess electrons, Δn, return to the valence band at a rate related to the carrier lifetime, τ, by the equation

$$\text{recombination rate} = \Delta n/\tau. \tag{2}$$

In the steady state

$$\Delta n = \alpha J_s \tau. \tag{3}$$

Since the signal response is proportional to Δn, (3) shows the importance of the absorption coefficient, determined by the generation process, and the lifetime, determined by the recombination process. These are discussed in turn.

Generation Process: Generation of carriers can occur by main band transitions or by transitions involving impurity levels. In a main-band transition [Fig. 1(a)], a photon is absorbed, exciting an electron from the valence band to the conduction band, creating a hole-electron pair. Detectors of this type include the lead salts and indium antimonide. The long wavelength limit of spectral response, λ_i, is determined by the intrinsic energy gap, E_i, of the material where

$$\lambda_i = hc/E_i. \tag{4}$$

The second mechanism of generation involves impurity levels which are located in the forbidden energy gap as shown in Fig. 1(b). In this type of detector, the long wavelength cutoff is determined by the impurity

level relative to the conduction or the valence band. Gold-doped germanium is the best known infrared detector of this type.

The radiation intensity decreases with the distance, x, into the semiconductor as

$$J_s(x) = J_{s0}e^{-\alpha x}. \tag{5}$$

If most of the radiation is to be absorbed, (5) shows that the thickness of the crystal should be of the order of $1/\alpha$.

In impurity-type detectors, the absorption coefficient is given by

$$\alpha = \sigma N_t \tag{6}$$

where σ is the cross section of the impurity level and N_t is the density of impurity level atoms. The cross section for simple impurity levels can be approximated by hydrogen atom formulas [2]. The density of impurity levels is usually determined by the solubility limits of the atoms in the semiconductors. In germanium, the maximum solubility of gold is about 2×10^{16} atoms/cm^3, giving an $\alpha\cong0.14$ cm^{-1}; therefore, a germanium crystal would have to be approximately 10 cm thick to absorb most of the radiation. This rather small absorption coefficient is characteristic of most impurity semiconductors [3].

In the intrinsic absorption process, the absorption coefficient near the main-band region is usually of the order of 10^4 cm^{-1}, and the radiation is effectively absorbed within about 1 micron of the surface. In the case of the lead-salt photoconductive detectors [4], the material is deposited in films approximately 1 micron thick. This assures that the radiation affects the total volume of the detector.

In broad-area diffused or alloyed p-n junction-type detectors [5], [Fig. 1(c)], such as indium antimonide, the main generation occurs within the first micron of the surface; however, it is not necessary to place the junction this close to the surface. The critical distance is set by the diffusion length, L, of the minority carriers and by the surface recombination velocity, S. For best performance, the distance, w, of the junction from the surface must satisfy

$$w \ll L, \tag{7a}$$

and

$$S \ll D/w, \tag{7b}$$

where $L=\sqrt{D\tau}$ and D is the diffusion coefficient for the minority carriers. The crystal can be much larger than either w or L.

Recombination Process: Some of the more important mechanisms by which carriers can recombine are discussed below and shown in Fig. 2.

The inverse of the main-band absorption process is the direct radiative recombination process where the electron falls from the conduction band to the valence band and gives up its energy by radiation [Fig. 2(a)]. It is desirable that the carrier lifetime be limited by direct radiative recombination; however, in most detectors the lifetime is limited by another mechanism.

In the normal recombination center (bulk and surface) shown in Fig. 2(b), the minority carrier is captured by an impurity center and then falls to the valence band in a two-step process described by Shockley and Read [6]. When the cross sections for the two steps are nearly equal, the rate limiting step is set by capture of the minority carrier by the impurity center, and the electron and hole lifetimes are equal.

Another type of impurity center is called a nonrecombining trap [7] (bulk and surface) and is shown in Fig. 2(c). This method of recombination differs from the normal recombination in that the cross section for the second step, the majority carrier, is relatively small. Under these conditions, the majority carrier is free for an extended period of time after the minority carrier is captured. The increase in majority carrier lifetime will be proportional to the time the minority carrier spends in the trap. Thus, minority carrier trapping is a mechanism for increasing the lifetime of majority carriers, which increases the signal response as shown in (3).

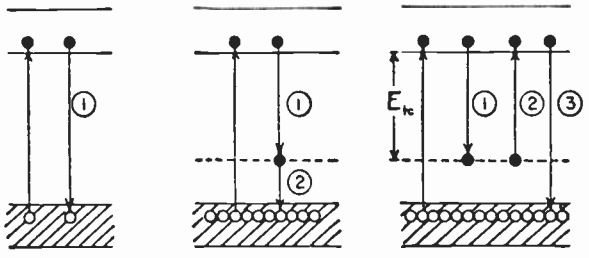

Fig. 2—Recombination processes in photoconductors. (a) Direct recombination. (b) Normal recombination center. (c) Non-recombining trap.

The recombination process can be used to classify the mechanism of detection. The impurity level detector deals with the majority carrier, and the time constant is the lifetime of the majority carrier. In the case of single crystal minority carrier detectors such as photovoltaic detectors, the important lifetime is that of the minority carrier.

Various researchers disagree on the basic recombination model in the thin-film lead-salt detectors. In one model [8], [9], the majority carrier lifetime is increased by the oxygen sensitization process which incorporates minority carrier traps. Another model [10] suggests that an array of p-n junctions is generated as a result of the oxygen sensitization process. The interested reader is referred to other sources, [4], [8]–[10], for further discussion of this subject.

Noise Properties

Noise mechanisms [11] that limit detector performance are considered in the following sections.

Background Radiation: An infrared detector must, if it is to be used in a physically interesting situation, have

background radiation of some sort fall upon it. For detectors used in laboratories, the background radiation is that of a blackbody at the ambient temperature. The background radiation has a random characteristic due to random arrival of photons which sets an ultimate limit to the smallest radiation signals that can be detected. The statistics of this noise have been analyzed by a number of authors, and a summary is given by Jones [12]. Background radiation is one source of generation-recombination noise; the other main source is the lattice (see below). An over-all goal of infrared detector physics and technology is to achieve detectors that are background radiation-noise limited.

Signal Fluctuations: In contemporary infrared detectors, the inherent fluctuations in the signal can be neglected, since background radiation fluctuations are of a much greater intensity. However, in future detectors which may operate in outer space, where effective background temperatures can be very low, conditions where fluctuations in the signal are of interest may be encountered. These signal fluctuations can be handled by the same methods used for background fluctuations.

Generation-Recombination Noise by Lattice Excitation and Recombination: Detector noise caused by fluctuations in the rate of generation of carriers by the lattice and the corresponding recombination process [13] can and usually does exceed background radiation noise. The magnitude of the lattice-induced noise is related to the lattice temperature, and cooling of the lattice reduces this noise.

Nyquist-Johnson Noise of Conduction Electrons: The electrons in the conduction band have velocity fluctuations which are generally the source of the Nyquist-Johnson noise, characteristic of all resistors [14]. This is the only noise present in the detector at equilibrium. In most photodetectors, the generation-recombination noise can be made to exceed the Nyquist-Johnson noise by proper biasing.

1/f Noise: Contemporary semiconductors have a component of noise power characterized by a $1/f$ spectrum which is proportional to the square of the biasing current. Considerable work is being directed toward determining the basic foundation of this noise and reducing its magnitude [15]. Experimental evidence indicates that $1/f$ noise is associated with surfaces, contact phenomena, and bulk phenomena such as dislocations. The subject is too complex to be discussed here, but $1/f$ noise must be recognized as an important source of noise in infrared detectors.

Amplifier Noise: The aim of amplifier design for use with infrared detectors is to assure that detector noise, not amplifier noise, limits the signal-to-noise ratio. This condition can usually be achieved by careful design [16].

Signal-to-Noise Ratio

The signal-to-noise ratio for an infrared detector is the basis for the absolute detectivity or sensitivity of a detector [17]. It can be calculated and/or measured with knowledge of the signal properties and the noise properties. For the purpose of characterizing detectors the concept of signal-to-noise ratio per unit of signal radiation, the detectivity, is useful. The concept of noise-equivalent-power, which is the radiation power required to give a signal equal to noise, is also useful.

Background Radiation Limited Condition of Operation (Blip)

As stated above, an important goal of infrared-detector physics and technology is the achievement of the true radiation limit of detectivity. In order to show the physics behind this condition, a discussion of the intrinsic photoconductor will be presented. This discussion is based on [13] where the background limited photoconductor was first analyzed with explicit consideration given to both the lattice-induced and the background radiation-induced noise. Recently, Burstein and Picus [18] have discussed the background limited condition for impurity level photoconductors and have coined the term *Blip* (background limited infrared photoconductor to describe it.

Intrinsic Photoconductor [19]

The instantaneous electrical conductivity of an intrinsic semiconductor is

$$\sigma(t) = a(\mu_e n(t) + \mu_h p(t)) = q\mu N(t)/V, \tag{8}$$

where

$$V = Ad, \mu = \mu_e + \mu_h, \text{ and } N = \mu V = pV.$$

Here, q is the electronic charge, $N(t)$ is the total number of conduction electrons, V is the volume, A is the surface area, d is the thickness of the detecting filament, and μ_e and μ_h are the mobilities of electrons and holes, respectively. The radiation signal is measured by the change in conductance caused by a change in N; therefore, the smallest signal that can be detected will be limited by the random fluctuation in N.

The two fundamental mechanisms by which N can fluctuate are phonon and photon absorption and emission, due to the lattice and background radiation. Other noise mechanisms present in the semiconductor are neglected for this discussion.

Since incident radiation will penetrate into the semiconductor to a depth of about $x=1/\alpha$, material at a depth greater than $1/\alpha$ sees little incident radiation and shunts the radiation effects. The analysis can be simplified if the filament thickness is assumed to be $d \leq 1/\alpha$ and the radiation is considered to be uniform over this region. Small densities of impurity levels, both bulk and surface, may be present for lattice excitation and recombination processes [Fig. 2(b)], but the electron and hole distribution is assumed to be that of the intrinsic semiconductor.

The small signal properties are governed by

$$d\Delta N_s/dt = A\eta_s J_s - \Delta N_s/\tau, \tag{9}$$
$$\Delta N_s = N(t) - N,$$

where N is the equilibrium number of electrons in the absence of the signal radiation J_s, η_s is the responsive quantum efficiency, and τ is the electron-hole lifetime.

These quantities can be expressed as

$$J_s = \frac{c}{4}\int_{E_i/h}^{\infty} n_s(\nu, T_s)d\nu, \tag{10}$$

$$\eta_s = \frac{c}{J_s 4}\int_{E_i/h}^{\infty} \eta(\nu) n_s(\nu, T_s)d\nu/, \tag{11}$$

$$\eta(\nu) = (1 - R)[1 - e^{-\alpha(\nu)d}]/[1 - Re^{-\alpha d}], \tag{12}$$

and

$$1/\tau = 1/\tau_r + 1/\tau_l, \tag{13}$$

where $n_s(\nu, T_s)$ is the density of photons in the radiation signal, T_s is the temperature of the signal source, $\eta(\nu)$ is the responsive quantum efficiency at the spectral frequency ν, R is the reflectance of the detector surface, τ_r is the radiative lifetime, and τ_l is the lattice lifetime which includes the effects of both bulk and surface recombination centers [Fig. 2(b)].

The solution of (9) for a sinusoidal signal of modulation frequency, $f=\omega/2\pi$, is

$$|\Delta N_s(f)| = A\eta_s J_s \tau/[1 + (\omega\tau)^2]^{1/2}. \tag{14}$$

The signal response can be increased by increasing the lifetime and by increasing the quantum efficiency. It can be seen that the carrier lifetime is the responsive time constant of the detector. The fractional change in conductivity is

$$\frac{|\Delta N_s(f)|}{N} = \frac{\eta_s J_s \tau}{nd[1 + (\omega\tau)^2]^{1/2}}, \tag{15}$$

showing the importance of making the equilibrium density of carriers as small as possible.

The fluctuation in N, which is the fundamental noise, is analyzed in Appendix A of [13]. The mean-square fluctuation of N in a small frequency interval, Δf, is

$$\langle \Delta N^2(f)\rangle = \frac{\Delta f 2\tau^2(F_r + R_r + F_l + R_l)}{1 + (\omega\tau)^2}. \tag{16}$$

F_r is the mean rate of generation of carriers by background radiation, R_r is the mean rate of recombination with emission of radiation, F_l is the mean rate of generation of carriers by absorption of lattice phonons, and R_l is the mean rate of recombination with emission of lattice phonons. F_r can be expressed as

$$F_r = \eta_r J_r A = \frac{Ac}{4}\int_{E_i/h}^{\infty} \eta(\nu) n_r(\nu, T_r)d\nu, \tag{17}$$

$$n_r(\nu, T_r) = \frac{8\pi\nu^2}{c^3(e^{h\nu/kT_r} - 1)}, \tag{18}$$

where J_r is the background radiation flux incident on the detector, and T_r is the temperature of the background radiation. A hemispherical field of view is assumed in (17).

When $E_i \gg kT_r$, the -1 in (18) can be neglected and

$$\eta_r J_r = B_r(T_r)e^{-E_i/kT_r}, \tag{19}$$

where

$$B_r(T_r) = 2\pi c\left(\frac{kT_r}{hc}\right)^3\left[\left(\frac{E_i}{kT_r}\right)^2 + 2\left(\frac{E_i}{kT_r} + 1\right)\right]. \tag{20}$$

In the absence of an exact distribution function for lattice phonons, an analogy with the radiation field yields,

$$F_l = \eta_l J_l A, \tag{21}$$

$$\eta_l J_l = B_l(T_l)e^{-E_i/kT_l}, \qquad E_i \gg kT_l, \tag{22}$$

where J_l is the lattice phonon flux and T_l is the lattice temperature. The lattice excitation involves the same activation energy, E_i, as the radiative process.

When a dynamic equilibrium has been established,

$$F_r + F_l = R_r + R_l \tag{23}$$

represents a state in which the total rate of generation must be equal to the total rate of recombination. Substituting (23) into (16),

$$\langle \Delta N^2(f)\rangle = \frac{\Delta f 4\tau^2 A(\eta_r J_r + \eta_l J_l)}{1 + (\omega\tau)^2}, \tag{24}$$

which expresses the noise in terms of the rates of generation of carriers by the radiative and lattice processes. The recombination rates can be expressed [13] in terms of the lifetimes as

$$R_r = N/2\tau_r, \qquad R_l = N/2\tau_l, \tag{25}$$

and

$$R_r + R_l = N/2\tau. \tag{26}$$

The detailed balance (23) can be expressed in terms of the semiconductor parameters by combining (23) and (25),

$$\eta_r J_r + \eta_l J_l = \frac{nd}{2}\left(\frac{1}{\tau_r} + \frac{1}{\tau_l}\right) = \frac{nd}{2\tau}. \tag{27}$$

When (27) is substituted into (24), an expression for the noise in terms of semiconductor parameters is obtained,

$$\langle \Delta N^2(f)\rangle = \frac{2\tau\Delta f nAd}{1 + (\omega\tau)^2}. \tag{28}$$

Combining (14), (24), and (28) two equivalent expressions for the signal-to-noise ratio are obtained:

$$\frac{|\Delta N_s(f)|}{\sqrt{\langle \Delta N^2(f)\rangle}} = \frac{\eta_s J_s \sqrt{A}}{[4\Delta f(\eta_r J_r + \eta_l J_l]^{1/2}}, \tag{29}$$

and

$$\frac{|\Delta N_s(f)|}{\sqrt{\langle \Delta N^2(f)\rangle}} = \frac{\eta_s J_s \sqrt{A}}{(2nd\Delta f/\tau)^{1/2}}. \tag{30}$$

Eqs. (29) and (30) allow for a discussion of the signal-to-noise ratio of an intrinsic photodetector under dy-

namic as well as thermal equilibrium. Eq. (29) is especially useful for analyzing the effects of cooling the background radiation and/or the lattice since J_r and J_l are functions of T_r and T_l, respectively, as shown in (19) and (22). Conversely, (30) is useful for discussing the effects of the semiconductor parameters on the signal-to-noise ratio. It is important to emphasize that (29) and (30) are equivalent because of the detailed balance condition (27). These equations will now be used to discuss actual and ideal detectors, and methods of obtaining an ideal detector.

Ideal Radiation Detector (Blip)

An ideal radiation detector must satisfy two criteria:

1) It must detect with unit quantum efficiency all of the radiation in the signal for which the detector is designed,

$$\eta_s = 1. \tag{31}$$

2) The noise should be that of the background radiation that comes from the field of view of the detector. In terms of (29) this means that

$$\eta_r J_r \gg \eta_l J_l; \tag{32}$$

that is, the carriers should be generated by background radiation, not by the lattice.

$\eta_r J_r$ is given by (17) for detectors which have a hemispherical field of view, but if apertures are used,

$$\eta_r J_r = (\eta_r J_r)_{FV} + (\eta_r J_r)_{EXT}. \tag{33}$$

In an ideal detector only $(\eta_r J_r)_{FV}$ should be present.

While (32) assures that lattice noise is dominated by radiation noise, it does not assure that the radiation noise dominates other noises such as $1/f$ noise. For this reason (32) is a necessary, but not a sufficient condition, for ideal operation. Background radiation must dominate all other sources of noise if ideal conditions are to be achieved. The term *Blip* [18] is quite suitable since it stresses the importance of the background radiation.

The signal-to-noise ratio for the ideal *Blip* detector for intrinsic photoconductors can be obtained by substituting (31) and (32) into (29):

$$(S/N)_{Blip} = \sqrt{A} J_s/(4\Delta f - J_r)^{1/2}, \tag{34}$$

where $\eta_r = 1$ is required over the spectral region of interest by definition of the *Blip* condition. For certain detectors the $\sqrt{4}$ in the denominator of (34) is replaced by $\sqrt{2}$. An example of this is the broad area p-n junction detector, where only excitation noise is present and the recombination term is absent. This point is further discussed by Pruett and Petritz [5].

Methods for Achieving Blip Operation

An optimization of the responsive quantum efficiency can be understood from an analysis of (12). For thick crystals, $\alpha d \gg 1$,

$$\eta(\nu) = 1 - R, \tag{12a}$$

while for thin crystals, $\alpha d \ll 1$,

$$\eta(\nu) = \frac{(1 - R)\alpha d}{[1 - R(1 - \alpha d)]} \tag{12b}$$

A loss in signal due to a low responsive quantum efficiency will result from a crystal that is too thin, while some of the signal will be shunted by a crystal that is too thick. A good compromise discussed after (5) is $\alpha d \cong 1$, where

$$\eta(\nu) = \frac{(1 - R)(1 - e^{-1})}{(1 - Re^{-1})}. \tag{12c}$$

A reduction of reflection by optical coating techniques will yield a further improvement in $\eta(\nu)$.

The reduction of noise to the condition of being generated only by background radiation will now be discussed. At room temperature, contemporary photoconductors have $\eta_l J_l \gg \eta_r J_r$; that is, the generation of carriers occurs primarily through lattice excitation. It can be seen from (22) that the generation of carriers through lattice excitation can be reduced by cooling the lattice. It has been shown experimentally that cooling the lattice, while keeping the background radiation constant, does improve the detectivity of the detectors toward the *Blip* condition.

It is of considerable interest to determine whether or not the *Blip* condition of operation can be achieved without cooling the lattice. At thermal equilibrium, there exist additional equations of detailed balance, other than (27), for radiative and lattice processes separately. These are

$$\eta_r J_r = \alpha d/2\tau_r \tag{35}$$

and

$$\eta_l J_l = \alpha d/2\tau_l. \tag{36}$$

These equations require a balanced condition of absorption and emission of photons and of lattice phonons separately. The over-all equation of detailed balance (27) is obtained by adding (35) and (36).

From (35) and (36),

$$\eta_l J_l/\eta_r J_r = \tau_r/\tau_l. \tag{37}$$

It is required that

$$\tau_r/\tau_l \ll 1, \tag{38}$$

and

$$\tau \rightarrow \tau_r, \tag{39}$$

to achieve the condition of (32). This means that the electronic system must be decoupled from the lattice to allow the lifetime to approach the radiative lifetime required in (39). If this can be done, the *Blip* condition can be achieved without cooling the lattice.

The next question is how the electronic system can be decoupled from the lattice. It may be possible to do this in single crystal detectors. In the case of germanium,

improved crystal technology has increased the lifetime from microseconds to the order of milliseconds. Improved crystal technology may lead to increases in carrier lifetime in single crystal detectors such as indium antimonide. It may be possible to achieve its calculated radiative lifetime of 3×10^{-7} second [20] at room temperature. However, it remains to be done and this is pointed out merely as an approach.

When the *Blip* condition is approached, (35) and (39) yield

$$\eta_r J_r = nd/2\tau. \tag{40}$$

Since $\eta_r J_r$ is fixed by the background radiation level, n and τ are no longer independent variables. Comparison of (40) with (27) indicates that in the *Blip* condition, the ratio n/τ has a minimum value. The necessary reduction from the value in (27) can be achieved by a reduction of n, an increase of τ, or both. When the lattice is strongly coupled to the electronic system and the lattice is cooled, n will decrease while τ remains essentially unchanged. If the lattice is decoupled from the electronic system and no cooling is employed, τ will increase and approach τ_r, the radiative lifetime. At the same time, n will remain constant because at thermal equilibrium n is a thermodynamic quantity in an intrinsic semiconductor.

Whether or not the complete *Blip* operation is achieved at room temperature is not the only point of this discussion. The degree of cooling necessary to achieve *Blip* operation is related to the strength of coupling to the lattice. If the carrier lifetime is increased by decreasing the lattice coupling, a corresponding lessening in the cooling requirement is obtained; thus, by improved crystal technology, the cooling requirement can be steadily reduced. One suggested goal would be an attempt to move the cooling requirement from the liquid nitrogen temperature to the dry ice temperature. The next few years of detector research and development may make this possible.

Blip Conditions for Other Types of Infrared Detectors

While the preceding discussion has been in terms of the intrinsic photoconductor, the requirements for *Blip* operation are basically the same for all types of infrared detectors. Analysis of impurity level detectors by Burstein and Picus [18] and the lead salts by Petritz [8] shows that (32) is a necessary condition for *Blip* operation. The over-all signal-to-noise ratio is reduced, due to increased noise, if the carriers are generated by a mechanism other than by background radiation.

While the intrinsic detector may reach *Blip* operation without extensive cooling, certain types of detectors require cooling for additional reasons.

Impurity Level Photoconductors [3], [18]: Impurity-type photoconductors are of interest for detecting infrared radiation beyond 3 microns. Since such impurities have very low energy levels in the semiconductor [see Fig. 1(b)], without cooling, the centers would be thermally ionized and very little absorption of radiation would take place at the impurity levels. Cooling is necessary in the case of impurity-type photoconductors, first, in order to have the carriers in the impurity levels where they may absorb radiation, and second, to reduce lattice noise (32).

Minority Carrier P-N Junction Infrared Detectors [5]: The *p-n* junction [Fig. 1(c)] infrared detectors are also of considerable interest for detection beyond 3 microns. In these detectors, notably indium antimonide, cooling is required to obtain good *p-n* junctions; the intrinsic numbers of carriers is so large at room temperature that the minority carrier effects are completely masked. Long-wavelength *p-n* junctions require cooling to obtain good *p-n* junctions and to reduce lattice noise. It is conceivable that shorter wavelength *p-n* junctions could reach the *Blip* condition without cooling.

Lead-Salt Film Detectors [4]: Lead sulfide is a very good photoconductor at room temperature although it does not reach *Blip* operation [21]. Cooling improves these detectors by reducing the lattice contribution to the noise, and the *Blip* condition is approached at solid carbon dioxide temperatures except for a component of 1/f noise which is usually present.

The longer wavelength lead-salt detectors such as lead selenide and lead telluride are far from the *Blip* condition at room temperature, and cooling improves these detectors in a more complex manner than in lead sulfide. Cooling appears to improve the signal response by an increase in the lifetime of the carriers [see (3)]. At temperatures of the order of 77°K, in both lead selenide and lead telluride, the carriers are generated principally by background radiation. However, both of these detectors still have 1/f noise at these temperatures, and the main improvement that can be obtained at low temperatures will be from a reduction of 1/f noise.

Photoelectromagnetic Detectors (PEM) [5], [22]: PEM detectors have been reported to operate quite well without cooling, and offer promise for still higher performance without cooling. This detector is a single crystal device. A magnetic field is used to separate photo-generated holes from electrons, causing a transverse voltage in the presence of radiation. The minority carriers are the important carriers, similar to the *p-n* junction detectors, but no *p-n* junction is required to separate the carriers. It is conceivable that this detector may approach *Blip* operation at or near room temperature, but further study is required to understand the competition between the Nyquist-Johnson noise of conduction electrons and the generation-recombination noise.

Information Capacity and the Blip Condition

When a detector is limited by generation-recombination noise, whether of lattice- or background-radiation origin, the frequency response of the signal and the spectrum of the noise are identical, as shown explicitly in (14) and (24). Under these conditions, electronic techniques can be used to boost the high-frequency response of both the signal and the noise without impairing the

signal-to-noise ratio; therefore, the information capacity of the detector is not limited by the carrier lifetime. Now, when the detector is in the *Blip* condition these arguments are still valid, and moreover the signal-to-noise ratio is a maximum. Thus *Blip* should be achieved even at the expense of an increased time constant. Electronic techniques can then be used to increase the information capacity of the system.

While this discussion has been in terms of intrinsic photodetectors, it is basic for all photodetectors and has been subjected to experimental proof in recent work on lead sulfide [23]. A lead-sulfide detector was studied at room temperature and at $-50°C$. The time constant changed from 500 microseconds ($f_c = 1/2\pi\tau = 310$ cps) at room temperature to 5 milliseconds ($f_c = 31$ cps) at $-50°C$. The 1-cycle NEP was improved more than a factor of 10 by cooling. This improvement was not gained at the expense of information capacity, since a bandwidth for the cooled detector greater than the original 310 cps was obtained by electronic techniques.

This experiment shows that a most important objective is to approach as nearly as possible the *Blip* condition of operation by whatever techniques must be employed. After this condition is achieved, one can then use electronic techniques to increase the bandwidth of the detector. Such an approach will achieve the maximum signal-to-noise ratio for a given bandwidth requirement.

These statements are based on the assumption that the noise is generation-recombination noise. Usually the noise will have a 1/f component at low frequencies, and at sufficiently high frequencies, must go into white noise of the resistor and amplifier. This limits the extent to which frequency compensation can be employed and requires a more detailed study. Such a study has been made in two papers on the information capacity of detectors [23], [24].

Noise Figure—A Figure of Merit for Detectors

The degree to which a detector approaches an ideal detector can be expressed by the noise figure, F, defined as

$$F = (S/N)^2_{Blip}/(S/N)^2_{\text{actual}} = (\text{NEP})^2_{\text{actual}}/(\text{NEP})^2_{Blip} = (D^*)^2_{Blip}/(D^*)^2_{\text{actual}}. \quad (41)$$

$(S/N)^2_{Blip}$ is the signal-to-noise ratio expected from an ideal detector, and $(S/N)^2_{\text{actual}}$ is the actual value of the ratio for the detector. D^* is the signal-to-noise ratio referred to unit radiation power, unit bandwidth and unit area [25]. F is called the noise figure since it corresponds to the noise figure as defined for microwave and radio-frequency receivers [26]. F approaches unity for a *Blip* detector and is greater than unity for a nonideal detector.

This can be seen in more detail by considering the theoretical expressions for the intrinsic detector operating under generation-recombination noise. Substituting (29) and (34) into (41) yields,

$$F = (\eta_r/\eta_s)^2[1 + (\eta_l J_l/\eta_r J_r)]. \quad (42)$$

F is greater than unity because of the two effects defined by (31) and (32).

When the detector is being limited by lattice noise,

$$F = \eta_l J_l/\eta_s^2 J_r, \quad (43)$$

where

$$\eta_l J_l \gg \eta_r J_r,$$

and increasing the quantum efficiency improves F as $1/\eta_s^2$. When the detector is background radiation noise limited,

$$F = \eta_r/\eta_s^2 \cong 1/\eta_s, \quad (44)$$

where

$$\eta_l J_l \ll \eta_r J_r,$$

and the improvement of F is with $1/\eta_s$ rather than $1/\eta_s^2$ because an improvement of quantum efficiency now affects the noise.

To facilitate the use of the noise figure, it is useful to have a plot of D^*_{Blip} as a function of the long wavelength threshold, λ_i. The definition of D^*_{Blip} is

$$D^*_{Blip}(\lambda_i) = (S/N)_{Blip}\sqrt{\Delta f}/(E_s J_s \sqrt{A}), \quad (45)$$

where $E_s = E_i = hc/\lambda_i$. Substituting (34) into (45)

$$D^*_{Blip}(\lambda_i) = \frac{1}{E_i\sqrt{4J_r}}, \quad (46)$$

where J_r is calculated from (17) with $\eta(\nu) = 1$ for $\nu \geq \nu_i$, and $\eta(\nu) = 0$ for $\nu \leq \nu_i$. A hemispherical blackbody radiation at $T_r = 300°K$ is assumed. A discontinuity exists as $E_i \to 0$, and

$$D^*_{Blip}(E_i \to 0) = (16\sigma k T_r^5)^{-1/2} = 1.81 \times 10^{10}, \quad (47)$$

has been calculated for an ideal blackbody thermal detector [12]; σ is the Stefan-Boltzmann constant. $D^*_{Blip}(\lambda_i)$ is plotted vs λ_i and E_i in Fig. 3.

While the question of the characterization of detectors requires more discussion than can be given here, it is suggested that the noise figure be considered as a figure of merit for detectors. The reasons are: F is a quantitative measure of the departure from an ideal detector, and the methods for determining F are consistent with methods used for other radiation receivers. Because of its generality and related uses in the microwave and radio-frequency bands, it is suggested that the noise figure, rather than its reciprocal [27], be employed in the infrared region in order to avoid new terms. For an example of the use of the noise figure for an infrared detector see Pruett and Petritz [5].

Thermal Detectors

The theory of thermal detectors is given in [12] and [28], and an up-to-date summary of their characteristics appears in this volume [29]. The discussion here will be confined to the basic characteristics of thermal detectors and to the possibilities for this type of detector to reach the *Blip* condition.

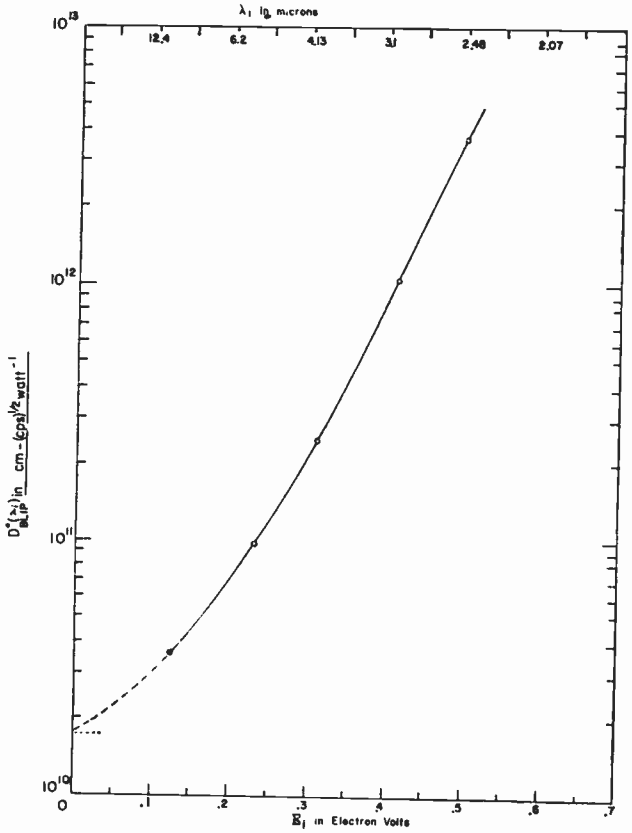

Fig. 3—Detectivity D^*_{Blip} of background-limited infrared photoconductors plotted against their long wavelength cutoff and corresponding energy gap. This curve assumes both generation and recombination processes contribute to the noise, if only one does, the values of D^*_{Blip} are increased by a factor $\sqrt{2}$.

Signal Properties

In general, thermal detectors can be considered as blackbody detectors; that is, they will absorb radiation rather uniformly over the infrared spectrum. Currently, they are the only detectors that will operate without cooling out to wavelengths as far as 14 microns. This is one of the inherent advantages of thermal detectors over photodetectors.

The photon absorption in thermal detectors causes a temperature rise in the lattice, which then causes a change in an electronic property. The rise in temperature will depend upon the thermal capacity of the system; therefore, great care is taken to make these detectors as small as possible.

Consider next how temperature equilibrium is established in the detector. If the detector is coupled to its environment only through the background-radiation field, temperature equilibrium is established by reradiation from the detector element. Such a condition in principle, could be achieved by suspending the detector in a high vacuum, with very low thermal conductivity leads attached to it. Such a detector has a very-long-time constant because the rate of reradiation is quite slow.

In actual practice, higher-speed detectors are desirable. These are made by mounting the sensitive wafer on a body which rapidly conducts heat away from the detector. Therefore, the total thermal conductivity is the sum of that due to reradiation plus that through the backing material. Usually the thermal conduction through the backing material completely dominates the reradiation effect. Much of today's technology on thermal detectors is to decrease the time constant by increasing the thermal conductance and by decreasing the thermal mass of the detector

Noise Properties

The ultimate noise of the thermal detector, as in all infrared detectors, is established by fluctuations in the background radiation. Such noise would manifest itself as a temperature fluctuation in the detector element. However, thermal detectors as presently manufactured do not approach this noise mechanism, but are limited by the Nyquist-Johnson noise of the conduction electrons.

Present thermal detector technology, which aims towards increasing the speed of response by thermal conduction to the backing plate, is going in the wrong direction to achieve the *Blip* operation. The temperature fluctuations under this condition will result from heat flow to the backing plate and will not be due to background radiation. The heat conduction to the backing plate plays an analogous role to the $\eta_i J_i$ term in the photodetector, [see (29)]; therefore, increasing this term leads away from the *Blip* condition. However, so long as these detectors are limited by Nyquist-Johnson noise, the speed of response improvements are achieved without raising the noise level; thus, they are entirely in order. This is pointed out to indicate that such approaches will not achieve the *Blip* condition.

The use of cooling to improve the performance of thermal detectors is discussed by Smith, Jones, and Chasmer [28], but the reported experimental results to date have fallen well below the theoretical expectations. One particular cooled thermal detector, the superconducting bolometer, has received considerable study, but for a number of reasons [28] has yet to be developed into a practical device.

An approach to the *Blip* condition in thermal detectors, which might not require cooling, is to suspend the detector element in a vacuum such that it is coupled predominantly to the radiation field. The resulting very-long-time constant could be tolerated and electronic means could be used to speed up the response of the detector if the true *Blip* condition were achieved. However, in addition, it would require the overcoming of the Nyquist-Johnson noise, which seems difficult in terms of present technology.

In summary, thermal detectors are of great importance for long wavelength detection at room temperatures, but rather difficult problems must be overcome before they will approach the *Blip* condition.

Future Trends

An important goal will be to develop *Blip* detectors to efficiently cover the infrared spectrum. It appears that cooling will be allowed for high-quality military and commercial detection systems; therefore his approach will be discussed first. Nearly all contemporary photodetectors are approaching the condition that the generation of carriers is mainly by background radiation if the detector is cooled sufficiently. However, none of these detectors has quite reached the total *Blip* condition because of 1/f noise. Therefore, more emphasis will be placed on improving the noise characteristics of detectors. This means more research on contact phenomena, surfaces and other sources of 1/f noise.

A second improvement in contemporary detectors will be to utilize fully the signal radiation; that is, to improve the responsive quantum efficiency, η_s. Antireflection coatings, optimizing detector thickness relative to absorption coefficient, and other techniques will lead to over-all improvements in η_s.

A third and important area will be that of increased emphasis on the physics and chemistry of detector preparation to optimize production yields. Better uniformity of response and methods of assuring no deterioration under adverse storage conditions will be realized.

Another goal will be to provide the user with a broader range of detectors that do not require cooling. Here the physics of hole-electron recombination processes becomes especially important and research will be done to decouple the electronic system from the lattice.

Concerning thermal detectors, further work aimed at improving their speed of response, uniformity of response, and general methods of preparation, can be expected. The present approach to achieve higher speeds of response does not appear to be compatible with reaching *Blip* conditions. However, good performance of thermal detectors at room temperature will make them valuable detectors for the indefinite future. More work will be done in the area of cooling thermal detectors and improvements in performance should result.

Finally, a completely new device, the infrared maser [30], can be expected to receive attention and it may have a large impact on the over-all infrared picture.

Acknowledgment

The author wishes to acknowledge the many stimulating discussions he has had with his colleagues and friends in the field of infrared. In particular, when at the Naval Ordnance Laboratory, his discussions with James Humphrey, Frances Lummis, Wayne Scanlon, and Robert Talley were invaluable. Discussions with Eli Burstein on the subject of *Blip* detectors have been very helpful.

Since joining Texas Instruments, the author's discussions with Werner Beyen and George Pruett have been especially helpful, both in regard to the subject of single-crystal detectors and to the preparation of this paper.

References

[1] A good general reference on the subject of photodetectors is "Photoconductivity Conference," eds., R. G. Breckenridge, B. R. Russell, and E. E. Hahn, John Wiley & Sons, Inc., New York, N. Y.; 1956.

[1a] G. A. Morton and S. V. Forque, "The photoconductive beam-scanning pickup tube," this issue.

[2] E. Burstein, G. Picus, and N. Sclar, "Optical and Photoconductive Properties of Silicon and Germanium," [1], pp. 353–413.

[3] For discussion and references to impurity-type photodetectors, see H. Levinstein, "Impurity photoconductivity in germanium," paper 3.3.6, this issue, p. 1478.

[4] For discussion and references to the lead-salt photoconductors, see R. J. Cashman, paper 3.3.4, this issue, p. 1471. Another recent review is, R. L. Petritz and J. N. Humphrey, "Research on photoconductive films of the lead salts," *Proc. IRIS*, vol. 3, pp. 65–79; March, 1958.

[5] For discussion and references to the indium antimonide photovoltaic and PEM detector, see F. F. Reike, L. H. DeVant, and A. J. Tuzzolino, "Single Crystal infrared detectors based upon intrinsic absorption," paper 3.3.5, this issue, p. 1475 and G. R. Pruett and R. L. Petritz, "Detectivity and pre-amplifier considerations for indium antimode photo-voltaic detectors," paper 4.1.9, this issue, p. 1524.

[6] W. Shockley, W. T. Read, Jr., "Statistics of the recombination of electrons and holes," *Phys. Rev.*, vol. 87, pp. 835–842; September, 1952. W. Shockley, "Electrons, holes, and traps," Proc. IRE, vol. 46, pp. 973–990; July, 1958. G. Bemski, "Recombination in semiconductors," Proc. IRE, vol. 46, pp. 990–1004; July, 1958.

[7] Nonrecombining traps have been discussed by A. Rose, *Phys. Rev.*, vol. 97, pp. 322–333; January, 1955, for insulator photodetectors; by J. R. Haynes and J. A. Hornbeck, *Phys. Rev.*, vol. 97, pp. 311–321; January, 1955, for silicon; by H. Y. Fan, *Phys. Rev.*, vol. 92, pp. 1424–1428; December, 1953, and vol. 93, p. 1434; March, 1954, for germanium; and by J. N. Humphrey and R. L. Petritz, *Phys. Rev.*, vol. 105, pp. 1736–1740; March, 1957, and R. H. Harada and H. T. Minden, *Phys. Rev.*, vol. 102, pp. 1258–1262; June, 1956, for the lead salts. Also Shockley [6] and Bemski [6].

[8] R. L. Petritz, "Theory of photoconductivity in semiconductor films," *Phys. Rev.*, vol. 104, pp. 1508–1515; December, 1956; Harada-Minden and Humphrey-Petritz [7].

[9] J. F. Woods, "Investigation of the photoconductive effect in lead sulfide films using Hall and resistivity measurements," *Phys. Rev.*, vol. 106, pp. 235–240; April, 1957.

[10] J. C. Slater, "Barrier theory of photoconductivity in lead sulfide," *Phys. Rev.*, vol. 103, pp. 1631–1644; September, 1956; G. W. Mahlman, "Photoconductivity of lead sulfide films," *Phys. Rev.*, vol. 103, pp. 1619–1630; September, 1956; E. S. Rittner, "Electron processes in photoconductors," in [1], p. 215.

[11] A recent review of noise in photodetectors, K. M. van Vliet, "Noise in semiconductors and photoconductors," Proc. IRE, vol. 46, pp. 1004–1018; June, 1958.

[12] R. C. Jones, "Performance of detectors for visible and infrared radiation," in "Advances in Electronics," ed. L. Marton, Academic Press Inc., New York, N. Y., vol. 5, pp. 1–96; 1953.

[13] R. L. Petritz, "The Relation Between Lifetime, Limit of Sensitivity, and Information Rate in Photoconductors," [1], pp 49–77.

[14] For a discussion of Nyquist-Johnson noise, see J. L. Lawson and G. E. Uhlenbeck, "Threshold Signals," McGraw-Hill Book Co., Inc., New York, N. Y., ch. 4; 1948.

[15] For reviews of 1/f noise, see: A. van der Ziel, "Noise in junction transistors," Proc. IRE, vol. 46, pp. 1019–1038; June, 1958. "1/f Noise and Germanium Surface Properties," "Semiconductor Physics," Ed. R. H. Kingston University of Pennsylvania Press, Philadelphia, Pa., pp. 207–225; 1957; R. L. Petritz, "Recent semiconductor noise studies," 5ª Rassegna Internazl. Elett.-Nuclear, Rome, Italy, pp. 217–226; 1958.

[16] For a discussion of preamplifiers for infrared-detectors, see G. R. Pruett and R. L. Petritz, [5].

[17] A good discussion and extensive bibliography of the statistical theory of detection is, D. Middleton and D. Van Meter, "Detection and extraction of signals in noise from the point of view of statistical decision theory," *J. Soc. Indust. Appl. Math.*, vol. 3, pp. 192–253; December, 1955, and vol. 4, pp. 86–119; June, 1956.

[18] E. Burstein and G. S. Picus, "Background Limited Infrared Detection," paper presented at IRIS; February 3, 1958.

[19] The analysis outlined here is based on [13], in particular, Sections 1, 3–7, and Appendix A. These sections can be read independently of the information theory aspects of the article; the latter has been superseded by [24].
[20] G. K. Wertheim, "Carrier lifetime in indium antimonide," *Phys. Rev.*, vol. 104, pp. 662–664; November, 1956. Also Bemski [6].
[21] F. L. Lummis and R. L. Petritz, "Noise-time constant, and Hall studies on lead sulfide photoconductive films," *Phys. Rev.*, vol. 105, pp. 502–508; January, 1957.
[22] O. Simpson and C. Hilsum, "The design of single-crystal infrared photocells," *Proc. IRIS*, vol. 3, pp. 115–120; September, 1958. P. W. Kruse, "Indium antimonide photoelectromagnetic infrared detector," *J. App. Phys.*, vol. 30, pp. 770–778; May, 1959.
[23] R. L. Petritz and I. Stiglitz, "Improved Use of Infrared Detectors by Methods Suggested by Information Theory," paper presented at IRIS; January 6, 1959. ("Statistics of Signal Detection," to be published.)
[24] R. L. Petritz, "Information theory of the performance of radiation detectors," *Proc. IRIS*, vol. 2, pp. 18–34; June, 1957.
[25] For the definition of D* see R. C. Jones, "Phenomenenological description of the response and detecting ability of radiation detectors," paper 4.1.1, this issue, p. 1481. Also Jones' paper, "Methods of rating the performance of photoconductive cells," *Proc. IRIS*, vol. 2, pp. 9–12; June, 1957.
[26] A. Rose, "A unified approach to the performance of photographic film, television pickup tubes, and the human eye," *J. Soc. Mot. Pict. Engrs.*, vol. 47, pp. 273–294; October, 1946. H. C. Torrey and C. A. Whitmer, "Crystal Rectifiers," McGraw-Hill Book Co., Inc., New York, N. Y., ch. 2; 1948.
[27] R. C. Jones, "Quantum efficiency of photoconductors," *Proc. IRIS*, vol. 2, pp. 13–17; June, 1957; "Quantum efficiency of detectors for visible and infrared radiation," in "Advances in Electronics and Electron Processes," vol. 11; 1959 (in press). Also [25], this issue.
[28] R. A. Smith, F. E. Jones, and R. P. Chasmar, "The Detection and Measurement of Infrared Radiation," Oxford University Press, Oxford, Eng., ch. 3; 1957.
[29] R. DeWaard and E. M. Wormser, "Description and properties of various thermal detectors," paper 4.1.3, this issue, p. 1508.
[30] A. L. Schawlow and C. H. Townes, "Infrared and optical masers," *Phys. Rev.*, vol. 112, pp. 1940–1949; December, 1958.

Paper 3.3.2

Infrared Photoemission*

G. A. MORTON, FELLOW, IRE†

PHOTOEMISSION is used as the basis of many devices which operate in the near infrared portion of the spectrum. The image tube (1P25) illustrated in Fig. 1, which was the essential component of the Sniperscope and Snooperscope used in World War II,[1] is an example of such a device. The infrared sensitive photocathode of this type of image tube is a sensitized semitransparent film of silver-oxygen-cesium on the optically-polished end-window of the tube. Radiation reaches this sensitive surface through the glass window and electrons are emitted from the other side into the vacuum within the tube and electrostatically focused onto the phosphor viewing screen. Opaque infrared sensitive photocathodes can also be formed using activated silver-oxygen-cesium layers very similar to those used as semitransparent cathodes. Such opaque cathodes are frequently employed in phototubes, certain types of photomultipliers, and similar devices.

The silver-oxygen-cesium photocathode was one of the first to be found which had sufficient sensitivity to long wavelength radiation to be useful for practical devices operating in the visible portion of the spectrum. Its application to phototubes was first described by Koller[2] in 1929 and, until the mid-1930's, was virtually the only cathode used for the detection of visible light.

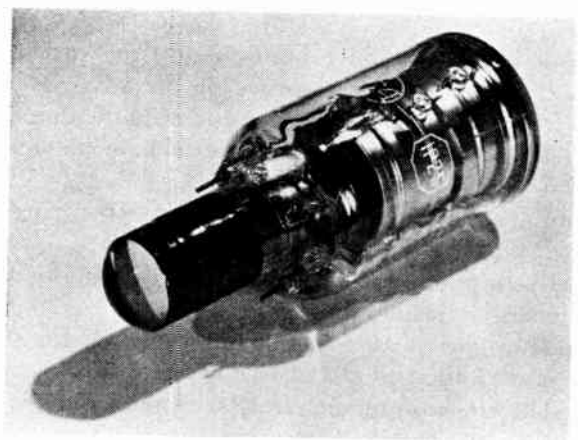

Fig. 1—The 1P25 image tube.

One procedure for preparing silver-oxygen-cesium photocathodes may be briefly described as follows.

Silver is evaporated in a thin film over the area to be activated. This silver is oxidized by means of a glow discharge in oxygen at a pressure of about 1 mm Hg. The surface is then exposed to cesium vapor and then baked at about 200°C. Further improvement in sensitivity can be obtained, as was pointed out by Asao and Suzuki,[3] by evaporating a small amount of Ag onto the

* Original manuscript received by the IRE, June 26, 1959.
† RCA Labs., Princeton, N. J.

[1] G. A. Morton and L. E. Flory, "An infrared image tube and its military applications," *RCA Rev.*, vol. 7, pp. 385–413; September, 1946.

[2] L. R. Koller, "Some characteristics of photoelectric tubes," *J. Opt. Soc. Am.*, vol. 19, pp. 135–145; 1929.

[3] S. Asao and M. Suzuki, "Improvement of thin film cesium photoelectric tubes," *Proc. Phys. Math. Soc. Japan*, vol. 12, pp. 247–250; 1930.

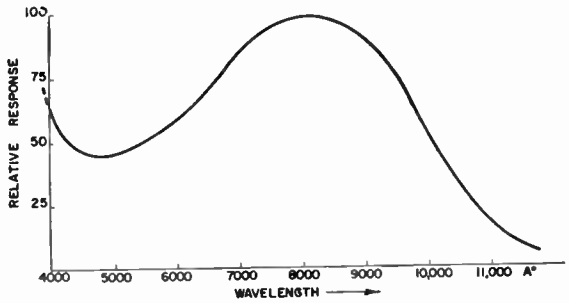

Fig. 2—Spectral response of the silver-oxygen-cesium photocathode.

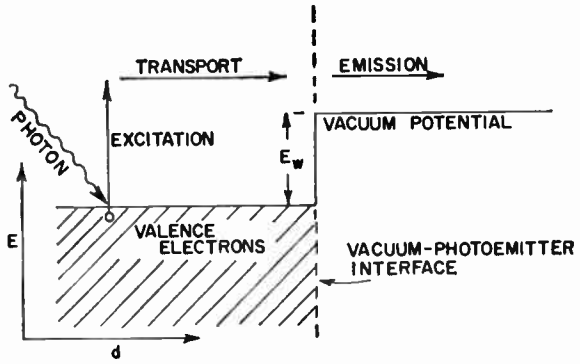

Fig. 3—Basic photoemission.

cesiated surface and subjecting it to additional thermal treatment.

The spectral response of the silver-oxygen-cesium cathode (designated by RETMA as Type S1) is shown in Fig. 2. The response has a minimum in the green portion of the spectrum and rises to a maximum between 0.8 and 0.9 microns from which it decreases to a practical threshold between 1.2 and 1.3 microns. At its maximum in the red, the quantum efficiency of this cathode is in the neighborhood of 1 per cent. Beyond 1-micron, the quantum efficiency falls exponentially with the reciprocal wavelength. With the aid of very sensitive measuring equipment, a well-activated silver-oxygen-cesium cathode shows some response out as far as 2 microns.[4]

Three hypotheses have been brought forward to account for the infrared response of the silver-oxygen-cesium photocathode. In order to evaluate these hypotheses, it is necessary to examine them in the light of present photoemitter theory.

Photoemission may be thought of as involving the following three steps:[5]

1) Excitation of an electron by the absorption of the energy of a photon.
2) Transport of the excited electron from the point of excitation to the surface of the emitter.
3) The emission of the electron through the surface potential barrier at the interface between emitter and vacuum.

This may be represented diagrammatically as shown in Fig. 3. In this figure, which represents a metallic emitter, energy is plotted vertically and distance horizontally. The shaded area represents the distribution of valence electrons (*e.g.*, in a metal). E_w, which is the energy difference between the top of the electron distribution and the potential barrier into the vacuum space, is the minimum energy an electron must have if it is to be emitted.

When a photon which enters the material is absorbed by an electron, it gives up an amount of energy which

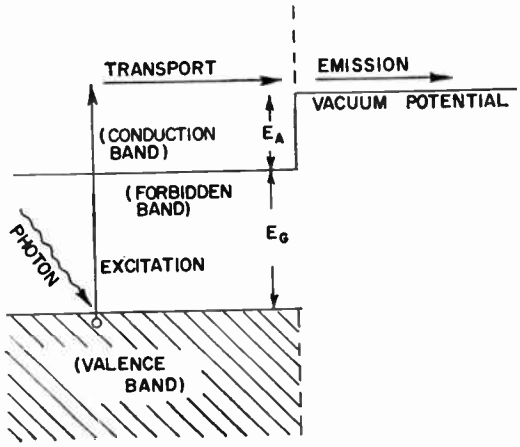

Fig. 4—Semiconductor photoemission.

is expressed by the Einstein relation $h\nu = hc/\lambda = E$. As has already been pointed out, emission can only occur when this energy E is greater than E_w. Therefore, any given photoemitter will have a long wavelength limit given by $\lambda_m = hc/E_w$.

If the excitation occurs at some distance within the emitter, a further condition must be satisfied, namely, that the loss of energy during transport between the point of excitation and the surface must be small enough so that when the electron reaches the surface, it still has an energy greater than E_w and can be emitted. This is a very important consideration and unless it is satisfied, the quantum efficiency of the emitter will be small inasmuch as only those electrons excited very near the surface can escape, while the majority of photons will be absorbed at depths too great to be effective in producing photoemission. This, together with optical reflection loss, is the reason why metals in general are poor emitters.

All efficient photoemitters are semiconductors. A characteristic of a semiconductor is that the valence electrons completely fill the valence band as indicated in Fig. 4. Between the valence band and the conduction band, there is a forbidden energy region in which (in the absence of impurities) electrons cannot exist. In the diagram, this forbidden gap is designated as E_G. The potential of the space surrounding the photoemitter is above that of the bottom of the conduction band by an

[4] "Study of Photoemissive Surfaces," ERDL Contract DA44-009-eng-2515.

[5] W. E. Spicer, "Photoemissive, photoconductive and optical absorption studies of alkali-antimony compounds," *Phys. Rev.*, vol. 112, pp. 114–122; 1958.

amount E_A. This energy difference is known as the electron affinity.

For photoemission to occur, the excited electrons must receive from the absorbed photons an energy equal to or greater than E_G+E_A. If the energy E_G of the forbidden band is greater than the electron affinity, an electron excited within the material to an energy only slightly greater than E_G+E_A can move through the material to its surface with only a small loss of energy. This is because electrons cannot exist in the forbidden band, and therefore the smallest amount of energy which can be accepted by a valence electron is E_G. An electron having the energy E_G+E_A does not have energy enough to give up an amount of energy E_G to another valence electron. During the transport there will be, of course, some loss of energy by the electrons moving through the material because of phonon and impurity scattering. However, this loss is relatively small so that semiconductors with small electron affinities may be very efficient photoemitters.

Examples of efficient semiconductor photoemitters are cesium antimonide (Cs_3Sb) photocathodes[6] and trialkali (Na_2KSb:Cs) photocathodes.[7] The forbidden band energy E_G, electron affinity and long wave limit of these emitters are:[5]

	E_G (ev)	E_A (ev)	λ_m
Cs_3Sb	1.6	0.45	6000 A
Na_2Ksb:Cs	1.0	0.55	8000 A.

The semiconductor in silver-oxygen-cesium cathodes is cesium oxide. Absorption measurements indicate that the band gap for this semiconductor is $E_G=2$ ev.[8] Even with an electron affinity $E_A=0$ volts, the intrinsic long wave limit would be about 4000 A. This satisfactorily accounts for the rise in the response of the silver-oxygen-cesium cathode at short wavelengths, but does not explain the infrared response.

The first model to be suggested attributes the infrared response to a surface layer of cesium which is partially polarized by the complex underlying material.[9] Recent experimental work which shows that infrared sensitivity is not found in very thin layers of silver-oxygen-cesium throws doubt on this explanation, but does not rule it out completely.[4] A second explanation is that the infrared emission is from colloidal particles of silver embedded in a cesium oxide matrix.[10] Electrons from the silver are emitted into the conduction band of the semiconductor and through it to the surface of cathode. The nearly uniform optical absorption of the material on the long wavelength side of the absorption edge of the semiconductor is a strong argument in favor of this explanation. Finally, the infrared response may be due to silver as a donor-type impurity in the cesium oxide semiconductor.[11] Donor levels 0.5 to 0.7 ev below the conduction band, together with the known very low electron affinity of the material, could readily account for its long wave response.

Active research is in progress, not only in this country but also in many others, directed both toward obtaining a better understanding of this type of photoemission and toward finding better long wavelength sensitive materials.

In view of the advances in the understanding of the phenomenon of photoemission as a result of the investigations made in the last few years, there is every reason for optimism for the possibility of greatly improved infrared photoemitters.

Acknowledgment

The author wishes to express his appreciation of the assistance given him by Dr. A. H. Sommer and Dr. W. E. Spicer in the preparation of this review.

[6] P. Goerlich, "On composite transparent photocathodes," *Z. Physik*, vol. 101, pp. 335–342; 1936.
[7] A. H. Sommer, "New photoemissive cathodes of high sensitivity," *Rev. Sci. Instr.*, vol. 26, p. 725; 1955.
[8] J. H. deBoer, "Electron Emission and Adsorption Phenomena," Cambridge University Press, Cambridge, Eng.; 1935.
[9] P. G. Borzyak, V. F. Bibik and G. S. Krameranko, "Distinctive characteristics of the photoeffect in Cs-O-Ag photocathodes," *Bull. Acad. Sci. USSR Phys. Ser.*, vol. 20, p. 1039; 1956.
[10] W. E. Spicer, private communication.
[11] J. E. Davey, "Thermionic and semiconducting properties of (Ag)-Cs_2O, Ag, Cs," *J. Appl. Phys.*, vol. 28, pp. 1030–1034; 1957.

Paper 3.3.3

Thermal Radiation Detectors*

R. DE WAARD† AND E. M. WORMSER†

INTRODUCTION

PREVIOUS sections have reported on detectors exhibiting various photo effects. The spectral response of these detectors is limited and generally not uniform. In thermal detectors, on the other hand, the radiant energy is absorbed in a thin blackened surface causing a minute rise in temperature in the blackened surface. Methods of blackening are such as to result in thermal detectors of uniform spectral responsivity throughout the spectral regions of principal interest, *i.e.*, from the visible to beyond 15 microns in the infrared.

Various physical phenomena are utilized to detect the minute rise in temperature in the thin blackened surface and to transduce this thermal energy into a corresponding electrical signal. Detectors utilizing these phenomena are described in the following sections. Also, elsewhere in this issue, various types of thermal radiation detectors are described in detail by the authors,[1] with emphasis on their systems applications.

THERMOELECTRIC DETECTORS

An electromotive force is generated at the junction of certain dissimilar metals or semiconductors in contact with a thin black absorbing foil as the temperature is changed. Since the thermal junction is of low resistance, a transformer is employed to couple the output to a conventional vacuum-tube circuit.

PNEUMATIC DETECTORS

A closed volume of gas is in close contact with the thin, blackened, absorbing membrane. The gas expands due to the temperature rise in the absorbing membrane. A flexible metallic membrane is distended by the gas expansion. The flexible metallic membrane may form one side of a condenser microphone which is in a suitable detection circuit. Alternately, the curvature of the flexible metallic membrane may be detected by an optical amplifying system which, in turn, modulates the light received by a photocell. The output from the photocell is amplified in a conventional manner.

BOLOMETER DETECTORS

In bolometer detectors, a thin strip of metal having a large positive change of resistance with temperature, or a thin strip of semiconductor having a large negative change of resistance with temperature, is placed in intimate contact with the thin, blackened surface. In bolometer detectors, in fact, the black-absorbing coating is usually applied directly to the thin bolometric strip. The minute change in temperature causes a small change in resistance in the bolometric strip. A dc polarizing voltage is applied across the bolometric strip to detect the change of resistance as a corresponding change in the polarizing voltage.

* Original manuscript received by the IRE, June 26, 1959.
† Barnes Engineering Co., Stamford, Conn.
[1] R. De Waard and E. M. Wormser, "Description and properties of various thermal detectors," paper 4.1.3, this issue, p. 1508.

Paper 3.3.4

Film-Type Infrared Photoconductors*

R. J. CASHMAN†

Introduction

PHOTOCONDUCTIVITY was first observed and correctly interpreted in 1873 by Smith.[1] Selenium rods, which served as high-resistance elements in circuits designed for testing long submarine cables, were found to decrease in resistance in the presence of light. Smith's discovery provided a fertile field of investigation for several decades, though most of the effort was of doubtful quality. By 1927, over 1500 articles and 100 patents had been listed on photosensitive selenium.[2] Selenium has a spectral response which extends slightly into the infrared to about 9000 A.

The first infrared photoconductor of high responsivity was developed by Case in 1917. He discovered that a substance composed of thallium and sulfur exhibited photoconductivity.[3] Later he found that the addition of oxygen greatly enhanced the response.[4] During the next fifteen years, many laboratories throughout the world engaged in research on photoconductivity and related phenomena.[5] In spite of all this activity, certain undesirable characteristics persisted in photoconductors. Instability of resistance in the presence of light or polarizing voltage, loss of responsivity due to overexposure to light, high noise, sluggish response and lack of reproducibility seemed to be inherent weaknesses. About 1930, the appearance of the Cs-O-Ag phototube, with its more stable characteristics, discouraged to a great extent further development of photoconductive cells until about 1940.

During World War II, the thallous sulfide cell was subjected to intensive development in the United States,[6] and its former shortcomings were largely overcome. Moreover, the detectivity was increased by almost two orders of magnitude. The cell was extensively used in communication and identification systems.[7-9]

Lead-sulfide photoconductors were brought to the manufacturing stage of development in Germany about 1943. They were first produced in the United States at Northwestern University in 1944[10] and, in 1945, at the Admiralty Research Laboratory in England.[11] Since the war, there has been extensive work on these cells and also on lead-selenide and lead-telluride types in the United States and other countries throughout the world.

Other substances which in film form at room temperature show infrared response in the 1- to 2-micron region include Ag_2S, MoS_2, In_2S_3, Bi_2S_3, SnS, In_2Se_3, and In_2Te_3. A great many films of other materials exhibit photoconductivity when cooled.[12] To date, none of these has shown as much promise as the lead-salt photoconductors.

Processing of Photoconductive Films

Thallous sulfide and lead telluride films are prepared by vacuum evaporation onto an insulating substrate, generally glass. Lead-sulfide and lead-selenide films may be prepared by vacuum evaporation[10,12,13] and also by chemical deposition.[13] Lead sulfide films are deposited chemically from a solution of lead acetate and thiourea made basic with sodium hydroxide. Lead selenide films may be deposited chemically from a solution of lead acetate and selenourea. In both methods, oxygen plays a role in producing a photoconductive film. This is accomplished in the evaporation method by controlled oxygen pressures and elevated substrate temperatures during film formation, or by oxygen-temperature treatments after the film is formed. In the chemical method, oxygen or oxygen-containing compounds are trapped in the polycrystalline film during film deposition. Subsequent baking in oxygen or vacuum may optimize the sensitization process.

* Original manuscript received by the IRE, June 26, 1959.

† Northwestern University, Evanston, Ill.

[1] W. Smith, "The action of light on selenium," *J. Soc. Tel. Engrs.*, vol. 2, p. 31; 1873.

[2] M. F. Doty, "Selenium, List of References, 1817–1925," New York Public Library, New York, N. Y.; 1927.

[3] T. W. Case, U. S. Patent No. 1,301,227; April 22, 1919.

[4] ———, U. S. Patent No. 1,316, 350; September 16, 1919.
———, "The thalofide cell—a new photoelectric substance," *Phys. Rev.*, vol. 15, p. 289; 1920.

[5] F. C. Nix, "Photoconductivity," *Rev. Mod. Phys.*, vol. 4, p.723; 1932.
R. J. Cashman, "Development of Sensitive Thallous Sulfide Photoconductivity Cells for Detection of Near Infrared Radiation," OSRD 1325, PB 27332; March 17, 1943. Available from Office of Technical Services, U. S. Dept. of Commerce, Washington, D. C. This report contains 176 references to photoconductors and related phenomena.

[6] R. J. Cashman, "Development of Stable Thallous Sulfide Photoconductive Cells for Detection of Near Infrared Radiation," OSRD 5997, PB 27354; October 31, 1945. Available from Office of Technical Services, U. S. Dept. of Commerce, Washington, D. C.
———, "Photodetectors for ultraviolet, visible and infrared radiation," *Proc. NEC*, vol. 2, p. 171; 1946.
———, "New photoconductive cells," *J. Opt. Soc. Am.*, vol. 36, p. 356; 1946.
U. S. Patent Nos. 2,448,517 and 2,448,518; September 7, 1948.

[7] J. M. Fluke and N. E. Porter, "Some developments in infrared communications components," PROC. IRE, vol. 34, pp. 876–883; November, 1946.

[8] W. S. Huxford and J. R. Platt, "Survey of near infrared communication systems," *J. Opt. Soc. Am.*, vol. 38, p. 253; 1948.

[9] V. K. Zworykin and E. G. Ramberg, "Photoelectricity and Its Applications," John Wiley and Sons, Inc., New York, N. Y., ch. 3; 1949.

[10] R. J. Cashman, "Development of Sensitive Lead Sulfide Photoconductive Cells for Detection of Intermediate Infrared Radiation," OSRD 5998, ATI 25740; October 31, 1945. Available from ASTIA Document Service Center, Dayton 2, Ohio. U. S. Patent No. 2,448,516; September 7, 1948.

[11] L. Sosnowski, J. Starkiewicz and O. Simpson, "Lead sulfide photoconductive cells," *Nature*, vol. 159, p. 818; 1947.

[12] R. A. Smith, F. E. Jones, and R. P. Chasmar, "The Detection and Measurement of Infrared Radiation," Oxford University Press, Oxford, Eng., p. 137; 1957.

[13] T. S. Moss, "Lead salt photoconductors," PROC. IRE, vol. 43, pp. 1869–1881; December, 1955.

Film Structure

The films formed by either of the above processes are of the order of 1 micron thick and consist of a composite of microscopic crystallites. X-ray and electron diffraction studies indicate that the crystallites have dimensions of the order of 0.1 micron and are separated by intercrystalline barriers of the order of 10 A thick. For the lead-salt films, the barriers are oxidation products such as PbO and $PbO \cdot PbSO_4$.

Role of Oxygen

Optical absorption[14] and electrical conductivity[15] measurements on single crystals of the lead salts have shown that the energy gap of the single crystal corresponds to the long wavelength limit of photoconductivity of the film. Thus, the photoelectric process in which free carriers are generated by absorption of photons involves a main-band transition in which an electron is raised from the full band to the conduction band, thereby leaving a hole in the full band. The role that oxygen plays in the photoconductive process therefore must be found in the recombination of charge carriers. Recombination processes are discussed generally in terms of the carrier lifetime of importance.[13,16-18] Three models will be discussed briefly.

In the *intrinsic-carrier model*,[16] oxygen acts as a *p*-type compensator impurity to balance the *n*-type impurities in the film. Both the lifetime and the number of free holes and electrons are equal. Recombination occurs between electrons and holes either directly or via recombination centers. Maximum response is obtained by minimizing the electron and hole densities by compensation and by maximizing the lifetime of hole-electron pairs.

The *minority-carrier model*[16,19] visualizes the film as a composite of microscopic *n-p-n* junctions. The crystallites are *n*-type with a thin layer of *p*-type material in between, presumably produced by the oxidation treatment. Barrier modulation plays an important role in this model. The diffusion of minority carriers across the *p-n* junctions results in lowering the space-charge barrier at the junction, thereby allowing more current to flow across the junction. This sort of secondary amplification is similar to *p-n* hook multiplication in a *p-n-p-n* junction transistor. A long minority-carrier lifetime and a low minority-carrier charge density are again necessary for high responsivity.

The *majority-carrier model*[20,21] depends on the presence of minority-carrier traps in the film which are due to oxygen or oxygen-containing molecules. The traps may be of either the surface or the bulk type. The free-minority carrier created initially by the photon, when trapped, leaves the majority carrier free to conduct. The increase in the majority-carrier lifetime is proportional to the time the minority carrier spends in the trap. High responsivity is obtained by optimizing the ratio of the majority-carrier lifetime to the majority-carrier density. Secondary amplification is also possible through lowering of the intercrystalline-barrier potential by the trapped minority carriers.

Many of the properties of photoconducting films have been explained by the last two models. It is not unlikely that both these processes and also possibly other mechanisms are present in the various photoconductive films.

Spectral Response

One of the most important characteristics of a photodetector is its spectral response. Fig. 1 shows the absolute spectral response of thallous sulfide, lead sulfide,[22] lead selenide,[23] and lead telluride[23] films at room temperature. In agreement with recent practice,[24]

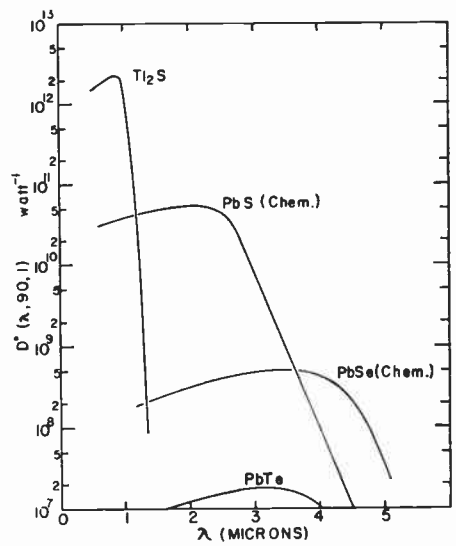

Fig. 1—Absolute spectral response of some infrared photoconductors at room temperature.

[14] W. Paul, D. A. Jones and R. V. Jones, "Infrared transmission of galena," *Proc. Phys. Soc. B*, vol. 64, p. 528; 1951.
M. A. Clark and R. J. Cashman, "Transmission and spectral response of PbS, PbSe and PbTe," *Phys. Rev.*, vol. 85, p. 1043; 1952.
A. F. Gibson, "The absorption spectra of single crystals of PbS, PbSe and PbTe," *Proc. Phys. Soc. B*, vol. 65, p. 378; 1952.

[15] W. W. Scanlon, "Interpretation of Hall effect and resistivity data in PbS and similar binary compound semiconductors," *Phys. Rev.*, vol. 92, p. 1573; 1953.

[16] A. Rose, E. S. Rittner, and R. L. Petritz in "Photoconductivity Conference," John Wiley and Sons, Inc., New York, N. Y.; 1956.

[17] A. Rose, "Performance of photoconductors," PROC. IRE, vol. 43, pp. 1850–1869; December, 1955.

[18] J. N. Humphrey and R. L. Petritz, "Photoconductivity of lead selenide," *Phys. Rev.*, vol. 105, p. 1736; 1957.

[19] J. C. Slater, "Barrier theory of photoconductivity of PbS," *Phys. Rev.*, vol. 103, p. 1631; 1956.

[20] R. H. Harada and H. T. Minden, "Photosensitization of PbS films," *Phys. Rev.*, vol. 102, p. 1258; 1956.

[21] R. L. Petritz, "Theory of photoconductivity in semiconductor films," *Phys. Rev.*, vol. 104, p. 1508; 1956.

[22] R. F. Potter and D. H. Johnson, "The Status of the Uniformity of Photodetectors in the U.S.A.," presented at 2nd Annual Natl. IRIS Meeting, Boston, Mass.; September 17, 1958.

[23] H. Levinstein, W. Beyen, P. Bratt, W. Engeler, L. Johnson, and A. MacRae, "Infrared Detectors Today and Tomorrow," presented at 2nd Annual Natl. IRIS Meeting, Boston, Mass.; September 17, 1958.

[24] R. C. Jones, "Phenomenological description of the response and detecting ability of radiation detectors," paper 4.1.1., this issue, p. 1495.

the detectivity D^* has been plotted as ordinate ($D^* = (A\Delta f/1\ \text{cm}^2 \cdot 1\ \text{cps})^{1/2} \cdot 1/\text{NEP}$, where A is the sensitive area, Δf is the amplifier bandwidth, and NEP is the noise equivalent power). The quantities in parenthesis (λ, 90, 1) refer to the test conditions; λ refers to monochromatic detectivity; 90, to the chopping frequency in cycles per second; 1, to the amplifier bandwidth in cycles per second.

Lead sulfide cells are now available from a number of manufacturers, and the spectral response may vary somewhat from that shown in Fig. 1. The peak detectivity may be higher by about a factor of 5 than that shown, but may be lower at 4 microns by a factor of 10 or more. Evaporated lead-sulfide films show greater variations in their spectral responses than do the chemically-deposited types.

The absolute spectral response of some cooled photoconducting films is shown in Fig. 2. The detectors are liquid nitrogen cooled, except for the lead selenide evaporated layer which is cooled with a dry-ice-alcohol mixture. This type of film is thinner than is used ordinarily and has a smaller long-wavelength cutoff than the chemically-deposited type of lead-selenide film[23] shown. The two curves for lead telluride films[23] give an indication of the "spread" in response to be expected among these detectors. The 900-cps chopping frequency used for these data is approximately the frequency which gives an optimum signal-to-noise ratio and hence optimum detectivity.

Lead sulfide cells from different sources may show considerable variation in their spectral response characteristics when cooled. This is due in part to the fact that a cell processed to give optimum detectivity at room temperature may not have the optimum detectivity possible when operated at dry-ice or liquid-nitrogen temperatures. Conversely, a cell processed to give optimum detectivity at dry-ice or liquid-nitrogen temperature may have a poor detectivity when operated at room temperature. When cooled-type lead-sulfide cells are so processed, their peak detectivity at dry-ice or liquid-nitrogen temperatures does not differ greatly from that of the uncooled cell of high detectivity shown in Fig. 1. The position of the peak and the long wavelength tail, however, shift to longer wavelengths as the temperature is lowered. If the wavelength is expressed in electron volts, the shift is about 4×10^{-4} ev/°C. The detectivity D^* of a liquid-nitrogen cooled cell may be as high as 10^{10} cm/watt at 4 microns or 100 times greater than that of the uncooled cell.

Time Constant

The speed of response of a photodetector is determined in two ways. The first consists of exposing the detector to square-wave radiation pulses and observing the rise and decay of the signal. The second consists of varying the chopping frequency of the incident radiation and observing the resulting changes in the signal. If the rise and decay are exponential and can be represented by a single time constant, τ, the two methods agree and the dependence of the signal S on the frequency, f, is given by the relation: $S = S_0(1 + 4\pi^2 f^2 \tau^2)^{-1/2}$. By observing the frequency, f_1, at which the signal voltage drops 3 db, one can obtain τ from the relation: $2\pi f_1 \tau = 1$. For the fast detectors ($\tau = 1$ to 10 μsec), this method may not be feasible due to the difficulty of modulating sources at high frequency. Some detectors, particularly cooled types, may exhibit more than one time constant, in which case the above expression for S is not valid.

The time constant of thallous-sulfide cells varies from about 300 μsec to 1 msec. The rise time is generally about one-half the decay time. Chemically-prepared PbS cells with a spectral response similar to that shown in Fig. 1 have a response time of 150–500 μsec. The rise time is generally faster than the decay time. Evaporated types are generally faster, ranging from 10 to 150 μsec. These are commonly used in motion picture sound reproduction.[25] Uncooled PbSe cells, both chemically-deposited and evaporated, and uncooled PbTe cells are very fast with time constants in the 1–10-μsec range.

Dry-ice-cooled evaporated PbSe cells with a spectral response like that shown in Fig. 2 have a 10–20-μsec time constant. Liquid nitrogen-cooled PbSe and PbTe cells generally exhibit two time constants and sometimes more. There is a fast component of 10–30 μsec and a slow component of the order of a millisecond. The most desirable of these cells are those in which the slow component contributes only a small percentage to the signal. The time constant of the PbTe detectors also frequently exhibits a wavelength dependence. The response to wavelengths of 1.5 μ and shorter is slower than for the longer wavelengths. Cooled PbS cells have time constants ranging from about 0.5 to 3.0 msec.

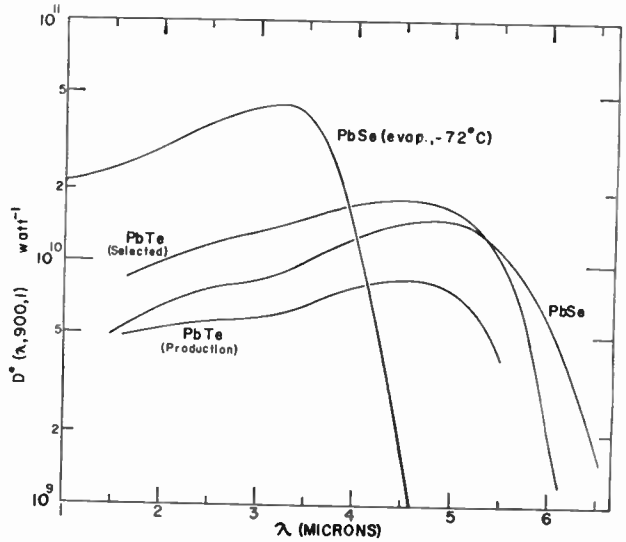

Fig. 2—Absolute spectral response of some cooled infrared photoconductors. The lead-telluride and chemical lead-selenide cells are cooled to −195°C.

[25] R. J. Cashman, "Lead sulfide photoconductive cells for sound reproduction," *J. Soc. Mot. Pic. Engrs.*, vol. 49, p. 342; 1947.

Noise

Present-day thin-film photoconductors exhibit several types of noise. These include Johnson or Nyquist noise, current noise which is of two types, flicker and generation-recombination noise, and radiation noise.

Johnson noise may often be made unimportant in practice by increasing the polarizing current until current noise predominates. Flicker noise is generally of the 1/f type, in which the noise power varies inversely with frequency. For some detectors, the noise power varies less rapidly than 1/f. Generation-recombination noise, which is due to fluctuations in the number of charge carriers in the crystallites, has the same frequency dependence as the signal response. Radiation noise, due to fluctuations in the rate of emission and absorption of background radiation, and which sets a fundamental limit on detectivity, provides one of the mechanisms by which generation-recombination noise is produced. The responsivity of thin-film photoconductors has not developed to the point where radiation noise overrides the other sources of noise.[26]

Thallous-sulfide and lead-telluride detectors exhibit a 1/f noise-power spectrum as do most evaporated lead-sulfide types. Chemically-deposited lead-sulfide cells generally are dominated by 1/f noise below 100 cps and by generation-recombination noise at higher frequencies. Chemically-deposited lead-selenide detectors have a noise power which decreases with increasing frequency but generally not as rapidly as 1/f. Occasionally the noise behavior is similar to that of chemically-deposited lead-sulfide detectors. Evaporated lead-selenide detectors are dominated at low frequencies by 1/f noise and by generation-recombination noise at higher frequencies.[27] Noise data for a detector of this type are shown in Fig. 3.

A quantitative expression may be derived for generation-recombination noise based on shot-noise theory and a one-carrier model.[28] If Ns is the ratio of generation-recombination noise power to thermal or Johnson noise power, then

$$Ns = \frac{e}{kT}\left(\frac{V}{d}\right)^2 \frac{\mu\tau}{1 + 4\pi^2 f^2 \tau^2}$$

where V is the potential difference applied across the detector, d is the electrode spacing, μ the charge carrier mobility and τ the carrier lifetime. The Hall mobility of photoconducting PbSe films has been measured[29] and at room temperature has the value of 10 cm²/volt sec. The carrier lifetime is taken as the measured time constant of these films which is 1 microsecond at room temperature. Substitution of values in the above equation gives a value of 15 for the noise-power ratio, which is in good agreement with the experimental value shown in Fig. 3. The agreement is probably somewhat fortuitous as the model is probably over-simplified. Moreover, experimental values may be as low as 3 for "quiet" cells and as high as 100 for "noisy" cells. The validity of the frequency dependence could not be determined at high frequencies because of equipment limitations.

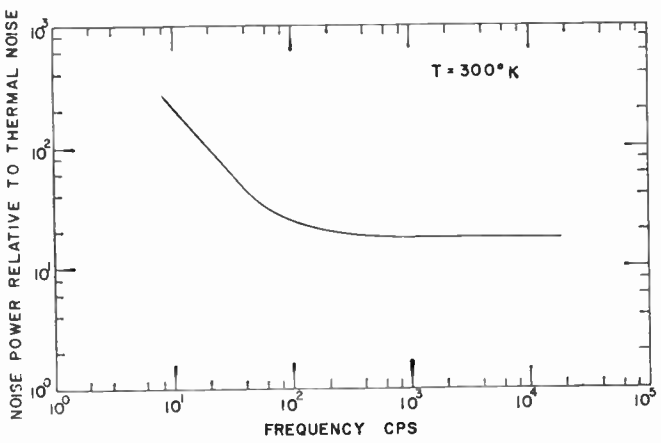

Fig. 3—Noise-power spectrum of an evaporated lead-selenide photoconductor.

Resistance

Uncooled lead-sulfide and evaporated lead-selenide cells have dark resistances of around 1 megohm, while chemically-deposited lead-selenide cells have values of about 50,000 ohms. Thallous-sulfide cells range from 1 to 10 megohms in dark resistance.

Liquid-nitrogen-cooled lead-telluride cells have quite high, dark resistances—50 to 1000 megohms. At this temperature, chemically-deposited lead-sulfide cells have resistances in the range of 10 to 20 megohms; those of evaporated types are around 100 megohms, and those of chemically-deposited lead-selenide cells are 2 to 10 megohms.

Other Cell Parameters

Cell users are frequently confronted with problems which bear on other cell characteristics than those discussed. One of these is the determination of the *optimum bias voltage*. Ordinarily, the signal response and noise of a cell increase linearly with cell bias voltage until a value is reached where either the signal increases less than linearly or the noise increases more than linearly. Further increase in bias potential beyond this optimum value results in a decreased signal-to-noise ratio.

Linearity of response to intensity of irradiation is important where the cell is used in quantitative flux measurements. Distortion-free sound reproduction also requires cells with a linear response. The maximum inten-

[26] F. L. Lummis and R. L. Petritz, "Noise, time constant and Hall studies on lead sulfide photoconductive films," *Phys. Rev.*, vol. 105, p. 502; 1957.

[27] R. J. Cashman, C. R. Betz, and L. J. Rose, unpublished data.

[28] A. van der Ziel, "Shot noise in semiconductors," *J. Appl. Phys.*, vol. 24; 1953.

[29] K. G. Halvorsen, "The Hall Effect in Lead Sulfide and Lead Selenide as a Function of Temperature," Ph.D. dissertation, Northwestern University, Evanston, Ill.; 1951. (Unpublished.)

sity beyond which nonlinearity sets in is not the same for all detectors, but is less for those of high responsivity than for those of low responsivity. If a cell is operating in the nonlinear range, the output signal depends on the image spot size on the cell. Lacking actual signal vs intensity of irradiation data for a given cell, it is still possible to estimate its linear range of response if detectivity data are known. From these data, the noise equivalent intensity, NEI, may be determined for a 1-cps bandwidth. It has been found empirically that cells are linear with intensity from NEI to 10^5 NEI. For many cells the range is greater.

In operation, there is *power dissipation* in the sensitive layer of the cell due to the incoming flux and I^2R heating. The maximum-safe-power dissipation for cells operated at room temperature is generally considered to be 100 milliwatts per cm^2 of cell area. A related subject is the maximum ambient temperature allowable during storage or operation that will not cause damage to the cell. Detector manufacturers will supply information on this subject and on most of the characteristics which have been discussed. Through control of processing parameters and by selection, manufacturers are able to supply cells with a wide range of characteristics.

Paper 3.3.5

Single-Crystal Infrared Detectors Based Upon Intrinsic Absorption*

F. F. RIEKE†, L. H. DEVAUX†, AND A. J. TUZZOLINO†

UNTIL the early 1950's, the development of infrared photodetectors revolved principally around polycrystalline films of PbS, PbSe, or PbTe, deposited either by evaporation or from solution. The success of semiconductor physics based on single-crystal techniques, culminating in the invention and development of the transistor, was an incentive to apply similar methods to the development of infrared detectors.

Photodetectors based on bulk crystals of germanium were described by Shive[1] in 1950. Although his devices had attractive features, the spectral response was restricted to the region covered by the intrinsic absorption of germanium, namely, wavelengths less than 1.7 microns.

It was evident that to develop a detector with response extending farther into the infrared, it would be necessary either 1) to "sensitize" Si or Ge to the infrared by introducing impurities that were normally unionized, but could be ionized by low-energy quanta, or 2) to employ a semiconductor with an energy gap considerably smaller than that of germanium.

Approach 1) has resulted in the development of the doped-germanium family of detectors, which is described elsewhere in this issue. Approach 2) is the subject of the present discussion.

* Original manuscript received by the IRE, June 26, 1959.
† Chicago Midway Labs., Chicago, Ill.
[1] J. A. Shive, *Bell Lab. Rec.*, vol. 28, p. 8; 1950.

The long wavelength limit to intrinsic absorption and photoconductivity, λ_c, in a semiconductor is inversely proportional to the energy gap E_g:

$$\lambda_c E_g = 1.24 \text{ ev} \cdot \text{microns}.$$

If one, somewhat arbitrarily, sets the goal of developing a detector with response extending at least as far into the infrared as that of lead sulfide ($\lambda_c \geq 3$ microns), one requires a semiconductor with energy gap of 0.4 ev or less; the number of such semiconductors now known is small. Of these, only indium antimonide has been extensively developed.

The primary consideration in improving the performance of a detector employing photoconductive phenomena is to minimize the rate at which free carriers are generated spontaneously within the active material. This requirement applies regardless of the chemical species or physical form of the semiconductor, or of the particular mode of operation. The generation rate affects the performance in two ways. First, through its inverse corollary, the lifetime of excess carriers, it determines the magnitude of the electrical response to the photogeneration of carriers. Secondly, through its effect on fluctuations in the total number of carriers, it influences the internal noise of the detector. The two effects combine in such a way that an increased generation rate tends to decrease the attainable signal-to-noise ratio. The significance of excess-carrier lifetimes has

been emphasized by Rose[2] and by Petritz.[3] The subject of noise in photoconductors has been reviewed recently in the PROCEEDINGS.[4]

Generation of carriers occurs by way of two mechanisms, one thermal, the other optical. Thermal generation results from the transfer of energy from lattice vibrations to electrons, either within the bulk of the semiconductor or at the surface. Surface generation and recombination of carriers is particularly important in detectors that depend upon intrinsic optical absorption, which is characterized by absorption coefficients of the order of magnitude of 10^4 cm^{-1}. In consequence of this strong absorption, the photoeffects originate primarily in a shallow surface layer, at most a few microns deep, from which the excess carriers can readily diffuse to the surface. Thermal generation is catalyzed by particular kinds of impurities and imperfections and is thus subject to some measure of control in the growth of the crystal and in the preparation of its surface. It generally can be greatly reduced by lowering the temperature of the crystal, and it is usually for this reason that many detectors exhibit enhanced performance when they are cooled.

The optical generation of carriers occurs through the absorption of radiation to which the detector is sensitive, and is a necessary accompaniment to the useful sensitivity of the detector. The generation of carriers by ambient radiation, however, lowers the signal-to-noise ratio. Ambient radiation can be minimized by placing the sensitive elements within a cooled cavity having an aperture that admits radiation from only the useful field of view, but such shielding will be rather ineffective if the performance of the detector is limited by thermal generation of carriers.

The single-crystal detectors that have been developed are of three types: photoconductor, *p-n* junction, and photoelectromagnetic (PEM).

PHOTOCONDUCTOR

A photoconductive detector employing simple photoconductivity is constructed by cementing a thin section of semiconductor to a backing, and attaching current leads. The backing is important in dissipating heat generated in the sample by the bias current, which is advantageous to make as large as possible without raising the temperature of the sample unduly. If the semiconductor is to be cooled, it is placed within the vacuum space of a Dewar flask.

Photoconductive detectors using indium antimonide have been described by Avery, Goodwin and Rennie.[5] Data on the performance of a typical cell[6] is given in Table I.

Photoconductive detectors have also been made using single-crystal tellurium cooled to 77°K. A noise equivalent power of 10^{-10} watts has been obtained for 500°K blackbody radiation at 85 cps with a 5-cps bandwidth. A minimum NEP of 10^{-11} watts occurs at a wavelength of 3.5 microns with a cutoff at 4.2 microns. The detector has an area of $1\times\frac{1}{2}$ mm^2, a resistance of approximately 1000 ohms and a time constant of 30 to 50 microseconds.[7] In terms of detectivity D^*[8] we thus have:

$$D^*(500°\text{K}, 85\text{ cps}) = 1.6\times10^9\text{ cm cps}^{1/2}\text{ watt}^{-1},$$

$$D^*(3.5u, 85\text{ cps}) = 1.6\times10^{10}\text{ cm cps}^{1/2}\text{ watt}^{-1}.$$

TABLE I

CHARACTERISTICS OF COOLABLE InSb PHOTOCONDUCTIVE CELLS (SENSITIVE AREA 1.4 MM^2, TIME CONSTANT LESS THAN 4×10^{-7} SECOND)

Temperature (°K)	90	195	249	292
Cell resistance (Ω)	20 K	1.8 K	490	120
D^*(cm cps$^{1/2}$ watt^{-1}) (λ_{peak}, 800 cps)	4.5×10^9	1.7×10^9	3×10^8	1.7×10^8
Wavelength of peak sensitivity (μ)	5.6	5.6	6.2	6.7
$\lambda_{1/2}(\mu)$	5.85	6.0	6.65	7.2
Responsivity (V/w)	1300	400	30	1

P-N JUNCTION

The theory and principles of operation of *p-n* junction detectors have been discussed elsewhere.[9,10] Photosensitive junctions can be produced by methods used in transistor technology, such as growth from the melt, vapor-phase diffusion, and alloying.

Grown *p-n* junctions are formed in a single-crystal bar of semiconductor with the *p-n* junction near the center. The junction plane is perpendicular to the major axis of the bar and is illuminated near its edge. The sensitive area is a small region surrounding the intersection of the junction plane with the surface of the bar and its magnitude is given by the product of the bar width and the sum of the minority carrier diffusion lengths. Diffused junctions can be formed by producing a thin *p*-type layer on an *n*-type semiconductor. Light is incident perpendicular to the resulting junction plane. The sensitive area can be varied by protecting a portion of the *p*-layer of the size and shape desired and etching away the remaining *p*-layer. *P-n* junction detectors sensitive in the intermediate infrared region generally require cooling to relatively low temperatures (~77°K). The detector can be operated with bias (photodiode) or without (photovoltaic), depending on which mode of operation leads to higher sensitivity.

[2] A. Rose, in "Photoconductivity Conference," John Wiley and Sons, New York, N. Y., pp. 3–48; 1955.
[3] R. L. Petritz, "Title," *Ibid.*, pp. 49–77.
[4] K. M. van Vliet, "Noise in semiconductors and photoconductors," PROC. IRE, vol. 46, pp. 104–118; June, 1958.
[5] D. G. Avery, D. W. Goodwin and A. E. Rennie, *J. Sci. Instr.*, vol. 34, p. 394; 1957.
[6] D. W. Goodwin, *Ibid.*, p. 368.
[7] G. Suits, private communication.
[8] D^* is defined as $\sqrt{A\Delta f}/\text{NEP}$ where the NEP is measured with bandwidth Δf, the nature of the radiation and the chopping frequency being indicated by the quantitites in parentheses.
[9] L. P. Hunter, "Handbook of Semiconductor Electronics," McGraw-Hill Book Co., Inc., New York, N. Y.; 1956.
[10] E. S. Rittner, "Photoconductivity Conference," John Wiley and Sons, New York, N. Y., p. 215; 1955.

Most of the development in the intermediate infrared region has been devoted to InSb *p-n* junctions. Detectors using grown junctions have been developed at Chicago Midway Laboratories.[11] Diffused-junction types have been developed and are manufactured by the Philco Radio Corporation and Texas Instruments, Inc. Grown-junction detectors have an inherently small sensitive area, whereas diffused-junction types can be made larger and of various shapes. The characteristics of the detectors are given in Table II.

TABLE II

Characteristics of InSb Grown- and Diffused-Junction Detectors

	CML, Grown-Junction Detector	Philco, Diffused-Junction Detector[12]	Texas Instruments Diffused-Junction Detector[13]
Temperature (°K)	77°K	77°K	77°K
Cell resistance (Ω)	22 K	50–200	1200–1500
Area (cm²)	3.2×10^{-1}	4.1×10^{-2}	4.16×10^{-2}
Time constant (μsec)	<1.8	<1	~0.1
Wavelength of peak sensitivity (μ)	5.5	5.3	5.35
D^*[14] (cm cps$^{1/2}$ watt^{-1})	9.4×10^{9} (500°K, 90 cps)	2.7×10^{9} (500°K, 800 cps)	5×10^{9} (500°K, 1000 cps)
Cutoff $\lambda_{\frac{1}{2}}(\mu)$	~5.7	~5.5	~5.5

Photoelectromagnetic (PEM) Type

The use of the PEM effect[15,16] leads to another type of single-crystal photodetector. When electrons and holes produced at the front surface of a semiconductor by light diffuse downward, a magnetic field applied perpendicular to this initial diffusion current will bend the electron and hole currents in opposite directions The resulting separation of charge gives rise to a photovoltage.

The strength of the PEM effect is determined by the product of the carrier mobility and the magnetic-field strength. For practicable magnetic fields, a semiconductor of high mobility such as InSb must be employed to achieve useful sensitivity. No bias current is required and the detector can be operated at room temperature. The detectors have been developed and manufactured by many agencies.

A typical room-temperature PEM detector made at Chicago Midway Laboratories has a peak noise-equivalent power of 8×10^{-10} watts at 6.2 microns with a cutoff wavelength at 7 microns. The detector has an area of 1.8×10^{-2} cm² and a resistance of 33 Ω. The detectivity D^*(6.2 μ, 90 cps) is thus 1.9×10^{8} cm cps$^{1/2}$ watt^{-1}. Although the time constant of the cell has not been measured directly, minority carrier-lifetime measurements indicate a value of less than 1 microsecond for the time constant.

In conclusion, we shall attempt to assess what has been done and what remains to be done. One can estimate how closely present-day intrinsic photoconductors can approach the radiation limit by introducing the noise figure, defined as the ratio of the detectivity limited by radiation fluctuations to peak detectivity. In principle, the noise figure $(NF)=(\tau^*/\tau)^{1/2}$, where τ^* is the radiation lifetime and τ is the actual lifetime.[3] Values of D^* and the noise figure of InSb and Te detectors are given in Table III.

The best cooled InSb cells have a noise figure of ten or less, and therefore the ultimate possibilities seem to have been approached. In this case, the future possibilities lie in improving design and reproducibility in manufacture. For the Te detector, the noise figure of 27 indicates that some improvement should be possible for this cooled detector. The uncooled InSb cells all have noise figures of the order of 300. For InSb at room temperature, $(\tau^*/\tau)=10$.[13] The reason for the large noise figure is not evident. It would appear that in this case a very

TABLE III

Values of D^* and the Noise Figure (NF) for InSb and Te Detectors

	Photoconductive			Photovoltaic			PEM		
	T°K	$D^*(\lambda_{peak}, 800$ cps) (cm cps$^{1/2}$ watt^{-1})	NF	T°K	D^*(5.4 μ, 90 cps) (cm cps$^{1/2}$ watt^{-1})	NF	T°K	D^*(6.2 μ, 90 cps) (cm cps$^{1/2}$ watt^{-1})	NF
InSb	90	4.5×10^{9}	10	78	2×10^{10}	5	292	1.9×10^{8}	300
	195	1.7×10^{9}	50						
	292	1.7×10^{8} (3.5 μ, 85 cps)	300						
Te	78	1.6×10^{10}	27						

[11] G. R. Mitchell, A. E. Goldberg, and S. W. Kurnick, *Phys. Rev.*, vol. 97, p. 239; 1955.

[12] M. E. Lasser, P. Cholet, and E. C. Wurst, Jr., *J. Opt. Soc. Am.*, vol. 48, p. 468; 1958.

[13] R. L. Petritz, private communication.

[14] The value of D^* for CML and Philco presented in the table is characteristic of their better detectors. The value for Texas Instruments is an average value.

[15] S. W. Kurnick and R. N. Zitter, *J. Appl. Phys.*, vol. 27, p. 278; 1956.

[16] C. Hilsum and I. M. Ross, *Nature*, vol. 179, p. 146; 1957.

great improvement in uncooled detectors is within the realm of possibility. Whether or not the same can be said for other single-crystal semiconductors must wait until results of lifetime measurements become available.

No other small-gap semiconductor has been so highly developed as InSb. There would probably not be much point in developing other materials having a cutoff wavelength ~6 microns. Detectors having cutoffs ~4 microns which might compete with PbS have not been extensively developed. The single-crystal-cooled Te detector discussed above has a cutoff at 4.2 microns, but further development on this detector will be necessary to determine whether or not it will compare with PbS. In addition, some work has been done on InAs where photoconductive, PEM, and photovoltaic responses have been reported.[17,18] Useful sensitivity is obtained out to 4 microns.

Little work has been done on intrinsic photoconductors having cutoff wavelengths ~10 microns. Some work has been done on HgTe-CdTe alloys in which appreciable sensitivity has been observed as far out as 13 microns.[19] Further development will be necessary before a comparison can be made of these intrinsic alloy detectors with the doped-Ge family of detectors.

[17] R. M. Talley and D. P. Enright, *Phys. Rev.*, vol. 95, p. 1092; 1954.
[18] C. Hilsum, *Proc. Roy. Phys. Soc. B*, vol. 70, p. 1011; 1957.
[19] W. D. Lawrence, *et al.*, *J. Chem. Phys. of Solids*, to be published.

Paper 3.3.6

Impurity Photoconductivity in Germanium*

HENRY LEVINSTEIN†

Spectral Response and Time Constant

INTRINSIC photoconductivity in Ge is produced when a photon interacts with a Ge atom producing an electron hole pair. Both electron and hole are then mobile until recombination takes place. The minimum photon energy required for the generation of hole electron pairs is 0.7 ev, and determines the long-wavelength threshold for photoconductivity ($\approx 1.8\ \mu$). When impurities are present in the Ge lattice, the energy required to free charge carriers from these impurities generally is less than that for electron-hole generation. This leads, in addition to intrinsic response, to extrinsic photoconductivity whose long-wavelength threshold depends on the type of impurity in Ge [1]. The time constant depends on the number of impurities which may act as recombination centers as well as the impurity-capture cross section. The smaller energy required for carrier excitation has the disadvantage that at room temperature, most charge carriers may be freed simply by the action of lattice vibrations, leaving none to be excited by incoming photons. This effect may be reduced by cooling the Ge, the required coolant temperature being determined by the ionization energy of the impurity. Ionization energies of a large number of impurities in Ge have been investigated [2]. Relatively few of these have been employed in the actual construction of detectors. Their selection is governed by the long-wavelength threshold required, the responsivity and time constant attainable, and the ease of preparation of the doped crystal. Fig. 1 shows the idealized spectral response curves (to constant photon flux) for Ge crystals containing various impurities and the temperature to which the detectors should be cooled.

* Original manuscript received by the IRE, June 26, 1959.
† Dept. of Physics, Syracuse University, Syracuse, N. Y.

Signal and Noise

A photoconductive detector is generally used in a circuit such as that in Fig. 2. The signal voltage V_S produced by a modulated photon flux is given by the expression

$$V_S = E \frac{R_C R_L}{(R_C + R_L)^2} \frac{G\tau}{n},$$

where E is the bias battery voltage, and R_C and R_L the detector and load resistances, respectively. G, the carrier-generation rate, depends on the incident-energy flux, the number of impurities from which charge carriers may be excited, and the probability of photon capture per impurity center. τ is the carrier lifetime and n is the number of dark carriers, which are excited thermally and by the background. When a detector is cooled to the point where the number of carriers excited thermally is small compared with that excited by background, the detector is background limited. Its signal is then relatively insensitive to variations in coolant temperature, but strongly dependent on the temperature of the background which the sensitive element "sees."

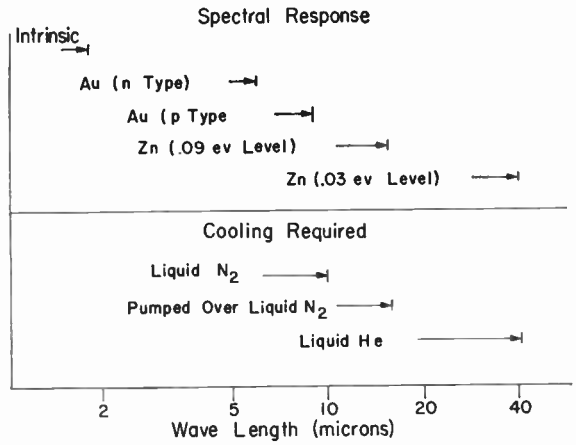

Fig. 1—Spectral coverage and cooling required for impurity photoconductivity in germanium.

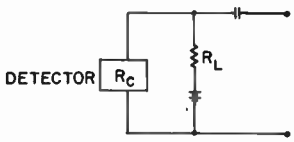

Fig. 2—Electrical circuit used with photoconductors.

This is the most desirable operating condition of a detector but not always attainable because of the limited number of coolants available between liquid N and liquid He.

The predominant types of noise found in impurity photoconductors are 1/f and generation-recombination noise. The 1/f noise appears to be due to the crystal surface and the contacts [3]. It can be reduced, and under certain conditions, virtually eliminated at frequencies above 10 cps by proper surface treatment and soldering techniques. Generation-recombination noise is determined by fluctuations in the generation and recombination rate of charge carriers and is inherent in the material. Generation-recombination noise voltage per cycle, V_n, is given by the expression [4]

$$V_n = 2E \frac{R_C R_L}{(R_C + R_L)^2} \frac{\tau^{1/2}}{n^{1/2}} \frac{1}{(1 + 4\pi f^2 \tau^2)^{1/2}},$$

where f is the frequency at which measurements are made. Other possible noise sources, such as Johnson noise, generally do not limit the performance of these detectors. The signal-to-noise ratio

$$\frac{V_S}{V_n} = \frac{G\tau^{1/2}}{2n^{1/2}}$$

appears independent of bias voltage. In practical applications, this is not the case. For low bias voltage, amplifier noise may exceed detector noise and thus limit its performance. For bias voltages which exceed specified values, noise introduced at the contacts will predominate over generation-recombination noise and limit-detector performance.

Detector Construction

Since all detectors in the Ge impurity group require cooling at least to liquid N temperature, the sensitive element must be mounted in a Dewar type container such as that shown in Fig. 3. Detectors requiring liquid He must be mounted in a double Dewar where an outer container with liquid N surrounds an inner container with liquid He. The Ge sample, which is in the form of a cube or rod, is generally soldered to a metal surface in contact with the coolant. The cooled shield surrounding the element serves a dual purpose. It reduces the background radiation which would normally strike the detector from the walls of the outer envelope, and serves to reflect back into the sensitive element those photons which have passed through the sample without being absorbed. Greater efficiency is obtained by having the inside of the shield as highly polished as possible and making its aperture as small as is permissible for the application under consideration. The choice of detector window depends on the long wavelength threshold of the detector. Sapphire is suitable for 6-μ detectors, BaF_2 and Si for 10-μ detectors, with various other materials such as AgCl for the long wavelength detectors.

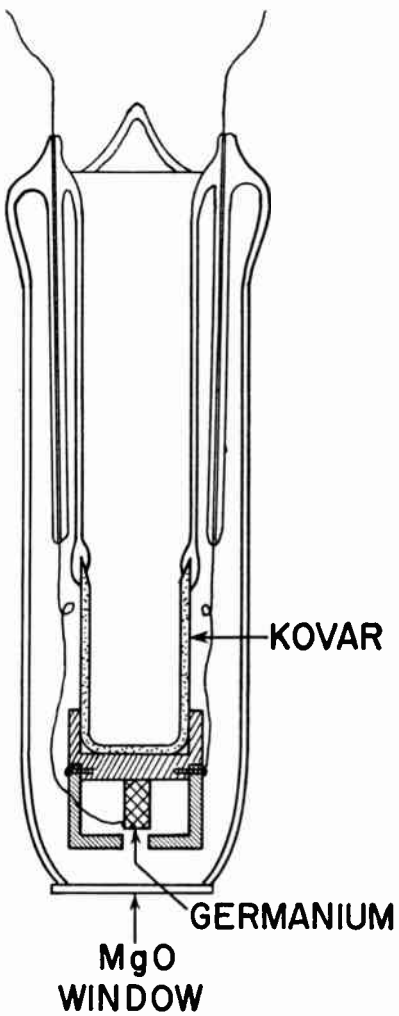

Fig. 3—Dewar mount for germanium detector.

The detector blank is generally evacuated to pressures less than 10^{-6} mm of Hg and gettered to avoid contamination of the surface and frosting of the window.

Typical Detectors

P-type Gold-Doped Germanium

The addition of gold to Ge produces a *p*-type crystal. The energy required to excite holes into the valence band, producing singly-charged negative ions, is 0.14 ev [5]–[7]. The detector thus has a long wavelength threshold at about 9 microns. The time constant is determined by the number of singly-charged gold ions where holes can recombine. This number consists of those atoms which have been ionized optically and thermally (by signal, background, and thermal excitation), and those which have captured electrons from *n*-type impurities generally present in the sample. The latter predominates at the operating temperature of the detector (80°K) producing about 10^{14} singly-charged gold ions/cc. Assuming a capture cross section (σ) of about 10^{7} cm per second, the time constant of the detector may be calculated from

$$\tau = \frac{1}{M\sigma v} = \frac{1}{10^{14} \times 10^{-14} \times 10^{7}} = \approx 0.1\ \mu\text{sec},$$

a number varying with the density of *n*-type impurities (M) but generally in agreement with measured results [8].

In the temperature range of operation (80°K), the density of dark carriers (n), is determined by thermal excitation. SNR may be increased by as much as a factor 4 when the temperature is lowered 10° below liquid N, such as is obtained by pumping on liquid N. The detector then becomes background limited and is no longer sensitive to changes in temperature. Further increases in sensitivity can only be achieved by decreasing the background radiation. This results in a smaller field of view, not always desirable. The carrier generation rate (G) for a particular photon flux depends on the concentration of gold atoms in Ge. Under normal crystal growth conditions, this number is less than 10^{16}/cc, producing less than 10 per cent absorption of the incident beam. Shaping the sensitive element and maintaining it in a highly-polished housing (integrating sphere) are two factors required to enhance the detector sensitivity.

N-type Gold-Doped Germanium

If the concentration of *n*-type impurities is equal to that of the Au, all Au centers become singly ionized. Further addition of *n*-type impurities produces doubly-charged negative Au ions and an *n*-type crystal. The energy of excitation of electrons from the doubly-charged Au ions to the conduction band is 0.2 ev, leading to a detector with a long-wavelength threshold at 6 μ. The magnitude of the signal depends on the number of doubly-charged Au ions. Since recombination of excited electrons can only take place at singly-charged Au ions, the time constant increases substantially as the number of singly-charged ions is decreased in favor of doubly-charged ions. Time constants as large as several milliseconds have been measured for detectors of this type. In actual practice, compensation is held at a point where a time constant of the order of 30 μsec at wavelengths longer than 2.3 microns is obtained [9]. Below that wavelength, the behavior is complicated by excitations and recombinations involving the valence, conduction bands and both Au states. This leads to quenching effects, and response times of the order of milliseconds under certain conditions [4]. Fig. 4 shows the absolute spectral response of the two types of Ge detectors as they are now available [10].

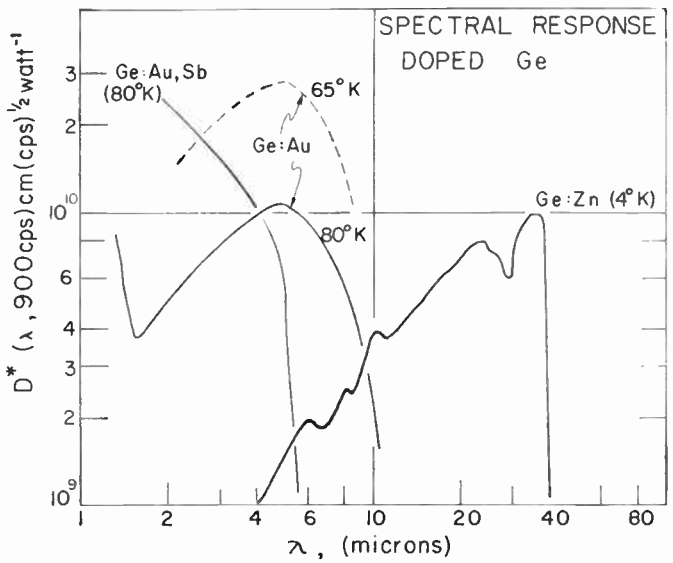

Fig. 4—Spectral response of impurity photoconductivity in germanium.

Germanium with Zinc Impurities

The addition of Zn to Ge produces *p*-type Ge. Excitation of holes requires an energy of 0.03 ev resulting in long-wavelength cutoff at 40 μ [11]. In order to avoid thermal excitation of carriers, the detector must be maintained in the temperature range of liquid He. In contrast to Au, Zn may be added in larger amounts to Ge. A large fraction of the incident photons are thus absorbed by the sensitive element, and an integration sphere is not required. Since the detector is background limited at liquid He temperature, it must be surrounded by a cooled cavity whose aperture determines the SNR of the detector. Time constants, as for *p*-type gold-doped Ge, are less than 0.1 μsec and D^* at the impurity spectral peak is in the range of that of gold-doped Ge [12].

A second type of Ge:Zn detector may be obtained when all Zn atoms in Ge become singly ionized by the addition of an equal number of *n*-type impurities. Ex-

citation of holes may then take place from the 0.09 level of Zn to the valence band, corresponding to a long-wavelength threshold at 15 μ. This type of detector has the advantage that it does not require the extreme conditions of cooling (pumped over N_2 is generally sufficient) and has D^* $(-, 900, 1)$ of the order of 10^{10}/watt [13] in the 9–13-μ atmospheric window.

Bibliography

[1] This was originally suggested by E. Burstein, at Prof. Nottingham's Photoconductivity Conference, March, 1949.
[2] For a summary, see R. Newman and W. W. Tyler, "Solid-State Physics," Academic Press, Inc., New York, N. Y., vol. 8.
[3] A. U. MacRae and H. Levinstein, *Bull. Am. Phys. Soc.*; March 30, 1959.
[4] W. Beyen, P. Bratt, H. Davis, L. Johnson, H. Levinstein, and A. MacRae, "Ge and PbTe IR Detectors," Syracyse Univ. Res. Inst. Final Report; February 1, 1957.
[5] G. Morton, Hahn and Schultz, "Phoconductivity Conference," John Wiley and Sons, Inc., New York, N. Y.; 1956.
[6] M. L. Schultz and G. A. Morton, "Photoconduction in germanium and silicon," Proc. IRE, vol. 43, pp. 1819–1828; December; 1955.
[7] W. C. Dunlop, *Phys. Rev.*, vol. 91, p. 1282; 1953; vol. 97, p. 614; 1955; vol. 100, p. 1629; 1954.
[8] J. R. Hansen, T. P. Vogl, and M. Garbuny, presented at 7th Eastern IRIS Symp.; December 3–4, 1958.
[9] M. E. Lasser and P. Chole, *J. Opt. Soc. Am.*, vol. 48, p. 468; 1958.
[10] W. Beyen, P. Bratt, H. Davis, L. Johnson, H. Levinstein, and A. MacRae, *J. Opt. Soc. Am.*, to be published.
[11] E. Burstein, J. W. Davison, E. E. Bell, W. J. Turner, and H. G. Lipson, *Phys. Rev.*, vol. 93, p. 65; 1954.
[12] G. S. Picas and S. F. Jacobs, presented at 7th Eastern IRIS Symp.; December 3–4, 1958.
[13] W. Beyen, P. Bratt, W. Engeler, L. Johnson, H. Levinstein, and A. MacRae, presented at 2nd Natl. IRIS Symp.; October, 1958.

Paper 3.3.7

Noise in Radiation Detectors*

R. CLARK JONES†

Introduction

THE kinds of noise we discuss in this paper are the kinds of electrical noise that one may find in the output of radiation detectors. The kinds of noise are distinguished by the physical source of the noise, not by any particular characteristic of the noise as measured at the output of the detector.

The discussion will be restricted to descriptions of the noise that relate to its mean-square amplitude. Other more complex measures may be used, but so far these have found little use in the application of radiation detectors.

The tool that will be used to describe the electrical noise is the power spectrum, defined as the mean-square fluctuation of the voltage (or current) about its mean value per unit frequency interval. A more general kind of spectrum is the mean-square fluctuation of Y (about the mean value $\overline{Y}$) per unit frequency interval measured in cycles per unit of X. Only when Y is a voltage or current is it appropriate to call this more general kind of spectrum a power spectrum. When Y is not a voltage or current, the term power spectrum is clearly inappropriate, and is obviously *wrong* when the variable Y is itself a power. The author recommends (and uses in this report) the name "Wiener spectrum" for the more general kind of spectrum. The name "variance spectrum" may also be used.

* Original manuscript received by the IRE, June 26, 1959.
† Res. Lab., Polaroid Corp., Cambridge, Mass.

The Power Spectrum

We use e to denote the instantaneous amplitude of a noise voltage. (The current i may be substituted for the voltage e throughout the following discussion.) The voltage is considered to be a function of the time t, where the epoch of the origin of t is supposed to be chosen arbitrarily. The mean value of $e(t)$ is supposed to be zero.

Consider that part of the noise voltage that occupies the time interval from $-T$ to T. The Fourier transform of this voltage is defined by

$$F(f) = \int_{-T}^{T} e(t)e^{2\pi ift}dt \tag{1}$$

where f is the frequency in cycles per second. Next we form the square of the absolute value of $F(f)$, divide by $2T$, and multiply by 2:

$$|F(f)|^2/T. \tag{2}$$

This expression is very close to what is meant by a power spectrum. To form what a mathematician means by a power spectrum, however, we must take an appropriate limit of this expression.

There are two different but equivalent ways to define the power spectrum. The first, and more simple, involves the average over an ensemble of independently generated noise voltages of the same kind. If an ensemble average is denoted by angular brackets, the power spectrum $P(f)$ is defined by

$$P(f) = \langle T^{-1} \mid F(f) \mid^2 \rangle. \quad (3)$$

The second equivalent definition of the power spectrum is formulated by first averaging the expression (2) over the bandwidth $2B$, and then taking the limit of the resulting expression as the time interval $2T$ becomes infinite and the bandwidth $2B$ approaches zero in such a way that BT becomes infinite:

$$P(f) = \lim_{\substack{BT\to\infty \\ B\to 0}} \frac{1}{2BT} \int_{f-B}^{f+B} \mid F(f') \mid^2 df'. \quad (4)$$

If the power spectrum determined by these operations turns out to be independent of the epoch of the origin of the time t, then the noise is said to be stationary. All of the noises discussed in this paper are supposed to be stationary.

The power spectrum defined above is defined for positive frequencies only. The total mean-square fluctuation of the voltage $\overline{e^2}$ is obtained by integrating $P(f)$ over positive frequencies:

$$\overline{e^2} = \int_0^\infty P(f)df. \quad (5)$$

Anyone who contemplates measuring a power spectrum or a Wiener spectrum would be well advised to read first the excellent pair of papers by Blackman and Tukey.[1]

Attention is called to an important paper by Callen and Welton.[2] These authors show, by use of quantum statistical mechanics, that wherever there is a dissipation process there is an associated fluctuation, and that the Wiener spectrum of the fluctuation can be calculated from the magnitude of the dissipation. Callen and Welton give three examples of the application of their theory. They show that the dissipation involved in the viscous drag on a moving airborne particle leads to a fluctuation in the position and velocity of the particle that is in exact accord with the accepted formulas for Brownian motion. They show that the radiation resistance offered to the acceleration of an electrical charge leads to a fluctuation of the electrical field that is equivalent to blackbody radiation; this is a particularly interesting and significant result. Finally, they show that the acoustic radiation resistance of an infinitesimal pulsating sphere leads to the accepted formulas for the pressure and density fluctuation of a gas. The author[3] has further exemplified their theory by using it to derive the Einstein formula for the fluctuation of the temperature of a small body that is in equilibrium with a radiation field or in contact with a heat reservoir; here, the dissipation process is the loss of negentropy in the thermal conductance between the body and its surroundings.

Eight Kinds of Noise

Table I names eight different kinds of noise that may be present in the output of a radiation detector. The table also indicates the kind of detector in which the noise may be important, and indicates briefly the mechanism.

Some of the kinds of noise listed in Table I have an ambiguous meaning. The term "temperature noise," for example, could mean either the fluctuation in the temperature of a bolometer element, or it could mean the consequent voltage fluctuation in the output of the detector. In this review, we avoid the ambiguity by using the eight names in Table I to mean always the *electrical* noise in the output of the detector.

TABLE I

The Eight Kinds of Noise, the Type of Detector in which the Type of Noise May Be Important, and a Brief Indication of the Physical Mechanism That Generates the Noise

Kind of Noise	Detector Concerned	Physical Mechanism
Shot Noise	Thermionic Detector	Random emission of electrons by thermionic emission
Johnson Noise	All Detectors	Thermal agitation of current carriers
Temperature Noise	Thermal Detectors	Temperature fluctuation
Radiation Noise	All Detectors	Bose-Einstein fluctuation of radiation photons
Generation-Recombination Noise	Photoconductive cells, Bolometers	Fermi-Dirac fluctuation of the current carriers
Modulation Noise		Resistance fluctuation in semiconductors
Contact Noise		Resistance fluctuation at contacts
Flicker Noise	Thermionic Detector	Fluctuation of the work function

The power spectra of the various kinds of noise must be added in order to obtain the power spectrum of the total electrical noise at the output of the detector. Thus, for example, the power spectrum of the total noise of a bolometer may be regarded as the sum of the power spectra of the Johnson noise, the temperature noise, the modulation noise, and perhaps also the contact noise.

Shot Noise

The usual expression for the power spectrum of the shot noise in a temperature-limited diode is

$$P_i(f) = 2e\bar{I} \quad (6)$$

[1] R. B. Blackman and J. W. Tukey, "The measurement of power spectra from the point of view of communication engineering," *Bell Syst. Tech. J.*, vol. 37, pts. 1 and 2, pp. 185–282 and 485–569; 1958.

[2] H. B. Callen and T. A. Welton, "Irreversibility and generalized noise," *Phys. Rev.*, vol. 83, pp. 34–40; 1951.

[3] R. C. Jones, "Performance of detectors for visible and infrared radiation," in "Advances in Electronics," Academic Press, New York, N. Y., vol. 5, pp. 1–96; 1953.

where ϵ is the absolute value of the charge of the electron, and $\bar{I}$ is the mean current. The subscript i on P indicates that the independent variable is the current —that is to say, the power spectrum $P_i(f)$ is the mean-square fluctuation of the current per unit bandwidth.

The above formula is derived easily if one supposes that the charge is transported discontinuously in quanta of size ϵ and that the transportations occur randomly in time. In a temperature-limited thermionic diode these conditions are quite well satisfied for frequencies above the range where flicker noise is significant.

The presence of space charge reduces the magnitude of the noise below that given by (6) without changing the flatness of the spectrum. The effect of finite transit time[4] within the diode and of shunt capacity causes the spectrum to fall off at high frequencies.

The idea behind shot noise—that the current carriers have a random element—has caused the term to be used to describe almost every noise except Johnson noise. Such a broad use of a term weakens its meaning. In this review, the term shot noise will be confined to the noise of a thermionic diode. More explicit terms are available for all of the other purposes for which the term is sometimes used.

In temperature-limited diodes, the existence of shot noise was predicted by Schottky[5] in 1918. The prediction was confirmed by Johnson[6] and by Hull and Williams,[7] and was confirmed later with high precision by Williams and Vincent[8] in 1926.

Johnson Noise

Johnson noise is the thermal agitation noise that appears at the output of every radiation detector. If the detector is in thermal equilibrium with its surroundings, both with respect to radiation and conduction, and if the steady electric current through the detector is zero, then the only noise at the output of the detector is Johnson noise.

The power spectrum of Johnson noise is given by

$$P_e(f) = 4kTR \cdot \frac{hf/kT}{e^{hf/kT} - 1} \tag{7}$$

where R is the real part of the electrical impedance. Except at very high frequencies, where hf is not very small compared with kT, the last factor may be omitted.

In 1906, Einstein[9] applied his recently developed theory of Brownian motion to the motion of the electrons inside of a wire. He found that the mean-square charge transported across any given cross section in the period τ was equal to

$$\overline{q_\tau^2} = \frac{2kT\tau}{R} \tag{8}$$

where the wire is supposed to be part of a loop of resistance R. This result was extended by de Haas-Lorentz.[10] She supposed that the transport of charge indicated by (8) was due to a fluctuating electromotive force in series with the loop. Let E be the instantaneous value of this electromotive force and let e_τ be the average value of E over a given period of duration τ. She showed that $\overline{e_\tau^2}$ is given by

$$\overline{e_\tau^2} = 2RkT/\tau. \tag{9}$$

The power spectrum of Johnson noise was not worked out until 1928. In that year, Nyquist[11] published a derivation of the expression (7) by a procedure that essentially involved counting the independent modes of vibration in a transmission line.

During the years between 1928 and 1941, the use of the equation for Johnson noise was pushed to higher and higher frequencies. According to Southworth,[12] it gradually became apparent to those working in the field that Johnson noise was the one-dimensional form of blackbody radiation. This was established in 1941 by Burgess.[13] He showed that if one connected an antenna through a transmission line to a resistor, the energy radiated from the antenna due to the Johnson noise fluctuation in the resistor was just balanced by the blackbody radiation received by the antenna, provided only that the temperature of the radiation field was equal to the temperature of the resistor.

Johnson noise is also called Nyquist noise, thermal noise, and sometimes thermal fluctuation noise.

Temperature Noise

Temperature noise is the electrical noise in the output of a detector due to the temperature fluctuation of the active element. Temperature noise is important primarily in connection with thermal detectors, which are defined as detectors whose conversion of incident radiation into an electrical output is mediated by a change in the temperature of the active element. Thermal detectors include the bolometer, the thermocouple, the Golay pneumatic detector, and the thermionic detector.

The Wiener spectrum of the temperature fluctuation is given by

[4] S. S. Solomon, "Thermal and shot fluctuations in electrical conductors and vacuum tubes," *J. Appl. Phys.*, vol. 23, pp. 109–112; 1952.

[5] W. Schottky, "Über spontane Stromschwankungen in verschiedenen Elektrizitätsleitern," *Ann. Physik.*, vol. 57, pp. 541–567, 1918.

[6] J. B. Johnson, "The Schottky effect in low frequency circuits," *Phys. Rev.*, vol. 26, pp. 71–78; 1925.

[7] A. W. Hull and N. H. Williams, "Determination of elementary charge from measurements of shot effect," *Phys. Rev.*, vol. 25, pp. 147–173; 1925.

[8] N. H. Williams and H. B. Vincent, "Determination of elementary charge e from measurements of shot effect in aperiodic circuits," *Phys. Rev.*, vol. 28, pp. 1250–1264; 1926.

[9] A. Einstein, "Zur Theorie der Brownschen Bewegung," *Ann. Physik.*, vol. 19, pp. 371–381; 1906.

[10] G. L. de Haase-Lorentz, "Die Brownsche Bewegung und einige verwandte Erscheinungen," Braunschweig, Ger.; 1913.

[11] H. Nyquist, "Thermal agitation of electric charge in conductors," *Phys. Rev.*, vol. 32, pp. 110–113; 1928.

[12] G. C. Southworth, "Microwave radiation from the sun," *Phys. Rev.*, vol. 239, pp. 285–297; 1945.

[13] R. E. Burgess, "Noise in receiving-aerial systems," *Proc. Phys. Soc. (London)*, vol. 53, pp. 293–304; 1941.

$$W_t(f) = \frac{4kT^2g(f)}{g^2 + (h + 2\pi fC)^2} \cdot \frac{hf/kT}{e^{hf/kT} - 1} \tag{10}$$

where C is the thermal capacity of the active element, and $g(f)+ih(f)$ is the complex thermal conductance of the active element to the environment, including the conductance due to radiation exchange. $W_t(f)$ is the mean-square fluctuation of the temperature about its mean value per unit frequency bandwidth.

It follows directly from a result given by Einstein[14] in 1904 that if two bodies, A and B, are in thermal contact with one another, and if they have been in contact long enough so that their mean temperatures are equal, the mean-square difference in their temperature is given by

$$\overline{t^2} = kT^2/C \tag{11}$$

where C is given by

$$C = \frac{C_AC_B}{C_A + C_B} \tag{12}$$

and C_A and C_B are the thermal capacities of the two bodies. Einstein's result may be derived from (10).

The Wiener spectrum of the fluctuation of the temperature was first determined by Milatz and Van der Velden.[15] The term temperature noise was introduced by the author[16] in 1949.

In order to obtain the power spectrum $P_e(f)$ of the temperature noise, the Wiener spectrum $W_t(f)$ must be multiplied by the square of factor $Q(f)$ that converts a change of temperature into a change of output voltage:

$$P_e(f) = Q^2(f)W_t(f). \tag{13}$$

Radiation Noise

Radiation noise is the noise in the output of a radiation detector that is due to the fluctuation in the radiant power that acts on the detector, and is often called photon noise.

The radiation noise may be formulated in a variety of ways, and several different methods are used in the discussion by Jones.[3] In a narrow band of radiation frequencies, the Wiener spectrum of the incident power is given by

$$W_p(f) = 2h\nu\overline{P}/(1 - e^{-h\nu/kT}) \tag{14}$$

where $\overline{P}$ is the mean incident power, and ν is the radiation frequency. $W_p(f)$ is the mean-square fluctuation of incident power per unit frequency bandwidth.

When the bandwidth of the radiation frequencies is not narrow, the right-hand side of the above expression must be integrated over the radiation frequency. If the radiation spectrum is that of blackbody radiation of temperature T, the result of the integration is

$$W_p(f) = 8kT\overline{P} = 8Ak\sigma T^5 \tag{15}$$

where A is the active area of the detector, σ is the Stefan-Boltman radiation constant, and where it is assumed that the detector is immersed in the blackbody radiation field.

In order to obtain the power spectrum $P_e(f)$ of the radiation noise, the Wiener spectrum $W_p(f)$ must be multiplied by the square of the responsivity $R(f)$:

$$P_e(f) = R^2(f)W_p(f). \tag{16}$$

The theory of the fluctuation of the power in a beam of thermal radiation was first worked out by Lewis,[17] although, as he points out, the theory is based on the older theory of the fluctuation phenomena in Bose-Einstein ensembles. Radiation noise is considered from a number of points of view by Jones.[3]

Generation-Recombination Noise

Generation-recombination noise is the noise in the output of a photoconductive cell or a semiconductor bolometer that is due to the fluctuation in the number and lifetime of the thermally-generated carriers.

Simple and general expressions for G-R noise do not exist. As Bernamont[18] showed, if the carriers are generated randomly in time and have an exponential distribution of lifetimes, the power spectrum of the noise can be expressed by

$$P_i(f) = 4\overline{I}^2\tau/n_0(1 + (2\pi f\tau)^2) \tag{17}$$

where τ is the mean lifetime of the carriers, and n_0 is the mean number of carriers in the semiconductor. This expression may also be written

$$P_i(f) = 4\epsilon\overline{I}G/(1 + (2\pi f\tau)^2) \tag{18}$$

where ϵ is the absolute charge of the electron, and G is the semiconductor gain[19] defined by

$$G = \tau/T_r = \tau\mu V/L^2 \tag{19}$$

where μ is the mobility, V is the voltage across the electrodes, L is the distance between electrodes, and T_r is the interelectrode transit time.

The factor 4 in (18) instead of the factor 2 in the shot noise formula (6) is brought about by the fluctuation in the lifetime of the carriers as well as in their number.

The above expressions for the power spectrum, based on Maxwell-Boltzmann statistics, do not have general

[14] A. Einstein, "Zur allgemeinen molekularen Theorie der Wärme," *Ann. Physik.*, vol. 14, pp. 354–362; 1904.
[15] J. M. W. Milatz and H. A. Van der Velden, "Natural limit of measuring radiation with a bolometer," *Physica.*, vol. 10, pp. 369–380; 1943.
[16] R. C. Jones, "Radiation detectors," *J. Opt. Soc. Am.*, vol. 39, pp. 327–356; 1949.
[17] W. B. Lewis, "Fluctuations in streams of thermal radiation," *Proc. Phys. Soc. (London)*, vol. 59, pp. 34–40; 1947.
[18] J. Bernamont, "Fluctuations de potentiel aux bornes d'un conducteur metallique de faible volume parcouru par un courant," *Ann. Phys.*, vol. 7, pp. 71–140; 1937.
[19] A. Rose, "Performance of photoconductors," PROC. IRE, vol. 43, pp. 1850–1869; December, 1955.

validity. In fact, the only special case where they are usually considered to be valid is an extrinsic semiconductor that is only slightly ionized. If the degree of ionization is γ, a simple argument due to van der Ziel[20] suggests that the factor $1-\gamma$ should be inserted in (17) and (18).

The analysis by Fermi-Dirac statistics of even a three-level system leads to complex relations.[21,22] These complications are beyond the scope of this short review.

Modulation Noise

The kinds of noises that have been discussed so far in this review have been rather fundamental in character. The three remaining types of noise, however, do not appear to be fundamental, and from some points of view can be considered as due to defects that, in principle, are avoidable. On the other hand, they occur so commonly in radiation detectors, and are of such great practical importance, that they must be included in any realistic discussion of noise in radiation detectors.

The term modulation noise introduced by Petritz[23] refers to noise in semiconductors that is due to modulation of the conductivity due to other causes than Fermi-Dirac fluctuations in the number of carriers. The power spectrum of modulation noise varies approximately as $1/f$:

$$P_i(f) = CI^2/f^\alpha \qquad (20)$$

where α is an exponent close to unity.

The frequency range over which modulation noise has been observed is remarkably large. In germanium filaments, it has been followed[24] down to 2×10^{-4} cps, and in point contact diodes it has been found[25,26] as low as 6×10^{-6} cps. Hyde[27] has observed $1/f$ noise in germanium crystals up to 4×10^{6} cps.

Unlike the first five kinds of noise discussed in this review, the physical mechanism of the last three is obscure.

The physical location of the source of at least part of the modulation noise is at the surface of the crystals; the level of modulation noise in single-crystal detectors can often be reduced by suitable treatment of the surface. The physical mechanism may involve shallow surface trapping states for carriers, or diffusion of impurity atoms, perhaps along dislocations.

Contact Noise

Contact noise is similar to modulation noise and is often confused with it.

Contact noise differs from modulation noise in that it has its source at the contacts and can sometimes be distinguished from modulation noise by the use of four-terminal methods. Like modulation noise, contact noise has a spectrum that often varies approximately as the inverse first power of the frequency:

$$P_i(f) = CI^\beta/f^\alpha \qquad (21)$$

where β is close to two, and α is near unity.

The noise in granular resistors and in carbon microphones is usually ascribed to contact noise. The first mention of contact noise appears to be that of Hull and Williams.[28] The first comprehensive study of contact noise was made by Christensen and Pearson.[29] They studied single carbon contacts, and carbon resistors. They found the average value of α and β to be about 1.0 and 1.85 at audio frequencies.

Flicker Noise

Flicker noise is the low-frequency noise that is in excess of shot noise in vacuum tubes. More specifically, when one measures the shot noise in temperature-limited thermionic emission, one finds that at low frequencies the power spectrum rises above the value predicted by the shot-noise formula (6).

Flicker noise was discovered by Johnson[6] in 1925, and was given its name by Shottky[30] in 1926. Johnson's measurements indicated that the power spectrum of flicker noise varied with frequency roughly as $1/f$ for oxide-coated cathodes, and roughly as $1/f^2$ for tungsten cathodes. He further found that the power spectrum of the fluctuation in the current was proportional to the square of the current, $\bar{I}$, whereas in shot noise, the spectrum is proportional to the first power of the current. Johnson suggested that the cause of flicker noise was a fluctuation in the state of the cathode.

Schottky pointed out that if the fluctuation in the state of the cathode was due to a diffusion process that was independent of the amount of the cathode current $\bar{I}$, then one would predict that the spectrum of the fluctuation should be proportional to $\bar{I}^2$. The most extensive investigation of flicker noise in the temperature-limited condition is that of Graffunder[31] in 1939. Graffunder studied the level of the flicker noise in a number of dif-

[20] A. van der Ziel, "Shot noise in semiconductors," *J. Appl. Phys.*, vol. 24, pp. 222–223; 1953.
[21] K. M. van Vliet, "Noise in semiconductors and photoconductors," PROC. IRE, vol. 46, pp. 1004–1018; June, 1958.
[22] S. Teitler, "Generation-recombination noise in a two-level impurity semiconductor," *J. Appl. Phys.*, vol. 29, pp. 1585–1587; 1958.
[23] R. L. Petritz, "On the theory of noise in *p-n* junctions and related devices," PROC. IRE, vol. 40, pp. 1440–1456; November, 1952.
[24] R. V. Rollin and I. M. Templeton, "Noise in semiconductors at very low frequencies," *Proc. Roy. Phys. Soc. B*, vol. 66, pp. 259–261; 1953.
[25] D. Baker, "Flicker noise in germanium rectifiers at very low frequencies," *J. Appl. Phys.*, vol. 25, pp. 922–924; 1954.
[26] T. Firle and H. Winston, "Noise measurements in semiconductors at very low frequencies," *J. Appl. Phys.*, vol. 26, p. 716; 1955.
[27] F. J. Hyde, "Excess noise spectra in germanium," *Proc. Roy. Phys. Soc. B*, vol. 69, pp. 242–245; 1956.
[28] A. W. Hull and N. H. Williams, "Determination of elementary charge *e* from measurements of shot effect," *Phys. Rev.*, vol. 25, pp. 147–173; 1925.
[29] C. J. Christensen and G. L. Pearson, "Spontaneous resistance fluctuations in carbon microphones and other granular resistances," *Bell Sys. Tech. J.*, vol. 15, pp. 197–223; 1936.
[30] W. Schottky, "Small shot effect and flicker effect," *Phys. Rev.*, vol. 28, pp. 74–103; 1926.
[31] W. Graffunder, "Das Röhrenrauschen bei Niederfrequenz," *Telefunken Röhre*, no. 15, pp. 41–63; 1939.

ferent types of commercial tubes, including tubes with pure tungsten, thoriated tungsten, bariated tungsten, and oxide-coated cathodes. His study was limited to the range of frequencies from 40 to 10,000 cps. He found that the measured power spectrum of the flicker noise accords fairly well with the 1/f law in this range of frequencies.

Many more investigators have studied the spectrum of flicker noise, but not in the temperature-limited condition. Among these investigators are Graffunder[31] Bogle,[32] Orsini,[33] Kronenberger and Seitz,[34] Brynes,[35] and van der Ziel.[36] Kronenberger and Seitz[34] have found the 1/f law to extend down to 0.1 cps for oxide-coated cathodes.

All investigators find that the flicker noise of pure tungsten and thoriated-tungsten cathodes is much less than that of most oxide-coated cathodes.

The power spectrum of the fluctuation in the current in temperature limited emission due to both shot noise and flicker noise may be written

$$W_i(f) = 2e\bar{I}\left(1 + \frac{F}{f}\cdot\frac{\bar{I}}{A}\right) \qquad (22)$$

where F is a constant that characterizes the nature of the cathode surface, and A is the surface area of the cathode. The appearance of the cathode area A in the formula follows from the assumption that the noises contributed by separate regions of the cathode are statistically independent.

The value of the constant F has been evaluated here for the various surfaces chiefly from the results of Graffunder.[31] The relatively small amount of data published by Johnson[6] and by Williams[37] has also been employed.

A summary of the results is shown in Table II. The first column shows the cathode surface, the second column the range of values of F, and the third column shows the number of tubes on which the evaluation is based.

TABLE II
VALUES OF THE PARAMETER F INTRODUCED IN (22)

Cathode	F in (cps-cm²/amp)	Number of tubes
W	250–2500	4
Th-W	1000–4000	4
Ba-O-W	2500–15,000	4
Oxide	$10^1 - 10^8$	7

Relations among the Various Kinds of Noise

Perhaps the most fundamental relation is that between radiation noise and Johnson noise. Radiation noise is due to the fluctuation in the power incident from a three-dimensional radiation field. Johnson noise is a one-dimensional form of blackbody radiation. Thus there is a sense in which radiation noise is the fluctuation in the power of the radiation field, whereas Johnson noise *is* the power of the radiation field.

Many efforts have been made to find a relation between shot noise and Johnson noise, but all of them have been unsuccessful.[38]

In the realm of validity of Wien's law, where $h\nu$ is is large compared with kT, the radiation photons are statistically independent. Thus in any detector that produces one current carrier for one effective photon (examples: photoemissive tubes, backbiased p-n junctions), the radiation will produce a noise current that accords with the relation given for shot noise. In this restricted sense, radiation noise and shot noise are identical. Indeed, the term shot noise is often used where the term radiation noise or photon noise would be more specific.

In the special case of the thermocouple radiation detector, the Peltier effect produces a coupling between the electrical and thermal circuits, whose result is that the effective resistance of the thermocouple is higher than it would be in the absence of the Peltier effect. The extra resistance has been called a dynamic resistance by Fellgett.[39] The noise generated by the dynamic resistance is the same whether it be viewed as the Johnson noise of the extra resistance or as the temperature noise of the detector. There is a similar dynamic resistance in a bolometer,[3] but in this case the extra noise due to the temperature fluctuation is *not* equal to the (calculated) Johnson noise of the dynamic resistance. (In general, the theory of Johnson noise is applicable only in situations where the detector is in complete thermodynamic equilibrium.)

In the special case where the active element of a thermal detector is in thermal contact with its surroundings only by radiation exchange, radiation noise and temperature noise are identical.

The term current noise, not used so far in this review, is a catch-all term that denotes the noise in excess of Johnson noise when current is passed through the element. The concept thus includes the temperature noise of bolometers, generation-recombination noise, modulation noise, and contact noise.

[32] R. W. Bogle, "Low Frequency Fluctuation Voltages in Vacuum Tubes," Applied Physics Lab., The Johns Hopkins University, Baltimore, Md., Tech. Monograph 137; 1948.

[33] L. de Queiroz Orsini, "L'amplification sélective en basse fréquence," *Onde Elec.*, vol. 29, pp. 408–413; 1949; vol. 29, pp. 449–456; 1949; vol. 30, pp. 91–102; 1950.

[34] K. Kronenberger and F. Seitz, "Experimentelle Untersuchung der Schwankungserscheinungen, die die Verstärking von Gleichspannungs- und Tiefstfrequenzverstärkern begrenzen," *Z. Angew. Phys.*, vol. 3, pp. 1–5; Month, 1951.

[35] F. X. Byrnes, "The effect of tube noise on the equivalent noise pressure of transducer systems," *J. Acoust. Soc. Am.*, vol. 24, 452(A); 1952.

[36] A. van der Ziel, "Study of the Cause and Effect of Flicker Noise in Vacuum Tubes," Electron Tube Res. Lab., University of Minnesota, Minneapolis, Minn., Quart. Repts. from October 15, 1951.

[37] F. C. Williams, "Fluctuation voltage in diodes and in multielectrode valves," *J. IEE*, vol. 79, pp. 349–360; 1936.

[38] An account of these efforts is given in Jones, footnote 3, pp. 14–15.

[39] P. B. Fellgett, "Dynamic impedance and sensitivity of radiation thermocouples," *Proc. Roy. Phys. Soc. B*, vol. 62, pp. 351–359; 1949.

Paper 3.3.8

Infrared Photography*

LEWIS LARMORE†

THE use of photography has been one of the principal methods for detecting and recording radiation in the near infrared region. Besides its use in spectroscopy, it has been applied to certain medical problems, aerial reconnaissance and photogrammetry, special artistic effects, and photography under "black light" conditions. Included in this section is a discussion of the response characteristics of infrared photographic emulsions, a comparison of infrared photography with other types of infrared detectors, and examples of some of its primary uses.

Photographic emulsions consist of one or more of the silver halides deposited in granular form within a gelatin. Both silver bromide and silver iodide are used for infrared-sensitive materials. If the only component deposited within the gelatin were the silver halide, the spectral response would be limited to wavelengths shorter than about 0.5 micron. However, in 1873, H. W. Vogel discovered that the addition of dyes produces sensitivity at longer wavelengths. Since this time, the wavelength limit has been pushed farther and farther until now photographic emulsions are available commercially which give response to wavelengths of 1.2 microns. Although no fundamental limitation exists for the extension of sensitivity to longer wavelengths, no suitable material has yet been found which gives any sensitivity to wavelengths longer than about 1.4 microns. Fig. 1

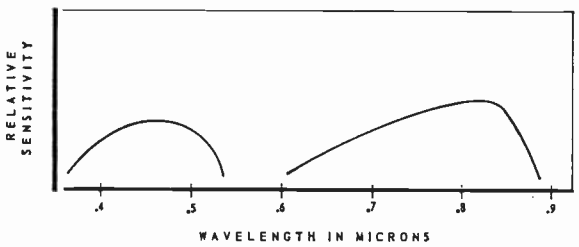

Fig. 1—Spectral response of typical commercial infrared film.

shows the spectral response of typical infrared film for pictorial use. The short wavelength sensitivity arises principally from the inherent characteristics of the silver halide, while the longer wavelength response is due to the addition of the proper dye. In use, the infrared characteristics are brought out by means of an optical filter which eliminates radiation of wavelength shorter than the desired amount. For example, for pictorial work in sunlight, infrared film will give an almost normal negative unless the short wavelength radiation is filtered out.

* Original manuscript received by the IRE, June 26, 1959.
† Lockheed Aircraft Corp., Burbank, Calif.

The limiting noise in a photographic system is usually formed by the granularity characteristics of the emulsion. Thus, in order to determine the noise equivalent power (NEP) and detectivity (D), we must have information concerning the granularity. No detailed analysis for infrared film has been made, but, following Jones' work,[1] we let $\overline{d^2}$ be the mean-square fluctuation of the density over an area A. Jones and Higgins[2] have shown that $\overline{d^2}$ is inversely proportional to A.

$$\overline{d^2} = \frac{\alpha^2}{A} \tag{1}$$

where α^2 is the proportionality constant and depends on the method of development and the amount of preexposure (if any). The square root of this quantity is thus a measure of the noise in the system. When radiation falls on the the film, an increase in density ΔD will result in the developed image. The amount of ΔD depends on the exposure provided (radiant energy falling on the film per unit area), and on the film "speed." Thus:

$$\Delta D = \frac{\beta P \tau}{A} \tag{2}$$

where P/A is the irradiance (watts-cm^{-2}), τ is the length of the exposure, and β is a proportionality constant dependent on the film "speed." For a signal-to-noise ratio of unity,

$$\sqrt{\overline{d^2}} = \Delta D \tag{3}$$

and

$$P = \frac{\alpha}{\beta} \frac{A^{1/2}}{\tau} \text{ watts.} \tag{4}$$

This value of P is the noise equivalent input (NEI) for the film, and its reciprocal is the detectivity D.

$$D = \frac{\beta}{\alpha} \frac{\tau}{A^{1/2}}. \tag{5}$$

Jones[1] has evaluated the constants α and β for various films used under reasonable conditions, but infrared film has not been included. If we assume that the granularity of infrared film is similar to Super-XX and that the β value is degraded because of lower film "speed," then

$$\frac{\beta}{\alpha} = 7.5 \times 10^{11} \text{ cm} \cdot \text{watt}^{-1} \cdot \text{sec}^{-1}. \tag{6}$$

[1] R. C. Jones, "Performance of Detectors for Visible and Infrared Radiation," in "Advances in Electronics," Academic Press, Inc., New York, N. Y., vol. 5; 1953.
[2] L. A. Jones and G. C. Higgins, "Photographic granularity and graininess. II," *J. Opt. Soc. Am.*, vol. 36, pp. 203–227; 1946.

Using $\tau = 0.01$ sec, and $A = 1$ cm^2 we have

$$D = 7.5 \times 10^9 \text{ watt}^{-1}. \quad (7)$$

Since the area was chosen as one square centimeter, this value also represents the nearest approach to a value of D^* (0.85, 100 cps) for the infrared film. The quantities in parentheses represent the wavelength of 0.85 microns and a chopping frequency of 100 cps (exposure time = 0.01 second). Infrared photography, then, does not show the detection performance which is present in other types of detectors in the near infrared region. However, it shares with other types of photography the ability to employ very long exposures and to utilize extremely small effective areas. In addition, it shares the unsurpassed ability of photography to record at an extremely high information rate.

The uses of infrared photography have been well documented, and information on this subject is available in a number of publications.[3] Most of the infrared emulsions produced are used in aerial photography. Comparison of infrared photographs with panchromatic film photographs yields information concerning camouflage and types of materials because of the variation of spectral reflectance between the visible and infrared. In addition, longer wavelengths penetrate the atmosphere considerably better than shorter wavelengths when the scattering follows the Rayleigh inverse fourth-power law. An example of the two effects is shown in Fig. 2. In Fig. 2(a), taken with panchromatic film, the grass and tree foliage appear dark; but in the infrared photograph, Fig. 2(b), these appear light. The result is due to the difference in the spectral reflectance characteristics of chlorophyl. Also, the haze penetration and difference in sky brightness are apparent. Infrared photography of documents is fairly common wherever obliteration or changes are suspected. Many invisible inks, chemical bleaching and mechanical erasure yield their presence by means of infrared radiation.

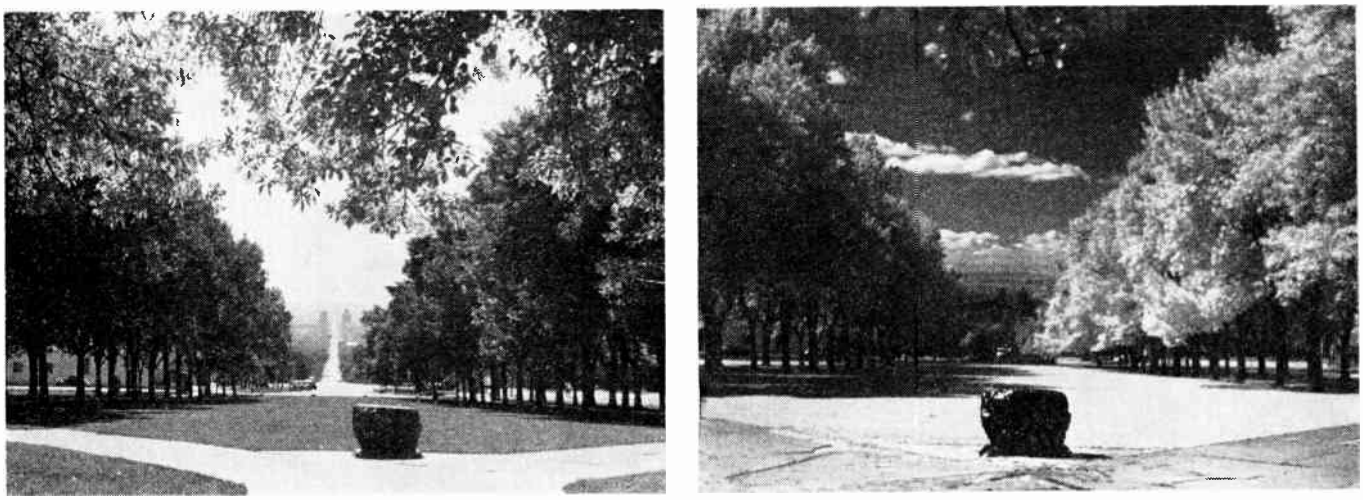

Fig. 2—(a) Photograph using panchromatic film (b) Photograph using infrared film.

It should be noted that the use of infrared film represents the first satisfactory attempt at "color translation." This technique has since been applied to observations in the ultraviolet region which are translated into the visible region. Also, the intermediate and far infrared regions have been similarily translated into the visible by means of scanners and readout devices described in this issue.

[3] See, for example, "Infrared and Ultraviolet Photography," Eastman Kodak Company, Rochester, N. Y.; 1955. Also L. Larmore, "Introduction to Photographic Principles," Prentice Hall, Inc., New York, N. Y., pp. 48–50; 1958.

Paper 3.4.1

Range Equation for Passive-Infrared Devices*

LEWIS LARMORE†

THE solution to the problem of determining the maximum range at which an infrared device can detect a target requires a detailed analysis of the spectral radiance properties of the target, the absorption in the intervening space, the characteristics of the radiation-gathering system, and the response of the detector. In this section, the general form of the passive-range equation is developed, while a detailed discussion of the parameters is included elsewhere. For example, target emission characteristics, atmospheric attenuation, and detector parameters are given in Section 3. Radiation collection systems and background characteristics are discussed in Section 4.

Radiation emitted by a target may have the spectral characteristics of a blackbody modified by the emissivity of the material; it may have those of a gaseous emission spectrum; or it may have a combination of the two. In any case, the spectral radiant emittance can be represented by

$$W_\lambda = E_\lambda(T)\epsilon(\lambda) \text{ watts} \cdot \text{cm}^{-2} \cdot \text{micron}^{-1} \tag{1}$$

where $E_\lambda(T)$ is the spectral radiant emittance at wavelength λ of a blackbody at temperature T, and $\epsilon(\lambda)$ is the emissivity of the material at wavelength λ. In most situations, however, the target cannot be characterized by a single temperature and values of W_λ must be obtained either from actual measurements or from an assumed temperature distribution over the target. In addition, the values of $\epsilon(\lambda)$ may change with temperature also, but this variation is not sufficiently large to warrant a detailed investigation.

At a distance R, which is assumed large compared with the source dimension, the spectral irradiance at the aperture of the infrared-detecting system is

$$H_\lambda = \frac{W_\lambda A \tau(\lambda)}{\pi R^2} \text{ watts} \cdot \text{cm}^{-2} \cdot \text{micron}^{-1} \tag{2}$$

where A is the projection of the target area and $\tau(\lambda)$ is the spectral transmittance of the intervening medium (usually air) between the target and receiving aperture. Note that the value of the spectral transmittance, $\tau(\lambda)$, is a function of the range.

In order to determine the amount of radiant power which actually falls on the detector, one must know the details of the detection system. However, these details can be represented by our making the assumption of a spectral transmittance for the system and multiplying it by the area of the aperture. Thus, the radiant power at wavelength λ falling on the detector is

$$s_\lambda = H_\lambda a \tau_0(\lambda) \text{ watts} \tag{3}$$

where a is the aperture area and $\tau_0(\lambda)$ is the spectral transmittance of the detecting system.

The response of most detectors is wavelength dependent, and they are unable to utilize all of the power which is incident on them. In order to allow for these response characteristics, we usually introduce the relative spectral response of the detector $\Sigma(\lambda)$ and apply it to (3). Hence, the effective radiation at wavelength λ falling on the detector becomes the signal to the detecting system from the target and is defined by

$$S_\lambda = H_\lambda a \tau_0(\lambda)\ \Sigma(\lambda) \text{ watts.} \tag{4}$$

The task now remains of putting together all of these relations and performing an integration over all wavelengths. Thus, the total signal provided to the detection system is

$$S = \int_0^\infty \frac{W_\lambda A \tau(\lambda) a \tau_0(\lambda)\ \Sigma(\lambda) d\lambda}{\pi R^2} \text{ watts} \tag{5}$$

where all terms have been previously defined.

In order to have an operating system which will detect a target, we must have two additional pieces of information: 1) the signal-to-noise ratio which can be tolerated, and 2) the value of the noise introduced into the system either by the background radiation, the electronics, or the detector itself. When the noise problem is introduced into (5), we have

$$\frac{S}{N} = \rho = \frac{Aa}{\pi R^2 N} \int_0^\infty W_\lambda \tau(\lambda) \tau_0(\lambda)\ \Sigma(\lambda) d\lambda. \tag{6}$$

As a rule of thumb, S/N values of unity can be handled for a tracking system while S/N values of from three to five are typical for scanning systems.

Only in special cases can (6) be solved for the range since the atmospheric transmittance is also a function of this parameter. Thus, graphical or numerical methods must be used in general. However, if only narrow windows of the atmosphere are used, or if, as in outer space, there is no attenuation, can we approximate a solution. In these cases the transmittance of the intervening medium can be removed from under the integral sign and a constant value assigned to it, and the maximum detection range becomes

* Original manuscript received by the IRE, June 26, 1959.
† Lockheed Aircraft Corp., Burbank, Calif.

$$R = \sqrt{\frac{\tau A a}{\pi N \rho} \int_0^\infty W_\lambda \tau_0(\lambda)\ \Sigma(\lambda) d\lambda} \qquad (7)$$

where ρ is the required signal-to-noise ratio. The noise, N, which limits the performance of the system is frequently one of the most difficult parameters to evaluate. Operation under daytime conditions usually leads to the conclusion that the background radiation furnishes the limiting noise, while night-time operations are limited by detector noise. A further discussion of these factors is included elsewhere in this text.[1]

Although the wavelength interval for integration in (6) and (7) is indicated to be 0 to ∞, in practice, some of the quantities under the integral are zero except over a fairly narrow wavelength region. Since the integration must be done either numerically or graphically, it is important to examine the values beforehand in order to limit the amount of work as much as possible.

[1] See R. H. Genoud, "Infrared search-system range performance," Paper 4.4.5, this issue, p. 1581.

Paper 3.4.2

Range Equation for Active Devices*

KENNETH V. KNIGHT†

ACTIVE infrared and optical ranging can be accomplished with the use of pulsed radiation in a manner analogous to that of radar in pulsed RF techniques. A very-high-intensity lamp at the focus of a collimating mirror is caused to flash, and the energy reflected from the target is collected in another mirror and focused upon a photodetector. The elapsed time between the emission of the pulsed light and the detection of its reflection from the target is, as in radar, a measure of the range to the target. This time can be measured on the face of an oscilloscope whose sweep is triggered with the firing of the flash lamp, or it can be measured and delivered as an analog voltage by more sophisticated automatic electronic techniques. Gating and integration techniques can be used to enhance performance when signal-to-noise ratios are low.

Greater range performance can presently be obtained using emission of flash lamps in the visual optical region and using photodetectors sensitive in this region. However, if it is desirable to operate totally within the infrared spectrum, flash lamps equipped with infrared filters can be employed together with suitably fast infrared photodetectors.

Farrand Optical Company, Inc., New York, N. Y., has been a leader in developing these techniques and has applied them to a wide variety of classified military equipments.

Although pulsed-light (visible or infrared) ranging is presently limited in comparison with pulsed radar, there are many attractive features to recommend its consideration where long-range performance is not required. Several of these are noted: the transmitter field of view can be very small and the receiver field of view can be very accurately defined and made as small as one pleases; consequently, the troublesome ground clutter of radar is not experienced in operating ground-to-ground. Side and rear radiation lobes are not present. Low power, size, and weight requirements further commend the techniques. High-range accuracy and range resolution are attainable with less difficulty than in RF technology. Because of high directivity and operation outside the RF spectrum, pulsed-light techniques are less susceptible to detection and jamming than are RF techniques. Rangefinders employing the technique are rugged and require little optical adjustment. Associated electronic circuits are usually relatively simple.

The basic range equations are also simple.

We recall from elementary physics that illumination upon a scene varies inversely with the square of the distance, R, from the illuminating source. If we place a collimating mirror behind a source in such a way that the target "sees" the mirror full of light, we have the familiar relationship

$$I_T = k_1 \frac{B_S D_T^2}{R^2} \qquad (1)$$

(ignoring atmospheric attenuation) where

I_T = irradiance of the target,
B_S = radiance of the source, and
D_T = diameter of the transmitting mirror.

* Original manuscript received by the IRE, June 26, 1959.
† Ramo-Wooldridge Corp., a division of Thompson Ramo-Wooldridge Inc., Los Angeles, Calif.

If the target is a perfectly diffuse reflector of reflectance r, its radiance can be expressed as

$$P_T = k_2 I_T r \tag{2}$$

and by substitution from (1)

$$P_T = k_3 \frac{B_S D_T^2 r}{R^2}. \tag{3}$$

We are interested, of course, in the reflected energy collected at the receiver mirror. This is expressed as

$$P_R = k_4 \frac{D_R^2 P_T S_T^2}{R^2} \tag{4}$$

where

D_R = diameter of the receiver mirror and
S_T = diameter of the target.

Upon substitution from (3), (4) becomes

$$P_R = k_5 \frac{B_S D_T^2 D_R^2 S_T^2 r}{R^4} \equiv S. \tag{5}$$

This is the basic equation for pulsed-light systems expressing the energy available for processing into electronic signals. Unfortunately, we must also recognize the existence of noise accompanying S and examine the familiar S/N ratio.

Pulsed-light systems are particularly affected by *external* noise, the principal source of which is random fluctuations in the level of energy received from the background in daylight operation, when sun reflections may be expected to occur in the background. Noise power can be expressed, assuming a typical exponent,

$$N = k_6 P_B^{1/2} \tag{6}$$

where P_B = background radiation collected by the receiver.

But

$$P_B = k_7 B_B \theta^2 D_R^2 \tag{7}$$

where

B_B = background radiance at the receiver, and
θ = field of view of the receiver.

Combining (6) and (7), we have

$$N = k_8 \theta D_R B_B^{1/2}. \tag{8}$$

Combining (5) and (8), we have the S/N ratio for a pulsed-light system operating against a perfectly diffuse target reflector.

$$\mathrm{S/N} = k_9 \frac{B_S D_T^2 D_R S_T^2 r}{\theta R^4 B_B^{1/2}}. \tag{9}$$

Pulsed-light system performance, therefore, is dependent upon the parameters: source radiance; apertures of the transmitter and receiver mirrors; target size and reflectance; background radiance; receiver field of view; and range.

Tacit in the development above is the assumption that the receiver field of view is larger than the angle subtended by the target, admitting background noise outside the target area. If we have a case where the angle subtended by the target is larger than the field of view, the effective target can be expressed as

$$S_T = \theta R \tag{10}$$

and, upon substitution in (9) we can obtain the result

$$\mathrm{S/N} = k_9 \frac{B_S D_T^2 D_R S_T r}{R^3 B_B^{1/2}} \tag{11}$$

which indicates that, for a condition where the receiver field of view is adjusted to encompass the target precisely, performance varies as the inverse *third*, rather than *fourth*, power of range.

The simplest control of background noise is to reduce the receiver field of view until it receives energy only from the target itself. Many targets are of such extent, however, that they subtend sizeable angles at the ranges at which pulsed-light systems operate best, and the problem is not severe. However, for targets of small angular extent, such as aircraft at a distance, reduction in the field of view establishes a requirement for a high degree of pointing accuracy.

Another source of external noise is the backscattering of the pulsed-emitted light from dust and other particulate matter between the transmitter and receiver. Ordinarily this is of less consequence in daylight than is background noise, but at night, when background noise is at a minimum, backscattered light may equal or exceed the signal energy at the longer ranges possible in darkness. However, as in RF techniques, electronic processing can extract signals which are considerably below noise.

There are many interesting and useful applications of pulsed-light techniques in which the "target" can be provided with a specular reflector. With r in the equations above increased considerably, S/N is similarly increased and range limits become greater. A flat mirror, suitably oriented, will return the projected pulse to the transmitter. In practice, however, corner reflectors, or triple mirrors, are used to obviate the need for accurate orientation of the target reflector.

Coaxial mounting arrangement of transmitter and receiver mirrors is preferable if a triple-mirror reflector is used as a target; otherwise, the reflected energy may be partially or wholly lost. Coaxial arrangements are generally used, however, even in the case of diffuse reflectors, to facilitate aiming the rangefinder.

In the case of a perfect triple-mirror target, the expression for S/N can be developed as

$$\mathrm{S/N} = k_{10} \frac{B_S A S_m^2}{\theta R^2 A_R^{1/2} B_B^{1/2}} \tag{12}$$

where

S_m = diameter of the triple mirror,
A = area of receiver mirror intercepting energy reflected from the triple mirror, and
A_R = whole receiver area which accepts background noise.

This equation should be compared with (9) for the similar case of a diffuse reflector smaller than the receiver field of view. Note that range affects S/N to the inverse *second*, rather than *fourth*, power. Range performance is markedly increased by this fact.

Atmospheric attenuation has not been treated in the foregoing development. It is a formidable factor affecting S/N, but it does not affect the relationship shown to exist between the parameters above.

Thus far, we have considered only the external optical characteristics of the pulsed-light system. Many of the unique advantages of optical pulse ranging derive from the fact that extremely short pulses of optical energy are generated and are detected on reflection and processed by even faster photodetectors.

Capacitors are discharged through pulse lamps of special design to insure that a maximum of the stored energy is dissipated in a single flash. This single flash may be of less than a half-microsecond duration, with a rise time of less than tenth of a microsecond.

Since optical energy is propagated at the same velocity as RF energy (3×10^8 meters per second, or 300 meters per microsecond), a microsecond delay in detection of an optical pulse corresponds to 300/2, or 150, meters in range. With modern electronic techniques, time resolutions are possible, permitting range measurements to an accuracy of less than one meter.

SECTION 4. INFRARED SYSTEM CONSIDERATIONS

SIDNEY PASSMAN†, EDITOR

Paper 4.0 Introduction*

THE design of infrared detection systems spans the technologies of optics, mechanics, and electronics. In addition, military systems often involve a host of other factors related to other disciplines such as aerodynamics and propulsion. The material in this section was selected to acquaint the reader with the system elements which are common to the design and utilization of infrared-detection devices. This will carry the logical development of the subject matter of this issue from the basic physical phenomena described in Section 3 to the system applications to be described in the following Section 5.

Since there are so many diverse systems making use of infrared techniques, a logical treatment requires some division into special categories. This we have done by means of the common categorization involving image-forming systems and nonimage-forming systems, as there are usually separate techniques involved in these two areas. However, it is realized that many of the subjects discussed, such as optical materials and optical systems, may be common to both areas. Within this framework, the nonimage-forming systems are described from the standpoints of their elements; namely, detectors and preamplifiers, optics and scanning systems, sources and backgrounds, and signal processing and signal presentation.

The point of view to be taken in these discussions will be mainly phenomenological, the theoretical groundwork having been prepared in the preceding section on physics. Thus, infrared detectors will be treated from the standpoint of their performance and effective integration into a system. This includes a description of detector response, detecting ability, and the measurement and interpretation of detector parameters. Thermal detectors will be treated as well as photodetectors. Since the latter detectors often require cooling in order to facilitate longer wavelength response, some discussion of cryogenic developments is given, restricted because of space limitations to the now common Joule-Thomson type gas coolers and the recently developed thermoelectric microrefrigerator. The discussion of detector-power supplies is limited to the recent development exploiting solar converters, especially for use in a space environment.

Naturally, environmental conditions will determine the components that can be used in any operational infrared system. Thus, the reduction of microphonism is described in the discussion of preamplifier circuits and transistorization; the effect of elevated temperatures is discussed in the paper on optical materials; and the deterioration of detector performance on immersion in a nuclear radiation field is treated separately in some detail. In keeping with the interests of IRE readers, a fairly detailed discussion of preamplifier considerations in connection with the new and promising indium-antimonide detector is given.

The next step in the synthesis of an infrared system, after the selection and integration of the appropriate detector, is concerned with the optics and scanning system necessary to meet the required system parameters. General infrared optical-design considerations and specific infrared telescope systems applicable to missile guidance are described, as well as the total ensemble of available optical materials for laboratory and field use. The scanning systems are treated with special regard to devices for search and reconnaissance systems. A novel discussion of basic considerations applicable to combined optical-microwave sensing systems is given. It is believed that this area is worthy of much increased effort, and it is hoped that one of the effects of publication of material in this issue will be the encouragement of workers in allied fields to exploit infrared systems in conjunction with their own technical efforts.

With regard to sources and backgrounds, little can be said here about particulars, since the various systems differ considerably in their choices of targets, and the ambient background clutter also varies with altitude and geometry of the tactical situation. Beyond the description of the physics of sources and backgrounds found in the preceding section, the situation would become clouded by security classification on any account. We therefore have chosen to emphasize the techniques for improving target-to-background contrast, prefaced with a fundamental description of the methods of background description and their utility.

Signal processing and signal presentation include the subjects of electronic filtering, infrared signal presentations, color-translation or multicolor presentations, and the automatic control of systems such as in missile-guidance servomechanisms. In addition, techniques for physical and electronic simulation of infrared-system

* Original manuscript received by the IRE, June 29, 1959.
† The RAND Corp., Santa Monica, Calif.

performance are described in detail. The complicated problem associated with the detection-range performance of infrared systems is discussed from a standpoint which emphasizes the statistics of the detection process, a subject which has previously been rather neglected in regard to infrared-system design.

The section on infrared image-forming systems is self-contained, drawing only upon material from the physics section for descriptions of the thermal or photoconductive retina's response mechanisms. A classification of the large ensemble of image-forming devices is given which places the entire subject in perspective for perhaps the first time.

Although electronically-scanned infrared-sensing retina devices offer promise for eventually replacing the more mechanically-complicated and bulky scanning systems, the limitation of system detectivity still makes such a changeover impractical for many present applications. Here again is a problem area where it is hoped that the interaction with the electronic community offered by the present publication will bring further advances and solutions.

In conclusion, it should be stated that space limitations have made it necessary to be selective in the choice of subjects incorporated in this section, as listed below.

4.1 *Detectors and Preamplifiers*

- 4.1.1 Phenomenological Description of the Response and Detecting Ability of Radiation Detectors
- 4.1.2 The Measurement and Interpretation of Photodetector Parameters
- 4.1.3 Description and Properties of Various Thermal Detectors
- 4.1.4 Cooling Techniques for Infrared Detectors
- 4.1.5 Lumped Parameter Behavior of the Single-Stage Thermoelectric Microrefrigerator
- 4.1.6 Infrared Detector Silicon Solar Cell Power Supply
- 4.1.7 The Behavior of Infrared Detection Elements Under Nuclear Radiation Exposure
- 4.1.8 Preamplifiers for Nonimage-Forming Infrared Systems
- 4.1.9 Detectivity and Preamplifier Considerations for Indium Antimonide Photovoltaic Detectors

4.2 *Optics and Scanning Systems*

- 4.2.1 Optics for Infrared Systems
- 4.2.2 Optical Design for Infrared Missile-Seekers
- 4.2.3 Optical Materials, Films, and Filters for Infrared Instrumentation
- 4.2.4 Optical-Mechanical Scanning Techniques
- 4.2.5 Infrared Search System Design Considerations
- 4.2.6 Combined Optical-Microwave System Considerations

4.3 *Sources and Backgrounds*

- 4.3.1 Methods of Background Description and Their Utility
- 4.3.2 The Technique of Spatial Filtering
- 4.3.3 Optical Filtering

4.4 *Signal Processing and Signal Presentation*

- 4.4.1 Special Electronic Circuits for Nonimage-Forming Infrared Systems
- 4.4.2 Infrared Data Presentation
- 4.4.3 Infrared Color Translation
- 4.4.4 Servomechanisms Design Considerations for Infrared Tracking Systems
- 4.4.5 Infrared Search System Range Performance
- 4.4.6 Simulation of Infrared Systems

4.5 *Image-Forming Systems*

- 4.5.1 Classification and Analysis of Image-Forming Systems
- 4.5.2 Photoemissive Image-Forming Systems
- 4.5.3 An Infrared Pickup Tube.

Because of the diverse uses and requirements for infrared systems, these contributions have been solicited in an attempt to cover those component areas applicable to the broadest possible utility and therefore may appear not sufficiently specialized to meet the particular needs of a specific system designer. Furthermore, the lack of space has made it necessary, in the case of several of these contributions, to edit the material drastically to fit these constraints. In cases where material suffered as a consequence, the present section editor must bear the responsibility. He wishes to thank all of those whose material is included in this section for their excellent cooperation and to apologize to the many whose material could not be used either because of the too-specialized nature of their contributions or because of space limitations. It is hoped that these articles can be published in future issues of the PROCEEDINGS.

Paper 4.1.1

Phenomenological Description of the Response and Detecting Ability of Radiation Detectors*

R. CLARK JONES†

I. Introduction

PREVIOUS articles discuss the nature of the physical processes that go on inside the active elements of radiation detectors. In this article, however, the radiation detector will be viewed as a black box with an input and an output.

Input and Output

The input of a radiation detector is radiant power, and the output is an electrical signal. Various applications will have appropriately different ways of describing both the input and the output. The input may be expressed in lumens, lumen-seconds, watts, ergs, or any of these quantities per unit area. The output is usually expressed as a voltage or a current. For the sake of specificity, we shall suppose that the input is expressed in watts of radiant power, and output is expressed in volts.

In the testing of radiation detectors, the input radiation is nearly always chopped at a uniform frequency. It is then desirable that the same measure be used for the input and the output. Usually the output is measured by the root-mean-square amplitude of its component of fundamental frequency; then the same measure is used for the input.

Responsivity

Most detectors have a range over which the output is proportional to the input, and over this range the ratio of the output to the input is called a responsivity. Even when the relation is not linear, one may still define an incremental responsivity as the ratio of a change in the output to a change in the input. The units of the responsivity R are volts per watt, usually rms volts per rms watt.

The responsivity, however, tells us nothing about the detecting ability of a radiation detector; that is to say, it tells us nothing about how small a radiation input is detectable.

Noise Equivalent Power

To evaluate the detecting ability, we must know the characteristics of the electrical noise in the output of the detector. If one divides the rms voltage of the noise by the responsivity (in volts per watt), one obtains the noise equivalent power P_N of the detector.

Thus it is clear that responsivity and noise equivalent power are important characteristics of radiation detectors. A detector that produces a greater output (from a given radiation signal) has a greater responsivity. But a detector that has a greater detecting ability has a *smaller* noise equivalent power. Thus the noise equivalent power is an upside-down measure of the detecting ability of a detector.

Detectivity

The reciprocal of the noise equivalent input is called the detectivity.[1] The detectivity D is a right-side-up measure of the detecting ability. The detectivity D is defined in general as the responsivity divided by the rms noise voltage.

If we use P to denote the radiation input power, S the voltage output, and N the rms noise voltage, then the following relations hold.

$$S = RP, \tag{1}$$

$$\mathrm{S/N} = DP. \tag{2}$$

That is to say, to determine the electrical signal output, multiply the radiation signal P by R, and to obtain the signal-to-noise ratio, multiply P by D.

The Term Sensitivity

There is a widespread tendency to use the term sensitivity to mean either the responsivity or detectivity, or their reciprocals. Just because the word sensitivity is part of everyday speech, there is a natural human tendency to use this word to mean whatever the writer happens to have in mind. In fact, it has been used to mean so many different concepts that its use in scientific and technical discourse is to be deplored.[1]

Individual Detectors and Types of Detectors

An individual detector is a single sample of a given type of detector. A type of detector is a class of individual detectors with some common properties. Heat detectors, bolometers, thermistor bolometers, photoconductive cells, and lead sulfide photoconductive cells with gold electrodes, are all examples of types of detectors.

* Original manuscript received by the IRE, June 29, 1959.
† Research Laboratories, Polaroid Corp., Cambridge, Mass.

[1] R. C. Jones, "Detectivity, the reciprocal of noise equivalent input of radiation," *Nature*, vol. 170, pp. 937–938; 1952. Also *J. Opt. Soc. Am.*, vol. 42, p. 286; 1952.

II. Parameters of the Radiation Signal

In testing the properties of detectors, one usually uses a radiation signal that is more or less monochromatic, or a radiation signal from a blackbody source. The radiation signal is thus described by its wavelength λ or by its blackbody temperature T_{bb}.

In testing detectors, it is also customary to modulate the signal at a given frequency f. It is advisable to state the amplitude of the modulated radiation power by its root-mean-square value. Most measuring systems respond only to the fundamental component of the detector output, and therefore if the source is not modulated in a sinusoidal manner, one should state the root-mean-square amplitude of the fundamental component.

In addition to the signal radiation that is to be detected or measured, there is usually additional steady radiation that is incident on the detector. Blackbody radiation from the environment, or daylight, are examples of steady ambient radiation. The power of this steady ambient radiation is denoted P_a.

III. Detector Parameters

Detector Temperature T

The detector temperature T is the temperature of the responsive element of the detector. Usually the temperature of the responsive element is substantially uniform over its volume, and there is no difficulty in defining the temperature of the responsive element.

Responsive Area A

Roughly speaking, we may say that the responsive area A of the detector is the area over which the detector is more or less equally responsive. In some types of detectors, such as wire-type thermocouples, there is no question of how the responsive area should be specified. In some other types of detectors, such as evaporated photoconductive films, there may be a real question how the area A is to be specified.

To define the area A more precisely, it is necessary to introduce the concept of the local responsivity of a detector. If the radiant power is concentrated on a very small area centered at the point x, y on the surface of the responsive element, the local responsivity $R(x, y)$ is the ratio of the electrical output to the incident power.

If the local responsivity has a flat maximum in the central region of the responsive area and decreases smoothly away from the center, then a useful measure of the responsive area A is

$$A = \int\int R(x, y)dxdy/R_{\max} \tag{3}$$

where $R_{\max}$ is the maximum value of $R(x, y)$.

If, however, the local responsivity is an irregular function (corresponding to the presence of small regions of particularly high responsivity), then the observer may elect to replace $R_{\max}$ in the above expression by a suitably chosen average over the central region of the detector.

Specifying the value of the responsive area A is particularly important because the original measurement of the responsivity usually involves measuring the ratio R_H of the electrical output to the irradiance of the cell. To obtain the responsivity R in the form electrical output divided by the incident power, R_H must be divided by A.

$$R = R_H/A. \tag{4}$$

In addition to having an area specified in square centimeters, the detector also has a size and shape. In many cases it will be sufficient to describe the two principal dimensions of a rectangular detector, but if the local responsivity is an irregular function, the only adequate way to express the shape of the local responsivity is to show a contour diagram or several profiles of the relative local responsivity.

The Gain g

Most kinds of individual detectors have externally adjustable parameters that permit variation of the responsivity (and of the detectivity). Examples of these adjustable parameters are the biasing current in bolometers and photoconductive cells, the applied potentials in multiplier phototubes and simple phototubes, the biasing voltage in back-biased junctions, the emitter current in phototransistors, the several adjustable parameters of the Golay detector, the pre-exposure of photographic films, and the magnetic field in photoelectromagnetic detectors. Indeed, only the thermocouple and photovoltaic detectors seem to be free of such adjustable parameters.

All of these parameters have the effect of varying the "internal gain" of the detectors, and as a generic way of referring to the variation of any of these parameters, we shall in the following refer to varying the gain g of the detectors. The gain g may be considered to mean any of the adjustable parameters. Since the gain g is used in this report only in a qualitative sense, we do not need to define g more precisely.

The Bandwidth Δf

The noise bandwidth Δf is the bandwidth in cycles per second of the noise that is effective in the measurement of the noise equivalent power P_N. If $N(f)$ denotes the mean-square-noise-voltage (or current) per-unit bandwidth [$N(f)$ is often called the power spectrum of the noise] at the point in the circuit where the noise equivalent power is measured, the bandwidth Δf is defined by

$$\Delta f = \int_0^\infty N(f)df/N_{\max} \tag{5}$$

where $N_{\max}$ is the maximum value of $N(f)$ with respect to variation of f.

Time Constants

The time constant of a detector is usually defined in terms of the way that the responsivity R depends on the frequency f. If, for example, the responsivity depends on f in accordance with the simple relation

$$R(f) = R_0/(1 + (2\pi f\tau_r)^2)^{1/2} \tag{6}$$

then τ_r is called the responsive time constant of the detector. More generally, the responsive time constant may be defined by

$$\tau_r = \frac{R_m^2}{4\int_0^\infty [R(f)]^2 df} \tag{7}$$

where R_m is the maximum value of $R(f)$ with respect to frequency.

Much more fundamental is the detective time constant, which is defined in general by

$$\tau_d = \frac{D^*{}_m^2}{4\int_0^\infty [D^*(f)]^2 df} \tag{8}$$

where $D^*{}_m$ is the maximum value of $D^*(f)$ with respect to f, and where $D^*(f)$ is defined by (20) below. The detective time constant τ_d cannot be changed by changing the gain vs frequency characteristic of the amplifier, and is thus an invariant measure of the speed of response of the detector.

IV. The Parameters on Which R, N and D Depend

The Responsivity R

The responsivity of an individual detector operated at a given temperature T and at a given gain g depends on these parameters and on the parameters of the radiation, giving

$$R = R(\lambda, f, P_a, T, g). \tag{9}$$

But the responsivity of a type of radiation detector, in which one is free to vary the detective time constant τ_d and the area A, will depend on these parameters also. Thus, one has

$$R = R(\lambda, f, P_a, T, g, \tau_d, A). \tag{10}$$

The Noise Power Spectrum N

The power spectrum N of the noise at the output of an individual radiation detector depends only on the modulation frequency f, the detector temperature T, and the gain g, provided that the noise is not affected by the amount of the ambient power P_a. But if the noise power does depend on the ambient power P_a, it also depends on the wavelength λ of this power. Thus, one has in general

$$N = N(f, T, g; \lambda, P_a). \tag{11}$$

The noise spectrum of a type of radiation detector, in which one is free to vary the detective time constant τ_d and the responsive area A, depends also on these variables.

$$N = N(f, T, g, \tau_d, A; \lambda, P_a). \tag{12}$$

The Detectivity D

The detectivity D of a radiation detector depends on the same parameters as the responsivity, and in addition it depends on the bandwidth Δf of the noise.

Thus, for an individual detector, one has

$$D = D(\lambda, f, p_a, T, g, \Delta f). \tag{13}$$

But if one is free to vary the detective time constant τ_d, and the area A, the detectivity of a type of radiation detector will depend also on these parameters

$$D = D(\lambda, f, p_a, T, g, \Delta f, \tau_d, A). \tag{14}$$

In terms of the responsivity R and the power spectrum N of the electrical noise, the detectivity D is defined in general by

$$D(\lambda, f, P_a, T, g, \Delta f, \tau_d, A) = \frac{R(\lambda, f, P_a, T, g, \tau_a, A)}{(\Delta f N(T, g, \tau_d, A; \lambda, P_a))^{1/2}}. \tag{15}$$

V. The Detectivity D^*, and the Figures of Merit M_1 and M_2

The Detectivity D in the Reference Condition E*

Most of the material in this section was condensed from the first three sections of a chapter[3] written in 1952. The material relating to D^* was first presented to an IRIS meeting on November 13, 1956, and later appeared in the *Proceedings of the IRIS*.[4]

In this section, it is supposed that the detectivity D does not depend appreciably on the ambient power P_a. The detectivity thus has the following functional dependence.

$$D = D(\lambda, f, T, g, \Delta f, \tau_d, A). \tag{16}$$

No one has yet been able to perceive any useful systematic trends in the dependence of the detectivity on the wavelength λ and the detector temperature T. But it is possible to perceive systematic relations between the detectivity and the other five parameters. For the present, we suppress the symbols λ and T, and consider that the detectivity has the following functional dependence.

$$D = D(f, g, \Delta f, \tau_d, A). \tag{17}$$

[2] R. C. Jones, "Performance of detectors for visible and infrared radiation," in "Advances in Electronics," L. Marton, ed., Academic Press, Inc., New York, N. Y., vol. 5, pp. 27–30; 1953. The responsive time constant τ_r was there called the physical time constant τ_p, and the detective time constant τ_d was there called the reference time constant τ.

[3] *Ibid.*, pp. 1–96.

[4] R. C. Jones, "Method of rating the performance of photoconductive cells," *Proc. IRIS*, vol. 2, pp. 9–12; June, 1957.

It is customary to adjust the gain g by varying the internal parameters of the detector so that the detectivity is maximized. To be sure, this maximum will usually depend on the frequency f, but some compromise adjustment is usually selected. Once this choice is made, the detectivity no longer depends on the gain g, so that one has

$$D = D(f, \Delta f, \tau_d, A). \tag{18}$$

We consider next the dependence of the detectivity D on the responsive area A. On the basis of certain idealized assumptions, one may prove that, other conditions being equal, D varies inversely as the square root of the area A.

$$DA^{1/2} = \text{independent of } A. \tag{19}$$

This relation is valid when the dominant noise of the detector is radiation noise. The relation also follows if the area A is varied by connecting together several identical adjacent detectors. In practice, one sometimes finds deviation from the above relation, and in all cases known to the writer, these deviations occur because the properties per unit area depend on the total area. 1) In thermistor bolometers, more power per unit area can be dissipated in very small detectors, because the lines of heat flow are then radial instead of normal to the surface. 2) In evaporated photoconductive cells, the surface often contains a small area of exceptionally high detectivity. With cells of very small area, one can select the cells that contain a "hot spot," and reject the others; in cells of large area that contain many hot spots, this is not possible. 3) In indium antimonide photovoltaic cells, there is often 1/f noise that arises from the boundary. This noise varies as the circumference of the cell and causes the detectivity to vary as $A^{-1/4}$, but the 1/f noise can be eliminated by suitable back bias or by use of a dc short circuit, in which case (19) is found to hold. In the first two examples, the exponent is greater than one-half; in the third, it is less than one-half. For comparing the performance of a wide variety of detectors, the exponent one-half in (10) is clearly a better choice than any other number.

Departures from (19) may also occur in a different kind of situation. Some detectors have a directivity pattern that is not Lambertian. With an antenna array, the quotient of the area A and the directive gain is a constant. The same relation holds when the effective area is changed by immersing the responsive element in a high-index medium. In both of these situations (19) fails, but may be made to hold by replacing A by the ratio of A to the directive gain.

We consider next the dependence of the detectivity on the noise bandwidth Δf. There are no perfectly general statements that can be made in this respect, because we have introduced so far no restrictions on the way that the power spectrum $N(f)$ of the noise depends on the frequency f. We now introduce the assumption that over the band of frequencies we wish to discuss, the power spectrum $N(f)$ is independent of f. (The amplifier can always be equalized so that this assumption is justified.) Then it follows that the detectivity D, other parameters being constant, varies as the inverse square root of the bandwidth Δf.

We now define $D^*(f, \tau_d)$ as the detectivity measured with a bandwidth Δf of one cycle per second and reduced to a responsive area of one cm^2. By the three preceding paragraphs, one has

$$D^*(f, \tau_d) = (A\Delta f)^{1/2} D(f, \tau_d, A, \Delta f). \tag{20}$$

D^* is pronounced "D-star." (An author may desire a formal name for D^*; the name "detectivity in the reference condition E" is recommended.) The dimensions of D^* are length-(frequency)$^{1/2}$/power. If A is measured in cm^2, and f in cycles/second, the units of D^* are cm-(cps)$^{1/2}$/watt. The writer recommends that these particular units be used for D^* unless there is specific indication to the contrary.

The Figures of Merit M_1 and M_2

For most detectors, including lead sulfide photoconductive cells, there is a systematic relation between the detectivity D^* and the parameters f and τ_d. In fact, detectors may be placed in two mutually-exclusive classes[5] on the basis of the way that D^* depends on the detective time constant τ_d. In order to define these two classes, we first introduce the quantity $D^*_m(\tau_d)$, which is defined as the maximum value of $D^*(f, \tau_d)$ with respect to the frequency f.

A Class I detector is then defined as a type of detector for which D^*_m is independent of the value of the detective time constant, and a Class II detector is a type of detector for which D^*_m is proportional to the square root of τ_d. It is an experimental fact that all detectors fall into one of these two classes, except for those types of detectors for which insufficient information is available to specify the Class membership.

Class I detectors include photoemissive tubes, ideal heat detectors, the Golay heat detector, radio antennas, and some photoconductive cells. Class II detectors include thermocouples and bolometers, photographic films, the human eye, and most lead sulfide cells. These statements are subject to a number of conditions and assumptions. A full discussion will be found in Jones.[3]

In 1949, a figure of merit was introduced[5] for each of the two Classes. The figure of merit M_1 for Class I detectors was defined as the ratio of the measured value of D^*_m to the value of D^*_m for an ideal heat detector at the temperature 300°K. M_1 may be written

$$M_1 = (5.52 \times 10^{-11} \text{ watt/cm-(cps)}^{1/2}) D^*_m \tag{21}$$

where D^*_m must be expressed in cm-(cps)$^{1/2}$/watt. M_1 is dimensionless. Similarly, the figure of merit for Class II detectors was defined[5] as the ratio of D^*_m to the value

[5] R. C. Jones, "Radiation detectors," *J. Opt. Soc. Am.*, vol. 39, pp. 327–356; 1949.

of D^*_m for a detector that accords with Havens' limit.[6,7] Havens' limit is an engineering estimate of the maximum possible detectivity of a thermocouple or bolometer. The value of M_2 may be written

$$M_2 = (6 \times 10^{-11} \text{ watt-sec/cm}) D^*_m / \tau_d^{1/2} \qquad (22)$$

where D^*_m must be expressed in cm-(cps)$^{1/2}$/watt and τ_d in seconds. M_2 is dimensionless.

Since the detective time constant is defined by

$$\tau_d = \tfrac{1}{4}(D^*_m)^2 \Big/ \int_0^\infty [D^*(f)]^2 df \qquad (23)$$

M_2 may also be written

$$M_2 = (12 \times 10^{-11} \text{ watt/cm-cps}) \left[\int_0^\infty [D^*(f)^2 df \right]^{1/2} \qquad (24)$$

where D^* must be expressed in cm-(cps)$^{1/2}$/watt, and f in cps.

In these expressions, the figures of merit M_1 and M_2 are dimensionless, and depend only on the wavelength λ (or the temperature T_{bb} of the blackbody source) and on the temperature T of the detector. (D^* depends on λ and T, and also on f and τ_d.)

M_1 and M_2 are plotted vs the wavelength for a number of different types of detectors in Figs 1 and 2. These figures are reproduced from Jones.[3]

VI. The Detective Quantum Efficiency Q_D

Most of the material in this section is condensed from the first four sections of a review written in 1958, to be published[8] in 1959. Some of the material has already been published.[9–12]

There are two kinds of quantum efficiency. The more familiar kind is always defined as the ratio of the number of output events to the number of input events. This kind of quantum efficiency is thus a ratio, and is moreover a ratio of the numbers of two kinds of countable events. A familiar example is the quantum efficiency of a photoemissive tube, which is usually defined as the ratio of the number of emitted photoelectrons to the number of incident photons. This kind of quantum efficiency is clearly related to the responsivity of a detector, and for this reason it has been named *responsive* quantum efficiency.

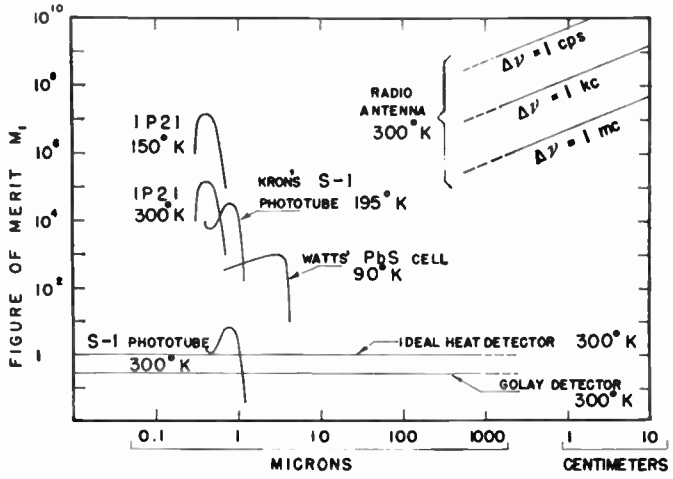

Fig. 1—The figure of merit M_1 as a function of the wavelength for several types of Class I detectors; both coordinate scales are logarithmic, but the ordinate scale is compressed relative to the abscissa scale. Of particular interest is the extent to which the detectivity of S-1 phototubes can be increased by cooling. The improvement of the 1P21 multiplier phototube by cooling is also marked.

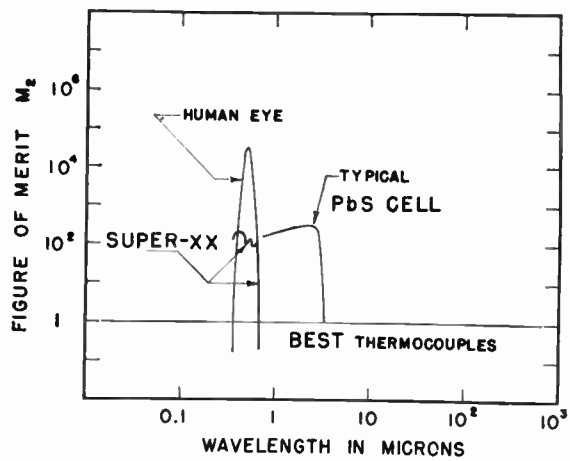

Fig. 2—The figure of merit M_2 as a function of the wavelength for several types of Class II detectors; the long-wavelength portions of the curves for human vision and for Super-XX film are coincident. References to the detectors described in Figs. 1 and 2 will be found in the literature.[3]

There is another kind of quantum efficiency that is related to the detectivity of a detector, and for this reason, it has been named *detective* quantum efficiency. The concept of detective quantum efficiency was first formulated by Rose[13] in 1946.

The detective quantum efficiency may be defined without regard to the amount of the ambient power P_a, but it acquires its chief interest only when the ambient power P_a is sufficient to affect appreciably the detectivity D. Thus the situation discussed in this section is complementary to that in Section V of this paper.

In the presence of a given amount of ambient power of the same wavelength as the radiation signal to be de-

[6] R. J. Havens, "Theoretical comparison of heat detectors," *J. Opt. Soc. Am.*, vol. 36, p. 355; 1946.
[7] R. J. Havens, "Theoretical limit for the sensitivity of heat detectors," *Proc. IRIS*, vol. 2, pp. 5–8; June, 1957.
[8] R. C. Jones, "Quantum Efficiency of Detectors for Visible and Infrared Radiation," in "Advances in Electronics and Electron Processes," Academic Press, Inc., New York, N. Y., vol. 12; 1959.
[9] R. C. Jones, "Quantum efficiency of photoconductors," *Proc. IRIS*, vol. 2, pp. 13–17; June, 1957.
[10] R. C. Jones, "On the quantum efficiency of photographic negatives," *Phot. Sci. Engrg.*, vol. 2, pp. 57–65; 1958.
[11] R. C. Jones, "Quantum efficiency of human vision," *J. Opt. Soc. Am.*, vol. 49, pp. 645–653; July, 1959.
[12] R. C. Jones, "On the detective quantum efficiency of television camera tubes," *J. Soc. Mot. Pict. Telev. Engrs.*, to be published.
[13] A. Rose, "A unified approach to the performance of photographic film, television pickup tubes, and the human eye," *J. Soc. Mot. Pict. Telev. Engrs.*, vol. 47, pp. 273–294; 1947.

tected, there is a very fundamental limit to the detectivity. This limit is due to the quantum fluctuations in the "steady" ambient radiation.

To bring out the nature of this limit in a simple way, we consider the number of photons in the radiation incident on a detector of area A in the period of duration T. The average number of signal photons is denoted M_s, and the average number of photons in the ambient radiation is denoted M_a. All of the photons are assumed to have the same wavelength. It is important to note that M_a is the average number, where the average is over a large number of successive periods, each of length T. In any given period, however, the number of actual photons $\mathfrak{M}_a$ will usually be different from the average number M_a. The number varies from period to period even in the most steady ambient radiation fields, because the individual photons arrive at random, like drops of rain on a roof. As shown by Fry,[14] the distribution of the number will be approximate to a Poisson distribution, from which it follows that the root-mean-square fluctuation of the number is equal to the square root of M_a.

$$N \equiv \Delta M = \langle \mathfrak{M}_a - M_a)^2 \rangle_{\mathrm{Av}}^{1/2} = M_a^{1/2}. \tag{25}$$

Since this fluctuation is a noise, it has been denoted by N in the above equation.

Similarly, the number S of signal photons is the number M_s,

$$S = M_s \tag{26}$$

from which one finds that the signal-to-noise ratio is given by

$$\frac{S}{N} = \frac{M_s}{M_a^{1/2}}. \tag{27}$$

This is the signal-to-noise ratio present in the radiation incident on the detector. Under the given conditions, no detector may have a higher signal-to-noise ratio in its output. In fact, no detector can have quite as high a signal-to-noise ratio.

The squared ratio of the actual signal-to-noise ratio $(S/N)_{\mathrm{meas}}$ to the maximum possible signal-to-noise ratio as given by (26) is the detective quantum efficiency,

$$Q_D = \frac{(S/N)_{\mathrm{meas}}^2}{M_s^2/M_a}. \tag{28}$$

Thus, one sees by its very definition that the maximum possible value of the detective quantum efficiency is unity.

The detective quantum efficiency must be defined as the *square* of the ratio of signal-to-noise ratios, in order to make the detective quantum efficiency equal to the responsive quantum efficiency of an ideal photoemissive tube. The details are here omitted.

[14] T. C. Fry, "Probability and its Engineering Uses," D. Van Nostrand Co., Inc., New York, N. Y., pp. 216–227; 1929.

The detective quantum efficiency is equivalently defined as the squared ratio of the noise equivalent power in the incident radiation to the noise equivalent power of the actual detector measured under the same conditions.

$$Q_D = (P_N)_{\mathrm{rad}}^2/(P_N)_{\mathrm{meas}}^2. \tag{29}$$

One may show that the mean-square fluctuation in the power of the ambient radiation is given by

$$(P_N)_{\mathrm{rad}}^2 = 2EP_a\Delta f \tag{30}$$

where E is the energy of a single photon. Combining the last two relations then yields

$$Q_D = 2EP_a\Delta f/(P_N)_{\mathrm{meas}}^2. \tag{31}$$

As indicated by (29) above, the reciprocal of the detective quantum efficiency Q_D^{-1} is a kind of noise figure. It is a noise figure in which the reference noise is the noise in the ambient radiation, whereas the noise figure ordinarily used in electronic equipment has Johnson noise as the reference noise. These two reference noise levels are in general different in amount and in concept. In a radio antenna, however, the two become identical.

The expressions for the radiation noise used above are based on Maxwell-Boltzmann statistics. Actually, ensembles of photons must be described by Bose statistics. So long, however, as hc/λ is large compared with kT_{rad}, where T_{rad} is the temperature of the source of the ambient radiation, the approximation used above is valid. The approximation is valid for the infrared spectrum (although it begins to break down for a high temperature source at wavelengths longer than about ten microns), but it is not correct in the radio spectrum. See Jones[8] for a full discussion.

Fig. 3 shows a plot with logarithmic scales of the detective quantum efficiency plotted vs the amount of ambient radiation M_a. The curve shown is for an imaginary detector. This plot has a number of interesting properties. On the plot, any detector that has a detectivity D independent of the ambient power is presented by a straight line with a slope of plus one. Thus the point on the curve where the detectivity has its maximum value is the point where the slope of the curve is plus one, as at the point A.

There is another kind of detectivity, named the contrast detectivity D_c, which is defined as the reciprocal of the noise equivalent value of the contrast M_s/M_a. D_c may be written

$$D_c = P_aD. \tag{32}$$

D_c is dimensionless. Any detector that has a contrast detectivity that is independent of the ambient power is represented in Fig. 3 by a straight line with a slope of minus one. Thus, the point on the curve where the contrast detectivity of the detector has its maximum value is the point where the slope is minus one, as at the point C.

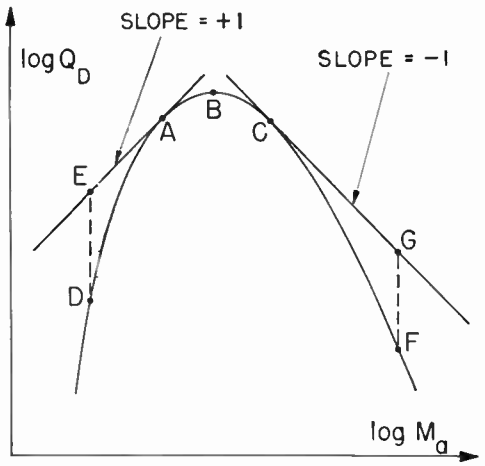

Fig. 3—A schematic plot showing the detective quantum efficiency Q_D plotted against the irradiation of the detecting surface; if the irradiation is less than at the point A (where the curve has a slope of plus one), the detector is underloaded, and Q_D can be increased by adding additional steady irradiation. If the irradiation is more than that at the point C (where the curve has a slope of minus one), the detector is overloaded, and Q_D can be increased by placing a neutral filter over the detector. All detectors can be overloaded, but not all detectors can be underloaded.

At any point on the curve where the slope is more than plus one, the detector is underloaded, which means that the detectivity D can actually be increased, as from the point D to E, by adding a local source of ambient radiation that raises the total ambient radiation to the value at A. Similarly, at any point on the curve where the slope is less than minus one, the detector is overloaded, by which is meant that the contrast detectivity can actually be increased, as from F to G, by placing an attenuating filter over the detector that reduces the ambient radiation to the value at C.

Thus, the range from A to C is the working range of the detector. Nothing is ever gained by operating outside of this range. All detectors can be overloaded, but most detectors cannot be underloaded. The classic example of a detector that is easily underloaded is the photographic film, where it is well known that it is necessary to pre- or post-expose the film to record the weakest images.

Figs. 4 and 5 show the detective quantum efficiency of human vision, two photographic films, and three television camera tubes. In Fig. 4, Q_D is plotted vs the ambient exposure with all of the parameters adjusted to their optimum values. In Fig. 5, Q_D is plotted against wavelength with all of the other parameters adjusted to their optimum values.

This section is concluded with the relation between the detective quantum efficiency Q_D and the detectivity D^*,

$$AQ_D = 2EP_a(D^*)^2. \tag{33}$$

This relation is easily derived from (31) and above, and holds for an individual detector in which the same conditions of measurements are used for Q_D and D^* (same values of λ, f, P_a, g and T).

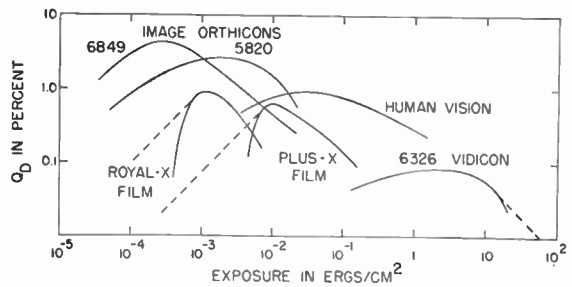

Fig. 4—The detective quantum efficiency Q_D plotted against the ambient exposure in ergs per square centimeter, for three varieties of image-forming detectors: television camera tubes, photographic negatives, and human foveal vision. The dashed lines have slopes of plus one and minus one, and correspond to the lines in Fig. 3. The results shown are for optimum choice of all of the other parameters that affect the value of Q_D, such as wavelength, size of signal area, signal duration, etc. The details of the method by which the curves are calculated are given in the literature.[8]

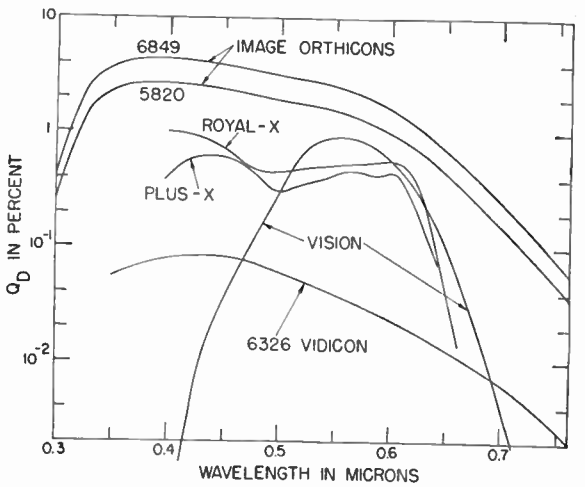

Fig. 5—The detective quantum efficiency Q_D plotted vs the wavelength for the same detectors as in Fig. 4. The results are for optimum choice of all of the other parameters that affect the value of Q_D, such as the amount of steady irradiation, size of signal area, signal duration, etc.

VII. Concepts Restricted to Photoconductive Cells

The great importance of photoconductive cells in infrared detection has led to a number of concepts and notations whose application is restricted to photoconductive cells.

"*Jones' S*"

The first concept proposed[15] specifically for photoconductive cells was "Jones' S." This concept is now obsolete, but it is still important because all of the detector reports issued by the Naval Ordnance Laboratory at Corona, Calif., use this concept. Jones' S is related to D^* by

[15] R. C. Jones, "A method of describing the detectivity of photoconductive cells," *Rev. Sci. Instr.*, vol. 24, pp. 1035–1040; 1953. Jones' S was proposed in a privately circulated report, "Proposal of a Figure of Merit for Photoconductive Cells," dated February 1, 1950, and the proposal was presented at Prof. Nottingham's Photoconductivity Conf. at Massachusetts Institute of Technology, Cambridge, Mass., March 28, 1950.

$$\text{Jones' } S = f^{1/2}/D^*. \tag{34}$$

Jones' S is defined as the noise equivalent power reduced to unit area and to a noise bandwidth in which the upper edge of the band has a frequency $e = 2.718$ times the frequency of the lower edge. Jones' S was intended to be used for low frequencies where S is constant if the responsivity is constant and the power spectrum $N(f)$ of the noise varies as 1/f. According to (34), Jones' S has the dimensions of power/length, and is usually expressed in watt/cm.

Specific Noise and Specific Responsivity

Shortly after Jones' S was proposed, Mundie and Kirk[16] proposed a specific noise N_1 and a specific responsivity S_1 defined by

$$N_1 = \frac{A^{1/2}V_{n,e}}{V} \cdot \frac{(R_c + R_L)^2}{4R_cR_L} \tag{35}$$

and

$$S_1 = \frac{V_s}{FV} \cdot \frac{(R_c + R_L)^2}{4R_cR_L} \tag{36}$$

where V is the bias voltage across the cell, V_s is the signal voltage produced by a signal irradiation of F watts per square centimeter, and $V_{n,e}$ is the rms noise voltage measured in a bandwidth with the frequency ratio e. R_c is the (variable) resistance of the cell, and R_L is the (variable) resistance of the load. They have the property that N_1 divided by S_1 is equal to Jones' S.

$$\text{Jones' } S = N_1/S_1. \tag{37}$$

Since Jones' S and N_1 were introduced, it has become increasingly evident that the power spectrum of the noise in many cases deviates quite importantly from a 1/f shape[17] and that, therefore, the appropriateness of the definitions of Jones' S and N_1 is reduced. Jones' S, S_1 and N_1 continue to be used in the Corona reports[17] up to the time of writing.

Petritz' Specific Noise

Petritz[18] has introduced a modified specific noise

$$N_s = \frac{A^{1/2}V_n}{(\Delta f)^{1/2}V} \cdot \frac{(R_c + R_L)^2}{4R_cR_L} \tag{38}$$

where V_n is the rms noise voltage measured within the bandwidth Δf. D^* is related to S_1 and N_s by

$$D^* = S_1/N_s. \tag{39}$$

N_1 is usually expressed in cm, S_1 in cm²/watt, and N_s in cm/(cps)$^{1/2}$.

[16] L. G. Mundie and D. D. Kirk, "Notes for Users of Photoconductive Detectors," NBS-Corona Rept. No. 30-E-109; August 15, 1952.

[17] See the papers by van Vliet and his co-workers in *Physica* and PROC. IRE, in 1956 and following years. Also see the NBS-Corona and NOL-Corona series of reports, beginning in 1952 and continuing through the present.

[18] R. L. Petritz, "Theory of photoconductivity in semiconductor films," *Phys. Rev.*, vol. 104, pp. 1508–1516; 1956.

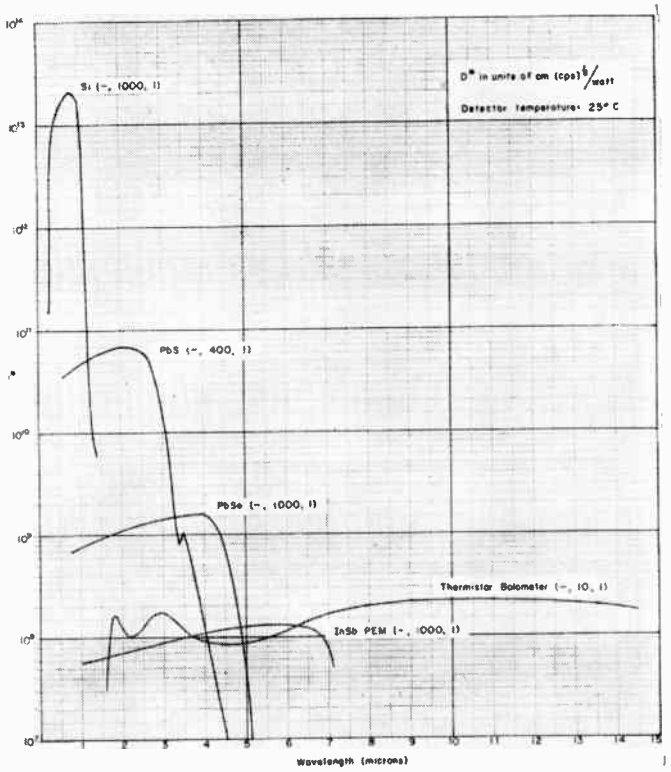

Fig. 6—Comparative spectral curves of several representative photodetectors at room temperature.

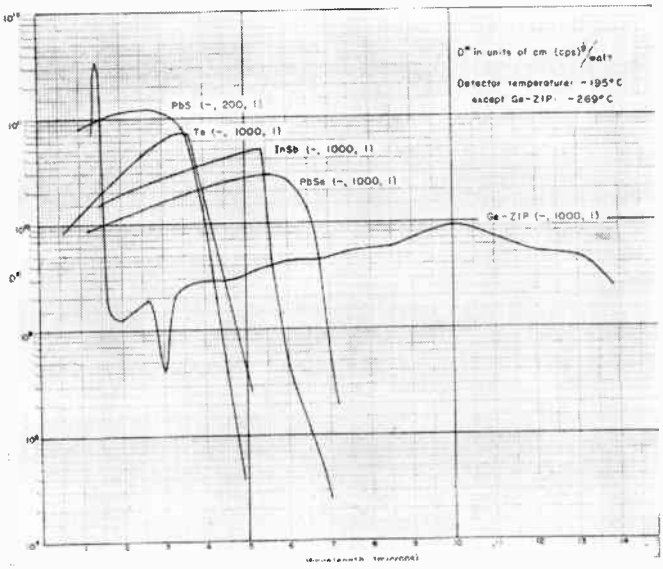

Fig. 7—Comparative spectral curves of several representative cooled photodetectors.

In conclusion, through the courtesy of R. F. Potter of the Infrared Division, U. S. Naval Ordnance Laboratory, Corona, Calif., it is possible to show, in Figs. 6 and 7, curves summarizing the current state-of-the-art of photodetectors. Detectivity in the reference condition E is plotted against wavelength. The hyphen in the parentheses following the label on each curve indicates that the data are for spectral measurements; the next number is the chopping frequency in cycles per second, and the final number is the frequency bandwidth, in each case unity.

Paper 4.1.2

The Measurement and Interpretation of Photodetector Parameters*

R. F. POTTER†, J. M. PERNETT†, AND A. B. NAUGLE†

Definitions of Symbols

J = rms value of the fundamental component of the energy flux measured in watts/cm².
V = rms value of the fundamental component of the signal voltage, as measured with the entire detector exposed.
N = rms noise voltage.
A = area of the cell, as defined by the electrodes, in cm².
P_n = noise equivalent power.
f = modulating frequency in cps.
Δf = frequency bandwidth in cps.
E = bias voltage applied across the detector and the load resistor.
R_c = detector dark resistance.
R_L = load resistance.

Introduction

INFRARED technology is including an increasing number of challenging problems within its domain. In order to meet and solve these challenges engineers and scientists must design and develop novel systems built on the physical principles and techniques of infrared technology. In many instances the key to the solution of an unexplored problem may be in understanding and realizing the potential utility of the photodetector.

The Infrared Sensitive Element Evaluation Program[1] which has been carried on for several years as a joint services effort at the U. S. Naval Ordnance Laboratory, Corona (previously known as the National Bureau of Standards, Corona Laboratories) is designed to provide up-to-date quantitative measurements on all types and kinds of photodetectors. For technical application, there are several important parameters which determine the detector's utility, and it is these parameters and the measuring techniques used at Corona which are described below.

In understanding and appreciating how these parameters are measured, the designer may find that particular detectors have more application potential than that utilized at present. The physical picture of photodetector operation has been presented in the preceding section on physics. In order to compare and evaluate detectors, several figures of merit[2] have been defined, and those in common use today, which are listed in the Corona reports, are given in Table I along with definitions of terms.

The following will be discussed: determination of optimum operating conditions, response to standard radiation sources, relative spectral response, determination of absolute response levels, frequency response, noise spectrum, and the sensitivity contours, as well as the manner of presentation of these data in the NOLC photodetector series of reports. In most instances, examples characteristic of a cooled PbSe photodetector will be given. This detector is one reported in NOLC detector series Report No. 36. There is a large variety of types of detectors with differing capabilities and operating conditions. This particular cell required cooling to −196°C.

TABLE I
Figures of Merit

Figure of Merit	Definition	Units
NEI	$\text{NEI} = \frac{JN}{V}$	Noise Equivalent Input in watts/cm².
NEP = P_n	$\text{NEP} = \frac{JNA}{V}$	Noise Equivalent Power in watts.
Jones' S	$S = \frac{P_n}{A^{1/2}} \left(\frac{f}{\Delta f}\right)^{1/2}$	Jones' S in watts/cm.
D^*	$D^* = \frac{A^{1/2}(\Delta f)^{1/2}}{P_n}$	The detectivity normalized to unit area and unit bandwidth in cm/watt.
S_1	$S_1 = \frac{V}{JE} \frac{(R_c + R_L)^2}{4R_cR_L}$	Specific Sensitivity in cm²/watt.

Optimum Bias and Standard Radiation Sources

The standard sources in use at Corona include a 500°K blackbody with a flux density of 7.7 μw/cm² at the detector plane, and a 1.1 μ He line with a flux density of 8.5 μw/cm². The flux density of the sources is obtained by comparison of the response of a radiation

* Original manuscript received by the IRE, June 26, 1959.
† Naval Ordnance Lab., Corona, Calif.
[1] NOLC Reports, "Properties of Photoconductive Detectors," a series of reports of measurements performed under the Joint Services Infrared Sensitive Element Testing Program, NE 120713-5; 1952–1959.
[2] For further discussion of these figures of merit, see R. C. Jones, "Phenomenological description of the response and detecting ability of radiation detectors," paper 4.1.1, this issue, p. 1495.

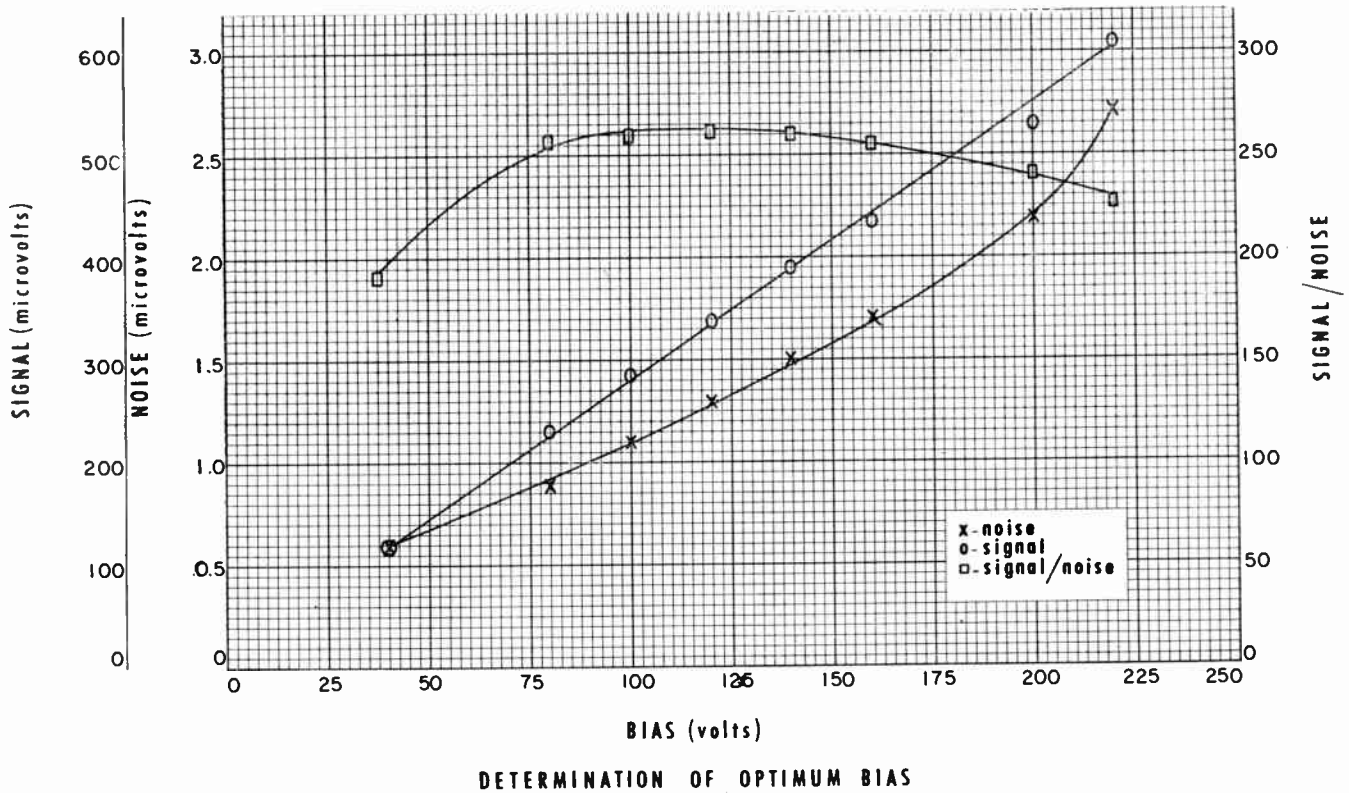

Fig. 1—The signal V and noise voltage N and the ratio V/N determined with a 1.1 μ He standard radiation source as a function of bias voltage. The dark cell resistance is 2.4 megohms and the load resistance is 2.4 megohms.

thermopile to the radiation from the sources, with the response to a National Bureau of Standards standard radiant energy lamp. The sources are mechanically modulated at 90 cps.

The signal and noise for the detector with load resistance is determined as a function of bias voltage with the 1.1 μ He radiation being used for the signal measurements. The amplifier consists of a cathode follower, a Tektronix model 122 preamplifier, and a General Radio model 736A wave analyzer tuned to 90 cps. The bias current found to give the highest signal-to-noise ratio is subsequently used for all other measurements of the detector. For most detectors the optimum bias does not appreciably change with the modulating frequency. Fig. 1 shows the bias graph for a cooled PbSe detector, with optimum bias at 24.5 μamps.

Relative Spectral Response

The relative spectral response is a very significant detector characteristic since it indicates over which portion of the infrared spectrum the detector will be useful. Two monochromators are in normal use at Corona; one, a Leiss double monochromator has CaF_2 prisms giving a range from 0.6 μ to 8 μ, the other a Perkin-Elmer Model 98 has NaCl prisms, giving a range from 2 μ to 15 μ.

The energy flux from the exit slit is kept at a constant value over that portion of the spectrum used, by comparing the flux at each wavelength with a thermopile or thermocouple. This is done with the internal thermocouple in the Model 98 while an external arrangement is used for the Leiss monochromator. For the latter, the light from the glower source is modulated at both 10 cps and 90 cps. The energy from the exit slit falls on a "black" thermopile and the signal is amplified with a 10-cps amplifier. The energy is raised or lowered to an arbitrary value by opening or closing the entrance slit, with the middle and exit slits usually remaining fixed. Once this level is set the energy flux is allowed to fall onto the detector and the response is rated with the same arrangement as for the standard source measurement.

The relative response curve in the example of Fig. 2 is normalized to unity at 1.2 μ. The interesting thing about detectors of this general type is their relatively high sensitivity out to 5 μ.

Using the Planck distribution function for a 500°K blackbody,[3] the detector response to such a source, and the relative spectral response, the absolute spectral response is determined in the following manner. The product of the fraction of blackbody energy in each 0.1 μ interval and the spectral relative response is numerically integrated over all wavelengths to give a factor γ which indicates how effective the detector is, compared to a "black" or "gray" detector (*i.e.*, a de-

[3] R. A. Smith, F. E. Jones, and R. P. Chasmar, "The Detection and Measurement of Infrared Radiation," Oxford Press, New York, N. Y., ch. 2; 1957.

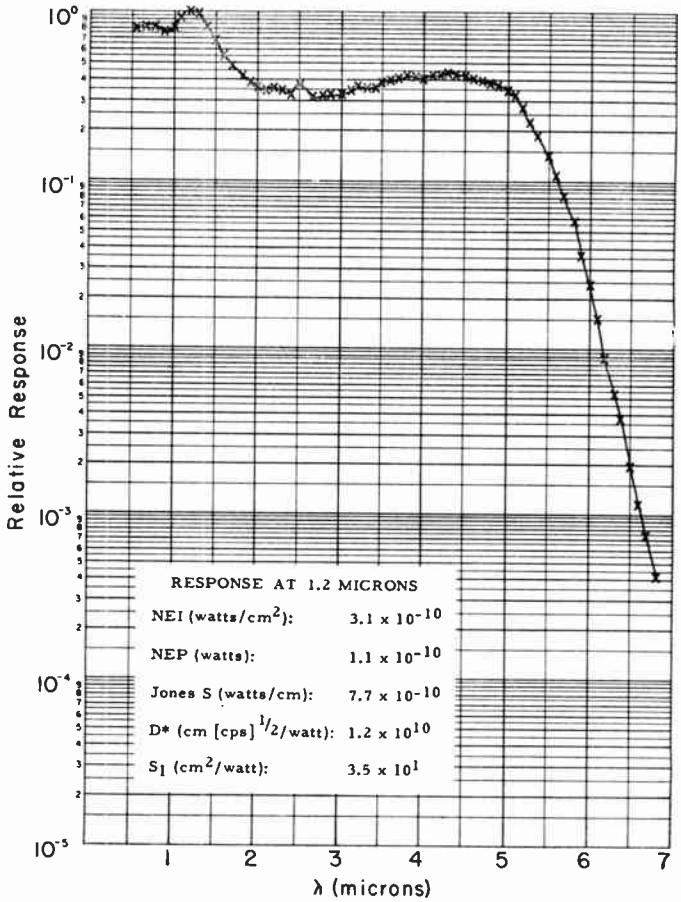

Fig. 2—The relative spectral response of the PbSe detector measured with the Leiss model monochromator. The curve was normalized to unity at the peak response at 1.2 μ. The detector has 40 per cent of its peak response at 4.5 μ.

tector with constant response at all wavelengths). The measured response of the detector to the 500°K blackbody is divided by this factor to determine the absolute response at the wavelength at which the relative response was normalized. The absolute spectral response is easily determined at any other wavelength from the relative spectral response. In practice, such figures of merit as S_i and D^* are evaluated at peak response by taking the quotient of the figure determined with the blackbody and the factor of effectiveness γ. Merit figures such as NEI and NEP are set by taking the product of the 500°K blackbody value and the effectiveness factor.

Frequency Response and Noise Spectrum

A knowledge of a detector's characteristic frequency response and noise spectrum are of great importance to the systems designer. They tell him at what frequencies he may operate the detector and still retain sufficient signal for his purposes; also at what frequencies the detector will operate to maximize the signal-to-noise ratio, V/N.

The frequency response is determined at Corona by means of a variable speed chopper giving a frequency range of 100 to 40,000 cps. Radiation from a Nernst glower is sinusoidally modulated by the chopper and is usually filtered by a selenium coated germanium window. The signal from the detector is measured by putting the output of a cathode follower and a Tektronix model 121 preamplifier into the y-axis input of a DuMont model 304-A oscilloscope. An incandescent tungsten source is simultaneously modulated by the chopper and activates a 931 photomultiplier tube whose signal is fed into a Tektronix model 121 preamplifier and a Hewlett-Packard model 500-A tachometer; the latter's output is proportional to frequency and is put on the Y axis of the oscilloscope. The screen display is photographed as the chopper slows down from its maximum speed.

When the photon excited carriers in the semiconductor have a simple decay mechanism[4] the response to a sinusoidal varying signal can be written

$$\frac{R(\omega)}{R_0} = [1 + \omega^2 T^2]^{-1/2}, \tag{1}$$

where $R(\omega)$ is the response as a function of $\omega = 2\pi f$, f is the frequency of the exciting signal, and T is the time constant for the decay mechanism. An effective time constant is reported in the NOLC reports based on (1) and the frequency response curves. The effective time constant is a very useful parameter for comparing frequency responses of different detectors. For example, the effective time constant from the curve of Fig. 3 is 28 μsec. A note of caution here: because there are distributed capacities present the load resistance must be kept as low as possible in order to approach the detector time constant. The practice at Corona is to reduce the load resistor to 1/10 the dark cell resistance, and this is noted in the report.

The noise spectrum, measured from 10 cps to 10,000 cps with a 5 cps bandwidth is shown in Fig. 4. As the noise theory has been treated in detail elsewhere in this issue, it will suffice to discuss the utility of the noise spectrum for evaluating detectors. In general, the noise has a negative frequency characteristic, but approaches a constant value at relatively high frequencies. For the systems designer, who is using a detector in a system which is cell noise limited, a great deal of flexibility in realizing greater detectivity is available by varying the chopping rate; most detectors may be operated at higher modulation frequencies with greatly improved detectivities. Of course, when system noise is the limitation, the signal response, S_i for example, is the important parameter. Complete information is presented in the Corona reports to permit the designer to determine V/N values for a wide frequency range; thus one can determine a value for D^* at any frequency, f, from the value at a given frequency (*e.g.*, 90 cps):

$$D^*_f = D^*_{90} \frac{(V/N)_f}{(V/N)_{90}} \tag{2}$$

[4] *Ibid.*, p. 141.

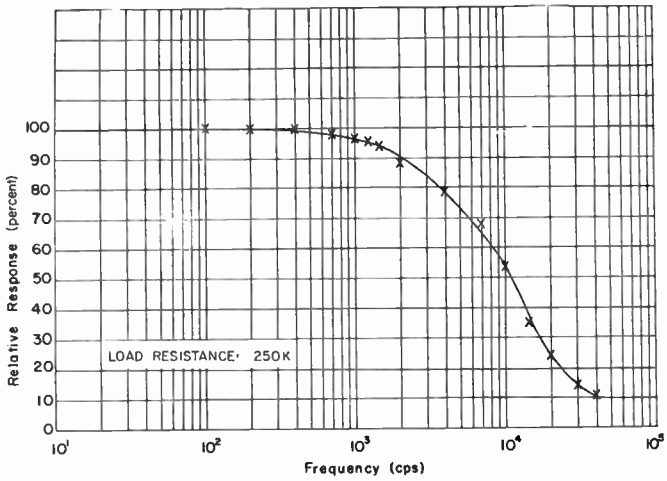

Fig. 3—The frequency response of the PbSe detector. The response is down 3 db at 58 kc.

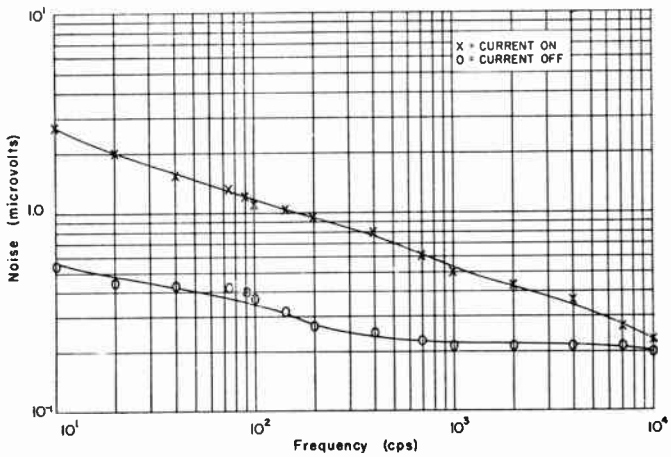

Fig. 4—The noise spectrum for the PbSe detector is shown with and without the bias current.

A similar relation applies for such merit figures as NEI and NEP.

$$(\mathrm{NEI})_f = (\mathrm{NEI})_{90}(V/N_{90}/V/N_f). \qquad (3)$$

By way of example, D^* for the PbSe detector for 500°K blackbody radiation is 1.0×10^9 cm/watt at 90 cps, and 2.0×10^9 cm/watt at 810 cps, with only a slight decrease in signal.

Sensitivity Contours

Contours of the sensitive areas of a detector are of principal concern when the optical system associated with the detector does not utilize the full area. The arrangement at Corona uses a microtable which allows the cell to be moved a small measured amount. The table is linked through a system of gears to a plotting table which gives up to a 36/1 increase in the scale. The exciting radiation is from an incandescent tungsten bulb chopped at 90 cps, and is passed in reverse through a microscope such that a spot 0.066 mm in diameter is focused onto the detector. As the detector is moved beneath this radiation, the relative response at 10 per cent

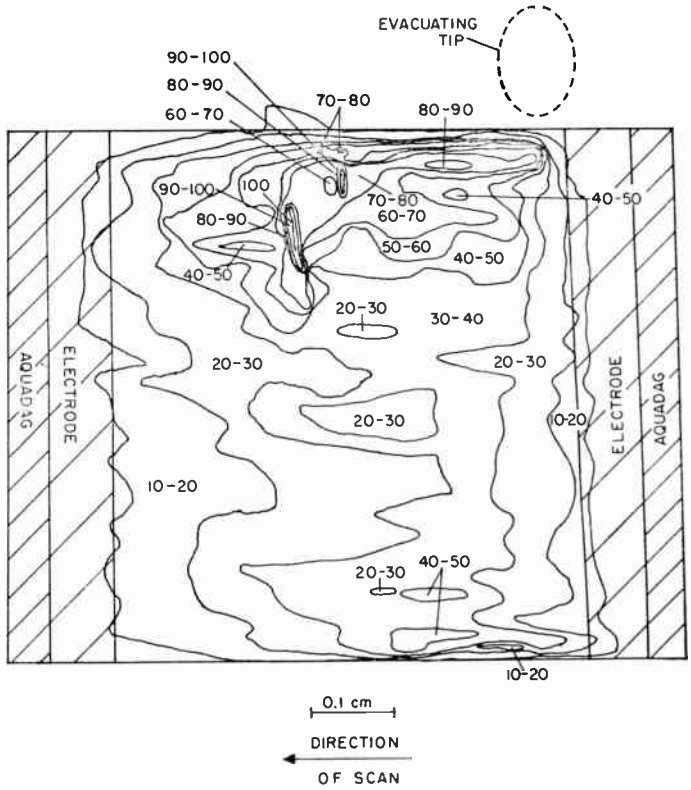

Fig. 5—The sensitivity contour for the PbSe detector. It appears that the uppor portion of the detector is more sensitive than the lower.

intervals is noted on the plotting table. Lines connecting points of equal sensitivity are drawn. Such a plot for the PbSe detector is shown in Fig. 5.

Conclusion

This brief discussion outlines the detector parameters and the methods used in measuring them as they appear in the NOLC photodetector series of reports. It has also indicated how the detector user can handle this information in order to determine which detector is best suited for his particular purposes. The completed data summary sheet as it appears in the Corona report is shown in Table II for the sample PbSe detector. Values of the figures of merit for these detectors are shown in Table III.

Test procedures, of course, must be modified, improved, and even replaced as the detectors themselves are modified and improved, and as new types become available. An example is the measurement of time constants which are generally getting shorter. Although effective time constants as short as 1.0 μsec can be determined with existing equipment at NOLC, designs are under study to modify the frequency response apparatus to enable measurements of time constants less than 0.5 μsec. A "flying shutter" device is now being tested which gives rise and decay time constants in this range and is expected to be of use for the range $10>T>0.1$ μsec.

TABLE II

DATA SUMMARY SHEET FOR PbSe DETECTOR AS IT WILL APPEAR IN PHOTOCONDUCTIVE SERIES REPORT

Cell Sensitivity	
Effective time constant (μsec):	2.8×10^{1}
500°K blackbody response:	
Noise equivalent input (watts/cm²):	3.8×10^{-9}
Noise equivalent power (watts):	1.3×10^{-9}
Jones' S (watts/cm):	9.4×10^{-9}
D^* (cm/watt):	1.0×10^{9}
Position of spectral peak (microns):	1.2
Response at spectral peak:	
Noise equivalent input (watts/cm²):	3.1×10^{-10}
Noise equivalent power (watts):	1.1×10^{-10}
Jones' S(watts/cm):	7.7×10^{-10}
D^* (cm/watt/sec$^{1/2}$):	1.2×10^{10}
"S_1" (cm²/watt) at 1.2 microns:	3.5×10^{1}
Sensitivity contour:	
Maximum sensitivity (volts/watt):	3.25×10^{4}
Masking factor:	

Conditions of Measurement	
Chopping frequency (cps):	90
Bandwidth (cps):	5
Humidity (per cent):	44
Cell temperature (°C):	−195
Dark resistance (megohms):	2.4
Load resistance (megohms):	2.5
Cell current (μamps):	24.5
Cell noise (μvolts):	1.3
Blackbody flux density (μwatts/cm², rms):	7.7
Spot diameter (mm):	0.066
Spot energy (μwatts, rms):	0.0295

Cell Description
Type: PbSe
Electrode material: Aquadag
Window: Sapphire
Method of preparation: Evaporated
Area (mm): 5.3×6.5
Age:

TABLE III

FIGURES OF MERIT FOR A PbSe PHOTOCONDUCTIVE CELL MEASURED AT 90 CPS

Figure of Merit	500°K Blackbody Response	Response at Spectral Peak (1.2 microns)	Response at 4.5 μ
NEI $\left(\frac{\text{watts}}{\text{cm}^2}\right)$	3.8×10^{-9}	3.1×10^{-10}	7.8×10^{-10}
NEP (watts)	1.3×10^{-9}	1.1×10^{-10}	2.8×10^{-10}
Jones' S $\left(\frac{\text{watts}}{\text{cm}}\right)$	9.4×10^{-9}	7.7×10^{-10}	1.9×10^{-9}
D^* $\left(\frac{\text{cm}}{\text{watt}}\right)$	1.0×10^{9}	1.2×10^{10}	4.8×10^{9}
S_1 $\left(\frac{\text{cm}^2}{\text{watt}}\right)$	2.9	3.5×10^{1}	1.4×10^{1}
T (μsec)	2.8×10^{1}		

ACKNOWLEDGMENT

The joint services program for detector evaluation has been carried on at the National Bureau of Standards and the U. S. Naval Ordnance Laboratory, Corona, with coordination and welcome assistance by O. H. Hunt and C. S. Woodside of the Bureau of Ships, U. S. Navy. Many of the basic procedures used in the program were developed by L. G. Mundie while at the Naval Ordnance Laboratories, Whiteoak, Md., and Corona, Calif. A. J. Cussen made significant contributions during his association with the program from its inception in 1952, until December, 1957, and provided leadership during much of that period. Finally the authors wish to acknowledge the aid and encouragement received from C. J. Humphreys, Head of the Research Department, U. S. Naval Ordnance Laboratory, Corona.

Paper 4.1.3

Description and Properties of Various Thermal Detectors*

R. DE WAARD† AND E. M. WORMSER†

RADIATION THERMOCOUPLES

IN principle a thermocouple offers a simple and direct means for measuring radiant energy. By blackening the junction of dissimilar metals, incident radiation is absorbed, causing a temperature rise at the junction and a resultant increment in the electromotive potential developed across the junction leads. To be useful in modern applications radiation thermocouples must both respond rapidly and offer receiver areas of controlled dimensions to match reasonably the image of a radiant source. For example, in spectroscopy, where monochromatic radiation levels are low, it is important that nearly all radiant energy defined by the slit falls on the sensitive area of the detector.

Most of the modern developments in radiation thermocouples have been aimed at achieving a combination of fast time response and good definition of receiver area. Techniques basically reduce to attempts to achieve minimum heat capacity in the receiver element and controlled heat loss from the element. These thermal characteristics, of course, must be commensurate with high thermoelectric power in the couple materials. In a recent book, Smith, Jones, and Chasmar[1] give a good account of both historical and modern developments in thermocouples, including theoretical treatments aimed at selecting materials with optimized electrical and thermal properties. Available commercial radiation thermocouples, in the main, fall into two categories. One type employs couple materials in bulk form[2]; the other type utilizes thin evaporated or sputtered films supported by a thin dielectric film.[3] In the first case a thin, low heat capacity gold foil, coated with an evaporated black, constitutes the actual receiver area; and couple materials are welded to the foil to form thermoelectric junctions. Thin evaporated coatings of gold or platinum black are also applied to the evaporated junctions to improve absorption of radiation.

Thermoelectric materials employed in commercial thermocouple devices are principally metals, *e.g.*, nickel, antimony, bismuth, or alloys of these. Metallic alloys with tellurium, a semiconductor, are also used. Much theory and experiment has gone into the choice of materials best suited for a given detector design. In general high thermoelectric power is desired, but thermal and electrical conductivity must also be considered. The latter should be high to minimize the resistance of the detector, and in some designs low thermal conductivity is desired to obtain high responsivity. Unfortunately, most materials with low electrical resistance tend to have low thermoelectric power. Intermetallic alloying of metals (including tellurium) produces materials which tend to utilize the best properties of individual components. A good tabulation of the pertinent properties of thermoelectric materials is given by Hornig.[2]

In the following sections several of the commercial radiation thermocouples will be briefly described and their properties and performance given.

Perkin-Elmer Pin-Type Thermocouple

This couple is designed[4] for fast response and ac operation in infrared spectrophotometric instrumentation. The receiver area is proportioned to match, as nearly as possible, the image (2×0.2 mm) of the exit slit in the monochromator. The receiver itself is a thin gold foil coated with gold black. The gold strip is welded at its ends on relatively massive wedge-tipped pins of special semiconducting thermoelectric materials. The combination of low thermal mass of the receiver strip, high thermoelectric power, and thermal conductivity in the junction materials is conducive to both fast response and high responsivity.

The evacuated detector is normally housed (Fig. 1)

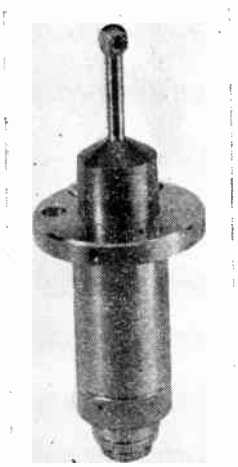

Fig. 1—Spectrometer-type thermocouple detector.

* Original manuscript received by the IRE, June 29, 1959.

† Barnes Engineering Co., Stamford, Conn.

[1] R. A. Smith, F. E. Jones, and R. P. Chasmar, "The Detection and Measurement of Infrared Radiation," Oxford Press, New York, N. Y.; 1957.

[2] D. F. Hornig and B. J. O'Keefe, "The design of fast thermopiles and the ultimate sensitivity of thermal detectors," *Rev. Sci. Instr.*, vol. 18, pp. 474–482; July, 1947.

[3] L. Harris, *Phys. Rev.*, vol. 45, p. 635; 1934.

[4] M. O. Liston, *J. Opt. Soc. Am.*, vol. 37, p. 515A; 1947.

behind a suitable window at the end of a stem-type mounting, the narrow stem construction being employed to minimize obscuration when the detector is located at the focal point of a fast mirror.

For ac operation 13 cps chopping of the radiation is considered a good compromise where couple responsivity has not been degraded much from its maximum at dc conditions and still provides a suitable frequency for amplification. The low impedance of the detector (10 ohms) calls for transformer coupling to a vacuum tube preamplifier. Short cabling is required to connect the detector and preamplifier in order to avoid introduction of electrical noise.

The nominal properties of this detector are listed below:

Receiver size = 2×0.2 mm
DC resistance = 10 ohms
Responsivity at 13 cps chopping = 2 volts/watt
Noise (Johnson noise of dc resistance to 1.5 times Johnson noise) = 4 to 6×10^{-10} volt rms in 1 cps bandwidth
Noise equivalent power (P_n) $P_n = 2$ to 3×10^{-10} watt for 1 cps bandwidth.

The Hornig Thermocouple

The design[2] of this type of thermocouple detector is based upon physical construction features involving a thin, low-heat capacity, blackened, gold-foil receiver joined by short fine thermoelectric wires, whose combined heat capacity is small in comparison to the foil receiver area. Thermal conduction losses through the short leads coupled with radiation losses from the receiver, and the aggregate small-heat capacity provide for both fast response and high responsivity. This detector is operated in a vacuum.

The Hornig type thermocouple is available commercially[5] usually in a single receiver size. It is housed in a stem-type evacuated mounting, not unlike the previously described detector, again for application principally in spectroscopic instrumentation. A potassium bromide window affords uniform transmission of radiation from the visible out to 25 microns. The unit carries a charcoal trap connected by a semiflexible tube for maintenance of good vacuum.

The Farrand-Hornig thermocouple has the following average performance characteristics:

Receiver size = 0.75×0.75 mm
dc resistance = 6–10 ohms
Absolute dc responsivity = 7–10 volts/watt
Responsivity at 5 cps chopping = 3–4 volts/watt
Responsivity at 10 cps chopping = 1.5–2.5 volts/watts
Noise (approximately Johnson noise of dc resistance) = 5×10^{-10} volt rms in 1 cps bandwidth
Noise equivalent power (P_n) (P_n) = 2 to 3×10^{-10} watts for 10 cps chopping frequency and 1 cps bandwidth.

[5] Farrand Optical Co., New York, N. Y.

Reeder Thermocouples

Thermocouples manufactured by the Charles M. Reeder Company[6] cover a wide range of receiver sizes and types of mountings. Models are available to fit commercial spectrometric instruments. In addition, special large area thermopiles designed for diversified laboratory applications are manufactured.

Extended development has gone into the design of these couples. Both pin type (Schwartz) and wire type (Hornig) and combinations of these basic constructions are employed in the Reeder detectors. Thermocouple materials used include bismuth, bismuth alloys, and alloys of tellurium. High responsivity is reported for these detectors and noise outputs are held substantially at the level of the Johnson noise of the thermocouple resistance.

Work is going on at the Reeder Laboratories on the development of spectrally selective thermopiles in the far infrared. Planned also are detectors extending into the 50 to 100 μ wavelength region.

Pneumatic Type Detectors

In its simplest form the pneumatic type detector is comprised of a small gas-filled chamber, equipped with an infrared transmitting window, some means for absorbing radiation admitted to the chamber, and finally a method for transposing pressure change in the chamber into measurable signal output, usually electrical or optical.

An early device of this type is described by Hayes.[7] A carbonized "fluff" material is sealed in the chamber to absorb radiation. One end of the radiation chamber is closed with a thin metal diaphragm which forms one plate of a condenser. Capacitance changes provide direct means for measuring the radiation input.

Zahl and Golay[8,9] are responsible for significant developments in the pneumatic detector. In effect, the carbonized fluff is replaced by a low-heat capacity-absorbing membrane, detection being accomplished by an optical amplification scheme.

Described briefly below are two commercially available pneumatic cells, along with some information on their performance.

The Golay Cell

The Golay type pneumatic cell, as manufactured by the Eppley Laboratory, Inc., is pictured schematically in Fig. 2. Operation is as follows. Radiation admitted through the infrared window (NaCl, K Br, KRS5 and others) is absorbed by a thin foil blackened receiver comprising one end of a small gas-filled chamber. Pres-

[6] Detroit 3, Mich.
[7] H. V. Hayes, "A new receiver of radiant energy," *Rev. Sci. Instr.*, vol. 7, pp. 202–205; May, 1936.
[8] H. A. Zahl and M. J. E. Golay, "Pneumatic heat detector," *Rev. Sci. Instr.*, vol. 17, pp. 511–515; 1946.
[9] M. J. E. Golay, "A pneumatic infrared detector," *Rev. Sci. Instr.*, vol. 18, pp. 357–362; 1947.

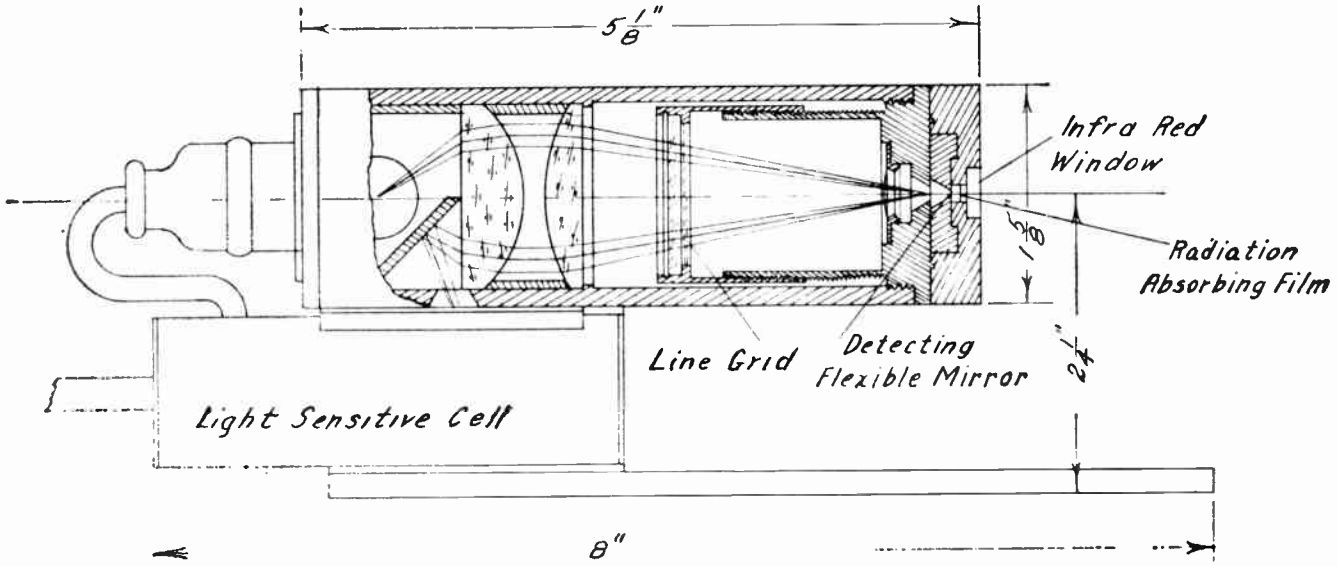

Fig. 2—Golay infrared detector.

sure changes distend a small flexible mirror located at the other end of the chamber. The optical system illustrated serves to detect distortions in the mirror. Light from an incandescent lamp, reflected by the flexible mirror, is imaged onto a photocell. A line grid is interposed to provide modulation of the light reaching the photocell. When the detecting mirror is undistorted the image of one-half the grid coincides with the other half in such a way that no light reaches the photocell. When the mirror membrane is distended the image defocuses and light energizes the photocell.

Drift common to all thermal detectors operated under dc conditions is eliminated by chopping the radiation and employing ac amplification. For spectrometric applications 10 cps chopping is suggested as optimum for the nominal detector time constant of about 15 milliseconds.

The standard receiver element has a 3/32-inch diameter absorbing disk, although other sizes and shapes can be obtained. Time constants can be made to range from about 2 to 30 milliseconds.

Operated in conjunction with a special synchronous-rectifier type amplifier, Noise Equivalent Input is quoted to be as small as 6×10^{-11} watt.

The Patterson-Moos Cell

In the Hayes and Golay type pneumatic cells the radiation absorbing elements are solid substances made as black as possible to absorb energy equally at all wavelengths. In another type of pneumatic cell the gas itself in the cell cavity absorbs radiation resulting in temperature and pressure increase in the chamber. By filling the cavity with gases having selective absorption bands, one can achieve detection only in certain preselected wavelength intervals, since the detector will only respond at wavelengths where the gas absorbs.

The Patterson-Moos[10] cell is of this type. Over-all physical size is determined largely by the size of the sensing area or entrance port. Typical gross dimensions of a cell with a 20 mm² sensitive area are about 1 inch long by ½ inch in diameter. The cell housing is metal and normally is hermetically sealed with a sapphire or germanium window. Capacitive or condenser type output serves to extract electrical signals. Time response is fast; hence these cells can be used with a radiation chopper up to 50 cps, or at higher frequencies with some loss in responsivity.

Bolometer Type Detectors

Bolometer type detectors consist of thin resistance elements exhibiting a large change of resistance with temperature. A dc polarizing voltage is applied across the bolometric strip to detect the change of resistance as a corresponding change in the polarizing voltage. The bolometer is hence seen not to be a transducer. Resistance change in the sensing element merely serves to modulate a steady potential applied across the bolometer.

Sensitive elements are either metals (nickel, platinum) or semiconductor (sintered metallic oxides). In the following paragraphs these two types of bolometers will be treated separately.

Metal Strip Bolometer

Metal bolometer elements have a positive temperature coefficient (α) of about 0.3 to 0.4 per cent per degree Centigrade. In order to make metal sensing elements both sensitive and fast in response, it is necessary to minimize their heat capacity per unit of area. In effect this means the sensing strip must be very thin.

[10] Jamaica 18, N. Y.

Other physical parameters importantly involved in making metal strip bolometers are heat conductivity in the element itself, thermal conduction losses from the element, and radiation exchange. Metal bolometer elements have been formed directly from the bulk materials. For example, Langton[11] has rolled small platinum wires into thin strips (less than one micron) and blackened them to form bolometer elements. The resistance of such bolometers is about 20 ohms and their time constant about 4 milliseconds. In order to reduce microphonics, the thin metal strip is mounted in a taut suspension under reduced pressure in hydrogen. Responsivity of 1 volt/watt is reported and noise is substantially the Johnson noise of the unit's resistance.

In order to reduce further the heat capacity of metal strip bolometers they have been formed by vacuum evaporation.[12] Evaporated films of nickel and bismuth in thicknesses less than 500 Angstroms were examined as bolometer elements. In the case of evaporated films, temperature coefficient and electrical conductivity deviate from those of the bulk metals, but useful bolometric elements are realized.

Because metal strip thermosensing elements have high reflectivity they must be coated with a black absorber to improve absorption of incident radiation. Coatings are usually thin evaporated layers of gold or platinum black. This coating treatment makes the metal bolometers substantially black from the visible to beyond 15 microns in the far infrared.

The inherent low impedance of metal strip bolometers makes it best to transformer-couple them to a vacuum tube amplifier. In modern practice chopping of the radiation beam accompanied with ac amplification is found best suited for maximum detectivity.

Metal bolometers, at present, are not available in a range of sizes and models. Baird-Atomic[13] markets a platinum strip bolometer (Model AT3) designed principally for infrared spectrometric application. This unit is housed in a steel-type mounting, equipped usually with a silver chloride window. The housing is permanently evacuated. The sensing element is a platinum ribbon coated with evaporated gold black. The standard receiver area is 7×0.3 mm. The resistance of the bolometer element is 40 ohms and it is reported to have flat response from 1 to 26 microns. Responsivity is quoted to be 4 rms volts per peak-to-peak watt of radiation. The thermal time constant is 16 milliseconds. Optimum beam chopping speed is 10 cps. Coupled to a high-gain transformer and a tuned narrow-band amplifier, detectivity is essentially limited by Johnson noise. Noise Equivalent Power (P_n) for this detector in a 1-cps noise bandwidth is of the order of 10^{-9} watt.

[11] W. G. Langton, "A fast sensitive metal bolometer," *J. Opt. Soc. Am.*, vol. 36, p. 355; 1946.

[12] B. H. Billings, W. L. Hyde, and E. E. Barr, "An investigation of the properties of evaporated metal bolometers," *J. Opt. Soc. Am.*, vol. 37, pp. 123–132; 1947.

[13] Baird-Atomic, Inc., Cambridge, Mass.

Thermistor Bolometers

The active element in thermistor type bolometers is a thin semiconductor film usually composed of oxidic mixtures of manganese, nickel, and cobalt. Unlike metal strip bolometers, the thermistor material itself is a good absorber of radiation, although some blackening agent is usually applied to improve absorption. Thermistors have a high negative temperature coefficient ($\alpha=4$ per cent per degree Centigrade) tending to provide high responsivity when used as a bolometric element. In common with the metal bolometer, the thermistor detector also operates by virtue of resistance change produced by incident radiation. In order to achieve fast time response, thermistor films or "flakes" are attached to good heat conducting thermal sinks. The normal bolometer bridge circuit comprises two identical thermistor elements mounted on the same base to effect compensation for changes in ambient temperature. One element, the active receiver, is exposed to radiation while the other is shielded from radiation. This circuit arrangement is ideally suited for ac operation, the signal junction being the common terminal between the two thermistors.

Initial development of thermistor detectors was carried out at the Bell Telephone Laboratories.[14] Manufacturing techniques were worked out and operating characteristics studied.[15] Later several organizations[16] continued manufacture and development of thermistor detectors.[17] Recent developments on thermistor detectors and their properties are described in a Navy Department Report.[18]

Two typical thermistor detector assemblies are pictured in Fig. 3. Bolometer elements are housed in a small (about 5/8 inch diameter $\times$ 3/8 inch long) evacuated capsule. Window materials are coated silver chloride, KRS5, or other infrared optical windows, depending upon the spectral range of interest.

Fig. 4 represents the performance of a family of modern high-quality thermistor detectors. They can be made in a range of time constants from less than one millisecond to the order of 15 milliseconds. This kind of behavior is typical of Class II detectors as defined by Jones.[19] Because they all have the same quality (Jones' $M_2=0.3$) one can trade responsivity for time constant and choose a detector best suited to the chopping speed associated with a particular detection problem. This

[14] W. H. Brattain and J. A. Becker, "Thermistor bolometers," *J. Opt. Soc. Am.*, vol. 46, p. 354; 1946.

[15] J. A. Becker, *et al.*, "Final Report on Development and Operating Characteristics of Thermistor Bolometers," OSRD 5991.

[16] Thermistor detectors are currently available from Barnes Engineering Co., Stamford, Conn., and Servo Corp. of America, New Hyde Park, N. Y. The properties of thermistors described in this paper refer to those manufactured by Barnes Engineering Co.

[17] E. M. Wormser, "Properties of thermistor infrared detectors," *J. Opt. Soc. Am.*, vol. 43, pp. 15–21; January, 1953.

[18] R. DeWaard and E. M. Wormser, "Thermistor Infrared Detectors: Part I—Properties and Developments," Navy Bureau of Ordnance, NAVORD Rept. 5495; April, 1958.

[19] R. C. Jones, "Phenomenological description of the response and detecting ability of radiation detectors," paper 4.1.1, this issue, p. 1495.

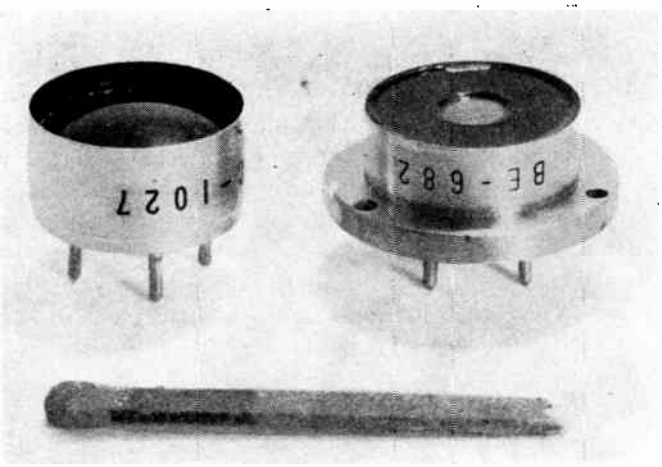

Fig. 3—Thermistor detector assemblies.

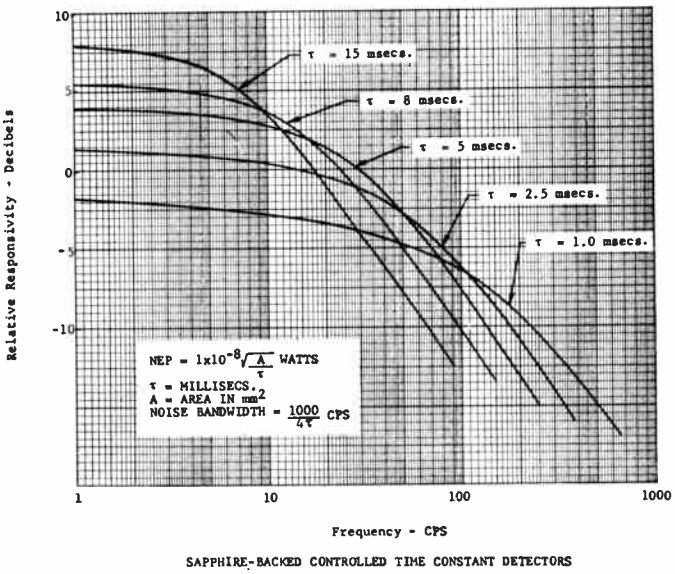

Fig. 4—Family of thermistor detectors.

family of detectors can be represented by a single simple relationship, given in Fig. 4, which states the noise equivalent power (NEP) as a function of detector area and time constant.

These detectors are available in a variety of sizes and rectangular shapes of the sensing element. Thermistors as small as 0.1×0.1 mm are being produced and it is possible to make them with linear dimensions as large as 10 mm. In the detection of small targets, however, it is advisable to keep the detector size as small as possible, since the larger detectors tend to decrease in detectivity.

The resistance of standard thermistor bolometers is high (1 to 5 megohms), making it convenient to couple them directly to vacuum tube amplifiers. Noise is substantially that attributable to the Johnson noise of the bolometer resistance. Noise levels in normal usage are of the order of 1 microvolt rms or less, hence it is advisable to provide close physical spacing between the bolometer and a vacuum tube preamplifier to avoid noise pickup.

Developments in Thermistor Bolometers

As a result of development work[20] carried on at Barnes Engineering Company in the past several years, thermistor detectors of new types and improved performance have evolved, and are now commercially available. These are briefly treated under separate headings below.

Optical Immersion Techniques

The detectivity of thermistor bolometers, in common with many other detectors, increases with decreasing receiver area. There are limits to the extent of optical gain one can practically achieve with conventional optical systems in the infrared. In the far infrared it is necessary to use reflecting optics exclusively and these become both expensive and bulky in large sizes. It is possible by means of optical immersion of the detector element to achieve substantial optical gain directly at the detector.

Thermistors have been optically attached to concentric germanium hemispheres to effect a large gain in detectivity. Fig. 5 illustrates the image reduction afforded by the high index ($N=4$) germanium optical element. The image at the plane face of the germanium element is reduced by a factor of 4 in linear dimensions from that of the image in space. This amounts to a reduction of 16 times in the area of the receiver and, since thermistor detectivity varies inversely with the square root of its area, a gain of a factor of 4 in detectivity results.

The thermistor is mounted centrally on the plane surface of the germanium hemisphere separated by a thin film which is transparent to infrared and electrically insulating. The insulating film has the important dual role of providing good optical contact and electrical insulation. Detector time constant is also determined by controlling the thickness of this layer. The germanium immersed bolometer is suitable for use in optical systems having an effective optical speed less than $f/1.0$. A typical immersed bolometer is shown in Fig. 6. Gross dimensions are about 5/8 inch diameter $\times$ 3/8 inch long. The bolometer carries a flange mounting base to facilitate precise location in an optical system.

Mosaic Techniques

A thermistor manufacturing process has also been worked out whereby it is possible to lay down a mosaic or matrix of a great number of small thermistor elements. Multiple thermistors are "printed" in desired patterns on ceramic substrates. Electrical junctions are likewise printed to provide signal and bias contacts. In Fig. 7 is pictured a printed assembly containing 100 thermistor elements arranged in a 10×10 matrix. Linear arrays of thermistor elements have also been produced by this technique. Individual bolometer element properties are comparable to those of the standard

[20] This work, in part, has been sponsored by the Navy Dept., Bureau of Ordnance.

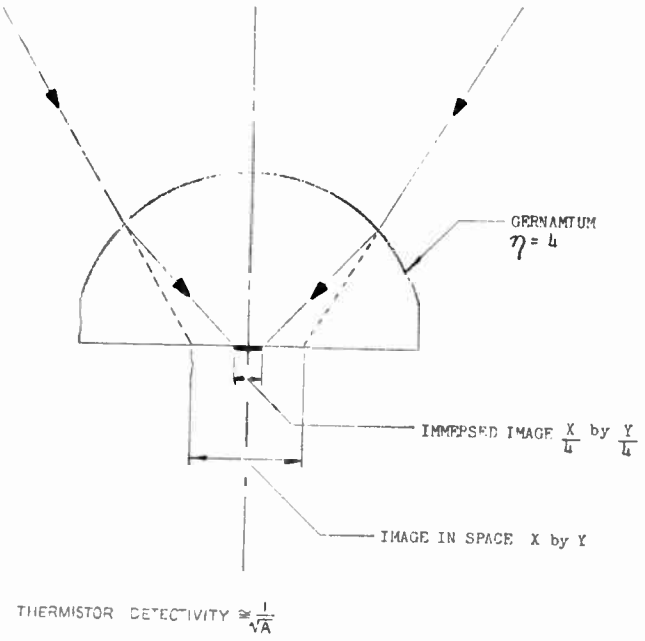

Fig. 5—Illustrating image reduction with germanium immersion.

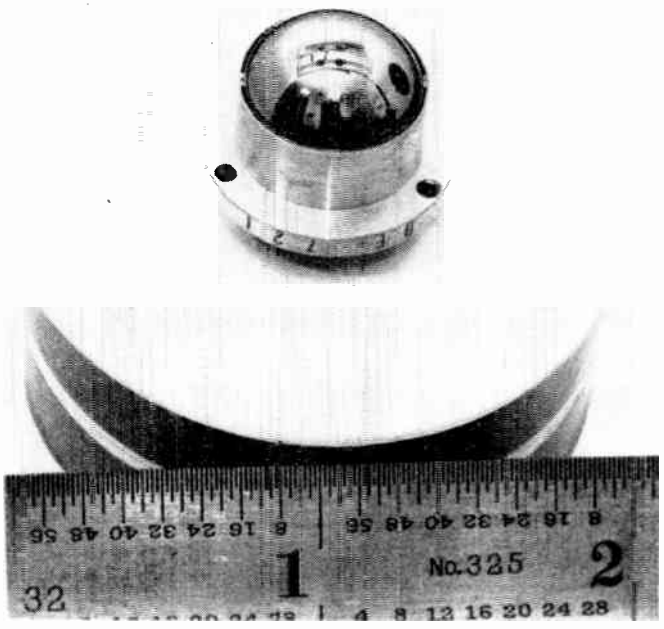

Fig. 6—Immersed bolometer.

thermistor detectors described above. At the present time, time constant cannot be varied much in the printing technique, 2 milliseconds being the nominal time constant obtained.

A feature worth mentioning of the printed-type thermistor is its adaptability to high-temperature operation. Because no organic cements or other temperature limiting materials are involved in construction, they can be exposed and used at high ambient temperatures.

Selective Wavelength Detectors

As already stated thermistor bolometers are uniformly black at all wavelengths in the infrared. Through special techniques it is now possible to make thermistor detectors spectrally selective; *i.e.*, they can be made to respond to radiation in certain specific wavelength regions. In brief, this is accomplished by first making the thermistor element completely reflective (overlay of evaporated gold). To achieve spectral selection the resulting blind thermistor element is coated with a material having appropriate absorption spectra. As coatings or sensitizers both organic films and powdered slurries of inorganic compounds have been employed. It is possible by this means to measure the radiant energy from a material by coating the detector with a thin film of the same material. In this case the detector senses only radiation emitted in characteristic absorption bands. Using an inorganic mineral as a sensitizer, a detector has been made with sensitivity at 15 microns extending one micron on either side, matching the strong CO_2 absorption band. Everywhere else in the infrared this detector is substantially insensitive. Selective detectors for other spectral regions can be similarly produced.

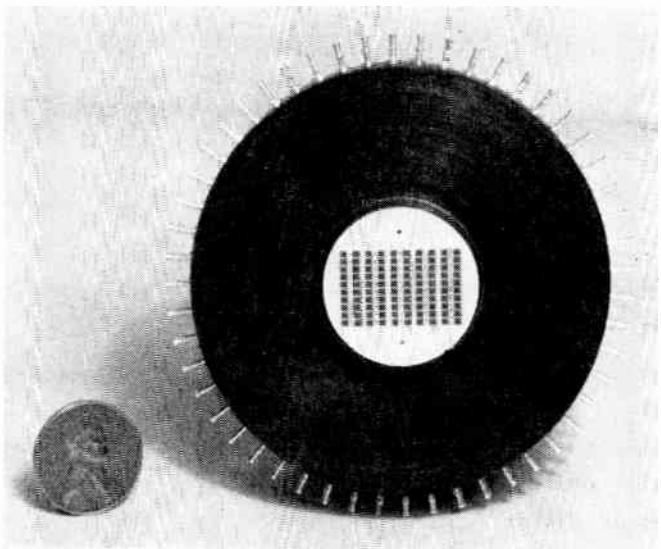

Fig. 7—100-element mosaic.

Thermistors for Matching Transistor Amplifiers

Most recently, spurred by developments in space technology and accompanying demands on small space and weight requirements, it has been desirable to employ transistor-type amplifiers with thermistor bolometers. The high impedance of the standard thermistor bolometer discussed above is not suitable for matching to transistor amplifiers. Theory and experiment show that the optimum resistance of thermistors for transistor coupling is of the order of 50K ohms. Suitable low impedance thermistors have been made and matched to transistorized preamplifiers. In general it has been possible to come within 6 db of theoretical detector noise (Johnson noise of the bolometer resistance).

Paper 4.1.4

Cooling Techniques for Infrared Detectors*

J. G. GOODENOUGH†

ALL of the semiconductor materials which are currently used as infrared detectors show a marked increase in detectivity to infrared radiation when cooled to low temperatures. However, the response of different detector materials to cooling varies. For example, no appreciable advantage is gained by cooling lead sulfide below approximately −70°C, whereas gold-doped germanium is increasingly sensitive down to about −218°C.

Considerable effort has been devoted to developing methods of cooling detectors to appropriate temperatures. Most of this development work has been directed toward airborne applications of the final product; minimum over-all size and weight, and reliability in service have therefore been prime considerations. The major effort has been directed along two lines:

1) Refrigeration by miniature coolers employing the Joule-Thomson effect, the refrigerant being a gas, bottled at relatively high pressure (after Parkinson).
2) Refrigeration by direct transfer of low-temperature liquified gas from a supply vessel.

Several typical Santa Barbara Research Center miniature coolers are shown in Fig. 1. All of these miniature coolers are based on the same design principles and operate by means of the Joule-Thomson effect.

The refrigerant gas flows through a small bore tube, which is finned externally and is wound spirally upon a mandrel. The outside diameter of the spiral is such that it fits precisely in the bore of a glass tube which carries the IR detector. The gas is allowed to expand either through an orifice or through a short length of unfinned tubing, after which the flow of gas is returned to atmosphere over the outside of the finned tubing. It is necessary, of course, that these glass tubes, which are open at one end and closed at the other, be provided with good thermal insulation, and they are commonly made as the inner member of a small Dewar vessel.

These miniature coolers have been developed to the point where they provide a reliable means of IR detector refrigeration, using commercially available gases, provided that the gas is thoroughly cleaned by a combination of fine mechanical filtering and a molecular sieve. The minimum operating pressure, and also the minimum rate of gas consumption for any specific application, is varied for operation at ambient temperatures which differ substantially from normal room values.

The second method of detector refrigeration which is being actively developed at Santa Barbara Research Center—the direct transfer of low-temperature liquified gas from a supply vessel to the detector flask—was devised for a particular airborne application in which space limitations prohibited the use of high-pressure gas storage containers.

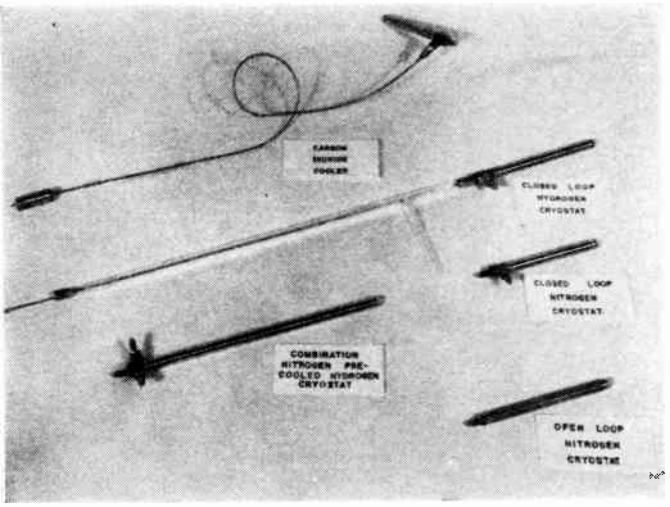

Fig. 1—Typical SBRC miniature coolers.

In this method, a small electrically energized heater is positioned in the supply vessel so that it is always submerged in liquid. The supply vessel is vented to atmosphere through a differential-pressure relief tube. The gas generated in the detector flask is vented to atmosphere through a calibrated orifice, and the heater circuit is controlled by a differential-pressure actuated switch, set to open at a slightly lower pressure than that at which the pressure relief tube opens. This method of refrigeration is illustrated in Fig. 2.

With an increase in the rate of flow of liquid, the pressure drop across the orifice will increase, and the internal pressure in the supply vessel will rise, opening the heater circuit. Conversely, a decrease in pressure closes the circuit. Thus the supply pressure and consequently the flow rate of liquid refrigerant can be maintained within tolerably close limits. This method of flow control has been used in the laboratory and in flight tests; it has marked advantages for airborne applications in that ambient pressure is used as a reference for both the exhaust orifice and for the pressure switch. Thus if the heater switch is set to give an operating pressure of, for instance, 5 inches Hg above ambient pressure, the resulting pressure in the liquid nitrogen system at an altitude of 50,000 feet is approximately 8.4 inches Hg, absolute. The boiling temperature of liquid nitrogen at this pressure approaches the critical temperature

* Original manuscript received by the IRE, June 29, 1959.
† Santa Barbara Research Center, Santa Barbara, Calif.

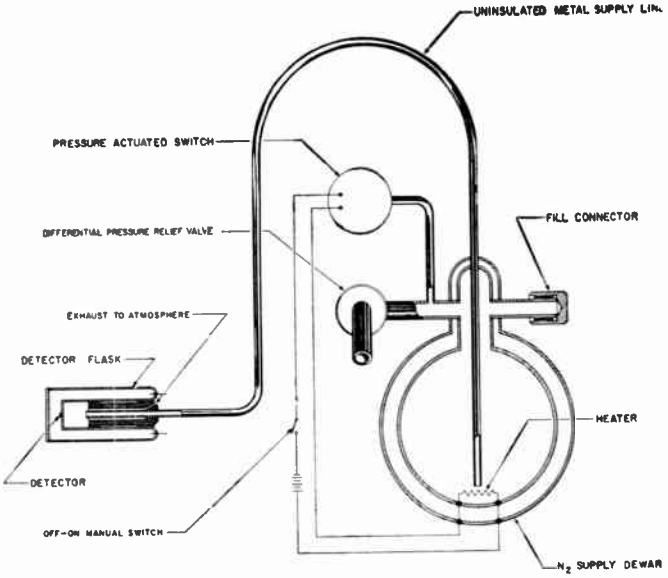

Fig. 2—Liquid nitrogen supply system using pressure-orifice control.

(−209°C) and is substantially lower than is the boiling temperature at sea level pressure. This decrease in boiling temperature with increase in altitude is reflected in a decrease in detector temperature.

Cool-down time is largely a function of orifice size and supply pressure. For example, the cool-down time of a six-detector flask with a running consumption of 100 cc per hour is approximately 45 seconds. If the pressure and orifice size are suitably changed, this time can be reduced to less than 20 seconds, at the expense of an increase in consumption to about 150 cc per hour. The shortest cool-down time which has so far been achieved is 7 seconds, with a small single-detector flask.

A typical container and controls weighing a total of about 7.5 pounds (filled) will endure a 24-hour standby period and will then adequately cool an eight-detector flask for a period in excess of 6 hours under simulated flight conditions. The volume occupied by the container and controls is approximately 500 cubic inches. This cooling supply unit has been tested under both simulated and actual flight conditions.

The work which has been conducted at SBRC both on miniature Joule-Thomson coolers using high-pressure gas as a refrigerant and on the direct liquid transfer method has progressed to the point at which it is possible to examine the individual requirements of any application involving detector cooling and to select the mode which offers the greater advantages. It appears that the use of a miniature cooler and high-pressure gas will always be advantageous in applications for which a very long standby period is mandatory. Also, the distance between the detector flask and the supply vessel is limited in the case of direct liquid transfer, whereas it is practically unlimited in the case of the high-pressure gas supply. By contrast, if weight and space limitations are critical, and if the supply vessel can be positioned within a reasonably short distance from the detector flask, the direct liquid transfer method is preferable, especially for use at very high altitudes.

Paper 4.1.5

Lumped Parameter Behavior of the Single-Stage Thermoelectric Microrefrigerator*

M. B. GRIER†, SENIOR MEMBER, IRE

Introduction

THE problem of adequate cooling in electronic systems is becoming ever more acute as greater system miniaturization is achieved. Adequate cooling is particularly important in the case of currently used infrared detectors, the sensitivity of which is far greater at very low temperatures than at ordinary ambients. Although relatively lightweight cryostats have been produced for the purpose of cooling to liquid nitrogen temperatures, difficulty often is experienced with miniature mechanical units in adequately purging moisture and impurities from the system.

Peltier refrigerators may well prove to be the most elegant solution to this problem since they can be constructed integrally with the detector itself, embody a system with no moving parts, and can be made highly reliable.

Although temperature drops larger than may be obtained with a single stage can be produced by cascading, useful cooling may be obtained by the use of a single-stage unit.

The following discussion summarizes some of the principal thermoelectric properties of the single-stage Peltier refrigerator.

* Original manuscript received by the IRE, June 29, 1959.
† Nortronics, A Division of Northrop Corp., Hawthorne, Calif.

The Lumped-Parameter Approach

The lumped-parameter equation governing thermoelectric cooling, making the assumption that half of the I^2R loss goes to the hot junction and half goes to the cold junction, was formulated by Altenkirch.

$$Q = IT_c(S_1 - S_2) - (\tfrac{1}{2})I^2\left(\frac{\rho_1 L_1}{A_1} + \frac{\rho_2 L_2}{A_2}\right) - \left(\frac{K_1 A_1}{L_1} + \frac{K_2 A_2}{L_2}\right)(T_h - T_c), \quad (1)$$

where subscripts 1 and 2 refer to the positive and negative legs of the couple, respectively, and

ρ = resistivity
A = cross-sectional area of elements, assume $A_1 = A_2$
L = length of a thermocouple element, let $L_1 = L_2$
K = thermal conductivity
T_h = temperature of hot junction, °K
Q = the useful cooling
$R_s = L/A(\rho_1 + \rho_2)$, the series resistance of the thermocouple.

Eq. (1) states that the useful cooling at the cold junction is equal to the Peltier cooling diminished by one-half the I^2R loss, and the thermally-conducted heat from the hot to the cold junction.

The amount of Peltier cooling, P, is given by

$$P = IT_c(S_1 - S_2) = IT_cS, \quad (2)$$

where

I = the current flowing through the junction
T_c = temperature of the cold junction
S_1 and S_2 = the Seebeck coefficients of dissimilar materials comprising the junction.

Thermoelectric refrigerators may be designed with two approaches in mind: to obtain optimum coefficient of performance, and to obtain maximum temperature drop. The design considerations and the resulting properties are somewhat different in the two cases.

For the case of cooling of small electronic components such as photosensors, the heat load is very small and the design may proceed along the lines of obtaining maximum temperature drop, rather than optimum coefficient of performance.

Calculation of Current to Yield Maximum Temperature Drop

Rearranging (1),

$$T_h - T_c = \Delta T = \frac{IST_c - Q - 1/2I^2\dfrac{L}{A}(\rho_1 + \rho_2)}{\dfrac{A}{L}(K_1 + K_2)}. \quad (3)$$

It is seen that the temperature drop is a function of current, I. At small currents, the Peltier cooling and the I^2R_s are both small; consequently ΔT is small. For large currents the Peltier effect increases, but the I^2R_s changes faster; as a result, there is a current which gives a maximum temperature drop, ΔT_{max}.

Assume Q, T_c, L/A constant. Then the current I_0, which yields the maximum temperature drop, is

$$I_0 = \frac{ST_c}{\dfrac{L}{A}(\rho_1 + \rho_2)} = \frac{ST_c}{R_s}. \quad (4)$$

Thus, the couple current, I_0, which produces the relative maximum ΔT is independent of the load, Q, at that ΔT_{max}.

This is shown in Fig. 1 for a typical single-stage microrefrigerator. The materials parameters are taken as typical of Bi_2Te_3:

$$S_1 - S_2 = 400\ \mu\text{volt}\cdot\text{deg}^{-1}$$
$$\rho_1 + \rho_2 = 2\cdot 10^{-3}\ \Omega\ \text{cm}$$
$$K_1 + K_2 = 0.04\ \text{watt}\cdot\text{cm}^{-1}\cdot\text{deg}^{-1}.$$

Materials with the above parameters will be assumed in the subsequent discussion.

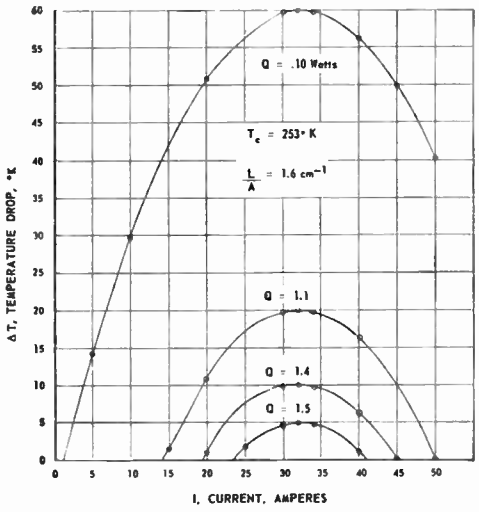

Fig. 1—Variation of temperature drop with current for constant load values.

Determination of Ingot Proportions

Having decided upon the value of I_0 desired, the optimum L/A to yield maximum temperature drop for the load Q may be calculated by differentiating (3), assuming that Q, T_c, and $I = I_0$ are constant. Thus,

$$\left(\frac{L}{A}\right)_{opt} = \left[\frac{ST_c}{I} - \frac{Q}{I^2}\right]\frac{1}{\rho_1 + \rho_2}. \quad (5)$$

A plot of L/A_{opt} vs Q for various values of I is given in Fig. 2 to show some of the relations among the parameters, the materials parameters being taken as above.

Eq. (5) may now be substituted in (3) to obtain the ΔT_{max} as a function of Q and I:

$$\Delta T_{max} = \frac{S^2}{2(\rho_1 + \rho_2)(K_1 + K_2)}\left[T_c - \frac{Q}{S^I}\right]^2. \quad (6)$$

It is seen that when $Q=0$,

$$\Delta T_{max} = 1/2(ZT_c^2) \quad (7)$$

where

$$Z = \frac{S^2}{(\rho_1 + \rho_2)(K_1 + K_2)}. \quad (8)$$

This is the largest temperature drop that can be attained with a single couple at the cold junction temperature, T_c.

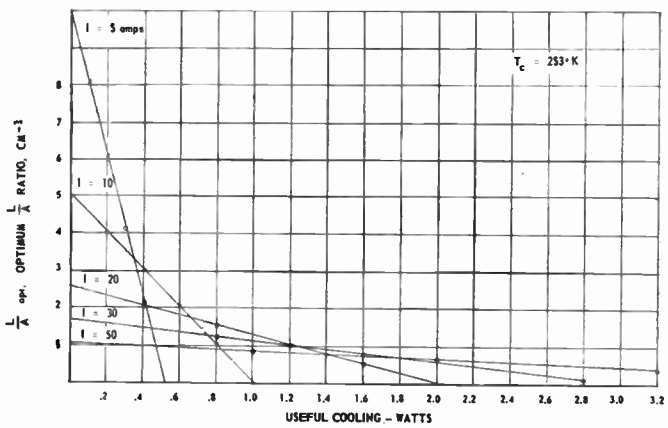

Fig. 2—Variation of optimum ingot proportions with load.

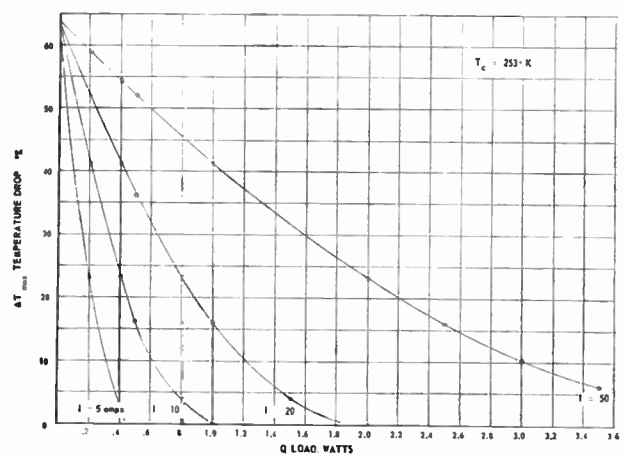

Fig. 3—Variation of optimum ΔT with load.

The relation (6) for ΔT is plotted in Fig. 3. By referring to Fig. 2 and Fig. 3, the following properties may be observed:

1) To obtain large temperature drops with relatively large loads, a high value of I is required. By reference to the L/A vs Q curves, it is seen that large values of I imply small values of L/A.
2) For each value of couple current, I, there is a maximum value of Q which may be pumped ($\Delta T=0$). This value of Q increases as the value of I increases.
3) From the L/A vs Q curves, it is seen that the absolute maximum temperature drop is obtained for a certain constant value of the product IL/A. Thus, I may be reduced by a given factor, providing that L/A is increased by the corresponding factor to maintain the IL/A constant.
4) For zero useful cooling, the maximum temperature drop is the same for all currents and for all corresponding values of L/A.

The Coefficient of Performance

By definition, the coefficient of performance, ϵ, is written:

$$\epsilon = \frac{SIT_c - \frac{1}{2}I^2\frac{L}{A}(\rho_1 + \rho_2) - \frac{A}{L}(K_1 + K_2)\Delta T}{I(S)\Delta T + I^2\frac{L}{A}(\rho_1 + \rho_2)}. \quad (9)$$

By substituting $(L/A)_{opt}$ in the above equation, we obtain the following expression for coefficient of performance.

$$\epsilon = \frac{\frac{1}{2}[SIT_c + Q] - \frac{(K_1 + K_2)(\rho_1 + \rho_2)I^2\Delta T_{max}}{IST_c - Q}}{IS\Delta T_{max} + [SIT_c - Q]}. \quad (10)$$

This expression is plotted as Fig. 4. It is seen that the maximum temperature drop is obtained when the coefficient of performance is zero, and vice versa.

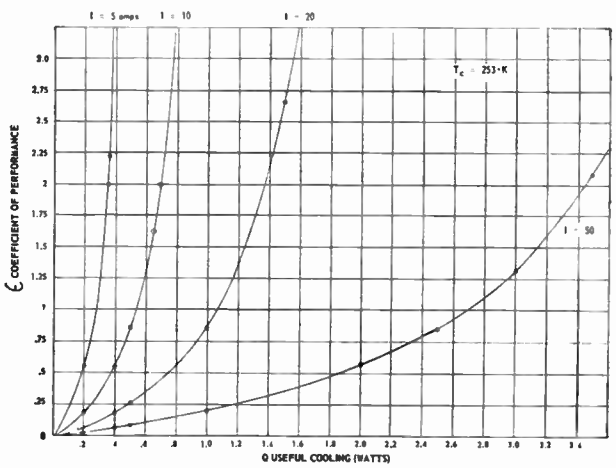

Fig. 4—Variation of coefficient of performance with load.

Variation of Heat Pumped with Change in Couple Current

Differentiating Q with respect to I in (1) and equating to zero, we obtain

$$I_{max} = \frac{ST_c}{\frac{L}{A}(\rho_1 + \rho_2)}.$$

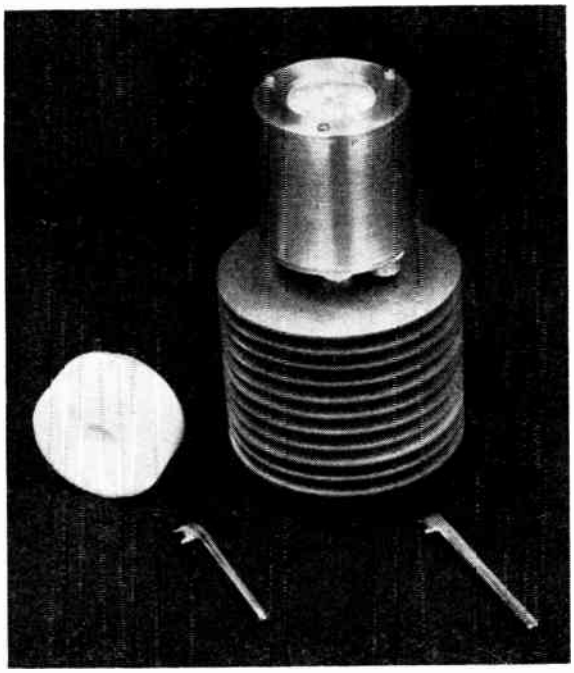

Fig. 5—Single-stage electronic microrefrigerator.

Thus, the couple current at which the relative maximum of heat pumped occurs is independent of the temperature drop, assuming the latter to be constant.

Indeed, referring to (4), it is seen that the I which yields a relative maximum heat pumping also yields relative maximum of ΔT. The absolute maximum of ΔT occurs when $Q=0$. And conversely, the absolute maximum of Q pumped occurs when $\Delta T=0$.

Thermoelectric Photocell Coolers

Single-stage photocell coolers with improved materials ($Z\sim 2.5$) have yielded a temperature drop of nearly 50°C. A photograph of an experimental model of such a single-stage refrigerator is shown in Fig. 5. Cooling of this magnitude is sufficient to increase considerably the sensitivity of current photoconductive detectors such as the lead sulfide cell (~threefold increase in S/N).

By comparison, early work in thermoelectric cascading in the Nortronics Laboratories has resulted in two-stage Peltier photocell coolers which gave a total drop of 50°C starting from a hot junction temperature of 20°C (Fig. 6). More recent two-stage units using improved materials ($Z\sim 2.5$) have yielded cooling of 79°C from 25°C. It is expected that still better materials will be available in the near future, ($Z\sim 3$) yielding correspondingly greater cooling for both single- and double-stage units.

Fig. 6—Two-stage photocell microrefrigerator.

Bibliography

[1] E. Altenkirch, "Elektrothermische kälteerzeugung und reversible elektrische heizung," *Physik. Z.*, vol. 12, pp. 920–924; 1911.

[2] H. J. Goldsmid and R. W. Douglas, "The use of semiconductors in thermoelectric refrigeration," *Brit. J. Appl. Phys.*, vol. 5, p. 386; 1954.

[3] H. J. Goldsmid, "Thermoelectric applications of semiconductors," *J. Electronics*, vol. 1, pp. 218–222; September, 1955.

[4] M. B. Grier, "Wide use foreseen for applied thermoelectricity," *Space/Aeronaut.*, vol. 31, p. 46; 1959.

[5] A. F. Ioffe, L. S. Stil'bans, E. K. Iordanishvili, and N. Fedorovich, "Thermoelectric refrigerator," *Kholodil'naya Tekh.*, vol. 33, pp. 62–63; 1956.

[6] A. F. Ioffe, L. S. Stil'bans, E. K. Iordanishvili, and T. S. Stavitskaya, "Thermoelectric cooling," *Acad. Sci. USSR*; 1956.

[7] A. Ioffe, L. Stil'bans, E. Iordanishvili, and E. Fedorovich, "Thermoelectric cooling in refrigeration technique," *Kholodil'naya Tekh.*, vol. 33, pp. 5–16; 1956.

[8] E. K. Iordanishvili and L. S. Stil'bans, "Thermoelectric microrefrigerators," *Zhur. Tekh. Fiz.*, vol. 26, pp. 945–957; 1956.

[9] R. M. Nolan, "Sun to cool spaceship electronic components," *Missiles & Rockets*, vol. 4, p. 40; 1958.

[10] L. S. Stil'bans, E. K. Iordanishvili, and T. S. Stavitskaya, "Thermoelectric cooling," *Izvest. Akad. Nauk SSSR., Ser. Fiz.*, vol. 20, pp. 81–88; 1956.

Paper 4.1.6

Infrared Detector Silicon Solar Cell Power Supply*

L. W. SCHMIDT†, ASSOCIATE MEMBER, IRE, AND J. I. DAVIS†, SENIOR MEMBER, IRE

THE silicon solar cell is a device that converts electromagnetic radiation into electrical energy through a photovoltaic conversion process.

Silicon has four valence electrons in its outer shell and it forms a stable tetrahedral or diamond crystal. In the pure, or intrinsic, state each silicon atom shares its four valence electrons with four electrons of four adjacent atoms. This sharing occurs as electron pairs and is called a covalent bond. The valence bonds are satisfied and the crystal is electrically stable.

Intrinsic silicon can be made to behave electrically different if a five-valence impurity, such as arsenic, antimony, or phosphorus, is added in quantities of one part in one billion to one part in one million. The impurity atom replaces a silicon atom in the crystal structure creating a "disordered" crystal lattice with an extra electron not needed for completion of the valence bonds. This "extra" electron is free to move about under the action of a comparatively small force such as might be supplied by thermal energy or energy from a photon.

These impurity materials are called "donors" because the conductivity of the silicon is enhanced by the "donation" of electrons, or negative charges, and the silicon known as *n*-type material. Similarly, the addition of a three-valence impurity, such as boron, gallium, or indium, will create a disordered crystal lattice with a deficiency of electrons necessary to complete the valence bonds. An electron that is free to move about may fall into the "hole" or space created by this deficiency leaving another "hole" and giving the appearance of motion to the "hole." The impurity material now is called an "acceptor" because the conductivity of the silicon is enhanced due to an absence of electrons (vacancies that will accept electrons), and the silicon is known as *p*-type material.

Consider a *p-n* junction formed by bringing together pieces of *n* and *p*-type material so that they form a perfect single crystal. Some of the holes and electrons in the vicinity of the junction intermingle by diffusion and recombine leaving behind a dipole layer due to the fixed charge of the impurities. Because of the dipole layer, *i.e.*, the electrons on one side of the junction and the holes confined to the opposite side, this will result in diffusion of electrons to the hole side and vice versa. This results in a net transfer of a charge which makes the *p* region negative with respect to the *n* region, and sets up an electric field in the direction to oppose further flow of electrons. In thermal equilibrium, this electric field will have built up to such a strength that further current flow is prevented; electrons are kept in the *n* region and holes are kept in the *p* region. Thus, there exists a potential gradient across the junction.

If sufficient electromagnetic radiation in the 0.4 μ to 1.2 μ spectral region (see Fig. 1) is incident upon the silicon *p-n* junction, electron-hole pairs are created. It has been experimentally proven that over a wide range of photon energies each photon absorbed in the crystal will create an electron hole pair. If the pair is created in the *p-n* junction, or close enough to the junction so that carriers can reach it by diffusion before recombination takes place, the electric field of the junction separates them, pushing the holes into the *p* region and the electrons into the *n* region, building up an external voltage on the device. Connecting the two ends of the junction by a wire causes current to flow in the wire from the *p* side to the *n* side.

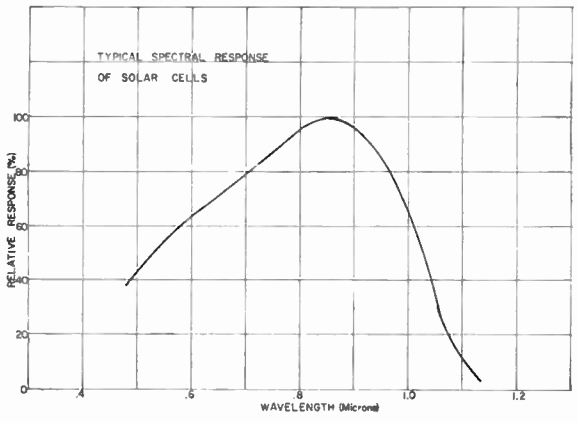

Fig. 1—Typical spectral response of solar cells.

Silicon solar cells have conversion efficiencies in excess of seven per cent, with efficiencies as high as fourteen per cent attained in laboratory samples. The use of silicon solar cells in solar converter systems with large electrical output requirements is well established.

In the Cleveland National Forest of California, a silicon solar cell power supply successfully powered a receiver-transmitter relay system for the U. S. Forest Service through the entire fire season. Energy was transferred to a 12-volt rechargeable battery system at rates as high as 125 watt hours per day.

A silicon solar cell power supply is presently operating a marine beacon light for the U. S. Coast Guard at the Los Angeles Harbor Light Station. Sufficient energy was

* Original manuscript received by the IRE, June 29, 1959.
† Labs. Div., Hoffman Electronics Corp., Los Angeles, Calif.

transferred to a 12-volt rechargeable battery to handle adequately demands of 20 watt hours per day during the winter months.

The Vanguard 1 satellite has been transmitting for approximately a year on energy supplied by silicon solar cells. For other satellite applications, solar cell power supplies have been designed and built to produce power on the order of 7 watts per square foot and 6.5 watts per pound.

As a power source for an infrared detector system, the silicon solar cell may fulfill two requirements—that of a voltage bias supply for the detector element and as a power supply for the signal amplifier. The impedance of a detector element of lead sulfide, lead telluride, or lead selenide is of such magnitude (order of 10^5 ohms) that it appears as an open circuit to a series string of silicon solar cells. The open circuit voltage of a solar cell is approximately 0.5 volt; hence, the number of cells required will be the bias voltage divided by 0.5. If the radiation level fluctuates, it may be desirable to shunt the solar power supply with a low current rechargeable battery to insure good voltage stabilization.

The minimum number of solar cells required to serve as a prime power source for a detector system is as follows:

$$n = \frac{\text{voltage required by system}}{\text{maximum power transfer voltage of cell}} \times \frac{\text{current required by system}}{\text{maximum power transfer current of cell}}$$

where the maximum power transfer voltage of the solar cell is 0.4 volt and the current is directly proportional to the active area of the cell.

If the activating radiation level is subject to change, or if the system is to operate when the radiation level is zero, then a rechargeable battery is necessary to meet the continuous power demand and to supply regulated voltage with the solar cells replacing the energy when the radiation level permits. Additional solar cells are required to compensate for battery inefficiencies, high temperature losses, if they exist, and losses through diodes used to prevent reverse current flow from the battery during dark periods.

It can be summarized that silicon solar cells may be used to supply electrical power for IR detectors or many other devices at remote areas either on earth or in space and will provide power substantially as long as solar energy is available.

Paper 4.1.7

The Behavior of Infrared Detection Elements Under Nuclear Radiation Exposure*

E. W. KUTZSCHER†

WHEN an infrared system has to operate in the presence of nuclear radiation, it must be made certain that such an environment will not seriously degrade the reliability of the system.

The behavior of many electronic parts which might be used as components in infrared devices has been investigated by operating them in a nuclear radiation field. The way in which optical characteristics, especially transmission properties, would change if certain optical materials were exposed to nuclear radiation has also been studied.

The heart of any infrared device is the detector element and it is of paramount importance for some applications to know if such a receiver would change its main characteristics, or even be damaged, if irradiated by gamma radiation or bombarded by neutrons.

* Original manuscript received by the IRE, June 29, 1959.
† Lockheed Aircraft Corp., Burbank, Calif.

In recent years, various laboratories have become interested in the subject and have carried out measurements in this field. The first investigations on various photoconductive cells, including lead sulfide, lead telluride, indium antimonide, and gold-doped germanium, and on thermistor bolometers, all operated in a nuclear radiation field, were conducted at Lockheed Aircraft Corporation, California Division.

The infrared receivers were exposed for a certain period of time to gamma radiation using relatively small flux intensities. The resistance, internal noise, and responsivity of these infrared detectors were observed during and after the exposure. The source for the gamma radiation was a 1500-curie cobalt-60 unit.

The radiation dose could be varied from approximately 5 to 21,000 roentgens (r) per hour. The total dose used was of the order of 15,000 to 35,000 r. The average photon energy of the radiation was approximately 1.2 to 1.3 mev. Similar observations were made

with the infrared receiver elements exposed to neutron bombardment. The neutrons were generated by a 9.6-curie polonium-beryllium source. The spectrum of this source has a maximum (in terms of neutrons per cm^2 /sec/mev) at an energy of approximately 3 mev and falls to approximately 50 per cent of the peak value at 1.0 mev and 6.5 mev.

The results of this investigation are indicated in Table I. It should be noted that only gold-doped germanium photoconductive cells changed their characteristics when exposed to either gamma radiation or neutron bombardment. The cells recovered immediately after the exposure was interrupted.

The Missile Division of Lockheed Aircraft Corporation studied the influence of cobalt-60 gamma radiation on the main photoconductive properties of lead sulfide cells up to a total dose of approximately 2×10^7 r. In this experiment the radiation intensity was about 1000 times greater than that used in the earlier investigations.

Contrary to the results obtained on lead sulfide cells exposed to relatively small gamma radiation intensities, it was observed that at greater intensities the resistance of this type of infrared receiver decreased somewhat and later showed a sharp increase at a total dose of approximately 2×10^7 r. In some cases the resistance increased by a factor of approximately 30, compared to the resistance before exposure. At the same time a decrease in time constant, an increase in noise, and a sharp decrease in responsivity to approximately 20 per cent of the original value were observed. When measured a certain time after exposure, the lead sulfide cells recovered completely and showed the original values for the various properties. The recovery time increased with the dose of gamma radiation used.

Other measurements on lead sulfide cells were carried out at Boeing Aircraft Corporation using gamma radiation dose rates up to 5×10^7 r. In addition, lead sulfide cell characteristics were investigated under neutron bombardment. During the exposure only the cell resistance was measured and it was assumed that both responsivity and resistance would change at the same rate. At a dose of about 5×10^7 r, resistance increased by a factor of approximately 100. It was then assumed that the responsivity would decrease by approximately 50 per cent at an exposure with a total dose of about 10^8 r. About the same decrease in responsivity was assumed after a total neutron dose of 10^{13} per cm^2. The resistance of the lead sulfide cells returned to normal approximately one month after the exposure.

Investigations on lead telluride photoconductive cells carried out at Syracuse University showed permanent damage to the cells after exposure to approximately 10^8 r of cobalt-60 gamma radiation.

TABLE I

	Co^{60} Gamma Radiation			PoBe Neutron Bombardment		
Cell	Strongest Dose Rate Used	Total Dosage	Influence	Strongest Flux	Exposure Time	Influence
PbS	20,800 R/h	22,000 R	None	2.2×10^6 N/cm^2 sec	215 min.	None
PbTe	17,600 R/h	35,200 R	None	$4.80\cdot10^5$ N/cm^2 sec	240 min.	None
InSb	10,300 R/h	15,450 R	None	$3.6\cdot10^5$ N/cm^2 sec	120 min.	None
Bolometer	10,300 R/h	14,450 R	None	$8.0\cdot10^4$ N/cm^2 sec	30 min.	None
Ge with either AgC or sapphire window.	0.8 R/h increased noise 4–6 times 6.6 R/h increased noise 9–12 times 422 R/h increased noise 65 times 1040 R/h increased noise 100 times 10,300 R/h increased noise 800 times (Compared with the internal noise without Gamma irradiation)			$3.3\cdot10^5$ N/cm^2 sec increased noise approximately 16 times if compared with the internal noise without neutron bombardment.		

Paper 4.1.8

Preamplifiers for Nonimage-Forming Infrared Systems*

J. A. JAMIESON†, MEMBER, IRE

Power Levels

THE most common form of photoconductive radiation detector used in infrared systems is the lead sulfide film. These films typically have a surface resistivity of about one million ohms and produce an output rms noise voltage of the order of 1 μv in a 100-cps pass band centered at 1000 cps. This corresponds to a noise power of 10^{-18} watts. The Johnson noise power from a resistor under similar conditions and at room temperature is 4×10^{-19} watts. The cooled, longer-wavelength sensitive detectors such as lead selenide and lead telluride may have resistances 3 to 100 times higher, but they exhibit a similar ratio of noise power to Johnson noise power. The more recent indium antimonide detectors are much lower-impedance devices, typically of the order of 200 ohms. The noise output of these cells may be even closer to Johnson noise and is therefore very low.

Evidently, it is quite difficult to design preamplifiers for use with these detectors in such a way that the combination is limited in detectivity by the noise of the detector. The considerations in such a design are not new, for the most part, but must be carefully observed.

Components

The first step is the choice of adequate components. In the case of tubes, the first consideration is that they shall have low susceptibility to microphonics. Many infrared systems are exposed to fairly severe vibrations. In some cases, this is particularly true of the preamplifier, since it may be required to move with the radiation detector in some form of mechanical scanning. Fortunately, the subminiature tubes desirable in restricted spaces available for preamplifiers are ruggedly built with spot-welded parts and tightly-strung, well-supported grids. They are relatively free of low-frequency resonances at the audio frequencies of interest in this work. Such tubes as the 6BY4, 6021, 6247, and particularly the 6533, give good results. Transistors inherently exhibit good microphonics performance, and such types as the Philco 2N207B and the TUNG-SOL TS628 are commonly used. Resistors in the first two stages must be low-noise types to avoid the excess current noise associated with carbon-composition resistors. Capacitors must be chosen to be stable and non-microphonic. The metalized-paper type tend to break down and heal at random times and are highly undesirable.

A particularly important consideration is the choice of interconnecting cabling. Simple shielded cable is vulnerable, under vibration or flexure, to changes in capacitance and to induction of charges on the dielectric by friction with the center conductor or shielding. In the case of cabling between the detector itself and the preamplifier, the bias potential often exists across the cable insulation. Consequently, changes in capacitance give rise to currents which flow through the load and appear as unwanted voltages. Several manufacturers (for example, Microdot Inc., of South Pasadena, Calif.) have materially reduced these problems by introducing cables which are treated with conducting materials between the outside sheaths and the dielectric, and, as far as possible, between the center conductor and the dielectric. These coatings tend to dissipate frictionally induced charge and to maintain rather constant capacitance.

Circuits

These carefully chosen components must be used in circuits selected for their low noise characteristics. In the case of transistors, the maintenance of a signal-to-noise ratio close to that of the detector usually requires the use of a transformer to match the detector impedance to the optimum source resistance of the transistor. Since this optimum source resistance is normally about 1.2 kΩ, the turns ratio may be quite large in the case of the higher-impedance detectors. Such a turns ratio of 20 or 30 to one, reduces signal levels to a point where both first- and second-stage noise must be considered. Individual stages are run at low current levels, and with small collector voltages to minimize the transistor's own noise.

Gain is limited in the first stage by the low current and by the need to keep the load resistor down to about 10 kΩ to be within reasonable range of the optimum source resistance of the second stage. Fortunately, the use of transformer input often makes it possible to obtain satisfactory bias stability at low current levels, and to bypass the bias resistors to remove their noise.

The common emitter connection appears to be most popular, in that its optimum source resistance from noise considerations is close to the optimum source resistance for maximum power transfer. Transistor circuits may, with careful design and selection of transistors, be used at noise figures of around 3 db in many applications.

Among tube circuits, the best appears to be the "cascode" circuit. This ingenious circuit uses two triodes, the second in grounded-grid operation acting as plate

* Original manuscript received by the IRE, June 29, 1959.
† Avionics Div., Aerojet-General Corp., Azusa, Calif.

load for the first which is a grounded-cathode amplifier. The first stage has little voltage gain, but considerable power gain. The over-all voltage gain is comparable with that of a pentode. Noise figures below 1.3 db are obtained with this circuit. One practical point about this circuit is that the cathode of the second tube is at the plate potential of the first. This imposes a strain on the heater-to-cathode insulation.

In addition to the careful design of the amplifying circuits, the power supplies, particularly for the detector and early stages, must be carefully filtered and decoupled. A part or all of the band-pass filter is often introduced into the preamplifier to remove power-supply ripple, signals at the scanning frequency, and transients due to uniform backgrounds at low voltage levels, before any circuit nonlinearities can give rise to cross products between these unwanted signals and noise.

Construction

The third general consideration in the design of preamplifiers is their construction. The preamplifier is usually placed close to the detector to avoid the cable noise previously considered. This may often place it close to scanning motors and other sources of stray fields. Since impedance levels may be high, this situation calls for extremely careful shielding, and despite the relatively low frequencies often involved, circuits should usually be as compact as possible.

Magnetic shielding, in particular, is sometimes a difficult problem. Electrostatic shielding of the detector itself is not easy. It has frequently been found necessary to drive the detector shield from a cathode follower amplifying the detector output, in order to reduce the charging current into its stray capacitance. In the case of cooled detectors, noise may be introduced by rapid temperature fluctuations, by microphonic vibrations between a cooling cryostat and the detector, and by vibration of the detector leads which change their capacitance to nearby structures.

These difficulties call for particularly careful mechanical design beyond normal packaging requirements. Systems which operate at very low frequencies may require attention to thermal voltages arising from changes of temperature at the junctions of dissimilar metals.

Special Techniques

The detectivity of an infrared system may be improved by using several detectors illuminated by one telescope. (This improvement in detectivity arises partly from the reduced area of each detector, consequent upon its seeing only a part of the instantaneous field of view, and partly from the reduced background signal at each detector.) If each detector must use a separate amplifier, the size and cost of the electronic package may become excessive. Therefore systems which use various means of sampling memory circuits attached to each detector are being developed. The memory circuits may, for instance, be resonant circuits or capacitors which integrate signal energy from their detector. Each memory circuit is sampled in sequence, and one amplifier is used to process the samples. For this purpose, very-low-noise switching circuits are required to perform sampling at rates of the order of a kilocycle per second. Various forms of mechanical rotating switches have been used for this purpose, but as the technique develops, solid-state circuits or light commutators may perhaps be used.

The use of maser preamplifiers at infrared wavelengths appears to be theoretically feasible, but the narrow optical bandwidth obtainable will probably limit them to rather special applications. Parametric amplifiers of various forms seem to be potentially capable of low-noise amplification, although they do not appear to have been applied in the infrared field as yet. The lead salt detectors have, in the past, produced noise levels high enough so that preamplifiers which did not degrade the signal-to-noise ratio excessively were possible. The introduction of the very-low-noise, wide-band, indium antimonide detectors may in the future require cooled-preamplifier stages, perhaps in the same package as the detector, to raise output signal and noise levels to a point where conventional amplification is adequate.

Paper 4.1.9

Detectivity and Preamplifier Considerations for Indium Antimonide Photovoltaic Detectors*

G. R. PRUETT AND R. L. PETRITZ†

INTRODUCTION

THE indium antimonide single-crystal photovoltaic detector[1] shows promise of reaching the ultimate limit of detectivity, termed the *Blip* condition of operation.[2] The detector has a lower impedance than the lead-salt detectors, and special attention must be given to the associated preamplifier. The detector signal, noise and detectivity characteristics as well as the preamplifier requirements will be discussed. Equations will be derived to show the conditions that must be fulfilled by the preamplifier in order to utilize the full detectivity of the detector. Equations which will simplify problems in design are derived, and a specific circuit is included with experimental data.

VOLTAGE-CURRENT CHARACTERISTICS

These detectors are prepared from single crystals of n-type indium antimonide. Diffusion or alloy techniques are used to create a thin p-type layer on the surface, and contact is made to the surface and base regions; thus, the model is a simple p-n junction with radiation incident normal to the junction. A more complete discussion of this type of detector is given elsewhere in this issue.[1]

In thermal equilibrium a p-n junction has voltage-current characteristics[3] given by

$$I_d = I_s(e^{qV/\beta kT} - 1), \tag{1}$$

where I_d is the junction current, I_s is the saturation current, q is the electronic charge, V is the drop in potential across the junction of the diode, k is Boltzmann's constant, T is the equilibrium temperature of the diode, and β is a factor[3] which is unity for an ideal diode, but is found to be greater than unity in cooled indium-antimonide junctions. Cooled indium antimonide appears to be similar to silicon at room temperature and to cooled germanium where the main generation of carriers occurs in the space-charge region of the junction, and where β is expected to be of the order of two.[4]

When radiation from a background with a temperature higher than the equilibrium temperature of the diode falls onto the detector, the voltage-current equation for the diode becomes[5]

$$I = -I_{sc} + I_s(e^{qV/\beta kT} - 1). \tag{2}$$

I_{sc} is the current induced by the incident background radiation. A derivation of (2) with an expression for I_{sc} in terms of basic semiconductor parameters is given by Rittner[5] in a treatment of the solar battery.

I_{sc} can be expressed in terms of the background-radiation flux as

$$I_{sc} = q\eta_r J_r A, \tag{3}$$

where

$$J_r = \int_0^{\lambda_i} J_\lambda d\lambda. \tag{4}$$

J_r is the radiation flux expressed in photons per second per square centimeter of area, A is area in square centimeters, η_r is the quantum efficiency with respect to background radiation, and $\lambda_i = hc/E_i$ is the long wavelength cutoff of the detector, corresponding to the energy gap, E_i. In indium antimonide, the energy gap at 77°K is 0.23 ev corresponding to a long wavelength cutoff of 5.35 microns. The radiation flux, J_r, and the current density, j_r, for an indium antimonide photodiode with an equilibrium temperature of 77°K while looking at 300°K radiation are

$$J_r = 2 \times 10^{16} \text{ photons/cm}^2 \text{ sec},$$

and

$$j_r = qJ_r = 3.2 \times 10^{-3} \text{ amp/cm}^2.$$

An additional path for current in diffused, alloyed, or grown photodiodes is a conductance, G_s, which is in shunt with the diode. When G_s is incorporated in the voltage-current equation, the latter becomes

$$I = -I_{sc} + I_s(e^{qV/\beta kT} - 1) + G_s V. \tag{5}$$

* Original manuscript received by the IRE, April 27, 1959; revised manuscript received, July 8, 1959.

† Central Res. Labs., Texas Instruments Inc., Dallas, Texas.

[1] A general discussion of indium antimonide infrared detectors is given by F. F. Rieke, L. H. DeVanx, and A. J. Tuzzolini, "Single crystal infrared detectors based upon intrinsic absorption," paper 3.3.5, this issue, p. 1475.

[2] For a discussion of the *Blip* (background-limited infrared photodetector) detector, see R. L. Petritz, "Fundamentals of infrared detectors," paper 3.3.1, this issue, p. 1458.

[3] J. L. Moll, "The evolution of the theory of the voltage-current characteristics of p-n junctions," PROC. IRE, vol. 46, pp. 1076–1082; June, 1958.

[4] C. T. Sah, R. N. Noyce, and W. Shockley, "Carrier generation and recombination in p-n junctions and p-n junction characteristics," PROC. IRE, vol. 45, pp. 1228–1243; September, 1957.

[5] E. S. Rittner, "Electron processes in photoconductors," in "Photoconductivity Conference," R. G. Breckenridge, B. R. Russell, and E. E. Hahan, eds., John Wiley and Sons, Inc., New York, N. Y., pp. 250–257; 1956.

Typical voltage-current curves for indium antimonide photodiodes are shown in Fig. 1. In curve A, the detector is at thermal equilibrium at 77°K with no excess background radiation; curve B shows the effect of adding 300°K radiation while the diode is held at 77°K, and curve C shows the effect of still more background radiation. Note that I_{sc} can be taken directly from Fig. 1 at the intercept with the current axis. The slope of the curve in the reverse biased condition would approach zero for an ideal photodiode, but in the actual photodiode this slope gives the value for the shunt conductance G_s. By plotting log $(I+I_{sc}-G_sV)$ vs V for the forward-bias condition, the values of β and I_s can be determined. The value of β has varied from 2 to 3.8 for the photodiodes measured.

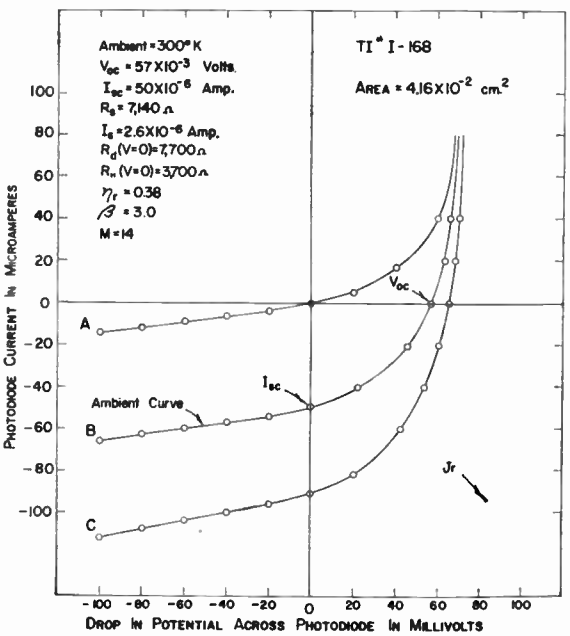

Fig. 1—Voltage-current characteristics for an indium-antimonide photodiode under several conditions of ambient radiation.

Small-Signal Properties

Response of the photodiode to a small radiation signal, ΔJ_s, in the presence of the background radiation, is obtained from (5) as

$$\Delta I = \left[-\frac{dI_{sc}}{dJ_s} + \frac{q}{\beta kT} I_s e^{qV/\beta kT} \frac{dV}{dJ_s} + G_s \frac{dV}{dJ_s} \right] \Delta J_s. \quad (6)$$

The small signal short-circuit current generator for a Norton representation is found by holding V constant:

$$i_s = \Delta I]_{V=\text{const}} = -\frac{dI_{sc}}{dJ_s}\Delta J_s = -q\eta_s A \Delta J_s, \quad (7)$$

where η_s is the quantum efficiency with respect to the signal radiation. The designation η_s is used to distinguish it from η_r because of the possible difference in the spectral character of the signal radiation and background radiation.

The impedance of the Norton equivalent circuit is found by differentiating (5) with respect to V while holding J_s constant:

$$\Delta I = (G_d + G_s)\Delta V, \quad (8)$$

where

$$G_d = \frac{qI_s}{\beta kT} e^{qV/\beta kT}, \quad (9)$$

$$R_d = \frac{1}{G_d}, \quad \text{and} \quad R_s = \frac{1}{G_s}. \quad (10)$$

At low frequencies (7) and (8) indicate the Norton equivalent circuit that is shown in Fig. 2.

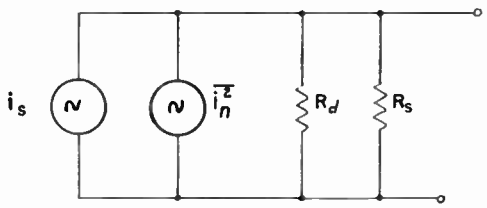

Fig. 2—Norton's equivalent circuit for indium-antimonide photodiode.

Noise Properties

The fundamental noise associated with an ideal narrow-base diode ($\beta = 1$) can be expressed[6] in terms of shot noise for each current:

$$\frac{\overline{i^2}}{\Delta f} = 2q[I_{sc} + I_s(e^{qV/kT} + 1)]. \quad (11)$$

When current is generated in the space-charge region ($\beta > 1$), (11) must be modified according to Schneider and Strutt,[7] who have recently made a study of this problem in silicon. When β is considered, the shot noise equation for the photodiode is

$$\frac{i^2}{\Delta f} = 2q\left[I_{sc} + \frac{I_s}{\beta} (e^{qV/\beta kT} + 1) \right]. \quad (12)$$

This equation is correct at thermal equilibrium ($I_{sc} = 0$, $V = 0$) since

$$\frac{\overline{i^2}}{\Delta f}\Bigg]_{\substack{V=0 \\ I_{sc}=0}} = \frac{4qI_s}{\beta} = 4kTG_d, \quad (13)$$

in agreement with the Nyquist result. Eq. (12) is valid for small bias near the $V = 0$ condition but needs modification for large forward bias. Since the bias condition near $V = 0$ is of the greatest interest for this discussion, (12) will be used throughout this paper.

[6] A recent review and extensive bibliography of the theory of shot noise in p-n junctions is by A. van der Ziel, "Noise in junction transistors," Proc. IRE, vol. 46, pp. 1019–1038; June, 1958.

[7] B. Schneider and M. J. O. Strutt, "Theory and experiments on shot noise in silicon p-n junction diodes and transistors," Proc. IRE, vol. 47, pp. 546–554; April, 1959.

The shunt conductance has a Nyquist noise,

$$\frac{\overline{i_s^2}}{\Delta f} = 4kTG_s. \tag{14}$$

Experiment has indicated that the main source of 1/f noise is the current which passes through the shunt conductance. An empirical equation for the 1/f noise can be written as

$$\frac{\overline{i_f^2}}{\Delta f} = \frac{1}{f}\left[k_1 G_s^2 V^2 + k_2(I - G_s V)^2 + k_3 I^2\right], \tag{15}$$

where

$$k_1 \gg k_2 \text{ and } k_3.$$

The values for k_1, k_2, and k_3 must be determined experimentally, since no quantitative theory of 1/f noise exists.

The equation for the total short-circuit noise generator is obtained from (12), (14), and (15).

$$\frac{\overline{i_n^2}}{\Delta f} = 2q\left[I_{sc} + \frac{I_s}{\beta}\left(e^{qV/\beta kT} + 1\right)\right] + 4kTG_s + \left[\frac{k_1 G_s^2 V^2 + k_2(I - G_s V)^2 + k_3 I^2}{f}\right] = N_n. \tag{16}$$

Signal-to-Noise Ratio and Detectivity

When (7) and (16) are combined, the signal-to-noise ratio for the photodiode can be expressed as

$$\frac{i_s}{\sqrt{i_n^2}} = \frac{qn_s \cdot 1 \Delta J_s}{\sqrt{\Delta f}(N_n)^{1/2}}. \tag{17}$$

Examination of (17) and (16) show that the S/N will be near a maximum when $V = 0$, and this has been verified by experiment. The chief reason for this is because the 1/f noise term due to the shunt conductance disappears at this bias. Another point is that the condition

$$I_{sc} \gg \frac{I_s}{\beta}\left(e^{qV/\beta kT} + 1\right) \tag{18}$$

is desirable, since I_{sc} reflects noise due to the background radiation, while the I_s term contains the lattice-induced noise.[2] Conditions for (18) can be obtained if the forward-bias state is avoided, since I_{sc} is usually much greater than $2I_s$.

The specific detectivity of the detector, D^*_d, is defined[8] as

$$D_d^* = \frac{(\mathrm{S/N_d})\sqrt{A\Delta f}}{E_s A \Delta J_s}, \tag{19}$$

where E_s is the energy per photon of the signal radiation, and N_d is the detector noise. This is a measure of S/N per unit of incident power, normalized to 1 cm² area and unit bandwidth.

When (17) is substituted into (19), and using (16),

$$D^*_d = \frac{qn_s}{E_s\left\{2q\left[j_{sc} + \frac{j_s}{\beta}\left(e^{qV/\beta kT} + 1\right)\right] + \frac{4kTG_s}{A} + \frac{1}{fA}\left[k_1 G_s^2 V^2 + k_2(I - G_s V)^2 + k_3 I^2\right]\right\}^{1/2}}, \tag{20}$$

where

$$j_{sc} = \frac{I_{sc}}{A} \text{ and } j_s = \frac{I_s}{A}.$$

If

$$\eta_s = 1, \quad \eta_r = 1, \quad j_{sc} \gg \frac{j_s}{\beta}\left(e^{qV/\beta kT} + 1\right),$$

and there is no 1/f noise, then this equation becomes that of the ideal radiation detector discussed elsewhere in this issue,[2] that is, the *Blip* (background-limited infrared photodetector):

$$D^*_{Blip} = \frac{1}{E_s\sqrt{2J_r}}. \tag{21}$$

Note that $\sqrt{2}$ appears in (21) whereas $\sqrt{4}$ appears in (46) of reference 2. This is because the photodiode registers only generation noise of the background radiation; the recombination of hole-electron pairs occurs in the base material and does not contribute to the noise.

D^*_{Blip} for indium antimonide facing hemispherical 300°K background radiation is

$$D^*_{Blip}(500^\circ\,\mathrm{K}) = 24 \times 10^9 \text{ watts}^{-1},$$

and

$$D^*_{Blip}(\lambda_i = 5.35\mu) = 13.6 \times 10^{10} \text{ watts}^{-1}.$$

Detector Noise Figure

A quantitative measure of the performance of a photodetector is the noise figure, F_d, defined[2] by

$$F_d = \frac{(\mathrm{S/N})^2_{Blip}}{(\mathrm{S/N})_d^2} = \frac{(D^*_{Blip})^2}{(D^*_d)^2}. \tag{22}$$

Substituting (20) and (21) into (22), one finds

$$F_d = \frac{1}{\eta_s^2}\left(\frac{N_n}{2qI_r}\right), \tag{23}$$

where Nn is defined in (16) and

$$I_r = qJ_r A.$$

Note that for a detector which is not limited at all by radiation noise, F_d depends on the quantum efficiency as $1/\eta_s^2$, but for detectors which see radiation noise, (23) can be written

$$F_d = F_d \text{ (quantum eff)} \cdot F_d \text{ (noise)}, \tag{24}$$

[8] For a discussion of the specific detectivity see R. C. Jones, "Phenomenological description of the response and detecting ability of radiation detectors," paper 4.1.1, this issue, p. 1495.

where

$$F_d \text{ (quantum eff)} = \frac{\eta_r}{\eta_s^2},$$

and

$$F_d \text{ (noise)} = 1 + \frac{2q\frac{I_s}{\beta}(e^{qV/\beta kT} + 1) + 4kTG_s + \frac{k_1G_s^2V^2 + k_2(I - G_sV)^2 + k_3I^2}{f}}{2qI_{sc}}. \quad (25)$$

For radiation signals of spectra $0 \leq \lambda_i \leq 5.35\mu$, η_s can be taken equal to η_r so that

$$F_d \text{ (quantum eff)} = \frac{1}{\eta_s}. \quad (26)$$

For the example of Fig. 1,

$$F_d \text{ (quantum eff)} = \frac{1}{0.38} = 2.6, \text{ or } 4.2 \text{ db}.$$

To calculate F_d(noise) precisely, the parameters specified in (25) must be determined. Of these, only k_1, k_2, and k_3 require direct noise measurements; all the other parameters can be taken from the voltage-current curves as previously discussed. It is of interest to calculate F_d (noise) at $V=0$, where the major source ($k_1G_s^2V^2$) of 1/f noise is zero. The 1/f noise associated with the terms containing k_2 and k_3 is neglected. Then

$$F_d \text{ (noise)}\big]_{\substack{V=0 \\ k_3=0}} = 1 + \frac{1}{M}, \quad (27)$$

where

$$M = \frac{qI_{sc}R_\parallel}{2kT} = 75I_{sc}R_\parallel. \quad (28)$$

$$1/R_\parallel = Gs + Gd$$

Eq. (27) is useful since it gives the lower limit of F_d (noise) for $V=0$. The presence of 1/f noise will cause F_d to be larger than this value.

For the example of Fig. 1,

$$F_d \text{ (noise)}\big]_{V=0} = 15/14, \quad \text{or} \quad 0.3 \text{ db};$$

thus the detector should be only 0.3 db from a 100 per cent radiation noise-limited condition if there is no 1/f noise present.

The total theoretical noise figure for the detector is

$$F_d = 2.6(15/14) = 2.8, \text{ or } 4.5 \text{ db}.$$

This indium antimonide detector should be only 4.5 db from the fundamental limit of detectivity; that is

$$D^*_d(500^\circ \text{ K}) = \frac{D^*_{Blip}}{\sqrt{2.8}} = 14 \times 10^9 \text{ watts}^{-1}.$$

With detectors having such high theoretical performance available, requirements on the preamplifier should is sufficiently stringent that the performance of the photodiode is not degraded by the preamplifier.

Effective Noise Figure of Preamplifier

When the detector is connected to a preamplifier, the problem becomes one of determining how the noise figure of the preamplifier affects the detectivity of the detector. The usual amplifier noise figure, F_a, is defined relative to the Nyquist noise of a resistor, R, at room temperature. The amplifier contribution to the noise can be represented in an equivalent circuit diagram as a series noise generator,

$$\overline{e_a^2} = 4kTR(F_a - 1)\Delta f, \quad (29)$$

as shown in Fig. 3(a).

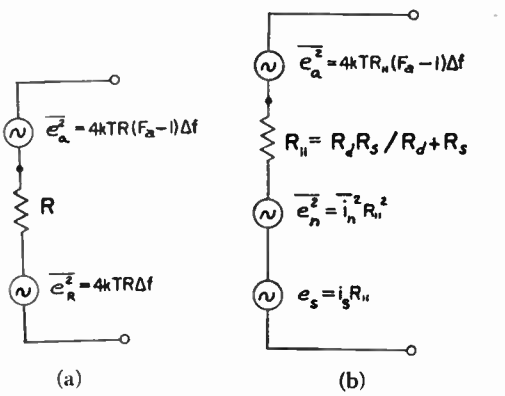

Fig. 3—Equivalent circuit for preamplifier input (a), and for detector-preamplifier combination (b).

When the indium antimonide detector is connected in place of the Nyquist noise resistor, a different situation exists: the detector is cooled, and the source noise is not that of a pure resistance but that of the detector. If the equivalent circuit of the detector, Fig. 2, is converted to a voltage equivalent circuit as in Fig. 3(b) and added in series with the amplifier noise generator, an effective noise figure, F^*_a, which has meaning relative to the cooled indium antimonide detector, can be defined. The effective noise figure of the amplifier can now be expressed in the same formal manner as the conventional noise figure,

$$F^*_a = \frac{(S/N)_d^2}{(S/N)_{d+a}^2} = \frac{(D^*_d)^2}{(D^*_{d+a})^2} = \frac{(N_{d+a})^2}{(N_d)^2}. \quad (30)$$

D^*_{d+a} is the detectivity of the detector including the amplifier noise:

$$D^*_{d+a} = \frac{S\sqrt{A\Delta f}}{N_{d+a}E_sA\Delta J_s}, \quad (31)$$

where N_{d+a} includes both the noise of the detector and preamplifier.

Substituting (16) and (29) into (30), and using the circuit of Fig. 3(b),

$$F^*_a = 1 + \frac{4kT_a(F_a + 1)}{R_{\|}N_n} \tag{32}$$

is obtained for the effective noise figure of the preamplifier. For indium antimonide detectors at the $V=0$ condition and assuming $k_2=k_3=0$, (32) becomes

$$F_a^* = 1 + \frac{T_a(F_a + 1)}{T_d(1 + M)}, \tag{33}$$

where $T_d=77°\text{K}$ and $T_a=300°\text{K}$. If the data from Fig. 1 are used along with $F_a=2$ (3 db) as an example, F^*_a is 1.27 or 1.0 db. This means that the detectivity as measured through this amplifier (D^*_{d+a}) is a factor of $\sqrt{1.27}$ less than the actual detectivity of the detector (D^*_d), as can be seen from the definition of F^*_a in (30):

$$D^*_{d+a}(500°\text{K}) = \frac{D^*_d}{\sqrt{1.29}} = 12.5 \times 10^9 \text{ watts}^{-1}.$$

To minimize the noise introduced by the amplifier, I_{sc} and $R_{\|}$ need to be as large as possible, and F_a should be as nearly unity as possible. A recent increase in detector impedance as a result of improved detector technology has helped in its direct effect in (33) as well as in its effect on transistor preamplifiers, which have better noise figures with source impedances of a few thousand ohms rather than a few hundred ohms.

Noise Figure of Detector-Amplifier Combination

The over-all noise figure of the detector with the amplifier can be defined as

$$F_{d+a} = \frac{(S/N)_{Blip}^2}{(S/N)_{d+a}^2} = \frac{(D^*_{Blip})^2}{(D^*_{d+a})^2}$$
$$= \frac{(D^*_{Blip})^2}{(D^*_d)^2} \times \frac{(D^*_d)^2}{(D^*_{d+a})^2}, \tag{34}$$

or

$$F_{d+a} = F_d \cdot F^*_a, \tag{35}$$

where F_d is given by (23) and F^*_a by (32). Using the example from Fig. 1,

$$F_{d+a} = 4.5 \text{ db} + 1.0 \text{ db} = 5.5 \text{ db (or the ratio, 3.54)}, \tag{36}$$

and

$$D^*_{d+a}(500° \text{ K}) = \frac{D^*_{Blip}}{\sqrt{3.54}} = 12.5 \times 10^9 \text{ watts}^{-1}, \tag{37}$$

in agreement with the results of the previous section.

This theoretical value for D^*_{d+a} is very satisfactory and indicates that contemporary indium antimonide photodetectors constitute very sensitive infrared detectors which can be connected directly into transistor preamplifiers without the use of a coupling transformer.

Measuring Technique and Preamplifier Application

Transistorized preamplifiers have been constructed, and measurements have been taken to investigate the above conclusions. A simple preamplifier circuit using a selected germanium transistor (2N185) is shown in Fig. 4. The characteristics of the amplifier as a function of frequency are shown in Fig. 5, and the dependence of F_a on source resistance is shown in Fig. 6. At present the noise figure for alloyed germanium transistors is superior to that of other transistors when operated in the "starved" condition[9] (low collector currents). Silicon transistors can be obtained with noise figures between 3 and 6 db.

Two methods are used for biasing to the zero-voltage condition. A choke can be placed across the photodiode to provide a dc short while maintaining a high impedance for ac signals, or the detector can be back-biased to the condition of zero voltage across the diode as shown in Fig. 4. The latter method has been used for making the experimental measurements. R_b should be large compared to R_s so that no Nyquist noise is introduced by the biasing resistor. If R_b is not large compared to R_s, the above formulas are still applicable provided R_s is considered to be the parallel combination of R_b and R_s.

The experimental values for D^*_{d+a} (500°K) are measured with the transistor preamplifier shown in Fig. 4 coupled directly into a standard amplifier. Signal and noise measurements are taken from a narrow-band wave analyzer, and the radiation signal is obtained from a standard calibrated 500°K blackbody chopped at 1000 cps. Both noise voltage and signal voltage are measured with the detector biased to the zero dc voltage condition with a 300°K ambient radiation. Thus D^*_{d+a} as defined in (31) is measured experimentally without transformers.

The value of D^*_{d+a} for the detector of Fig. 1, as measured under the condition noted above was

$$D^*_{d+a}(500°\text{K})\big]_{\substack{V=0 \\ f=1000 \text{ cps}}} = 8.7 \times 10^9 \text{ watts}^{-1}, \tag{38}$$

and

$$F^*_{d+a}(500°\text{K}) = \frac{24}{8.7} = 2.76, \text{ or } 8.8 \text{ db}. \tag{39}$$

When the value from (39) or (38) is compared to the theoretical value from (36) or (37), it is found that the experimental value of D^*_{d+a} is 3.3 db below the theoretical value. The difference is due to the neglect of 1/f noise in calculating D^*_{d+a} (theoretical). In the measurement of a large number of detectors, results such as those of (38) and (39) are typical. A difference of 3 to 6

[9] R. D. Middlebrook and C. A. Meed, "Transistor ac and dc amplifiers with high input impedance," *Semiconductor Products*, vol. 2, pp. 26–35; March, 1959.

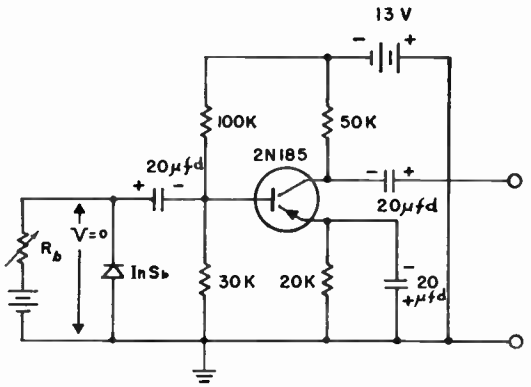

Fig. 4—Circuit diagram for transistor preamplifier with an indium antimonide photodiode back-biased to the $V=0$ operating point.

db between the experimental and the theoretical value of D^*_{d+a} is common and is attributable to 1/f noise in the detectors.

Summarizing the values obtained for the example of Fig. 1, it is found that

$$D^*_{d+a}(\text{exp}) = 8.7 \times 10^9 \text{ watts}^{-1},$$

and

$$F^*_{d+a}\,(\text{exp}) = 8.8 \text{ db}$$

of which

$$\begin{aligned} F_d \text{ (quantum eff)} &= 4.2 \text{ db}, \\ F_d \text{ (noise other than 1/f)} &= 0.3 \text{ db}, \\ F_d \text{ (1/f noise)} &= 3.3 \text{ db}, \\ F^*_a &= 1.0 \text{ db} \\ &\overline{\quad\quad 8.8 \text{ db}.} \end{aligned}$$

Conclusion

Contemporary indium antimonide detectors can be used to nearly their full potentialities directly with germanium or silicon transistor preamplifiers; no coupling transformer or choke is required. With further increase in detector impedance and I_{sc}, the amplifier noise contribution can be reduced to negligible proportions for even relatively noisy preamplifiers. The formulas which have been derived for calculation of the noise figure of the detector and the preamplifier separately should be useful in the design of both preamplifiers and detectors. These formulas should also provide guidance in detector and preamplifier research and development.

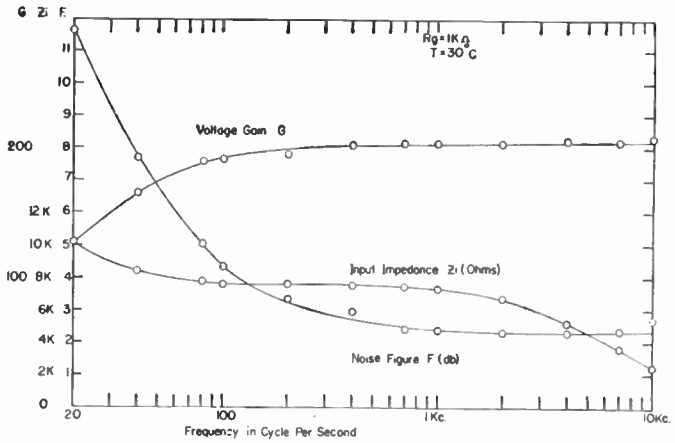

Fig. 5—Preamplifier characteristics as a function of frequency for an input of 1000 ohms at 30°C.

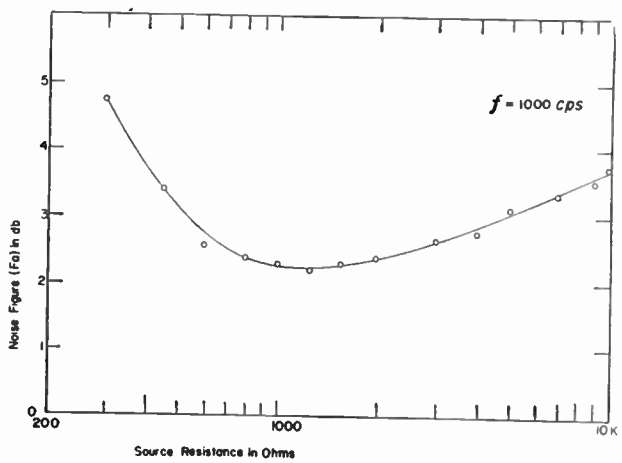

Fig. 6—Preamplifier noise figure as a function of source resistance at 1000 cps.

Acknowledgment

The authors wish to acknowledge the contributions to this subject of W. A. Craven, Jr., and R. H. Genoud, who kindly gave us a preprint of their paper, "Characterization of Indium-Antimonide Photodetectors," presented before the Optical Society of America on April 3, 1959. We would also like to acknowledge the aid given by the personnel at Texas Instruments Inc. who were associated with the development and production of infrared detectors, especially B. R. Pagel and R. Fewer, who designed the transistor preamplifiers, and L. G. Sloan, who supervised the construction of the detectors used in collecting the experimental data.

Paper 4.2.1

Optics for Infrared Systems*

R. M. SCOTT†

THE principal differences between the optics of infrared systems and visual optical systems result from the image-size requirements in the two portions of the spectrum. In the visible and near infrared, photoelectric detectors, photographic plates and the eye are capable of resolutions in the tens of microns and smaller range of dimensions. In the deep infrared, beyond two microns wavelength, the current state of the art yields detectors with effective resolution areas from the order of millimeters down to one hundred microns in size. Thus, the optics required for the latter region need not produce the high resolution common in visual optics. Great advantage is taken of this fact to make the optics simpler.

Any optical system, no matter how perfect in design or construction, will be limited in its resolution by diffraction. The effect of this limitation depends on the size of the optics and the wavelength of the radiation forming the image. An image of a point source produced by an ideal optical system has a central maximum of intensity surrounded by diffraction rings. The effective diameter of the central maximum is given by

$$\delta_d = \frac{1.22\lambda}{D}, \tag{1}$$

where δ_d is measured in radians. The wavelength, λ, and the diameter of the aperture, D, of the optical system are measured in the same units. This relation may be rewritten

$$\frac{d}{\lambda} = 1.22N. \tag{2}$$

In this form the diameter of the central maximum is in the same dimensions as the wavelength, while N is the F number defined as $N=f/D$. Here f is the effective focal length of the system and D, as before, is the diameter of the aperture. Fig. 1 and Fig. 2 show the effects of aperture and F number on resolutions as limited by diffraction at various infrared wavelengths.

The simplest optical systems for use in the infrared contain either a simple lens or a mirror to produce the image which falls on the detector. In many cases the image produced by a spherical mirror is small enough to be of use. A simple but useful approximation for the image size produced on axis by a spherical mirror is

$$\delta_s = \frac{7.8 \times 10^{-3}}{N^3}. \tag{3}$$

As before, δ_s is in radians. At $F/1$ this approximation gives a value too small by only three per cent, and in slower systems the agreement is much closer. In many systems it is inconvenient to place the detector in the entering beam or to deflect the energy; thus, transmission optics are often desirable. The image size due to spherical aberration of a simple lens of two spherical surfaces is given approximately by

$$\delta = \frac{7.8 \times 10^{-3}}{N^3} A, \tag{4a}$$

where

$$A = \frac{n+2}{n(n-1)^2}\sigma^2 - \frac{4(n+1)}{n(n-1)}\sigma + \frac{3n+2}{n} + \frac{n^2}{(n-1)^2} \tag{4b}$$

and

$$\sigma = \frac{R_2 + R_1}{R_2 - R_1} = \frac{\frac{R_2}{R_1} + 1}{\frac{R_2}{R_1} - 1}. \tag{4c}$$

R_1 and R_2 are the radii of curvature of the lens surfaces. Note that the factor A depends on the index of refraction, n, and a relation between the two radii. The minimum value of A, and, therefore, of the image size, occurs when

$$\frac{R_2}{R_1} = \frac{2n^2 + n}{2n^2 - n - 4}. \tag{5}$$

This relation is shown in Fig. 3, in which values for several materials of infrared interest appear. Fig. 4 shows the image size to be expected from lenses of optimum form for various F numbers.

Here again the approximations by these simple formulas gives an image size somewhat smaller than will be obtained in practice. Strong curves on the lenses, small F numbers, or low index of refraction of the material makes the approximation worse than for weaker curves in slower systems or for materials of high index. For SiO_2 at $F/1.5$ the actual image will be about 35 per cent larger than shown, while for germanium at $F/1$ the image is 23 per cent larger. However, for F numbers twice as large, $F/3$ for SiO_2 and $F/2$ for Ge, the approximations become very close indeed.

In the design of any optical system one of the important parameters is focal length. For the mirror case the approximate focal length is given by

* Original manuscript received by the IRE, June 30, 1959.
† The Perkin-Elmer Corp., Norwalk, Conn.

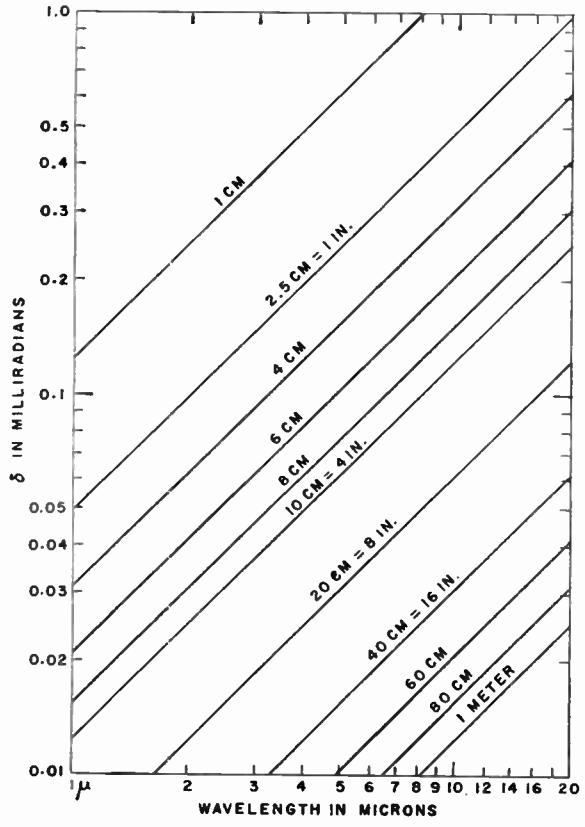

Fig. 1—The angular diameter of the diffraction image of an optical system as determined by the aperture of the system and the wavelength of the radiation.

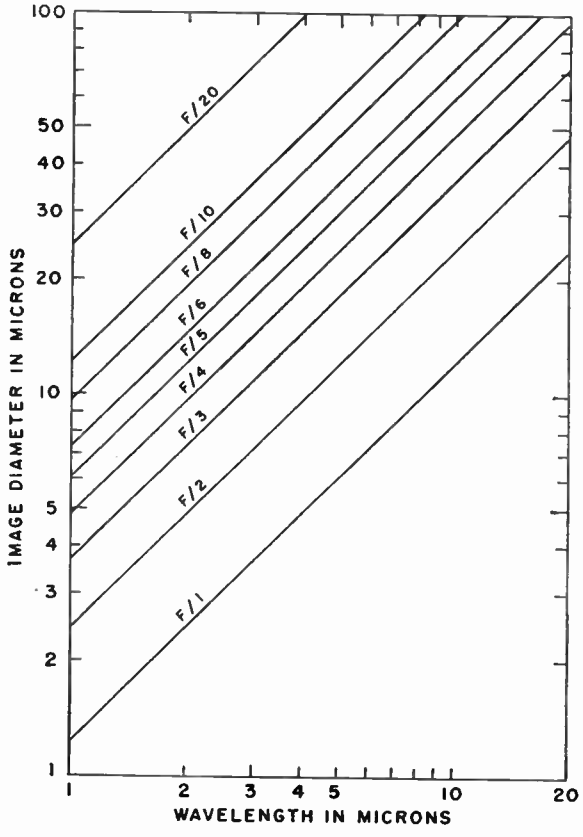

Fig. 2—The linear diameter of the diffraction image of an optical system as determined by F number and wavelength.

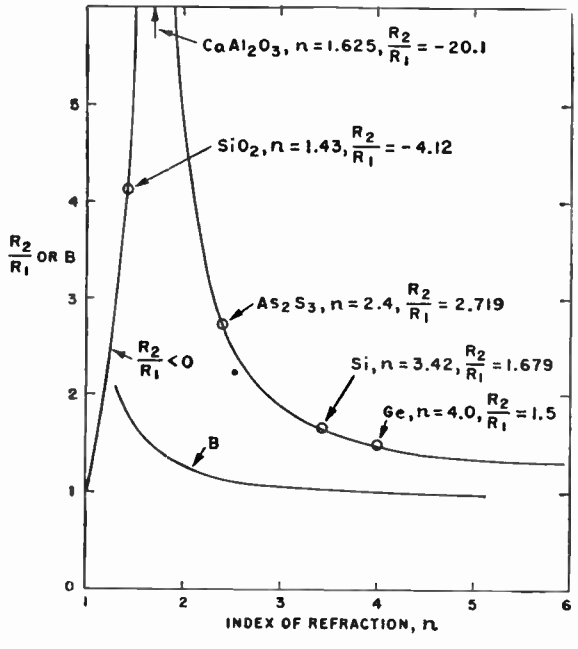

Fig. 3—Ratio of radii of the surfaces of lenses for minimum spherical aberration and the value of the constant, B, in (8), as they depend on the index of refraction.

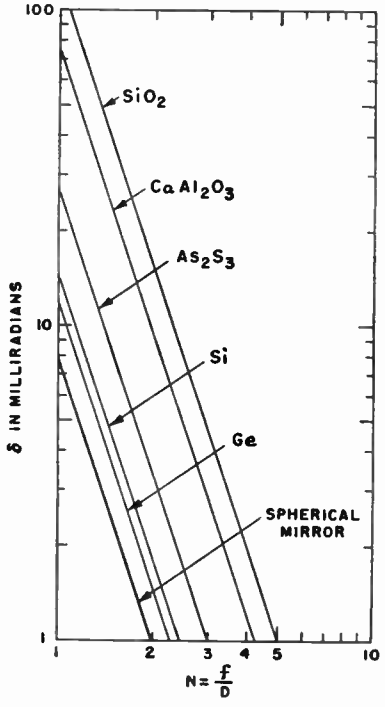

Fig. 4—The angular diameter of images produced by lenses of typical materials with spherical surfaces chosen for minimum spherical aberration as dependent on the F number of the system.

$$f = \tfrac{1}{2}R. \tag{6}$$

For fast systems the position of best energy concentration will be a bit closer to the mirror than one focal length due to spherical aberration. For lenses the relation is

$$f = \frac{-R_1R_2}{(n-1)\left(R_1 - R_2 - \dfrac{n-1}{n}t\right)}. \tag{7a}$$

If the effect of thickness, t, of the lens is neglected, the relation becomes

$$f = R_1 \frac{1}{(n-1)\left(\dfrac{R_1}{R_2} - 1\right)}. \tag{7b}$$

For the case of minimum aberration, the value of the constant B in

$$f = -BR_1, \quad \text{here} \quad B = \frac{1}{(n-1)\left(\dfrac{R_1}{R_2} - 1\right)}. \tag{8}$$

is plotted in Fig. 3. The neglect of the thickness in (7a) results in a small error of focal length. For the case of quartz at $F/1$, the worst case of the lot, (7b) gives $1.87R_1$ whereas (7a) gives $1.91R_1$.

In a particular system, even the most advantageous choice of radii may not produce images small enough to be satisfactory. While more complex systems could be designed with additional elements, the normal practice in the infrared is to utilize nonspherical surfaces. For the case of the mirror the sphere becomes ideally a parabola. The height of the surface, x, at a radius, r, from the axis, for a mirror of focal length f is given by

$$x = r^2/4f. \tag{9}$$

At a radius, r, the departure, τ, from a spherical surface of radius R, touching the parabolic surface at the center, and at r_0 is

$$\tau = \frac{r^2}{8R^3}(r^2 - r_0^2). \tag{10}$$

In order to define the amount of material to be removed to convert a sphere to a parabola, the relation between F number, N, of the mirror and the depth of the difference between the sphere and the parabola in units of the focal length is

$$\frac{\tau}{f} = \frac{1}{2^{10}N^4}\left(\frac{r}{r_0}\right)^2\left[\left(\frac{r}{r_0}\right)^2 - 1\right]. \tag{11}$$

If the mirror is manufactured precisely to the curve described by (10) and (11), the image will be of the size indicated by diffraction, as in (2). In many cases, images smaller than produced by a simple sphere are required, but the absolute perfection of the parabola is not justified. The aspheric curve may be prescribed as a parabola with tolerances set by the required image size. These tolerances may be estimated from (11).

As an example, consider an $F/2$ mirror system, 8-inch focal length, to work at 4 microns with an image requirement of 0.5 milliradian. It can be seen from Fig. 4 that a spherical mirror of $F/2$ will produce an image of one milliradian diameter, while a parabola will produce one of 0.05 milliradian, as shown in Fig. 1. The surface of the parabola at the 0.7 radius zone, the greatest departure, is 0.000125 inch below that of the sphere as given by (11). It follows then that a surface described by

$$x = \frac{r^2}{32} \pm 6.2 \times 10^{-5} \text{ inches} \tag{12}$$

should give the required 0.5-mil image, provided that the surface is smooth and axially symmetrical. In the vicinity of the diffraction limit the diameter of the central maximum does not change very much with errors in the surface. Rather, there is a change in the energy distribution between the central disk and the outer rings. This effect holds for errors up to about $\frac{1}{4}$ wavelength; about 4×10^{-5} inches for our example. Fig. 5 diagrams these relations.

Aspheric lenses for the infrared are now becoming widely used. There are two refracting forms which employ simple conic sections for focusing collimated energy. The first of these resembles in shape the optimum spherical case for high-index materials. It has a convex ellipsoid on the first surface and a concave sphere centered at the focus on the second surface. The shape of the ellipsoid is given by

$$x = f\frac{n(n-1)}{(n^2-1)}\left[1 - \sqrt{1 - \frac{1}{4N^2}\frac{(n+1)}{(n-1)}\left(\frac{r}{r_0}\right)^2}\,\right], \tag{13a}$$

$$x = \frac{nf}{(n-1)}\left[\frac{1}{8N^2}\left(\frac{r}{r_0}\right)^2 + \frac{1}{2^7N^4}\frac{n+1}{n-1}\left(\frac{r}{r_0}\right)^4 + \cdots\right]. \tag{13b}$$

Only the first term is worthy of consideration here; thus

$$x = \frac{n}{(n-1)}\frac{f}{8N^2}\left(\frac{r}{r_0}\right)^2. \tag{13c}$$

This parabolic approximation to the desired ellipsoid is very attractive because it may be generated with high accuracy by natural optical manufacturing methods. This ellipsoid departs from the sphere whose radius is the same at the axis by approximately

$$\frac{\tau}{f} = \frac{1}{n(n-1)}\frac{1}{2^7N^4}\left(\frac{r}{r_0}\right)^4. \tag{14}$$

Here again, the tolerance may be computed by a method analogous to the mirror case exemplified above.

The other conic section case, that of a flat first surface and a convex hyperboloid second surface, has proved of

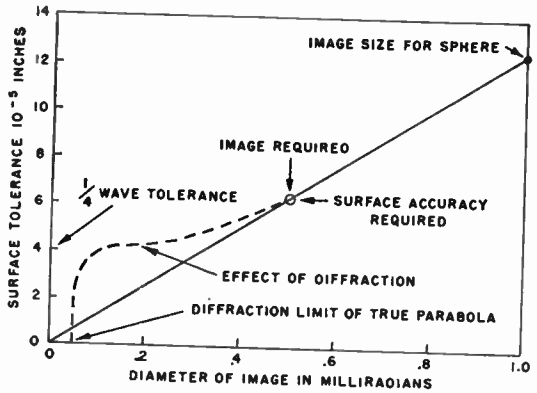

Fig. 5—The dependence of image size on surface tolerance for an $F/2$ mirror of 8-inch focal length at 4 microns wavelength

very little interest for infrared work because of its difficulty of manufacture and its unfavorable shape for coma. The optimized spherical case of (5) may be improved to the diffraction limit by applying an aspheric correction to one of the two surfaces. The convex surface, if there is one, is chosen generally for ease of manufacture. The exact computation of such a surface is not simple and it is most often carried out on an electronic computer by ray tracing methods.

One other case is of interest. The spherical aberration of a spherical mirror can be corrected by a thin corrector plate of nearly zero power, containing only the aspheric contribution. This is the Schmidt principle, and if the plate is placed at the center of curvature of the mirror, the correction of the image is good over very large field angles. The plate must, of course, be transparent to the radiation of interest. One side is most often flat and the other is worked to a compound curve. The material to be removed from a plane parallel plate is

$$\frac{\tau}{f} = \frac{1}{2^9(n-1)N^4}\left(\frac{r}{r_0}\right)^2\left[\left(\frac{r}{r_0}\right)^2 - 1\right]. \qquad (15)$$

Note that when $n=-1$, the convention for a mirror, (15) is equivalent to (11). The mirror for the Schmidt system has a radius $R=2f$, and the focal plane is curved to a sphere of radius $R_f=f$.

An approximate method developed from the Schmidt, useful for estimating tolerances on aspheric lenses, is as follows. The two radii of the lens are selected by the use of (5) and (8) to provide a minimum of spherical aberration and the proper focal length. Through the use of (4c), (4b), and (4a), the size of the image produced by the spherical lens may be computed. This is analogous to the spherical mirror image in the tolerance already discussed. The F number for a mirror of the same focal length as the lens and producing the same image size is found by

$$N_m^3 = N_L^3/A_L. \qquad (16)$$

Here N_L and N_m are the F numbers for the lens and equivalent mirror, and A_L is the A of (4b). This value of N_m in (15) will give the aspheric correction to give a diffraction image. Now the tolerance method already described for the mirror may be applied to the lens.

Since the infrared region of the spectrum covers several octaves, an error equivalent to chromatic aberration increases the size of the image of lens systems as a result of the variation of index with wavelength. As each material has a variation of index peculiar to itself, Table I is presented to provide a guide to image size.

TABLE I

Material	Ge		Si		As_2S_3	$CaAl_2O_3$		SiO_2		
Wavelength range in microns	2.5–7	2.5–9	3–7	3–9	2.5–9	1–3	1–4	1–2	1–2.8	1–3.5
Image size actor K	0.010	0.011	0.0025	0.0030	0.0060	0.0185	0.0345	0.0125	0.029	0.047

The relation giving image diameter in the same dimensions as the focal length is

$$\delta = \frac{Kf}{N}. \qquad (17)$$

In most simple, but fast, lens systems, unless the wavelength range of sensitivity is restricted by additional filters or by the sensitivity of the detector combined with the emission of the source, the effective image size from this effect will greatly exceed those sizes resulting from the previous considerations. Where wide wavelength ranges are required, a mirror and mirrors with corrector plates provide color free systems. In addition, some doublets have been designed for the infrared. A Si-Ge doublet is described by Trenting[1] and an As_2S_3-LiF doublet is described by Thielens.[2]

Thus far we have considered systems which are required to produce images only on, or very close to, their optical axes. For systems where the image of an extended object is required, additional optical errors produce images of object points of greater size. The error which first enlarges the image as one moves away from the axis is coma. The coma of a spherical mirror is zero if the entrance pupil of the system is at the center of curvature. The coma of a parabola is independent of the location of the pupil and is equal to that of a sphere with the pupil at the sphere. The effective angular size of the comatic image for spheres and parabolas with the pupil at the surface is

$$\delta_c = \frac{U}{16N^2}, \qquad (18)$$

[1] R. G. Treuting, "An achromatic doublet of silicon and germanium," *J. Opt. Soc. Am.*, vol. 51, pp. 454–456; July, 1951.
[2] E. H. Thielens, U. S. Patent No. 2,863,253; December 23, 1958.

where U is the field angle between the axis of the system and the direction from the system to the object point in question.

For lenses the coma depends on the shape of the lens. A lens free of third-order coma has radii in the ratio given by

$$\frac{R_2}{R_1} = \frac{n^2}{n^2 - n - 1}. \tag{19}$$

The focal length of such a lens is given in (8). Eq. (19) is plotted in Fig. 6. The spherical aberration for a lens of zero comma is given by (4a)–(4c), and is uniform over the field. This may be removed by aspheric treatment as through the equivalent mirror and Schmidt formulas, (16) and (15), respectively.

Eq. (5) gives the ratio, R_2/R_1 which makes A of (4b) a minimum. The value of A, therefore, will be insensitive to small variations of R_2/R_1. On the other hand, the amount of coma due to departures from the value of R_2/R_1 given by (1) is essentially linear. In situations where coma is important, it is, therefore, preferable to use the value of R_2/R_1 given by (19) to that given by (5). Fortunately, the values obtained by the two equations are not far apart, particularly for the high index materials used in the infrared as shown in Table II.

TABLE II

Index of Refraction	R_2/R_1 [From (5)]	R_2/R_1 [From (19)]
1.5	−6.0	−9.0
2.0	5.0	4.0
3.0	1.91	1.80
4.0	1.50	1.45

At even larger field angles, astigmatism begins to enlarge the image. Again, a pupil at the center of a spherical mirror frees the system of astigmatism. In addition, a parabola with a pupil one focal length ahead of the mirror has no astigmatism. However, a sphere or parabola with the pupil at the mirror does suffer from this error.

Astigmatism is an optical error of such nature that the image of an off axis point source becomes a line perpendicular to the direction to the axis of the optics at one point in image space. At another point, a bit further along the ray, there is another line image perpendicular to the first. On a plane perpendicular to the optical axis of the system and containing the axial focal point, the image is an elliptical area. The image of smallest size lies at some point between the two line images. The angular length of the elliptical image along the radial direction from the center of the field is

$$\delta_{a_p} = \frac{U^2}{2N}\left(\frac{1}{n} + 3\right). \tag{20}$$

The angular width of this ellipse is

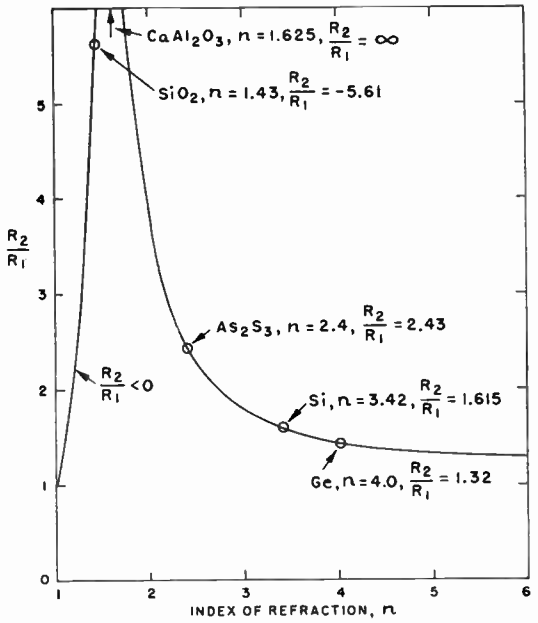

Fig. 6—Ratio of radii of the surfaces of lenses to produce zero coma.

$$\delta_{a_s} = \frac{U^2}{2N}\left(\frac{1}{n} + 1\right). \tag{21}$$

The first (primary) line image falls on a spherical focal surface whose radius is

$$R_{f_p} = f\frac{n}{3n + 1} \tag{22}$$

and the radial line image (secondary) is on a surface of radius

$$R_{f_s} = f\frac{n}{n + 1}. \tag{23}$$

For a mirror $n = -1$ and the relations are

$$\delta_{a_p} = \frac{U^2}{N}, \quad \delta_{a_s} = 0, \quad R_{a_p} = \frac{f}{2}, \quad R_{a_s} = \infty. \tag{24}$$

In this case the image is a radial line on the flat focal plane. The tangential line lies on a surface with a radius of half the focal length. The smallest image thus falls on a surface between these two. It may be considered a sphere of radius equal to the focal length centered at the center of the aperture of the mirror. The smallest image for lens or mirror is round and has a size

$$\delta_a = \frac{U^2}{2N}. \tag{25}$$

It falls on a surface of radius

$$R_f = f\frac{n}{2n + 1}. \tag{26}$$

For most purposes in infrared optics, the image sizes arising from the various effects, diffraction, spherical

aberration, coma, astigmatism, and color may be simply added to give a resulting effective image size. Most often one effect will dominate and the others may be neglected. The optical component may now be considered as just one more element in the information transmission line from scene to presentation. The optics have a transfer characteristic equivalent to a low-pass filter network. If the image of a point source is considered as a disk of uniform brightness, the transfer characteristic is given by

$$T = 2\frac{J_1(\pi\delta\nu)}{\pi\delta\nu}. \qquad (27)$$

Here δ is the image diameter in radians as before and ν is the angular spatial frequency in the object in cycles per radian. The response of the optical system to a given space modulation of the energy from an object as a function of spatial frequency, is given by

$$M_i = TM_o. \qquad (28)$$

M_i is the modulation in the image while M_0 is that of the object. Modulation is defined as

$$M = \frac{I_{max} - I_{min}}{I_{max} + I_{min}} \qquad (29)$$

where I_{max} and I_{min} are the maximum and minimum values of the component of spatial frequency ν in the scene modulation. Fig. 7 is a plot of (27). As an example, consider our mirror whose image is 0.5 milliradian in diameter. For a spatial frequency in the scene of 2 cycles per milliradian even 100 per cent modulation of the energy will produce modulation in the image of only 0.175, because $\delta\nu = 1$ and for this value $T = 0.175$. For a spatial frequency of one cycle per milliradian, $\delta\nu = 0.5$; 100 per cent modulation in the object will produce 70 per cent modulation in the image. For the same object frequency 10 per cent modulation in the scene will produce 7.0 per cent modulation in the image.

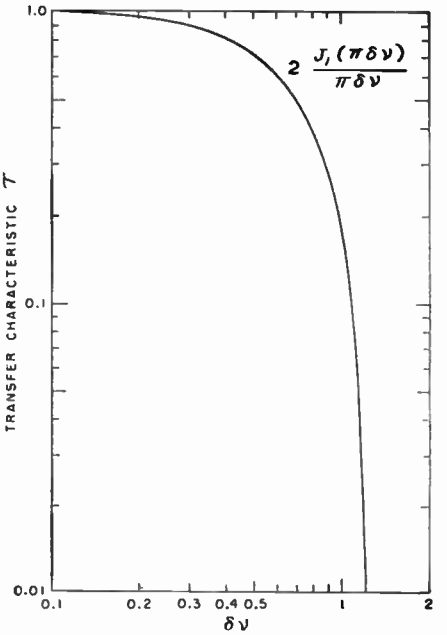

Fig. 7—The transfer characteristic of an optical system whose images of point sources are disks of uniform illumination.

Formulas

Diffraction:

$$\delta_d = \frac{1.22\lambda}{D}$$

diameter of image in radians
D diameter of pupil
$N = F$ number $= f/D$

$$d = 1.22\lambda N$$

d = diameter of image in same units as λ

Spherical aberration for spherical mirror:

$$\delta_s = \frac{7.8 \times 10^{-3}}{N^3}$$

for simple lens:

$$\delta_s = \frac{7.8 \times 10^{-3}}{N^3} A$$

$$A = \frac{n+2}{n(n-1)^2}\sigma^2 - \frac{4(n+1)}{n(n-1)}\sigma + \frac{3n+2}{n} + \frac{n^2}{(n-1)^2}$$

$$\sigma = \frac{R_2 + R_1}{R_2 - R_1} = \frac{\frac{R_2}{R_1} + 1}{\frac{R_2}{R_1} - 1}$$

n = index of refraction

minimum spherical:

$$\frac{R_2}{R_1} = \frac{2n^2 + n}{2n^2 - n - 4}$$

minimum coma:

$$\frac{R_2}{R_1} = \frac{n^2}{n^2 - n - 1}$$

Focal length of mirror:

$$f = \frac{1}{2}R$$

Focal length of lens:

$$f = \frac{-R_1R_2}{(n-1)\left(R_1 - R_2 - \frac{(n-1)}{n}t\right)}$$

t = thickness

$$f = R_1\frac{1}{(n-1)}\left(\frac{R_1}{R_2} - 1\right) \qquad t = 0$$

Shape of parabolic mirror surface:

$$x = r^2/4f$$

x = height above vertex
r = radius from axis

Departure from a sphere matching at $r=0$ and $r=r_0$:

$$\tau = \frac{r^2}{8R^3}(r^2 - r_0^2)$$

or

$$\frac{\tau}{f} = \frac{1}{2^{10}N^4}\left(\frac{r}{r_0}\right)^2\left[\left(\frac{r}{r_0}\right)^2 - 1\right]$$

Shape of lens with zero spherical aberration:

Ellipsoid on R_1,

Sphere on $R_2=f$:

$$\frac{x}{f} = \frac{n(n-1)}{(n^2-1)}\left[1 - \sqrt{1 - \frac{(n+1)}{4N^2(n-1)}\left(\frac{r}{r_0}\right)^2}\right]$$

$$\frac{x}{f} \simeq \frac{n}{(n-1)}\left[\frac{1}{8N^2}\left(\frac{r}{r_0}\right)^2 + \frac{1\,(n+1)}{2^7N^4(n-1)}\left(\frac{r}{r_0}\right)^4 \cdots\right]$$

Departure from sphere:

$$\frac{\tau}{f} = \frac{1}{n(n-1)}\,\frac{1}{2^7N^4}\left(\frac{r}{r_0}\right)^4$$

Schmidt plate:

$$\frac{\tau}{f} = \frac{1}{2^9(n-1)N^4}\left(\frac{r}{r_0}\right)^2\left[\left(\frac{r}{r_0}\right)^2 - K\right]$$

$K = 1$ least glass removed

$K = 1.5$ least chromatic error

Coma:

$\delta_c = 0$ spherical mirror, pupil at center of curvature

$\delta_c = \dfrac{U}{16N^2}$ pupil at mirror for sphere any pupil for parabola. U is field angle.

Astigmatism:

Size of ellipse on flat focal plane:

$$\delta_{a_p} = \frac{U^2}{2N}\left(\frac{1}{n} + 3\right) \quad \text{radial direction}$$

$$\delta_{a_t} = \frac{U^2}{2N}\left(\frac{1}{n} + 1\right) \quad \text{tangential direction}$$

Smallest image:

$$\delta_{\min} = \frac{U^2}{2N}$$

Radii of surfaces of line images:

$$R_{f_p} = f\frac{n}{3n+1} \quad \text{radial direction}$$

$$R_{f_t} = f\frac{n}{n+1} \quad \text{tangential direction}$$

$$R_{f_{\min}} = f\frac{n}{2n+1} \quad \text{smallest image}$$

for mirror $n=-1$:

$$\delta_{a_p} = \frac{U^2}{N}, \quad \delta_{a_t} = 0, \quad R_{a_p} = \frac{f}{2}, \quad R_{a_t} = \infty$$

Smallest image:

$$\delta_a = \frac{U^2}{2N},$$

Transfer characteristic for disk image:

$$T = 2\frac{J_1(\pi\delta\nu)}{\pi\delta\nu}$$

$$M_i = TM_o$$

M_i = modulation in image

M_o = modulation in object

$$M = \frac{I_{\max} - I_{\min}}{I_{\max} + I_{\min}}.$$

ACKNOWLEDGMENT

The author wishes to express his appreciation to A. Offner for supplying some of the material, for guidance in proper emphasis, and for suggestions as to content of this contribution; to Dr. H. Polster, R. Shack, and A. Offner for reading the manuscript; and to Miss Grace Schroeder for preparing the figures.

Paper 4.2.2

Optical Design for Infrared Missile-Seekers*

HARVEY DUBNER†

Introduction

THE OPTICS used in an infrared missile-seeker result from a series of design compromises involving sensitivity, resolution, and geometry. Since the optics must be a part of a gimbal system and must be contained in a prescribed enclosure, the geometry problem is the most dominant.

Fig. 1 shows the seeker configuration of an IR missile. The folded optical system consists of a dome, primary mirror, secondary mirror, correcting lens, focal plane (which generally contains a reticle or a light chopper), and detector.

The sensitivity, S, of such systems varies, in general, with the aperture diameter, D, optical efficiency, e, and the ratio of focal length to aperture diameter, $f^{\#}$, in the following way: $S \alpha De/f^{\#}$.

A system with resolution on the order of a four-milliradian circle of confusion at two degrees off-axis would be useful in an unsophisticated missile, while a high performance missile would require a more sensitive seeker, one with resolution of perhaps one milliradian at five degrees off-axis.

Most infrared seekers operate in the 2–3 or 3–5 micron spectral regions, but rarely over both bands.

Domes

A simple optical system, consisting of a dome and a primary mirror, is shown in Fig. 2. A flat secondary mirror is located between the spherical mirror and the dome, to fold the system.

The primary mirror introduces spherical aberration, and since this element is used as the aperture stop, coma and astigmatism are also introduced. For instance, an $f/1$ mirror would have about ten milliradians resolution on-axis. Coma contributes about three milliradians per degree off-axis, and astigmatism would contribute about two milliradians at four degrees off-axis, a small amount compared to coma.

The dome introduces spherical aberration opposite to that of the primary mirror. It also produces significant amounts of higher-order on-axis aberrations. It is interesting to note that although the paraxial power of the dome may be 1/20 that of the mirror, the aberrations of the dome are equal and opposite to those of the primary mirror. This means that the dome is a highly nonlinear element, with much aberration and little power.

Chromatic aberration is also introduced; for instance, a quartz dome working in the 2–3 micron region would add another milliradian over the whole field.

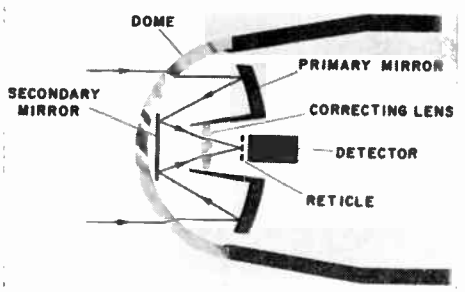

Fig. 1—Seeker configuration.

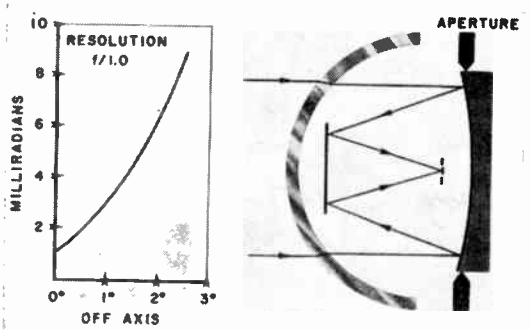

Fig. 2—Simple dome and mirror optical system.

From symmetry considerations, since the dome center is near the center of the aperture, the dome affects the off-axis rays almost identically as the on-axis rays. In optical terms, the principal ray of the system is perpendicular to the dome surfaces so that almost no off-axis aberrations are generated by the dome. The dome might be called a Maksutov corrector, based on the work Maksutov has done on thin meniscus elements.[1]

Primary Mirrors

In attempting to improve the resolution, the first logical step was to investigate the use of a more complicated primary mirror. This was done by using thin-lens formulas.[2] A study of a mangin (back surface) mirror (Fig. 3) showed that by keeping the power of the lens constant and just bending the lens, the astigmatism remains constant, the coma decreases, and the spherical aberration decreases through zero and then increases negatively as shown. If this mirror were used to correct coma, the spherical aberration would have reversed sign, and the dome would no longer be able to correct the residual spherical aberration. Therefore, a correcting lens is required to cancel the remaining spherical aberration.

* Original manuscript received by the IRE, June 30, 1959.
† Avion Div., A.C.F. Industries, Inc., Paramus, N. J.

[1] D. D. Maksutov, "New catadioptic meniscus systems," *J. Opt. Soc. Am.*, vol. 34, pp. 270–284; 1944.
[2] A. E. Conrady, "Applied Optics and Optical Design," Dover, New York, N. Y.; 1957.

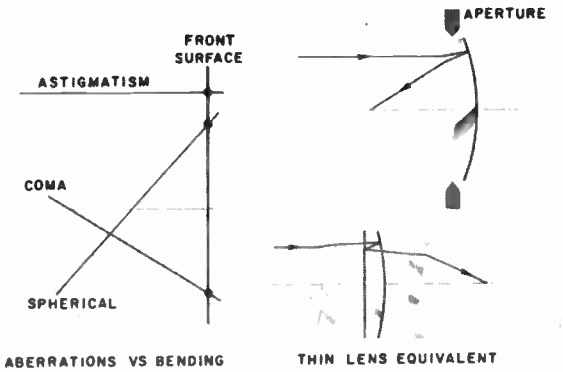

Fig. 3—Mangin primary mirror system, and its thin lens equivalent.

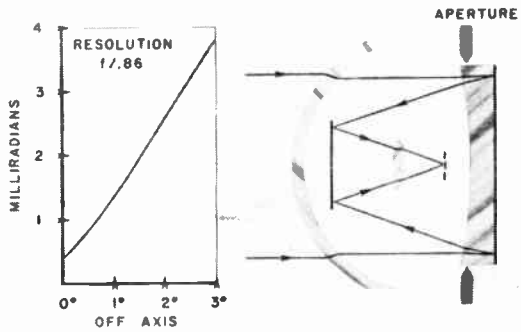

Fig. 4—Mangin primary mirror system with correcting lens.

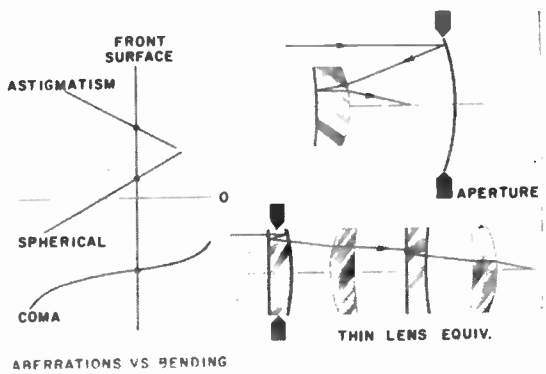

Fig. 5—Mangin secondary mirror system and its thin lens equivalent.

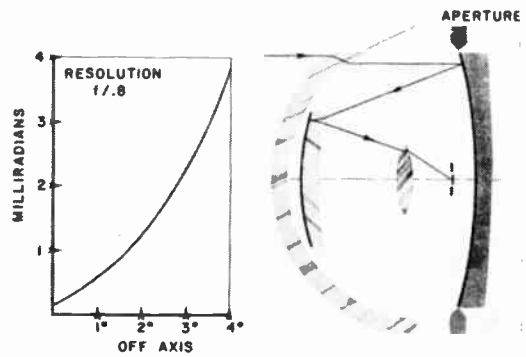

Fig. 6—Mangin secondary mirror system with correcting lens.

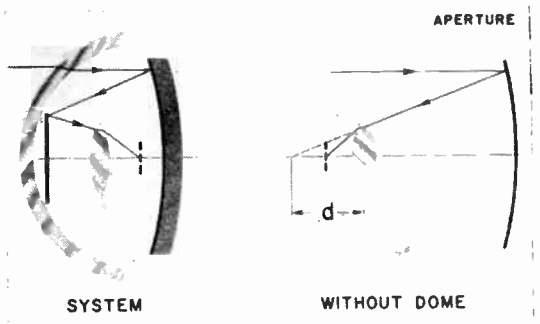

Fig. 7—Correcting lens.

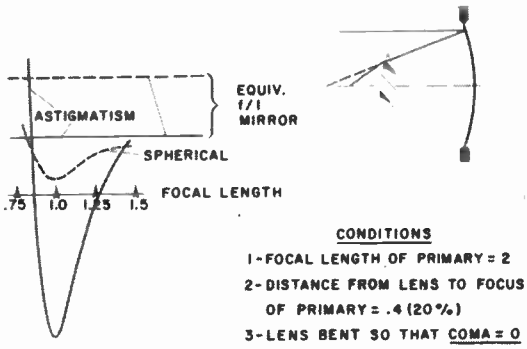

Fig. 8—Astigmatism and spherical aberration vs lens power, for zero coma.

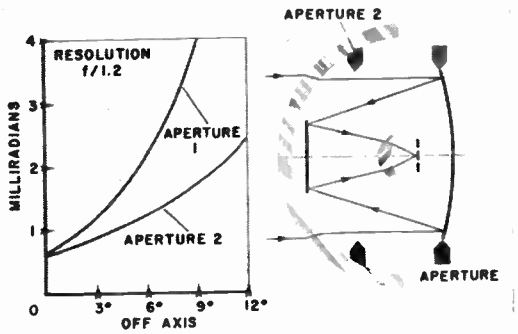

Fig. 9—Lens-only optical system.

The system shown in Fig. 4 consists of a calcium-aluminate glass dome, an arsenic-trisulfide mangin primary mirror, which provides most of the power of the system, a flat secondary mirror, which folds the telescope, and an arsenic-trisulfide correcting lens. The resolution of this system at two degrees off-axis is approximately two milliradians, much better than the resolution of the simple dome-mirror, which had well over six milliradians. However, the mangin primary mirror introduces much chromatic aberration which would add one milliradian to the resolution.

Secondary Mirrors

Using thin-lens formulas, an investigation was made on a mangin secondary mirror. The study of a system composed of the primary mirror and a mangin secondary mirror (Fig. 5) showed that spherical aberration varies

rapidly as a function of lens bending. At the point where spherical aberration is near zero, the mangin secondary mirror behaves in much the same manner as the dome; that is, for large changes in spherical aberration there is little change in either coma or astigmatism. Thus, a dome can now be chosen independent of the spherical aberration required; the mangin mirror can supply the residual spherical aberration. However, another optical element is required to reduce the off-axis aberrations. Such a system is shown in Fig. 6. It consists of a fused-quartz dome whose parameters were chosen to make fabrication easy and economical, a spherical primary mirror, a back-surface-silvered arsenic-trisulfide mangin secondary mirror, and an arsenic-trisulfide correcting lens which was designed to minimize coma. This is a useful system for many purposes; for instance, at four degrees off-axis the resolution is better than four milliradians. Chromatic aberration would add, at most, a half milliradian to the spot size.

Correcting Lens

Since both the mangin primary and the mangin secondary mirrors required a correcting lens in front of the focal plane, a thorough analysis was made of a system consisting of a dome of Corning No. 0160 glass, a primary mirror, a plane secondary mirror, and an arsenic-trisulfide lens (Fig. 7).

The first objective was to find a configuration which would yield zero coma. It was found that for any particular lens power, the lens can be bent so that there is no coma. Next, for zero coma, astigmatism and spherical aberration were plotted as a function of lens power (Fig. 8). This showed that astigmatism goes through zero twice and the spherical aberration decreases but does not change sign. Therefore, a dome can correct the residual aberration. For geometric reasons, the 1.25 cross-over point was analyzed more carefully: by choosing a position of the lens and solving for the lens power and the lens bending, primary coma and astigmatism can be reduced to zero.

It was found that for wide variation in lens position, the effective focal length remains close to 1.25. This means that coma and astigmatism can be kept at zero and that this last parameter (lens position) can be used to reduce the field curvature to zero. A plot of curvature of focal surface as a function of lens position showed that to produce zero curvature, the position of the lens should be approximately 20 per cent of the effective focal length. This leads to a very desirable geometry: the lens is close to the focal plane.

Finally, a dome was added to cancel the spherical aberration; the resultant system is shown in Fig. 9. With the aperture at the primary mirror, the resolution is about two milliradians at six degrees off-axis. However, with a slight movement in aperture, the resolution is better than two and one-half milliradians at twelve degrees off-axis. Since all the primary aberrations are zero, this circle of confusion is due entirely to higher-order aberration.

In summary, this is a system which has no primary spherical aberration, no coma, no astigmatism, no field curvature, and negligible chromatic aberration.

Conclusion

Only variations of the optical properties of the primary mirror, the secondary mirror, and the lens have been considered. Naturally, many other types of optical systems can be designed. For instance, aspheric surfaces can be used, but their higher cost makes them less desirable than spherical components; also, refracting, rather than reflecting, systems can be designed. Our objective has been, however, to improve the resolution of the systems and still maintain simplicity of configuration.

Paper 4.2.3

Optical Materials, Films, and Filters for Infrared Instrumentation*

W. L. WOLFE† AND S. S. BALLARD‡

Introduction

FOR infrared instrumentation, special problems arise in the design of appropriate optical systems and in the choice of satisfactory window materials. In the visible part of the spectrum, which covers a comparatively narrow wavelength range, relatively little difficulty has been encountered in developing optical materials with desirable properties. Many varieties of glass and transparent crystals are available for the design, for instance, of color-corrected lenses, polarizing prisms, and strong, chemically resistant windows. In contrast, the infrared spectrum covers an extremely broad wavelength interval, one that is many times that of the visible; therefore, the spectrally dependent properties of materials can be expected to vary considerably, and no one substance can be expected to be completely satisfactory over the entire range. Thus, although there are many crystals, glasses, and plastics available, the designer must usually make an engineering decision based on a variety of compromises. Some of the data upon which the design choices must depend are presented and discussed, several materials which at present best meet the criteria for some common applications are enumerated, and the logic for each selection is briefly outlined.

Whereas the entire infrared spectrum is of interest to the laboratory research scientist, it is convenient to consider military infrared technology in terms of three separate wavelength ranges based on the spectral sensitivity of the several detector types and the transmission of the atmosphere. These ranges are 1–3μ, 3–6μ, and 8–13μ; they are often called the near, intermediate, and far infrared regions. Some workers prefer to consider 0.8 to 1.2μ the near region, and designate four realms of interest, but this shortest wavelength interval presents few problems to the worker in choosing satisfactory optical materials.

In this very near band (to 1.2μ), ordinary glass can be used for most applications. However, for some so-called active infrared operations it is necessary to prevent the source from being observed visually. Thus a cut-on filter at about 0.9μ is necessary. This filter can be either a specially treated glass, or a reflecting mirror with an appropriate coating; sometimes both are used. The basic criterion in the design is high infrared transmission and very low visible transmission, with a sharp transition between them. The present components for this spectral region are, in general, quite satisfactory; and although some slight optical improvement might be obtained with crystals, the thermal, mechanical, and size restrictions thus imposed are intolerable.

The other wavelength regions are much less satisfactorily supplied with materials which can be used for good refractive elements; therefore a judicious choice must be made by the instrument designer from among the available substances that best meet his particular requirements.

Properties of Optical Materials

Transmission

The transmission regions of most of the materials which have been used for various infrared instrumentation problems are presented in Fig. 1 roughly in order of increasing long-wavelength transmission limit. The range of good transmission, the primary choice criterion for an optical material, has been arbitrarily defined as the spectral region in which the external transmittance is greater than 10 per cent for a sample 2 mm thick. These conditions approximate a mean between the characteristics of a window used as part of a detector cell, located inside an instrument, and one used as a larger, external window for the field equipment.

The transmission, or more precisely the external transmittance, of an optical component depends on both internal absorption and the reflection loss at the surfaces. Substances with a high refractive index, of course, have a high reflectivity; in this case, a reflection-reducing coating is often used and the external transmittance is thus increased. The effects of such coatings are not included in the data illustrated in Fig. 1. The absorption of a material is, in general, a function of its purity and its temperature. This is particularly true for semiconductors, in which the tendency toward metallic properties is increased by both decreasing purity and increasing temperature. Thus for data like those of Fig. 1, not only the thickness of a sample should be specified, but also its purity and temperature; the values quoted here are generally for relatively pure material at room temperature. Although the effects of impurities on transmission are important in the search for better components, materials can generally be supplied in rather pure form if this is necessary. Of more practical importance is the change of transmission with increasing temperature; this effect on a sample of germanium is shown in Fig. 2. Since many of the current applications of military and civilian infrared technology require the

* Original manuscript received by the IRE, July 6, 1959.
† Willow Run Labs., Univ. of Michigan, Ann Arbor, Mich.
‡ Univ. of Florida, Gainesville, Fla.; also Consultant to Willow Run Labs., Univ. of Michigan, Ann Arbor, Mich.

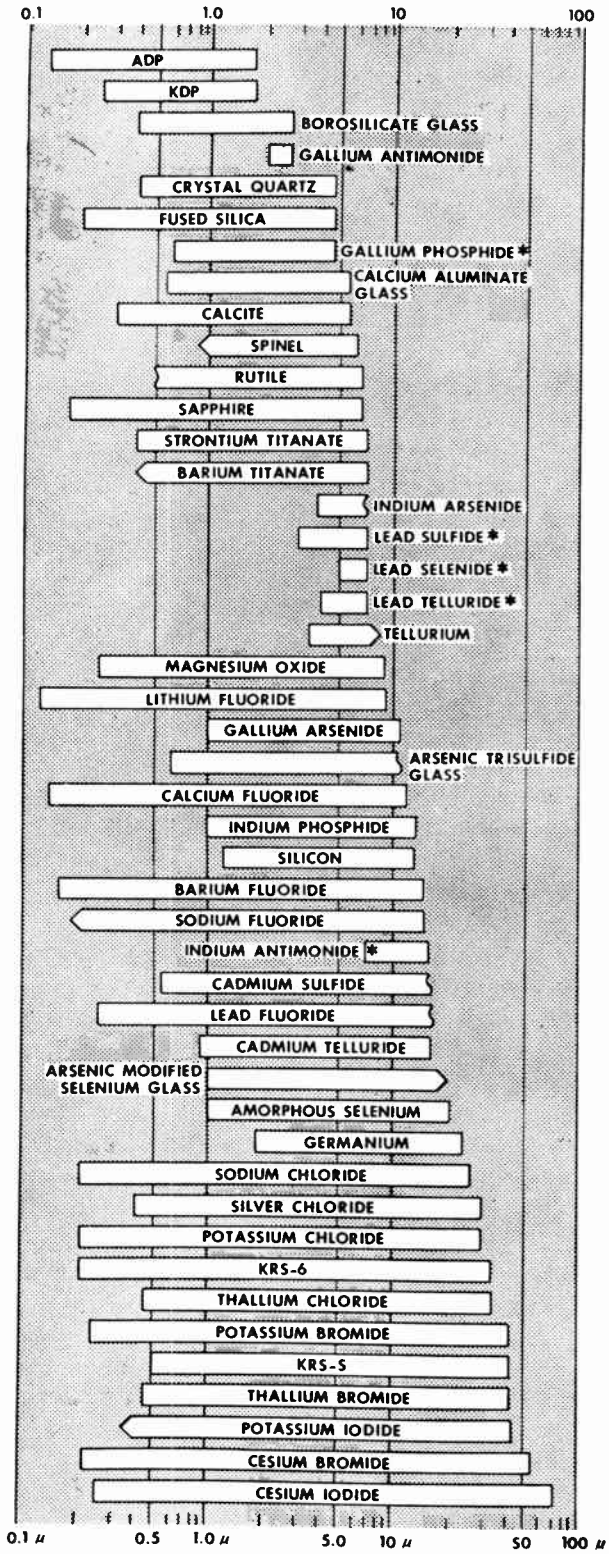

Fig. 1—The transmission regions of selected optical materials. (Regions are for 10 per cent external transmittance or better, for a 2-mm sample at room temperature.)

instruments to operate in elevated-temperature environments, the optical materials and other components can be expected to encounter rather severe operating difficulties. The effect of temperature on the transmission of a semiconductor is illustrated in Fig. 2; glasses

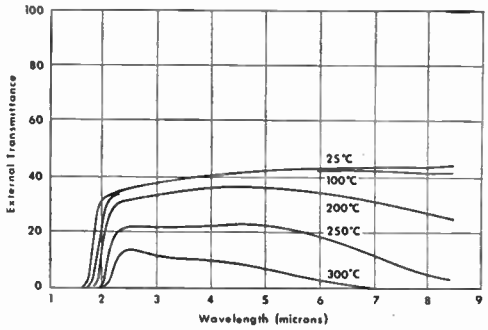

Fig. 2—The transmission of germanium for several different temperatures; resistivity, 30 ohm-cm.

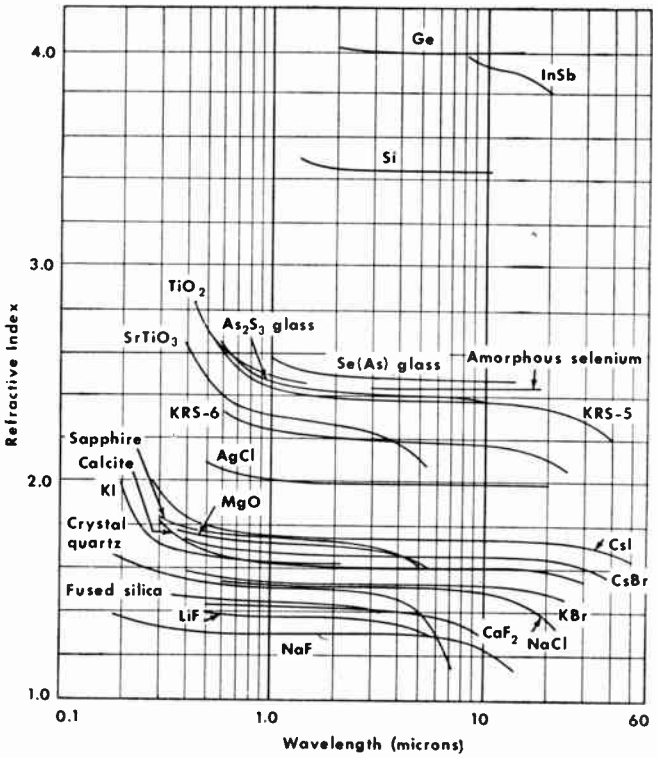

Fig. 3—The refractive indices of selected optical materials.

react somewhat differently: although the over-all transmission does not decrease appreciably (in a few cases it may actually increase) the deep absorption bands will emit infrared radiation significantly. This effect can be a serious one, causing spurious signals and perhaps even saturation of the detector.

Thus, for most high-temperature applications one should choose either an insulating crystal or a semiconductor with a low temperature coefficient of absorption; and the good transmission region of the material should extend well beyond the wavelength limits of the detector response.

Refractive Index

A second optical property of importance is refractive index. Indices of many materials are illustrated in Fig. 3. The wide range of values from about 1.3 to greater

than 4.0 should be contrasted with those of the optical glasses, which generally range from 1.5 to about 1.7. The high values of index offer both an advantage and a problem; thinner lenses of equal power can be fabricated, and a wider range of materials for achromat design is available, but the reflection losses are greatly increased.

Other Properties

Not all the physical and chemical properties of the many materials can be enumerated here, but Tables I–III list values for some of the important nonoptical properties which should be considered in instrument design. These are surface hardness, melting temperature, and strength (Young's Modulus); their importance is obvious. The reader is referred to a recent compilation[1] for more complete data.

Materials for Specific Applications

The choice of a material for a particular application can be based on information of the type just mentioned. The following discussion presents some of the more favorable choices (based on such data) for a number of common uses, in each of the three wavelength regions listed above.

Thermal Region

The far infrared or thermal region, from 8 to 13μ, is the most critical one as far as satisfactory optical materials are concerned. Windows can be fabricated of rock salt, potassium bromide, and several other "conventional" materials, but these are generally water soluble or even hygroscopic. Silver chloride can withstand moisture and even solarization, if pure enough and properly coated for protection, but its homogeneity leaves something to be desired and it is also rather soft. The synthetic single crystal commonly called KRS-5 has a melting temperature of 415°C, exhibits cold flow, is sometimes inhomogeneous, is somewhat toxic, is expensive, and is of high specific gravity, so optical elements constructed from it are heavy. Arsenic trisulfide glass, which is often used as a window material, loses transmission significantly in the middle of the 8 to 13μ region, and softens at a temperature that is too low for many applications. Crystalline germanium and silicon might be used here except for size restrictions and for the fact that the transmission of germanium drops rapidly with increasing temperature, starting at about 100°C (*cf.* Fig. 2); silicon can be used up to about 300°C, although it is not completely nonabsorbing throughout the 8–13μ atmospheric transmission "window."

Some of these materials are useful as corrector plates, lenses, and prisms in optical systems, but are not as satisfactory as they might be because of the limitations that have been indicated. Filtering is generally not as important in this portion of the spectrum, and fortunately so; there are few materials with sharp cut-on characteristics, and interference filters with adequate ruggedness and a sufficient variety of bandpasses for these wavelengths are not available. So-called immersion lenses for radiation detectors have been made from germanium and selenium; this is probably the least restricted of the applications in the thermal region, because of the less stringent mechanical and thermal requirements.

The Intermediate Region

In this portion of the spectrum, 3 to 6μ, the situation is somewhat improved. Of course the above-listed materials can be used as far as their limitations permit, and in addition, calcium aluminate glass, sapphire, and periclase are available. Again, the IR dome problem is the most critical. Calcium aluminate glass still shows absorption in the wide water band centering at 2.8μ, and this fact should be considered with regard to the reemission problem already discussed. Sapphire may soon become available in large enough sizes for many applications, but it is expensive. Flat plates and segmented domes of magnesium oxide, arsenic trisulfide glass, Kel-F, etc., have also been used; but these materials are, at best, usually a compromise because of their mechanical limitations.

Optical elements in this region can be constructed from germanium, silicon, rutile, sapphire, and the glasses mentioned, plus arsenic-modified selenium glass. Care must be taken to avoid or correct for the problems inherent in a high refractive index, and to use its advantages properly. Silicon and germanium not only show this high refractive index but also low dispersion; thus they are promising as lens and prism materials that possess high power and little chromatic aberration. The reflection-reducing coating problems, however, must not be overlooked. Selenium, germanium, and strontium titanate have been used for immersion lenses. Other materials are available for this use; they should be chosen to best "match" the physical properties of the particular detector. The use of a filter is more important in this region than in the thermal region, and fortunately there are many more possibilities. Not only are there better interference filters available, but many different semiconductor cut-on wavelengths lie here, and it appears that a desired cut-on can even be "manufactured" by a proper mixture of materials.

The Lead Sulfide Region

This region, which can be considered as extending from the visible to 3μ, is by far the most satisfactory one from the optical materials point-of-view. Most of the materials mentioned above are available for consideration; fused silica and some optical glasses can also be used. Fused silica, because of its excellent thermal, chemical, mechanical, and optical properties, is the

[1] S. S. Ballard, K. A. McCarthy, and W. L. Wolfe, "IRIA State-of-the-Art Report, Optical Materials for Infrared Instrumentation," Univ. of Michigan, Ann Arbor, Rept. No. 2389-11-S; January, 1959.

TABLE I

HARDNESS

Material	Hardness (Knoop Number)	Direction	Indenter Load (gm)
Potassium bromide (KBr)	5.9	⟨110⟩	200
	7.0	⟨100⟩	200
Potassium chloride (KCl)	7.2	⟨110⟩	200
	9.3	⟨100⟩	200
Silver chloride (AgCl)	9.5		200
Thallium bromide (TlBr)	11.9	⟨110⟩	500
	11.9	⟨100⟩	500
Thallium chloride (TlCl)	12.8	⟨110⟩	500
	12.8	⟨100⟩	500
Sodium chloride (NaCl)	15.2	⟨110⟩	200
	18.2	⟨100⟩	200
Sodium nitrate ($NaNO_3$)	19.2	Perpendicular to cleavage planes	200
Cesium bromide (CsBr)	19.5		200
Thallium bromide-chloride (KRS-6)	29.9	⟨110⟩	500
	38.5	⟨100⟩	500
Thallium bromide-iodide (KRS-5)	40.2*		200
	39.8	⟨100⟩	500
	33.2	⟨110⟩	500
Barium fluoride (BaF_2)	82		500
Lithium fluoride (LiF)	102–113		600
Arsenic trisulfide glass (As_2S_3)	109		100
Calcium fluoride (CaF_2)	158.3	⟨110⟩	500
	158.3	⟨100⟩	500
Fued silica (SiO_2)	461		200
Strontium titanate ($SrTiO_3$)	595		
Magnesium oxide (MgO)	692	Perpendicular to cleavage planes	600
Crystal quartz (SiO_2)	741	Perpendicular to *z*- and *x*-cut faces	500
Titanium dioxide (TiO_2)	879	Random	500
Spinel ($MgO \cdot 3.5\ Al_2O_3$)	1140	Random	1000
Silicon (Si)	1150		
Sapphire (Al_2O_3)	1370	Random	1000
Calcite ($CaCO_3$)	3†		
Cadmium telluride (CdTe)	43.5‡		
Barium titanate ($BaTiO_3$)	200–580‡		

* Machined surface. † Moh Number. ‡ Vickers' Scale.

TABLE II

MELTING OR SOFTENING TEMPERATURE

Material	Temperature (°C)
Amorphous selenium (Se)	35*
Arsenic modified selenium glass; Se(As)	70*
Arsenic trisulfide glass (As_2S_3)	210*
Potassium dihydrogen phosphate (KDP)	252.6
Sodium nitrate ($NaNO_3$)	306.8
Gallium arsenide (GaAs)	400†
Thallium bromide-iodide (KRS-5)	414.5
Thallium bromide-chloride (KRS-6)	423.5
Thallium chloride (TlCl)	430
Tellurium (Te)	449.7
Silver chloride (AgCl)	457.7
Thallium bromide (TlBr)	460
Gallium phosphide (GaP)	>500
Indium antimonide (InSb)	523
Cesium iodide (CsI)	621
Cesium bromide (CsBr)	636
Gallium antimonide (GaSb)	720
Potassium iodide (KI)	723
Potassium bromide (KBr)	730
Potassium chloride (KCl)	776
Sodium chloride (NaCl)	801
Borosilicate crown glass	820*
Lead fluoride (PbF_2)	855
Lithium fluoride (LiF)	870
Calcite ($CaCO_3$)	894.4†
Cadmium sulfide (CdS)	900‡
Lead telluride (PbTe)	917
Germanium (Ge)	936
Indium arsenide (InAs)	942
Sodium fluoride (NaF)	980
Cadmium telluride (CdTe)	~1040
Indium phosphide (InP)	1050
Lead selenide (PbSe)	1065
Lead sulfide (PbS)	1114
Gallium arsenide (GaAs)	1238
Barium fluoride (BaF_2)	1280
Calcium fluoride (CaF_2)	1360
Silicon (Si)	1420
Crystal quartz (SiO_2)	<1470
Barium titanate ($BaTiO_3$)	1600
Fused silica (SiO_2)	~1710
Titanium dioxide (TiO_2)	1825
Sapphire (Al_2O_3)	2030
Spinel ($MgO \cdot 3.5Al_2O_3$)	2030 to 2060
Strontium titanate ($SrTiO_3$)	2080
Magnesium oxide (MgO)	2800

* Softening temperature † Dissociation temperature. ‡ Sublimation temperature.

TABLE III

YOUNG'S MODULUS

Material	Young's Modulus (10^6 psi)	Remarks
Cesium iodide (CsI)	0.769	Measured in flexure
Thallium bromide-iodide (KRS-5)	2.3	Measured in flexure
Cesium bromide (CsBr)	2.3	Measured in flexure
Arsenic trisulfide glass (As_2S_3)	2.3	
Silver chloride (AgCl)	2.9	Measured in flexure
Thallium bromide-chloride (KRS-6)	3.0	Measured in flexure
Potassium bromide (KBr)	3.9	Measured in flexure
Thallium bromide (TlBr)	4.28	Calculated
Potassium chloride (KCl)	4.30	Measured in flexure
Potassium iodide (KI)	4.57	Calculated
Thallium chloride (TlCl)	4.60	Calculated
Barium titanate ($BaTiO_3$)	4.90	Single crystal
	16.50	Ceramic
Sodium chloride (NaCl)	5.80	Measured in flexure
Indium antimonide (InSb)	6.21	Calculated
Barium fluoride (BaF_2)	7.70	Measured in flexure
Gallium antimonide (GaSb)	9.19	Calculated
Lithium fluoride (LiF)	9.40	Measured in flexure
Calcite ($CaCO_3$)	10.50*	Minimum value
	12.80†	
Fused silica (SiO_2)	10.60	
Calcium fluoride (CaF_2)	11.0	Measured in flexure
Crystal quartz (SiO_2)	11.1†	Minimum value
	14.1*	
Germanium (Ge)	14.9	Calculated
Silicon (Si)	19.0	Calculated
Magnesium oxide (MgO)	36.1	Calculated
Sapphire (Al_2O_3)	50.0	

* Young's modulus measured parallel to *c* axis. † Young's modulus measured perpendicular to *c* axis.

usual choice. Thus, satisfactory refractory-type windows or domes can be obtained for this wavelength region, lens systems can replace reflecting or catadioptic systems, and virtually any desired spectral band can be isolated by an interference filter.

Coatings

The use of coatings on refractive and reflective components is an established practice in the optical industry. One type of coating is used to protect the elements from atmospheric and environmental effects—water and water vapor, abrasion, solarization and the like—while a second kind of thin film is used to improve the light-transmitting properties of refractive elements or the reflection of mirrors. Silicon dioxide and magnesium fluoride are frequently evaporated onto lenses and windows or mirrors; titanium dioxide and silicon monoxide have been used to protect the silvered surfaces of reflectors; thin plastic films are often used on sodium chloride to protect it from moisture, and coatings of stibnite or silver sulfide are deposited on silver chloride elements as a protection against solarization.

The use of reflection-reducing and reflection-enhancing layers is somewhat more novel but is becoming of considerable importance in infrared instruments. The theory of these thin, quarter-wave films is described by Strong.[2] The criteria for a reflection-elimination film are that its refractive index be equal to the square root of the substrate index and that the phase difference between the incident wave and the reflected wave be an odd multiple of π. Thus,

$$n = \sqrt{n'}$$
$$\Delta\phi = 4\pi nd \cos r/\lambda = 2\pi(m+\tfrac{1}{2}).$$

The second of these conditions reduces to

$$nd \cos r = (\lambda/4)(2m+1),$$

where

n = the refractive index of the film,
n' = the refractive index of the material,
$\Delta\phi$ = the phase change of the incident light,
λ = the wavelength of the incident light,
d = the thickness of the film,
r = the angle of inclination, in the film, of the ray to the film normal,
$m = 1, 2, 3, \cdots$.

The properties of reflection-reduction coatings can be inferred from the third equation, which states that for best reflection reduction the optical path length in the film must be an odd number of quarter wavelengths of the incident light. Since the variation of refractive index with wavelength in regions of high transmission is small and since d is a constant, reflection reduction is maximized for only a very narrow spectral band at normal incidence. The third equation also points out that best reflection reduction occurs for only a single angle of incidence; normal incidence is usually chosen for design purposes. Finally it should be pointed out that the broadest useful spectral region is obtained for $m = 1$, and that for m larger than 3 or 4, a channel spectrum is observed.

Several different coatings have been used for refractive elements in the infrared. Silicon monoxide is coated on a variety of materials—particularly silicon, germanium, and arsenic trisulfide glass; magnesium fluoride is used in both the visible and the infrared for coating glass; and for some high-index materials, lead fluoride and zinc sulfide are used. These films may be chosen because they protect the material from atmospheric effects as noted above. An interesting example is the coating often used for silicon: *i.e.*, silicon monoxide. This film can be formed by a chemical reaction, in which some silicon dioxide is usually formed as well; a reasonably good, stable, protective coating that also provides satisfactory reflection-reduction is thus obtained.

In certain applications—particularly in reflecting systems for near-infrared sources—it is desired to obtain spectrally selective reflection, *i.e.*, to enhance the reflection in a given wavelength region. This can be done by the proper design of a reflection-enhancing film or H layer, or by a number of properly designed H layers. These techniques have been discussed recently in some detail by Hass[3,4] who reports that TiO_2 is a particularly good material for many of these applications. An H layer should also have an optical thickness of one-quarter wavelength, but its refractive index should be higher than that of its substrate.

For both the high- and low-reflection coatings, a number of layers laid on top of each other and optimized for different wavelengths provide enhancement over a wider spectral range.

Filters

Spectral filters can be classified by either their transmission characteristics or the physical phenomenon upon which their action is based. One can designate long-wave-pass, short-wave-pass, and band-pass filters. By this is meant, respectively, a filter which transmits all radiation with wavelengths greater than some preselected value (and extending beyond the region of interest), a filter which passes all radiation with wavelengths shorter than the selected value, and finally a filter which transmits only between two chosen wavelengths. The Bausch and Lomb Optical Company has prepared an informative brochure[5] describing the no-

[2] J. Strong, "Concepts of Classical Optics," W. H. Freeman and Co., San Francisco, Calif., pp. 242–253; 1958.

[3] G. Hass and A. P. Bradford, "Anodically produced multiple oxide films for increasing the reflectance of evaporative aluminum," *J. Opt. Soc. Am.*, vol. 44, pp. 810–815; October, 1954.

[4] G. Hass, "Filmed surfaces for reflecting optics," *J. Opt. Soc. Am.*, vol. 45, pp. 945–952; November, 1955.

[5] "Near Infrared Transmission Filters," Bausch and Lomb Optical Co., Rochester, N. Y., Infrared Progress Rept. No. 3; September 8, 1958.

menclature often used with filters to delineate their parameters.

Some of the physical phenomena upon which filters can be based are absorption, refraction, scattering, and polarization.[6] A discussion of many of these, and of the filters resulting from their application, has been given by Greenler.[7] He includes Lyot, Christiansen, and polarization types along with the absorption and interference filters of more practical importance in field instrumentation. The latter two types will be discussed here.

Following Greenler, it can be stated that there exists an abundance of short-wave-pass filters, although certain difficulties are encountered in obtaining sufficiently sharp cut-offs. This is an optimistic way of stating that materials do not transmit very far into the infrared. The filters for the very near infrared are usually the absorption type utilizing a base material impregnated with an appropriate dye. Cut-off and band-pass filters of this type are available with a wide variety of spectral characteristics. A technique for utilizing certain plastics which form both the substrate and the absorber has been described by Blout[8]; such filters are illustrated in Fig. 4.

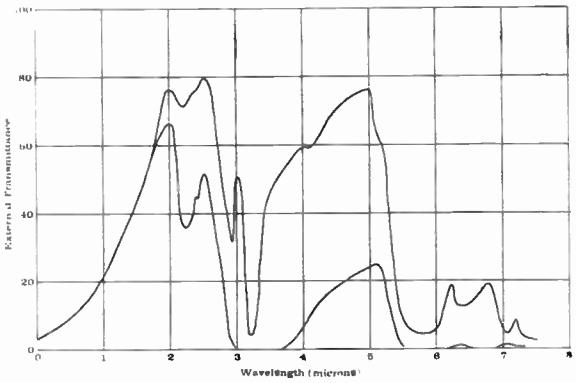

Fig. 4—The transmission of Polaroid Type C infrared filters. The top curve presents the transmission of an unlaminated plastic filter, the bottom left that of a glass-laminated filter, and the bottom right, that of an unlaminated filter coated with a scattering mixture.

Cut-on or long-wave-pass filters are less easily obtained. A number of semiconducting crystals have appropriate absorption edges and long-wavelength transmission. The variety of cut-on wavelengths that can be obtained by proper choice is illustrated in Fig. 5, which also illustrates the sharpness of these cut-ons. By proper "doping," *i.e.*, introducing known amounts of impurities, the location of this absorption limit can be moved, although the edge usually becomes less sharp and the material more opaque with greater impurity concentration. A recent technique for obtaining a sharp cut-on at a desired wavelength has been discussed by Greene and Kingston[12] and by Schroeder.[13] They both indicate that an alloy of two similar compounds has an absorption edge located between those of the pure materials, and that its position is a linear function of the ratio of the compounds; the slope of the absorption edge of the mixed crystal seems to remain as steep as that of its pure components.

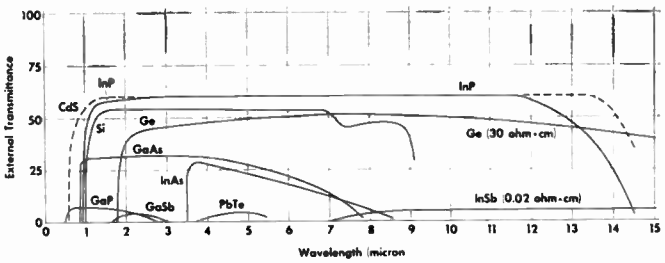

Fig. 5—The transmission of selected semiconductors. Some data are derived from absorption constants; others are found in the literature.[9–11] Resistivity is specified on some curves in ohm-cm.

Interference filters can also be fabricated with a variety of cut-on characteristics. The simple, solid Fabry-Perot type might be considered the earliest of those utilizing the phenomenon of interference. Other modifications of it are the reflection filter described by Hadley and Dennison,[14] and finally, the dielectric multilayer filters[15,16] consisting of the proper arrangements of a number of alternating high- and low-reflecting layers. In Fabry-Perot filters, interference of light between two parallel half-silvered plates provides spectral discrimination; the sharpness of the filter is proportional to the reflectivity of the plates, but the peak transmission is reduced markedly as the reflectivity is increased. The all-dielectric filter consisting of alternate *H* and *L* layers provides better peak transmission for the same pass band, but one of the difficulties inherent in these multilayer interference filters is that there are always regions of secondary transmission which must be eliminated by the use of the so-called blocking filter or blocking layer.

The brochure of Bausch and Lomb mentioned above[5] describes pertinent nomenclature and also the characteristics of a number of commercially available filters.

[6] N. M. Mohler and J. R. Loofbourow, "Optical filters," *Am. J. Phys.*, vol. 20, pp. 579–588; December, 1952.

[7] R. G. Greenler, "Optical filters," in J. Strong, "Concepts of Classical Optics," W. H. Freeman and Co., San Francisco, Calif., Appendix O; 1958.

[8] E. R. Blout, R. S. Corley, and P. L. Snow, "Infrared transmitting filters, II. The region 1 to 6 μ," *J. Opt. Soc. Am.*, vol. 40, pp. 415–418; July, 1950.

[9] H. Welker and H. Weiss, "Group III-Group IV compounds," *Solid State Physics*, vol. 3, pp. 1–78; 1956.

[10] F. Oswald and R. Schade, "The determination of the optical constants of semiconductors of the type A^{III} B^{IV} in the infrared," *Z. Naturforsch.*, vol. 9A, pp. 611–617; 1954.

[11] C. D. Salzberg and J. J. Villa, "Index of refraction of germanium," *J. Opt. Soc. Am.*, vol. 48, p. 579; August, 1958.

[12] L. C. Greene and D. L. Kingston, "Absorption edge in single crystals of alloys of ZnS-CdS," *Bull. Am. Phys. Soc.*, ser. II, vol. 4, no. 3, p. 157; March 30, 1959.

[13] F. Schroeder, Ohio Semiconductors, Cleveland, Ohio, private communication; April, 1959.

[14] L. N. Hadley and D. M. Dennison, "Reflection and transmission interference filters," *J. Opt. Soc. Am.*, vol. 37, pp. 451–465; June, 1957, and vol. 38, pp. 483–496; June, 1948.

[15] H. D. Polster, "A symmetrical all-dielectric interference filter," *J. Opt. Soc. Am.*, vol. 42, pp. 21–24; January, 1952.

[16] R. G. Greenler, "Interference filters for the infrared," *J. Opt. Soc. Am.*, vol. 47, pp. 130–131; February, 1957.

One can generally obtain a band-pass filter from one of the several suppliers[17] with a half width of about 10 per cent of the cut-on wavelength, in the region 1–5μ. Smaller band-passes result in reduced transmission. Long-wave-pass filters are available in the same spectral range with a transmittance of about 85 per cent or more of the uncoated substrate. They have slopes of about 10 per cent of the cut-on wavelength; *i.e.*, the wavelength difference between the 5 per cent and 85 per cent transmission points is 10 per cent of the nominal cut-on wavelength. Band-pass filters are available in a form which includes both the filter element and the blocking filter on a single disk. Generally the band-pass filter is deposited on one side of the disk and the blocking filter on the opposite side, although it has been stated by one group that both filters can be deposited on the same side, with the advantage that the filter can be mounted so that its fragile part receives greater protection.

[17] Baird-Atomic, Inc., Cambridge, Mass.; Bausch and Lomb Optical Co., Rochester, N. Y.; Eastman Kodak Co., Rochester, N. Y.; and Infrared Industries, Boston, Mass., for example.

Paper 4.2.4

Optical-Mechanical Scanning Techniques*

M. R. HOLTER† AND W. L. WOLFE†

THE characteristics of reflecting and refracting optical systems for collecting and focusing infrared radiation do not complete the characterization of infrared equipment used for military and industrial applications. These telescopes usually have relatively small fields of view because of their optical limitations; thus, for many applications (*e.g.*, reconnaissance, mapping, thermal photography, tracking, and missile guidance), some method is needed to make this small field of view cover a much larger one. The process by which this is often accomplished is a programmed space-scan or scanning, which can be done in a number of ways. Each of these is defined and described briefly, and the conceptual constraints on a scanner used for air-to-ground mapping are derived to demonstrate the methods by which engineering comprises are made.

An equipment which employs electronic scanning is in principle identical to standard television systems: an image is focused on a photosensitive surface which is in turn scanned by an electron beam. The major constraints in this system are the properties of the surface. If a satisfactory material is available, the properties of the electron optics and scanning techniques well known in the television industry are applicable. This type of system is very satisfactory in many respects, but a useful sensitive surface is not readily available. These image-forming systems are described in detail in papers 4.5.1 and 4.5.3 of this issue.

An alternative technique is to cause a single detector, or a one- or two-dimensional detector array (mosaic), to "see" a series of small parts of the field of view. This type of sampling is generally called optical-mechanical scanning or simply "scanning," as opposed to electron-beam scanning, the process described above. There are, in principle, two types of scanning—image plane and object plane. The first of these is so termed because an image of the total object field is formed by a collecting telescope; this image is then sampled point-by-point by a second optical system containing the transducer, the infrared detector. It is clear that the scanning device, the optical element that changes the instantaneous field of view of the detector, can be simple, small, and easily designed. On the other hand, a high quality image of the entire field must be formed by the collecting optic. The problems involved in performing such a feat over fields larger than some 10° or 20° are quite difficult to overcome; it is mainly for this reason that image-plane scanning systems are difficult to design and construct.

Object plane scanning, of course, also has its advantages and disadvantages; however, the problems are not those of improving optical systems, but of designing the proper scanning device. It is for this reason that this method has been quite successful to date and will be discussed further.

Many types of scan patterns and scan methods can be visualized. They all fit into several general classes, however—circular or spiral, cycloidal, and rectilinear or raster. Each of the scan patterns has certain characteristics that make it more suitable for some applications than for others. For instance, one should probably use a regular, repetitive raster or simple circular scan to construct an image, the particular geometry depending upon the shape of the object field. A search system or tracking system does not require the construction of an image; therefore, a scanning system that searches more critical areas more frequently may be desired.

To illustrate the versatility of the scanning systems,

* Original manuscript received by the IRE, July 6, 1959.
† Willow Run Labs., Univ. of Michigan, Ann Arbor, Mich.

several types are described below. First, a hypocycloidal pattern can be generated simply by superimposing one circular scan upon another. If an offset mirror is rotated about a shaft, and the shaft in turn has a locus which is a circle, then the scan pattern shown in Fig. 1(a) is obtained. A more interesting and versatile scanning system is that of a pair of prisms or wedges. If these are counter-rotated at the appropriate rates, a rosette pattern somewhat similar to the hypocycloid is generated. [See Fig. 1(b)]. But if the wedges are rotated in the same direction different rates, a spiral [Fig. 1(c)] is developed. Other patterns are possible, the most interesting of which is probably the simple sinusoid [Fig. 1(d)]. If this pattern is appropriately set up, one can obtain a scan very similar to a television raster (no flyback or interlace, however) and thus obtain an image. The possibilities for other types of scan, servo-corrected pseudo-sine waves, circular scan, Palmer scan, and others are virtually limitless. The particular application determines the form of the scan; the values of detector time constant, required frequency of coverage, total field of view, resolution, and physical limits on moving parts, among other things, generally limit the system.

As an example, since not all scanning applications can be considered, and since other techniques are discussed elsewhere in this issue, an air-to-ground reconnaissance mapping device will be briefly considered here. Its features and constraints illustrate most of the design problems of object plane scanning. The scan pattern is illustrated in Fig. 2.

An airborne vehicle traveling with speed v at altitude h carries a scanner having an instantaneous field of view (resolution element) of angular size β in both dimensions. To provide a good quality image, β (Fig. 2) is typically quite small, on the order of milliradians. This instantaneous field of view is caused to scan through an angle (α) at right angles to the aircraft path by a rotating element in the scanner. The motion of the vehicle carries the scanner forward so that successive scans cover different strips of the ground. The portion of ground swept over during a single scan through angle α is called a "line." If successive lines are not contiguous (if between the lines there are parts of the ground which are not scanned), the condition is termed "underlap." This can occur if the vehicle speed is too high or if the rotating elements revolve too slowly. If successive lines scan partly over the same terrain the condition is called "overlap." Underlap is clearly undesirable, since information is not obtained between successive lines. Contiguous scanning is desirable in that no ground remains unscanned, and there is a certain economy in not scanning more than once over any part of the ground. Under certain circumstances overlap is useful since the redundancies can be used to increase signal-to-noise ratio.

A typical device for obtaining such a scan pattern is illustrated in Fig. 3. A mirror in the form of a prism with n faces rotates at a rate r about an axis which is

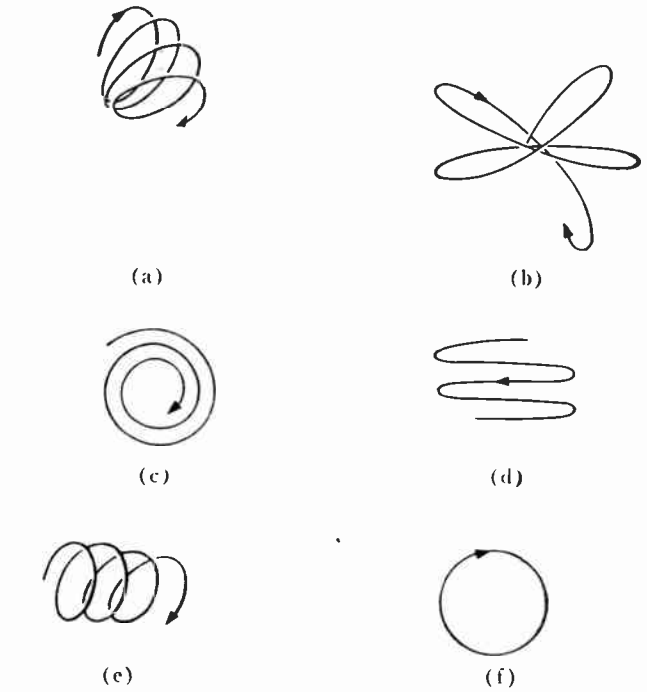

Fig. 1—Examples of representative scan patterns. (a) hypocycloid; (b) rosette; (c) spiral; (d) sinusoid; (e) Palmer; and (f) circular.

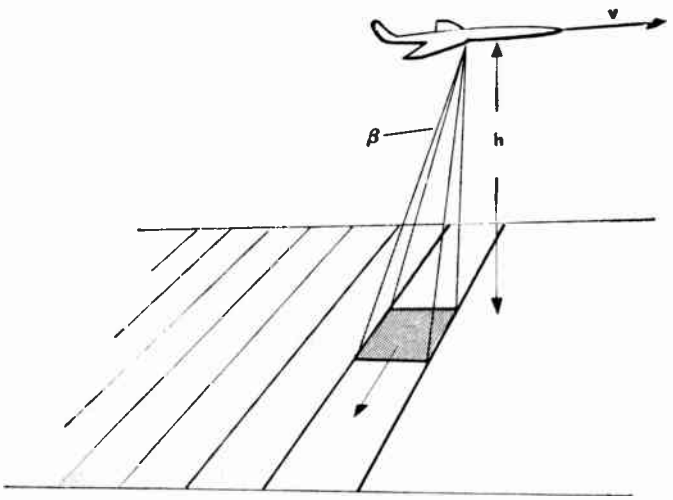

Fig. 2—Representation of the scan pattern for a typical prism scanner.

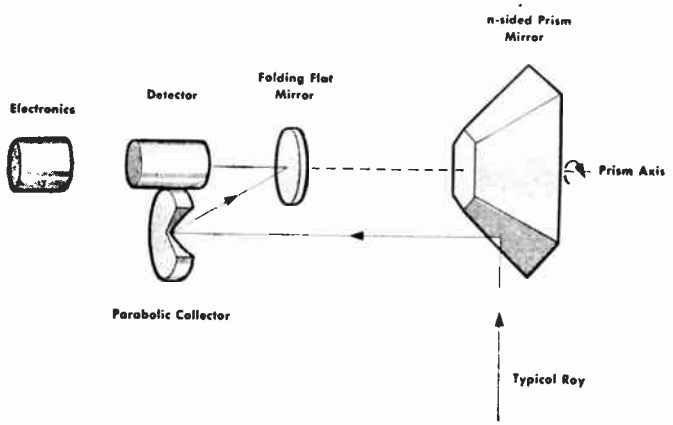

Fig. 3—Schematic illustration of a typical prism scanner.

parallel to the flight path of the aircraft. Hence n lines are scanned per revolution when a single element detector is used. Each face of the prism is inclined 45° to the axis of rotation. Normally, the detector acts as the field stop of the system, determining the angular dimensions of the instantaneous field of view. If the detector, instead of being a single element, consists of l identical elements arranged in a closely-spaced linear array, then l contiguous lines will be swept out simultaneously by each face of the prism. Thus $n \times l$ lines will be scanned per revolution. The principal detector characteristic of significance here is the time constant τ. It will be assumed that the scanner must dwell on each resolution element for time not less than $k \times \tau$, where k is a positive dimensionless number, representing the dwell time in terms of the detector time constant.

The operation of such a scanner must meet two conditions: 1) The scanner must dwell on each resolution element for a time not less than $k\tau$. The number of resolution elements scanned per second is $2\pi r/\beta$, so the dwell time is $\beta/2\pi r$. Hence, $(\beta/2\pi r) \geq k\tau$. 2) The scanner must be operated at such a rate that no underlap occurs, (overlap may be permitted). In the direction of aircraft travel, the width of the strip scanned by each face of the prism is βhl; the width of the strip scanned each second is $\beta hlnr$. If no underlap is to occur, this expression must be greater than or equal to the vehicle speed, $\beta hlnr \geq v$. Rearranging these two expressions we obtain

$$r < \frac{\beta}{2\pi k\tau},$$

$$r \geq \frac{v}{hln\beta},$$

in which all quantities are positive.

Thus r has an upper limit set basically by the detector time constant and a lower limit set by the zero underlap requirement (by v/h). A third constraint upon r is also important: the maximum rotation rate permitted by mechanical considerations such as strength of materials, vibrations, and allowable distortions.

Eliminating r from the above inequalities we obtain a constraint upon β

$$\beta \geq \sqrt{\frac{2\pi k}{nl} \cdot \frac{v}{h} \cdot \tau}.$$

Unlike r, β is only constrained by a lower limit. This constraint is imposed by the joint action of v/h and τ.

Under the limiting condition of contiguous lines the inequalities become equalities and the relations become

$$r = \sqrt{\frac{1}{2\pi knl} \cdot \frac{v}{h} \cdot \frac{1}{\tau}},$$

$$\beta = \sqrt{\frac{2\pi k}{nl} \cdot \frac{v}{h} \cdot \tau}.$$

The individual terms in these expressions warrant some discussion. The designer usually will have little or no control over v, h, τ, and k. The first two are usually set by considerations relative to vehicle operation. The properties of the detector materials determine τ and these are not subject to change. Some small choice is available by selecting different detector materials. The amount of information degradation which is tolerable determines k, which is usually not less than 2. Thus, the only free variables are n, l, and to a lesser extent β in that it is constrained by a minimum value but not by a maximum value, except as the picture quality is degraded. As noted above, r is constrained by both greatest and least values as well as by mechanical considerations.

The value selected for n determines α, the total angular width of the scan, since $\alpha = 360°/n$. Note that since $n = 1, 2, 3, \cdots$, then $\alpha = 360, 180, 120, \cdots$, degrees.

In the reconnaissance of large areas it is desirable to spend as little time as possible flying over the area. Therefore, α should be as large as possible, so n should be as small as possible, *e.g.*, $n = 2$ so $\alpha = 180$ deg.

Inasmuch as the maximum detail is usually desired, β should be as small as possible. Also, for mechanical reasons it is desirable to minimize r. In order to minimize both β and r the designer has at his complete disposal only the factor l. Thus, in a sense this factor lies at the heart of the scanner design process.

Two types of reconnaissance missions appear to permit reasonable safety to the aircraft. These are very low, very fast flight or very high, very fast flight. The first, a low-altitude, high-speed reconnaissance system, is represented by the following parameters: $k = 2$, $n = 2$, $v = 1000$ ft/sec, $h = 1000$ ft and $\tau = 10^{-5}$ sec, then

$$r = 63 \frac{1}{\sqrt{l}} \text{ rps}, \qquad \beta = 7.8 \times 10^{-3} \frac{1}{\sqrt{l}} \text{ rad}.$$

If $l = 1$, the simplest configuration to implement, then $r = 3780$ rpm, and $\beta = 7.8$ milliradians.

An r of 3780 is reasonable, since apertures commonly used in such devices are of the order of 6-inch diameter, and such mirrors can be rotated at rates up to 6000 rpm without undue difficulty in holding distortion within optical limits (to the order of 25 μ).

A β_{min} of 7.8 mrad is larger than is desirable, since optical components can be made with resolution better than 1 mrad. If, in an attempt to improve β without increasing l, the fastest detector readily available is selected (*i.e.*, $\tau = 10^{-6}$ sec), then $r = 12{,}000$ rpm and $\beta = 2.5$ mrad. This has still fallen short of the desired instantaneous field of 1 mrad, and the rotation rate is becoming a serious problem. Thus, decreasing detector time constant cannot greatly improve the performance of single element detector scanners operating with large α.

If, on the other hand, l is increased to achieve a β no greater than 1 mrad, it must be at least 9, and in this case $r = 4000$ rpm and $\beta = 0.8$ mrad for $\tau = 10^{-6}$ sec. Both

of these are achievable values. Note again that further decreasing τ would result in unrealistic values for r.

The second example concerns itself with very high-altitude reconnaissance. At present it is not unreasonable to think of flight altitudes of 100,000 feet, an increase by a factor of 100 over the 1000-foot altitude considered in the above example. An increase in v by the same factor does not seem possible at present. Considerations relative to propulsion units and aerodynamics seem to restrict v to about 3000 to 5000 feet/sec. In addition, if these limitations are neglected there is another limit on v on the order of 25,000 to 30,000 feet/sec. speeds quite close to escape velocity. Thus, very high and very fast operation must result in a reduction of the ratio, v/h. But due to the manner in which v/h enters the expressions for r and β, this results in values for these quantitites which are relatively easy to obtain. Thus, the low and fast operation considered in the example is the most difficult to achieve in terms of scanner use. Therefore, any other method of operation is bound to be easier in terms of scanner implementation.

There is one exception to the last statement. If it is desired to maintain, at very high altitudes, the same linear resolution on the ground that is obtainable at low altitudes, a difficulty arises. At an altitude of 1000 feet an angular resolution of 1 milliradian implies a linear ground resolution of 1 foot at an altitude of 100,000 feet; a ground resolution of 1 foot implies an angular resolution of 10^{-2} mrad. But the Rayleigh criterion states that for a circular aperture of diameter d, the best obtainable resolution at a wavelength λ is given by $\beta = 1.22\lambda/d$. At a wavelength of 10μ, a desired β of 10^{-2} mrad requires a circular aperture with a diameter of 120 cm, or about 40 inches. This aperture lies barely within the range of those which can be employed in airborne vehicles. However, the Rayleigh criterion is an idealized limit assuming a perfect optical system. In practice such performance cannot be realized. Thus at very high altitudes linear ground resolution may have to be sacrificed due to fundamental physical limitations.

There are two features of the operation of the scanner described above which must be considered in the display of the information. First, although the angular resolution is constant, the linear resolution on the ground is not; it becomes progressively larger as the optical axis of the scanner is inclined at larger angles from the vertical, and it does not change isotropically. Secondly, when a linear detector array is employed, the projection of the instantaneous field of view of the array on the ground rotates as the scan angle increases. These effects are discussed below; the mechanism of resolution change in direction of aircraft travel as a function of angle of view away from the vertical is sketched in Fig. 4.

In Fig. 4, and in the following text, a flat earth approximation is assumed. The angle away from vertical is designated by θ, the range from the scanner to the earth at any instant is designated r, and p is the length of the instantaneous field of view in the direction of aircraft travel. It can be seen from the figure that $p = \beta r$ and $r = h \sec\theta$ so that $p = \beta h \sec\theta$.

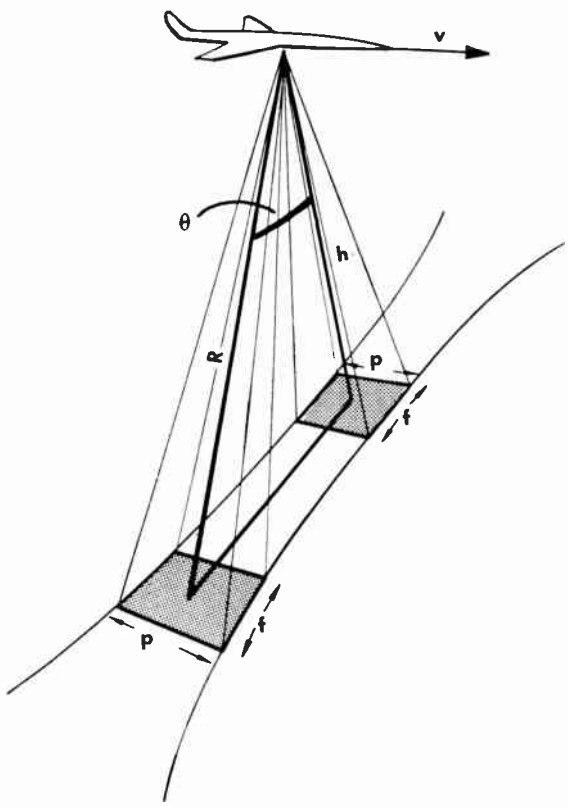

Fig. 4—Geometry for the determination of resolution change in the direction perpendicular to the flight direction.

To obtain an expression for the change in the other dimension of the instantaneous field of view as a function of θ, see Fig. 5. From this figure

$$s_2 = h \tan(\theta + \phi) = h \frac{\tan\phi + \tan\theta}{1 - \tan\phi \tan\theta},$$

and

$$s_1 = h \tan(\theta - \phi) = h \frac{\tan\theta - \tan\phi}{1 + \tan\theta \tan\phi}.$$

But $\tan\phi \approx \phi$ for small ϕ. Therefore,

$$s_2 \approx h \frac{\phi + \tan\theta}{1 - \phi \tan\theta}$$

$$s_1 \approx h \frac{\tan\theta - \phi}{1 + \phi \tan\theta}$$

$$f = s_2 - s_1 \approx 2h\phi \frac{1 + \tan^2\theta}{1 - \phi^2 \tan^2\theta}.$$

For values of θ not more than 85°, $\tan\theta$ is not much larger than 10. Since ϕ is about 10^{-3} rad, $\phi^2 \tan^2\theta$ can be ignored.

Thus,

$$f \approx h\beta(1 + \tan^2\theta) = h\beta \sec^2\theta.$$

We therefore have the result that the field of view

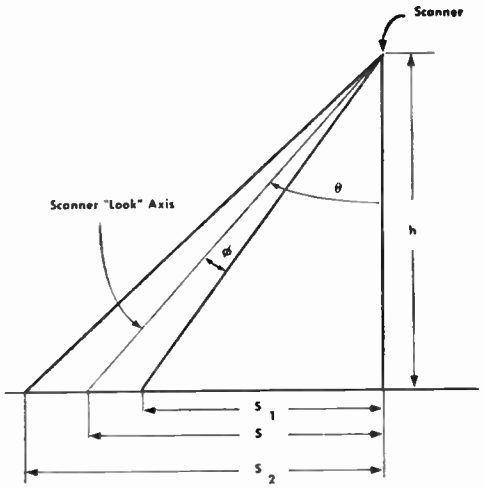

Fig. 5—Geometry for the determination of resolution change in the direction parallel to the flight direction.

changes as $\beta h \sec \theta$ in one direction and $\beta h \sec^2 \theta$ in the other.

It is also true that when a linear detector array is used with a rotating prism scanner of the type discussed here (*i.e.*, with prism faces inclined at 45° to the axis of prism rotation), the projection of the elements of the linear array upon a flat earth rotates as the projection moves laterally to the aircraft flight path. The angle of rotation of the projected array elements is just equal to the angle θ away from the vertical through which the element prism face has rotated.

In summary, the example has shown that the parameter l is of central importance in the design of scanners of the rotating prism type. By the use of linear detector arrays with small numbers of elements, of the order of 10, any reasonable resolution, β, can be obtained at reasonable rotation rates, r. There seems to be no immediate need in this type of scanner for detectors having much shorter time constants than those now used. The design of this equipment involves several unusual geometrical factors which should be corrected if undistorted presentation of information from a scanner operating over wide ($\alpha = 120°$) total fields of view is to be obtained.

The example given here does not include an assessment of all the variables involved in the design of optical-mechanical scanning equipments, since these devices in general are used not only for air-to-ground reconnaissance but also for air-to-air guidance and warning, ground-to-ground search and detection, and a variety of different military and civilian problems. Many factors must be considered in their design. Thus, although the example given here encompasses only a small part of the plethora of problems facing the infrared instrumentation engineer, it illustrates several of the basic design decision processes, and yields practical results for a specific application.

Paper 4.2.5

Infrared Search System Design Considerations*

R. H. McFEE†

THE primary function of an infrared search device is to search for and to indicate the presence, location, and IR radiance of targets within a prescribed field of view. An IR search system is one which observes and indicates the direction and/or radiance of infrared-radiating objects by either sequentially or simultaneously detecting IR radiation from elements of the field, and which presents the information in a manner correlated with the field observed.

The design of the search system is determined by mutual consideration of the operational requirements and the capabilities of infrared. The operational mission for which the equipment is intended governs the requirement for field coverage, information rate, types of targets, detection range, resolution, and size and weight. Limitations of the detection system may demand a compromise solution to the operational requirements, for the most useful design within the over-all system constraints. It may then be desirable to adjust the tactical approach so as to make effective use of the equipment capability.

The nature of the present requirements of IR search systems is such that the combined demands for field coverage, range capability, and resolution exceed present capabilities. As a result, it is difficult in many instances to arrive at a design which approaches the operational requirements, and yet is not excessively complex, costly, and unreliable. The design usually results from a system of successive approximations, hopefully made on paper, to produce the most reasonable compromise.

There are three basic categories of search-system scanning designs: 1) the scanning spot, 2) the multiple-scanning spot, and 3) the mosaic. The first type [Fig. 1(a)] designates systems in which the field is repeatedly

* Original manuscript received by the IRE, June 30, 1959.
† Avionics Division, Aerojet-General Corp., Azusa, Calif.

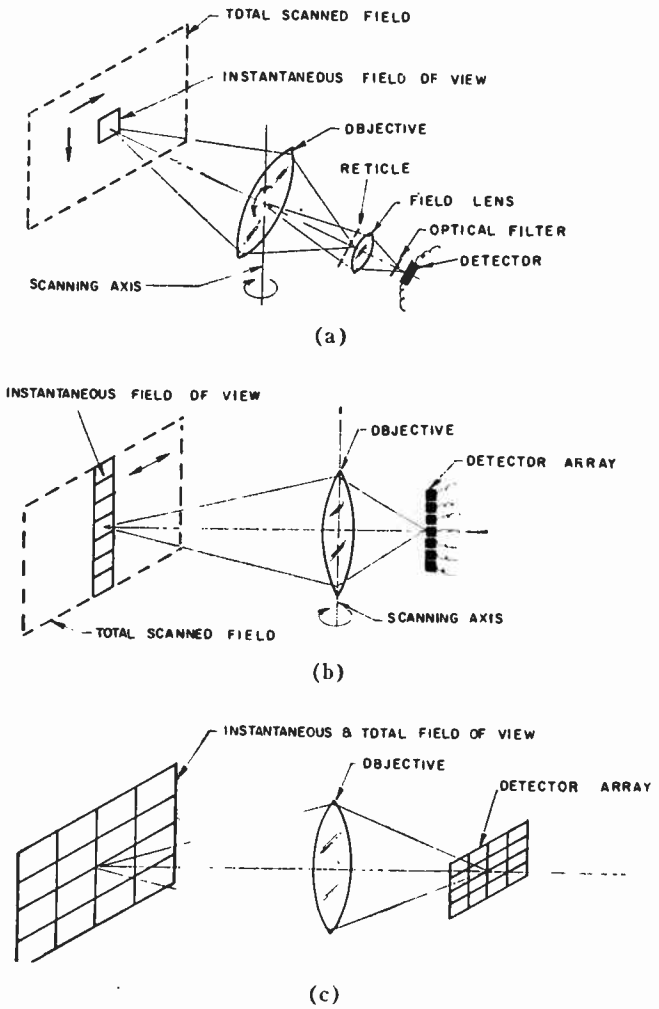

Fig. 1—Basic types of infrared search system designs. (a) Scanning spot system. (b) Multiple-scanning spot system. (c) Mosaic system.

scanned by successively observing single elements until the total field is covered.

The multiple-scanning spot system [Fig. 1(b)] effectively divides the field into sections. Each section is scanned by a detector channel in the manner of the scanning spot device.

The mosaic approach [Fig. 1(c)] is basically not that of a scanner. It is a system where the field is subdivided into smaller regions, each of which is observed by a single stationary detector element. The detector unit takes the form of a two-dimensional matrix of elements.

Each of the three types of scanners has its advantages for certain applications. The single scanning-spot devices, useful where high sensitivity is not required, have relatively simple electronic circuitry requirements with only a single detector to operate and maintain. The multiple-scanning-spot systems can provide high sensitivity with considerable flexibility of design. The mechanical aspects of scanning can be simplified over the single-element system by covering one dimension with multiple detectors and scanning the array about one axis.

The mosaic system is useful in situations where the source of radiation appears briefly at an unknown time and location within the field. Thus all elements of the field must be continually observed in order not to miss the phenomenon when it occurs. This system, although mechanically simple, is complex electronically and employs an elaborate and expensive detector.

Several varieties of scanning-spot systems have been devised, differing only in their mechanical and/or optical means of scanning the field. The field-sampling process may be accomplished either by use of a moving pinhole aperture in the image plane, or by reorientation of the external optical axis of the elemental-field detection system.

The pinhole-aperture scanner [Fig. 2(a)] originally developed by Nipkow as a television pickup device, employs a moving disk or drum containing many small apertures. The pinholes are made to travel one at a time across the field in successive lines, describing a raster covering the field. The single detector generates a signal proportional to the irradiation from the elemental fields as they are observed. Information is usually presented by means of a cathode-ray, television-type display. Since the optical system of the simple Nipkow scanner must be capable of covering the total field of view at once, this device is limited to relatively small scanned fields.

The oriented optical axis approach takes many forms. Various means of pointing the look direction can be employed, each with its set of advantages and limitations. Most common is the method of moving plane mirrors before the objective in the optical system [see Fig. 2(b)]. With this scheme, a small-field system is made to observe elements of the total field by scanning in a systematic fashion over the field. Either one mirror is used, which oscillates about one axis while nodding about another, or two mirrors are located in a series to perform independent scanning about the two axes.

The most direct approach to the scanning-spot mechanization is to mount the entire optical system on gimbals and to drive it through a program of field coverage by changing its orientation. Fig. 1(a) illustrates this type.

The objective lens or mirror can be reoriented for scanning by using an inclined plane mirror between the objective and the detector system, such that the optical axis on the detector side of the flat intersects the detector at all positions of the scanning objective [Fig. 2(c)]. Multiple objectives can be used with a single detector system to provide more efficient field scanning.

Deviation of the optical axis by prism elements can be used as a scanning mechanism [Fig. 2(d)]. Chromatically corrected prisms can be located in front of the objective as a single pair counter-rotated at the same rate for linear scan, or two pairs rotated at different frequencies for Lissajou pattern scanning. This device, known as a diasporameter, has the advantage of compactness, and the disadvantage of extra transmission

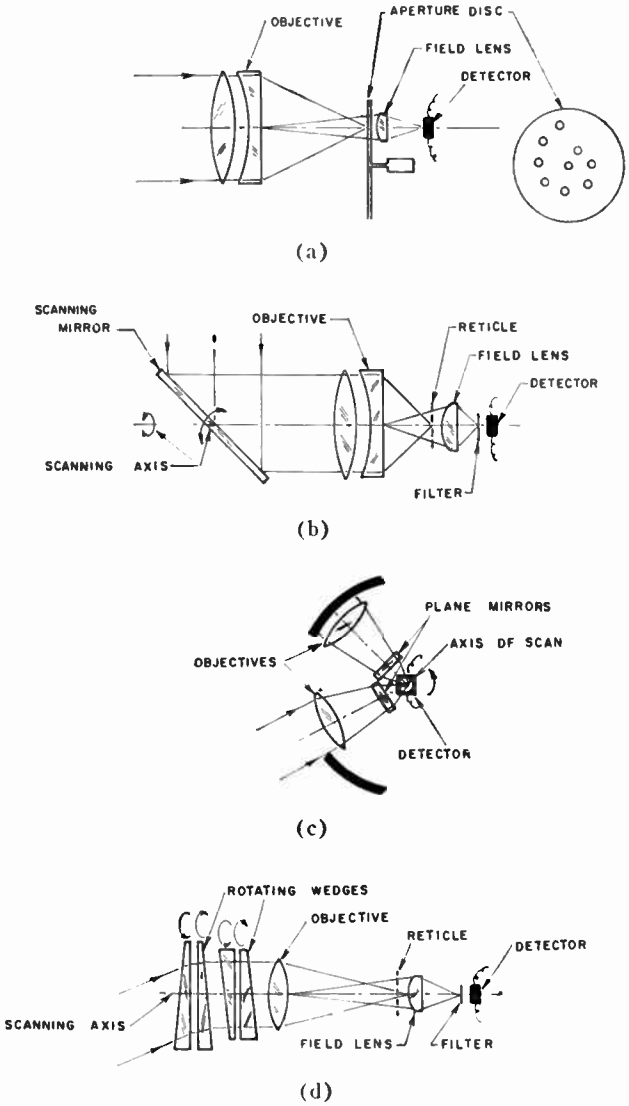

Fig. 2—Representative scanning spot systems. (a) Nipkow scanner. (b) Plane mirror scanner. (c) Moving objective scanner. (d) Rotating wedge scanner.

elements, with their reflection and transmission losses.

Scanning of multiple-spot systems can be accomplished with a linear array of detectors which are made to move over the focal surface of a concentric optical system in a direction perpendicular to the detector alignment. This system has the advantage of small moving parts, with disadvantages of moving-detector difficulties and a large primary mirror.

Scanning systems designed for particular applications may consist of combinations of the basic designs described above. Hybrid designs which incorporate two or more of the basic schemes, will often result in effective solutions to complex requirements dictated by the application. For example, a pair of rotating wedges can be used to scan about one axis while a plane mirror is used for another axis, or a multiple channel detector system can be used with a Nipkow scanner.

The characteristics of the available components of the search system have a strong influence on the choice of the scanning system design. The characteristics of the detector, for example, can determine the size of the optical aperture, the number of detector channels necessary, the type of optical transmission elements, or the mechanical scanning approach. The sensitivity of the detector required for response to the available target radiation can govern whether or not an optical system of practicable size can provide the system sensitivity necessary. The speed of response of the detector directly influences the mechanical scanning design as well as the number of detectors required to cover the field in the specified time with adequate sensitivity.

Techniques of discrimination against unwanted background radiation can be introduced into search-system designs in several forms. Spectral filtering may be employed, which, together with the spectral response of the detector and the spectral transmission of the optics, can provide favored response to the target radiation over the background. These filters may be located either in the parallel radiation in front of the objective, or directly before the detector.

Space filtering is usually obtained by locating a suitably designed reticle in the image surface of the objective optics. The reticle may be stationary and provide modulation of the target image by the scanning motion of the system, or a moving reticle may be used to chop the image at a higher frequency than would be produced by a stationary reticle.

Mechanical considerations play a very prominent part in the design of search systems. Practical solutions must be found to problems such as space or roll stabilization of the scanning system, slip-ring pickoff of signals from rotating elements, and general packaging in compact form of dynamic configurations, with maintenance of the basic-performance capability of the detection system.

Paper 4.2.6

Combined Optical-Microwave System Considerations*

S. H. CUSHNER†

I. Introduction

THIS PAPER presents a discussion of locating systems employing both infrared and microwave energy as intelligence carriers. The actual wavelength regions which are of interest here are 3×10^{-5} cm to 3×10^{-3} cm and 0.3 cm to 30 cm. Emphasis is on a particular class of such systems, called "dual systems," in which the functions of the several components are combined insofar as possible. This first section will present the dual concept and will consider some general applications. Section II discusses various components which prove useful in system design.

Speaking broadly, there are two approaches to the system problem of employing infrared and microwave energy. As previously mentioned, we will concentrate on the dual approach. The alternative is the parallel approach, which simply means two separate detection systems—one for each wavelength region. This approach is a good choice in surface-based systems. Without too much anticipation of the results of Section II, we compare the elements and functions which characterize airborne infrared and radar detection and direction finding systems.

Each system has a "dome" or entrance window, which must be transparent to the radiation and must give protection to the rest of the system. Each type of system then has what is termed an antenna or energy-collecting system, the function of which may be stated in various ways. In a microwave system, it can be considered to match the impedance of free space to the remainder of the system. It performs this by deforming the wavefronts. In the infrared, we may speak meaningfully of rays; and in this case, parallel rays are transformed into converging rays.

After a scanning scheme for determining the angular coordinates of the source being viewed, the next element in both systems is the detector. At this point, it is clear to workers in either field that there must be something which directs the two spectral regions to appropriate detectors. We assume, for the time being, that the detectors are necessarily different.

The last step is the information-processing system. The data derived from infrared homing or tracking devices are the instantaneous target angular coordinates and the corresponding angular rates. Radars get this data and, in addition, can measure range and range rate. Determining the best method for weighting the data which are common to both systems would require study for a given tactical situation, since some or all information could be spurious.

Each of the foregoing items will be discussed in more detail in later sections.

* Original manuscript received by the IRE, June 30, 1959.
† Ramo-Wooldridge Corp., a division of Thompson Ramo-Wooldridge, Inc., Los Angeles, Calif.

II. Dome

Since all infrared transparent materials are low-loss dielectrics, they are, in principle, transparent to microwaves. However, the problem is the large dielectric constants which materials such as quartz, sapphire, and magnesium oxide have in the microwave region. These materials have dielectric constants relative to vacuum in the range of five to ten. For normal incidence, the power losses due to reflection are in the range of 44–67 per cent. This difficulty may be avoided by making the electrical pathlength through the material such that it behaves as its own low-reflectance layer.

This condition is fulfilled for normal incidence on a loss-free nonmagnetic homogeneous isotropic dielectric of refractive index n when the thickness d is given by

$$d = N\frac{\lambda_0}{2N}$$

$$N = 1, 2, 3 \cdots$$

λ_0 = free space wavelength.

In transmisson line parlance, this is the condition for an impedance match. The spectral bandwidth over which the reflection loss for two surfaces is less than 20 per cent is typically ± 5 per cent of the center frequency for first-order interference ($N=1$).

Separating Elements

There are two general approaches to the problem of separating infrared radiation from microwave radiation. One can reflect the microwave and transmit the infrared or one can reverse the functions. The methods of realizing these alternatives are as follows:

Transmit infrared, reflect microwaves
1) wire grating or mesh
2) dielectric structure.

Transmit microwaves, reflect infrared
1) metallic array
2) dielectric structure.

A wire grating will reflect incident microwaves when the electric vector is parallel to the grating elements, and have negligible effect if the wires are perpendicular to the electric vector of the incident waves. Such a structure is almost perfectly transparent to infrared waves. The electromagnetic complement of the grid, which is obtained by replacing the grid wires by spaces and the grid spaces by metal, can be made to be transparent to microwaves and to reflect 90 per cent or more of incident infrared energy.

Another type of beamsplitter is the all-dielectric structure. This is simply a slab of dielectric which has a high-reflectance coating in the infrared. These coatings are also nonconducting and contribute a negligible amount to the thickness of the slab. The entire structure can therefore be made a low-reflectance thickness for the microwaves; or the alternative, if desired, can have a low-reflectance infrared coating and be made a thickness which reflects all the microwave radiation.

Energy-Collecting System

It has been mentioned that the operation of the energy-collecting elements of the system may be stated in several ways. In the microwave case, where the diameter of the main collector element is usually a small (~ 20) number of wavelengths, the full machinery of vector diffraction theory must be used to predict the efficiency and characteristics of antennas. In the infrared, where the size of the collecting elements is a few times 10^5 wavelengths, the geometrical-optics approximation of straight-line propagation may be used. In the case of very high resolution systems such as are used for reconnaissance or precision tracking, there may be a stop which is small enough to spread the waves by diffraction. In this case, additional optical elements called field lenses, which can collect energy distributed over large angles, are used to gather the energy and bring it to focus on the detector. Field lenses are often used in optical systems to produce high-quality images in the absence of diffraction phenomena. There is a wide variation in the quality of the surfaces required to collect energy in the two wavelength regions. It is only asserted here that the surface quality of an optical reflector is more than adequate for use in the microwave region. The typical vacuum-evaporated aluminum film used to make the reflecting surface on optical elements has a conductivity great enough to be a satisfactory reflector of microwaves.

Detectors and Scanning

In the previous discussion, reference has been made to a separating element which directs the microwave radiation and the infrared radiation to their respective detector. Present-day technology dictates the silicon crystal and catwhiskers for a microwave detector and a photoconductive cell or bolometer for the infrared system.

A mechanical scanning system for the microwave portion of a dual system is less desirable than for a conventional radar. The reason for this is the considerably smaller latitude of vibration which can be tolerated by optical-type systems. For dual systems, an electronic scanning system such as the ferrorod type would be more desirable.

Paper 4.3.1

Methods of Background Description and Their Utility*

DAVID Z. ROBINSON†

Introduction

In order to design or evaluate a given infrared system, it is necessary to know the characteristics of the potential targets and backgrounds with which it is expected to deal. The information desired can be put in the form of questions.

1) What is the probability of detecting a target in the presence of a given background with a given IR system?
2) What is the probability that a given background will not give a false signal when no target is present?
3) How can one design the system to increase these probabilities?

Note that it is not only the properties of the background which are involved here. Of vital importance also are the properties of both the target and the IR system which is being used.

It is the hope of those working in the field to find a concise description of backgrounds which will work with any system and with any target. If the method of de-

* Original manuscript received by the IRE, June 30, 1959.
† Office of Naval Res., London, England. Formerly with Baird-Atomic, Inc., Cambridge, Mass.

scription does not work for all targets and systems, it is of value to see under what circumstances the description is adequate.

It is obviously possible to describe completely the spatial distribution of radiance from a single background. It is also obvious that such a complete description for all possible background conditions involves a large amount of data, essentially infinite in scope. It would be very desirable to condense the information.

There have been a number of incomplete descriptions of backgrounds proposed. The Working Group[1,2] defines three such methods: the single line scan and the one- and two-dimensional Wiener transforms. It is the conclusion of this paper that these particular incomplete descriptions are only of value for a very restricted class of backgrounds. With most backgrounds and most systems, these methods are useless insofar as they can be used to predict performance.

In this paper, a start is made toward some descriptions which may well be more adequate for certain purposes. However, the problem is of sufficient magnitude to warrant further work in this field.

After a brief survey of the present methods of describing backgrounds, the main operations of infrared systems now in use will be described. The backgrounds will be classified into various types, and the utility of the proposed descriptions for each type will be examined. Finally, other possible descriptions will be briefly examined. Many of the mathematical conclusions are presented without rigorous proof. These proofs can be found in standard works on stochastic processes.[3]

Present Methods of Describing Backgrounds

Complete Descriptions

An individual scene can obviously be described completely as far as the spatial distribution of radiance is concerned. The two-dimensional function, $R(x)$ where R is a radiance and x is the vector representation of position, gives all the available information. The information is usually collected with a system which has a certain limiting resolution and, therefore, the variation in radiance at points spaced more closely together than this limit is not revealed. As long as the ultimate system which will be used resolves points spaced no closer together than the system used to collect the information, this limitation is not important. The data can be presented as a tabulation, a thermal photograph or a contour map.

These methods all have the disadvantage that each background must be described by many numbers. Since there are many possible type of backgrounds and, many conditions of viewing, it would be extremely difficult to use such methods to evaluate an infrared system even if this information were collected. The parameters of any infrared system are few. It seems illogical to require such a vast amount of data to fix such a relatively small number of parameters. For this reason and others, many authors have tried to reduce the work necessary to obtain the performance of given systems by summarizing the data in some way.

Incomplete Descriptions

Single Line Scan: If, instead of making a two-dimensional scan of the field, a one-dimensional scan is made, we obtain a single line scan (see page 6 of Jones[1]). This scan is very easy to obtain, but it obviously leaves out all of the two-dimensional aspects of the information. It is impossible to distinguish between a point and a line, or to get much information about shapes unless they are very simple.

The One-Dimensional Wiener Transform. It is possible to perform a Fourier analysis on the data obtained from a single line scan and obtain the one-dimensional Fourier spectrum. Usually the phase information is removed by taking the square of the absolute value of the Fourier coefficients. The function thus obtained is called the one-dimensional Wiener transform. (See pages 7–9 of Jones,[1] for an extensive discussion of this function.) The function is analogous to the power spectrum of an electronic noise signal.

The One-Dimensional Autocorrelation Function: Another description of the radiance distribution is the autocorrelation function. The autocorrelation function of the single line radiance scan is defined by the equation:

$$\phi(x') = \frac{1}{A}\int R(x)R(x + x')dx, \qquad (1)$$

where $\phi(x')$ is the autocorrelation function, $R(x)$ the radiance signal obtained from a line scan, and the integral is taken over the whole line. A is the length of the line. The autocorrelation function of an argument x' is simply obtained by multiplying the function by itself, shifted by the value x', and then integrating over the area of overlap. The autocorrelation function at the origin is the integral of the square of the function. For x' larger than the distance over which the value of one point in R has an influence on the other, ϕ approaches the square of the average value of the original function. There is an important relationship between the Wiener transform of a function and the autocorrelation function. If $W(f)$ is the Wiener transform and $\phi(x')$ is the autocorrelation function of $R(x)$, then $W(f)$ is the Fourier transform of $\phi(x')$. From the point of view of

[1] R. C. Jones, ed., "Report of The Working Group on Infrared Backgrounds, Part I," IRIA Rept. 2389-7-S; July, 1957.

[2] R. C. Jones, ed., "Concepts and Units for the Presentation of Background Information," in "Report of The Working Group on Infrared Backgrounds, Part II," IRIA Rept. 2389-7-S; November, 1956.

[3] (a) S. Goldman, "Information Theory," Prentice-Hall, Inc., Englewood, N. J.; 1953.
(b) S. O. Rice, "Mathematical analysis of random noise," *Bell Sys. Tech. J.*, vol. 23, pp. 282–332; July, 1944.
(c) ——, vol. 24, pp. 45–156; January, 1945.
(d) J. Bendat, "A general theory of linear prediction and filtering," *J. Soc. Indust. and Applied Math.*, vol. 4, pp. 131–151; September, 1956.
(e) C. E. Shannon, *Bell Sys. Tech. J.*, vol. 27, pp. 379–423, 623–656; 1948.

contained information, there is no difference between the autocorrelation function and the Wiener transform. The relative utility of each is merely a matter of convenience in understanding the functions or in measuring them.

The Two-Dimensional Wiener Transform: The two-dimensional Wiener transform can be obtained from the two-dimensional radiance function $R(x)$ by performing the Fourier transformation (which is itself two-dimensional) and obtaining the square of the absolute value of the individual Fourier coefficients. The transform is described in more detail by Elias, *et al.*[4]

The Two-Dimensional Autocorrelation Function: The two-dimensional autocorrelation function[4] is related to the radiance distribution function by

$$\phi(x') = \frac{1}{A}\int\int R(x)R(x + x')dx. \tag{2}$$

Physically, the autocorrelation function for any argument x' can be obtained by displacing two radiance distribution functions $R(x)$ by the vector x' and obtaining the average product of the displaced values. A is the area of overlap. The two-dimensional autocorrelation function is also the Fourier transform of the two-dimensional Wiener spectrum.

All the incomplete methods of description remove some of the original information present in the field of view. Their value depends upon whether or not the information left is of any importance in describing the performance of a particular system with a particular target, or whether it can aid in the design of such a system.

Operations in Infrared Systems

There are a large number of infrared systems used for the detection of targets against backgrounds. There are, however, a relatively small number of individual operations; even these can be divided into two main classes, linear and nonlinear.

Linear Operations

A linear operation is one for which superposition of inputs gives superposition of outputs. Properties of a linear operator are such that the relationship between input and output can be characterized by a superposition integral

$$o(x) = \int i(x')h(x - x')dx', \tag{3}$$

where i is the input, o is the output and h is the operator response function. It can be shown that the Fourier transform of i and the Fourier transform of o are related by an equation of the form

$$O(f) = H(f)I(f) \tag{4}$$

where the capital letters refer to Fourier transforms. H is often called the transfer function of the operation and is the Fourier transform of h.

An infrared system is usually made up of a number of operations. Often, a large fraction of these operations are linear. For example, the scanning of the field of view with a detector produces an output which is not exactly the same as the original input, since the detector averages the input signal over its angular field. If the detector is operating over its linear range, then the averaging operation is linear. An electronic filtering system after a detector is usually linear, as is a rotating reticle placed in front of it. A lens acts as a linear operator in the sense that the superposition integral is still valid in any one small area, but very often the aberrations are such that the blur circle (which is related to the operator response function) varies over the field of view. Such an operator is a *space-varying linear operator*, and it is not characterized by a simple transfer function. The usual method of dealing with these operators is to divide the field into zones where the response function is approximately constant over the zone.

Nonlinear Operations

There are a number of important operations which are inherently nonlinear. Rectifying, clipping, and squaring are good examples of such operations. A very important nonlinear operation is the "decision-making" one. A yes or no answer is inherently nonlinear, since each output corresponds to a very large number of possible inputs. A given input i_1 may give an output "don't fire," and half this input may give exactly the same signal. The transfer function is not simply defined for nonlinear operations.

For example, scanning systems for search purposes are linear in the processing of the entering picture. The final output step, however, is nonlinear, since it is decision making. It may be a *peak* reading signal, in which a target is said to be present if a voltage level goes above a given quantity. Other final decision-making operations may involve a human element in which a particular target is chosen from background. The latter step is complex, nonlinear, and two-dimensional.

Types of Background Ensemble

In order to describe adequately the utility of a given infrared system against backgrounds, it is necessary to obtain the probability of satisfactory performance against various types of background configurations. An individual background is not the only problem. There is interest in all possible backgrounds depending on their probability of occurrence. This whole group of backgrounds (past, present and future) is called the *background ensemble.* Only a small part of the possible ensemble of backgrounds can be studied, but it is hoped

[4] P. Elias, D. S. Grey, and D. Z. Robinson, "Fourier treatment of optical processes," *J. Opt. Soc. Am.*, vol. 42, pp. 127–134; February, 1952.

that as the number studied increases, it will be possible to make generalizations.

There are two kinds of averaging operations that are used with ensembles. The first is called the "ensemble average" and the second is called the "spatial average." The ensemble average radiance, for example, is the average radiance which would be expected to be obtained by looking in a given direction. It would be measured by selecting a large number of backgrounds at random and taking the average value of $R(x)$ on those backgrounds. Note that it is possible for the ensemble average radiance to be different for different directions.

In addition to the ensemble average, there is also the spatial average. This is the average which can be obtained by integrating over the spatial coordinates x for an individual picture. This average radiance is a function not of the ensemble but of an individual picture. $\overline{R}$ does not depend on x, but does depend on the particular member of the ensemble. In most cases, it is the ensemble average which is the important property and the more fundamental of the two.

Ensembles can be classified in many ways. There are a few types of particular importance upon which the utility of the various incomplete descriptions depends. The definitions are not rigorous, but will give an idea of the difference between types. These classes will now be defined for the background case, and examples will be given.

Stationary Ensemble of Backgrounds

A stationary ensemble of backgrounds is an ensemble for which the properties do not vary with the direction of view.

The stationary property of a background ensemble simplifies the description of the ensemble. The average radiance is not a function of direction x, and the ensemble autocorrelation function is only a function of the separation variable x' and not of the direction variable x.

In sky backgrounds, the properties do not vary much out to 45° from the zenith. Similarly, for air-to-ground backgrounds, the ground looks very much the same so long as one is looking more or less straight down. This type of background ensemble would then be stationary.

With the normal definition of backgrounds, however, which considers the radiance reaching the detector, the properties of backgrounds differ as one approaches the horizon. Atmospheric emission and absorption increase rapidly, changing both the average radiance values and their variations. Furthermore, the effect of aspect increases. Clouds that looked like circles when overhead look like ellipses at the horizon. The horizon itself always adds a nonstationary aspect to backgrounds. Although the mathematical implications of nonstationarity on the Wiener transform are difficult to describe rigorously, it does mean that an individual Wiener transform of a complete picture may not be a useful description of that picture, since it describes only average effects.

An Ergodic Ensemble of Backgrounds

An ensemble of backgrounds is called *ergodic* if the statistical properties of any background are the same as those of any other.

The chief implication of the ergodic property is that it makes it possible to replace an average over the ensemble as a whole with an average over an individual member. Thus, if we wish to know the average radiance of an ensemble of backgrounds, it is merely necessary to take the average over any given example chosen for convenience.

A stationary ensemble of backgrounds can often be subdivided into ergodic sub-ensembles (thus the clear sky ensemble might be subdivided into day and night sub-ensembles), but it is obvious that a stationary ensemble is not necessarily ergodic. The ocean may look the same in all directions in a single picture, but that does not mean that the ocean today will look like the ocean tomorrow.

A Gaussian Ensemble of Backgrounds

There is an important class of backgrounds which is termed Gaussian. The properties of these backgrounds are analogous to the electrical noise that is generated in radiation detectors. The Gaussian ensemble is completely specified to the greatest possible accuracy consistent with its random nature by the values of its autocorrelation function, and thus by its Wiener transform.

No one has measured the statistical properties of the ensemble of backgrounds, but it is probable that such things as sea backgrounds and forest backgrounds may approach the Gaussian type. Possibly, either clear or completely overcast skies are reasonably close to this ideal. A partly cloudy sky, on the other hand, has a probability distribution of radiance centered either around the blue sky value or around the cloudy sky value and is therefore highly non-Gaussian. (See Fig. 1.)

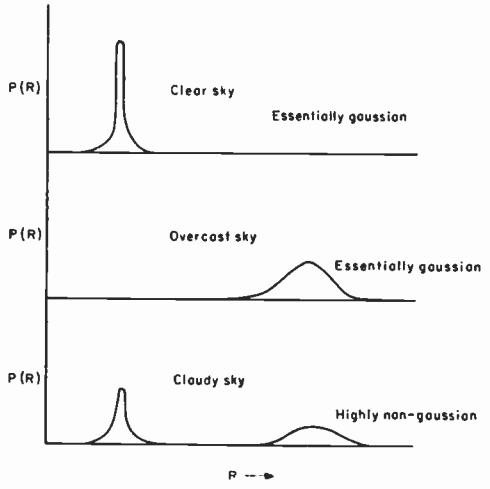

Fig. 1—Schematic probability distribution of radiance for clear sky, overcast sky, and cloudy sky.

Utility of Some Incomplete Methods of Background Description

The utility of various proposed methods of describing the backgrounds greatly depends upon the type of background ensemble being dealt with. Various cases will be considered.

Utility of the Autocorrelation Function and Wiener Transform

Stationary, Ergodic and Gaussian Backgrounds: The autocorrelation function completely describes all the probability distributions of stationary, ergodic and Gaussian backgrounds. Since the Wiener transform has the same information content as the autocorrelation function, it too can be used to describe the function completely.

In this case, if the autocorrelation function is known, it is, in principle, possible to find the average number of zero crossings in the signals, the distribution of maxima, and any other property which one may desire.

Stationary, Ergodic But Non-Gaussian Backgrounds: With any stationary, ergodic background, whether Gaussian or non-Gaussian, it is possible to get certain information from the Wiener transform or the autocorrelation function. If all the operations of the system are linear, then

1) It is possible to compute the rms signal obtained from scanning any background.

2) It is possible to design the system which will give the minimum mean-square difference between the target signal and the output. (The transfer function of this system is the ratio of the target Wiener spectrum to the input Wiener spectrum.)

3) It is possible to design the linear system which will give peak signal to rms background signal. (The transfer function of this system is the ratio of the Fourier transform of the target to the Wiener spectrum of the the noise.)

These properties of the Wiener transform have been apparently so useful that many people have overlooked two important questions:

1) How important is rms noise as a measure of the performance of a system?
2) What will happen if nonlinear systems are used?

In many cases of non-Gaussian backgrounds, the true measure of performance is the peak noise signal which cannot be obtained from the autocorrelation function. And in many nonlinear systems, discrimination based on shape is possible. For these systems, the Wiener spectrum is useless.

The fact that the rms noise is not a good criterion can be determined by the following example. Consider a number of small pulses of any shape spaced at random. As long as the spacing is random, the Weiner spectrum of this background is independent of the relative heights and spacing. Thus, a background consisting of a few strong pulses will have exactly the same Weiner spectrum as one consisting of a large number of small pulses, so long as the total power is the same in both cases. A peak reading system will obviously have a great deal more trouble from the first of these than from the second, but it would be impossible to know this from the spectra alone. The rms noise value tells nothing about the peak signals, even though the spectrum is given.

In visible reconnaissance systems, it is quite easy for a human observer to locate an airport in the field of view even if there is a great deal of background clutter at other portions of the field of view. This is particularly true if the clutter consists of objects (such as cities) which also have recognizable shape. In such cases, the rms background noise level can be a great deal higher than the signal and not cause trouble.

In summary, therefore, for non-Gaussian ensembles, the rms noise criteria can be misleading in two ways:

1) The peak-to-peak noise can be much higher than would be expected for Gaussian backgrounds. (Performance worse than one might think.)
2) The nonlinear systems can discriminate against a larger number of background signals than might be expected. (Performance better than one might think.)

Thus, the Wiener spectrum, or the autocorrelation function, does not even give a limit to the performance of any given nonlinear system with a particular background, if that background is non-Gaussian. If the system is linear, however, it does give an upper limit to the performance.

As an example of near "optimum" linear space filtering, consider a target one unit in size and a background consisting of a square 10×10 units in size. These are both in a field 20×20 units square. The intensity of the target is taken to be one-half unit and the intensity of the background is taken to be four units. (See Fig. 2.) Before any filtering occurs, the following numbers describe the system

$$\text{Peak target signal/peak noise} = 0.125.$$
$$\text{Peak target signal/rms noise} = 0.3.$$

The field is scanned with a nine-element array, whose center is weighted at one; the signals from the corners are weighted by $\frac{1}{4}$ added to the center signal, and the signal from the four edge elements is weighted by $\frac{1}{2}$ subtracted from the signal. (This array is near enough to the "optimum" designs to give apparently improved performance.[5]) After scanning with this array, we obtain a new field shown also in Fig. 2.

The general effect of this filter is to eliminate completely the edges of the background, to blur out the

[5] The particular array is optimum only if nine elements are used. It would be possible to scan the field with a much larger array and completely eliminate the signal from this particular square (but not from squares of the same size and other orientations). The author is grateful to R. C. Jones for pointing this out.

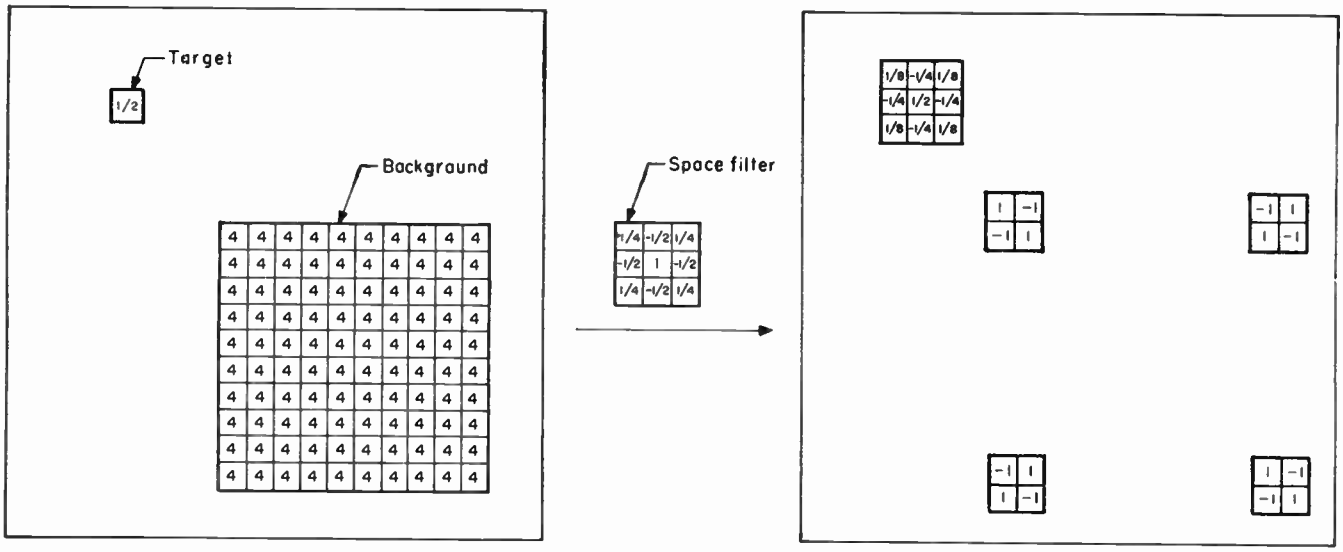

Target and background before space filtering

Peak signal / RMS background = 0.3
Peak signal / peak background = 0.125

Target and background after space filtering

Peak signal / RMS background = 2.5
Peak signal / peak background = 0.5

Fig. 2—Effect of space filtering with a near-optimum nine-element array on a target and background.

target and enhance its contrast a little, and to reduce the signals at the corners by a factor of two. Signal-to-noise ratios become

$$\text{Peak target signal/peak noise} = 0.5.$$
$$\text{Peak target signal/rms noise} = 2.5.$$

The filter has increased the signal to rms noise ratio by a factor of eight, and has even increased the peak signal to peak noise ratio by a factor of four. There would seem to be no question that this filter has greatly improved the probability of finding the target.

This, however, is not the case. With a linear system, it would be impossible to find the target without also getting a signal from the corners of the background area even after filtering. This is so even though the S/N ratio as normally stated is 2.5. The peak-to-peak signal is still less than one.

With a nonlinear system which involves looking at the signal obtained on a cathode-ray screen, there is no difficulty in finding the target and ignoring the background completely without the filtering. After the filtering, the target and the corners would look very much alike, and it becomes much more difficult for the observer to distinguish between target and background signals. Thus, a near "optimum" linear filter has actually *decreased* the probability of finding the target, even though it has greatly increased the signal to rms noise ratio.

Furthermore, it is not difficult in this particular case to use the same array in a nonlinear manner to find the target directly. If, instead of using a weighted linear combination of the signals from the array, we weight each of them plus one and look at the signals separately, the following rule should be used:

1) If a signal is obtained from the center element and no signal is obtained from the other elements, the signal is then passed.
2) If a signal is obtained from the center element and a signal is obtained from any other element, the signal is rejected.

With such an array, it is possible to scan the field of view and find the target without *any* interference from the background. Of course, this filter is nonlinear, and it is difficult to prove that it is optimum, but that is a small price to pay for successful operation.

If the background had been Gaussian, with the same space frequency distribution, it would not have been possible to use the second filter with success. It is only because we took into account the phase relationships for the Fourier components (in other words, the *shape* of the background), that we were able to succeed.

In reconnaissance systems of all kinds, the user is usually interested in a non-Gaussian background, that is to say, in the shape of objects. In these cases, the Wiener spectrum is of very little value.

Line Scan Information

Line scan information is one-dimensional. This means that a great deal of the information concerning shapes is removed. It keeps some account of the amplitude distribution, and, as such, has an advantage over the Wiener transform.

Unfortunately, line scan information must be obtained with an element of a given angular size. It is difficult to predict the type of signal which would be obtained from an element of another size, even from a larger one (larger in both dimensions), unless the background is Gaussian and isotropic. In this case, the Wiener

spectrum, or the one-dimensional autocorrelation function, suffices.

The line scan is particularly useful in treating the performance of one-dimensional scanning systems where the angular size of the element used in the one-dimensional system does not differ from that in the scan used to study the backgrounds. Even if the scanning system scans in two dimensions but does not take advantage of the two-dimensional quality of the information, and looks only for peak signals, the one-dimensional scan gives the complete description.

In conclusion, there are certain types of systems for which a line scan at the same resolution is adequate to aid in design and production. For many systems and for non-Gaussian backgrounds, the line scan is inadequate.

Other Possible Incomplete Descriptions of Background Ensembles

Since it is the contention so far that the complete descriptions of backgrounds contain far too much data to enable them to be handled adequately, and that the incomplete descriptions are inadequate for non-Gaussian backgrounds which may make up the majority of important cases, are there any other methods of description which might be more useful, particularly for the two-dimensional nonlinear system?

Before discussing other possibilities, it might be well to separate the treatment of nonstationary backgrounds and nonergodic ones from non-Gaussian ones. It is usually possible to divide the nonstationary background into stationary zones where the properties are more or less the same. Whatever description is used in these zones, it should be kept separate, because the combining of them into one average removes the possibility of treating different directions differently. Thus, if a designer is making an instrument to search the sky, he might like to design something different for operation near the horizon; if the horizon description parameters are lumped in with the description of the rest of the field, this possibility will be removed.

The same statement can be made about nonergodic stationary ensembles. These ensembles can usually be divided into ergodic sub-ensembles, and the sub-ensembles studied separately. Again the various descriptions should not be lumped together.

It might be best to pinpoint the information missing from the incomplete descriptions of non-Gaussian backgrounds; it is the amplitude of the radiance, the $R(x)$ itself. More particularly, it is the amplitude differences between various objects in the field of view that are important. In any Gaussian ensemble, these differences can, of course, be computed from the autocorrelation function, or Wiener transform.

Any incomplete background ensemble description should give some indication of the radiance differences and the radiances themselves. Unfortunately, these values may be a function of the angular size of the objects in the field, if the angular size of objects in the field is less than that of the measuring radiometer.

In order to give some idea as to the direction in which the search for better methods might go, a few examples of functions giving more information is presented. It is not thought that these functions are by any means the best that can be considered, but they are presented to stimulate the thinking of people working in the field.

The Probability Distribution of Radiance, $P(R)$

The probability distribution of radiance for a given angular-size radiometric measuring device can be obtained by making a line scan with this device and measuring the fraction of time used when the signal falls between various radiance values.

The advantage of this function for certain non-Gaussian backgrounds is that it gives the peak signals which may be obtained directly. If the object of search gives a radiance higher than any radiance values in the field of view, then it can be detected by a system which has a built in clipping level.

Probability of Point Target Detection

One of the important target types is the point target. This type of target is characterized merely by the intensity of radiation reaching the detector, and by the fact that its angular size is less than the minimum resolvable element of the system. For these targets, where shape is not a factor, it is possible to devise methods of collecting data which will aid in the analysis of both linear and nonlinear systems.

The chief characteristic of a point target is that when the scanning system passes over it, a signal is received which is one resolvable element in size; that is, that all around the target, the signal is less than the target by an amount equal to the target signal. Any system which examined the area in the immediate neighborhood of a suspected target and found that the signals from all points in the area were lower, would show that a point target was present. This is the system which was postulated for the perfect scan of the example in Fig. 2.

Therefore, if the field of view is scanned with a nine-element array, which weights each element equally, and signals from the outer elements are *simultaneously* less than the signal from the center element by a value R, a point signal greater than R is present. It should then be possible to draw a graph showing the probability of obtaining a false point signal of a given size from the background as a function of the signal size. The probability will obviously be very high at zero signal and decrease as the signal size increases. This plot gives the probability of obtaining a false signal for a nonlinear system of the same resolution used in the scan with a nine-element array. It does not give the probability of obtaining a false signal for a scan or picture system of any other resolution. In order to describe such backgrounds completely, it is necessary to scan with arrays of the desired resolution.

The instrumentation of such a system is not so easy to assemble as the instrumentation needed to perform the measurements needed for Wiener transforms, but it would directly give the probability of obtaining a false signal from a particular background, which would be much more useful. Moreover, if the information from complete line scans were recorded, the data could be analyzed in this way.

In theory, then, it would be possible to design a scanning system which would directly give the probability of finding a point target as a function both of the intensity of the target signal and of the angular resolution of the system. It should be emphasized that these curves can be obtained from any Gaussian background if the autocorrelation function or Wiener transform is known. It is only necessary to do this fairly complicated scanning procedure with non-Gaussian backgrounds.

Summary and Conclusions

1) The autocorrelation function and the Wiener transform are very good means for describing background ensembles which are Gaussian.

2) In all background ensembles, these functions enable a designer to predict the rms noise over the whole field of a given *linear* system.

3) The autocorrelation function and Wiener transform enable a designer to "optimize" the linear system, either in the least squares sense, or in the peak target signal to rms noise sense.

4) For non-Gaussian ensembles, such as cloudy skies, or ground backgrounds, these functions give no indication of peak noise signal even with a linear system.

5) These functions do not predict performance of nonlinear systems (almost all real systems are nonlinear).

6) The line scan gives information concerning the performance of many systems where the angular size of the scanning element approximates the angular size of the element used to study the background. In these cases, it can give the probability of detection for any system which does not take the two-dimension property of the background into account.

7) For point target detectivity, it is suggested that the probability of finding a point of a given magnitude and angular size in the field of view be determined.

8) Another function worth considering is the probability distribution of radiance.

Acknowledgment

The author would like to thank Dr. Peter Elias for his many helpful suggestions and criticism.

Paper 4.3.2

The Technique of Spatial Filtering*

GEORGE F. AROYAN†, MEMBER, IRE

Introduction

SPATIAL filtering is a method for improving the detectability of a particular object or set of objects in an optical or electro-optical system. The space filtering itself permits a convenient and rapid method of converting or filtering the useful input into interpretable form with minimum loss of information.

In a typical application, an optical system may be employed to detect and determine the position of an object from which some form of detectable energy is emanating. This detection and position determination function is analogous to radar systems and frequently may take the form of a search or track system, a combination of these systems, or a reconnaissance system. In contrast to radar systems, considerable freedom in the design and selection of an instantaneous field of view is permitted the optical system designer because of the extremely short wavelength of infrared or visible radiation. Relatively narrow-beam optical systems may be used for search, track, or track-while-scan systems or, alternatively, wide field surveillance systems employing an array or mosaic of detectors in the focal plane may also be used for similar purposes.[1]

In practice, the object one wishes to detect is usually located in the presence of radiation from extraneous sources. The fundamental objective of space filtering, then, is to filter or highlight the salient dimensional or space features of a particular object—such as an airplane—at the expense of dimensional detail received from undesired radiation—such as that received from clouds, horizons, lakes, etc. This space filtering is most frequently performed by the field stop and/or reticle located at the focal plane of an optical imaging system.

* Original manuscript received by the IRE, June 30, 1959.
† Ramo-Wooldridge Corp., a division of Thompson Ramo-Wooldridge Inc., Los Angeles, Calif.

[1] M. R. Holter and William L. Wolfe, "Optical-mechanical scanning techniques," paper 4.2.4, this issue, p. 1546. See also R. H. McFee, "Infrared search system design considerations," paper 4.2.5, this issue, p. 1550.

A fundamental limitation of conventional electromagnetic radiation detectors is that they transduce the two-dimensional incident energy into a one-dimensional electrical time signal. This reduction in the degrees of freedom of space filtering requires that the combination of space filtering and subsequent time base filtering be performed in a particular manner to maximize the two-dimensional space characteristics of the desired object or target and to minimize detector bandwidth for maximum system detectivity.

There are two convenient and alternative methods of analysis which permit a study of the space discriminating ability of optical systems—space and space frequency. The detail of light distribution across the object or image, whether from the background or target, can be expressed mathematically as a function of its intensity and the linear position in that plane, such as x and y. It may also be expressed mathematically as a function of inverse space or $1/x$ and $1/y$; it is then analogous to frequency in the true sense, and is called space frequency. These equivalent descriptions of a function are analogous to the study of electrical networks in either the time domain (impulse and correlation function) or frequency domains (frequency response and transform analyses). The appropriate mathematical relations involved in space filtering are described more fully in the following section.

Mathematical Analysis

In general, an object has a particular location in space and time and also has particular reflection or emission characteristics for electromagnetic energy. The electromagnetic energy is generally incoherent in the visible and infrared spectrums and thus only the intensity is of interest. The optical imaging system is further assumed to be linear (displacements from center of field and intensities are proportional in object-image), as is the transmission factor of the optical elements; *i.e.*, they are isoplanatic.

The total optical processing from the object plane to the cell is illustrated in Fig. 1. A lens or mirror forms a two-dimensional image, which, grossly speaking, is linearly related to the object. The blur circle or aberration in the image plane is defined by the light distribution which arises from a point source and is analogous to the impulse response in electrical networks. The image of an extended object is formed by the summation of many blur circles arising from the many point sources in the object. This resulting addition to describe a function in a linear system is known as the superposition integral and is conveniently dealt with mathematically by use of the Fourier transforms. Therefore, the object can be expressed in terms of its two-dimensional space-frequency content, the lens or mirror has a space-frequency transfer characteristic (the transform of the blur circle) or "pass band," which is an ability to translate this object detail into image detail, and the resulting image has a quality or space-frequency content which is

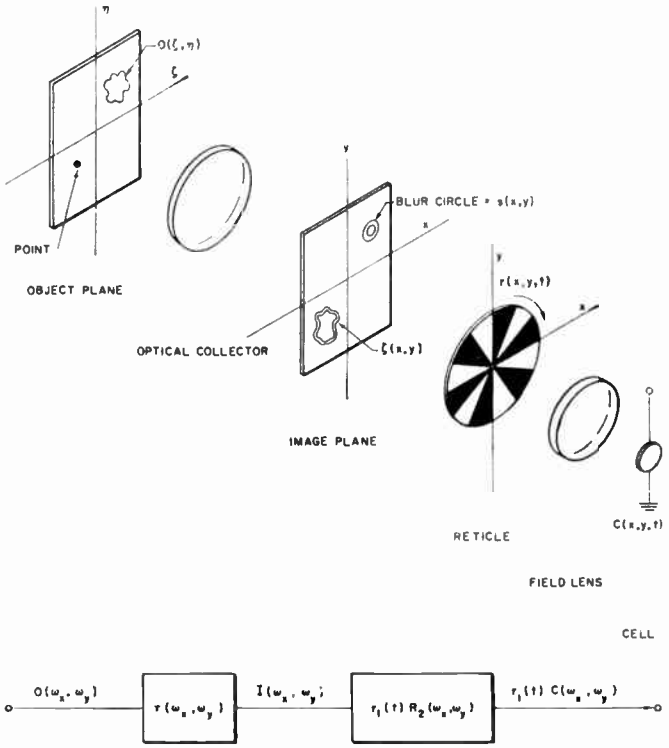

Fig. 1—Linear optical imaging system.

simply the product of the object function and lens function. This dependence on the object-image function has been described by Duffieux,[2] Elias,[3] and others.[4]

In real space, the reticle and field stop combination multiplies its transmission function by that of the image. The field lens subsequently integrates the total light intensity which passes through the reticle by imaging the primary collector. The reticle function itself, however, must be separated into its time and space variables if it is simultaneously chopping and scanning. The resulting integrated space-frequency multiplication effects a real convolution which is modulated at a time frequency depending on the separated time variable in the reticle function.

Mathematically, the output of a cell or detector, $c(x, y, t)$, is desired as a function of: 1) the object intensity distribution corresponding to the background or target, $o(\xi, \eta)$; 2) the transmission factor of the optics, $s(x, y)$, which corresponds to the "spread function," or the blur circle pattern of a point object as seen on the image plane; and 3) the reticle function, $r(x, y, t)$, which may be simultaneously scanning and chopping the image.

The spread function, $s(x, y)$, is the light intensity distribution of a point object in the image plane. An extended, incoherently illuminated object, $o(\xi, \eta)$, has a

[2] P. M. Duffieux, "L'Integral de Fourier et ses Application a l'Optique," Besancon, Faculte des Sciences; 1946.
[3] P. Elias, "Optics and communication theory," *J. Opt. Soc. Am.*, vol. 43, pp. 229–232; April, 1953.
[4] See, for example, D. Z. Robinson, "Methods of backgrouud description and their utility," paper 4.3.1, this issue; p. 1554.

resulting image, $i(x, y)$, composed of the integral of many point sources in the object modified by the transmission function. If unit magnification is assumed, then

$$i(x, y) = \int\int_{-\infty}^{+\infty} s(x - \xi, y - \eta)o(\xi, \eta)d\xi d\eta. \quad (1)$$

The light distribution immediately behind the reticle is the real space multiplication of the reticle and image. The field lens integrates this total light intensity distribution upon a cell or detector. Furthermore, relative motion of the reticle in space imparts a real space convolution to the two space functions when combined with the integrating effect on the cell-condenser combination. The reticle function itself is separated into orthogonal time and space variables in a manner analogous to traveling-wave theory.[5] The total light intensity falling on the cell is the product of each individual differential area summed or integrated over the various reticle displacements x', y', and modulated at the time frequency of the reticle.

$$c(x, y, t) = r_1(t) \int\int_{-\infty}^{+\infty} r_2(x', y')i(x - x', y - y')dx'dy'$$
$$= c(t)c(x, y). \quad (2)$$

The functional relationships in (1) and (2) may also be related to each other in space-frequency terms by employing the two-dimensional Fourier transform of a function, $f(x, y)$, defined as follows:

$$F(\omega_x, \omega_y) = \int\int_{-\infty}^{+\infty} f(x, y)e^{-j(\omega_x x + \omega_y y)}dxdy.$$

The resultant spatial transform of the cell output related to all the optical and reticle components is then

$$C(\omega_x, \omega_y) = R_2(\omega_x, \omega_y)S(\omega_x, \omega_y)O(\omega_x, \omega_y). \quad (3)$$

In summary, the total image processing from the object plane to the detecting element can be treated conveniently with Fourier transforms, as shown in the block diagram at the bottom of Fig. 1. The light intensity modulation on the cell is the product of the two-dimensional transform or space frequency of the object, the lens, and the reticle or field stop, all modulated at a time frequency determined by the separated time function of the reticle.

It is interesting to note that both the blur circle or transmission function of the lens and the field-stop reticle combination are initially evidenced by their equivalent space description. This space description, or equivalent impulse function, is manipulated directly in space filtering synthesis, and is at variance with the ordinary electrical network method of altering the frequency response in order to shape the impulse function. Some authorities, therefore, have worked directly with equivalent correlation functions in optical systems. Karr[6] investigates the interrelation of background, $B(r, \theta)$, and reticle, $R(r, \theta)$, in terms of an output correlation function or the ensemble average of reticle outputs, $c(t)$ and $c(t+\tau)$ at times t and $t+\tau$. As an example, he examines a star reticle rotating at an angular rate ω, and being translated at a velocity V in the direction of zero angular reference on polar coordinates r, θ. The resulting ensemble average over various samples of the background is

$$\langle c(t)c(t + \tau)\rangle$$
$$= \int_0^a dr \int_0^a dr' \int_0^{2\pi} d\theta \int_0^{2\pi} d\theta' rr'R(r, \theta)R(r, \theta' - \omega\tau)$$
$$\langle B(r, \theta)B(r'\theta')\rangle.$$

The evaluation of the above relationship can be extremely difficult and requires the implementing of particular background and reticle measuring programs. As pointed out by Karr,[6] assumptions may be used to simplify the analysis, such as the reasonable assumption of an isotropic background; *i.e.*, the autocorrelation function of the background is a function only of the scalar distance between points. Further simplifying assumptions are that the function of the star reticle is a function of θ only, and that the scanning speed r is small compared with the speed of the rotating reticle. This latter assumption imposes real limitations on some system designs, especially in high-speed search systems, as will be pointed out in the subsequent applications and examples section of this paper.

In summary, there are advantages in employing correlation and impulse function techniques to space filtering. The transmission function of the optics and of the reticle itself is defined in terms of their space configuration. The freedom associated with readily manipulating an impulse function coupled with subsequent time base or frequency filtering opens up especially attractive possibilities. For example, optimum analytic predictor functions frequently take the form of impulse functions, and they may be physically realized optically and subsequently combined with electrical filtering in special reconnaissance or TV systems.

Background Noise and Signal Characteristics

Conventional system-design procedure requires measurement and specification of the input signal and noise characteristics. Then and only then can filters be optimized to transmit useful information and suppress unwanted noise. Furthermore, noise in one set of conditions may be defined as signal under different circumstances. For example, in a TV or reconnaissance system all image detail is of importance; both large and small objects should be reproduced with equal fidelity. In an aircraft or missile surveillance system, however, details of gross objects such as clouds are not desired; only a

[5] J. A. Stratton, "Electromagnetic Theory," McGraw-Hill Book Co. Inc., New York, N. Y., chs. 5, 6, 7, 9; 1941.

[6] P. R. Karr, "Mathematical Study of Background Noise," presented at East Coast Infrared Information Symp., Wright Air Development Center, Dayton, Ohio; April, 1957.

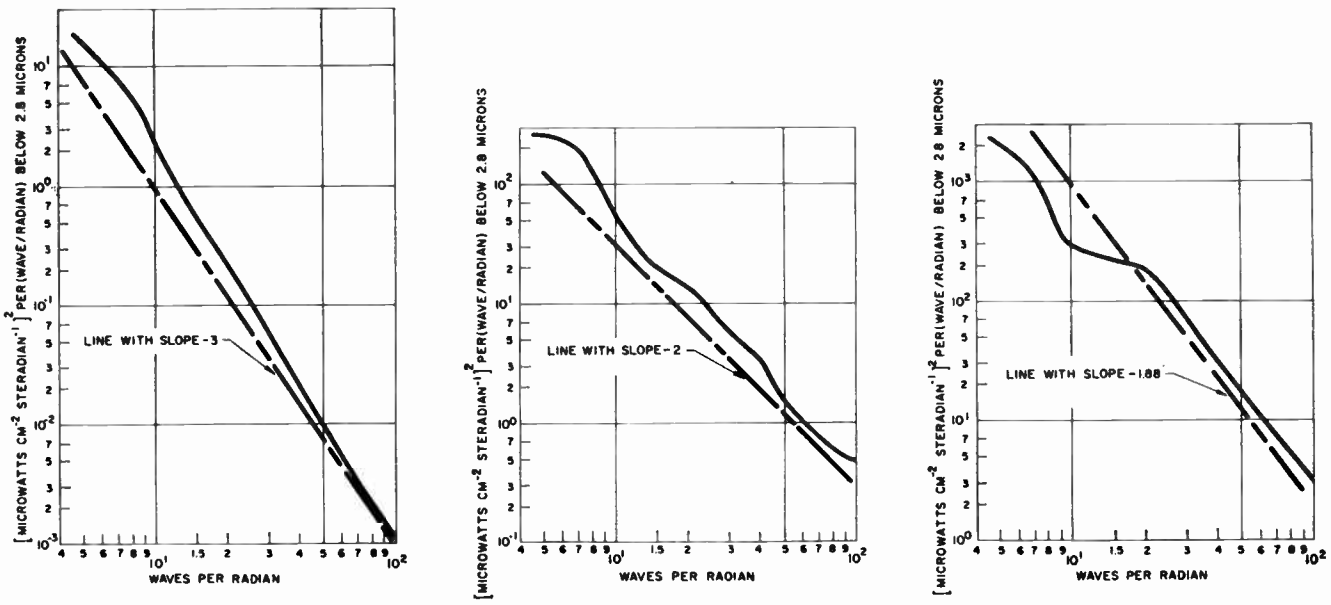

(a) (b) (c)

Fig. 2—Average power densities for sky background: (a) blue sky, (b) hazy sky, (c) cloudy sky.

filtered image of small object size emphasis is desired.

The background radiation is most frequently considered as a two-dimensional function of space random variables in a manner described by Jones.[7] This model has been used extensively to measure, by gradient meters, the background in various infrared sky background measuring programs. Figs. 2 and 3 are typical results of background gradient measurements conducted at Ramo-Wooldridge and illustrate the approximate inverse space-frequency dependence of space power spectra in typical backgrounds.[8]

This method of measurement gives only a partial description of the background since the value of the signal at any location in space is dependent on the adjacent signal levels, *i.e.*, clouds or a horizon are well defined with continuous borders. For typical backgrounds, therefore, higher-order probability distribution functions are necessary to describe completely all the statistical characteristics. Existing background measurements are also unable to show the extremely low space-frequency function dependence.

A heuristic description of the nature of earth and sky background was made for rationalizing existing measurements and predicting further interesting characteristics of backgrounds.[9] This model assumed that, grossly speaking, clouds of constant emissivity or temperature are located against an approximately uniform sky. There are then basically two levels of reflected intensity —the "white" of the cloud or the "blue" of the sky and two emission levels corresponding to the "temperature" of the cloud and that of the surrounding cold sky. The lengths of the background pulse widths in space were assumed to be the particular probability function, $4 \times e^{-2x}$, where x is the linear dimension in space. This agrees, to some extent, with our intuitive notion of cloud lengths; *i.e.*, cloud distributions over π radians in length are rare (except for overcast or cloudless days) while cloud lengths of extremely small size are also rare. The normalized one-dimensional power distribution of this assumed distribution of cloud lengths or pulses are derived in a manner described by the M.I.T. Radiation Laboratory,[10] and was shown to vary inversely with higher space frequencies.

$$S(\omega) = 8\,\frac{(\omega^2 + 8)}{(\omega^4 + 64)}.$$

There is, in addition, an ambient or average intensity level encountered in nature which appears as a delta function at the origin. The step or abrupt change in intensity—which was assumed in the model—is not encountered in practice due to the fuzziness of the edges of clouds, especially in the longer wavelength thermal emission band. This assumed model would then indicate that background power will attenuate with an inverse fourth power of space frequency at higher space frequencies in lieu of the second-power dependence occurring at lower space frequencies. To date, insufficient data have been accumulated to fully substantiate this prediction or the prediction of a breakpoint at one-

[7] R. C. Jones, "Four Methods of Describing Infrared Radiance Distribution," Polaroid Corp., Cambridge, Mass.; March 7, 1956.

[8] "Infrared Sky Background Investigation," Ramo-Wooldridge, Los Angeles, Calif., Contract AF 33(600)30489, RW 1631.70, .84, .87; 1957.

[9] G. F. Aroyan, "A Theoretical Model for Describing Background Spectra," Ramo-Wooldridge, Los Angeles, Calif.; 1958.

[10] J. L. Lawson and G. E. Uhlenbeck, "Threshold Signals," M.I.T. Rad. Lab. Ser., McGraw-Hill Book Co. Inc., New York, N. Y., vol. 24, chs. 3, 8; 1950.

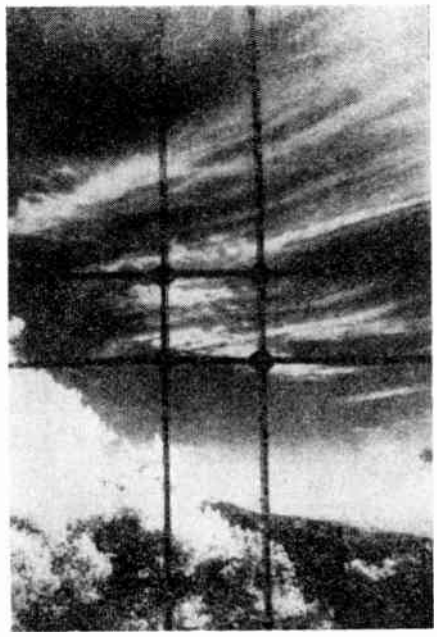

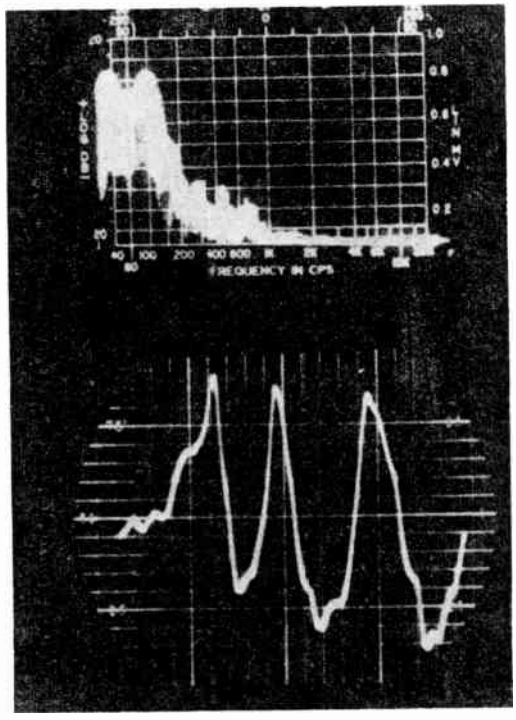

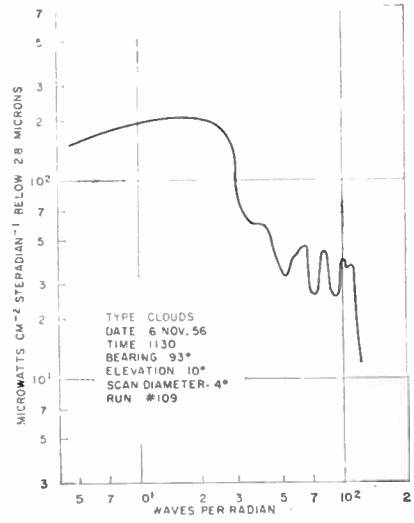

Fig. 3—Illustrative gradient data.

half a wave per radian at the lower space frequencies. It is obvious, however, that the inverse space-frequency dependence cannot continue to zero space frequency.

The spectrum or transform of particular objects or targets and the transmission function of the optics in contrast to backgrounds are straightforward derivations of the object shapes. In Fig. 4, for example, an inverse background power spectrum dependence is shown, as are typical transforms of a small circular object and a diffuse blur circle that may ordinarily arise in the optics. The blur circle fundamentally makes all optical systems behave like low-pass filters and, therefore, the high frequency detail of both the background and particular objects are attenuated. The design of the subsequent filtering must maximize the particular object or target detail at the expense of background noise in the presence of finite optical transmission functions.

Applications and Examples

The design of theoretical optimum space filters and the more practical design of usable physically-realizable filters are described in this section. Several examples of typical reticles are used to illustrate their two-dimensional space-frequency spectra, the effects introduced

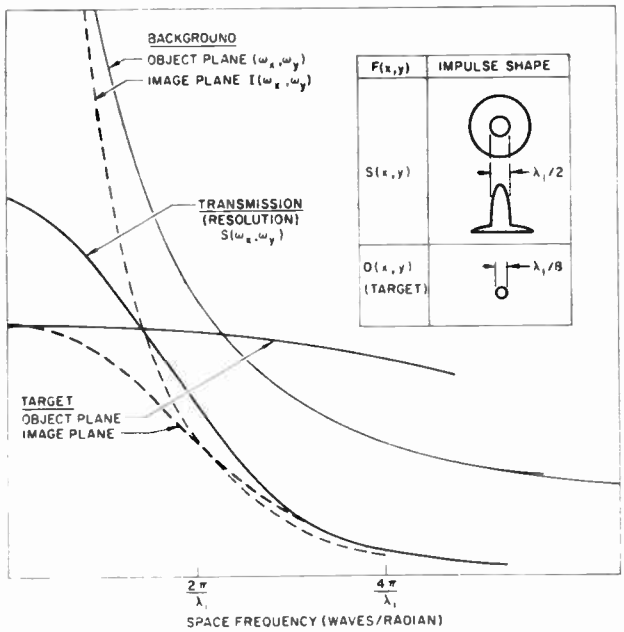

Fig. 4—Object-image transforms.

by parameter variation, and the corresponding detection capabilities of the reticles.

The optimum space filter for detection of a particular object may be derived in a manner analogous to that of a North filter.[8] However, the background noise spectrum, as shown in Figs. 2 and 3, is not "white," but possesses some inverse space-frequency dependence. The ratio of a disk-shaped object spectrum in the presence of an inverse space-frequency noise spectrum rises from zero space frequency to a broad maximum near the frequency whose period is approximately twice the object width, and then falls off again towards the null of the object transform. There are subsequent humps and nulls in the optimum filter which may fall off or remain at the same level of the fundamental characteristic, depending on the relative attenuation rates of the background and object transforms. Additive internal cell detector noise, however, usually prevents utilization of any space filtering beyond the initial broad signal maximum.

In simple scanning systems, the resulting time frequency response equals the product of scan velocity and space frequency in the direction of scan. Since no negative intensity exists, the attenuation of low space frequencies for optimum filtering can only be obtained with related time-frequency filtering or the artificial addition and subtraction of multiple cell or detector outputs. The optimum filter may be physically realized, therefore, by having a field-stop aperture of the same size as the object one wishes to detect and by then utilizing subsequent time-frequency filtering to shape the response to that of an optimum filter. Reconnaissance systems utilize maximum permissible bandwidths to permit high-fidelity reproduction of the image with as small a field of view as possible. The loss of information is then directly calculable as a function of field stop and bandwidths, although some methods of compensation are occasionally used to reconstruct the original image.

In most infrared systems the object one wishes to detect is extremely small, and it would be extremely tedious and mechanically difficult to scan any appreciable field with a field stop as small as, for example, 0.1 milliradian. Actual fields of view are usually significantly larger than the object one wishes to detect.

As the field of view is increased in size, the following changes occur. The background noise increases as a function of the size of the field of view, but the signal energy remains constant. The space-frequency energy reinforcement is also independent of the area of the field stop, and thus an increase in size, although accompanied by narrower space-frequency bandwidths, also increases the amount or height of its peak value. The resulting shift of space-frequency reinforcement to ever lower space frequencies with increasing aperture size does not permit acceptable spatial filtering by the time filter, which is associated with scanning velocity and field-stop aperture, alone. Reticles are conventionally used in such systems for both signal modulation and space filtering. The reticle is located in the focal plane and effectively splits the space-frequency reinforcement from the extremely low space-frequency modulation of the field-stop aperture alone to a space frequency corresponding to the region where maximum object signal-to-noise occurs; *i.e.*, at the peak of the optimum filter described earlier. The maximum object signal-to-noise occurs in a region corresponding roughly to where the reticle spoke width equals the object size one wishes to detect. The 50 per cent transmission of the reticle reduces the incident energy proportionately, but the improvement of space filtering by the concentration of reticle reinforcement in the region of peak signal-to-noise space frequencies more than compensates for the energy loss involved.

The particular space-filtering properties associated with typical picket fence, checkerboard, and star reticles, as they operate in square or circular field stops, are shown in Figs. 5 and 6. The two-dimensional Fourier transforms of the reticles are shown, but since the reticle spacings are usually made to "match" the blur circle, the higher harmonics (3rd, 5th, etc.) which would arise from the square reticle are attenuated to an indistinguishable level and are not shown. The fundamental, itself, of the square-wave modulation is also partially attenuated by the blur circle transform.

The following general observations concerning all the reticles and their transforms may be made, using the square field, picket fence reticle as a model. The space configuration is short in the x direction, and long in the y direction. The corresponding two-dimensional Fourier transform or space-frequency content of this reticle consists of two primary regions of reinforced space frequencies—at the ambient level and region of high inverse x and low inverse y space frequencies. If the field stop or total size of the aperture is increased, but the

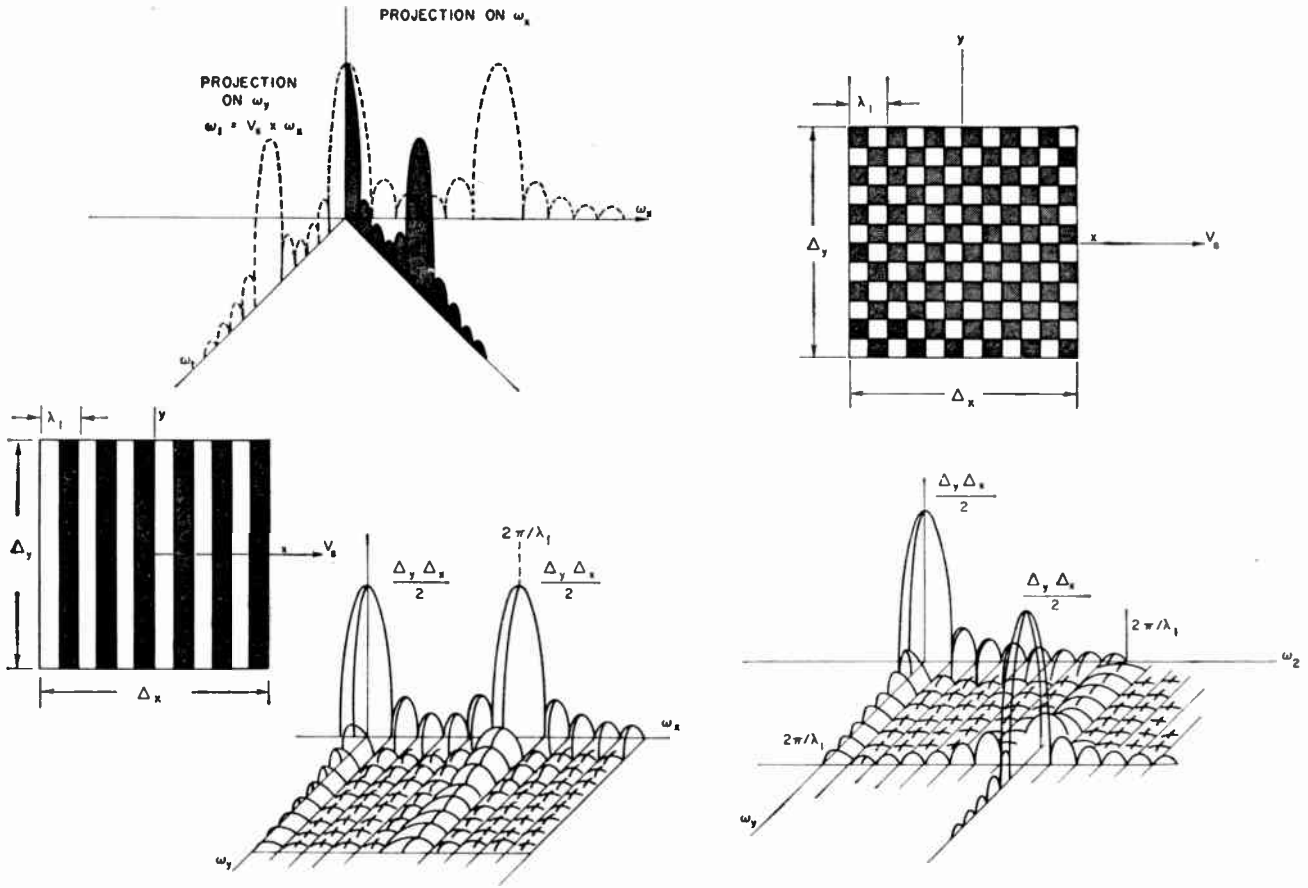

Fig. 5—Comparison of checkerboard and picket fence reticle.

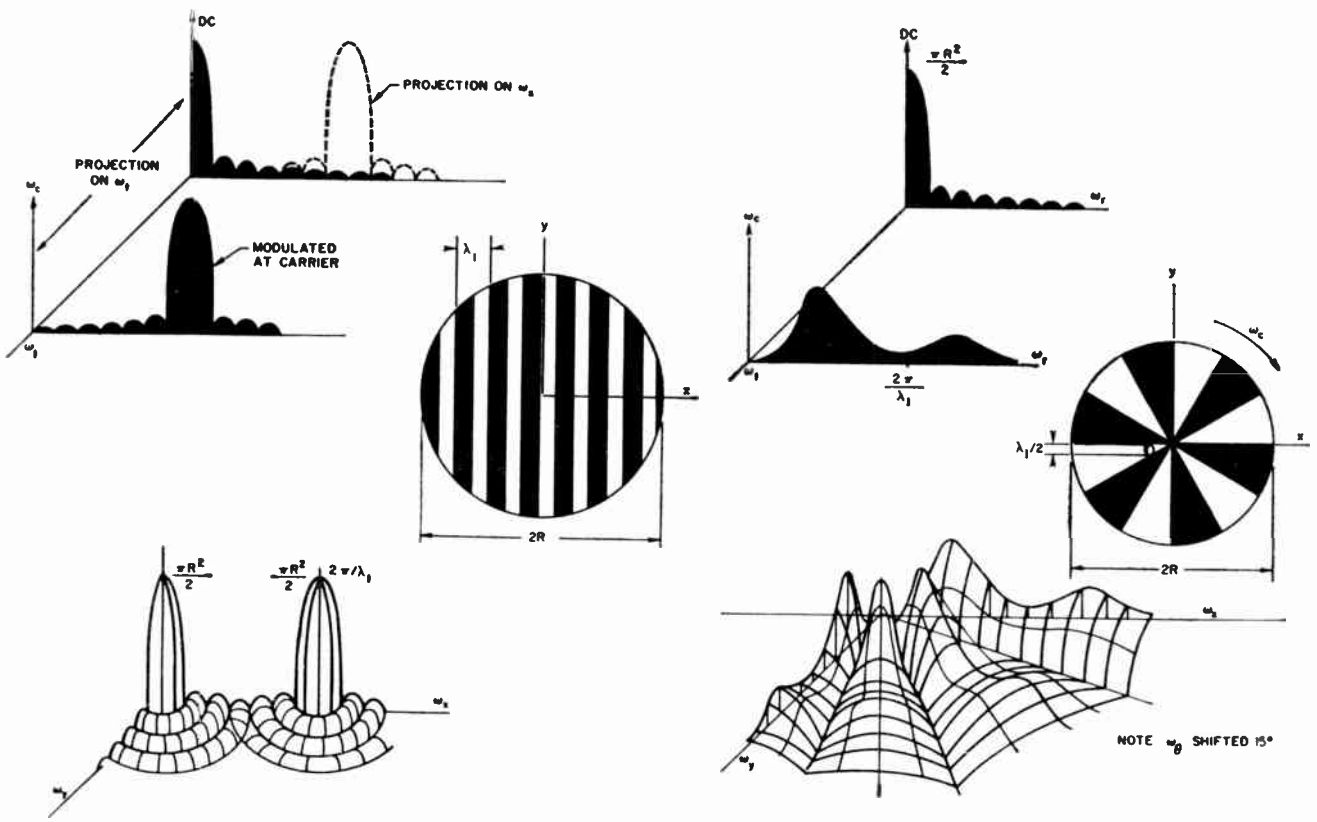

Fig. 6—Transform of parallel slit and radial reticles.

same reticle width spacings are maintained, the effect on the transform is to narrow the concentration of reinforced energy, or bandwidth, at the two main reticle reinforcement regions, and to peak them up higher. If the same size aperture or field stop is retained, but the reticle spacings are made finer, there is a shift in the concentration of high inverse x energy to higher space frequencies, but the same effective bandwidth or envelope of modulation remains around the two primary regions of reticle reinforcement. In this example, the envelope is determined by the field-stop transform, but of only one-half the magnitude. The actual size of the field stop is usually determined by physical considerations such as realizable optical resolution, convenient mechanical-optical scan velocities, and minimum acceptable means of space filtering.

The actual chopping action or time frequency developed in the detecting amplifier is derived from translating the reticle in space with a finite velocity. The time-frequency developed is actually equal to the product of scan velocity and space frequency in the direction of scan for each and every point on the reticle. The time-frequency modulation of a particular space-frequency function may therefore take on considerable flexibility for optimum filtering. For example, if the field stop is moved at a relatively low velocity and the associated reticle has a high velocity relative to the aperture itself, then the corresponding time modulation of the ambient space-frequency modulation is low, and the high space frequencies are modulated at high time frequencies, as shown in Fig. 6. If the field stop and reticle are fixed with respect to each other however, then the time-frequency modulation and one-dimensional space-frequency function are proportional to each other.

The star reticle can be readily shown to produce poor space-frequency discrimination and wide time-frequency modulation. The poor space-frequency discrimination is shown to arise from the diverging spoke widths. The space transform of the star reticle is actually illustrated with only the spoke modulation shown—the field-stop aperture ambient space frequency is identical to that shown for the circular aperture, picket fence reticle, and is omitted for clarity. The poor time-frequency modulation is due to the associated wide frequency variations when the scan velocity vector combines with the rotating angular velocity throughout the field; for example, they add at the top of the field and subtract at the bottom. A combination of velocity vectors, however, can be used to good advantage in conventional track systems when modulation is required to define or locate the relative position of an object within the instantaneous field of view. This track modulation is most frequently performed by velocity vector manipulation, such as combining a nutation and rotation motion, or by varying the reticle spacings themselves if a constant velocity vector exists in the track system.

Space-frequency content alone is not entirely satisfactory for describing space filtering ability unless actual space functions or higher-order probability distributions are also considered. Therefore, the filtering effect of the reticles should also be examined when scanning extended objects such as clouds or horizons in real space. Although the space-frequency reinforcement may statistically average out the same, the actual time modulation may look considerably different for various scan and chopping orientations. This difference is important in assessing the effectiveness of supplementary time or pulse bandwidth filtering techniques. For example, if the scan direction is normal to the slits, lines or extended objects parallel to the slit are modulated for the same dwell time as a point target. Background lines or horizons, which are parallel to the scan direction and would normally have long dwell times, are not modulated or chopped by the reticle and thus supplementary time base filtering is ineffective; *i.e.*, both targets and backgrounds have the same resultant power spectra and pulse widths.

There is a method of obtaining effective two-dimensional space filtering with subsequent time filtering; this is by scanning the picket fence reticle parallel to the spokes, and having the reticle chop in a direction normal to the spokes. Long lines normal to the scan direction are not modulated or chopped by the reticle. Lines parallel to the spokes are chopped by the reticle, but with dwell times considerably longer than for point targets. Thus, long lines in any direction are eliminated, since dwell time and spectra for both time bandwidth filtering and Pulse Length Discrimination (PLD) are different between the target and background.

In summary, space filtering is performed in optical and infrared systems by a combination of optical resolution, field-stop aperture, and reticles located in the focal plane. Subsequent time filtering must also be made in a particular manner to maximize signal-to-noise ratios. For detection of small-sized objects, fields of view approaching the same dimensions as the target object should be used, but with added time filtering to adequately shape the linearly-related space-frequency function. However, since extremely small instantaneous fields of view are physically difficult to mechanically instrument when scanning large fields, reticles are used in the focal plane for optimum filtering with discrete field-stop apertures, as well as for simple signal modulation. The parallel spoked reticle, in particular, has relatively good and uniform spatial filtering characteristics, and, if combined with chopping and scanning motion in mutually perpendicular directions, results in maximum effective use of pulse length discrimination or pulse bandwidth filtering in one direction, and reticle spatial filtering in the orthogonal direction.

Paper 4.3.3

Optical Filtering*

L. W. NICHOLS†

ONE of the most severe problems facing a designer of infrared equipment is that of subduing background radiation. This interfering radiation may be sunlight reflected from clouds or mountains, it may be emitted by the background objects themselves, or it may even arise from the inner surfaces of the detection instrument. Whatever its source, this unwanted radiation limits the desired performance of the equipment and requires some compromise in design.

An obvious technique for reducing background radiation is the use of optical filters. If the spectral characteristics of the target source and the background are known, it is often possible to select filters which will admit most of the target radiation and reject the bulk of the background radiation. A familiar example of this technique is found in photography where filters are used to enhance the contrast of chosen objects.

Fortunately, in the past few years, a large selection of good optical filters has become available to the designer of infrared equipment. Some of these filters are absorbing types which became available as a result of work done in the development of semiconductors. A family of transmission curves of such materials is shown in Fig. 1. Other useful filters are of the interference type. These filters are made by depositing many alternating layers of materials of the proper thickness on a transparent substrate. Here, the manufacturer can control the cutoff wavelength and transmission efficiency over a wide range of frequencies by his choice of materials and the thickness of the layers. A family of transmission curves demonstrating a selection of available interference filters is shown in Fig. 2. By choosing one or more of the various filters, the designer is able to isolate a wavelength band most suited to his purpose.[1]

If the equipment under consideration is to be used out-of-doors and under daytime conditions, the most serious background radiation will most likely be reflected sunlight or scattered sunlight. The sun, being an approximate blackbody radiator at a temperature of 6000°K, has its radiant energy peak at 0.5 micron; the wavelength of yellow-green light in the middle of the visible spectrum. Half of its radiant power occurs in the infrared wavelengths, or in wavelengths longer than 0.7 micron, 25 per cent of its energy is at wavelengths longer than 1.0 micron, and 2 per cent of its energy is radiated in wavelengths longer than 3.0 microns. Studies of the spectral appearance of sunlight reflected from clouds, land, and sea, show that it is much like the radiation directly from the sun itself, and therefore, the distribution given above still applies.

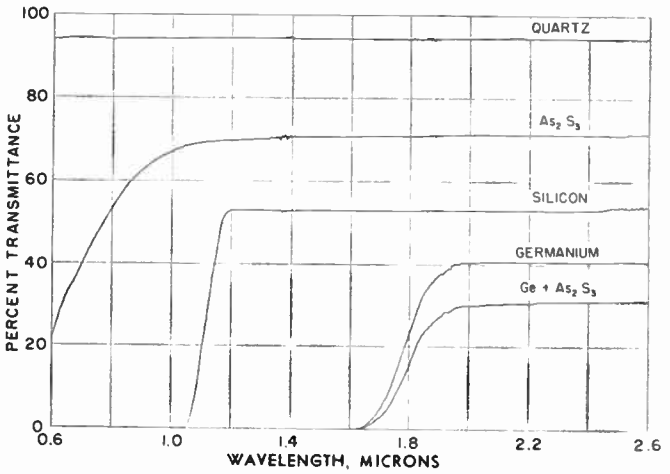

Fig. 1—Transmittance plot of wavelength cutoffs for five materials: quartz, As_2S_3, silicon, germanium, and Ge+As_2S_3.

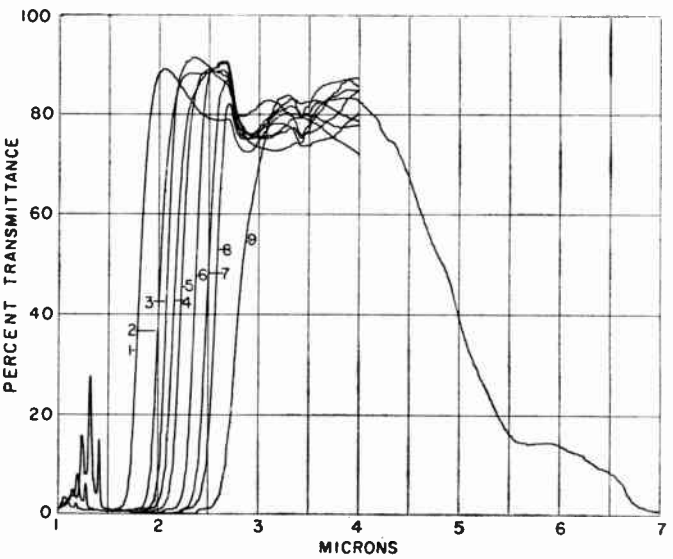

Fig. 2—Transmittance plot for Bausch and Lomb interference-filter series.

Now, if the source to be detected by the infrared receiver is observed against a sunlit background, the problem becomes one of filtering out as much sunlight as possible while admitting as much radiation from the source as possible. The source of interest will certainly be an object at a temperature much less than the sun, and consequently its radiation will occur predominantly at wavelengths further out in the infrared. A suitable filter for eliminating background radiation in this case would be a "low-pass filter," one which eliminates short wavelengths and passes long wavelengths. Examples of low-pass filters are shown in Figs. 1 and 2.

* Original manuscript received by the IRE, June 30, 1959.
† Naval Ordnance Test Station, China Lake, Calif.
[1] Additional filters are described by W. L. Wolfe and S. S. Ballard, "Optical materials, films, and filters for infrared instrumentation," paper 4.2.3, this issue, p. 1540.

The proper cut-off wavelength for such a filter can only be selected when the spectra of the source and the background are known. For example, a filter cutoff wavelength would be shorter for a device detecting a hot object, such as a light bulb, than for a device detecting a cooler radiator, such as a soldering iron. Furthermore, in selecting the filter, the transmission of the atmosphere and the spectral response of the detector must be considered, as both affect the amount of useful source radiation accepted by the receiver and the amount of interfering radiation from the background.

If the infrared equipment is intended for use at night, or in a wavelength band at approximately 4.0 microns or longer, the sunlight may not be a problem, as might ambient temperature radiators such as land, atmosphere, or the instrument itself. Now the problem becomes one of eliminating the longer wavelength radiation while passing the shorter wavelengths. Filters for this application are found among the absorbing types such as quartz, sapphire, or some of the glasses. These materials often can be incorporated into the system as optical elements. Also, the filtering action of the infrared detector itself can be considered, as its spectral response at the longer wavelengths may cut off abruptly.

Optical filtering is not the only means of enabling an infrared receiver to work in the presence of background radiation. Other techniques, such as discrimination on the basis of source size, or variation of source radiant intensity, may be used. However, it is perhaps the most powerful technique, and the skill with which it is employed directly affects the performance of the equipment.

Paper 4.4.1

Special Electronic Circuits for Nonimage-Forming Infrared Systems*

J. A. JAMIESON†, MEMBER, IRE

Introduction

To catalog completely the ingenious electronic circuits which have been used in infrared systems would be a long task. For this paper, three circuits of particular interest have been chosen. The three circuits deal with extraction of small signals from noise, suppression of background signals, and logical operations on high-level signals.

Matched Filters

A number of authors[1–3] have considered the detection of small signals in noise in the light of statistical decision theory as developed by Wald.[4] This theory is concerned with a voltage at a suitable point in a receiver circuit, as a sample function of a stochastic process for which the multidimensional, probability-density function is not completely known. (If the bandwidth and duration of the voltage are finite, only a finite number of dimensions are required.) Optimum detection then requires the testing of a hypothesis that the sample function was drawn from a population of signals and noises, against the hypothesis that the sample function was drawn from a population of noises alone. If the signal shape is known and the noise is supposed to be Gaussian, band-limited, additive, and white, then the appropriate test consists in computing the cross correlations of the expected signal with the observed sample, multiplying by a constant which depends upon the noise power and the signal energy, and comparing against a threshold.

The operations may be implemented in electrical circuitry by constructing a filter, its impulse response being the time image of the expected signal shape. The unknown voltage is fed into this filter, and the output is compared against a voltage threshold; its value, in practice, is chosen with respect to the prevalent noise level.

This theory may be applied to infrared search (pulse) systems, with the reservations that the noise is not usually white and may not be Gaussian if background noise is included. The first consideration may be overcome by conceiving of the filter as a cascade connection of three filters. The first converts the nonwhite noise (the power spectral density is assumed known) to a white spectrum, but distorts the signal. The second and third filters together form the optimum cross-correlating filter for the distorted signal. The second filter is then

* Original manuscript received by the IRE, June 30, 1959.
† Avionics Div., Aerojet-General Corp., Azusa, Calif.
[1] W. W. Peterson, T. G. Birdsall, and W. C. Fox, "The theory of signal detectability," IRE Trans. on Information Theory, vol. IT-4, pp. 171–212; September, 1954.
[2] P. M. Woodward, "Probability Theory and Information Theory with Applications to Radar," McGraw-Hill Book Co., Inc., New York, N. Y.; 1955.
[3] D. Middleton and D. Van Meter, "Detection and extraction of signals in noise from the point of view of statistical decision theory," *J. Soc. Industrial and Applied Math*, pt. I: 3, pp. 192–253, December, 1955; pt. II: 4, pp. 86–119, June, 1956.
[4] A. Wald, "Statistical Decision Functions," John Wiley and Sons, Inc., New York, N. Y.; 1950.

chosen as the inverse of the first, and the resulting cascade reduces to the third filter alone, which is a new form of matched filter for the original signal and non-white noise spectrum.[5]

Where the noise-power spectral density depends on the inverse first power of the frequency, this procedure results in a simple criterion for designing optimum filters. This criterion states that the optimum filter should be such that its response to a step input should be the delayed time image of the expected signal. For distant targets, the shape of the expected signal is determined by the distribution of energy within the image of a point source in the system telescope, and by the shape and motion of the system reticle or detector arrangement. For many systems, the signal is well approximated by a sinusoidal pulse train at a frequency determined by the number of reticle bars crossed per second by the target image, and of a duration determined by the dwell time of the signal on the system detector.

The approximate filter for the signal and noise described is illustrated in Fig. 1. This filter, followed by a threshold circuit, forms a good receiver under the given assumptions.[6] The level of the threshold is, in practice, chosen according to the methods of Marcum[7] to satisfy the system requirements for average false-alarm time and signal-detection probability.

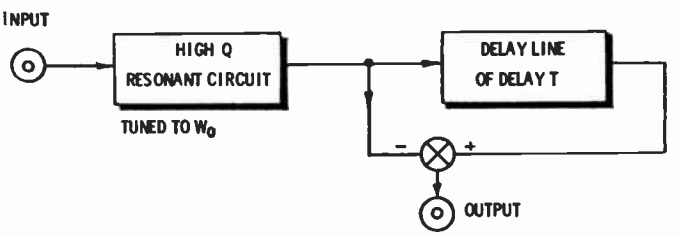

Fig. 1—Optimum filter for a signal $S(t)=A \sin W_0 t$; for $0 \leq t \leq T$ and noise with power spectral density proportional to W^{-1}.

The filter described forms a standard for comparison of other filters. It is rarely used in practice, because of the size and complexity of the required delay lines. Computation from theory and experiment shows that simpler resonant circuits of optimum "Q" are capable of attaining 90 per cent of the output signal-to-noise ratio achieved by the standard filter.

The previously described filter optimized the peak signal-to-rms-noise ratio for a particular signal and noise spectrum. It is of interest to ask whether this form of signal is the best that could be chosen. The statistical decision analysis shows that the efficacy of a signal (of fixed bandwidths) for maximum detectivity depends only on the energy content. This radiation flux density at the entrance aperture of the system cannot be changed by operations on the system. The maximum peak value of the signal is proportional to this flux density (with a constant of proportionality set by the system aperture, optical gain, detector responsivity, etc.) and consequently, for a given dwell time, the best that can be done with the signal is to maintain it near the peak value for the greatest possible fraction of its duration.

However, system detectivity may not be the only design criterion. The output of the optimum filter for a pulse train has several local maxima (corresponding approximately to the maxima of the signal auto-correlation function). These several maxima may give rise to ambiguity in detecting the time of occurrence of the signal, and, hence, the bearing of a target. It turns out that the theory of error-correcting codes supplies criteria for selecting signals whose auto-correlation functions have only one large local maximum. These signals offer an escape from ambiguity errors in accurate resolution of targets, particularly where large dynamic ranges are encountered, at some sacrifice in detectivity.

Background Signal Rejection

The detectivity of many infrared systems is limited more by irrelevant radiation signals from clouds, the ground, etc., than by noise generated inside the system itself. One way in which such background radiations may sometimes be distinguished from target radiations is by their spectral distribution of energy.[8] To exploit this characteristic, where it exists, systems have been designed to use multiple radiation detectors, some of which are made sensitive to radiation at one wavelength and some at another. These detectors may be physically separate, sharing the aperture of the telescope, or they may be the same detectors operating in one mode at one time and in the other in the succeeding interval. This type of background rejection may be instrumented optically or electronically. It may, for instance, be arranged that a change in the ratio of the signals from one set of detectors to the signal from another set indicates that a target is in the field of view, while a change in the level of all signals merely indicates a change in the level of background radiation.

It has been proposed to compute such ratios by the use of two channels of logarithmic amplification, one from each set of detectors with subtraction of their outputs, or, in the time-sharing case, with subtraction of a direct signal and a delayed signal. However, logarithmic amplifiers may become cumbersome, and may not be suitable for inclusion in the other operations of a processing chain. Consequently, other nonlinear circuits have been developed in which the two sets of signals are

[5] L. A. Zadeh and J. R. Raggazzini, "Optimum filters for the detection of signals in noise," Proc. IRE, vol. 40, pp. 1223–1231; October, 1952.

[6] This receiver is not ideal unless previous knowledge about the amplitude and phase of the signal is used in applying the threshold decision.

[7] J. I. Marcum, "A Statistical Theory of Target Detection by Pulsed Radar," The RAND Corp. Research Memorandum RM-754, December, 1947; Mathematical Appendix R113, July, 1948.

[8] L. W. Nichols, "Optical filtering," paper 4.3.3, this issue, p. 1569.

amplified in AGC amplifiers, subtracted, and fed back through integrators or lag circuits to control the gain of the AGC amplifiers. By suitable selection of gains and of the form of the feedback in the AGC gain circuit, the difference of the outputs of the AGC amplifiers can be made to be very small under steady-state conditions but to show a sharp transient when the ratio of the inputs changes abruptly.

New-Target Circuits

Search and surveillance systems may be required to follow multiple-target situations and to be able to determine when a new target appears in the field of view. Memory and logic circuits have been developed for this purpose. A byproduct of the use of these circuits is an improvement in detectivity of the system by virtue of the two-dimensional correlation function allowed by the circuit.

These circuits use two memories. The signals obtained on one frame are amplified, filtered, checked for amplitude relative to noise, and recorded in one memory. On the next frame, the signals received are compared with the recording of the previous frame and recorded on the second memory. At the end of the second-frame time, the first memory is erased and the second prepared for reading. Comparison between present signals and those from a previous frame make possible a variety of logical operations. It is also possible to use rapid read-out for presentation on a short persistence (frame time) display.

Paper 4.4.2

Infrared Data Presentation*

RICHARD K. McDONALD†

INFRARED displays are as varied as the equipments they symbolize. In some devices, the problem of display is solved by the basic detection process itself. Among these are the thermal imaging tubes, such as the evaporograph and the metascope. The infrared image, projected on one side of a membrane, is recognized on the reverse side by a change in one of the optical properties of the film; *e.g.*, by differences in surface reflection, transmission, or the emission of a phosphor coating. Such a convenient process is lacking in the case of most detectors and applications of infrared.

Logical groupings of equipment can be based on display requirements; particularly, how rapidly the data must be processed and how much information about the target is needed. All that may be needed is warning that an object is approaching from a certain aspect, or, at the other extreme, a photograph may be wanted of the same area with all possible detail. Sample groupings are shown below.

Data Type	Target Variables	Usual Display	Representative Equipments
Perishable	One	Neon flash lamp pips	Gun sight Proximity warning indicator
Perishable	Many	Cathode-ray tubes	Air-to-air search Battlefield surveillance
Permanent	One	Oscillograph	Railroad "hotbox" detector Rapid scan spectrometer
Permanent	Many	Film	Air-to-ground mapper Commerical camera

* Original manuscript received by the IRE, June 30, 1959.
† Boeing Airplane Company, Renton, Wash.

In actual practice, more than one display mode may be encountered; one to monitor equipment functions, and the other for permanent records. Seldom are simple meter readings adequate, as they are in radiometry and range finding.

Cathode-Ray Tubes

Radar and infrared are continually being compared to each other. Regarding displays, infrared is associated with a greater variety of techniques, but none are as complex as the general category of radar scopes. There are no range or velocity gates, moving target indicators, or jamming to affect displays. Rather than the familiar dimensions of range vs horizontal angle found with radar scopes, infrared has vertical angle vs horizontal angle.

In sophisticated infrared systems, as with airborne early warning, other information may be simultaneously displayed; the past history of the subjects, or correlative data from radar, television, or a second infrared set responding to other wavelengths. Cathode-ray displays for infrared require the customary variable controls such as amplitude gating level, clipping level, and gain.

Memory or variable persistence tubes are useful, much as for radar; target enhancement occurs by integration of the signals and by cancellation of the noise. This is accomplished by the eye with cathode-ray tubes, or by the gray scale retention of the memory tube.

With their characteristic narrow beamwidths, infrared systems aboard ship or aircraft are sensitive to platform attitude. Display corrections can be made electrically by shifting the raster up and down for pitch, and right and left for roll in synchronism with the platform

movements. Targets within the frame will appear to remain stationary, although the picture frame moves about.

Usually, the only times PPI type scopes (horizontal angles displayed radially) are encountered is when the scanner actually moves through a circular total field of view. Distance from center represents vertical angle. An interesting variant is to split the scope into four concentric rings, each ring belonging to a different scan. The history of the three previous scans is then always available for comparison with the most recent trace.

Neon bulbs have been incorporated into another PPI-like configuration. In this apparatus, six concentric phosphor rings on the display panel are activated by six rotating neon lamps. Each ring associated with one detector represents a specific elevation sector seen during the 360° azimuthal scan.

Neon Glow Tubes

A common engineering problem with infrared is that of processing the information from multiple detector systems. Hundreds of detectors wtih individual amplifiers may be employed. When each output needs to be retained intact to the display, oscilloscopes and oscillographs are replaced by arrays of neon glow tubes with each lamp's intensity modulated by the detector it represents.

The bank of stationary neon lamps can be viewed directly. One multiple detector unit built for the Navy has an oscillating presentation mirror phased with the radiometer's line-of-sight. To the observer, the lamps appear to flash at angular positions corresponding to the actual target coordinates. Where geometry prevents direct viewing, the lamps can be watched with a television camera or a scanning phototube.

Infrared gun sights must meet severe restrictions in weight, volume, and configurations. Advantage is usually taken of the persistence-of-vision effect of the eye to simplify the equipment. A common shaft drives the chopping reticle in front of the detector and a similar mask before a flash lamp which can be seen by the operator. Should the reticle have pairs of slits like sides of a "V," the two flashes of light generated as the detector spots the target successively through the two sloping lines appear to the observer as an "X." The target's position is at the center of the intersection. Aiming the gun is accomplished by orienting the intersection over internal crosshairs.

This procedure, using synchronously rotated masks over detector and flash lamp for direct viewing, works equally well for multiple detectors. There are many ways of coding the presentation symbols—triangles, bars, circles, etc.—to show the target location. In general, the principle is that an off-centered target causes only one or two aperture images to be activated, while an on-center target activates all apertures in a symmetrical pattern.

Film Methods

With their flat frequency response from dc to 150,000 cps, neon tubes have become indispensable when the goal is to record the best possible detail on film. Commercial use has been made in one infrared camera wherein the radiometer makes a raster-type scan over the field of view. Coupled to the back of the large panning mirror is a small mirror that causes the image of the modulated neon lamp to sweep across a Polaroid film in direct correspondence with the radiometer's position.

One airborne mapper of the pushbroom variety has a line of fixed detectors oriented crossways to the aircraft heading. During flight, a strip of ground parallel to the aircraft path is viewed by the system. The display uses multiple neon lamps placed at right angles to photographic film that is moving at a velocity to match the aircraft ground speed.

The need for individual neon tubes arises because it is not always possible or desirable to combine multiple sources into a single channel. The use of switching devices requires each output to be sampled once per dwell time with no signal distortion. In addition, where the display is a cathode-ray tube, the sampling rate must be high enough to minimize flicker.

An alternate way to obtain a moving film record is to photograph the intensity-modulated, single-line trace of an oscilloscope. One airborne mapper uses this procedure. The electron beam is deflected to make a line trace corresponding to the radiometer's scanning motion, with beam intensities governed by the strength of the infrared signal. As it moves perpendicularly to the line trace, the film reproduces a strip map of the ground.

Paper 4.4.3

Infrared Color Translation*

M. B. GRIER†, SENIOR MEMBER, IRE

The Nature of the Color-Translation Process

THE principle of color translation seems to have developed earliest for the ultraviolet portion of the spectrum. The first successful applications lay in the field of microscopy.[1–3] It was observed that some objects which show little contrast in the visible spectrum have marked absorption bands in the ultraviolet, so that by photographing such objects in ultraviolet radiation, contrast and visibility are increased.

The principle has been applied to a restricted region of the near-infrared spectrum in the form of color-translating infrared color film, where it has demonstrated successful ability to detect camouflage.

Color translation may be considered to be a method of abridged spectrophotometry. In a typical spectrophotometric analysis, absorption or emission spectra are observed over the region of interest as a means of identification. The infrared portion of the spectrum has been particularly fruitful in furnishing spectral structure for this purpose. Usually, the object of interest is a small uniform sample. When it becomes desirable to analyze complex distributions of matter, it is difficult to record complete emission or absorption spectra of all objects of interest.

An abridged method, therefore, presents spectral behavior from selected spectral regions, and by optically superimposing the data upon a visual screen, the spectra may be visually integrated and interpreted by the observer. In this fashion, the spatial distributions of the unknown objects of interest are preserved, and spectral data are also available for identification of the unknown.

Selective thermal emission occurs in the same spectral regions in which selective absorption of radiant energy takes place; therefore, a substance will selectively emit at the location of its absorption bands. Analysis by color translation may be described as a method of abridged absorption spectrophotometry for observation with external illumination (active mode) and a method of abridged emission spectrophotometry for observation by thermal emission from an object (passive mode).

* Original manuscript received by the IRE, June 30, 1959.

† Nortronics, a Division of Northrop Corporation, Hawthorne, Calif.

[1] E. M. Brumberg, *Compt. Rend. Acad. Sci., URSS*, vol. 25, p. 473; 1939.

[2] E. H. Land, E. R. Blout, D. S. Grey, M. S. Flower, H. Husek, R. C. Jones, C. H. Matz, and D. P. Merrill, "A color translating ultraviolet microscope," *Science*, vol. 109, pp. 371–374; April 15, 1949.

[3] V. K. Zworykin and Fred L. Hatke, "Ultraviolet television color-translating microscope," *Science*, vol. 126, pp. 805–810; October 25, 1957. (The present author independently discovered the principle of color translation in 1949.)

System Function

The principle of operation of a color-translating system is demonstrated in the simplified schematic shown in Fig. 1. A scanning system projects the image to be observed through an optical analyzer, distributing the optical energy into three channels. Each channel contains information from a portion of the spectrum essentially different from that of the other two. After amplification, the images are reproduced in three visual channels and combined in an optical synthesizer. For example, the three channels may peak at 3.6 microns, 4.5 microns, and 5 microns, respectively. The image in each extravisual channel is thus converted to a primary color image in the visible region of the spectrum. By this process, spectral bands in the invisible portion of the spectrum are shifted to corresponding spectral bands in the visible portion of the spectrum, rendering the invisible "colored" image visible in color to the human eye.

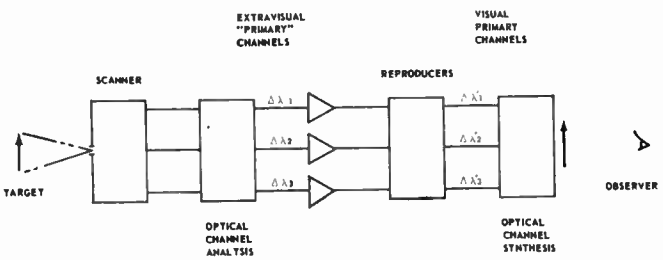

Fig. 1—Basic elements of a color-translating system.

Infrared Tristimulus Values

We may write for the infrared tristimulus values $(X)_{IR}$, $(Y)_{IR}$, and $(Z)_{IR}$, of a Planckian radiator

$$(X)_{IR} = \frac{1}{\pi}\int_{\lambda}\iint N_b(\lambda)R_1(\lambda)\tau_0(\lambda)\tau_a(\lambda)\frac{\cos\alpha_s\cos\alpha_r}{r^2}dS_s dS_r d\lambda$$

$$(Y)_{IR} = \frac{1}{\pi}\int_{\lambda}\iint N_b(\lambda)R_2(\lambda)\tau_0(\lambda)\tau_a(\lambda)\frac{\cos\alpha_s\cos\alpha_r}{r^2}dS_s dS_r d\lambda$$

$$(Z)_{IR} = \frac{1}{\pi}\int_{\lambda}\iint N_b(\lambda)R_3(\lambda)\tau_0(\lambda)\tau_a(\lambda)\frac{\cos\alpha_s\cos\alpha_r}{r^2}dS_s dS_r d\lambda$$

with analogous equations for non-Planckian radiators, where

λ = wavelength
$N_b(\lambda)$ = spectral radiance of a "complete" or Planckian radiator
$R_K(\lambda)$ = relative response of channel K to equal energy spectrum
$\tau_0(\lambda)$ = spectral transmittance characteristic of the optical system
$\tau_a(\lambda)$ = spectral transmittance characteristic of the atmosphere
α_s = angle made with the normal to a source by the direction of propagation
α_r = angle made with the normal to a receiver by the direction of propagation
r = distance between the source and receiver
dS_s = area of the source
dS_r = area of the receiver.

Calculation of the Color-Translated Trichromaticity Coordinates

The tristimulus values of the visual primary colors (phosphors) under excitation by the target signals may be obtained in a manner similar to that used for determining the color-translated tristimulus values. Then, the tristimulus values X_{ct}, Y_{ct}, and Z_{ct} of the color-translated image will be

$$K_1(Y_1)_{IR}X_1 + K_2(Y_2)_{IR}X_2 + K_3(Y_3)_{IR}X_3 = X_{ct}$$
$$K_1(Y_1)_{IR}Y_1 + K_2(Y_2)_{IR}Y_2 + K_3(Y_3)_{IR}Y_3 = Y_{ct}$$
$$K_1(Y_1)_{IR}Z_1 + K_2(Y_2)_{IR}Z_2 + K_3(Y_3)_{IR}Z_3 = Z_{ct}$$

where

$X_k, Y_k, Z_k \equiv$ tristimulus values of visual primary color, K
$(Y_n)IR \equiv$ normalized response of infrared channel, n
$K_1\ K_2,\ K_3 \equiv$ over-all channel gain values, chosen so that the reference radiator will appear as the desired visual reference source.

If we let

$$X_{ct} + Y_{ct} + Z_{ct} = \Sigma_{ct},$$

the chromaticity coordinates of the color-translated image are

$$x_{ct} = \frac{X_{ct}}{\Sigma_{ct}}, \qquad y_{ct} = \frac{Y_{ct}}{\Sigma_{ct}}, \qquad z_{ct} = \frac{Z_{ct}}{\Sigma_{ct}}.$$

Color-Translated Planckian Radiators

As an example of the application of color translation theory, we may consider the appearance of Planckian radiators.

When the chromaticity coordinates of Planckian radiators at various temperatures are plotted in the visual system on the CIE chromaticity diagram, a color temperature locus[4] is obtained, as indicated in Fig. 2.

A Planckian radiator of temperature 600°C appears on this locus close to the spectrum locus in the red. As the temperature of a Planckian radiator is increased, its position on the locus shifts in succession to the orange, yellow, white, and blue, as indicated on the diagram. Planckian radiators of high temperature converge to the infinity point on the locus.

In the color-translated system, this locus is altered in a characteristic and useful way. This may be explained by considering the radiance peak of a blackbody radiator according to Wien's Displacement Law. This peak migrates to shorter wavelengths as the temperature is increased. Assume that the channel peak responses of the color-translating system lie at 3.6, 4.5, and 5 microns, and that these channels represent visual blue, green, and red, respectively. Relatively cold objects peaking at long wavelengths will appear red, while hotter objects peaking at shorter wavelengths appear blue. Objects of intermediate temperature tend to remain a neutral color or white.

Fig. 3 shows the color-translated chromaticity coordinates of a series of Planckian radiators of varying temperature superimposed on measured values obtained with filters of the above peaks. The theoretical values were obtained with ideal filters, while the measured values were obtained with corresponding real band-pass filters with a PbSe detector.

The reference Planckian radiators were 400°K and 394°K, respectively. It is seen that the correspondence between the theoretical and the observed values is close. The chromaticity coordinates for the color-translated Planckian radiators thusoccupy a locus similar to the visual system, but in the former case, the locus is much elongated, particularly at ordinary ambient temperatures.

Applications

The color-translation process is versatile, the applications being manifold. There are possibilities in the observations of astronomical, terrestrial, and microscopic subjects.

In space flight, a particular use is color-translation photography of the planets. By this means, it may be possible to map the location of the various substances comprising the planetary surface and the constituents of the planetary atmospheres.[5] Contrast may be enhanced by the selection of each of the three channels in such manner as to coincide with a characteristic absorption band of interest. For example, oxygen, water, and CO_2 might thus be mapped in a planetary atmosphere.

[4] Committee on Colorimetry, Optical Society of America, "The Science of Color," Thomas Y. Crowell Co., New York, N. Y., p. 304; 1953.

[5] See for example G. P. Kuiper, "The Atmospheres of the Earth and Planets," The University of Chicago Press, Chicago, Ill., p. 326; 1949.

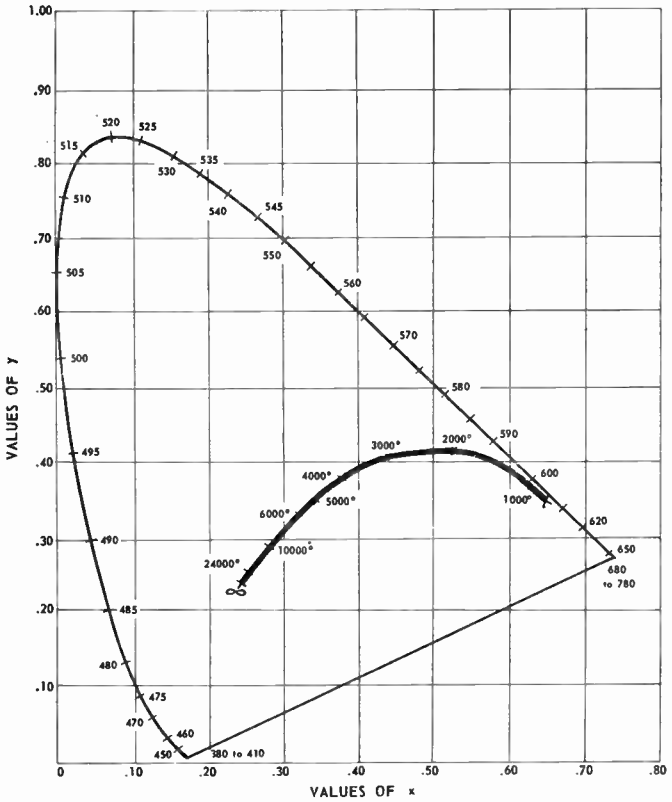

Fig. 2—Chromaticity diagram showing locus of color temperature (in degrees Kelvin) of Planckian radiators in the visual system.

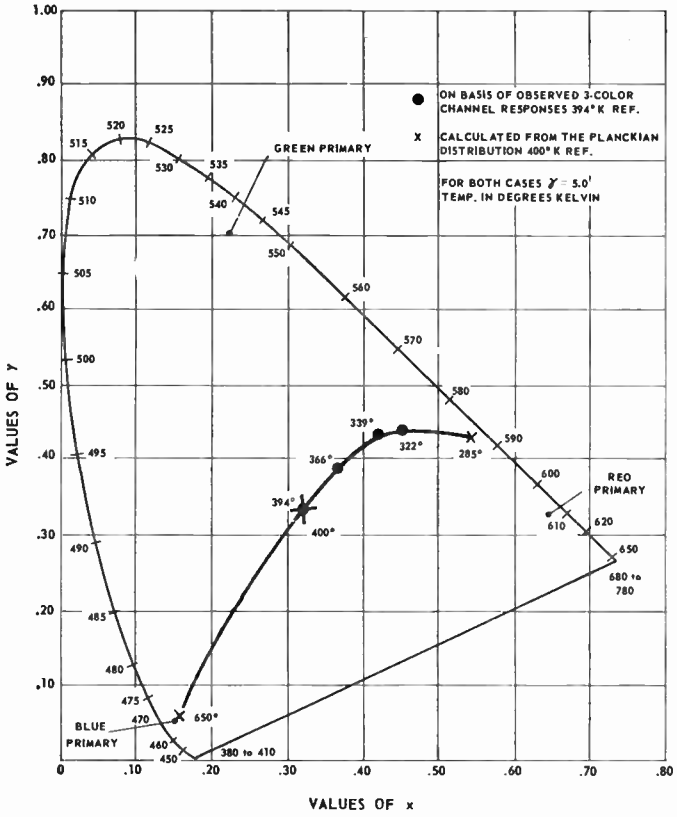

Fig. 3—Observed and theoretical color-translated trichromaticity coordinates of Planckian radiators.

It is thus possible to map the location of poisonous constituents, such as methane, that may exist in a planetary atmosphere.

The mode of operation in this case may be by reflection of the solar radiation from the planetary surface in the region up to three microns, and by passive thermal emission in the region beyond about three microns. Among many military applications,[6] the possibilities for the detection of camouflage are of considerable importance.

[6] The pioneer work of H. Dauber and associates at SRDL, Ft. Monmouth, N. J., has been outstanding in this field.

Applications in the field of microscopy have, as mentioned above, been confined to the ultraviolet region. However, due to the great abundance of detailed spectral structure of substances in the infrared,[7,8] the potentialities of color translation in this portion of the spectrum may be more fruitful than on the short wavelength side of the visual. The use of infrared stains may add to this versatility.

[7] R. Wegmann, "Spectrographie dans l'infrarouge. VIII. Les acides desoxyribo-et ribonucleiques du noyau," *Acta Histochem.*, vol. 4, pp. 132–140; 1957.

[8] G. B. B. M. Sutherland, "Infrared analysis of the structure of amino acids, polypeptides, and proteins," *Advances in Protein Chem.*, vol. 7, pp. 291–318; 1952.

Paper 4.4.4

Servomechanisms Design Considerations for Infrared Tracking Systems*

J. E. JACOBS†, SENIOR MEMBER, IRE

Introduction

THE objective of an infrared tracking system is to provide information on the angular location of a real or apparent source of radiation. Such information may be in the form of estimates of the direction angles of the line-of-sight (*i.e.*, the line in space joining the source centroid[1] and the radiation aperture of the tracker), estimates of the angular rates of the line-of-sight, or both. The tracking system will have an optical axis, *i.e.*, that unique direction such that a fixed point source located in this direction produces the static equilibrium state of the tracking system.

Two general classes of systems can be used to provide the requisite information, namely open-loop systems and closed-loop systems. In the open-loop system, the optical axis is oriented in a known direction, and the angular difference (error angle) between this axis and the line-of-sight causes an output signal from which the error angle can be estimated by a predetermined calibration. In the closed-loop system, the signal caused by the detected error angle actuates a drive mechanism to rotate the optical axis toward the line-of-sight. The drive ceases when signals corresponding to the equilibrium state are achieved. Angle pick-off devices provide information on position of the optical axis, and electrical signals corresponding to drive rates provide read-outs on angular rates. In applications where unattended, automatic tracking is desired over sizeable ranges of line-of-sight angles, a closed-loop system offers significant performance advantages, in that information can be maintained with small field-of-view optical systems. Only this type of system will be considered in what follows.

The information flow for a closed-loop system is shown in Fig. 1. A brief description of each of the processes follows. The radiation receiver and optical processor has the function of gathering the radiation, performing spectral selection or filtering, encoding for error angle and pattern (size and shape of image) recognition, providing spatial selectivity (field-of-view limiting), and transmitting the processed radiation to the detector. The detector converts the radiation to a corresponding electrical signal, a typical conversion being output voltage proportional to incident radiation power. The electrical processor acts to select the error angle information pertinent to the source being tracked from the signal, noise, and other perturbing signals (introduced from competing sources, channel disturbances, or system noise). The compensating network filters the signal as necessary to obtain from the tracking system the desired dynamic performance. The electromechanical transducer transforms these electrical signals to the desired motions which orient the telescope so that its optical axis coincides with the line-of-sight.

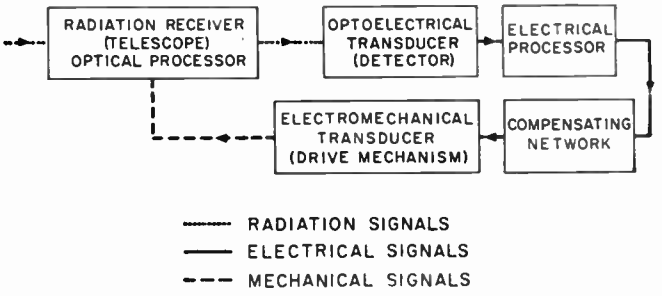

Fig. 1—Infrared tracking system information flow.

Orientation of the telescope requires all of the above processing to be done for each of the two degrees of freedom of the system. (These can be thought of as the two independent-direction cosines, the polar and azimuth angles in spherical coordinates, or as any other two variables convenient for the problem). In general, then, two channels or two sets of processors are required although certain components can be common. For example, one telescope might encode two-dimensional information as amplitude and phase of the radiation waveform envelope, permitting the use of one detector and common equipment for much of the electrical signal processing. The use of as much common processing as possible is usually urged by considerations of space, weight, power consumption, and economy. Associated with this type of system is an inevitable interchannel coupling, or crosstalk. For purposes of simplicity, we shall assume such coupling to be nonexistent or negligible and consider only a one-dimensional tracking system.

Linear Servo Design

The synthesis of the servo system must begin with a specification of required performance. For most systems, some degree of proportional control is desirable, and hence a reasonable procedure is to synthesize a linear servo system and modify its parameters as necessary to

* Original manuscript received by the IRE, June 30, 1959.
† Hughes Aircraft Co., Culver City, Calif.
[1] The term source centroid refers to the location in the object plane where a point source of radiation could replace the actual source with no detectable change of the line-of-sight direction as seen by the tracking system.

maintain adequate performance in the regions of nonlinear operation. A set of specifications for a linear servo appropriate to the task would include, as a minimum, numerical limits on bandwidth, damping of the dominant poles, and appropriate values for the error coefficients. Other constraints may be imposed by the intended application. The values of the limits must be derived from the required performance and the physical situation which obtains at system employment.

The servo bandwidth can be related to the information rate which is necessary to do the desired tracking. To give a brief example of this calculation, consider the following optical or infrared missile guidance application. Let the guided missile be at range R, moving with a relative velocity, V_R, in a coordinate system fixed to the target. V_R is directed toward the point of closest approach which is a distance M from the target. The geometry is shown in Fig. 2.

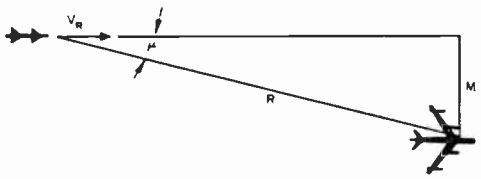

Fig. 2—Guided missile geometry.

The angular rate of the line-of-sight due to geometry factors is

$$\dot{\mu} = \frac{V_R \sin \mu}{R} = \frac{V_R M}{R^2} . \tag{1}$$

Assume the seeker to be of a scanning type with a scanning period of τ_s; then the change in μ per sample is $\dot{\mu}\tau_s$, or

$$\Delta\mu = \frac{V_R M \tau_s}{R^2} . \tag{2}$$

Suppose we desire the tracking accuracy to be maintained to an angular error of less than δ_μ. Since the problem is really in two dimensions, the number of solid-angle cells, n, which the tracker must choose on each scan is

$$n = \frac{(\Delta\mu)^2}{(\delta_\mu)^2} = \frac{V_R^2 M^2 \tau_s^2}{R^4 (\delta_\mu)^2} . \tag{3}$$

The amount of information transfer, I, in such a choice is log n or

$$I = 2 \log \frac{V_R M \tau_s}{R^2 \delta_\mu} \tag{4}$$

and the information rate, C, since the transfer occurs in each τ_s time interval, is

$$C = \frac{2}{\tau_s} \log \frac{V_R M \tau_s}{R^2 \delta_\mu} . \tag{5}$$

The relationship between this information rate and the required bandwidth is given by Shannon's mean-power theorem[2,3]

$$C \leq W \log (1 + P/N); \tag{6}$$

where

C = the maximum channel capacity or information rate as above,

W = the bandwidth in cycles per second,

P = the mean signal power, and

N = the mean noise power.

The equality in the Shannon theorem holds only for optimum coding. In missile guidance applications, simple, "instantaneous" coding is ordinarily employed. We may account for this by artificially depressing the signal-to-noise ratio. In the case of the missile seeker, we may assume the true signal-to-noise power ratio varies approximately as R^{-4} due to the R^{-2} law of energy propagation and the square-root-law behavior of photoconductive detectors; *i.e.*, voltage output is proportional to incident power.

With these considerations in mind, an applicable form of the theorem is

$$C = W \log \left[1 + K \left(\frac{R_0}{R} \right)^4 \right], \tag{7}$$

where

K = the signal-to-noise correction factor for nonoptimum coding,

R_0 = the range at which the true signal-to-noise ratio is unity.

Equating (5) and (7), the required bandwidth is found to be

$$W = \frac{2 \log \dfrac{V_R M \tau_s}{R^2 \delta_\mu}}{\tau_s \log \left[1 + K \left(\dfrac{R_0}{R} \right)^4 \right]} . \tag{8}$$

It can be seen that the bandwidth requirements decrease with increasing range and, in fact, become negative at long ranges. This merely reflects the fact that the angular change in target position due to relative motion becomes smaller than the allowed error, δ_μ, at long ranges. For a nonadaptive or fixed bandwidth servo, the requirement will be determined then at the minimum range which is, of course, the miss distance M.

[2] A. E. Puckett and S. Ramo, eds., "Guided Missile Engineering," McGraw-Hill Book Co., Inc., New York, N. Y., ch. 6; 1959.

[3] C. E. Shannon, "Communication in the presence of noise," PROC. IRE, vol. 37, pp. 10–21; January, 1949.

Substituting M for R and noting that

$$K\left(\frac{R_0}{M}\right)^4 \gg 1,$$

$$W_{max} = \frac{2\log\left(\frac{V_R\tau_s}{M\delta_\mu}\right)}{\tau_s \log\left[K\left(\frac{R_0}{M}\right)^4\right]}. \quad (9)$$

Taking as representative values:

$V_R = 10^3$ ft/s
$\tau_s = 10^{-2}$ s
$M = 10$ ft
$\delta = 10^{-3}$ rad
$K = 10^{-1}$
$R_0 = 10^{-5}$ ft,

we obtain $W_{max} = 40$ cps.

The treatment in this example is incomplete. No account has been taken of other factors which tend to increase the apparent line-of-sight rates and hence require additional bandwidth. An example of these factors is the coupling of missile body motion into the seeker. Thus, to conserve bandwidth, this coupling should be minimized, *i.e.*, the seeker should be space stabilized. We have also neglected the dynamics of the missile and the seeker look angle limitations, which may preclude any effective use of information during the terminal stages of flight and hence allow the use of a larger minimum range in (8) to reduce bandwidth requirements.

To return to a discussion of the servo specifications, we mention next the damping factor for the dominant poles of the system. The requirement here is determined by the permissible rise time and overshoot which can be tolerated in the transient response of the tracking system. A thorough discussion of the relationships of these characteristics and damping in second-order systems is contained in the literature of servomechanisms.[4] The second-order system approximation is compatible with the simplifications employed in the initial synthesis consideration presented here. The values of rise time and overshoot allowable will depend on the application and possibly on the tie-in of tracking to the over-all system function. In a missile guidance application, the latter factor is certainly important and the lack of definition of an over-all system precludes any quantitative discussion here. It might be pointed out, however, that two perturbations influencing the choice of this specification are: 1) the transients due to positioning errors in initial acquisition of the target by the seeker, usually dominating the damping requirements at low signal-to-noise ratio, and 2) the transients due to resolution of multiple sources at close approach to the target, usually dominating the damping requirements at high signal-to-noise ratio. Application of analysis to the usual missile guidance situation yields a range on damping factor of $0.5 \leq \zeta \leq 1.0$.

The error coefficients[5] specified for an infrared or optical tracking system merit some special attention. The error coefficients of a servo system are inversely related to the steady-state errors experienced in the servo for unit disturbances of position, velocity, acceleration, etc.; *i.e.*, a large error constant implies a small steady-state error.

Since in the systems of interest here, a limited field-of-view is desired (for background interference reduction) and must be positionable over an extended angular range from any reference direction, a large position error constant is probably implied. A second consideration is that accurate line-of-sight rate information may be a required system output. If this is so, a nonzero velocity error coefficient is required. It is customary practice, because of these considerations and the desire to avoid undue complexity, to specify an infinite position error coefficient, a finite, nonzero velocity error coefficient and zero values for higher derivative error coefficients. Stated in another way, it is customary to use velocity-coupled servomechanism systems for optical or infrared tracking.

Having translated the system performance into servomechanism specifications, the designer may proceed with the system design by standard synthesis techniques.[6]

Nonlinear Considerations

Nonlinearities appear in the tracking system both by intent and by inadvertence. In the former category are design features, such as field-of-view limiting and optical axis angular-rate limiting, which are often included to accomplish specific performance objectives. The latter category includes departures in realizable component behavior from the desired idealistic behavior as, for one example, the unintended "wiggles" or "fine structure" appearing on the error characteristic,[7] due to space filtering and signal-processing filter characteristics or, for a second example, the dependence of electromechanical device parameters on driving signal levels. In any case, the effects of these nonlinearities on the performance of the tracking system may be of significance; hence some analysis is usually in order.

Simplifying approximations, which make the mathematical description of the system tractable for parametric studies, are usually justified by the insight into system operation which is obtained when such studies can be performed. Evaluation of nonlinear system dynamics of higher accuracy than is available by the "pen-

[4] H. M. James, N. B. Nichols, R. S. Phillips, "Theory of Servomechanisms," McGraw-Hill Book Co., Inc., New York, N. Y., sec. 4.2; 1947.

[5] *Ibid.*, sec. 4.4.

[6] J. G. Truxal, "Automatic Feedback Control System Synthesis," McGraw-Hill Book Co., Inc., New York, N. Y., ch. 5; 1955.

[7] The error characteristic is the functional relationship (usually expressed graphically) between the error angle and the input signal to the compensating network.

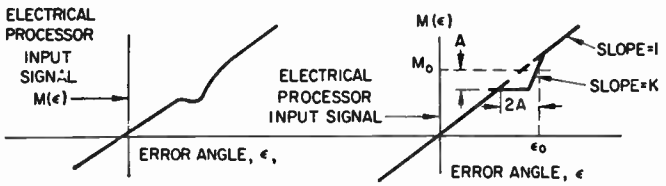

Fig. 3—Error characteristic, and its approximation for analytical purposes. (a) error characteristic; (b) error characteristic approximations.

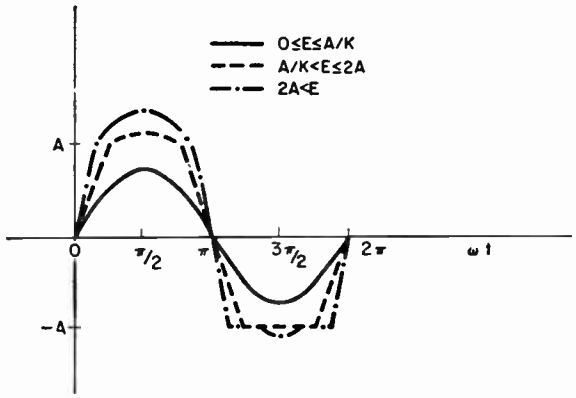

Fig. 4—Waveform of $M'(\epsilon)$.

cil and paper methods," or manual analysis techniques, referred to above, is in general performed by system simulation.[8] An example of approximate analysis by manual techniques is described to illustrate the point.

In the example, we are concerned with the effect of the "wiggles" referred to above on the tracking system stability. In Fig. 3(a), we show a portion of an actual error characteristic, and in Fig. 3(b), the approximate representation for analysis purposes. This characteristic is observed in the optical processor of a velocity-coupled tracking servo. The question posed is, "What values of the notch parameters A and K are permissible consistent with system stability?" To answer this question, the following technique may be used. The system is assumed to be tracking a source moving at a constant angular rate so that, because of the velocity coupling, a steady-state error of ϵ_0 ensues. (Constant input signal of M_0 to the drive mechanism gives an optical axis angular rate equal to the assumed line-of-sight rate.) Since we are interested in perturbations from this steady-state equilibrium point, we generate the describing function[9] for the nonlinear characteristic model about this point. The describing function, N, is a gain factor whose value depends on the amplitude of the assumed sinusoidal driving function. For a given value of N, the amplitude of the fundamental component of the output depends only on A and K. A root-locus plot of the system poles with N as the variable gain defines the value of N for which instability ensues. For this value of N,

[8] H. F. Meissinger, "Simulation of infrared systems," paper 4.4.6, this issue, p. 1586.
[9] J. G. Truxal, *op. cit.*, ch. 10.

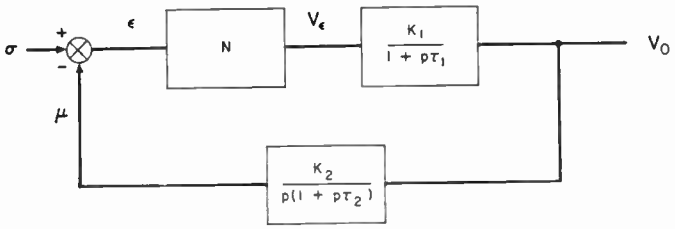

N — DESCRIBING FUNCTION OF THE NON-LINEARITY
K_1 — 100
τ_1 — 0.01 SEC
K_2 — 0.167 DEG/VOLT-SEC
τ_2 — 0.0075 SEC
σ — LINE-OF-SIGHT ANGLE
μ — OPTICAL AXIS ANGLE
ϵ — TRACKING ERROR ANGLE
V_ϵ — ERROR SIGNAL VOLTAGE
V_0 — OUTPUT SIGNAL VOLTAGE

Fig. 5—Simplified one-channel tracking system.

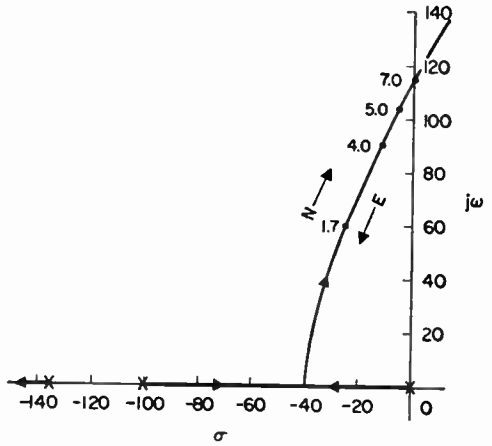

Fig. 6—Root locus of tracking system.

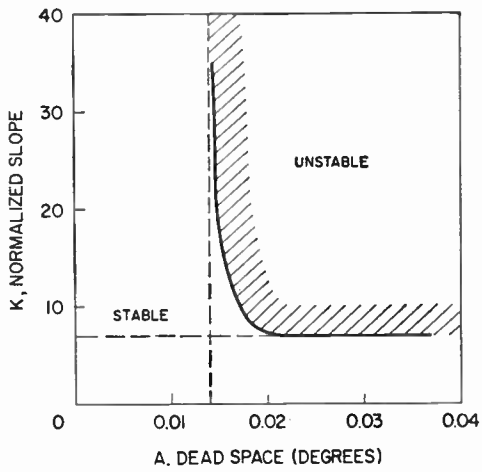

Fig. 7—Permissible values of notch parameters.

the region of the A, K-plane, compatible with the stability of the system, is defined.

To illustrate specifically, consider the waveform of $M'(\epsilon) = M(\epsilon) - M_0$ for a sinusoidal variation of ϵ about the mean value ϵ_0; *i.e.*, $\epsilon(t) = \epsilon_0 + E \sin \omega t$. This waveform is sketched in Fig. 4 with E as a parameter. The amplitude of the fundamental component can be determined by Fourier analysis. The symmetry of the waveforms about the peak value indicates that this fundamental

has no phase shift, so that the "gain," or describing function, of the nonlinear characteristic is a real number, independent of frequency. The dependence of N on the parameters A and K and the amplitude E is obtained as a result of the Fourier analysis.

The gain N appears as an element in the block diagram which represents the tracking system for the fundamental component only of the signal. A one-channel tracking system in which the compensating network has been omitted for simplicity is shown in Fig. 5 along with nominal parameter values. The root locus for this system for variable N is shown in Fig. 6. It can be seen that the system becomes unstable for $N \geq 7$. It then remains only to define what values of the notch parameters A and K are consistent with $N < 7$. The results are shown in Fig. 7. In application, the measured notch characteristic is bounded by tangent lines at zero slope and at the maximum slope, and the values of A and K defined by the tangents are compared with Fig. 7 for acceptability.

Acknowledgment

The author wishes to acknowledge the helpful suggestions of his colleagues in the Missile Systems Department of the Systems Analysis Laboratory of the Hughes Aircraft Company, both in the development of the technique applications and in the editing of the article. In particular, Dr. Harold Davis and Lawrence Kittiver have been very helpful.

Paper 4.4.5

Infrared Search-System Range Performance*

RICHARD H. GENOUD†

I. Introduction

IN ITS elementary form, a passive infrared search system consists of a telescope with instantaneous field of view or resolution element ω (steradians) that scans the total or search field Ω (steradians) in a time T (second) called the frame time. Whenever a radiating target appears in the instantaneous field of view, the radiation detector produces an electrical signal that allows an azimuth-elevation description of the position of the target in the search field. The basic question to be answered is: "What is the single-look probability of detecting the target at range R for any pre-assigned false alarm rate?"

For the search system considered, the target and background are focused by the telescope of entrance pupil diameter D (cm) on a rectangular field stop of dimensions x_0, y_0 (radians), the field stop serving as a simple space filter. The energy that passes through the stop is then relayed optically to the radiation detector of area A (cm²) which produces a voltage proportional to the radiant flux. The electrical output is amplified, filtered to maximize peak signal-to-rms-noise subject to the constraint of reasonable output signal-pulse fidelity, biased to reduce the false alarm rate to any required level, and displayed in elevation and azimuth on a z-axis modulated scope. Fig. 1 offers a pictorial description of the optical and electrical system.

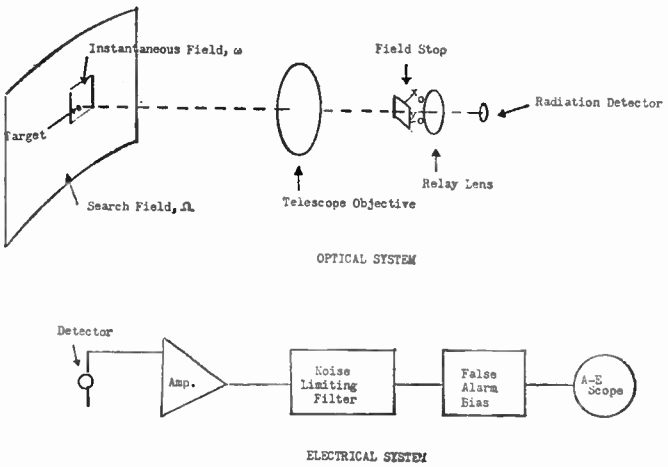

Fig. 1—Elementary passive infrared search system.

II. The Range Equation—Detector Noise Predominating

The maximum range at which a target can be detected clearly depends upon whether the target can be distinguished from the noise appearing with the signal. Distinguishing signal from noise is, of course, a statistical problem; when signal and noise are comparable, the chance for mistaking a noise pulse for a real target is appreciable. This chance for error is conveniently described in terms of the signal-to-noise ratio (S/N). The signal produced by a photoconductive detector is closely proportional to the radiant flux falling upon its sensitive surface. When the system noise is due almost

* Original manuscript received by the IRE, June 30, 1959.
† Hughes Aircraft Co., Culver City, Calif.

entirely to the detector, the calculation of signal-to-noise ratio is straightforward. One calculates the target energy collected by the optical system and compares this to the internal noise of the system. At first thought, it might appear that S/N should be proportional to the square of the entrance pupil diameter, since the collected energy is proportional to the area of the collector. It turns out, however, that the signal-to-noise ratio is proportional only to the first power of entrance pupil diameter. Essentially, this is due to the fact that scaling up linear dimensions of an optical system requires a corresponding increase in detector size (to maintain the same instantaneous angular field of view), with a consequent increase in detector noise.

It will be proved later that the ratio of the peak signal voltage V_p to the rms noise voltage V_n of an infrared search set is given by

$$\frac{V_p}{V_n} = \frac{\pi}{2}\,\frac{\delta J}{R^2}\,\frac{(NA)D}{S_s}\left(\frac{VC}{\dot{\Omega}}\right)^{1/2} \tag{1}$$

where

C = number of detector channels $\leq \Omega/\omega$, where ω is the instantaneous field of view and Ω the total field to be scanned,
D = diameter of the entrance pupil (cm),
J = radiant intensity of the target (watts/steradian in the wavelength band to which the set is sensitive),
(NA) = numerical aperture of the optical system = [2 (over-all f number]$^{-1} \leq n$ where n is the index of refraction of the medium surrounding the detector; in general, $NA = n \sin \alpha$ where α is the semi-angle of the cone of rays leaving the exit pupil of the optical system,
R = range to target (cm),
S_s = detector sensitivity (rms watts), defined below,
V = visibility factor, defined below,
δ = optical transmission, including obscuration by mirrors, atmospheric transmission, etc.,
$\dot{\Omega} = \Omega/T$ (steradians/second) where T is the frame time.

Except for the visibility factor, this expression is implicit in Jones' paper.[1]

The specific sensitivity of the detector S_s is defined by

$$S_s = \text{NEP}/\sqrt{A\Delta f'} = 1/D^*;$$

where NEP (noise equivalent power) is the power (rms watts) incident on the detector that gives an rms-signal-to-rms-noise voltage of unity for certain conditions of measurement. A is the detector area (cm^2), and $\Delta f'$ (cps) is the noise bandwidth of the measurement, assumed to be small. A full discussion of D^*, the reciprocal of S_s, and its magnitude for different infrared detectors can be found in several papers in this issue.

The visibility factor V of a pulse input is defined by

$$V = (V_p/V_{ss})^2/t\Delta f;$$

where V_p is the peak pulse output voltage, V_{ss} is the steady-state output amplitude (*i.e.*, the amplitude approached by a pulse of infinite duration), Δf is the noise bandwidth of the detector/noise filter combination, and t is the duration of the input pulse (t = detector dwell time = $\omega TC/\Omega$ = time that the target spends in the instantaneous field). As Δf is increased, V_p increases to a constant value V_{ss}. Thus V attains a maximum for some Δf, and for this Δf, the signal is most easily distinguished from the noise.

Let $x = (V_p/V_n)^2$, and $R/R_0 = 1/x^{1/4}$, then

$$R_0 = \text{idealized range} = \left(\frac{\pi}{2}\,\frac{J(NA)D}{S_s}\right)^{1/2}\left(\frac{VC}{\dot{\Omega}}\right)^{1/4}; \tag{2}$$

i.e., a range for which the peak signal-to-rms-noise is unity.

The problem now is to determine at what range the target can be detected with high probability, provided a time τ_D, called the detection time, is allowed for a decision, and false alarms due to noise are separated by a time τ_{fa}, the false alarm time. To this end, let

n = total number of noise pulses in τ_{fa}
= $(\dot{\Omega}/\omega)\tau_{fa}$ = (number of picture elements) $\cdot$ (τ_{fa}/T)
= C/t,
γ = total number of signal pulses in $\tau_D = \tau_D/T$
= number of frames in τ_D.

III. Statistical Ideas

If the search set is not a carrier system, no nonlinear process is involved in signal detection. Therefore, the the output noise will be considered to be distributed normally with zero mean and variance V_n^2. The carrier case is considered in standard radar theory.[2,3]

The probability that the signal plus noise will exceed any value y for a single noise pulse is

$$P(x, y) = \frac{1}{\sqrt{2\pi}}\int_{y-x^{1/2}}^{\infty} \epsilon^{-u^2/2}du; \tag{3}$$

where $x = (V_p/V_x)^2$ is the normalized signal strength = $(R_0/R)^4$, and $y = (V_b/V_n)$ is the normalized bias level. The probability that a noise pulse alone will exceed the bias level y is

$$\Gamma = \frac{1}{\sqrt{2\pi}}\int_{y}^{\infty} \epsilon^{-u^2/2}du. \tag{4}$$

[1] R. C. Jones, "A new classification system for radiation detectors," *J. Opt. Soc. Am.*, vol. 39, pp. 327–342; May, 1949.

[2] J. I. Marcum, "A Statistical Theory of Target Detection by Pulsed Radar," The RAND Corp., Research Memorandum RM-754; December 1, 1947.

[3] D. L. Drukey and L. C. Levitt, "Radar Range Performance," Hughes Aircraft Co., Systems Dev. Labs., Technical Memorandum 560; August 1, 1957.

Since there are n noise pulses in the false alarm time τ_{fa}, the probability that the bias level is not exceeded in τ_{fa} will be $P_0=(1-\Gamma)^n$. If $n\gg1$, which is generally true in practice, $\Gamma\simeq(1/n)\ln 1/P_0$; and for $P_0=0.5$, which will be assumed in the following numerical calculations, $\Gamma=0.693/n$. Finally, the probability that at least one of the signal pulses will exceed the bias level is $P_\gamma=1-(1-P)^\gamma$. Fig. 2 is a plot of P_1 for $n=10^2$, 10^3, 10^4, and 10^8.

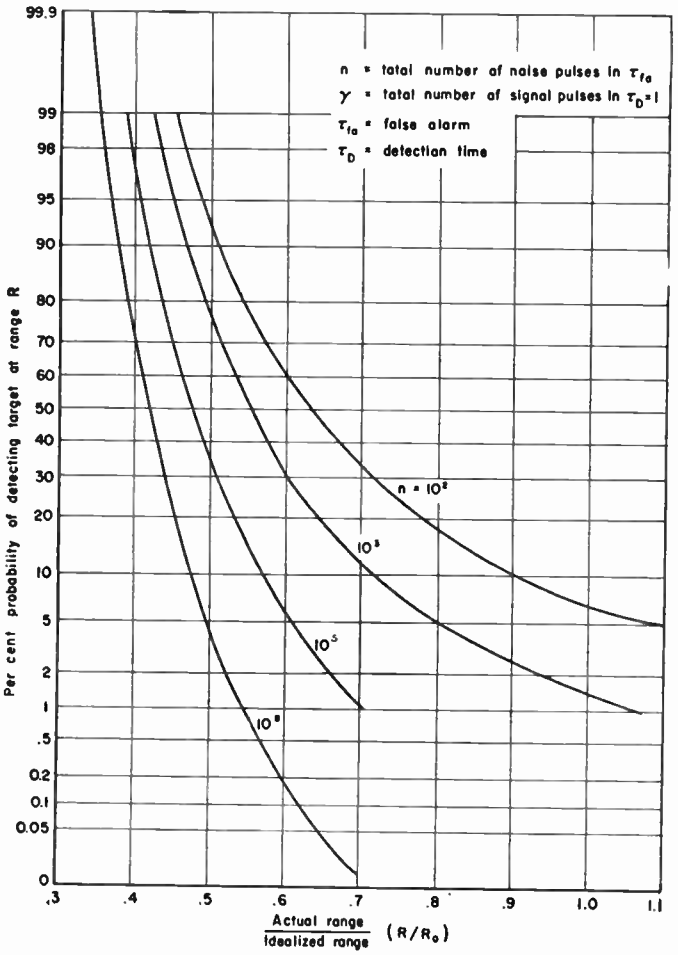

Fig. 2—P_1 vs R/R_0.

IV. Visibility Factor

For any given pulse input to the search set detector, the visibility factor is a function of the detector/noise filter combination. Suppose the detector is characterized by a responsivitiy (see papers on detectors in this issue).

$$(f) = \Re_0/(1 + (2\pi f\tau_d)^2)^{1/2} \text{ rms volts/rms watt;} \quad (5)$$

where τ_d is the detector time constant, and a white noise spectrum of spectral density $N(f)=N_0$ mean square volts/cps. The noise filter transfer characteristic will be assumed to have the form

$$|V_{out}/V_{in}| = |T(f)| = \sqrt{1 + (2\pi f\tau_d)^2}/(1 + (2\pi f\tau)^2). \quad (6)$$

The filter characteristic is chosen to compensate for the falloff in responsivity of the detector. This has the effect of allowing accurate reproduction of the pulse but, at the same time, of increasing the noise spectral density at high frequencies. A 12-db-per-octave falloff is introduced to limit noise but tends to have an adverse effect on pulse reproduction. The problem now is to maximize the peak signal-to-rms-noise by a suitable choice of τ while still retaining good output shape; *.i.e.*, the angular resolution implicit in the input pulse.[4,5]

For a rectangular radiation pulse of duration t and height P applied to the cell (it is assumed that the target image is a point)

$$V_p/V_n = \left(\frac{\Re_0 P}{\sqrt{N_0}}\right) t^{1/2} \left\{ \frac{2\sqrt{2}(\epsilon^x - 1)}{x^{1/2}(1 + u^2x^2)^{1/2}} \cdot \exp\left(-\frac{x\epsilon^x}{\epsilon^x - 1}\right)\right\} \quad (7)$$

where P is the peak radiant flux (watts) incident on the detector, $x=t/\tau=$ input pulse duration/filter time constant, and $u=\tau_d/t=$ detector time constant/input pulse duration. Since $N_0\Delta f=V_n^2$ and $\Re_0 P=V_{ss}$,

$$V=(V_p/V_{ss})^2/t\Delta f=\left\{\frac{8(\epsilon^x-1)^2}{x(1+u^2x^2)}\exp\left(-\frac{2x\epsilon^x}{\epsilon^x-1}\right)\right\}. \quad (8)$$

This expression is plotted in Fig. 3, which also shows the fractional output pulse half-width (the width at half-height) $t_{0(1/2)}/t$.

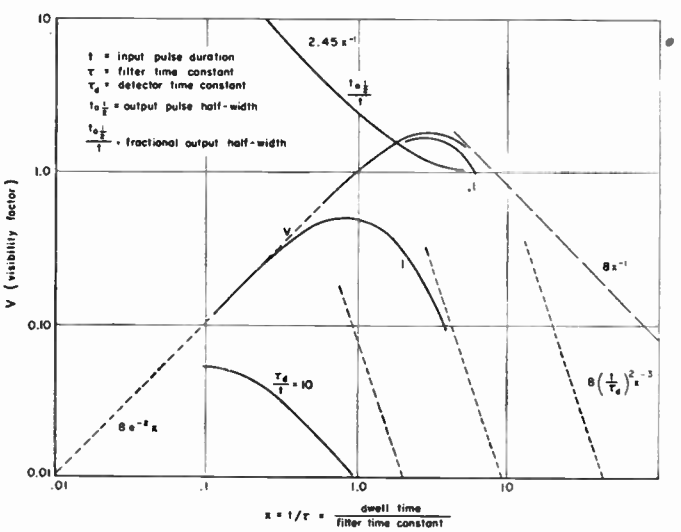

Fig. 3—Visibility factor for detector—noise filter combination.

If the detector time constant is very small compared to the pulse duration (the dwell time), the visibility factor can be maximized for $x=3$; *i.e.*, the noise filter time constant is one-third the pulse duration. This choice for

[4] L. A. Zadeh and J. R. Ragazzini, "Optimum filters for the detection of signals in noise," Proc. IRE, vol. 40, pp. 1223–1231; October, 1952.

[5] B. M. Dwork, "Detection of a pulse superimposed on fluctuation noise," Proc. IRE, vol. 38, pp. 771–774; July, 1944.

τ gives good pulse fidelity, and little angular information is lost. For $\tau_d = 0.1\ t$, roughly the same situation is obtained. Now, however, if $\tau_d = \tau$, the choice of x for maximum visibility causes about a three-fold increase in output-pulse half-width. The important point is that it is *not* possible to maximize V by varying τ and still retain resolution if τ_d/t is large.

Using the expression for V in (8), the derivation of (1) follows if the following substitutions are made in (7):

1) $S_s = \sqrt{N_0}/\mathfrak{R}_0\sqrt{A}$.
2) $\pi(NA)^2 \cdot 1 = \omega(\pi D^2/4)$, ω small (from the optical sine theorem and ultimately the second law of thermodynamics).
3) $P = \delta J \pi D^2/4R^2$.
4) $\omega = \dot{\Omega} t/C$.

The above example treated a detector with a white noise spectrum. Many photoconductivedetectors show a 1/f noise characteristic, at least at low to medium audio frequencies. The analysis for search sets using detectors with an 1/f noise characteristic would proceed in a similar fashion except that the noise bandwidth Δf appearing in the visibility factor would have to be suitably modified.[6] When the appropriate visibility factor has been calculated for the detector and filter, (1) relating S/N to the constants of the search set is still valid.

V. The Range Equation—Background Noise Predominating

A similar treatment may be applied to noise whose source is the spatial fluctuation in background radiance. The scanning of the instantaneous field transforms the fluctuations of radiance into electrical fluctuations. The field-stop aperture acts in a manner analogous to an electrical filter; a small aperture accepts fluctuations of smaller spatial extent and hence gives rise to higher frequency components than a larger aperture system.

The methods for treating this problem have been developed in general terms by Elias, *et al.*,[7] and somewhat more specifically by Jones.[8] Use is made of the two-dimensional autocorrelation function, or its Fourier transform called the Wiener transform, of the spatial variations of background radiance. The utility of this method of background description (especially in its implied restriction to the Gaussian random process) is discussed in detail in Robinson's paper.[9]

Suppose the Wiener transform $\Phi_N(k_x, k_y)$ of the background radiance $N(x, y)$ is uniform

$$\Phi_N(k_x, k_y) = B\ (\text{watts/cm}^2 - \text{steradian})^2/(\text{cycle/rad})^2;$$

where k_x, k_y, the transform variables (cycles/rad), run from $-\infty$ to $+\infty$. To obtain the electrical noise generated in the detector, we must multiply $\Phi_N(k_x, k_y)$ by the square of the magnitude of the Fourier transform of the transmission function of the field stop aperture and average over y (which gives us $(\text{watts/cm}^2)^2/(\text{cycle/rad})$), then divide by the scanning velocity $\dot{x}$ (which gives $(\text{watts/cm}^2)^2/(\text{cycle/sec})$). Use of the filter of (4) results in the expression of the signal-to-noise ratio in terms of the background radiance noise spectral density B, the instantaneous field of view ω, and a new visibility factor which depends on both the electrical filter and the field stop shape.

Proceeding as in the derivation of (1), one can show that

$$V_p/V_n = \delta J V^{.5}/R^2\sqrt{2B\omega}; \qquad (9)$$

where δ is the atmospheric transmission (the transmission of the optical system is not included since signal and noise are affected identically). The visibility factor for a rectangular aperture, rectangular signal pulse, and the electrical filter of (4) is

$$V = \frac{2x(\epsilon^x - 1)^2 \exp\left(\dfrac{-2x\epsilon^x}{\epsilon^x - 1}\right)}{(x - 3/2 + 1/2(x+3)\epsilon^{-x})}, \qquad x = t/\tau \qquad (10)$$

and is plotted in Fig. 4. This figure shows that for a filter time constant $\tau \gg t$ (the dwell time), S/N is poor. As τ approaches the dwell time, S/N improves and peaks at about $\tau = t/6$. Further increase in the electrical bandwidth results in little change in V, since the noise bandwidth is now determined by the space filter. In actual practice, for large bandwidths, the internal noise could become a dominating factor. The requirement of good pulse reproduction is seen to be consistent with a maximum visibility factor.

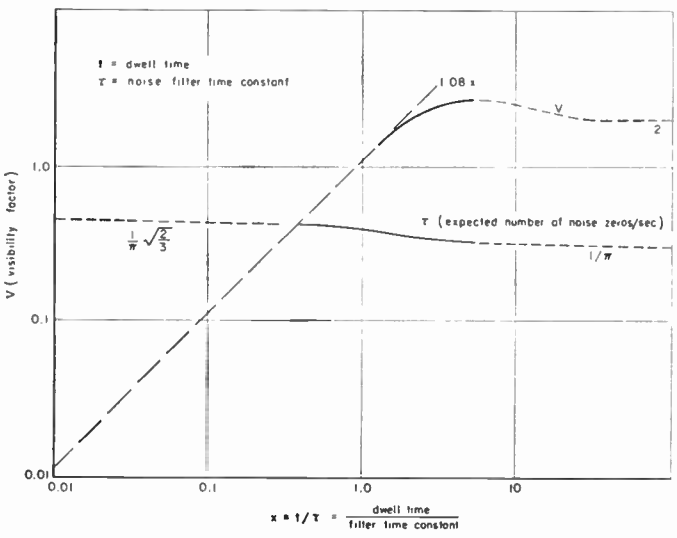

Fig. 4—Visibility factor for white sky noise, rectangular scanning aperture, and noise filter.

[6] G. Rohringer, "Noise limitations of passive search systems," *Proc. IRIS*, vol. 3, pp. 48–56; June, 1958.
[7] P. Elias, D. S. Grey, and D. Z. Robinson, "Fourier treatment of optical processes," *J. Opt. Soc. Am.*, vol. 42, pp. 127–134; February, 1952.
[8] R. C. Jones, "New method of describing and measuring the granularity of photographic materials," *J. Opt. Soc. Am.*, vol. 45, pp. 799–808; October, 1955.
[9] D. Z. Robinson, "Methods of background description and their utility," *Proc. IRIS*, vol. 3, p. 102; March, 1958. Also, paper 4.3.1, this issue, p. 1554.

The idealized range R_0 now depends on new variables

$$R_0 = (\delta J\sqrt{2B})^{1/2}(V/\omega)^{1/4} \quad (11)$$

and the previously-derived statistics are directly applicable, since it is assumed that the background radiance is normally distributed about the mean radiance.

VI. Elaboration

In Section II of this paper, it was assumed that the number of independent noise pulses per second in each channel $= 1/t$; this is a good approximation for white noise and a uniform amplifier gain to a frequency $f_0 \sim 1/t$. For cases when the noise is colored, the number of independent noise pulses per second equals $1/t_c$, where t_c is the correlation time of the output noise. Unless the noise is of a very unusual spectral distribution, t_c will not be very different from t. In practice, the amplifier bandwidth f_c must be chosen to be of the order $1/t$ so that a pulse of duration t can be reproduced accurately. If the white noise bandwidth is f_0, the average noise frequency is $f_0/2$. Since for each cycle of noise there are two noise pulses, one positive and one negative, the number of independent noise pulses is equal to $2(f_0/2)$ or $1/t$. Even if the noise spectrum is strongly colored, the requirement that f_0 be of the order $1/t$ means that the average noise frequency will generally not be moe than a factor of three from $f_0/2$. Fig. 2 shows that even an error in n as large as a factor of ten produces only a relatively small change in the probability of detection. Calculation of the number of noise zero-crossings[10] or the autocorrelation function of the noise provides a general method of estimating the number of independent noise pulses per second.

In general, the optical transmission is a function of range. Fig. 2 is actually a plot of $P(x^{-1/4})$. The relation between R/R_0 and $x^{1/4}$ is

$$R/R_0 = [\delta(R)/\delta(R_0)]^{1/2}x^{-1/4} \quad (12)$$

where R_0 must be determined by trial and error, such that

$$R_0 = (\pi\delta(R_0)J(NA)D/2S_s)^{1/2}(VC/\dot{\Omega})^{1/4}.$$

The probability of detection as a function of entrance pupil irradiance, H, may be discussed as follows:

1) $H/H_0 = x^{1/2}$

2) $$H_0 = (2S_s/\pi\delta(NA)D)(\dot{\Omega}/VC)^{1/2}\text{watts/cm}^2; \quad (13)$$

where δ is independent of range since it does not include the atmospheric transmission. $\dot{\Omega}$ is a measure of the information received per unit time.

The requirements on $\dot{\Omega}$ might not be rigid in some cases; *i.e.*, $\dot{\Omega}$ might vary over fairly wide limits and still satisfy the system requirements. An increase in $\dot{\Omega}$ allows the possibility of integrating the signal and noise. If the integration time is equal to the former frame time, the resulting improvement in S/N offsets the decreased single look detection range. For Gaussian noise and perfect integration, the two effects cancel each other exactly.

VII. An Example

Consider the following search system:

Optical:

$\delta = .55$ (atmospheric transmission = 1),

$(NA) = .5(f/1)$,

$D = 20$ cm.

Detector:

$S_s = 5 \times 10^{-10}$ rms watts,

$\tau_d = 20$ μsec.

System requirements:

$\Omega = 600$ sq deg, $\quad T = 1.5$ sec $= \tau_D$.

$\omega = .5$ sq deg.

Electrical:

$V = 1.80$, since $\tau_d/t = 1.6 \times 10^{-2}$

$C = 1$.

Then

$$H_0 = (J/R_0^2) = 1.5 \times 10^{-11} \text{ watts/cm}^2$$

and

$$n = 4.8 \times 10^4 \tau_{fa} \text{ (min)}.$$

Fig. 5 is a plot of detection probability vs entrance pupil irradiance for $\tau_{fa} = 12.5$ seconds 35 hours ($n = 10^4$, 10^8).

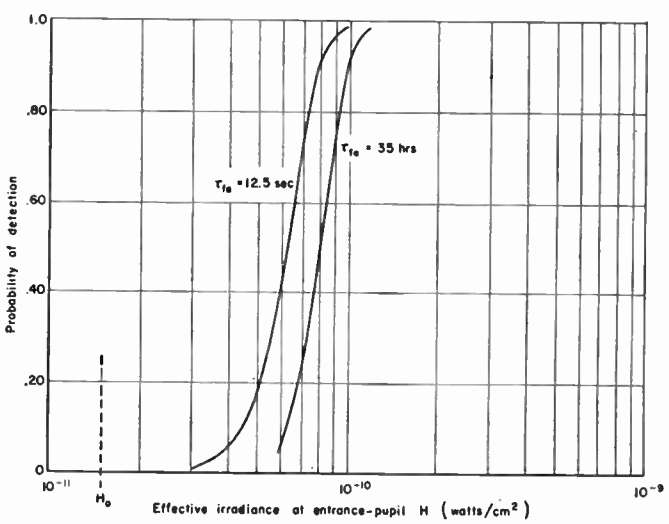

Fig. 5—Probability of detection vs effective entrance-pupil irradiance for an infrared search set.

[10] S. O. Rice, "Mathematical analysis of random noise," *Bell Sys. Tech. J.*, vol. 24, pp. 47–156; January, 1945.

VIII. Target Noise

A basic limitation to search-set sensitivity lies in the quantum nature of the target radiation. The average number of target quanta, $\overline{N}$, arriving at the detector in a frame time T will be

$$\overline{N} = (H/h\nu)\delta(\pi D^2/4)t = H/H_0'$$

where t is the dwell time and $h\nu$ the energy of a target photon.

$$H_0' = 2.5 \times 10^{-19}\dot{\Omega}/\lambda\delta D^2\omega C \qquad (14)$$

where $\lambda(\mu)$ is the wavelength of the target radiation. For the foregoing example, $H_0' = 2.3\times10^{-19}$ watts/cm^2 ($\lambda = 4\mu$).

If the product of target temperature (°K) and wavelength (cm) is sufficiently small ($<.5$, say), the target photons may be assumed to obey classical statistics, and the probability that at least one photon arrives at the detector in the frame time T will be

$$P_1 = 1 - \exp(-\overline{N}). \qquad (15)$$

Acknowledgment

The author is indebted to Dr. R. W. Gelinas of The RAND Corporation for assistance in the preparation of this paper.

Paper 4.4.6

Simulation of Infrared Systems*

H. F. MEISSINGER†, SENIOR MEMBER, IRE

I. Introduction

INVESTIGATION of infrared tracking and guidance systems by means of simulation studies is often necessary to supplement theoretical analysis. This approach enables the systems analyst to study more effectively the behavior of complex multi-loop feedback systems and provides him with a more realistic picture of the effects of nonlinear characteristics in the infrared detection and information-processing circuits. Thus, it becomes feasible to study such typical problems as complex physical phenomena in the seeker relating to discrimination between several infrared sources; tracking stability under varying operational conditions; lock-on capability, especially for sources of low radiant intensity; and prediction of performance limitations in the presence of severe tracking rate requirements and system disturbances, notably thermal noise and drift.

These examples illustrate the great variety of phenomena and problem areas to be considered for analysis and simulation. A flexible approach is required by the analyst to take advantage of all the simulation equipment and techniques available. Literature on this subject is widely scattered; an attempt has been made here to glean pertinent information from available sources and present this material in the form of a survey.

II. Objectives of Infrared Simulation

Simulation is a practical tool for evaluation of system performance as well as for system synthesis, optimization, or modification to meet desired performance criteria. Simulation studies are often made at an early stage in order to fully understand all phases of the tracking process and the effects of component interactions, or to assess the importance of critical system parameters and the effects of parameter changes. System tolerances that are compatible with practical design and production methods can thus be established. Finally, as will be discussed in greater detail below, the statistical influences peculiar to infrared tracking systems may be investigated comprehensively in the simulation laboratory under controlled experimental conditions, at a fraction of the cost of actual system tests in the field and, usually, with more conclusive results.

Simulation should not be viewed as a substitute for theoretical systems analysis but rather as a supplementary effort. It serves to verify preliminary assumptions, check or synthesize theoretical models, and confirm tentative conclusions derived from test data. This is equally true for the two major classes of simulation techniques, mathematical and physical. In the former, the entire system is represented in terms of mathematical relations that can be programmed into conventional analog or digital computers; the latter uses computing equipment in combination with system hardware subjected to physical stimuli much like those experienced during normal operation. The computer then simulates those phenomena which cannot be implemented in the laboratory, such as the aerodynamic reactions of a vehicle steered by an infrared guidance unit, and the kinematic relations which govern the relative motions between vehicle and target source. Mathematical and

* Original manuscript received by the IRE, June 30, 1959.
† Systems Dev. Labs., Hughes Aircraft Co., Culver City, Calif.

physical simulation will be discussed in detail in Sections III-A and III-B of this paper.

Obviously, the degree of complexity of the simulation model must be adapted to the objectives of the investigation and depends on how realistically the pertinent phenomena are to be represented. Considering the example of missile guidance, the simulation may only be concerned with maneuvers in two dimensions, with the main emphasis on limitations of tracking system performance. On the other hand, a complete three-dimensional model of missile motion may be required in which all significant cross-couplings in the guidance and control system as well as in the aerodynamic equations are taken into account, and where the dynamic constraints, crosstalks and imperfections of the IR tracking system are fully represented. Simulation studies may follow a step-by-step approach progressing from a simple, idealized mathematical simulation model through an intermediate stage to a highly complex final representation incorporating many physical components of the system, together with a sizeable amount of analog computer equipment.

Good judgment must be exercised at this point to prevent the simulation model from expanding beyond reasonable proportions; otherwise, phenomena of primary interest tend to become obscured by a combination of lesser effects or masked by accumulated inaccuracies having their source in the computers, the system hardware, and the auxiliary simulation components used in the experiment. However, the opportunity for observation of unexpected interactions or malfunctions in the system under controlled laboratory conditions provides a valid argument in favor of highly realistic and, hence, complex simulation models. Sources of trouble can often be detected and eliminated at an early stage before they lead to costly failures of the system in field operation.[1] Apparently, no general rule defining acceptable limits of complexity in simulation can be given. The specific requirements of each individual problem must be used as a guide.

III. Specific Problem Areas and Simulation Techniques

The problems discussed in this section are taken from the field of IR guided missile development, but typify representative areas of investigation to which simulation can be applied. It will become apparent that the line between mathematical and physical simulation problems cannot be clearly drawn. The method selected depends on the primary objective of the study and on such factors as

1) availability and capacity of analog computer equipment and auxiliaries needed to perform physical simulation;
2) frequency response characteristics of the simulation equipment and of the system to be studied, which may preclude physical simulation, since a representation in real time is required;
3) time available for conducting the study since physical simulation, as a rule, is considerably more time-consuming than the corresponding mathematical operation.

Various problem areas classified according to applicable simulation techniques and phenomena of principal interest are listed in Table I.

A. Mathematical Simulation

The fundamental response characteristics of the tracking system or of the over-all system, including the tracking unit as a subsystem, can usually be determined by mathematical simulation. The study is performed in terms of an idealized, linear model, unless a more realistic representation is indicated to take into account the inherently nonlinear features of infrared tracking. The range of excursions of system variables from a given operating point influences the choice of linear vs nonlinear representation. Whenever possible, the linearized model should be used, since this leads to simpler, more economical and, usually, more accurate computer operation. Furthermore, the results are more easily interpreted and normalized, and the effects of various disturbances may be predicted on the basis of the superposition principle.

Linear simulation, usually involving time-varying coefficients due to range closure, is concerned with the following basic problem areas:

1) Stability of the tracking system and the over-all control loop. In time-variant linear systems, conventional methods of frequency response and transient analysis cannot be applied, whereas the simulation approach easily yields stability boundaries and damping characteristics. The destabilizing influence of various cross-couplings and undesired feedback terms can be assessed.
2) Guidance accuracy in the presence of initial and intermittent disturbances, drifts, and noise signals can be determined in terms of residual guidance errors, trajectory deviations, and miss distances from a desired terminal position.

A very useful device in the analysis of linear, time-invariant or time-variant systems is the weighting function or unit impulse response, $h(t, t_1)$, which represents the output at time t caused by a unit impulse applied to a specified input point of the system at time t_1. The response to an arbitrary input function $f(t)$ can then be expressed by the superposition integral

$$y(t) = \int_{-\infty}^{t} f(t_1)h(t, t_1)dt_1.$$

The weighting function is of particular interest in the

[1] G. Hintze, "Mathematical vs physical simulation," *Proc. First Flight Simulation Symp.*, White Sands Proving Grounds, N. M., pp. 3–9; September, 1957.

TABLE I

INFRARED TRACKING PROBLEMS AMENABLE TO SIMULATION

Problem Area	Type of Simulation	Phenomena of Special Interest	Remarks Concerning Simulation Procedure
Linear system studies	Mathematical	Tracking system performance and guidance accuracy in the presence of step input disturbances and noise.	Trajectory and stability analysis. Determination of impulse response functions by adjoint computer method.
Problems associated with nonlinear characteristics of IR tracking system	Mathematical	Lock-on capability, especially in case of low signal-to-noise ratio. Effects of late target acquisition on guidance accuracy. Problems associated with false lock-on. Effect of nonlinear crosstalk.	Realistic representation of IR seeker characteristics by flexible arbitrary function generators.
Multiple target discrimination	Mathematical or physical	Effect of resolution transients on guidance accuracy.	Linear and nonlinear models of source resolution. Study in terms of a) detector output waveform fine-structure and frequency spectrum or b) seeker response functions in the presence of source interaction.
Background discrimination	Mathematical or physical	Deterioration of lock-on capability and guidance accuracy.	Study of detector output waveform fine-structure and frequency spectrum.
Effects of seeker optics and range variation	Physical	Optical distortions such as defocusing, astigmatism and collimation error. Effects of image size variation in relation to geometrical structure and dimensions of space filter. Variation of source characteristics caused by change in aspect angle.	Display of simulated sources, *e.g.*, incandescent lamps, oscilloscopic images, heated disks, etc. Use of photomultipliers or actual seeker hardware for source detection.
Statistical influences	Mathematical or physical	Interaction of multiple sources varying with source-intensity ratio. Variation of seeker response with roll attitude. Random fluctuations of seeker response due to environmental conditions. Fluctuations of parameters in production samples.	Representation of statistically characterized nonlinearities by mathematical model or by use of empirical results using recording and playback techniques. Use of samples of seeker hardware and of statistically varying operating conditions.

determination of rms-miss due to random noise and is frequently used in the determination of optimum parameters. It can be found either by a point-by-point simulation using impulse disturbances at various times of application, or by the more elegant technique of adjoint computation which uses a modified simulation program directly derivable from the conventional model.[2,3] When using the adjoint technique in missile simulation, the various contributions to rms-miss and even the over-all probability of hit can be plotted as functions of the launching range in a single run of the computer. Stationary character of the noise signal is not a prerequisite for applying this technique, but simplifies the procedure considerably by reducing the evaluation of miss dispersion to simple integrals of the form

$$\sigma^2 = N_0 \int_0^t h^2(t, t_1)dt_1$$

where N_0 is the low-frequency spectral density of the noise input signal.

The above considerations are not applicable when the analysis proceeds to the inherently nonlinear properties of infrared tracking. Typical examples of problem areas requiring nonlinear simulation are discussed below.

Tracking Capability in the Presence of Large Initial Tracking Errors and/or Large Line-of-Sight Turning Rates: In contrast to radar tracking systems, the angular range of response of infrared systems is extremely narrow (a typical range is of the order of a few degrees), and over most of this range, the correction signal produced by the tracker is a highly nonlinear function of the tracking error. A response curve typifying tracking systems used in missile guidance may take the form shown in Fig. 1, where the correction signal is plotted as a function of the tracking error. Lock-on capability of the tracker (*i.e.*, the ability to recover from initial aiming errors or from severe angular disturbances occurring during tracking operation) is a point of major interest in system analysis. In a typical tracking system, the output, or correction signal, produces a proportional angular rate of the optical axis in order to keep track of a rotating line-of-sight. It can be seen that, in the presence of large rotation rates, the net effective angular range over which lock-on is possible may be substantially smaller than the nominal range. Fig. 1 shows a horizontal line corresponding to some required angular rate which shifts the point of tracking equilibrium to the right of the origin and displaces the cross-over point at which lock-on is lost to the left of the nominal position.

Other significant factors affecting lock-on are caused by local depressions in the seeker characteristics, as illustrated in Fig. 2. Such depressions may be intentionally imposed for purposes of source discrimination.

[2] J. A. Aseltine and R. R. Favreau, "Weighting functions for time-varying feedback systems," PROC. IRE, vol. 42, pp. 1559–1564; October, 1954.

[3] J. H. Laning and R. H. Battin, "Random Processes in Automatic Control," McGraw-Hill Book Co., Inc.; New York, N. Y., chs. 5, 6, and Appendix C; 1956.

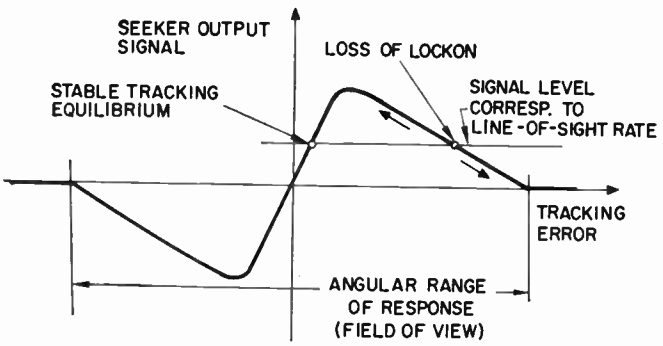

Fig. 1—Idealized seeker response characteristic.

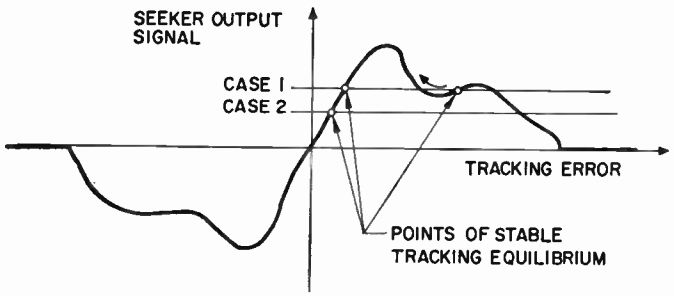

Fig. 2—Seeker characteristic exhibiting local depressions.

In the presence of a line-of-sight rate, a temporary stable equilibrium point may exist at a relatively large tracking error which is eliminated as soon as the line-of-sight rate decreases below the value corresponding to the local minimum. In the subsequent tracking process, a sharp transient peak may occur in the correction signal as the seeker nulls on the true equilibrium point near the center of the seeker characteristic.

The simulation of these nonlinear effects calls for a realistic representation of seeker characteristics by means of flexible function generators. Diode function generators or curve followers are suitable for this purpose,[4] the latter type having a capacity for a larger number of maxima and minima that occur in empirical data.

Simulation studies involving nonlinear seeker response characteristics may be conducted to determine the probability of loss of lock-on caused by continuous or intermittent disturbances and by extreme target maneuvers. Along with a realistic representation of the nonlinear seeker characteristics, it may be necessary in these cases to insert other nonlinearities such as tracking rate limits and receiver AGC characteristics into the simulation program. A further refinement may then take into account the variation of the seeker characteristic with signal-to-noise ratio. Function generators suitable for handling arbitrary bivariant functions are required for this purpose. Fig. 3 illustrates a block diagram used in the mathematical simulation of the essential nonlinearities of the tracking system assuming a

[4] G. A. Korn and T. M. Korn, "Electronic Analog Computer," 2nd ed., McGraw-Hill Book Co., Inc., New York, N. Y., ch. 6; 1956.

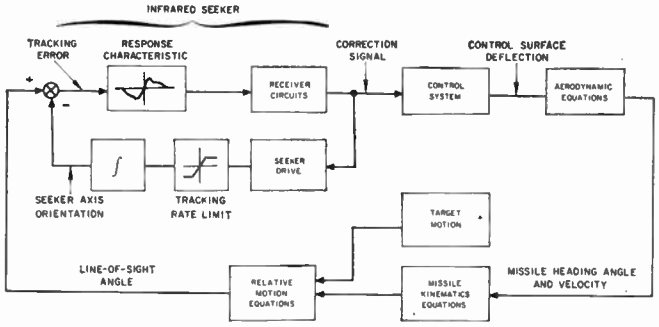

Fig. 3—Block diagram of simplified closed-loop simulation of single-channel missile guidance problem.

single axis of rotation. For a representation of three-dimensional guidance and control, the second axis of rotation having similar characteristics and introducing nonlinear cross-coupling effects must be included. Furthermore, variations of seeker response produced by changes in roll attitude of the mounting platform strongly affect the performance characteristics and lead to a still more complicated simulation program. The feasibility of realistic mathematical simulation may become questionable under these conditions, and physical simulation should be considered.

Discrimination Between Multiple IR Sources: Discrimination problems arise between sources of the same type which appear simultaneously within the field of view of the tracking system when only a single source should be tracked, as in the case of missile guidance against a target aircraft flying in formation with others. Moreover, as a prerequisite for successful operation, the tracking system must be able to discriminate the desired IR source from its background radiation environment such as clouds, layers of haze in the atmosphere, or sources on the ground if the target is viewed from above. Finally, discrimination is an essential requirement in cases where the tracking system must distinguish a bona fide source of radiation from false sources that may be employed by a target aircraft as a defensive measure or decoy.

The dilemma facing the infrared seeker is to decide at an early stage which one of several sources appearing in the field of view ought to be tracked. In target interception, a delayed resolution and lock-on phase will have deleterious effects on terminal guidance accuracy and, hence, on the success of the mission.

A useful concept involving linearized simulation is the representation of the resolution process as an instantaneous effect occurring at the range where a specified difference angle is subtended between the lines of sight from tracker to target sources. The results of studies using such a step-resolution model tend to give more or less optimistic results, depending on the assumed magnitude of the threshold angle of resolution.

A more realistic model of the resolution process is based on a source interaction principle derived from laboratory measurements. These results can be ap-

proximated mathematically by a linear combination of individual nonlinear response functions, each response corresponding to that obtained with only one source in the field of view. Fig. 4 shows schematically how this combination may be programmed on the simulator. For the study of two-axis (azimuth and elevation) tracking, a more complicated scheme is required which simulates the interaction of responses in two channels, *i.e.*, seeker crosstalk, in addition to the effects produced by the multiple sources. The approximations made here must remain relatively crude, since a simulation of the complete interaction phenomena would involve function generators capable of handling arbitrary functions of four variables. The addition of roll attitude and AGC effects would call for a dramatic increase in the complexity of the mathematical simulation program. Here again, physical simulation methods offer a more practical approach to laboratory evaluation of the over-all system.

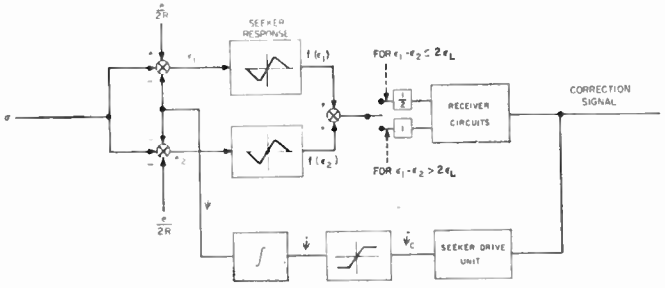

σ—LINE-OF-SIGHT ANGLE REFERRED TO CENTER OF SOURCES
ψ—SEEKER AXIS ORIENTATION
c—SOURCE SEPARATION
R—RANGE TO CENTER OF SOURCES
ϵ_1, ϵ_2—TRACKING ERRORS OF SOURCES 1 AND 2
ϵ_L—LINEARITY RANGE OF SEEKER RESPONSE CURVE $f(\epsilon)$

Fig. 4—Block diagram of seeker simulation for two-source resolution problem.

It is interesting to consider the results obtained in the case of a two-axis mathematical simulation study involving resolution of two IR sources of equal intensity. All nonlinear effects in the seeker response were expressed by combinations of functions of single variables according to the approximation scheme mentioned above. Stability criteria derived from this simulation as well as conclusions on guidance accuracy and influences of critical parameters were confirmed by physical simulation studies and field test results within acceptable experimental errors. It was recognized in the course of these experiments, however, that statistical factors noticeably affect the infrared information-gathering process, such as the exact superposition in the detector of radiation energy received from the various sources, especially in view of expected differences in source intensity. This aspect of infrared simulation requires further discussion.

Statistical Considerations Applying to the Simulation Model: The fine structure of the impulses of IR energy detected by the tracking system could, in theory, be described in a deterministic manner. The superposition of waveforms resulting from background radiation or from multiple discrete sources could then be performed in detail. Amplitude and phase relations of the individual component waveforms must be established for this purpose. In practice, this approach would be very complicated and, in fact, quite fruitless, since the waveform characteristics are made uncertain by lack of information on the geometrical configuration and radiant intensity of the sources and by the arbitrary phase relation imposed by roll attitude as a parameter. In addition, fluctuations of the photoelectric cell sensitivity due to environmental conditions plus thermal noise in the receiver circuits introduce statistical properties into the tracking system output signal, which further reduce the significance of a deterministic fine-structure analysis. As a result of these effects, the output can be considered to contain nonlinearities of a statistical nature which are repeatable functions of tracking error under fixed environmental conditions, but vary practically at random as conditions are changed. This variation in measured seeker characteristics may be assumed as normally distributed with zero mean and fixed standard deviation for a given test specimen. A model of this statistical nonlinearity having specified spectral characteristics can be constructed and programmed on the simulator.[5] Its use adds statistical significance to the predicted behavior of the over-all system.

Several methods of mechanization of the statistical model have been used experimentally. One method uses recorded output samples from a Gaussian noise generator which are reproduced by means of a curve follower. The random variable may then be played back to the simulator as a function of tracking error rather than as a function of time. In another approach, the statistical function is represented as a harmonic sum of sines or cosines with tracking error as argument. Uniformly-distributed random phase angles or normally-distributed amplitudes of the individual components are chosen to reproduce the desired random characteristics of the waveform.

B. Physical Simulation[6]

The primary purpose of performing physical simulation studies where components of the infrared seeker are connected in a closed loop with real-time analog computing equipment is to put the representation of the inherently nonlinear and hard-to-formulate system response characteristics on a realistic basis. Physical simulation models considered here are primarily concerned with data-gathering and -processing phenomena in the seeker. The methods used involve the presentation, by electronic or electromechanical means, of moving infra-

[5] R. B. McGhee, "Statistical characterization of control system nonlinearities," to be presented at the Natl. Control Conf., Dallas, Tex.; November, 1959.

[6] E. D. McAlister, Eastman-Kodak Co., Rochester, N. Y., has contributed some information for this section in private communication with the author.

red or optical sources and incorporate seeker components in open- or closed-loop operation. In some applications, only a small amount of analog computing equipment and physical simulation auxiliaries is required, making this procedure very attractive from an economical and practical standpoint.

The simulation can be considered valid only if the detection process taking place in the artificial laboratory environment gives rise to phenomena in the seeker system which are identical to those encountered under the corresponding normal operating conditions. As a less stringent requirement, it will often be sufficient to stipulate that all pertinent seeker output characteristics be realistically duplicated in the laboratory equipment.

Criteria for a satisfactory representation of infrared sources and background are: 1) proper radiation energy levels, scaled down to correspond to the small source-to-detector distances used in simulation; 2) correct spectral properties of source and background in relation to the detector bandwidth; 3) appropriately scaled size and geometrical configuration of the source, or sources. Range variation occurring during normal seeker operation must be reflected in the simulation model by a corresponding variation in intensity and size, although the latter requirement may sometimes be sacrificed in the interest of simplicity; *i.e.*, sources are represented as approximate point sources with a time-varying intensity program. Spectral characteristics of the source outside the narrow band of wavelengths detected by typical seekers are usually of no concern as long as the artificial source emits sufficient radiation in this bandwidth.

Realistic simulation of backgrounds is a considerably more complicated task than source simulation because of the large variety of background characteristics to be considered and changes of intensity and spectral qualities within the background specimen seen by the seeker. A recent development in background simulation is the use of photographic slides suitable for projection in the laboratory, together with radiometric data obtained simultaneously with the photograph for the purpose of intensity calibration.

Apart from the quality of source simulation, an essential requirement for obtaining valid results from physical simulation is the distortion-free operation of the auxiliary equipment which provides mechanical displacement of the system components under test. Obviously, any systematic inaccuracies of the auxiliary equipment could mask the system responses to be investigated. Typical examples of equipment errors which must be kept within close tolerances are phase lag, linearity errors, dead space, and velocity limits occurring in flight tables used for angular positioning of system components. Dynamic performance requirements for flight tables have been discussed by Blanton.[7] Similarly, errors in line-of-sight orientation, as seen by the seeker, which are caused by angular distortions in the optical path between source and detector, may invalidate the simulation and must be minimized.

Oscilloscope Source Simulation: The ease and speed of manipulation of light sources on the screen of a CRT by suitable input signals to the horizontal and vertical deflection plates and by control of image brightness and focus, have made the oscilloscope a flexible and inexpensive means of IR source simulation. Kantner and Cameron[8] have described the use of this device in the analysis of circularly-scanning reticles employed in IR seekers. Fig. 5 shows a simplified block diagram of the simulation loop incorporating a CRT, a lens system for proper focusing of the source into the plane of the reticle, the reticle itself, signal-processing circuits of the seeker, and analog computer channels for the dynamic and kinematic equations of motion of the vehicle carrying the seeker.

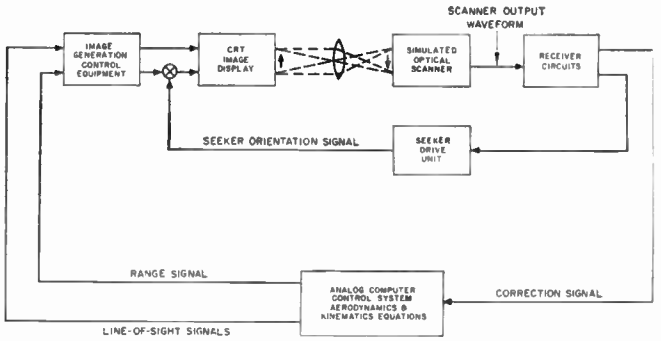

Fig. 5—Physical simulation of seeker using oscilloscope technique (Kantner and Cameron).

The objective of this simulation program was the evaluation of the effect of a large number of system parameters upon over-all performance of the seeker in the presence of multiple IR sources and specified background intensity distributions. Techniques similar to those commonly used in television practice were employed to control image brightness characteristics and magnification. The seeker components were broken up into subsystems in order to facilitate substitution of new reticle specimens and other optical parts. The photodetector time constant was modified to correspond to the time constant of the photocell employed in the seeker. In the experimental unit having simulated seeker components, it was possible to use an arbitrarily reduced time-scale of operation, since no hardware of the actual seeker had to be tied in. In a modified experiment using the same source display but integral seeker hardware, a 1:1 time scale had to be adopted.

Using the above procedure, the quality of over-all system performance can be evaluated in terms of guid-

[7] H. E. Blanton, "Performance requirements for flight tables," *Proc. Natl. Simulation Conf.*, Dallas, Tex., pp. 5.1–5.7; January, 1956.

[8] H. H. Kantner and S. H. Cameron, "Laboratory evaluation of systems incorporating scanning reticles," *Proc. Natl. Simulation Conf.*, Dallas, Tex., pp. 9.1–9.4; January, 1956.

ance accuracy by closed-loop system studies. A similar use of CRT techniques can be made for studying the specific signal-processing characteristics of the seeker. This program involves open-loop (seeker only) and closed-loop (seeker and vehicle) simulation using a CRT for circular scan of an enlarged reticle pattern. The reticle is placed over the oscilloscope screen and modulates the illumination of a photomultiplier tube by one or several moving images. Spectral characteristics of the waveforms produced by the photomultiplier are evaluated by a low-frequency wave analyzer or by harmonic analysis circuits programmed directly on the analog computer. The optics of the seeker can be investigated in detail, and phenomena such as defocusing, astigmatism, and eccentricity of the scan pattern can be represented. Interaction of source and background radiation are reflected in the waveforms. Output signals from various stages of the receiver circuitry can then be analyzed and a fuller understanding of the influence of design constants may be gained.

It should be noted that circular scan and modulation phenomena in the reticle and photodetector as represented by the CRT simulation are subject to experimental inaccuracies caused by nonuniform phosphor coating of the CRT screen, by nonlinearity in the deflection plate response causing eccentricity of the scan pattern, and by the inability of the experimenter to achieve perfect concentric alignment of the scan circle with the reticle. Hence, an unwanted amplitude modulation of 5 to 10 per cent is encountered in the simulation. Such errors are not critical, however, when viewed in comparison to the deviations of the actual seeker system from ideal alignment and response.

Electromechanical IR Source Simulation: In the simulation facility built by Eastman Kodak[9] for multiple-source interaction studies, a set of servo-driven incandescent lamps move over tracks extending across the field of view of a seeker unit which is mounted on a two-axis flight table, as illustrated in Fig. 6. These light sources may be used, for example, to represent the exhaust of engines aboard a target aircraft. The relative spacings of the sources and their brightness are controlled by feedback from the simulation loop to reflect range closure, whereas relative lateral motion between seeker and center of radiation yields line-of-sight rotations in azimuth and elevation, which are reproduced by mirrors rotatable around vertical and horizontal axes, respectively. Equations of the control system, missile aerodynamics and kinematics are handled by a general purpose computer which contains a large complement of function generators, trigonometric resolvers, and other nonlinear elements. A flight table receiving its input signals from the aerodynamics portion of the simulator provides attitude angles for the seeker platform mount and thus establishes the relative orientation of the line-of-sight with respect to seeker platform coordinates. Thus, kinematic conditions are provided which yield representative crosstalks and nonlinearities in the seeker drive mechanism and affect system stability and performance.

In addition to the equipment listed above, the facility includes accessories for automatic sequencing, remote control, readout and seeker hardware monitoring. Special extrapolating circuits are employed to predict trajectory and miss data in cases where the simulated flight must be terminated some finite time interval before interception, since excessive angular rates of change which normally occur immediately before interception would tend to overload some of the electromechanical computing elements. It can be shown that for representative range closure and turning rates and for typical system time constants, an extrapolation range of several hundred feet gives results of sufficient accuracy.

Since the physical simulation experiments performed on this facility are affected in a realistic manner by receiver noise and random photocell sensitivity fluctuations, a statistical sample of computer runs is required for each configuration and environmental condition. Automatic sequencing of computer operations assists the analyst in the performance of his duties.

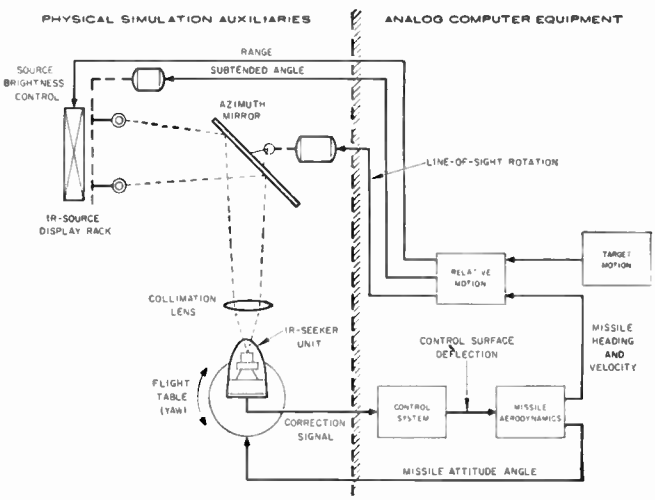

Fig. 6—Physical simulation of IR guidance problem using incandescent light sources (Eastman Kodak). Only one rotational degree of freedom is illustrated.

IV. Acknowledgment

This survey of simulation techniques useful for infrared system evaluation and synthesis reflects current practice as employed in the field of guidance and control with which the writer is acquainted. Unfortunately, owing to the nature of the development projects of interest here, only scant recognition to significant detail and specific problem areas could be given in an unclassified report such as this. The writer wishes to acknowledge valuable suggestions received in discussions with J. E. Jacobs, D. Mayers, R. B. McGhee and B. Ulrich of the Missile Systems Department, Hughes Aircraft Company, and technical material contributed by E. D. McAlister of Eastman Kodak Company.

[9] Navy Ordnance Div., Rochester, N. Y.

Paper 4.5.1

Classification and Analysis of Image-Forming Systems*

W. K. WEIHE†, SENIOR MEMBER, IRE

I. General Survey and Classification

THIS paper will discuss devices which are capable of producing a visible, two-dimensional image of a scene under conditions where vision is restricted due to insufficient ambient illumination.

Information about the individual elements of the scene is available in the form of radiation composed of two components: the radiation which is being emitted by each individual element and which has its origin inside or outside the scene. This information reaches the image-forming device through the intervening atmosphere, which modifies it by selective absorption and selective emission at its own temperature. The radiation component added by the latter source can be considered as constant, or, at the most, as changing rather gradually across the field of view. These three radiation components constitute the total information from object space present at the aperture of the system. Finally, the detector of the imaging system is affected by radiation from its own surroundings, or by a radiation and heat exchange with them; the control of this influence of the detector surroundings lies, to a substantial extent, in the hands of the designer. The image-forming device transcribes, therefore, within the range of its spectral response, the information received into a visible record presenting an intensity pattern.

The statistical fluctuations in the radiation received set the ultimate limit to the performance of the imaging system. No imaging system has been constructed, so far, approaching this limit; rather, the performance of practical systems is restricted by system noise, either of fundamental character or due to imperfections in the system, and finally by the limit in the discernibility of one part of the record from an adjacent one, as set by the ability of the eye to perceive intensity differences. This ability is reduced when the average intensity of the record increases due to a uniform addition of intensity to all parts of the record. In imaging systems where the recorded intensity increases with an increase of incident radiation (positive image), it is therefore necessary to suppress any information which merely increases the average recorded intensity without adding information about the individual elements. This can be achieved by optical means or, where applicable, by electronic means. The recognition capability of imaging systems which present a negative image suffers, all conditions being equal, from the drawback that the record obtained has a substantial average intensity.

A first point of view for classification of image-forming devices is to typify them with respect to the kind of detector used. At the present state of the art, the following types are of importance:

1) the photon sensitive imaging devices, specifically the photoemissive device with a response in the visible and the near-infrared, and the photoconductive device with a response extending into the intermediate infrared;
2) the temperature sensitive imaging devices which use thermal detectors and have, over wide limits, a nonselective spectral response.

The prime application of the photoemissive image-forming device is for the detection of the reflected component of the radiation available from the elements of the scene. The sources of this radiation are either natural sources such as the stars, or the moon reflecting the sun's radiation, or artificial sources which increase the natural ambient illumination in a certain spectral range selected according to the spectral sensitivity of the detector and, in military applications, selected by additional considerations of security. Contrast is established by differences in reflected radiation due to reflectivity differences and, in the case of directional sources, by differences in the direction of illumination of the individual elements (shadow effects).

No similar general statement can be made with respect to photoconductive imaging systems. In their present form, they have a performance approaching the photoemissive device or the temperature sensitive device, which will be discussed first.

The temperature sensitive imaging device does not depend for its operation on the presence of sources illuminating the scene; it is able to respond to the radiation emitted from the elements themselves due to their temperatures and emissivities. What is actually recorded by the thermal imaging device will, in general, be influenced by reflected radiation also. Since most of the objects encountered in practical applications are essentially blackbody radiators, the contribution of the reflected radiation will be small.

A second point of view for classification is an operational one, based on the way in which the transducer of the image-forming device receives and processes the information about the different elements of the field of view. We define the transducer as that specific component which performs in its most general form the following functions:

1) It absorbs the radiation from the different elements of the field of view.

* Original manuscript received by the IRE, June 30, 1959.
† U. S. Army Engr. Res. and Dev. Labs., Fort Belvoir, Va.

2) It undergoes changes in its characteristics under the influence of the radiation absorbed.
3) It converts these changes into a physical quantity (output of the transducer) which is amenable to reading out the information for further processing and which results finally in the presentation of a two-dimensional picture.

Not all of these functions might be separable in a specific transducer. With respect to the classification to be discussed, it is necessary to state that components used for the further processing of the output of the transducer are not included in what is defined as the transducer of the device. Examples of transducers are, therefore, a photoconductive or a photoemissive layer with its electrode(s), a thermosensitive layer coated with a radiation absorbing film, etc.

There are a number of ways of reading into the transducer the information from each of the elements of the field of view. These possibilities will be classified with respect to the degree of simultaneity with which the information is read-in. This may be done:

1) simultaneously, for all the elements of the field of view (simultaneous read-in); or
2) by scanning the field of view successively from one element to the other (sequential read-in); or
3) simultaneously for a conveniently arranged group of elements, and (by a scanning process) successively for the other groups of elements composing the field of view (mixed read-in).

For simultaneous read-in, the transducer obviously has to be of a size which covers the total field of view. It may be either in the form of a continuous layer or of a mosaic. For this type of read-in, there are the same three possibilities, as listed above, to read-out the information. Only simultaneous read-out or sequential read-out seem to be of technical importance. Examples of systems with simultaneous read-in and simultaneous read-out are the photoemissive imaging systems in one group; the absorption edge image converter, the thermosensitive phosphor imaging system, and the Evaporograph in another group. In the first group, the read-out information is carried by electrons; in the latter group, it is carried by visible light. An example of a system employing simultaneous read-in and sequential read-out is the photoconductive beam scanning pick-up tube.

Systems with sequential read-in (and consequently sequential read-out) contain, in their most efficient form, a single detecting element of a size corresponding to the resolution desired. A movement of the optical system in two coordinates is necessary to scan all elements of the field of view. Examples are the "Barnes Far Infrared Camera" and the "Thermoscan," manufactured by Radiation Electronics Corporation, Skokie, Ill.

Systems with mixed read-in usually employ a set of detectors arranged in a row of a length corresponding to one dimension of the field of view. These systems have to use a movement of optical components in one coordinate in order to scan all parts of the field of view. The type of read-out may be such that all detectors are read out at the same time in parallel channels; they carry the information in the form of a number of concurrently-running sequences (mixed-read-out). Alternatively, the read-out may be completely sequential by gathering the information point by point along the row and repeating this process successively (sequential read-out). An example of the first type (mixed read-in and read-out) is the Eastman Kodak "30-Element Scanner System."

The process by which the transducer performs its functions under the influence of irradiation can be described as an integration process, either with or without a weighting time function. Integration with a weighting function is substantially the same as that performed by an RC-network: the weighting time function is $1/\tau \exp(-t/\tau)$. Usually the time constant of one of the processes by which the action of the transducer has been defined is the predominant one, and τ is then equivalent to this time constant. For best performance, τ should be matched to the time available for integration. This time is given by the type of read-in and read-out which the device uses, and the integration process occuring in the different devices is referred to as element storage, line storage and frame storage. Frame storage operation obviously offers the promise of greatest sensitivity. In practice, matching τ to the available integration time might be difficult to achieve, and at the present state of the art it is this restriction in obtainable values of τ that determines the integration time.

The photoconductive beam scanning pick-up tube is a special case. Here, the transducer function that establishes the predominant time constant is the one converting the change in conductivity of the transducer elements into an output in the form of local charges accumulated on the scanned side of the transducer. Storage occurs by the action of an RC network formed by the elemental areas of the photoconductor. The input voltage of the network is a constant voltage, and in order to obtain an output reflecting the conductivity changes, it is necessary to choose τ at least 5 times as large as the frame period. The beam scanning pick-up tube is remarkable in another respect: in an ideal way, it solves the problem of recovery of the quiescent state; the read-out process itself clears the transducer of the stored information.

Integration without a weighting time function occurs in the transducer of the Evaporograph. Here the storage process produces an output which increases in proportion to the amount of absorbed energy up to the physical limitations of the transducer.

II. Specific Systems

A. Photoemissive Image-Forming Systems

For a discussion of these devices the reader is re-

ferred to the paper by Wiseman and Klein elsewhere in this issue.[1]

B. Photoconductive Image-Forming Systems

1. Sequential Read-in and Read-out: We assume that the image-forming device scans, in successive lines, a total field of view of $\Omega_1 \cdot \Omega_2$ steradians in a frame time of t_F seconds with an instantaneous field of $\omega \cdot \omega$ steradians. The scanning process will have a certain time efficiency, p, which expresses the fact that a time of pt_F seconds is used for the actual scanning, the remaining time being required to reset the device for the scan of the next line. The detecting element has a size of A cm² determined by the instantaneous field, the diameter D_0 of the optical system and its F/number

$$A = \omega^2 D_0^2 F^2. \tag{1}$$

The output of the detector is fed into an amplifier with an upper frequency cutoff at f_2 cps and a lower frequency cutoff at f_1 cps. We first determine these two frequencies.

f_2 is fixed, in the customary way, by assuming that the field of view is a checkerboard configuration of squares, each of a size of $\omega \cdot \omega$ steradians. With this, we obtain

$$f_2 = \frac{1}{2} \frac{\Omega_1 \cdot \Omega_2}{\omega^2} \frac{1}{pt_F}. \tag{2}$$

The lower-frequency limit f_1 is set by the requirement that the system should be able to handle an extended target of a certain angular length Ω_T taken in the scanning direction. If we permit the output to decay to $(1-e^{-1})$ during the time it takes to scan the angle Ω_T, we obtain

$$f_1 = \frac{1}{2\pi} \frac{\Omega_1 \cdot \Omega_2}{\omega \Omega_T} \frac{1}{pt_F}. \tag{3}$$

For the rms value of the flux falling on the detector at the wavelength λ, and in a wavelength interval $d\lambda$, we obtain

$$(P_\lambda d\lambda)\text{-}rms = \frac{1}{\pi\sqrt{2}} t_A(\lambda) t_0(\lambda) D_0^2 \omega^2 \epsilon_T(\lambda) \cdot [N_\lambda(T_T) - N_\lambda(T_S)] d\lambda,$$

under the assumption that the detector looks alternately at a target of a size $\omega \cdot \omega$ and at the target surrounds. This results in the radiant flux having the form of a triangular wave. $t_A(\lambda)$ and $t_0(\lambda)$ represent the percentages of radiation of wavelength λ transmitted through the atmosphere or through the optics respectively. $\epsilon_T(\lambda)$ is the emissivity of the target and $[N_\lambda(T_T) - N_\lambda(T_S)]$ is the difference between the spectral radiance of a blackbody at the temperature of the target (T_T) and a blackbody at the temperature of its surrounds (T_S).

[1] R. S. Wiseman and M. W. Klein, "Photoemissive image-forming systems," paper 4.5.2, this issue, p. 1604.

We now introduce the relative spectral responsivity $R_r(\lambda)$ of the detector normalized with respect to its peak spectral response and its noise-equivalent-power (NEP) at its spectral peak, and for a bandwidth extending from f_1 to f_2 cps. Then the ratio (S/N) of the rms output voltage of the detector in the wavelength band $\lambda_1 \cdots \lambda_2$ to its rms noise voltage is given by

$$\left(\frac{S}{N}\right) = \frac{1}{\pi\sqrt{2}} \frac{D_0^2 \omega^2}{(NEP)} \int_{\lambda_1}^{\lambda_2} t_A(\lambda) t_0(\lambda) R_r(\lambda) \epsilon_T(\lambda) \cdot [N_\lambda(T_T) - N_\lambda(T_S)] d\lambda.$$

In order to simplify this equation, we assume now that $t_0(\lambda)$, $R_r(\lambda)$, $\epsilon_T(\lambda)$ can be replaced by average values $\bar{t}_0$, $\bar{R}_r$, $\bar{\epsilon}_T$, valid for the spectral band under consideration. We obtain

$$\left(\frac{S}{N}\right) = \frac{1}{\pi\sqrt{2}} \frac{D_0^2 \omega^2}{(NEP)} \bar{t}_0 \bar{R}_r (\Delta N_{app})_{\lambda_1}^{\lambda_2},$$

where

$$(\Delta N_{app})_{\lambda_1}^{\lambda_2} = \bar{\epsilon}_T \int_{\lambda_1}^{\lambda_2} t_A(\lambda) [N_\lambda(T_T) - N_\lambda(T_S)] d\lambda$$

will be called the apparent target radiance difference in the wavelength band $\lambda_1 \cdots \lambda_2$.

The noise equivalent apparent target radiance difference in the wavelength band $\lambda_1 \cdots \lambda_2$ is given by

$$(NER)_{\lambda_1}^{\lambda_2} = \pi\sqrt{2} \frac{(NEP)}{D_0^2 \omega^2} \frac{1}{\bar{t}_0 \bar{R}_r}. \tag{4}$$

The noise-equivalent-power of the detector (NEP) is a function of A, ω, Ω_1, Ω_2, pt_F. In order to show this dependence, we compare the detector, as used in the device, with a reference detector of the same kind and material for which the following quantities are known:

a) Responsive area: A_c.
b) rms noise voltage, $N_c(f)$, as a function of frequency and measured for a small bandwidth Δf_c.
c) Noise-equivalent-power at the spectral peak $(NEP)_c$, measured at a chopping frequency f_0 and for the bandwidth Δf_c.

From this we obtain the following value for the noise-equivalent-power (NEP) of the detector as operated under the conditions of the special system under investigation:

$$(NEP) = \sqrt{\frac{A}{A_c}} \sqrt{\frac{\int_{f_1}^{f_2} N_c^2(f) df}{N_c^2(f_0) \Delta f_c}} (NEP)_c$$

or

$$(NEP) = \sqrt{\frac{A}{A_c}} \frac{\sqrt{\overline{N_c^2}}}{N_c(f_0)} \sqrt{\frac{f_2 - f_1}{\Delta f_c}} (NEP)_c \tag{5}$$

where $\overline{N_c^2}$ is an average value of $N_c^2(f)$ in the frequency range $f_1 \cdots f_2$. Combination of (1)–(5) results finally in the following equation for $(NER)_{\lambda_1}^{\lambda_2}$:

$$(\mathrm{NER})_{\lambda_1}^{\lambda_2} = \pi\left[\frac{\sqrt{\overline{N_c^2}}}{N_c(f_0)}\,\frac{(\mathrm{NEP})_c}{\overline{R}_r}\,(A_c\Delta f_c)^{-1/2}\right]\left[\frac{1}{\bar{t}_0}\,\frac{F}{D_0}\right]\left[\omega^{-2}\sqrt{\frac{\Omega_1\Omega_2}{pt_F}\left(1-\frac{\omega}{\pi\Omega_T}\right)}\right]. \quad (6)$$

This integral has been computed by Berler [1] for different spectral bands, and a set of temperatures T_S. Values for $t_A(\lambda)$ were taken from published data on atmospheric transmission for ground-to-ground paths, available for two amounts of precipitable water. Table I gives an example of the results for $T_S = 300°\mathrm{K}$. The values from this table can then be used to calculate, in a first approximation, the noise-equivalent target temperature difference (NET), with respect to a background temperature of 300°K by

$$(\mathrm{NET})_{TS} = \frac{(\mathrm{NER})_{\lambda_1}^{\lambda_2}}{\bar{\epsilon}_T(\Delta_T N_{\mathrm{app}})_{\lambda_1}^{\lambda_2}}.$$

TABLE I

Wavelength Range	0.7 mm Precipitable Water	17 mm Precipitable Water
2.75 · · · 3.25 microns	1.2×10^{-7} W cm^{-2} ster^{-1} deg^{-1}	3.5×10^{-8} W cm^{-2} ster^{-1} deg^{-1}
3.25 · · · 3.75 microns	5.9×10^{-7} W cm^{-2} ster^{-1} deg^{-1}	4.3×10^{-7} W cm^{-2} ster^{-1} deg^{-1}
3.75 · · · 4.35 microns	1.2×10^{-6} W cm^{-2} ster^{-1} deg^{-1}	1.1×10^{-6} W cm^{-2} ster^{-1} deg^{-1}
4.35 · · · 4.85 microns	2.4×10^{-6} W cm^{-2} ster^{-1} deg^{-}	1.4×10^{-6} W cm^{-2} ster^{-1} deg^{-1}
4.85 · · · 5.35 microns	3.0×10^{-6} W cm^{-2} ster^{-1} deg^{-}	9.6×10^{-7} W cm^{-2} ster^{-1} deg^{-1}
5.35 · · · 5.85 microns	6.2×10^{-7} W cm^{-2} ster^{-1} deg^{-1}	$<1.0.10^{-9}$ W cm^{-2} ster^{-1} deg^{-1}
5.85 · · · 6.05 microns	9.5×10^{-9} W cm^{-2} ster^{-1} deg^{-1}	$<1.0.10^{-9}$ W cm^{-2} ster^{-1} deg^{-1}

This is the most reduced quantitative expression, when we are concerned with photoconductive detectors in general. The situation is different from the one to be discussed in section 1 of II-C, where the possibility exists of selecting a transducer of such a frequency response that it yields a minimum value of the noise-equivalent-power at a certain frequency, and where the dependence of the noise-equivalent-power on this selection is well established. This is not the case for photoconductive detectors in general. The last bracket in (6) shows the influence of the instantaneous field and of the solid angle scanned per second, $\Omega_1\Omega_2/t_F$, on the value of $(\mathrm{NER})_{\lambda_1}^{\lambda_2}$, when it is assumed that the quantities in the first bracket of the equation are not affected by changes of these two parameters, and that we stay in a reasonably flat portion of the frequency response curve of the detector for these changes. The dependence of $(\mathrm{NER})_{\lambda_1}^{\lambda_2}$ on the size of the instantaneous field is essentially of the form (ω^{-2}) and is due to the smaller amount of radiation received from the smaller target area seen by the detector when $\omega\cdot\omega$ is decreased; the beneficial effect of a decrease of the detector area necessary to obtain a smaller instantaneous field is compensated by the effect of a larger bandwidth required when Ω_1, Ω_2 and pt_F are kept constant. The dependence of $(\mathrm{NER})_{\lambda_1}^{\lambda_2}$ on the solid angle scanned per second is given by the square root of this quantity, providing that the instantaneous field of view is kept constant.

It should be pointed out that (6) is valid only if the frequency response of the detector is reasonably flat up to the frequency f_2. When this is not the case, an obvious correction of the value of (NER), as calculated from (6), has to be made.

Finally, the question arises as to what apparent radiance difference in the wavelength band $\lambda_1 \cdots \lambda_2$ can be expected from the scene for a certain target temperature difference. For this we need an evaluation of the integral

$$(\Delta_T N_{\mathrm{app}})_{\lambda_1}^{\lambda_2} \equiv \int_{\lambda_1}^{\lambda_2} t_A(\lambda)\left(\frac{\partial N_\lambda(T)}{\partial T}\right)_{T_S} d\lambda, \text{ watts cm}^{-2}\,\text{ster}^{-1}\,\text{deg}^{-1}.$$

A scanning device of the kind discussed above has been developed by the Radiation Electronics Corporation under the name "Thermoscan." Scanning is performed by moving two plane mirrors. The following data are characteristic of the performance of the system [2]:

Collecting optics: 4-inch diameter, $F/1.5$:
Instantaneous field of view: 5 mrad × 5 mrad;
Frame time: 2 seconds;
Presentation: Cathode-ray tube and photographic recording;
(NET) with respect to a background temperature of 20°C;
0.25°C for a dry-ice-cooled photoconductive indium antimonide detector;
4°C for an uncooled PEM indium antimonide detector.

2. Simultaneous Read-in, Sequential Read-out: An example of a system of this kind is the photoconductive beam scanning pick-up tube. For details on this tube the reader is referred to the paper by Morton and Forque.[2]

3. Mixed Read-in and Read-out: An example of this type of system is the "30-Element Scanner System" developed by the Eastman Kodak Company [3]. The transducer consists of a linear array of 30 cells positioned in the focal plane of an $F/2$ Cassegrainian optical system with a 6-inch diameter, spherical, primary mirror. The array covers a vertical field of about 5°. Scanning in the horizontal direction is provided by a rocking motion of the plane secondary mirror around a

[2] G. A. Morton and S. V. Forgue, "An infrared pickup tube," paper 4.5.3, this issue, p. 1607.

vertical axis. The total horizontal field covered is 15°. The adjustable sweep rate is normally chosen at 10 per second. Each individual cell is connected to an individual amplifier. Its output voltage is used to fire a corresponding individual neon lamp in an on-off fashion. The neon lamps, also arranged in a linear array, are viewed by a second rocking mirror moving in synchronism with the first rocking mirror. Either direct visual observation, or recording on photographic film, is provided.

The cell array is produced by depositing a continuous strip of conventional lead sulfide or plumbide material on a glass substrate, by evaporating electrodes at the desired separation on the layer, and by dividing the layer into individual cells by mechanical means. This method guarantees the utmost in uniformity of the characteristics of the individual cells. The individual elements are 0.025-inch square with a gap of 0.010 inch separating them. Means to cool the cells to dry ice temperature are provided.

Practical performance tests showed that the resolution of the system is nearly 6 milliradians. This is approximately twice the field of view of an axially-located cell, and is due to the fact that the off-axis imperfections of the optical systems make a compromise defocused adjustment of the cell array necessary, in order to provide constant resolution for a substantial portion of the scanned field. The blackbody temperature, just observable with the device, was established by photographic observation only. For uncooled lead sulfide and a photographic integration time of 5 seconds, a threshold temperature of slightly less than 0.5°C at an ambient temperature of 23°C was determined. From this, a threshold temperature difference for visual observation of about 5 times this value, may be estimated. The use of plumbide cells, cooled to the temperature of dry ice, can be expected to result in an improvement by a factor of about three.

Systems of the mixed read-in and read-out type are superior to systems of the sequential read-in and read-out type, with respect to noise-equivalent target radiance difference. The reason for this is that they are operated with a substantially reduced bandwidth. Their upper cutoff frequency, f_2, is given by

$$f_2 = \frac{1}{2}\,\frac{\Omega_1}{\omega}\,\frac{1}{pt_F},$$

using the same nomenclature as used in section 1 of II-B, and assuming that of the field of view in the scanning direction is Ω_1 radians. For the lower cutoff frequency, f_1, we obtain

$$f_1 = \frac{1}{2\pi}\,\frac{\Omega_1}{\Omega_T}\,\frac{1}{pt_F}.$$

With the same reservations as listed in connection with (6) of section 1 of II-B, we can then describe the influence of the instantaneous field and of the solid angle imaged per second on the noise-equivalent-target radiance difference:

$$(\mathrm{NER})_{\lambda_1}^{\lambda_2} \sim \omega^{-2}\sqrt{\frac{\omega}{\Omega_2}}\sqrt{\frac{\Omega_1\Omega_2}{pt_F}\left(1-\frac{\omega}{\pi\Omega_T}\right)}.$$

Comparison of this equation with (6) shows that the reduction in the values of $(\mathrm{NER})_{\lambda_1}^{\lambda_2}$ and (NET) is, other factors remaining constant, given by the square root of the number of detectors contained in the linear array, (ω/Ω_2).

C. Temperature Sensitive Image-Forming Systems

1. Sequential Read-in and Read-out: Here both thermocouples and bolometers are used as the transducer. It has been established that these detectors belong to a class which offers the possibility of obtaining a minimum value of the noise-equivalent power for a signal of frequency f, by adjusting their time constant to an optimum value of $(2\pi f)^{-1}$. Omitting numerical factors, the (NEP) is then proportional to $(Af)^{1/2}$ for a detector area A.

Under these circumstances, we are able to develop further the equations derived in section 1 of II-B, so that they show how, for this class of detectors, the noise-equivalent apparent target radiance difference depends on the solid angle scanned per second and on the instantaneous field. The optimum value of the time constant is equal to $(2\pi f_2)^{-1}$, and we assume that it is physically possible to obtain this value for the limits between which f_2 might change due to changes in $(\Omega_1\cdot\Omega_2)/t_F$ and ω^2. Then the (NEP) of the device is proportional to

$$(\mathrm{NEP}) \sim [Af_2(f_2 - f_1)]^{1/2}$$

where numerical factors and terms not affected by $(\Omega_1\cdot\Omega_2)/t_F$ and ω^2 have been omitted. Introducing the values for f_1 and f_2, we write

$$(\mathrm{NEP}) \sim A\omega^{-2}\sqrt{\frac{\Omega_1\cdot\Omega_2}{pt_F}}\sqrt{\frac{\Omega_1\Omega_2}{pt_F}\left(1-\frac{\omega}{\pi\Omega_T}\right)},$$

with

$$A \sim \omega^2$$

and

$$(\mathrm{NER})_{\lambda_1}^{\lambda_2} \sim \omega^{-2}\cdot(\mathrm{NEP});$$

and for

$$\frac{\omega}{\pi\Omega_T} \ll 1,$$

we then obtain

$$(\mathrm{NER})_{\lambda_1}^{\lambda_2} \sim \omega^{-3}\,\frac{\Omega_1\Omega_2}{pt_F} = \omega^{-1}\,\frac{\Omega_1\Omega_2}{\omega^2 pt_F}.$$

The first part of this equation shows that the noise-equivalent apparent target radiance difference (or the noise-equivalent target temperature difference) is pro-

portional to ω^{-3} when the rate at which the total field is scanned remains constant; the second part indicates a proportionality to ω^{-1} when the rate at which the number of picture elements is scanned stays constant. Furthermore, the equation shows that (NER) and (NET) are proportional to the scan rate.

A thermocouple-type device of this kind has been developed in France by Bayle [4]. In this device, the thermocouple is positioned in the focal point of a mirror telescope of 12-inch aperture. The telescope performs a line scan in the vertical direction with a fast return and is moved slowly in the horizontal direction by a rotation around a vertical axis. The output of a second thermocouple exposed to the radiation of the full field of view is put in opposition to the output of the first thermocouple. The instantaneous output of the combined thermocouples is then proportional to the difference of a local apparent radiance and the average apparent radiance of the full field of view. This instantaneous output is continuously recorded, during the scanning process, on a photographic plate or, in a model improved by Delbord, on paper of the Alfax type. Though no quantitative performance data are given, the published examples of thermal images taken show good performance.

A first model of a bolometer-type scanning device was developed by L. L. Horrell in 1951 at the U. S. Army Engineer Research and Development Laboratories. A thermistor-type bolometer was chosen due to its stability, ruggedness and relatively fast response. This device is the forerunner of the more spohisticated "Far Infrared Camera," which has recently been described by Astheimer and Wormser [5]. With 8-inch diameter optics and an instantaneous field of view of 1 mrad$\times$1 mrad, the following values are characteristic for its performance:

Time to scan a field of 10°$\times$10°; 17 minutes
(NET); 0.15°C for unimmersed thermistor bolometers,
0.04°C for immersed thermistor bolometers.

The instrument permits a quantitative evaluation of the signal recorded on photographic paper. For this purpose, the signal received from the different elemental areas of the field is continuously compared with the signal from an internal reference blackbody of controlled temperature, and a calibrated gray scale is produced together with the thermal image. The radiance of the reference blackbody is given by its temperature setting and by a calibrated electrical bucking voltage which is fed into the amplifier and which permits one to adjust the effective blackbody radiance to a desired value.

2. Simultaneous Read-in, Simultaneous Read-out: We will consider here devices where the transducer is of a type which undergoes, under the influence of irradiation, some change in its characteristics that can be sensed by direct visual observation. We can distinguish two types of transducers. In the first type, the changes which are observed attain (after a transient process) a constant value for constant irradiation; we will call a transducer of this type a "power proportional transducer." In the second type, the changes which are observed increase proportionally to time, up to the physical limitations of the transducer; therefore this type of transducer will be called an "energy proportional transducer."

D. Devices Using "Power Proportional Transducers"

Several effects have been investigated in this group of devices. We list as the most interesting the following.

The thermosensitive phosphor imaging system has been described by Urbach, Nail, and Pearlman [16]. It makes use of the dependence of the luminous intensity of a phosphor upon its temperature. The phosphor is illuminated uniformly by ultraviolet radiation and the emitted visible radiation is observed. When a local temperature change is produced by absorbed radiation, the conversion efficiency of the phosphor decreases and the area of higher temperature appears darker than its unaffected surrounds. The paper referred to lists a brightness change of about 20 per cent for a temperature change of 1°C, measured with zinc-cadmium sulfide phosphors. The authors give a value of about 5.10^{-4} W cm^{-2} as the smallest detectable energy flux on the phosphor surface, obtained for phosphors of this type.

The absorption edge image converter was invented in 1953 by Northrop [6] and is discussed further in a paper by Harding, Hilsum and Northrop and in a comprehensive study on the thermal-imaging process by Hilsum [10]. This device uses a transducer which has, as the temperature sensitive element, a layer of a semiconducting material that has its absorption edge in the visible portion of the spectrum. The location of the absorption edge depends on the temperature of the semiconductor. When monochromatic light of a wavelength in the region of the absorption edge is transmitted through the transducer and viewed by the eye, local variations in the temperature of the layer will be detected. In order to produce temperature changes in the semiconducting layer, the transducer contains a layer that is in intimate contact with the semiconductor and absorbs the radiant flux entering the optical elements of the device, but is transparent to the wavelength of the observation light.

In the device reported on, amorphous selenium was used as the semiconductor. The absorption edge of this material happens to be at such a spectral location that the wavelengths of the sodium *D*-lines are in the highly absorbing range, a fact which makes for experimental simplicity of the device. A schematic diagram of the imaging device is shown in Fig. 1. The mirror, *M*, images the radiation from the scene on the transducer, *T*, which is mounted in an evacuated vessel. The collimated light of a sodium arc lamp, *S*, passes through a filter, *F*, which eliminates the sodium lines of longer wavelengths, and then passes through the transducer. The

eye directly views the 1:1 image of the transducer produced in the plane of the field lens, *F.L.* Local variations of the light transmitted by the transducer are a record of the temperature pattern set up in the transducer by the radiance pattern of the scene to be imaged.

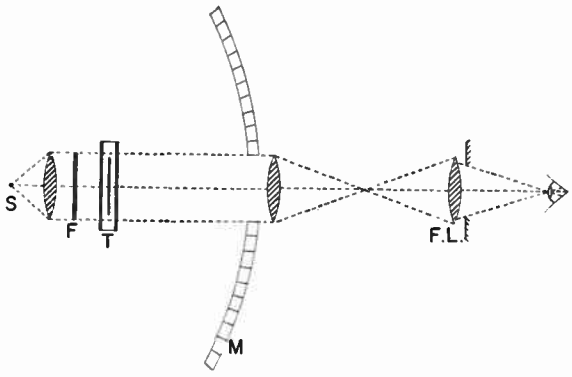

Fig. 1—Schematic diagram of the absorption-edge image converter.

We will now proceed to make an assessment of the performance of this device. This will give us an opportunity to discuss the general problems pertinent to thermal-image-forming devices with simultaneous read-in and simultaneous read-out For this assessment, the selection of operating conditions and materials was dictated by the availability of data and not by an attempt to arrive at a device of optimum performance. In this sense, silicon monoxide, which has well determined absorption bands in the wavelength range of the 8- to 14-micron atmospheric window, was selected as the infrared absorbing layer. The data for the optical constants of Se and SiO were taken from [7] and [8], and the behavior of the transducer was calculated for thicknesses up to 5 microns of each component layer.[3] The reservation made on the availability of data applies especially to data available for the contrast threshold of the human eye. Here, data published by Blackwell [9] will be used. They assume a pattern in the form of a circular spot located in a field of uniform brightness. The assessment will be made for this simple situation. Obviously, this will lead to very optimistic results relative to the possibility of observing details in a complex scene.

The assessment will lead to limits of the observable temperature differentials of objects in the scene. At the present state of the art, the limits are set by the capability of the human eye to observe relative brightness differences; other more fundamental limitations do not need to be taken into account at the present. It will be assumed, furthermore, that the transducer has uniform performance for all its elementary areas.

We will first calculate the smallest temperature difference, ΔT_{min}, that, occuring locally in the transducer, can be observed under conditions varying with the individual thicknesses of the SiO and the Se layer composing the transducer. We assume that the sodium arc lamp provides an apparent luminance of 5000 foot-lamberts without the transducer being inserted. The absorption of the transducer is predominantly given by the thickness of the selenium layer, the influence of the SiO layer being negligible for the purpose of this assessment. Using the computed absorption values, we get the values of the apparent background luminance, B, and from an interpolation of Blackwell's results, the minimum perceivable relative contrasts $(\Delta B/B)_{min}$ for different angles (in minutes of arc) subtended by the diameter of the circular spot as a function of the thickness of the selenium layer. We then calculate the relative change of B due to a small temperature change. Disregarding any interference effects in the transducer and assuming no absorption of the sodium D-lines in the SiO layer, the relative change $\Delta B/B$ for a small temperature increment ΔT is given by

$$\frac{\Delta B}{B} = - h_1 \left(\frac{d\alpha}{dT}\right) \Delta T \qquad (7)$$

where h_1 is the thickness of the Se layer and $(d\alpha/dT)$ is the temperature coefficient of the absorption coefficient α of the selenium. This coefficient has been determined by Hilsum [11], as 190 cm^{-1} deg^{-2} at the wavelengths of the D lines and a temperature of the specimen of 30°C. Evaluating this equation, we can calculate (by comparison with the values obtained for $(\Delta B/B)_{min}$) values for the smallest observable temperature difference, ΔT_{min} in the transducer. These values are tabulated in Table II. The table shows a result which can be

TABLE II
VALUES OF ΔT_{min} (0°C)

Spot Size (Minutes of Arc)	Se Thickness			
	2	3	4	5 microns
9.68	0.50	0.40	0.47	0.75
18.2	0.34	0.26	0.24	0.35
55.2	0.23	0.15	0.13	0.13
121.0	0.19	0.13	0.10	0.10

expected: increasing the thickness is advantageous on the one hand since $\Delta B/B$ is proportional to the thickness, disadvantageous on the other hand in so far as the increasing absorptance moves the luminance of the operating point into a region of increasing $(\Delta B/B)_{min}$. The result is an optimum thickness of the Se layer which varies with the spot size.

The next step will connect the temperature which establishes itself in an element of the transducer to the temperature of an element of the scene. Fig. 2 shows a description of the situation. We assume that an elementary area dA_T in the scene has a temperature T_T and an emissivity $\epsilon_T(\lambda)$, and that it is surrounded by objects of temperature T_S. The area will radiate with a

[3] The author is indebted to P. H. and J. A. Berning, of the U. S. Army Engr. Res. and Dev. Labs., for setting up and carrying out the computations.

spectral radiance of $\epsilon_T N_\lambda(T_T)+(1-\epsilon_T)N_\lambda(T_S)$, where $N_\lambda(T)$ is the spectral radiance of a blackbody at a temperature T. We characterize the influences of the atmosphere and the optics by transmittances $t_A(\lambda)$ and $t_0(\lambda)$, respectively. The transducer is contained in an evacuated enclosure with walls of emissivity $\epsilon_B=1$, and at a constant temperature T_B. The transducer has absorptances $a(\lambda, v)$ and $a'(\lambda, v')$ which, in general, will be a function of the wavelength and of the angle of incidence, v or v', defined by Fig. 2. The maximum angle of incidence for radiation passing through the optics is v_1. The elementary area of the transducer onto which the area dA_T is focused is designated by dA, and we assume that a temperature T establishes itself in this area. We are not so much interested in the absolute value of this temperature as we are in its change with respect to a certain reference condition. We choose as this reference condition the temperature T_0, which is established in the transducer when the area dA_T has the temperature of the surrounding objects, *viz.*, T_S.

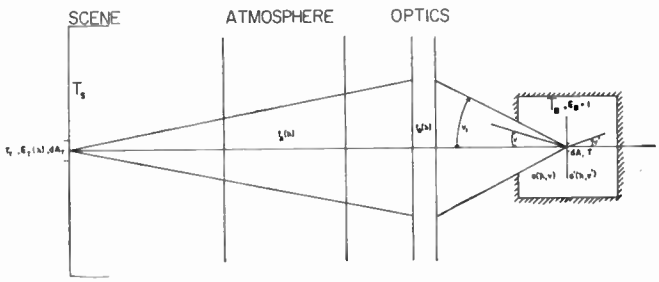

Fig. 2—Schematic diagram for the derivation of the radiation balance of the transducer.

We first calculate the increment of energy $d(\Delta U_a)$, absorbed by dA in a time element dt, with respect to the reference condition. The increment of the apparent spectral radiance of dA_T is $\epsilon_T[N_\lambda(T_T)-N_\lambda(T_S)]$, and this radiance is the only one contributing to $d(\Delta U_a)$, since radiation from the atmospheric bands, the optics, and the enclosure are the same for $T_T \neq T_S$ and $T_T = T_S$. For small temperature differences $T_T - T_S = \Delta T_T$, we obtain

$$d(\Delta U_a) = \pi dA\, dt \Delta T_T \int_0^{v_1} E_a(v) \sin 2v\, dv, \tag{8}$$

where

$$E_a(v) = \int_0^\infty \epsilon_T t_A t_0 a(\lambda, v) \left(\frac{\partial N_\lambda(T)}{\partial T}\right)_{T_S} d\lambda.$$

The increment of energy $d(\Delta U_e)$, emitted by dA in a time element dt, with respect to the reference condition is, for small differences $T - T_0 = \Delta T$, given by

$$d(\Delta U_e) = \pi dA\, dt \Delta T \left[\int_0^{\pi/2} E_e(v) \sin 2v\, dv + \int_0^{\pi/2} E_e'(v') \sin 2v'\, dv'\right] \tag{9}$$

where

$$E_e(v) = \int_0^\infty a(\lambda, v) \left(\frac{\partial N_\lambda(T)}{\partial T}\right)_{T_0} d\lambda$$

$$E_e'(v') = \int_0^\infty a'(\lambda, v') \left(\frac{\partial N_\lambda(T)}{\partial T}\right)_{T_0} d\lambda. \tag{10}$$

For the special case of the SiO-Se layer combination, under consideration here, computations showed that the influence of the angle of incidence on $a(\lambda, v)$ and $a'(\lambda, v')$ can be disregarded; in this case, these quantities can be written as $a(\lambda)$ and $a'(\lambda)$, and (8) to (10) transform to the following:

$$d(\Delta U_a) = \pi dA\, dt \Delta T_T \sin^2 v_1 E_a, \tag{11}$$

$$d(\Delta U_e) = \pi dA\, dt \Delta T E_e \tag{12}$$

where

$$E_a = \int_0^\infty \epsilon_T t_A t_0 a(\lambda) \left(\frac{\partial N_\lambda(T)}{\partial T}\right)_{T_S} d\lambda$$

$$E_e = \int_0^\infty (a(\lambda) + a'(\lambda)) \left(\frac{\partial N_\lambda(T)}{\partial T}\right)_{T_0} d\lambda. \tag{13}$$

In the absence of significant lateral heat conduction in the transducer, these two terms alone establish the steady-state energy balance for the element dA. This results in the following formula for the temperature difference $(\Delta T)_R$ in the transducer for predominantly radiation cooling:

$$(\Delta T)_R = \sin^2 v_1 \frac{E_a}{E_e} \Delta T_T, \tag{14}$$

where $\sin^2 v_1 = 1/(1+4F^2)$. (F = F number of optics.) Eq. (14) shows that, were it only for increasing $(\Delta T)_R$, the temperature T_0 should be made small compared to T_S, in order to decrease the value of the integral E_e in the denominator. This becomes more apparent when we assume that all quantities in (13) except $N_\lambda(T)$ and $t_A(\lambda)$, are independent of wavelength. With the further assumption that $t_A(\lambda)=0$ for wavelengths outside a band $\lambda_1 \cdots \lambda_2$, we obtain:

$$(\Delta T)_R = \frac{1}{1+4F^2} \epsilon_T t_0 \frac{a}{a+a'} \phi(\lambda_1, \lambda_2, T_S) \left(\frac{T_S}{T_0}\right)^3 \Delta T_T, \tag{15}$$

$$\phi(\lambda_1, \lambda_2, T_S) = \frac{\pi}{4\sigma T_S^3} \int_{\lambda_1}^{\lambda_2} t_A \left(\frac{\partial N_\lambda(T)}{\partial T}\right)_{T_S} d\lambda \tag{16}$$

(σ = Stefan-Boltzmann constant).

For a temperature $T_S = 300°\text{K}$ and a wavelength band from 8 to 14 microns, the latter expression has a value of about 0.5 for an air path containing 0.7 mm precipitable water, and of about 0.3 for one containing 17 mm precipitable water.

Since conductive cooling has to be ruled out so long as we want the transducer to be an unsupported film, the only method to reduce T_0 is by radiation cooling from the enclosure. The efficiency of this cooling method

depends on the F-number of the optics. It can be estimated that the minimum temperature to which the film can be cooled in this way cannot be smaller than

$$(2 + 8F^2)^{-1/4} \cdot T_S;$$

that is, 0.56 T_S for $F/1$-optics and 0.41 T_S for $F/2$-optics.

We turn now to a discussion of the influence of lateral heat conduction in the layer. We assume that the thickness of the transducer is small enough so that no temperature gradient is present in the direction vertical to its surface. The amount of heat flowing, during a time dt, into a volume element in excess of the amount flowing into the same volume element in the reference state is given by

$$-(k_1h_1 + k_2h_2)\nabla^2(\Delta T)dA\,dt,$$

where k_1 and k_2 are the thermal conductivities of the two materials and h_1 and h_2 are their respective thicknesses. In the steady state, we have now

$$-(k_1h_1 + k_2h_2)\nabla^2(\Delta T)dA\,dt + d(\Delta U_e) = d(\Delta U_a),$$

or

$$-\frac{k_1h_1 + k_2h_2}{\pi E_e}\nabla^2(\Delta T) + \Delta T = \Delta T_T \sin^2 v_1 \frac{E_a}{E_e} = (\Delta T)_R. \quad (17)$$

ΔT depends now on the pattern of the temperature distribution, ΔT_T, or the corresponding pattern of ΔT_R. Solutions of this equation for a number of patterns have been given by Eberhardth [12], Edmond and King [12], and by Jones [13]. In view of the pattern on which the earlier discussion was based, we take the solution given when $(\Delta T)_R$ has the form of a circular spot of diameter $2r_0$. Then

$$\Delta T = (\Delta T)_R\left[1 - \frac{r_0}{L_0}K_1\left(\frac{r_0}{L_0}\right)\cdot I_0\left(\frac{r}{L_0}\right)\right] \text{ for } r \leq r_0$$

$$\Delta T = (\Delta T)_R \frac{r_0}{L_0} I_1\left(\frac{r_0}{L_0}\right)K_0\left(\frac{r}{L_0}\right) \text{ for } r \geq r_0, \quad (18)$$

where $I_0(z)$, $K_0(z)$, $I_1(z)$, $K_1(z)$ are the modified Bessel functions of zero and first order, and where the quantity

$$L_0 = \sqrt{\frac{k_1h_1 + k_2h_2}{\pi E_e}} \quad (19)$$

defines a "characteristic length." (See [8].) If r_0 is not too small, with respect to L_0, the drop in ΔT at distances larger than r_0 is very rapid, and it is permissible to define a temperature difference $\overline{\Delta T}$ as the average taken over the nominal area of the circular spot. We obtain

$$\overline{\Delta T} = (\Delta T)_R\left[1 - 2K_1\left(\frac{r_0}{L_0}\right)I_1\left(\frac{r_0}{L_0}\right)\right]. \quad (20)$$

The relationship between $\overline{\Delta T}/(\Delta T)_R$ as a function of r_0/L_0 is plotted in Fig. 3.

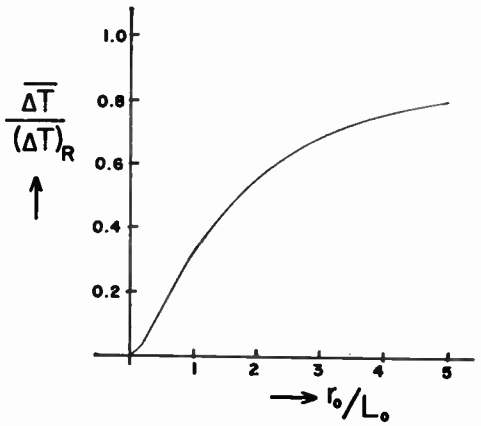

Fig. 3—Dependence of $\overline{\Delta T}/(\Delta T)_R$ on r_0/L_0.

We are ready now to combine the two steps of our investigation and obtain the following expression for the minimum apparent target temperature differences observable in the simple scene we have assumed;

$$\Delta T_{T_{\min}} = (1 + 4F^2)\frac{E_e}{E_a}\frac{\Delta T_{\min}}{1 - 2K_1\left(\frac{r_0}{L_0}\right)I_1\left(\frac{r_0}{L_0}\right)}. \quad (21)$$

This equation was evaluated for Se thicknesses ranging from 2 to 5 microns and SiO thicknesses ranging from 1 to 5 microns, both in 1-micron steps. The thermal conductivity of amorphous selenium was taken to be 5.10^{-4} cal sec^{-1} cm^{-1} deg^{-1}, [14], while, due to lack of available data, the thermal conductivity of SiO was assumed to be about that of fuzed quartz (3.10^{-3} cal sec^{-1} cm^{-1} deg^{-1}). For the computation of E_e, the lower limit of the integral was taken to be 8.5 microns, since contributions of smaller wavelengths to the integral are negligible due to the transparency of the transducer (between 8.0 microns and the wavelengths of the absorption edge of Se), and/or due to the small values of the factor

$$\left(\frac{\partial N_\lambda(T)}{\partial T}\right)_{T_S}$$

for short wavelengths; the upper limit of the integral was chosen as 30 microns, since the influence of the same factor keeps contributions of longer wavelengths to the integral small. E_a was calculated for the 8- to 14-micron atmospheric window and values for the spectral transmittance of the atmosphere were taken from published data on the atmospheric transmission in a ground-to-ground path. Two situations were evaluated, one for 0.7 mm precipitable water and one for 17 mm precipitable water. Finally it was assumed that the image of the transducer is observed by the unaided eye. (See Fig. 1.) This establishes nominal spot radii of 0.35 mm, 0.60 mm, 2.0 mm, and 4.4 mm on the transducer, corre-

sponding to the spot sizes of 9.68, 18.2, 55.2, and 121.0 minutes of arc as used in [7]. Furthermore an emissivity $\epsilon_T = 1$ and $F/1$ optical system with $t_0 = 1$ were assumed.

The following summarizes the results of the computations:

a) The characteristic length L_0 was found to change from 0.88 mm for the 1 μ Se-2μ SiO combination, to 1.23 mm for the 5 μ Se-5 μ SiO combination. This means that the nominal spot radii considered are about 4 times and about 0.3 times the characteristic length for the largest and the smallest spot, respectively.

b) Optimum performance is little affected by having the infrared radiation incident on the Se or on the SiO layer.

c) Subtended angle of circular spot, 121.0′: in this case, the change of the characteristic length with the composition of the layer is of little influence on the value of $\Delta T_{T\min}$ because the change in r_0/L_0 takes place in the range of small slope of Fig. 3. $\Delta T_{T\min}$ is mainly determined by the value of $\Delta T_{\min}$ tabulated in Table II. It leads to an optimum thickness of the Se layer of 5 microns. Since the expression E_a/E_e was found to decrease slightly with increasing thickness of the SiO layer, an optimum performance can be expected for thicknesses of this layer from 1 to 3 microns. For such a layer, values for $\Delta T_{\min}$ of 1.7°C and 2.5°C for 0.7 mm and 17 mm precipitable water respectively, were calculated.

d) Subtended angle of circular spot, 55.2′: in this case, with r_0/L_0 changing around 2.0, the influence of the characteristic length is greater, ruling out thicker SiO layers, since this material contributes most to the lateral heat conduction. The optimum layer is one with a Se thickness of 4 or 5 microns and a SiO thickness of 2 microns. $\Delta T_{T\min}$ has values of 3.0°C and 4.2°C, respectively, for the two amounts of precipitable water.

e) Subtended angle of circular spot, 18.2′: here, the influence of r_0/L_0 is increased. $\Delta T_{T\min}$ has a value of 16°C and 23°C for a layer of Se, 3 or 4 microns thick, and of SiO, 2 microns thick.

f) Subtended angle of circular spot, 9.68′: the small value of r_0/L_0 of about 0.3 leads to such small values of $\overline{\Delta T}/(\Delta T)_R$ that the application of the approximations used and the reasoning for the derivation of (19) are not permissible any more.

g) A combination of a 4-micron Se layer and a 2-micron SiO layer is the best. It results in the following assessment for $\Delta T_{T\min}$ as a function of angular spot size.

Spot Size:	18.2′	55.2′	121.0′
0.7 mm precipitable water:	16°C	3.0°C	1.7°C
17.0 mm precipitable water:	23°C	4.2°C	2.5°C

In order to characterize the resolution of the transducer in a way which lends itself to laboratory measurements of the same kind as used to determine the resolution of image tubes, we will now discuss its performance when subjected to a periodic pattern of line pairs, each pair composed of one line at a temperature T_S and one line at a temperature $T_S + \Delta T_T$. A solution for this pattern is found in the form of a series representation in [12] and [13]. It can be shown that this solution corresponds to the solution

$$\Delta T = \frac{(\Delta T)_R}{2} + (-1)^{2n}\frac{(\Delta T)_R}{2}\left\{1 - \frac{\cosh\dfrac{x - (k+n)\Gamma}{L_0}}{\cosh\dfrac{\Gamma}{4L_0}}\right\}, \tag{22}$$

for

$$k - \frac{1}{4} + n \le \frac{x}{\Gamma} \le k + \frac{1}{4} + n$$

$$(k = 0; \pm 1; \pm 2; \pm 3; \cdots; n = 0 \text{ or } 0.5),$$

where x is the coordinate perpendicular to the lines and Γ is the width of the line pair, measured on the transducer. It follows from (22) that the peak-to-peak value ΔT_{pp} of the periodic component of the solution is given by

$$\Delta T_{pp} = (\Delta T)_R\left(1 - \frac{1}{\cosh 4\Gamma_0}\right). \tag{23}$$

We will use (23) to calculate the relationship between target temperature difference and minimum detectable value of the line pair width, the latter expressed in number of line pairs per mm. The evaluation will be made for the layer composed of 4-μ thick Se and 2-μ thick SiO. We make the assumption that the contrast threshold of the human eye for observing the line pattern is the same as for observing a circular spot when the angle subtended by one line of the line pair is equal to the angle subtended by the diameter of the circular spot. The data in Table I mean that 0.38, 0.13, and 0.06 line pairs per mm are just observable when temperature differences of 0.24, 0.13, and 0.10°C are present in the transducer. Using (23) with $L_0 = 1$ mm and $\Delta T_T/(\Delta T)_R = 13.3$ (for 0.7 mm precipitable water), we are able to express these temperature differences by apparent target temperature differences. We obtain the following values:

	$\Delta T_T =$ 20°C	2.4°C	1.4°C
Maximum observable number of line pairs/mm =	0.38	0.13	0.06.

It remains now to calculate the transient behavior of the device. The amount of heat stored in a volume element in excess of that stored in the same volume element in the reference state is given by

$$C_1 dA d(\Delta T),$$

where C_1 is the thermal capacity per cm² of the layer. Again, we assume first that the effects of lateral heat conduction can be neglected. In this case we obtain, with (12) and (14),

$$\Delta T + \frac{C_1}{\pi E_e} \frac{d(\Delta T)}{dt} = (\Delta T)_R.$$

The process has a time constant

$$\tau_R = \frac{C_1}{\pi E_e}.$$

For the 4- μ Se-2- μ SiO layer, C_1 has a value of $8.34 \cdot 10^{-4}$ W sec cm^{-2} deg^{-1} (see [14]) if, due to lack of available data, constants for SiO_2 are used for the SiO layer. E_e was calculated to be $1.08 \cdot 10^{-4}$ W cm^{-2} deg^{-1}. This results in a value of τ_R of about 2.5 seconds.

We turn now to the transient behavior of the transducer when lateral conduction is present. It seems that a solution is available only for a periodic pattern of line pairs. The solution is in the form of a series representation where each term changes with a time constant descreasing with increasing order of the term. (See reference [13].) Restricting ourselves to the first term of the series, we obtain

$$\tau_1 = \frac{\tau_R}{1 + 4\pi^2 \frac{L_0^2}{r^2}}.$$

For the selected layer, we obtain with $L_0 = 1$ mm the following values for τ_1 for different values of line pairs per mm:

Line pairs/mm	0.38	0.13	0.06
τ_1	0.37	1.5	2.2 second.

The analysis made is sufficient for the attempted performance estimate; therefore a discussion of the influence of the absorption of the sodium arc lamp radiation in the Se layer was omitted.

As was pointed out in the beginning, it was not intended to make an attempt to optimize the transducer. In [10], it has been reported that a transducer, consisting of a combination of a metal layer and a selenium layer, was used. Such a film can be made so that it exhibits a high absorption for infrared radiation striking the selenium side of the film within angles of incidence up to 50°, and a low absorption for all other angles of incidence. This asymmetrical behavior of the film results, then, in an improvement of the ratio E_a/E_e in (13) (for further details see papers by Hilsum on this subject [10], [15]. This feature, and the fact that the thickness of the metallic absorbing layer is substantially less than that of the dielectric absorber considered above, result in a performance superior to that of the transducer configuration discussed here: objects 15°C above ambient temperature could be seen in a laboratory device using $F/1$-optics; a time constant of less than 0.5 second was measured; the imaging device showed a resolution of 2 line pairs/mm, which is probably not due alone to lateral conduction effects but also due to imperfections of the optical system used.

E. Device Using an "Energy Proportional Transducer"

This device has become known under the name "Evaporograph." Its underlying principle was first described in detail by Czerny [17], and was conceived as an aid for spectrometry in the infrared portion of the spectrum.

The transducer consists of a very thin nitrocellulose membrane, blackened on one side to absorb radiation, and with a thin layer of oil on the other side. This configuration is kept in an enclosure connected to a vacuum pump. The conditions are chosen so that for room temperature, the oil film is in equilibrium with its vapor, so far as is experimentally possible. This means that in the ideal case, the number of molecules leaving the oil film is equal to the number of molecules striking the oil film from its vapor. When the radiation absorbed is increased, the former balance is upset, the temperature of the irradiated part of the transducer increases, and a localized evaporation of the oil occurs. The process of evaporation continues so long as the irradiation prevails; the thickness of the oil layer decreases continually proportionally to time, and it is this change of thickness which is observed by the change of interference colors. Obviously, it is necessary to restore the oil film to its original state every time an observation has been made.

The rate of decrease of thickness is proportional to the radiant power falling on the transducer in excess of that establishing the original state of equilibrium, and inversely proportional to the heat of vaporization and the density of the oil. This assumes that the excess radiant power is consumed mostly for the evaporation of the oil and to a negligible amount only to cover increased re-radiation and conduction losses.

Baird-Atomic, Inc., Cambridge, Mass., has developed this principle into a commercial instrument. With optics of 8-inch focal length and $F/2.25$, blackbody temperature differences from a few tenths of a degree up to several hundreds of degrees against ambient temperature can be determined. The observation time to image a blackbody source of 1°C above ambient temperature is given as 6 seconds. The resolution was determined to be 10 to 14 lines per mm if a 10° blackbody temperature differential is viewed. The company proposes two modes of operation, depending on the temperature of the objects viewed. This becomes necessary due to the fact that the conditions of exact equilibrium between evaporation and condensation cannot be met without prohibitively extensive stabilizing measures. The conditions of the device are such that, in general, for object temperature of 80°C and above, the absorbed radiation is sufficient to cause evaporation of the oil at a faster rate than condensation occurs. In this case, a uniform film of oil is to be deposited, with the shutter of the instrument closed. The shutter is then opened and the local changes in interference colors are evaluated with visual or photographic techniques. For objects below 80°C, Czerny's original idea is used in

a varied manner [18]. The method has been called the "condensograph method." In it, the oil film is first removed from the membrane by flooding it with intense radiation from a lamp in the instrument. When the local lamp is turned off and the shutter is opened, oil will start to condense on the membrane at a faster rate on portions of the membrane subjected to smaller irradiation, and at a slower rate at portions subjected to larger irradiation. In this way, a pattern of different interference colors is obtained once again.

Acknowledgment

The author is indebted to Dr. G. A. Morton at RCA, Princeton, N. J., and to L. M. Biberman at the Chicago Midway Laboratories, Chicago, Ill., for valuable discussions on certain aspects of this paper. Also, the assistance of the staff of the Far-Infrared Branch, U. S. Army Engineer Research and Development Laboratories, is gratefully acknowledged.

References

[1] S. Berler, "Blackbody Radiance Differentials as Influenced by the Atmosphere," U. S. Army Engr. Res. and Dev. Labs., Ft. Belvoir, Va., to be published.
[2] Communication from the Radiation Electronics Corp., Skokie, Ill.
[3] C. F. Gramm, A. Prasil, and G. W. Hammar, "An Image Scanner Using Lead Sulfide Cells," Eastman-Kodak Co., Rochester, N. Y.; Contract NOrd 9979, Task II, Phase III; December 15, 1953.
[4] A. Angot, "Le rayonnement infra-rouge," *Mém. artillerie franc.*, vol. 2, pp. 455–457; 1955.
[5] R. W. Astheimer and E. M. Wormser, "Instrument for thermal photography," *J. Opt. Soc. Am.*, vol. 49, pp. 184–187; February, 1959.
[6] D. C. Northrop, "Quart. Rept. No. 31," Services Electronics Res. Lab., Bladock, Herts., Eng.; July, 1953.
[7] W. F. Koehler, F. K. Odencrantz, W. C. White, "Optical constants of evaporated selenium films by successive approximation," *J. Opt. Soc. Am.*, vol. 9, pp. 109–115; February, 1959.
[8] G. Hass and C. D. Salzberg, "Optical properties of silicon monoxide in the wavelength region from 0.24 to 14.0 microns," *J. Opt. Soc. Am.*, vol. 44, pp. 181–187; March, 1954.
J. T. Cox, "Optical constants of SiO for wavelengths from 14.0 to 30.0 microns," verbal communication.
[9] H. R. Blackwell, "Contrast thresholds of the human eye," *J. Opt. Soc. Am.*, vol. 36, pp. 624–643; November, 1946.
[10] W. R. Harding, C. Hilsum, and D. C. Northrop, "A new thermal image-converter," *Nature*, vol. 181, pp. 691–692; March 8, 1958.
C. Hilsum, "Tech. Rept. No. M.16," Services Electronics Res. Lab., Bladock, Herts., Eng.; April, 1959.
C. Hilsum, Ph.D. dissertation, London University, England; 1959.
[11] C. Hilsum, "The absorption edge of amorphous selenium and its change with temperature," *Proc. Roy. Soc. B*, vol. 69, pp. 506–512; 1956.
[12] E. H. Eberhardt, "The Distribution of Temperature in Thin Films," ITT Labs., Fort Wayne, Ind., Rept. No. 188, Contract NObsr 42080; December, 1949.
J. Edmond and P. G. R. King, "Addendum to Quart. Rept. No. 17," Services Electronics Res. Lab., Bladock, Herts., Eng.; January, 1950.
[13] R. C. Jones, "Temperature Distribution in Thin Films," Polaroid Corp., Cambridge, Mass., Interim Tech. Rept., Contract DA-44-009 Eng-1727; 1955.
[14] A. V. Kurtener and E. K. Malyshev, "Thermal conductivity of selenium and Hutchins alloy," *J. Tech. Phys. (USSR)*, vol. 13, p. 641; 1943.
[15] C. Hilsum, "Infrared absorption of thin metal films," *J. Opt. Soc. Am.*, vol. 44, pp. 188–191; March, 1954; vol. 45, pp. 135–136; February, 1955.
[16] F. Urbach, N. R. Nail, and D. Pearlman, "Observation of temperature distributions and of thermal radiation by means of non-linear phosphers," *J. Opt. Soc. Am.*, vol. 39, pp. 1011–1019; 1949.
[17] M. Czerny, *Z. physik*, vol. 53, p. 53; 1929.
[18] D. Z. Robinson, unpublished work.

Paper 4.5.2

Photoemissive Image-Forming Systems*

R. S. WISEMAN† AND M. W. KLEIN†

Introduction

THE devices described in this paper all use the evaporated, semitransparent photoemissive surface as the infrared-sensitive element. The photoemissive surface in the device converts the infrared radiation image into an electron emission, which is accelerated and focused either on a phosphor of an image tube or on the storage target of an image orthicon television-camera tube. In the case of the image tube, the phosphor screen converts the electron image into a visible picture which can be viewed directly. In the case of the image orthicon tube, its storage target develops a pattern of charges corresponding to the electron image, and an electron scanning beam is modulated by this charge pattern producing a visual picture on a kinescope.

The Photoemissive Surface

Photoemissive surfaces are formed by evaporating thin films of various metals under controlled conditions. Their response does not depend upon a rise in temperature in the surface, but on an emission of electrons caused by the absorption of radiation quanta. These surfaces have the following general characteristics:

1) The photo-current is directly proportional to the intensity of the radiation until saturation.
2) The energy of the emitted photo-electron is linearly related to the frequency of the exciting radiation.
3) The energy of the photo-electron is independent of the intensity of the exciting radiation.

* Original manuscript received by the IRE, June 30, 1959.
† U. S. Army Engr. and Dev. Labs., Fort Belvoir, Va.

The kinetic energy, E, of the photo-electron can be calculated from Einstein's fundamental photo-electric equation

$$E = hf - ew$$

where f is the frequency of the radiation and w is the work function of the material.

The first practical photoemissive surface was formed by evaporating layers of silver and cesium in proper thicknesses with controlled oxidation and temperature to obtain maximum sensitivity. This silver-oxygen-cesium surface, designated S-1, is sensitive to radiation of 0.3–1.2 microns with dual peaks at 0.36 and 0.8 micron, as shown in Fig. 1. When irradiated with radiation from a tungsten lamp operated at 2870°K (color temperature), it has a typical integrated response of 25 μa/lm and a maximum observed integrated response of 60 μa/lm. At 0.8 micron, its absolute sensitivity is 2.2 mμa/μw for a typical surface and 5.5 mμa/μw for the best surface. Its quantum efficiency at 0.8 micron is only 0.84 per cent.

Because of its broad spectral response, the S-1 photoemissive surface has been usable in devices designed to receive ultraviolet, visible, and near-infrared images and signals. However, research advances resulted in the development of the cesium-antimony photoemissive surface, which has greater luminous sensitivity (48–88 mμa/μw at 0.44 micron), greater quantum efficiency (25 per cent), and a spectral response curve extending to 0.7 micron, matching more closely that of the eye. Thus, the cesium-antimony photoemissive surface, called the S-4, -5, -9, -11, -13, or -17 when evaporated on different materials (*e.g.*, glass, quartz, or aluminum backing), became the standard surface for visible and ultraviolet sensitive devices; and the silver-oxygen-cesium photoemissive surface, S-1, became the standard for near-infrared sensitive devices.

In the past few years, a new surface has been developed which has even greater sensitivity than the cesium-antimony surface and has greater response in the red, out to 0.79 micron. This surface, called the S-20 or multi-alkali photoemissive surface, is formed by proper evaporation of antimony, potassium, sodium, and cesium. Its luminous sensitivity to a 2870° K color-temperature tungsten lamp is from 150 to more than 225 μa/lm. Its absolute sensitivity at its peak, 0.44 micron, is 65–98 mμa/μw, and its quantum efficiency is 28 per cent. Its dark current caused by thermionic emission is only 0.03×10^{-15} amperes per square centimeter, as compared to 70×10^{-15} for the S-11 cesium-antimony surface and 900×10^{-15} for the S-1 silver-oxygen-cesium surface.

The S-1 photoemissive surface is, at present, the surface used in near, infrared image-forming devices for the military, since these systems are designed to operate only at wavelengths longer than 0.85 micron, in order to prevent visual detection by the enemy.[1]

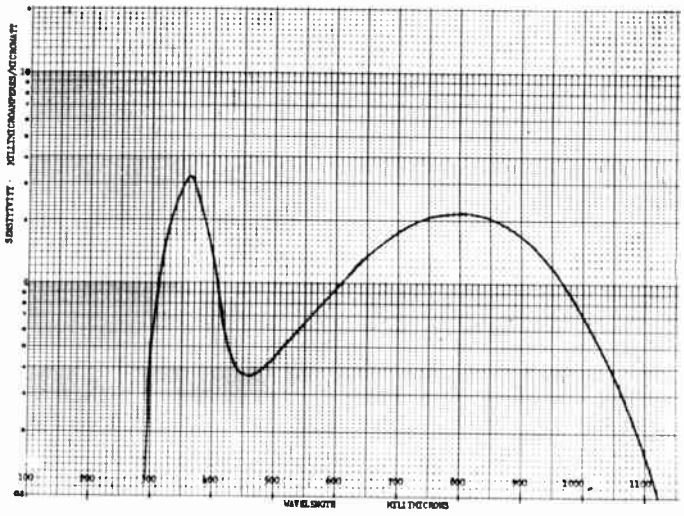

Fig. 1—Spectral response of S-1 photoemissive surface.

The Image Tube

Development of image tubes was started in the United States in 1942. Since that time, there has been a continuing improvement in sensitivity, image quality, and simplicity of construction and operation.

Basically, an image tube is an evacuated cylindrical glass tube, one end of which bears a photoemissive surface, while the other is coated with a phosphor screen. Radiation incident on the photoemissive surface causes the photoelectrons to be emitted in a density pattern equivalent to the incident radiation image. These photoelectrons are accelerated toward the phosphor screen and given added energy by applying 6–20 kv, dc. In addition, the electrons are focused by either an electrostatic or a magnetic field to form an electron image on the phosphor screen. The phosphor then converts this electron image into a visual image whose brightness distribution is equivalent to the radiance distribution in the original infrared image. Since the photoemissive surface responds to quanta and not to thermal effects, the resultant infrared and visual images are similar to all other images formed by reflected light.

As indicated, the electron optics used to form the electron image within the image tube can be either electrostatic or magnetic. At the present time, most image tubes are electrostatically focused; and whereas formerly, this type of tube required intermediate focusing electrodes, the latest designs are unipotential. Magnetic-focused image-tube development for the military has been hampered by the unavailability of permanent magnets in small light-weight sizes, sufficiently strong to create the necessary field strengths to control the electrons when accelerated by the high voltages required to obtain high-brightness images.

The phosphor used in military image tubes is the P-20, zinc-cadmium-sulfide, which, although producing a yellow-green picture, is the most efficient phosphor in converting the electron energy into visible light. This

[1] R. S. Wiseman and M. W. Klein, "Infrared viewing systems," paper 5.1.6, this issue, p. 1617.

phosphor has short persistence, so that moving objects may be seen clearly without smearing. If desired, long persistent phosphors or phosphors of other compositions may be used to obtain different output characteristics.

The over-all sensitivity or gain of an infrared image tube is measured in terms of its "conversion index." The conversion index is determined by projecting one-tenth (0.1) lumen of 2870°K color-temperature radiation from a tungsten lamp onto the photoemissive surface. A standard RETMA (Radio, Electronic and Television Manufacturers Association) #2540 infrared-transmitting filter is placed between the source and photoemissive surface to eliminate visible radiation shorter than 0.8 micron. The lumen output of the phosphor is then measured, and the ratio of the output to the input flux is called the conversion index of the tube. The early infrared image tubes of World War II had a conversion index of less than 0.5, but improvements in photoemissive-surface sensitivity, increased operating voltages, and increased phosphor sensitivity have resulted in tubes with conversion indexes sometimes as high as 40.

The original tube developed for use in military equipment was the 1P25 image tube, illustrated in Section 3. Representative of the latest type of tube is the 6914, Fig. 2. Both are electrostatically focused tubes, and a comparison of the two is given in Table I.

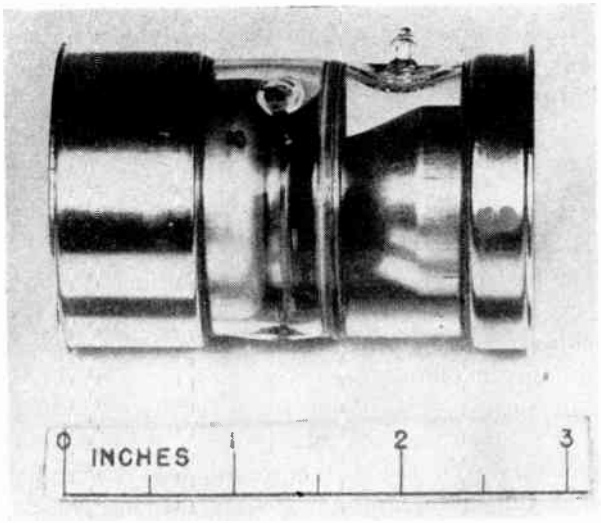

Fig. 2—6914 image tube.

TABLE I
COMPARISON OF 1P25 AND 6914 IMAGE TUBE

	1P25 (1942 design)	6914 (1959 design)
Length	4.6 inches	2.75 inches
Diameter	1.7 inches	1.75 inches
Operating voltage, over-all	4000 volts	16,000 volts
Intermediate focusing voltages	3	none
Magnification, cathode to phosphor	0.5	0.8
Resolution	8 line pairs/mm	28 line pairs/mm
Conversion index	0.4	30
S-1 Photoemissive surface	20–30 μa/lm	30–40 μa/lm

FUTURE DEVELOPMENTS

The U. S. Army Engineer Research and Development Laboratories have a continuing program directed toward improving the conversion index, picture quality, and over-all performance of infrared image tubes. Studies are being conducted to improve the sensitivity response of photoemissive surfaces, to reduce thermal and field emission background noise, to improve phosphor resolution and efficiency, and to increase image-contrast rendition. New image-intensifier techniques, such as the cascading of two-image tubes, are being developed to achieve an even greater conversion index. The literature contains information on many new image-tube techniques being used in developing low light-level image-intensifier tubes for use in moonlight and starlight viewing systems.[2] Since the only difference between a low light-level intensifier image tube and an infrared image tube is the evaporation of a different photoemissive surface, the techniques described previously are all applicable to future infrared image-tube developments.

Although the silver-oxygen-cesium photoemissive surface was first used in early image-orthicon television-camera tubes for visible operation, it is not known what sensitivity they achieved beyond 0.7 micron. Recent attempts to make infrared image orthicons with silver-oxygen-cesium photoemissive surfaces have failed to produce any tubes with usable near-infrared sensitivity. Perhaps future studies will furnish information which can be used to make image orthicons with infrared sensitivity, and infrared television will then be available for military use.

[2] M. W. Klein, "Image converters and image intensifiers for military and scientific use," PROC. IRE, vol. 47, pp. 904–909; May, 1959.

Paper 4.5.3

An Infrared Pickup Tube*

G. A. MORTON†, SENIOR MEMBER, IRE, AND S. V. FORGUE†, FELLOW, IRE

THERE are a number of ways in which infrared photoconductors, modified to give them the required electrical characteristics, may be used in simultaneous read-in imaging devices.[1] The most promising of these were examined in detail and the method finally selected as most satisfactory was that using frame storage and sequential read-out. This is the principle employed in the television pickup tube known as the vidicon. In order to obtain a longer wavelength response than can be achieved with any known *photoemitter*,[2] lead sulfide was chosen as a suitable *photoconductor* for the initial investigation.

The pickup tube contains a sensitive target surface in the form of a thin layer of the photoconductor on a transparent window forming one end of the tube. For reasons that will become apparent, the photoconductor employed must have a very high resistance when the material is in darkness. At the other end of the tube, there is an electron gun producing a low velocity beam of electrons. Electrons returning from the target enter a secondary emission multiplier which is coaxial with the gun, and the greatly amplified return current is supplied to the signal lead. Fig. 1 shows the arrangement of this tube. The electron beam is focused by an axial magnetic field and deflected by a system of orthogonal deflecting coils producing fields at right angles to the motion of the beam.

The operation of this type of pickup tube is illustrated in Fig. 2 and may be described as follows. First, assuming the tube is in complete darkness, any small element of area of the photoconductor under the beam receives electrons and becomes increasingly negative until it reaches approximately the potential of the gun cathode. Thereafter, the beam electrons can no longer reach this element, but are turned back by the negative charge on it and are collected by the multiplier. As soon as the beam moves away from this element in the course of its scanning cycle, the dark current flowing between the conducting substrate (which is maintained at a positive potential), and the surface tends to charge the surface positive. This charging continues until the beam returns to this element at the start of the next frame, when it is again returned to cathode potential. Now, if radiation falls on the target in the area in question, the surface charges positive more rapidly, due to the photoconduction of the material, and reaches a higher positive potential during the period of one frame. Consequently, when the beam passes over this area and returns it to its equilibrium (gun cathode potential), more electrons will be extracted from the beam and fewer returned to the multiplier. It is evident, then, that if the radiation image is focused upon the target, the output current from the multiplier will fluctuate as the beam passes over the illuminated and unilluminated areas of the image, the current being larger for the dark areas and smaller for the illuminated regions. This is the video signal output of the pickup tube.

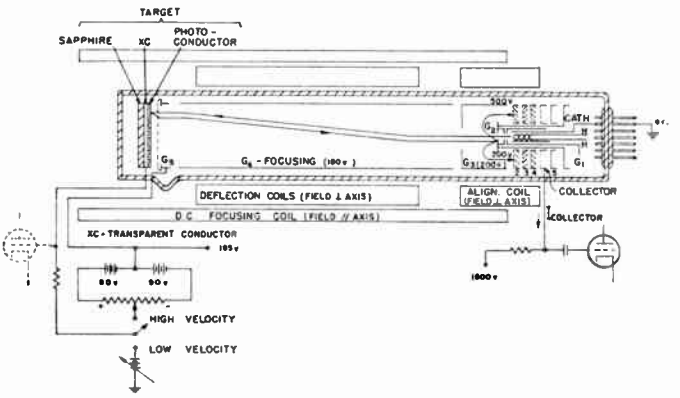

Fig. 1—Basic arrangement of infrared photoconductive beam scanning pickup tube.

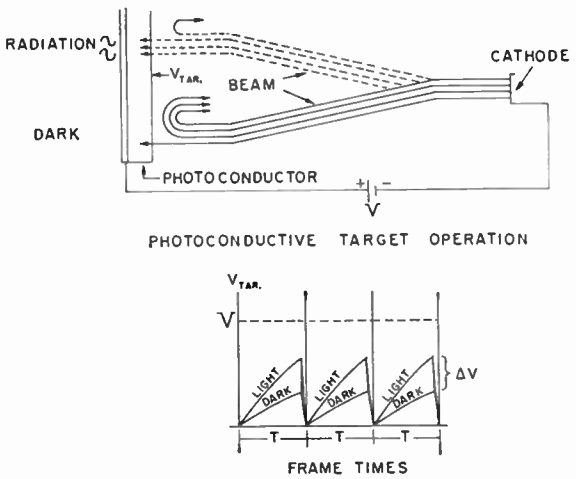

Fig. 2—Photoconductive target operation, and frame time.

An important point to notice in connection with this type of operation is that every picture element of the target which is illuminated conducts a photocurrent during the entire time and stores the accumulated information as a positive surface charge for the frame period while the beam is elsewhere on the target. This storage operation leads to a gain in signal-to-noise ratio proportional to the square root of the number of picture ele-

* Original manuscript received by the IRE, June 30, 1959.
† RCA Labs., Princeton, N. J.
[1] W. K. Weihe, "Classification and analysis of image-forming systems," paper 4.5.1, this issue, p. 1593.
[2] R. S. Wiseman and M. W. Klein, "Photoemissive image-forming systems," paper 4.5.2, this issue, p. 1604.

ments in the image area, as compared to the same photoconductor used in a system where point-by-point scanning is employed; *e.g.*, where the photoconductor is used with a Nipkow disk or other similar system.[3] For a high definition picture, such as the tube under discussion is capable of producing (*e.g.*, a 400-line picture), the gain in signal-to-noise ratio is of the order of 500 times.

The critical element of the infrared pickup tube is the photoconductive target which must satisfy two rather conflicting requirements; namely, it must be of a material which is sensitive to relatively long wavelength infrared radiation, yet it must have the high resistivity required for storage operation. A simple calculation reveals that for a target of material having a dielectric constant of 3, the resistivity must be of the order of 10^{10} ohm-centimeters. In order to make clear the difficulty which arises in attempting to satisfy these two conditions, it is necessary to examine briefly the physics of photoconductivity.

As has been discussed earlier in Section 3.4, a photoconductor is a material whose conductivity increases when electromagnetic radiation of appropriate wavelength is incident upon it. They are members of the class of substances which are known as semiconductors. In these substances, which are in general crystalline in nature, the conduction electrons (and holes) are weakly bound to their parent lattice atoms, thereby differing on the one hand from an insulator where the binding is strong, and on the other hand from a metal where the conduction electrons are free. At low temperatures and in the absence of radiation, semiconductors have very high resistance. However, electromagnetic radiation of short enough wavelength and therefore constituted of photons of sufficient energy, can cause the release of charge carriers and consequently cause conductivity. The relationship between radiation wavelength, λ, in microns, and photon energy, E, in electron volts (ev) is:

$$E = \frac{1.234}{\lambda}.$$

If a photoconductor is to be sensitive to radiation of 2-micron wavelength, the binding energy of the charge carriers must be 0.617 ev or less. A normal semiconductor, with an activation or binding energy as small as this, will have a very low resistivity at room temperature. Therefore, for application in a storage type pickup tube, the basic material must be prepared in very special ways. The resistivity of normal lead sulfide at room temperature is only a few ohm-centimeters. This, as has been shown above, is 9 or 10 orders of magnitude lower than the resistivity required for storage operation; therefore the lead sulfide must be greatly modified for use in this type of pickup tube.

[3] M. R. Holter and W. L. Wolfe, "Optical-mechanical scanning techniques," paper 4.2.4, this issue, p. 1546. Also, R. H. McFee, "Infrared search system design considerations," paper 4.2.5, this issue, p. 1550.

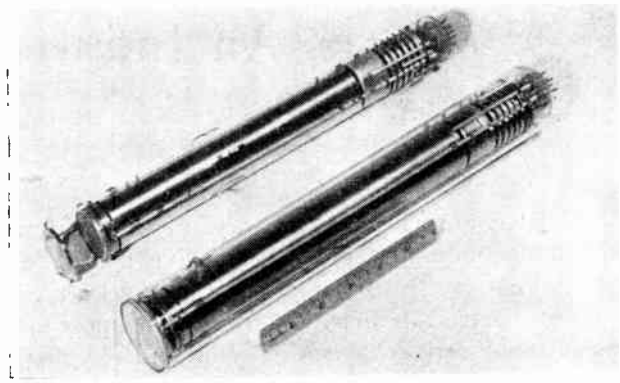

Fig. 3—Infrared beam scanning pickup tube (2 inch noncooled).

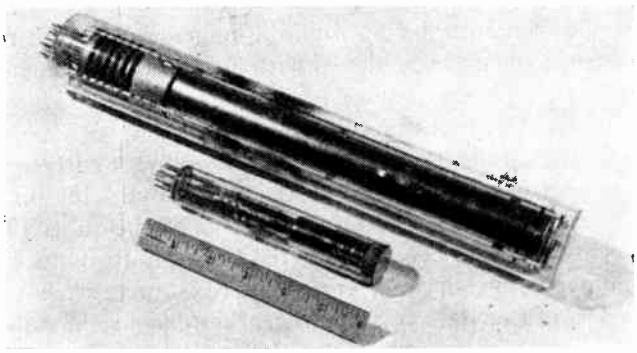

Fig. 4—Infrared pickup tubes using modified lead sulfide (2-inch and 1-inch sizes).

Targets for the tube under discussion are prepared by evaporating, on an appropriate substrate, layers of lead oxide which are then activated with sulfur and a suitable thermal treatment, followed by a final layer of lead oxide. This results in a surface film which has a very high resistance and which has an extremely complex structure in terms of a solid-state model. The fraction of lead sulfide centers in the layer is relatively small, but sufficient so that the optical absorption of the film is adequate for the purpose. The presence of the lead oxide increases the ionization energy of the basic lead sulfide and, furthermore, it introduces barriers in the form of *p-n* junctions.

The completed tube with the modified lead sulfide target is shown in Fig. 3. It fits into a focusing coil and deflecting yoke which is very similar to that used for the image orthicon and, except for the fact that it does not require image section voltages and a higher target voltage is used, the voltages applied to the tube electrodes are also approximately those used with the image orthicon.

In addition to the 2-inch-size tube shown in the preceding figure, smaller tubes of the 1-inch vidicon size were also made. The tubes of this size did not have a multiplier and employed standard vidicon basing so that they could be used directly in ITV cameras. Fig. 4 shows a side-by-side comparison of the 2-inch and 1-inch-size tubes.

In order to evaluate these tubes, a field camera based on a closed-loop ITV unit was constructed. This camera

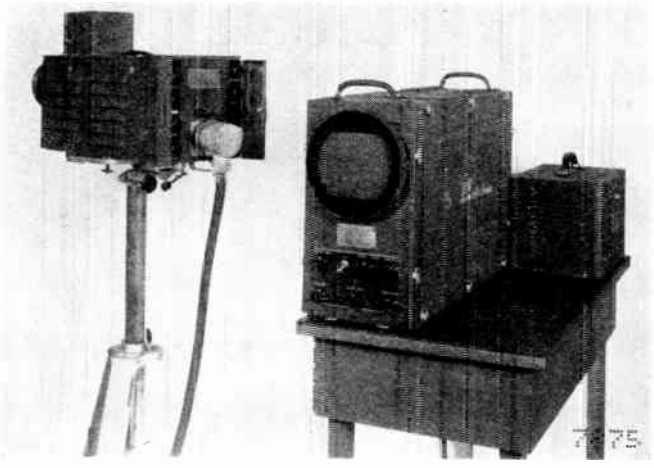

Fig. 5—Infrared field camera chain.

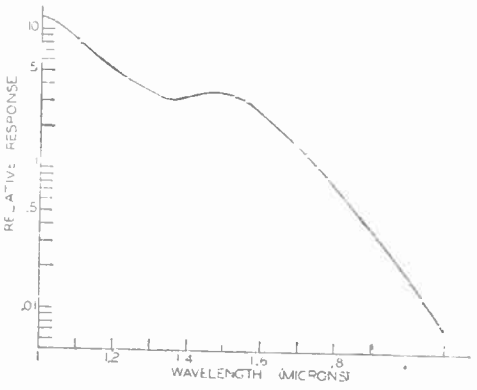

Fig. 6—Spectral response of infrared pickup tube.

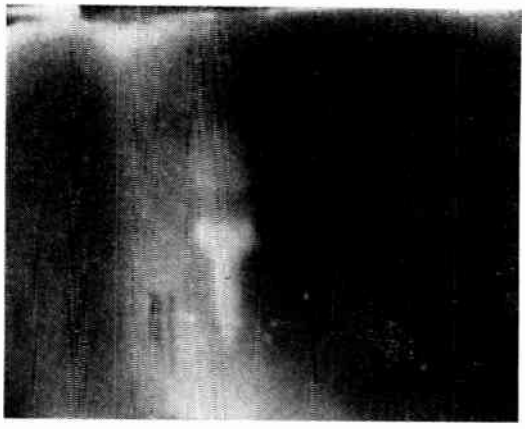

Fig. 7—Soldering iron at 200°C.

Fig. 8—Human subject illuminated with radiation beyond 1.3 microns (Corning 2540/4060 combination).

is shown in Fig. 5. The spectral response of the system is shown by the curve given in Fig. 6. The response reflects the contributions of a form of lead oxide response, having its maximum in the middle of the visible spectrum, and the lead sulfide response, which peaks in the near-infrared and extends out to about 2.1 microns.

The sensitivity of these tubes is sufficient to image objects which are at 150°C, by their own radiation. Fig. 7 shows the reproduced image of a soldering iron operated at 200°C. The long wavelength limit extends far enough into the infrared so that it is possible, with the use of an appropriate infrared filter (a combination of Corning 2540 and 4060 passing radiation beyond 1.2 microns) and an illuminator, to see with radiation which is invisible to the World War II image tubes. Fig. 8 shows a human subject illuminated with such an illuminator. It is interesting to note that the flesh tones are completely black, due to the fact that there is a strong water absorption band in the vicinity of 1.8 microns where the reflectivity is very low.

The sensitivity and long wavelength response of tubes of this type are sufficient so that they can be used for the study of the thermal area distribution of objects operated at a relatively high temperature, such as boilers, nuclear reactor cores, and certain types of electrical equipment. With an appropriate illuminator, they may be used in the preparation and processing of infrared films, since such films have a long wavelength cut off considerably above the cut off of the tubes in question. Another interesting application of these tubes is in the examination of the semiconductor germanium. Germanium becomes transparent at 1.8 microns. Thus, these tubes can be used together with appropriate optics for examining strain patterns, making microscope studies of the material, etc. They have also proved to be a useful tool for rapidly adjusting near infrared optical systems for maximum performance. A final example of the application of these tubes might be cited in their employment by spectroscopists for the rapid study of near-infrared spectra, beyond the wavelength that can be covered either with an image converter tube or by photographic plates.

Acknowledgment

The writers wish to acknowledge the contributions of G. Krieger, G. Bain and Dr. M. Schultz to the development of this tube. The program of research at RCA Laboratories which led, in 1952, to the development of this tube was sponsored by the U. S. Army Engineer Research and Development Laboratories, Fort Belvoir, Va.

SECTION 5—INFRARED APPLICATIONS

Paper 5.0 Introduction*

PAUL J. OVREBO†, EDITOR

THE material on infrared military applications is not all-inclusive, but rather a general treatment within limited categories, which hopefully describes the application of the physics of infrared and the use of the components described in the two preceding sections. Furthermore, this Section serves to indicate the development of the practical art which has taken place following the close of the time period covered in Section 2 on the early history of infrared technology.

It should be remembered that the requirements of security have of necessity limited the scope and extent of the treatment of military applications. However, it is hoped that the general discussion of this material which has reached the public domain will give the reader an appreciation for the methods already employed and the future potential of this art.

Beyond this, it has been an interesting experience to collect data on industrial and medical applications. Whereas the emphasis of development has in the recent past been predominantly in the military area, the future will see an increasing trend toward the utilization of infrared technology in the satisfaction of human needs.

It is desired to acknowledge the cooperation of the several companies in furnishing technical data and to thank the individual contributors for preparing their portions of the manuscript. Special recognition is due R. W. Powell for his editorial assistance at several important stages during the preparation of Section 5, which follows.

* Original manuscript received by the IRE, July 13, 1959.
† Wright-Patterson Air Force Base, Dayton, Ohio.

Paper 5.1

Military Applications of Infrared Techniques*

L. W. NICHOLS,[I] W. A. CRAVEN,[II] MEMBER, IRE, R. W. POWELL,[III] R. S. WISEMAN,[IV] M. W. KLEIN,[IV] W. L. WOLFE,[V] M. R. KRASNO,[VI] W. R. WILSON,[VII] M. ARCK,[VIII] G. JANKOWITZ,[VIII] AND P. J. OVREBO[IX]

5.1.1 MISSILE SEEKERS AND HOMERS

by L. W. Nichols and W. A. Craven

Introduction

THE application of infrared (IR) techniques to missile guidance is a natural one, since most targets of military importance emit large amounts of thermal radiation. The earliest efforts toward such applications were in Germany, where in the early 1930's, the forerunners of the present-day lead sulfide cells were developed. Also during this period, basic research was done on the transmission of infrared through the atmosphere, and measurements were made of the infrared radiation from various targets and backgrounds.

During World War II, the Germans devised a number of systems using infrared, including several types of anti-aircraft missiles. Scanners were developed to the point where they were able to detect piston-engine bombers at distances up to 5000 meters.

The United States and British efforts during the war were partly directed toward infrared surveillance systems, such as the "sniperscope," with a minor effort on the development of guided devices such as guided glide-bombs. Most of the effort in the United States to develop infrared seekers for missiles has occurred since the end of World War II. This effort was spurred somewhat by the advent of turbojet aircraft and the production of lead sulfide cells whose performance surpassed that of the earlier German cells. The effort was slow at first, but increased rapidly when evidence of success became apparent.

A wide variety of specific types of missiles to which IR may be applied are: air-to-air, ground-to-air, air-to-ground, and ground-to-ground missiles. Of these many possibilities, the most successful application has been to the air-to-air homing missile, where the tailpipe of a turbojet aircraft serves as the radiant target source. For this type of missile, the infrared seeker provides a compact passive-guidance capability with sufficient angular accuracy to provide precision guidance.

* Original manuscript received by the IRE, July 13, 1959.
[I] Naval Ordnance Test Station, China Lake, Calif.
[II] Guided Missile Lab., Hughes Aircraft Co., Culver City, Calif.
[III] Avionics Div., Aerojet-General Corp., Azusa, Calif.
[IV] Warfare Vision Branch, Elec. Engrg. Dept., U. S. Army Res. and Dev. Labs., Ft. Belvoir, Va.
[V] Willow Run Labs., Univ. of Michigan, Ann Arbor, Mich.
[VI] Raytheon Co., Santa Barbara, Calif.
[VII] Northwestern University, Evanston, Ill.
[VIII] Barnes Engrg. Co., Stamford, Conn.
[IX] Wright-Patterson Air Force Base, Ohio.

Function of Missile Seekers

The primary function of an infrared missile seeker is to provide information on the target's location in a form suitable to guide the missile to the target. The usual missile guidance system causes the missile to follow a collision course to the target, as illustrated in Fig. 1.

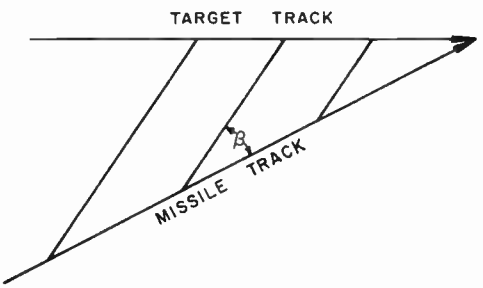

Fig. 1—Target and missile tracks for collision-course guidance.

The characteristic feature of the collision course is the constancy of the line-of-sight angle to the target, β. For such collision-course guidance, it is therefore necessary that the infrared seeker provide information so that the missile steering can be so instrumented as to maintain a constant value of β. It normally is most convenient to obtain constancy of β by maintaining its first time derivative $\dot{\beta}$ equal to zero. Therefore, the missile-seeker's function can be reduced to the accurate measurement of the deviation of $\dot{\beta}$ from the desired value of zero. This value of $\dot{\beta}$, then, serves as an error signal to actuate the missile-steering mechanism; the result is the desired collision course with the target. Such a guidance system can be represented as a simple servo system, as shown in Fig. 2.

An important conclusion from the above is that an absolute measurement of angle is not required for missile guidance, only accurate angular rates being significant.

The seeker may now be shown as a subsidiary servo-loop, as in Fig. 3.

The infrared scanner generates an error signal if the target does not coincide with its null axis; the amplifier amplifies this error and drives a mechanical transducer, which realigns the scanner null axis with the target by a suitable means. Depending on the particular implementation of this tracking loop, a measure of $\dot{\beta}$ is obtained which can be used for steering.

From the above description, it is possible to further define the function of the optical scanning system as the

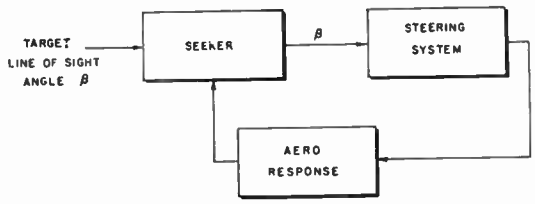

Fig. 2—Block diagram of missile-guidance system.

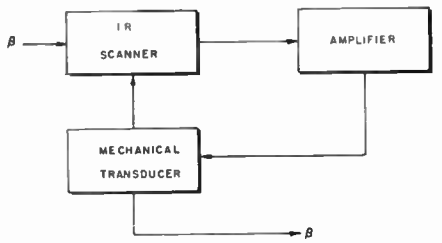

Fig. 3—Functional diagram of typical missile seeker.

measure of the deviation of direction of the line of sight to the target from a null position. The absolute accuracy of this measurement is of importance only insofar as it affects the measure of the rate of deviation in the particular implementation of the seeker loop.

General Characteristics

Although intuitively, the angular measurement which the seeker performs is a simple function, it should be recognized that this function need normally be performed by equipment which operates under extreme environmental conditions in a small space and with minimum weight. To illustrate the types of conflicting requirements that need to be reconciled, a tabulation of a few is given in the following table.

Desired Characteristics	Requirements of Missile Application
Large aperture for maximum sensitivity	Limit of missile diameter
High-resolution optical system	Short axial length of optical path
Adjustable optical elements to maximize resolution	Fixed elements for stability and easy production
Thick, rigid optical elements	Low weight and inertia required and small space available
Constant temperature control and stable mounting platform	Wide range of ambient temperatures; severe vibration
Fixed high-quality cables for signal leads to minimize microphonics	Light, flexible cables in high-vibration environment

The resultant design, based on such considerations, will usually have the following general features:

Weight: Minimum weight is attained by use of relatively thin optical elements, the normal thickness-diameter ratio of about 1/4 being reduced to as little as 1/10 in some cases. Supporting structures are also reduced to a minimum, using high rigidity-to-weight configurations wherever possible. Low-density materials are used where suitable.

Size: The design is carefully executed to maximize the optical system size, resulting in small clearances and rigid tolerance on mechanical structures; normally, the available axial optical path is shorter than the aperture diameter.

Resolution: By astronomical standards, resolution is usually poor, 10 to 100 times the diffraction limit being typical.

Optical tolerances: Tolerances on optical surface quality can be rather loose, but lack of adjustment of spacing or centering requires abnormally tight tolerances on thicknesses, edged diameters, and centering.

Electrical circuits: Since photodetectors typically operate in the microvolt region, extreme care is taken to rigidly mount detectors, and to use high-quality connectors, specially-treated low-microphonic cables, and shock-mounted high-quality tubes or transistors.

Typical Optical Scanner

A typical scanner consists of an image-forming optical system, a reticle or chopper in the image plane to modulate or "chop" the radiation, an infrared detector, and an amplifier, as shown schematically in Fig. 4.

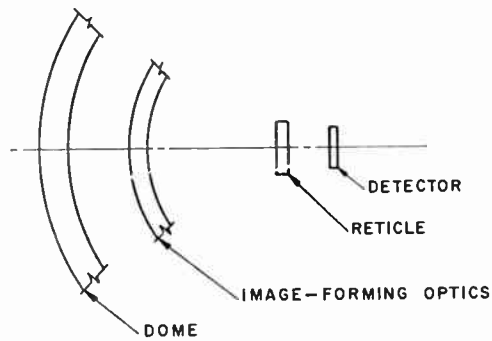

Fig. 4—Typical optical scanning system (schematic).

The image-forming optical system performs the functions of collecting radiation from the target and focusing it on the reticle. The optics may be a lens system or mirrors. Usually the missile nose window itself is utilized as one of the optical elements. If the dome is a concentric shell of some infrared transmitting material, it will act as a negative lens and offer the designer a degree of freedom in correcting spherical aberration. When the dome can be used in this fashion, optical systems of relative aperture f/1 or less can be designed which still have adequate image quality. Optical systems for missile seekers are discussed in detail elsewhere in this issue.[1]

[1] H. Dubner, "Optical design for IR missile seekers," paper 4.2.2, this issue, p. 1537.

The reticle or modulator element in a seeker lies in the focal plane of the image-forming optics. Its function is to modulate the incoming radiation into an ac signal, which confirms the presence of the target and also furnishes directional information. The modulated wave form produced by the chopping reticle is used for automatic tracking in much the same way that a modulated radar-return signal is used in a tracking radar.

There are a number of ways in which the chopping reticle may be used. The two most common are a nutating system and a rotating system. In a nutating system, the optical axis of the collector is rotated at an angle to the axis of the reticle. This causes the image to move about on the reticle in a circular fashion; and, if there is a target in the field of view, it will be modulated by the reticle pattern as its image moves about. In a rotating system, the optical axis of the collector and the axis of the reticle are common, but the reticle rotates in the image plane. In this case, the rotating pattern in the image plane will modulate the target image to give the error signal.

After the radiation from the collector passes through the modulating reticle, it is allowed to strike the infrared detector. Here it is converted to an electrical signal.

A number of detectors are now available for use in seekers. Among them are lead sulfide, lead selenide, gold-doped germanium, and indium antimonide. Each has characteristics favoring particular applications.

The lead sulfide cells are sensitive to radiation in the visible wavelengths and out to wavelengths as long as 3μ. They can be operated in an uncooled state and are perhaps the best detectors for use against targets whose temperatures are above 350°C.

The lead selenide, gold-doped germanium and indium antimonide cells are particularly sensitive in the 3- to 5-μ wavelength region. They all have shorter time constants than lead sulfide and, because of their long wavelength response, they can detect cooler targets than lead sulfide cells. These cells have to be operated in a cooled condition, however, to realize their best performance, and this imposes some problems in their application to military devices.

The size of the detector used in a seeker is usually made as small as possible in an effort to increase the seeker sensitivity. The ratio of the collector area to the detector area is termed the optical gain of the system. The greater the optical gain, the less the energy density need be for the seeker to track, and hence, the farther it can "see" a target.

Whichever cell is chosen, the threshold signal generated by it will be of such small amplitude that severe requirements are imposed on the electrical connections and the amplifier used with it. It is desired for best performance to have the cell noise level, which is usually a few microvolts, be the limiting noise of the system. Since cell noise figures are usually in the range 3 to 12 db above thermal noise, amplifier noise can, under static conditions, be made small in comparison. The more difficult problem is the elimination of microphonics and electrical pickup under operating conditions.

The present-day infrared seeker has undergone sufficient developments so that its threshold sensitivity is close to the limit imposed by the detector. Infrared-power densities less than one-billionth of a watt per square centimeter are sufficient to lead the seeker to its target. This high sensitivity is desirable, but it brings with it many problems related to background clutter. Reflected sunlight from clouds, mountains, or the sea may be seen by some seekers. Even self-emitted radiation from clouds or mountains may be a background problem. There are many techniques available to enhance the contrast of the target while subduing the background. These include various forms of optical filters, and space filtering. The problem here is to achieve the most favorable compromise so that the seeker can operate at useful ranges against daytime background clutter.

Fig. 5—SIDEWINDER infrared missile fired from F9F-8 Cougar hitting flare on wing-tip of F6F Drone.

Operational Infrared Seekers

At present, there are two examples of infrared air-to-air missiles in operational status: the Navy's SIDEWINDER and the Air Force's FALCON. Both are successful and show extremely high accuracy.

The accuracy of the SIDEWINDER is demonstrated in Fig. 5, which shows a SIDEWINDER missile hitting a flare mounted on the wingtip of an F6F drone. This technique leaves the drone undamaged for another test. The SIDEWINDER missile is 5 inches in diameter,

Fig. 6—Infrared FALCON air-to-air missile.

about 9 feet long, and weighs approximately 150 pounds. It can be carried by a variety of aircraft, including the F8U-1, the FJ-4, and the F104. The SIDEWINDER has been used recently by the Chinese Nationalists with marked success against the Communists in combat over the Taiwan Straits.

The FALCON GAR-2A infrared missile was designed to complement a similar radar-guided missile, the GAR-1. These missiles are about 6½ inches in diameter, about 6½ feet long, and weigh slightly more than 120 pounds (see Fig. 6). The prime mission of these missiles is air defense, and they are currently used in the F102A and F-8911 interceptors. A variety of loadings of the interceptor can be utilized, but the normal usage is a mixed load of radar and infrared missiles for more versatility.

The seeker used in the FALCON GAR-2A is a compact, sealed unit. This unit is able to "look" over a large solid angle, providing maximum flexibility in attack geometry. The tracking range of the seeker is sufficient to allow the missile to be launched many miles from the target.

5.1.2 FIRE CONTROL

by R. W. Powell

Introduction

As a result of new developments in infrared scanners, the importance of infrared missile- and gunfire-control equipment to the military has been increased tremendously. The infrared scanner is used in fire-control operations to perform the functions of "search," "acquisition," and "tracking." The "search" function implies the systematic examination of space for the purpose of locating and identifying targets of interest. "Acquisition" implies the process that occurs between the location of a target in the search phase and the final alignment of tracking equipment on the target. The "tracking" function implies the continuous and precise observation of the target to collect sufficient information to permit predictions about the target (such as an expected future trajectory) to be made.

Fire-control systems and surveillance equipments using visual sights are essentially limited to daylight operation. Infrared fire-control equipments can extend the capability of these systems throughout the hours of darkness by optically and electronically converting the invisible infrared radiation of hot targets, such as aircraft and motor-driven vehicles, into visible target information or into signals suitable for automatic fire control.

Modern radar equipment provides an effective means for the firing of guns and rockets. However, there are dangers associated with sole reliance on radar fire-control equipment. Since radar systems are active, *i.e.*, transmit signals, the enemy can obtain from them considerable information on the presence, location, intention, and tactics of the attack. This information can then be used to guide any of several types of countermeasures, including maneuvering, electronic countermeasures (ECM), and decoying. Also, radar is susceptible to electronic countermeasures. In addition, fire-control radar is costly, and its complexity makes it susceptible to failure.

Advantages of IR Fire Control

Infrared fire-control equipment has the following inherent advantages as compared with radar equipment.

It is simpler, smaller, and less expensive.
It has greater angular accuracy.
It has no minimum-range limitations.
It can be used for low-angle operation near the ground or sea.
It requires very little auxiliary equipment.
It is passive (does not transmit signals that might betray its position).
It is difficult to jam.

Design Considerations

In the designing of radar fire-control equipment, the search and fire-control functions are usually combined in one device. Because of different functional requirements, such a combination necessarily results in some undesirable compromises.

Search equipment should be able to detect targets at a long range but need not be capable of highly-accurate angular resolution, and it should be able to search through a large volume of space in a short period of time. On the other hand, fire-control tracking equipment must be capable of extremely high angular accuracy, but need not have the long ranges and large field of view of search devices.

Another fundamental difference is that, to be tactically useful, search equipment must be able to detect and present multiple targets within its field of view, while tracking equipment is concerned with only one target in most situations.

Because of the small size and simplicity of the infrared equipment, it is entirely feasible to use separate search and tracking systems, each designed for its specific function without the detrimental compromises demanded by the opposing requirements. Systems of separate, specialized scanners having the two separate functions of search and tracking can even be used in airborne applications in which space and weight are at a premium. In addition to the attainment of high performance by specialization, search while tracking is achieved, thereby providing the operator with additional combat information.

Equipment

Fig. 7 shows the construction of typical infrared receiving equipment, an airborne scanner.

Fig. 7—Airborne infrared scanner, and associated electronics.

The use of the visual gunsight on interceptor aircraft for the firing of guns and rockets has recently been extended to include both day and night operation by the addition of infrared equipment. The infrared sight (IR sight) for fire-control use is an example of infrared equipment which performs the "search" and "tracking" functions. The pilot performs the "acquisition" function by selecting a particular target for tracking.

An IR sight is in operational use in this country; it is being used by the F-104 Starfighter interceptor. The sight is a single unit containing the infrared detection system, the electronic amplifiers, and the visual-display projection system for the combining glass of the visual gunsight. The complete unit, weighing 14 pounds (without the power supply), is shown in Fig. 8.

Mounted in the cockpit of the F-104, the IR sight receives infrared energy through a small window under the windshield canopy. The target is presented, as a visual display, directly onto the combining glass in front of the pilot. The pilot sees the display in the same position as the visual image of a target would normally be observed. He flies the aircraft to superimpose upon the

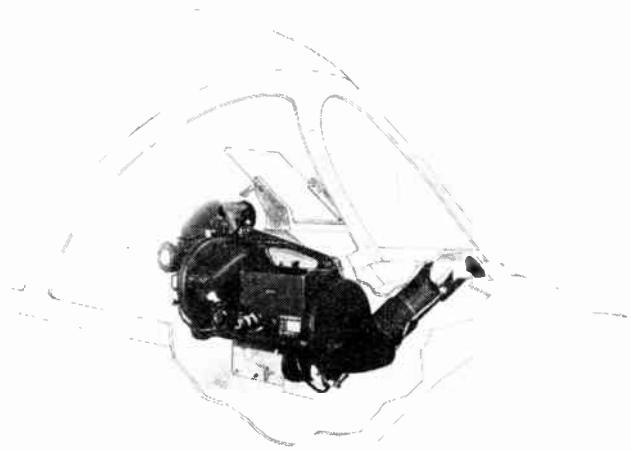

Fig. 8—Infrared sight installation in fighter aircraft.

IR display the "pipper" of the computing sight, and thus is able to conduct the attack as if the enemy aircraft were directly visible to the eye.

As the speed and power of targets continue to increase and the cross sections of targets continue to decrease, the future contributions of passive, infrared, scanning equipment for airborne fire control are expected to be highly significant.

Infrared fire-control equipment is applicable to surface installations to provide night, as well as day, search and tracking capability, and to avoid the sea-return and ground-clutter problems that are associated with radar in use against surface or low-altitude targets.

5.1.3 BOMBER DEFENSE

by R. W. Powell

BOMBER-defense studies have shown that fighter aircraft equipped with IR missiles and IR search-track gear pose a dangerous threat to a bomber. Unlike AI radar, the IR equipment of the fighter is passive and does not reveal even the presence of the fighter to the bomber. To establish fighter presence, intention, and capabilities for countermeasure purposes, the bomber crew has to choose between

a) employing active radar, with the attendant weight, complexity, revelation of bomber presence and location, and susceptibility to countermeasures and to home-on-radar missiles; or

b) employing passive IR equipment.

An infrared scanner can extend the capability of the bomber-defense system by providing increased detection ranges against interceptors, indicating the launching of missiles from the interceptor, and providing information for the initiation of countermeasures.

After the initial detection of threatening interceptors and missiles by a search scanner, it is important that the potential threat be continuously monitored or tracked to permit the defense to be evaluated further. An infrared tracker can also be used to provide a defense-system operator with accurate information on the

angular positions of targets as well as on the rate of change of the target positions. With this type of precise information as a basis, the choice of the active or passive defense to be used becomes simpler and more certain of success.

5.1.4 AIRBORNE EARLY WARNING

by R. W. Powell

Introduction

THE systematic surveillance of areas of anticipated attack by static warning devices such as the Distant Early Warning (DEW) line and the Texas towers is being supplemented with airborne-warning lines extending over large areas of the oceans. The addition of high-performance IR search equipment to the search radar in these systems offers a number of potential advantages for the Airborne Early Warning (AEW) system.

Target-Detection Range

High-speed aircraft with effective long-range armament are among the weapons to be detected in the near future. The high operating altitude of the picket aircraft is conducive to long-range IR detection, due to the associated reduction in atmospheric attenuation of the IR energy of the target. In addition, increases in intruder speed seriously increase the burden on an AEW aircraft line equipped with radar alone, whereas IR detection ranges tend to increase rapidly as target speed is increased.

Sight-Line Accuracy

Target sight-line measurements to within a fraction of a degree appear highly desirable for AEW equipment, especially if the radar is less accurate in either a normal or a countermeasured environment. For example, high accuracy and fine resolution in target sight-line angles should be useful in establishing the number and approximate spacing of intruders in a raid formation, and in providing refined target-bearing data for use in interceptor control.

Countermeasure Resistance

Unlike the search radar, the IR equipment is completely passive; its operation does not reveal the presence of AEW airplanes to the enemy.

Additional Target Data

The IR search equipment can provide redundant data on intruders which might be used in a number of ways. For example, the comparison of IR signals with radar search signals might assist in classifying the target. The IR equipment also represents a limited but potentially important source of data for use in the event of radar search degradation due to component failure or severe enemy ECM activity.

Installation

The passive infrared scanner, with its capability of providing large areas of coverage, can be easily installed in high-altitude-picket aircraft because of its small power, space, and weight requirements.

The sensitivities reported in the literature for infrared detection systems have been increasing rapidly with the development of new detectors, materials, and techniques. In addition, to obtain higher speeds, the trend in aircraft equipment has been to provide increasingly greater engine power, thereby releasing more and more infrared energy as well as the increase in IR radiation resulting from the heating of the leading edges of the aircraft due to the higher speeds. This indicates that although the achievable detection ranges of IR equipment are very good today, extraordinary increases can be predicted for the future.

5.1.5 BALLISTIC-MISSILE DETECTION

by R. W. Powell

THE natural progress in the field of tactical weapons indicates that future warning systems must be able to detect the launching and re-entry of ballistic missiles (ICBMs and IRBMs) as well as manned aircraft. The continuing improvements in the range and resolution of infrared scanner systems indicate that such equipment may be capable of meeting the detection requirements of the future. The small size, weight, and cost will permit the extensive utilization of infrared equipment for warning lines maintained from aircraft, ships, and satellites.

In the spring of 1958, the U. S. Army announced that the infrared radiation from a Jupiter IRBM re-entering the earth's atmosphere was measured by infrared equipment aboard missile-tracking ships off the coast of the Lesser Antilles island group in the Atlantic Ocean. The missile had been launched from the Air Force Missile Test Center at Cape Canaveral, Fla. An Aerojet-General field radiometer (Fig. 9) was used as a manual tracker in this program.

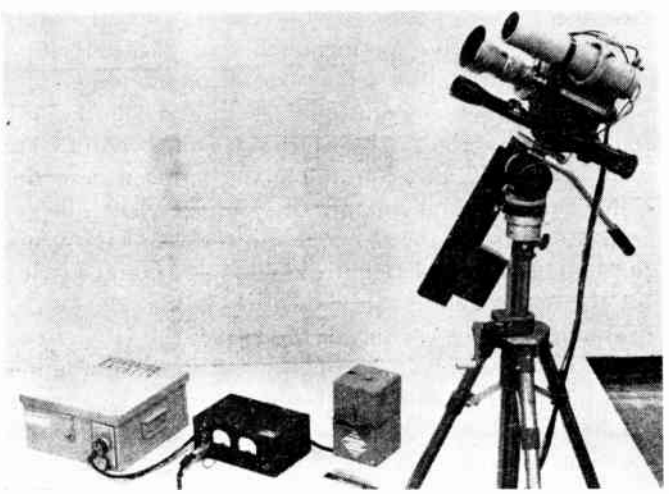

Fig. 9—Field radiometer.

The tracking of long-range ballistic missiles during the launching phase should be an even greater contribution because of the highly-accurate angular measurements that can be made with infrared trackers. It is possible that with such data, the point of re-entry may be determined. Furthermore, the tremendous amount of infrared radiation emitted by large rocket engines and the high altitudes to which burning persists should permit the observation and accurate tracking of ICBMs, IRBMs, and submarine-launched missiles at extreme ranges.

5.1.6 INFRARED VIEWING SYSTEMS

by R. S. Wiseman and M. W. Klein

Introduction

TWO TYPES of infrared viewing systems are presently being used or studied by the U. S. military. One is the near-infrared system utilizing radiation in the 0.8- to 1.5-μ spectral region which is reflected from the target and converted to a visible image by use of a photoemissive image-converter tube. The other is the far-infrared system utilizing radiation in the spectral region from 1.5 μ to beyond 14 μ which is emitted from the target itself. The far-infrared invisible heat image is converted to a visible image by using various techniques which relate an electrical, magnetic, physical, or chemical change of special materials to temperatures in the image.

Near-Infrared Viewing Systems

Fig. 10 shows the basic components common to all near-infrared viewing systems. The first requirement is a source of near-infrared radiation, such as a searchlight which irradiates the target to be viewed. Depending on the specific requirements, tungsten lamps, carbon arcs, or xenon arc lamps are used as the source. Since these sources emit not only infrared, but visible radiation as well, it is necessary in military applications to use a filter to eliminate the visible radiation of wavelengths shorter than 0.85 μ so as to obtain security from visual detection. The near-infrared projected by this searchlight is reflected by the target, and an infrared image is formed by the objective lens (either refractive or reflective type) of the viewing device on the infrared-sensitive, cesium-silver-oxide photoemissive cathode surface of the image-converter tube. The image tube converts the infrared image into electrons which are focused (electrostatically or electromagnetically) to create a visible picture on the phospher viewing screen. An eyepiece is used to view this visible picture directly. A high-voltage, low-current power supply is required to operate the image tube. Typical power ratings are 12 and 16 kv, dc, with a current of about 0.01 μa. The power source is a type C dry cell in a transistorized blocking oscillator-type power supply.

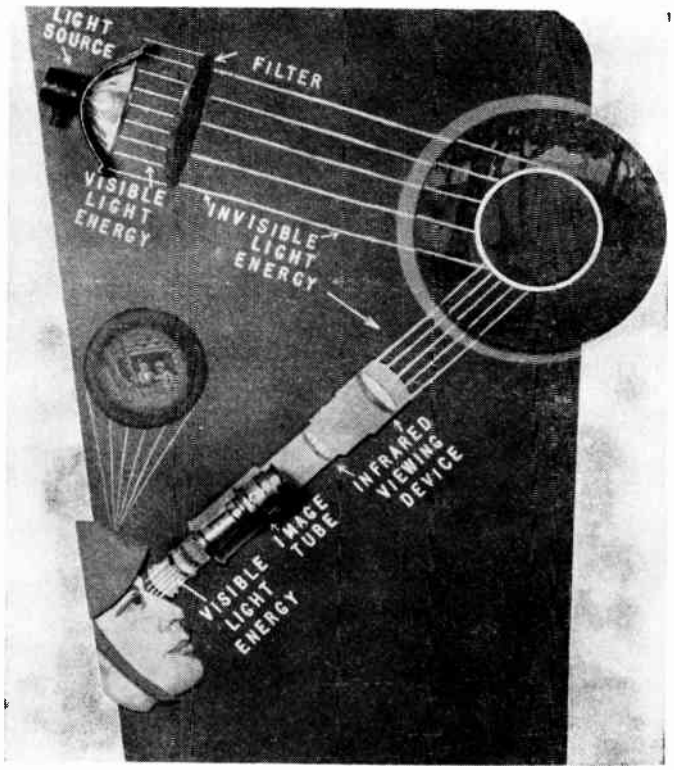

Fig. 10—Operating principles of near-infrared detecting systems.

Military Applications

The first U. S. military use of a near-infrared viewing system was demonstrated at Fort Belvoir, Va., in 1942, when a hand-held infrared telescope was used to drive a truck along a darkened road in an attempt to improve blackout driving of military vehicles. Since that time, numerous other military applications have proved successful, and great improvements have been made in the image-tube performance. Sensitivity and image quality have been greatly improved, along with dependability and simplicity of operation. An entire family of near-infrared viewers has been developed by the U. S. Army Engineer Research and Development Laboratories and are being found extremely useful in a wide variety of military tasks. Lightweight, helmet-mounted, near-infrared binoculars were developed for use in driving vehicles. By simply snapping a set of infrared filters over the conventional headlights of the vehicle, a soldier equipped with these binoculars can drive at moderate speeds with confidence and good security. These lightweight binoculars are also used with auxiliary infrared sources for performance of activities where freedom of movement and use of both hands is required. With them, equipment and material can be moved and assembled in forward areas under infrared floodlights.

Probably the most famous near-infrared viewer is the "sniperscope" of World War II. The original issue was fairly heavy and bulky. The high-voltage power supply for the image tube and the low-voltage power supply for the tungsten source mounted on the viewer were both contained in the pack worn on the back. The latest

sniperscope, now called the "weapon sight" (Fig. 11), not only has improved performance, but also is much lighter in weight. The high-voltage power supply for the image tube is integral with the viewer. The low-voltage batteries for the tungsten lamp are in the small pack which is worn on the belt. The light source can be demounted from the viewer and the viewer used with auxiliary infrared sources placed in strategic positions to irradiate critical military targets or areas.

The near-infrared image metascope (Fig. 12) was developed for use in reading maps and signs, in detecting the enemy use of near-infrared sources, and in signaling and communicating between individuals. For example, patrols can be sent through their own lines and re-admitted upon their return using infrared-filtered flashlights for signaling. The power supply for the image tube in this device is a tiny internal hand-cranked generator which charges a condenser for 30- to 45-minute operation.

Infrared image tubes have also been used to convert the periscopes and telescopes used in Army tanks for night operation. Such a system consists of a dual-purpose, infrared-visible searchlight, driver's periscope, gunner's periscope, commander's periscope, and hand-held infrared binoculars. It permits the tank crew in the so-called "buttoned up" condition to drive, to locate targets, and to fire its guns with accuracy and effectiveness necessary in modern warfare. The latest in the series of USAERDL-developed, near-infrared devices is the Unit Commander's Infrared Observation System. This system consists of a dual-purpose, infrared-visible searchlight and an infrared telescope with a 10-inch objective. This tripod-mounted telescope enables a military commander to study a tactical situation, to deploy his forces effectively, and to observe the progress of a night encounter from some remote vantagepoint.

Fig. 11—Infrared weapon sight.

Fig. 12—Metascope.

Scientific Uses

Use of near-infrared image tubes in scientific applications has been hampered in the past because of the poor performance of early tubes and the military security restrictions on the new and improved models. Now that certain of the new tube types have been declassified and good tubes are commercially available, there should be many applications in scientific research as well as in commercial fields.

Medical research has profited by the use of infrared image tubes in microscopes, in the ophthalmoscope and pupilometer for study of the eye without affecting adaptation, in studying frog-eye retinas without bleaching of the visual purple, in observing the action of animals, in sensory isolation, and in studies dealing with the blood.

The U. S. Department of Agriculture has used infrared viewing systems for studying the habits of rats and in observing the breeding habits of sheep. Spectrometers have been adapted using the image tube to permit direct observation of infrared spectral lines. Other viewers have been used for inspection of products, *e.g.*, film, during processing and for observing low-temperature radiation. Of course, near-infrared viewers have also been used for the overt surveillance of critical areas by police and guard forces.

Future Photoemissive Viewing Systems

Improvements in infrared image tubes can be expected to expand the use of the viewers to greater applications. All near-infrared viewers can be converted for visible or ultraviolet use by substituting the same type of image tube equipped with a different photoemissive surface. Image tubes can be made not only with the infrared-sensitive S-1 surface, but also with a visible-sensitive S-11 or S-20 (multialkali) surface, as well as an ultraviolet-sensitive surface. A new ultraviolet microscope has just been marketed using ultraviolet-transmitting optics and an ocular which includes an image tube having an ultraviolet photoemissive surface coated on its ultraviolet-transmitting face plate.

Development of infrared television has been delayed because of the inability to achieve good, sensitive S-1 photoemissive surfaces in the image-orthicon pick-up tube. Models made thus far have showed such low infrared sensitivity that they are unusable. Infrared-sensitive Vidicon pick-up tubes have been made with a lead oxide-lead sulfide photoconductor. Although their sensitivity is adequate, they are found to be unusable at low irradiation levels because of image persistence.

Far-Infrared Viewing Systems

Far-infrared viewing systems have been built around several widely different kinds of detectors. There are both scanning and nonscanning types. These viewers may be used to obtain thermal patterns of areas at temperatures generally from below 0°F to 500°F.

The Thermograph

One far-infrared image-forming device, the Thermograph (Fig. 13), obtains a two-dimensional thermal image by scanning the far-infrared image over a thermistor bolometer detector which has uniform sensitivity over a large wavelength range. The electrical output signal from the thermistor bolometer is amplified and modulates the light from the lamp. This light beam, in addition to being modulated, is scanned across a photographic film in synchronism with the initial pick-up scanning system and produces a picture in a manner similar to the wirephotos used in newspapers. The scanning time can be varied from a minute to a half hour, depending on requirements for over-all field of view, resolution, and sensitivity to temperature differences. Fig. 14 is a photograph of a scene made with the thermograph.

The Evaporograph

This instrument (see discussion of the Evaporograph later on) is a nonscanning far-infrared viewer. In principle, the thermal pattern is imaged on a thin membrane which absorbs the incident radiation and forms a heat picture. This heat picture, by causing evaporation, changes the point-to-point thickness of an oil film on the back of this membrane. White light projected on this varied-thickness film produces an interference color picture which is viewed directly or photographed without the requirement for electronic circuitry. The effect is the same as observed when sunlight is reflected from an oil film on water, and the colors can be related to the temperature-emissivity radiation from the original object.

The far-infrared viewers, in addition to obvious military applications, can be used in industry to inspect temperature distributions over engines, boiler housings, electrical connections, conductors, and components, and other objects where temperature is an important indicator. The Thermograph has also been used in medical research to determine the condition of body tissues by detecting areas of abnormal temperature.

Fig. 13—Thermograph.

Fig. 14—Thermograph picture of an airport scene.

5.1.7 INFRARED RECONNAISSANCE

by William L. Wolfe

EARLY methods of infrared reconnaissance were very similar to standard photography; special films and filters were used in aerial cameras to provide sensitivity to a wavelength of about one micron. These techniques provided information about the area viewed that could not be obtained by standard photography, especially camouflaged military objects, because sunlight in the near infrared is reflected differently than is visible sunlight. Infrared photography useful in the 0.8- to 1.2-μ-wavelength range is still of considerable importance. It has been extensively described in detail in other literature.[2] The interesting and useful techniques in the longer-wavelength regions of the spectrum (1 to 15 μ) provide information about energy radiated by a scene rather than reflected by it, and make possible new and powerful applications.

Three categories of reconnaissance, particularly in the military sense, may be delineated: ground-to-ground,

[2] W. Clark, "Photography by Infrared, Its Principles and Applications," John Wiley and Sons, Inc., New York, N. Y., 2nd ed.; 1945.

air-to-ground, and space-to-ground. Each of these is characterized by its own type of equipment, its own specific applications, and its unique problems.

Ground-to-Ground Reconnaissance

Each soldier or small unit has a need for information about his opposing number, the other individual soldier or small unit. He can usually take considerable time—minutes or even hours—to obtain this information, but he cannot afford to be logistically encumbered. His need for detection range can be assumed to somewhat exceed the range of his weapons, but it is essentially equal to this range. The enemy's activities should be known at all times so that no "sneak attacks" are possible. Thus, ground-to-ground surveillance equipment should have the following characteristics:

A capability for detecting objects of interest (soldiers, vehicles) at ranges of several hundred to a few thousand yards.
Simple logistics.
Continuous viewing capability.
Reaction time on the order of minutes.
Ability to operate in a clandestine manner.

These requirements have led to the investigation of equipments which operate passively,[3] and do so either by scanning techniques or by thermal-imaging techniques similar to those described in the preceding paper, and papers 4.5.1 and 4.5.3 in this issue. The purpose of these reconnaissance devices is to provide a visible representation of the thermal structure of the field of view.

Air-to-Ground Reconnaissance

As in the case of photographic observation, an aerial platform provides greater surveillance capability than a ground-based observing station. The problems are correspondingly more complex, but their solution pays greater dividends. The compromises that are available and the constraints limiting the design of an air-to-ground reconnaissance equipment have already been discussed.[4]

Scanners used for reconnaissance might have the general configuration of the Reconofax camera developed by Haller, Raymond, and Brown, Inc.[5] The Reconofax camera was originally designed as a photoelectric system that could operate under low light levels and utilize whatever advantages accrue from flying-spot scanning. Later, the equipment was modified for use with a lead sulfide detector. The scanner is illustrated schematically in Fig. 15. Radiant energy from a source at a distance enters the system as collimated light. The beam is folded by the scanning mirror into the collecting and focusing optics. The energy is transduced by the phototube, and after appropriate electronic amplification, the electrical signal modulates the output of a glow tube. (For simplicity, the schematic diagram combines the functions of the infrared-electrical transducer and the electrical-light transducer into a single phototube.) The resulting light signal is scanned across a film strip in synchronism with the scanning mirror. The scan is thus reconstructed, and an image is produced.

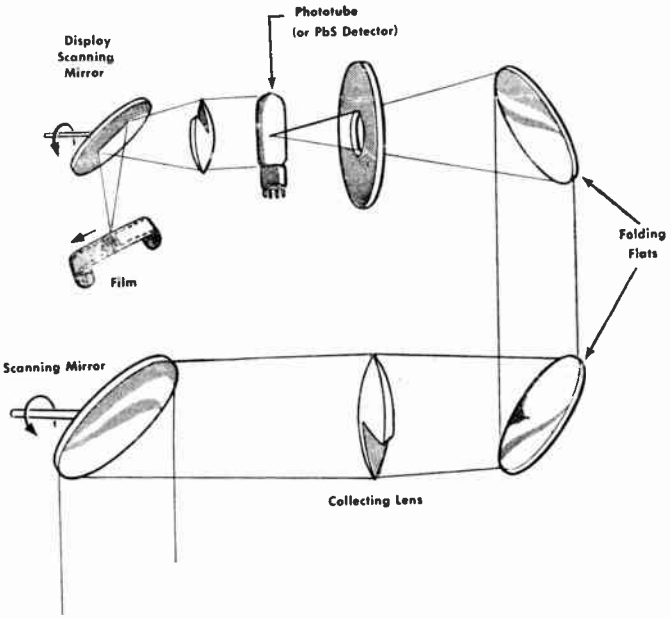

Fig. 15—Diagram of optical and scanning system of the Reconofax camera.

In the same way that stereoscopic photography and color film increase the information obtainable from photo-reconnaissance films, one can anticipate increased capabilities on the part of airborne infrared reconnaissance. Stereoscopic presentation is possible if the same scene is viewed from two places an appropriate distance apart. This can be accomplished if two telescopes are used, or even if one is properly designed to look at a scene from two different places at two different times. Similarly, "multicolor" presentation is possible if the different spectral responses of the various detectors are utilized or if appropriate filters with a single type of detector are used. Multicolor techniques permit inferences to be made about the temperature as well as the radiant heat from objects since, most terrain features are essentially "gray-body" sources.

Reconnaissance from Space

There are several important reasons for, and advantages in, performing reconnaissance from space, *e.g.*, from a satellite. These result from the tremendous altitude involved, which makes possible the surveillance of large parts of the earth's surface at a time. A properly

[3] "Passive operation" denotes detection by target-emitted radiation. "Active operation" denotes detection of the energy from an illuminating source reflected by the target, such as with the sniperscope described above by R. S. Wiseman and M. W. Klein, "Infrared viewing systems," paper 5.1.6, this issue, p. 1617.

[4] M. R. Holter and W. L. W. Wolfe, "Optical-mechanical scanning techniques," paper 4.2.4, this issue, p. 1546.

[5] J. B. Cannon, W. B. Birtley, and J. E. Bogen, "Interim Engineering Report on Development of Experimental Reconofax Camera," Haller, Raymond, and Brown, Inc.; January, 1953.

oriented satellite (polar orbit) will, in fact, scan the entire earth in a relatively short time, thus providing information about the cloud and storm structure, the radiant-heat exchange, temperature distributions on the earth, and many of the other important parameters related to heat and temperature.

Although increased height provides the advantage of increased coverage, it also limits the linear resolution capabilities. Some of the scanners which might be used for this purpose have angular resolution (instantaneous field of view) from 1 to 10 milliradians. An angular resolution of 1 milliradian from a satellite in a low orbit (10^6 foot altitude) provides a ground resolution of about 1000 feet. Although it is possible to improve this resolution, for representative optical systems, 0.1 milliradian probably represents the engineering limit, if not the Rayleigh (theoretical) resolution limit.

Other Applications

Although the above discussion is related primarily to military applications of infrared reconnaissance, other important related uses are being made of these techniques and still others can be anticipated. It is entirely feasible to search for schools of fish, and to map thermal currents in the ocean. The National Bureau of Standards has reported[6] on infrared techniques for determining rust in crops, and it seems possible to map water tables and to detect the flow of refuse disposal in rivers and water basins.

Infrared reconnaissance and mapping techniques are valuable in a variety of military and civilian applications. The equipments and methods are relatively new, and the promise of significant advancement is high. However, there are many interesting areas of research and development which need investigation. Techniques for the interpretation of the output of reconnaissance devices, the nature of the thermal radiation from many items of interest, and the investigation of new optical systems, better scanning techniques, improved optical materials, and better detectors all merit extensive investigation.

5.1.8 INFRARED COMMUNICATION

by M. R. Krasno and W. R. Wilson

Introduction

BETWEEN the red limit of the visible light spectrum and the cutoff wavelength of lead sulfide cells lies the near-infrared region generally used in infrared communications. If these wavelength limits are taken as 0.8 and 3.5 μ, the corresponding frequencies are 3.75×10^{14} and 8.57×10^{13} cps. This bandwidth of 289 megamegacycles must seem to the radio engineer enormously wide, and perhaps suited for a very large number of useful communication channels. Unfortunately, the usual number of channels obtained in this bandwidth is *one*. Practical methods of producing coherent radio waves are only now invading the EHF millimeter spectrum, which is still several orders of magnitude away from the near infrared in wavelength or frequency.

Considerations

Most sources available for use in the near-infrared radiate over a very broad spectral region. An example is the tungsten filament, which closely approximates a graybody radiator. For a typical lamp operating at 2900 K, 80 per cent of the radiation lies in the near-infrared; 10.7 per cent consists of visible wavelengths, 0.1 per cent is ultraviolet, and 92 per cent are longer infrared wavelengths.

A few lamp types having somewhat less extended spectral output are available. An example is the relatively very efficient cesium-vapor lamp, which radiates especially strongly in two lines at 8521 A and 8944 A (0.85 and 0.89 μ). However, only 22 per cent of the input energy appears in the two lines. Moreover, the lines are very close to visible wavelengths and the normal operating power requirements and the resulting equipment tend to be large.

The compact high-brightness arc lamp to some extent combines the characteristics of the two lamps mentioned above, producing a strong continuum much like that of a black- or graybody, but having superimposed on this continuum an intense infrared line spectrum concentrated between 0.8 and 1.0 μ.

Considering the spectral bandwidth of tungsten lamps and other IR sources, narrow-band "tuned" receivers would be very inefficient because they would respond to only a small fraction of the source radiation. Fortunately, the "receivers" or detectors available for the infrared are also generally very broad in their spectral response. Moreover, a detector can usually be chosen to be a reasonable spectral match to the source. For example, lead sulfide is an excellent match for a tungsten lamp and a good match for a xenon arc. Thallous sulfide, usable only at night, is an excellent match for a cesium-vapor lamp.

As used to communicate by infrared, the radiation is usually amplitude-modulated, either directly by current modulation of the source, or by modulating the steady beam of radiation from a constant source. The receiver cell, usually a photoconductive detector, responds to the amplitude-modulated infrared radiation by changing its resistance in correspondence to the modulation. The receiver electronics reconvert these resistance changes to the original electrical modulating signal.

Advantages

Privacy of communication is the chief advantage of IR communications. This privacy is a result of the

[6] H. J. Keegan, J. C. Schleter, W. A. Hall, Jr., and G. M. Haas, "Spectrophotometric and Colorimetric Study of Diseased and Rust Resisting Cereal Crops," U. S. Dept. of Commerce, National Bureau of Standards Rept. No. 4591; July, 1956.

narrow beamwidths easily and naturally achieved in infrared, the lack of side lobes and forward atmospheric scatter, and the ease with which the visible part of the radiation can be removed by optical filters. A second advantage is freedom from interference, also a result of narrow beamwidth. A third advantage is that it affords added channels over and above radio channels already in use and of a kind which cannot interfere with them. A fourth advantage is the lack of requirement for FCC licensing or regulation. This quite tremendous advantage for a large variety of users would seem incontrovertible, because of the lack of interference possibilities. A fifth advantage is its simplicity and potentially low cost. And finally, its sixth advantage is that with small size, simplicity, and low cost, it will give quite usable ranges of 6 to 10 miles in fair weather. Thus, it offers very convenient private communication for distances from just beyond voice range to as far as one can see. A diagram of a typical Infrared Communication System is shown in Fig. 16.

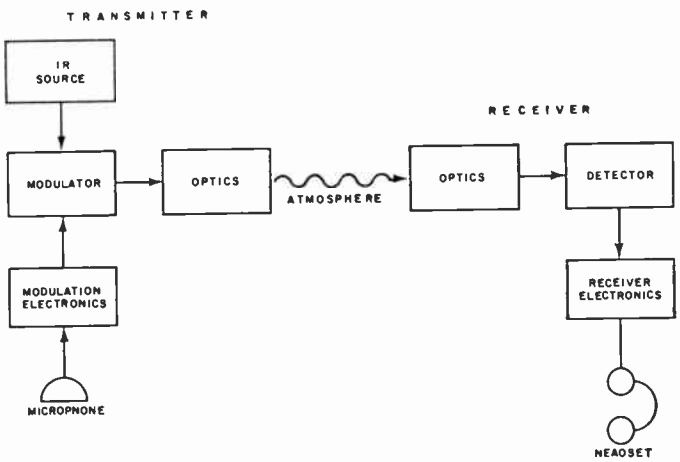

Fig. 16—Block diagram of infrared communication system.

Present State

The simple, low-power, light-weight equipment types with relatively narrow transmitting and receiving beams have become smaller, lighter, more efficient, and more reliable. The heavier, higher power, broad-beam and omnidirectional equipment types have been considerably reduced in size and weight while attaining long-range capability for both day and night operation. The newer and more unusual modulation schemes have not yet been reduced to really practical equipment, although some show considerable promise.

Contributing to the improvement of all this equipment, but especially to the very-light-weight types, has been the improvement in infrared components over those used ten years ago or less. Detector cells for communication purposes, especially lead sulfide types, have improved greatly in sensitivity, lowered noise level, uniformity, shortened time constant, and in their ability to withstand temperature, moisture, etc. Infrared filters with sharper cutoffs and less loss in the transmission region are now available. Mirror galvanometers have improved in frequency response and ruggedness. Optical materials with better infrared transmission and better resistance to the elements are available. Mirrors especially, which when used as objective optics may be made smaller because of other improvements in the system, are also available in lighter-weight types than were once thought possible. Better arc sources have made great improvement possible in the performance of some equipment.

The electronic art has also contributed to the rather considerable advance in infrared equipment. Thus, new and excellent equalization techniques allow the bandpass characteristic to be given almost any desired configuration. The development of smaller, lighter-weight amplifiers with better linearity and less distortion makes a considerable contribution to smaller size and better performance.

Finally, the growth of knowledge and understanding of the effects on the operation of infrared communication equipment of the transmission of the atmosphere, shimmer, background brightness, and also of optical-system losses and defects, has led to considerable design improvements in present equipment. Advanced input circuitry has diminished the apparent cell saturation problem. Both operational and equipment techniques have lessened the effects of shimmer, while careful design has improved the linearity of modulation.

5.1.9 RANGE INSTRUMENTATION

5.1.9.1 INSTRUMENTATION AIDS[7]

INFRARED seekers and trackers have proven useful in applications other than ordnance. For instance, when long-focal-length camera lenses are used to photograph missiles or other distant objects, a camera directed by means of a seeker-directed servo can often give better pictures than one directed by a human operator. Such an application implies the use of targets which are good infrared sources, but these are often encountered in the form of rocket motors or even sun-illuminated satellites.

In one series of tests at the Naval Ordnance Test Station, an infrared seeker was used to direct cameras by feeding its error signal into a conventional tracking radar set. In this instance, the reflector dish of a SCR-584 radar was removed and a large instrument platform was installed in its place. An infrared seeker was mounted on this platform along with several cameras and other instruments. The apparatus is shown in Fig. 17. One azimuth phase-reference signal and one elevation phase-reference signal generated by the seeker were introduced into the 584 system much as had been done with the same signals from the replaced antenna. The operator would merely acquire the target manually

[7] Prepared by L. W. Nichols.

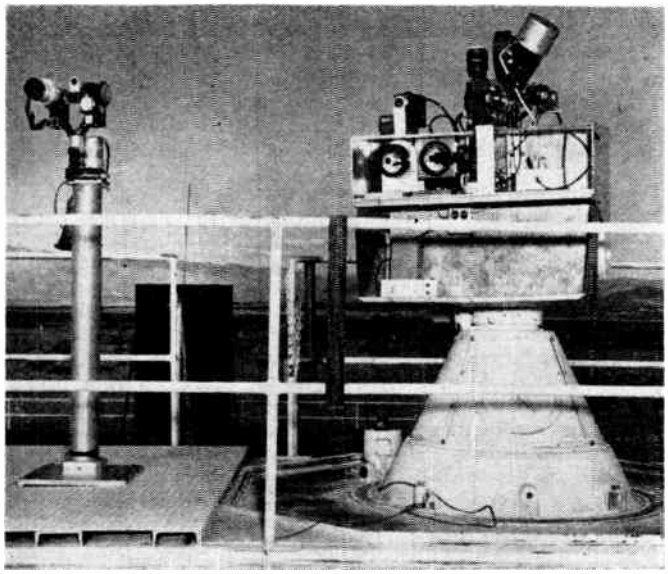

Fig. 17—Infrared automatic tracking equipment on servo-driven camera platform.

through an optical sight and then switch the system to auomatic track, and the cameras were accurately directed by the existing servo motors on the pedestal.

The tracking accuracy of this arrangement amounted to one or two rms mils, a limit imposed by the servo units. With a precision tracking telescope and an improved servo system, this accuracy would be improved.

5.1.9.2 HIGH-RESOLUTION INFRARED TRACKING SYSTEM[8]

THE extensive testing of missiles has resulted in an application for infrared. Missile testing requires tracking throughout flight in order to provide data for performance analysis. Safety requirements make it important for the Range Safety Officer to know of any deviations from the preselected flight path, so that missile destruction can be accomplished when necessary. Radar has been used for tracking and has performed well at long ranges. At short ranges, however, radar performance is degraded by ground clutter. The large amounts of obscuring smoke and dust often prevent early tracking by optical equipment.

Infrared provides a feasible alternate method of tracking. An infrared tracker developed at Barnes Engineering Company was installed at the Air Force Missile Test Center, Cape Canaveral, Fla. This equipment has been used for automatically tracking Atlas, Jupiter, and a wide variety of other missiles in powered flight to ranges in excess of 10 miles, at which time tracking can be switched over to radar. The equipment operates equally well during day or night.

The major units of the system include a tracker head mounted on the radar antenna yoke and an electronics unit mounted on the antenna pedestal. Also included in the system, but not vital to its function, are a television camera mounted next to the tracker head and a monitoring console located inside the radar van. The console includes the television monitor and oscilloscope unit which indicates both radar and infrared tracking-error signals. By means of a manual or automatic switch, tracking can be controlled by either radar or infrared. In addition, the operator can track the target by means of manual controls, using the television monitor as a finder.

When the infrared tracking system is used at Cape Canaveral, the television monitor is used to train the field of view upon the missile before take-off. As soon as the exhaust flame appears, the tracker locks onto it and automatically follows the flame throughout powered flight. At ranges of over 10 miles, there is a switchover to radar tracking. Infrared tracking is so accurate that the missile remains locked at the exact center of the TV screen. If the operator purposely deflects tracking, the infrared system rapidly re-acquires the target and brings it back to the center of the field of view.

[8] Prepared by M. Arck and G. Jankowitz.

5.1.10 FOREIGN MILITARY APPLICATIONS

by P. J. Ovrebo

WHILE it is not possible to discuss foreign military applications in technical detail, it is of interest to quote briefly several statements from abroad which possibly reflect the degree of foreign interest in infrared technology. In 1954, the Air Fleet Herald (Soviet Journal) wrote as follows:

> Optical phones are particularly useful for operations in a mountainous region because of their high operational secrecy. As a matter of fact, the beam of infrared rays thrown across such a region practically cannot be intercepted by the enemy if it passes at a considerable distance from the earth surface. The operation principle of apparatuses used for that purpose was based upon the infrared beam produced by a special generator and modulated with an acoustic frequency. The receiver, installed on the opposite end of the line, converted the vibrations of the radiant energy into electrical vibrations of an acoustic frequency which, in turn, brought into action an electroacoustic or special printing apparatus.[9]

This journal continued to discuss several types of infrared direction-finding equipments known as "thermopeloruses" which were alleged to be of greatest interest to foreign armies. The precision of "sea peloruses" was indicated to extend up to 0.01° and to permit the finding of the direction of ships at a distance of 30 to 35 km.

> Airplane thermopeloruses usually have a somewhat lesser precision (0.10°), with a radius of action of about 20 km.

The final paragraph states:

> The above-mentioned designs of thermopeloruses and other infrared apparatuses, used for Air Force purposes, do not cover all inventions in the field of infrared technology during the last years, but give merely a general idea of the possible ways of solving certain problems raised by the needs of Modern Air Forces.[9]

[9] N. Grigor'yev and L. Filippovsky, "Infrared technology and its use in aviation," *Air Fleet Herald*, no. 11, pp. 57–70; 1954.

In 1955, Vafiadi commented as follows:

The appearance of infrared direction finders doubtless calls for the development of methods for lowering the heat radiation of airplanes and ships, but this in turn, will call for still more sensitive infrared direction finders.[10]

In 1958, Rykov[11] wrote an article entitled "Infrared Aircraft Equipment (Based on Materials From the Foreign Press)." The article included the following:

The infrared devices, installed aboard modern aircraft, can be used for detection and interception of aerial targets, and for plotting the distances between aircraft in flight, in order to prevent collision. . . .

Any substance, whose temperature differs from absolute zero (−273°C), is a source of infrared rays. The radiation of such objects as sea-going vessels, tanks, aircraft, rockets, industrial establishments, etc., are of highest interest for military purposes. No signals or pulses have to be sent, as it is done by radar devices, in order to discover the sources of infrared radiation. It is only necessary to know how to receive and discern, among all the variform radiations, these rays which arrive from the necessary target. Thereupon, these radiation forms have to be converted into visible rays, or electrical signals which can enter, for instance, the self-guidance automatics of the missile.[11]

Inasmuch as the frequency of electromagnetic waves of the infrared range exceed by many times (approximately by 1,000 times) the highest frequency employed in radar, it is possible to obtain by infrared rays a good resolving capacity, *i.e.*, to discern between the objects situated close to each other. If, for instance, the millimeter-range radar is capable to distinguishing between two aircraft flying 400 m apart from each other, at 8-km distance between the radar station and aircraft, the infrared sights are capable of discerning not only the aircraft themselves but also their power plants.[11]

Continuing to discuss "Thermo Direction Finders," Rykov states:

Aircraft or rockets in flight constitute powerful sources of the infrared rays. At low velocities they are radiated directly by the heated-up parts of power plants and exhausts. They can be revealed only in the rear hemisphere, and this fact determines the interception tactics with respect to such targets.[11]

With increase of the velocity of flight, especially at the transition through the velocity of sound, there begins strong radiation from the heated covering (skin). With increase of velocity, the intensity of radiation increases. Thus, the skin temperature of the aircraft, whose flying speed at the 10-km altitude constitutes 0.8 Mach, is equal to −23°C; this temperature increases up to 227°C at the speeds corresponding to 2.4 Mach number. The radiation energy increases by 16 times, and the signal intensity on the maximum radiation wave (peak) by 32 times. Thus, at high speeds, the entire aircraft constitutes a torch of infrared rays, which facilitates its detection from other directions as well, besides the rear hemisphere.[11]

Rykov's article ends with a comparison of "Infrared Technology and Radar":

The extensive development and assimilation of the radar technology in the aviation, which made it possible to perform the aircraft guidance, interception of aerial targets, fire delivery, bombing, etc., in any meteorological condition, created the impression that all the problems can be solved by radar. It is far from actual truth. First of all, the radar devices are subjected to the effect of variform interferences. In addition, its resolving capacity and accuracy of determining the coordinates are rather low. The operation of radar devices is complex, and their over-all dimensions and weight are excessively large.[11]

The ever-increasing demands of aviation, paired with the deficiencies of the radar system, evoked the necessity of concentrating on the technology of infrared rays. As known, the infrared equipment weighs less and possesses smaller over-all dimensions, in addition to simpler design. Thus, the infrared guidance system contains the total of seven tubes, whereas the corresponding radar system employs several dozens. No great expenses are required for the development and expanded production of the infrared-ray equipment.[11]

The infrared technology can emerge in numerous cases as a rival for the radar, and sometimes as its assistant. Nevertheless, it should not be assumed that one of these branches of the contemporary radio-electronics will completely replace the other; both of these branches possess enormous potentialities for further development and application in the military business and, particularly, in the field of aviation.[11]

Soviet Air Force news articles refer to the possibilities of airborne infrared reconnaissance. One[12] describes an airborne Arctic ice-pack reconnaissance device that can measure and record the temperature of the ice. The equipment reportedly weighs 3000 pounds. It is ordinarily flown at an altitude of 600 meters, and it portrays a viewing band of 5-km width (an extremely large angle of ±76° at a 600-meter altitude); and reportedly can determine the temperature, thickness, and structure of the Arctic ice pack.

[10] V. Vafiadi, "Infrared direction finders," *Red Star;* November 19, 1955.

[11] S. Rykov, "Infrared Aircraft Equipment," *Soviet Aviation*, p. 3; September 16, 1958.

[12] A. Strizhak, "With a televisor over the Arctic," *Soviet Aviation. USSR.*

Paper 5.2

Astronautical Applications of Infrared Techniques*

P. J. OVREBO†, R. ASTHEIMER‡, AND E. WORMSER‡

5.2.1 CELESTIAL TRACKING

INFRARED trackers can track the sun for positioning of astronomical instruments and collectors for solar furnaces. For navigational purposes the moon and stars, as well as the sun, are tracked.

Unmanned aircraft, missiles, and drones can be preprogrammed and then controlled by reference to celestial objects. Satellite vehicles can also use the earth's atmosphere as a reference for attitude control. This is especially important to prevent vehicle tumbling when manned. Space vehicles can use infrared for attitude control during launch and landing, for navigation during flight, and for mapping and photography during orbit around the moon or planets such as Venus and Mars.

5.2.2 SATELLITE TRACKING[1]

THE infrared radiation of artificial satellites in orbit around the earth has been tracked and measured by scientists and engineers from Barnes Engineering, Aerojet-General, and the Royal Radar Establishment of the Ministry of Supply of Great Britain. These experiments were conducted to obtain the radiation characteristics of satellites, to aid in establishing the sensitivity and optical requirements for specialized infrared trackers to track a satellite at every passage over a monitored area.

The present methods of tracking rely on complex radar facilities or on simpler radio and optical sighting stations of the "Minitrack" and "Moon Watch" observer teams. The latter groups can track only satellites that have radio transmitters or that are illuminated favorably by reflected sunlight. Visual observation from the earth is impossible except at dawn or dusk because of atmospheric scattering of the reflected sunlight in the daytime, and the lack of reflected sunlight at night.

Since all objects with a temperature above absolute zero (−273°C) emit infrared radiation, the logical development of the infrared tracker is to provide an instrument that can "see" the radiated energy of the satellite. During the sunlit period of a satellite's orbit, the reflected and emitted energy make infrared observation relatively simple. Because the satellite is heated in the sunlit period, it will continue to radiate some of its stored heat during a dark passage. In addition, most satellites carry instruments or experimental animals; this means that the interior of the satellite must be maintained at a relatively high temperature. Even with the best techniques of insulation, such a satellite will have a temperature different from its environment.

Fig. 1 shows an infrared-tracker recording of Sputnik III made by an Aerojet team that sighted the satellite at 4:18 A.M. (PDST) on July 26, 1958, over Southern California. A time-exposure photograph was taken simultaneously with a Leica camera fitted with an 8-inch lens. The photograph shows the satellite as a dotted line (caused by the tumbling of the satellite as it passed). The top recorder trace is the reflected solar energy of the Sputnik III cylinder and shows two "bright" periods of approximately 0.8-second duration, separated by a 7.5-second "dark" period, similar to the visual effect captured by the camera in the sky photograph.

The Aerojet infrared tracker shown in Fig. 2 is a small instrument with a folded, reflecting optical system. Although this optical system is only 6 inches in diameter, it has the same configuration as the Palomar and Mt. Wilson telescopes. The infrared-sensitive detector used in the experiment was a lead sulfide cell cooled to −78°C.

The Avion Division of ACF Industries is developing, with the support of Air Force Cambridge Research Center, a test device to aid in the definition of satellite infrared radiation. It provides wide-angle, high-speed search capabilities to supply rapid acquisition information on satellite position as the satellite appears on the horizon. This Multi-Cell Search Unit consists of three parts: the mount, the optical head, and the presentation. The unit will have a three-axis mount, chosen to afford any search path in the sky. With this mount, a standard equatorial-type astronomical mount can be duplicated, and provisions are made so that a clock drive may be incorporated.

The optical head is shown in Fig. 3. The optics will be a folded, concentric, catadioptric system of f/0.85 speed. The aperture of the system will be 3 inches and located at the combination window and filter of the system. Scanning will be accomplished by rotation of the optics at 30° per second, reversing direction by means of a reversing switch at the end of the preselected scan angle. The scan angle will be manually adjustable from 30° to 210° throughout the full rotation about the scan axis, with slip rings provided on this axis.

An array of 30 cell elements will be located at the focal plane. Each cell element will have a field of view 0.92° square. The 30 cell elements will be mounted perpendicular to a scan of 27.5° and will be sampled by

* Original manuscript received by the IRE, July 13, 1959. Material not otherwise identified has been assembled by the Section Editor, P. J. Ovrebo.

† Wright-Patterson Air Force Base, Dayton, Ohio.
‡ Barnes Engrg. Co., Stamford, Conn.

[1] Obtained from reports supplied by Aerojet-General Corp. and Avion Div. of ACF.

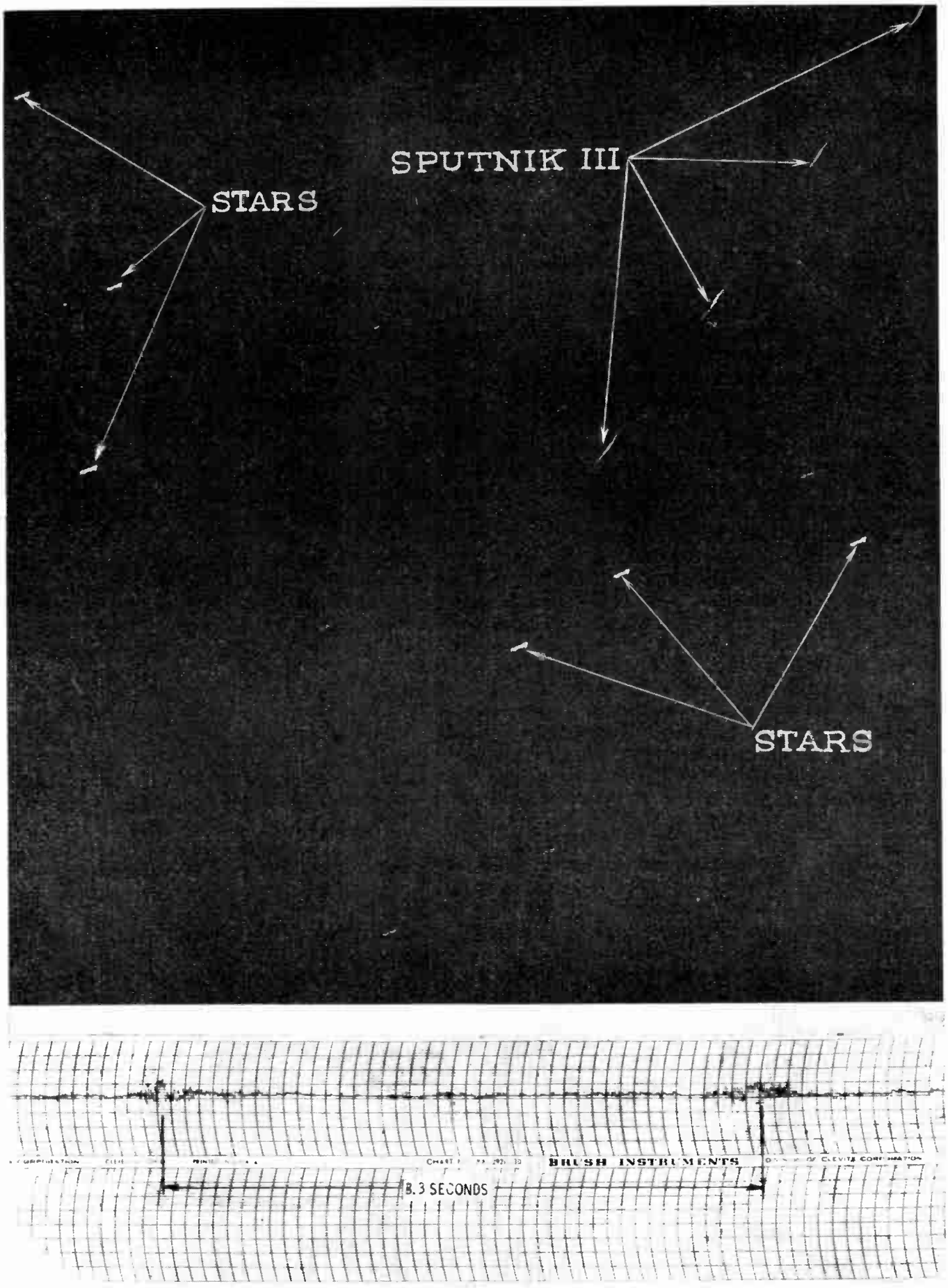

Fig. 1—Sputnik III by photography (upper part) and by infrared tracker (recorded signal, lower part).

Fig. 2—Satellite tracker.

means of a commutator at 40 cps, yielding 1200 bits of information per second. In addition, a chopper located in front of the cells will modulate the signal at a frequency of 1000 cps.

Information will be presented on a Dumont #304A Oscilloscope, or equivalent, with long-persistence phosphor. Overlays on the tube face will be calibrated to afford identification with respect to initial mount settings. A control box will also be located at the presentation scope.

5.2.3 WEATHER FORECASTING

VALUABLE data for long-range weather forecasting may be obtained by infrared surveillance of the earth's cloud coverages. The infrared equipment can be mounted in a satellite and continuously survey the earth's atmosphere

Of more immediate use, airborne or satellite-borne infrared surveillance equipment can detect the masses of hot air associated with thunderstorms and hurricanes. The early warning of impending danger thus obtained may result in the saving of lives as well as the reduction of property damage.

A satellite orbiting around the earth would provide an excellent platform for making radiation measurements of the earth's atmosphere and surface. Since these measurements could be made over a large portion of the earth's surface they would have important meteorological applications. Repeated measurements over this area would record the major features of the earth's surface, over which will be superimposed the motion of cloud masses and major weather fronts. Such information would be invaluable in long-range weather prediction.

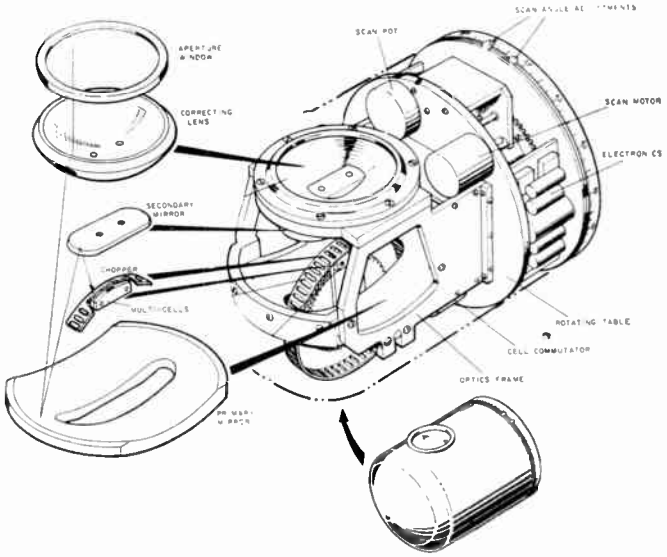

Fig. 3—Satellite infrared radiation test device.

5.2.4 SPACE INFRARED OBSERVATIONS[2]

The principal hindrance to extraterrestrial observation has been the confusion offered by the earth's atmosphere. Observations from immediately outside the atmosphere will permit examination of planetary atmospheres with sufficient precision to study the environment that future planetary explorers will have to cope with.

Similarly, infrared observations from an orbiting vehicle will permit measurements of cloud cover, water vapor, and carbon dioxide concentrations, and the like, which will be valuable from the meteorological observations. In addition, infrared sensors in similar vehicles may have some utility for military reconnaissance and surveillance of the earth. In particular, especially large sources of infrared energy such as afterburning engines of supersonic vehicles and exhaust flames of ballistic missiles may be detectable from orbital platforms.

Infrared detection range is severely limited within our atmosphere by scattering and absorption, so that most military applications, such as guidance for air-to-air missiles of the Sidewinder type are of a short-range (*i.e.*, less than 10 miles) nature. However, the space environment will permit full exploitation of the ultimate sensitivity of infrared detectors, permitting extension of detection range by several orders of magnitude. Of course, celestial sources will be detectable at even greater ranges.

Infrared sensors will permit the surveillance of space vehicles in a manner distinct from either optical detection, based on reflected sunlight, or radar, based on reflection of radio waves. The utility of this technique will be dependent in part upon the amount of heat expended in future vehicle power supplies and propulsion systems. One advantage of infrared for ground-based observations of space objects is the ability of infrared to produce a clear image even through haze and scattered sunlight.

Since sunlight has an appreciable portion of its spectrum in the infrared region, it is also possible to observe space vehicles with systems that combine both optical and infrared sensors. A detector such as lead sulfide is sensitive to both these classes of radiation, and may therefore be better in some applications than a narrow sensor limited to a single region of the spectrum.

Infrared can also be useful for detection of celestial objects in space navigation. For such an application, infrared possesses many of the advantages of optical techniques, such as angular accuracy and small equipment size and weight; however, it has one important and unique advantage due to the temperature-magnitude relationship inherent in celestial objects. The tremendous number of optically-detectable objects may tend to cause confusion if an optical system

[2] Statements extracted from 1958: "Space Handbook: Astronautics and its Applications," RAND Rept. No. RM-2289-RC; Published as a Staff Report on "Astronautics and Space Exploration," by U. S. Government Printing Office under No. 33660; 1959.

is used for navigation or surveillance, unless some method for logical discrimination on the basis of space relationship is built in or is available by virtue of the human element. A properly filtered infrared detection system, however, will be limited to detection of a much smaller number of celestial objects which, fortunately, include the most interesting near objects such as the planets, thus offering a simplified background problem. When combined with a measure of spectral analysis, infrared sensors would permit clear identification of a planet, for example, which may be of considerable value in navigation and terminal guidance of space vehicles.

For tracking certain objects, some advantage is gained by using the infrared portion of its spectrum. Infrared radiation from the object being tracked may provide a better contrast with the background radiation, and certain fog and haze conditions are more readily penetrated. In general, however, infrared radiation is also absorbed by the lower atmosphere and the range and general utility of infrared tracking are enormously increased by carrying equipment in high-altitude vehicles essentially above the earth's atmosphere. The use of photoelectric detection and scanning techniques permits automatic read-out of angular position information.

A rather new development in optical and infrared tracking is the use of television techniques to improve sensitivity, selectivity, and rapid read-out characteristics of the tracker. Work in this field is being done both in this country and abroad. Essentially, a tracking telescope is fitted with the front end of an image orthicon followed by an image intensifier for amplification of photoelectrons. The results provide selectivity to "chop off" the sky background and permit tracking in daylight as well as tracking of fainter objects at night.

In the Vanguard II satellite, instrumentation was used in the near infrared region (0.6 to 0.9 μ) for cloud-cover measurements. This region was selected to give maximum contrast among land, sea, and clouds.[3]

5.2.5 WIDE-ANGLE HORIZON SENSOR[4]

THE Wide-Angle Horizon Sensor is a compact and sensitive passive infrared device which can detect the thermal discontinuity between the earth and space. Two of these sensors can be used to establish a stable vertical reference for control of the orientation or attitude of a missile or satellite in space.

Infrared and electro-optical techniques have been used in the design of this sensor. It employs thermistor detectors that respond to far-infrared wavelengths, and filters that cut out visible and near-infrared radiation, so that the sensor responds to the earth's self-emitted radiation, and not to reflected solar radiation. Sharp clipping and sensitive phase-detection circuits are used, so that the sensor output is precise and is practically independent of variations in the temperature and radiance of the earth.

The Horizon Sensor has been designed for minimum size, weight, and power requirements, and has been constructed to operate with maximum reliability under severe environmental conditions. The sensor is a completely self-contained unit, enclosed and sealed by a single cylindrical cover. Transistor electronics are used exclusively, and all circuits are potted. The sensor weighs 2.5 pounds and consumes 4 watts of power. It is designed to scan space in a conical pattern and detect radiation discontinuities such as those existing at horizons.

When the vehicle in which the sensor is mounted is oriented so that the earth is present in the scanning path, there will, in general, be two points where the scan intersects the earth's horizon. The sensor detects the thermal discontinuity, or change in radiation level, between the earth and space at the two horizon points. It bisects the included angle from itself to the two horizon points, compares the direction of the bisector with that of a fixed reference in the vehicle containing the sensor, and generates linear error signals proportional to the angle between the bisector and the fixed reference. These linear error signals may be used to control attitude in one plane by valving jets or by spinning reaction wheels, which will orient the vehicle so that its fixed reference is made to coincide with the bisector of the angle between the two horizons.

Two Horizon Sensors properly oriented in a space vehicle can establish a local vertical with respect ot the earth or other close celestial object. The linear error signals can then be used to control roll and pitch of the vehicle to orient it with respect to the local vertical.

[3] J. A. Van Allen, "Scientific Uses of Earth Satellites," University of Michigan Press, Ann Arbor, ch. 13. Also, *Electronics;* March 20, 1959.

[4] Prepared by R. Astheimer and E. Wormser.

Paper 5.3

Industrial, Technical, and Medical Applications of Infrared Techniques*

P. J. OVREBO[I], R. R. SAWYER[II], R. H. OSTERGREN[III], R. W. POWELL[IV], AND E. L. WOODCOCK[V], SENIOR MEMBER, IRE

THE commercial applications of infrared equipment were, until recently, limited to infrared heat sources for artificial sunbathing and cooking and to infrared cameras for photography and mapping. Infrared began being used for control of chemical processes in 1936.

The first military application to catch the public's fancy was the infrared "sniperscope," which consisted of an infrared source to illuminate the target and an infrared telescope to observe the target. This "seeing" in the dark was immediately conceived by the public as being applicable to police and nightwatchmen-type work. The mass production of infrared components and the simplification of techniques are rapidly increasing the number and types of infrared commercial applications.

5.3.1 INFRARED SPECTROPHOTOMETRY[1]

WHEN the first industrial infrared spectrometers were installed in the 1936–1937 time period, it was not anticipated that infrared spectroscopy would become widely accepted as an industrial tool. However, during the war years important applications were found in the petroleum and synthetic-rubber programs. With commercial availability of recording-type spectrophotometers, there has been widespread adoption of infrared analysis techniques by many industrial and university laboratories.

Spectrophotometers

Although they may not be universally recognized as such, spectrophotometers, currently in use or available commercially, are sophisticated systems. In general, a systems analysis of all available spectrophotometers reveals that they are of two types, namely open-loop systems, referred to as single-beam spectrophotometers, and closed-loop systems, referred to as double-beam systems. These two systems can be categorized by two block diagrams which differ in only a few aspects. In the single-beam or open-loop system, the functional aspects can be illustrated as in Fig. 1. The single-beam system records absorption spectra on an arbitrary transmission scale, so that data must be referred to a zero curve by calculation and point-by-point plotting. The double-beam instrument, Fig. 2, automatically refers data to a true zero and yields spectrograms on a transmission-vs-wavelength chart. The source of the radiation is usually a silicon-carbide rod (Globar) or a Nernst glower, either of which, when heated by conducting an electric current, emits the required radiation. This radiation is then passed through the sample, which may be a gas, a liquid, or a window or filter material. The scanning of the spectrum is accomplished by rotating some optical component, such as a "wavelength mirror." The dispersion of the radiation is accomplished by a prism or combination of prisms, and in some cases by a grating.

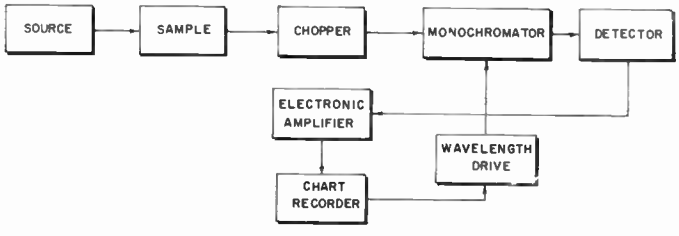

Fig. 1—Single-beam spectrometer (open-loop).

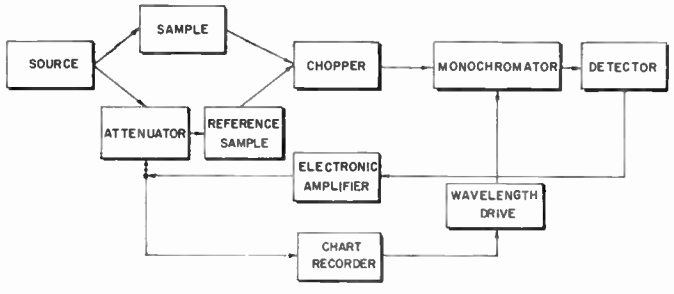

Fig. 2—Double-beam spectrometer (closed-loop).

Since ordinary glasses do not transmit infrared beyond 2.5 μ, other infrared dispersing materials such as various synthetic crystals are used.[2] Similarly, front-surface mirrors must be used. The dispersed radiation is then detected by a thermocouple or bolometer and the resulting signals are recorded on a suitable pen-type drum recorder.

When the spectrum of sensitivity of some type of detector, such as a photoconductive cell, is to be obtained,

* Original manuscript received by the IRE, July 13, 1959. Material not otherwise identified has been assembled by the Section Editor, P. J. Ovrebo.

[I] Wright-Patterson Air Force Base, Dayton, Ohio.
[II] Instrument Div., Perkin-Elmer Corp., Norwalk, Conn.
[III] Beckman Instruments, Inc., Fullerton, Calif.
[IV] Perkin-Elmer Corp., Norwalk, Conn.
[V] Aerojet-General Corp., Azusa, Calif.

[1] Much of the technical information included herein was obtained from manufacturers' literature. W. G. Driscoll of Baird-Atomic, Inc., assisted in preparing the discussion of spectrophotometers.

[2] See W. L. Wolfe and S. S. Ballard, "Optical materials, films, and filters for infrared instrumentation," Paper 4.2.3, this issue, p. 1540.

the spectrometer's detector is replaced by the detector to be tested, together with its own type of amplifier. On the other hand, when a source of radiation is to be tested for its spectral distribution, the spectrometer's source is replaced by the one to be tested. In this case, the detector associated with the spectrometer is used.

It may be stated that in spectrophotometer systems, as with all systems, the information content and the time required to obtain the information may be traded one for the other. Accordingly, if the system is not energy-limited, optically inferior, detector-limited, etc., the spectral information that can be recorded is proportional to the time taken to scan the spectrum and simultaneously record it.

The problem of designing a good infrared spectrometer involves difficulties going beyond those experienced in the design of a visible-light spectrometer, since all parts of the spectrometer emit and/or reflect infrared radiation which may fall in the spectral range of interest. Consequently, great pains are taken to obtain a clean spectrum containing a minimum of stray radiation. Despite these difficulties of design, there are today a number of good spectrometers available on the commercial market whose quality is attested by the great range of problems to which they are applied.

While spectrophotometers are in fact sophisticated, improvements in such instrumentation can still be anticipated in the future. For instance, spectral data as presently collected are grossly redundant. Consequently, when ways and means become available to recognize these redundancies and other effects which are saturating the present information or channel capacities, improvements in data handling should be forthcoming. Studies in this direction should result in significant improvements in each of the subsystems of the over-all spectrophotometer. More intense sources with higher output in the longer-wavelength regions, or with different spectral characteristics, are desirable. Similar improvements in detector characteristics would obviously improve the system performance. New and more effective monochromator designs using prisms, filters, interferometers, and/or combinations of these dispersing elements might be significant.

Infrared Absorption Spectroscopy

Infrared absorption spectroscopy takes advantage of the fact that molecules of substances to be tested vibrate at various frequencies which are dependent on their atomic mass, type of chemical bond, and the geometry of the molecules. Hence, when infrared radiation is passed through the sample, its molecules will absorb in varying degrees the infrared frequencies which are characteristic of the sample's own molecules. Thus, the end result of the test is an infrared absorption curve, or a spectrogram, with bands or peaks which represent the absorbed energy. These bands are then characteristic of the sample being irradiated and may be measured for their exact position in the wave number or wavelength spectrum.

Beer's Law is the fundamental law of quantitative absorption spectrophotometry. This law provides a theoretical relationship between concentration of an absorbing substance and the amount of radiation absorbed. Those substances which obey Beer's Law can be quantitatively analyzed by calculation directly from the spectrophotometer data by means of simple systems of linear equations. Substances which do not obey Beer's Law can be analyzed only by the use of analytical curves —empirical calibration curves obtained by measuring known concentrations of the substance at an appropriate wavelength and then plotting concentration vs transmittance, or concentration vs absorbance. In all methods discussed, greatest accuracy can be obtained by working with special bands showing transmittances between 25 per cent and 60 per cent.

Beer's Law describes the absorption of a beam of parallel monochromatic light in a homogeneous isotropic medium.

$P/P_0 = 10^{-abc}$, where

P_0 = "incident" power
P = transmitted radiant power
a = absorptivity
b = path length
c = concentration of the absorbing component.

Or,

$\log_{10} P_0/P = abc$ = absorbance, A, or optical density.
P/P_0 is the transmittance, T, of the sample, and is often expressed in per cent.

An infrared spectrophotometer directly measures the (external) "transmittance," which is the ratio of the radiant power P transmited by a sample to the radiant power P_0 incident on a sample, both measured at the same spectral position with the same slit width. "Absorbance," A, is the logarithm to the base 10 of the reciprocal of the transmittance: $A = \log_{10} 1/T = \log_{10} P_0/P$. "Absorptivity," a, is the ratio of the absorbance to the product of concentration and length of path: $a = A/bc$, where b is the path length and c the concentration. This term is a specific quantity expressing the absorbance per unit path length, per unit concentration. It has also been called the absorption coefficient.

It is significant to note that as many as ten to twelve constituents can be analyzed simultaneously, at great savings of time and expense. The infrared spectrum of a compound, according to Sutherland and Thompson, is the most characteristic physical property of that compound. Hence, the spectrum is in fact a "fingerprint" whose probability of duplication for some other compound is practically zero.

However, while nearly all materials give infrared spectra (materials composed of molecules of three or more atoms and some with two), the problem is to apply usable sampling techniques. Liquids and gases are gen-

erally the simplest states for easy and rapid sampling. Hence, some of the advances in infrared analysis have, in fact, been due to ingenious innovations in sampling techniques, and it has become possible to examine samples weighing as little as five millionths of a gram. Such a capability is important in cancer research, where tiny samples of hormones and other steroids must be identified.

5.3.2 INDUSTRIAL APPLICATIONS OF INFRARED SPECTROSCOPY[3]

by R. R. Sawyer

Agriculture

Qualitative and quantitative analysis of liquid and solid fertilizers, limestone, urea-formaldehyde, organic-phosphorus, organic sulphur and fluorine compounds, insecticides and insecticide residues; identification of nitrates, chlorides and ammonium salts in soil; investigation and control of silica and alumina in soil and their effects on fertilizers.

Aircraft and Missiles

Infrared analysis of complex propellant mixtures used in aircraft and missile programs, including many of the high-energy fuels such as organo-boron compounds; infrared kinetic investigations of reactions and breakdown of fuels when burned; identification of exhaust gases; compositional analysis of aircraft greases essential to solution of lubrication problems.

Air Pollution

Analysis of oxidants, ozone, oxides of nitrogen, petroleum hydrocarbons, mercaptans, end products in organic combustion, and exhaust gases; rapid identification of aldehydes, ketones, and organic acids present in smog conditions; measurement and control of the concentration of carbon monoxide, atmospheric fluorides, hydrogen sulfide, and oxides of sulphur emitted from factories into the surrounding air; study of effluents halides; especially powerful in conjunction with gas chromatography or other preseparation or collection systems; used with long path cells to follow very dilute reactions or reactions at simulated high altitudes.

Atomic Energy

Identification of products formed during radiation decomposition of organic compounds; identification and analysis of impurities of solvents used in experimental process studies; analysis of impurities in gases, such as borontrifluoride used in neutron counters and in structural investigations of complex ruthenium compounds and other solid materials; most valuable tool in the production of heavy water where strict analytical control of the deuterium content is necessary.

Biochemistry

Identification and molecular-structure determination of enzymes, amino acids, indoles and nitrogen compounds; analysis of lipides, porphyrins, proteins, hemoglobin, vitamins, sterols and sugars; measurement of carbon dioxide, phenobarbital and diphenylhydantoin in blood, trace quantities of boric acid in blood and urine, urinary lead compounds, methanol in body fluids.

Coal

Studies of the composition and structural features of coal and bituminous coal; identification of minerals, bituminous anthraxylons, carbohydrate chars, petroleum asphalt, and coal extracts; correlation of changes in the spectral data of residues from vacuum distillation with changes in rank; detection of the presence of chemical groups to preclude or limit the existence of proposed structures and to demonstrate similarities or differences in chemical structures of coals and coal-like products.

Coatings

Infrared examination of monomers, polymers, epoxy resins for information on problems concerning curing rates, blending conditions and ionic forces involved in holding coating to material. Composition of polymer blends and co-polymers can be determined by the infrared quantitative analysis of the pyrolyzates of these blends. Rapid identification of oils, fatty acids, oxirane rings, urea-formaldehyde resins, silicone elastomers, and phenolic resins; analysis of organic constituents of paints, varnishes, automotive lacquers, pigments.

Cosmetics and Essential Oils

Checking essential oils and mixtures for identity, constancy of composition, adulteration and dilution; evaluation of organic sulfur compounds in cold waves, studies of the swelling of hair; control of the purification of oils; analysis of the composition of natural oils.

Dairy Products

Control of the amount of water in butter, of the ratio of fat components; quantitative determination of concentrations of triglycerides in milk and butterfat; studies of dried full-cream milk, dried separated milk, casein, lactose, butterfat have revealed much concerning the protein-carbohydrate systems involved. Infrared is the most important factor in the control of dried milk manufacture.

Drugs and Narcotics

Infrared plays a most important role in the identification of narcotics: illicit, synthetic, or natural. The spectra of alkaloids, their hydrochlorides and their derivatives reveal much information concerning purity, concentration of narcotic present, and even origin. For example, opium contains 24 different alkaloids; if the relative proportion of each should vary with the place the plant was grown, it should be possible to pinpoint the source of the plant.

[3] Prepared by R. Sawyer.

Education

Infrared spectroscopy is widely used in universities and colleges both for research and as part of the chemistry student's training in instrumentation. With the increasing availability of low-cost infrared instruments, the undergraduate is now being trained in infrared techniques in some of his elementary courses. The importance to the student of acquiring an early familiarity with the physical aids available to him is well-recognized—for a fundamental appreciation of both molecular structure and infrared's applied role.

Emulsions

Rapid identification of resins, waxes, polymers, and emulsifiers in emulsions; the qualitative and quantitative determination of the formulation of emulsions; compositional analysis of emulsions for shellac, colloidal silica, sodium soaps, carnauba wax, ionized carbonyl groups, polystreme polymers, resin-maleic, anhydride resins, vinyl acetates and the vinyl acrylates; phenolic resin content and ester wax content is readily determined.

Food

Analysis and identification of proteins, amino acids, fats, oils, inorganic ions, enzymes, carbohydrates, acids and vitamins in foods; identification of various yeasts, tocopherols in natural oils and food stuffs, and sugars in candies; analysis of food products for vitamins A, D, niacin, B_6, B_2 and pantothenic acid; analysis of starch in apples or meat products, crude fibers in foods; detection of the presence of antibiotics in milk, inhibitory substances in milk and residual pesticides on food materials.

Inorganic Compounds and Minerals

Identification of minerals, polymineralic sediments, and inorganic chemicals. Qualitative determination of the major constituents of rocks can be made rapidly. Quantitative analysis of impurities in clays, minerals, etc.; correlation of structural groups within different minerals relates much concerning environment and history of the mineral. Soil samples and sedimentary rocks can readily be qualitatively analyzed.

An infrared spectroscopic method has been developed for the qualitative and quantitative analysis of the mineral constituents of sedimentary rocks for use in petroleum exploration research. The method consists of grinding rocks to a fine powder and examining the powder as a film on a conventional sodium chloride window. The mineral constituents of the rocks are identified by comparing their spectra with the spectra of pure minerals. Quantitative analysis within 10 per cent of the amount present can be made for minerals which have sharp, well-defined absorption bands, such as quartz, kaolinite, orthoclase, calcite, and dolomite. Errors in the analysis are caused by nonuniformity of the sample film and scattering of the infrared radiation. The technique has been used in analyzing oil-well cuttings, cores, drilling mud, and surface samples that are obtained in connection with various geological problems related to petroleum exploration.

Medical Field

Infrared techniques provide the medical researcher or technician with much information regarding the identity and purity of the material under examination, information regarding the amounts of various constituents, and information regarding molecular structure. Identification of chemical compounds extracted from animals, an organ, individual cells or cell fragments, or isolated enzyme systems; measurement of steroids in serum by micro infrared methods; identification of specific barbiturates in serum. The widespread and rapid advance in the use of the new antibiotics can at least be partially attributed to infrared investigations, where it played a large role in deciding the configuration of atomic groups in such new molecules as penicillin, aureomycin, terramycin, and others. The first successful attempt to synthesize penicillin G produced about one milligram of sample. Half of this was immediately used for infrared sampling to establish identity with the natural product.

Petroleum Industry

Identification and structural determinations of hydrocarbons in oils, quantitative analysis of oils; determination of octane numbers of gasoline; checking the composition of lubricating-oil additive blends. Quantitative determination of trace components, anti-icing additives in motor gasoline and bicyclic sulphur compounds in a kerosene-extract tar oil is done mainly by infrared. Identification of synthetic oils, viscosity improvers, anti-wear additives, extreme pressure additives, pour-point depressants, and corrosion preventatives.

Pharmaceuticals

Pharmaceutical laboratories employ infrared most extensively for qualitative functional group analysis, identification of compounds, molecular-structure determinations, and quantitative analytical control of products and intermediates. Infrared is the most common tool used for determination of structures of new synthetic compounds, alkaloids, antibiotics, steroids, growth substances; it is used for positive identification of ingredients prior to formulation into pharmaceutical preparation and for identity control of compounds entering or in process in the plant.

Polymers

Rapid identification of polymers used as lacquers, enamels, paints, varnishes, rubbers, adhesives, glues, plastics, and insulating materials; for identification and measurement of additives such as plasticizers, waxes, flame-proofing agents and co-polymers, stabilizers, antioxidants, and accelerators for determining aging factors; condensation polymerization reactions and residual impurities in plant processing.

Rubber

Infrared has been extensively applied to structural problems in the rubber industry. Spectroscopic correlations for different patterns about the C:C have aided greatly in the investigations of the structure and reactions of monomers, polymers, and synthetic polydienes; study of rubber oxidation and rubber derivatives; to control sulphur vulcanization, to follow reactions of sulphur with model compounds; study of crystallinity and chain configuration. In identifying the types of polyisoprene from different plants; in following the chlorination and hydrochlorination of rubber.

Silicone Chemistry

Infrared spectroscopy is the most important tool used in the study of silicone compounds. Identification of substituents such as methyl, ethyl, or phenyl groups, halogens, ethoxy groups, etc., on the silicone atom; differentiation between linear and cyclic siloxanes and of cyclic structures, *e.g.*, trimer, tetramer, pentamer, etc., and detection of combination structures such as linear-cyclic linkage. Molecular weights of polymers, structure of silicone elastomers, residual hydroxyl or conjugation in silicone polymers, nature of bonding forces in amino-silicone coatings, and presence of ionic structures can be determined quickly by infrared.

Textiles

Infrared has contributed both to fundamental research and to applied problems in textile materials. Study of structure, orientation, and degree of crystallinity in fiber materials; investigation of intermolecular forces within the fiber structure, interactions of functional groups of fiber molecules with other molecules; effects of chemical breakdown due to exposure to light or excessive heat, or tendering by dyestuffs. Quantitative measurements of crystallinity and amorphism.

Tobacco

Rapid identification and measurement of components such as carbonyl compounds, methanol, hydrogen cyanide, carbon monoxide, carbon dioxide, and the higher-molecular-weight hydrocarbons: identification of the complex mixture of susbstances derived from the combustion and pyrolysis of tobacco. Infrared analysis of the condensable and noncondensable fractions of tobacco smoke reveals much concerning concentrations of ammonia, cyanogen, hydrogen sulfide, aldehydes, and ketones.

Toxicological Analysis

Infrared analysis provides a method of classification and identification of different organic poisons. Because barbiturates are so frequently encountered in toxicological examinations, a reliable procedure for their identification is essential. Chemical methods are not available for differentiating between the barbiturates. In a study of the infrared absorption spectra of these compounds, the spectra of the purified compounds, run at optimum concentrations in chloroform solution, showed significant deviations in the minor absorption bands. The variations permitted a classification and a method of identification of the different members of the series based on their infrared absorption characteristics. Barbiturates encountered in organs and body fluids can be quantitatively analyzed. In toxicological analysis of tissue extracts containing organic compounds, infrared is usually the only effective method.

Waxes

Identification of carnauba wax and candellila wax, long-chain ester groups, long-chain acid groups, hydroxy acids and alcohols found in waxes; quantitative measurements of carbonyl content, aromatic content, petroleum-derived wax, oxidized micro-crystalline wax in solid waxes; formulation of complex waxes can be determined, and control of formulation during mixing and plant processing can be followed by infrared.

5.3.3 INDUSTRIAL NONDISPERSIVE ABSORPTION ANALYZERS[4]

IN spite of its firmly established value as a qualitative and analytical tool, even the most rugged and stable infrared spectrometer or spectrophotometer is not generally suitable for plant stream use where the identity of the components to be measured are known. Simplified, ruggedized, reliable, accurate and sensitive instrumentation is needed which can be procured and maintained at lower costs. Furthermore, in the interests of speed of application of control, relief from mathematical computation is needed. These parameters are provided by infrared absorption analyzers using nondispersive techniques without the use of prisms or diffraction gratings.

Analyzer Principles[5]

Two general ways of applying the self-filter principle have evolved from these original conceptions, known respectively as the "negative-filter" method and the "positive-filter" method.

In the negative-filter method, two equal beams of radiation are passed through a common sample cell. One of the beams passes through a filter cell and the other through a compensator cell. The resultant two beams then fall on two detectors, which form part of an electrical bridge circuit. In analyzing a mixture of gases for a component A, a high concentration of A, (usually 100 per cent) is put into the filter cell. Thus this beam of radiation, on passing through the filter cell, is reduced in intensity by an amount equal to the integrated sum of all the infrared absorption bands of A. The gas mixture being analyzed is put into the sample cell. Theoretically, from Beer's Law, if the concen-

[4] W. A. Patterson, *Chem. Engrg.;* September, 1952.
[5] Obtained from manufacturers' literature.

tration in the filter cell is high enough, any variation in component A in the gas sample will not appreciably affect the intensity of this beam of radiation. On the other hand, the intensity of the other beam will vary with the concentration of component A. Absorption due to other components in the gas sample would affect both beams by the same amount, so the difference in the intensity of the two beams is a measure of the concentration of component A. In this simple explanation, it is assumed that the absorption bands of other components do not overlap those of component A.

In the positive-filter method, the radiation is similarly split into two equal beams. One beam passes through a sample cell, the other through a cell containing an inert gas such as nitrogen. These two beams fall on either side of a detector cell, which is divided into two parts by a thin membrane or diaphragm. Here, component A is put into both sides of the detector cell; it will absorb only that radiation corresponding to its infrared absorption spectrum, excluding all other radiation. When radiation is absorbed, the gas is heated and will expand. If there is a difference in the amount of energy absorbed on the two sides of the detector cell, then the membrane will be displaced. This displacement can be measured by making the membrane one plate of an electrical condenser, the other plate being fixed in position. The presence of component A in the sample cell would reduce the amount of effective radiation reaching that side of the detector cell, and the resulting displacement of the thin membrane would be a measure of the concentration.

Basically, the difference in the two methods is as follows: In the negative-filter method, the detector measures the energy of the beam reduced by an amount equal to the absorption of the sensitizing component. However, in the positive-filter method, only that energy absorbed by the sensitizing component is measured. Instruments based upon these two methods are also known respectively as "nonselective" detector and "selective" detector analyzers, according to the role played by the respective detectors.

Commercial Instruments

An instrument manufactured by Baird-Atomic, Inc., is shown schematically in Fig. 3. The sample cell is readily removed from its case for cleaning. The two components on each side of the sample cell are screwed to the sample cell compartment and enclosed in cases. The cells may be of brass or stainless steel, depending on the application; and the cell windows are of quartz, calcium fluoride, rock salt, or other materials depending on the problem. A single mirror in the source compartment serves to align the two beams. The optical unit is enclosed in a copper box, which in turn is placed in an insulated explosion-proof box.

Another instrument of the negative-filter type is made by the Leeds and Northrup Company. The instrument is similar to the Baird instrument, but there are

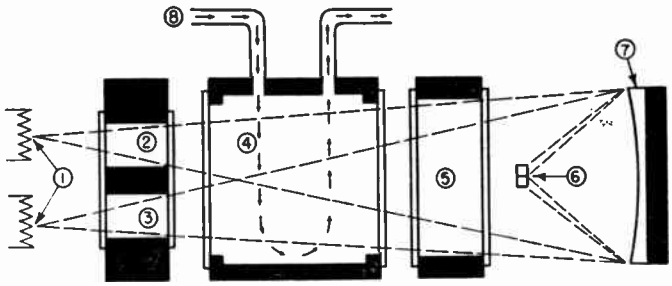

Fig. 3—Diagram of commercial absorption analyzer.

considerable differences in the instrumental components. Thermopiles are used instead of bolometers, and an attempt has been made to funnel the energy from each beam onto the respective thermopiles by cone-shaped filter and compensator cells. A gold-coated boro-silicate-glass sample cell is used to converse energy.

The first positive-filter type instrument was developed by K. F. Luft in 1943. It is the forerunner of all modern "positive-filter" type instruments. Because the general arrangement is typical of a number of instruments produced by different manufacturers, the name Luft-type Infrared Analyzer (*i.e.*, LIRA) has been given to them. The instrument has an interference cell and a compensator cell. A characteristic of this instrument common to all commercial positive-filter type instruments is the light interrupter. In this particular instrument, the two infrared beams from two Nichrome wire spirals are chopped simultaneously and an amplifier is tuned to respond only to the frequency of interruption. This modulated system increases considerably the stability of the instrument, and additional freedom from ambient temperature effects is obtained by providing a slow leak between the two halves of the detector cell.

Positive Vs Negative Types

In comparing the two general types of instruments, many of the differences are mainly due to what each manufacturer believes is the best approach to satisfy plant conditions. The present instruments manufactured by Baird-Atomic, Inc., and the Leeds and Northrup Company have no moving or vibrating parts in key positions, on the theory that this design makes for ruggedness. Detectors based on the heat expansion of gases, as in the positive-filter type instruments, may have linearity problems, but this may not be serious, as the temperature differential would be small. On the other hand, the detectors used in negative-filter type instruments have a lower signal-to-noise ratio. The positive-filter type of instrument is definitely limited in analyzing liquids since a suitable sensitizing gas must be used in the detector, but such a gas or mixture of gases could probably be found for many applications. Application to liquids is relatively simple in the negative-filter type, but thermostating at a sufficiently low tempera-

ture for some liquids can cause trouble and a chopped-beam system may be more feasible for protection from ambient temperature fluctuations.

One of the advantages claimed for the positive-filter instruments is that there is no background signal, whereas in the negative-filter method there is a large background signal. In other words, a large amount of the radiation detected is not directly concerned in the analysis. This is especially true for simple gas mixtures. However, for complex mixtures, the background signal in the negative-filter instrument becomes much smaller because of the high absorption of the other components and the desensitizing gases used. It is possible that ways may be found to eliminate it altogether.

Analyzers vs Spectrometers

For plant process analysis and control, the nondispersive infrared analyzers have a number of advantages overinfrared spectrometers; these include greater ruggedness and stability, lower cost, and elimination of mathematical treatment for interfering bands. In addition, they are more sensitive, detecting smaller concentration of a given component in a given path length because of their use of the integrated energy of the entire infrared absorption spectrum of the component. Because they have no slits or dispersing elements they have theoretically infinite resolution, giving greater selectivity. They have shown measurable and significant differences on gas mixtures which give apparently identical infrared spectra.

All this adds up to a decidedly useful instrument for chemical plant analysis. With the development of liquid analyzers, their potential seems unlimited. To reach this potential means further improvements and better knowledge of sensitizing and desensitizing, as well as of the specific applications in the plant. Properly used, such instruments not only can give continuous and instantaneous analytical results, but also can often control the process as well.

5.3.4 ABSORPTION-SPECTRA HYGROMETERS[6]

THERE have been many approaches to the problem of measuring atmospheric water vapor. One of the most promising ones is a method of measurement by absorption-spectra analysis, employing as a sensing element a beam of infrared radiation. Due to the nature of the absorption function, the method results in high sensitivity at low vapor concentrations where other systems fail. This is particularly true under Arctic and high-altitude conditions. Other areas may include: continuous monitoring of short-term atmospheric variations, ice-fog studies in the Arctic, evaporation studies over reservoir surfaces, and plant process monitoring and control. Prototype instruments employing interference band-pass filters for isolating the particular wavelengths of interest have been built by the U. S. Weather Bureau. These instruments make use of the 1.38-μ absorption band of water vapor and utilize a reference wavelength at 1.24 μ. They are essentially experimental types and have not been produced commercially.

An improved model has been designed and built by R. C. Wood of the Mechanical Division of General Mills. One of the most important design features affecting improved hygrometer performance has been the use of the 2.6-μ absorption band, the most sensitive water-vapor band that can be used in an instrument employing glass optics. There are several advantages of this feature. High sensitivity can be obtained with a short sensing path; this in turn results in a more rugged optical platform that is less sensitive to alignment errors. In addition, light scattering due to particles in the path or dust on optical surfaces has less effect than at shorter wavelengths. Carbon-dioxide absorption, which becomes significant beyond 2.65 μ is avoided by choosing filters which do not transmit appreciably beyond that wavelength.

If an optical material transmits differently at two wavelengths, the energy ratio between the two wavelengths can be altered by changing the thickness of the material.

In the hygrometer, the balancing filter is didymium glass which has a higher transmission at 2.60 μ than at 2.45 μ. By constructing this filter in the form of a long wedge and mounting it in the path normal to the optical axis of the beam, the ratio of absorption- and reference-band energies can be made to vary as a function of its position (thickness). Thus, a departure from an absorption/reference-band ratio of unity due to a variation of water vapor is quickly compensated by an appropriate change in position (thickness) of the glass wedge. A second wedge indentical to the servo-operated wedge, adjusted manually, serves to correct the calibration for instrument drift. The detector is a lead sulphide Kodak "Ektron" photocell with a 4×4 mm area. At low concentrations of 0.2 gram per cubic meter or less, the hygrometer can detect variations of one milligram of water vapor per cubic meter, or approximately one part per million by volume. Above dewpoints of 32°F, the accuracy has been found to exceed plus or minus 0.5°. At lower concentrations, the absolute accuracy is uncertain because of the calibration method. The repeatability, however, is equivalent to plus or minus 1° at −20°, and plus or minus 2° at −50°. In 5 seconds or less, the instrument will indicate 95 per cent of a given change assuming an instantaneous sample change not greater than 50 per cent of the initial volume. Accuracy and sensitivity at lower sample concentrations can easily be increased through the use of a longer path.

An item under internal development at the U. S. Army Signal Research and Development Laboratory,

[6] Obtained from manufacturers' literature and from the following: R. C. Wood, "Improved infrared absorption spectra hygrometer," *Rev. Sci. Instr.*, vol. 29, pp. 36–42; January, 1958. R. C. Wood, Foskett and Foster, "The Infrared Absorption Hygrometer in Progress Report," Instr. Soc. Am., Paper No. 54-36-1; R. H. Ostergren and K. G. Halvorsen, Paper presented at the Instr. Soc. Am. Conf., New York, N. Y., September, 1957.

Fort Monmouth, N. J., is an infrared absorption-hygrometer for the measurement of atmospheric water vapor content, which is designed to be sensitive and accurate enough for use at the low temperatures and pressures encountered by aircraft.

Airborne Hygrometer[7]

The U. S. Air Force has formulated basic specifications for an airborne infrared absorption-type instrument to measure humidity for meteorological research. Beckman Instruments, Inc., has undertaken the task of extending accuracy, range, reliability, speed, compactness, lightness, and ruggedness to meet these airborne requirements.

Water-vapor bands of varying width and absorption exist at numerous points in the infrared spectrum. Each of these bands is in reality a group of lines. A high-resolution spectrophotometer would indicate a large variation in absorption with change in bandwidth at different wavelengths. For a measuring instrument, however, it is more practical to utilize the average, or integral, absorption of a band of 20- to 40-mμ width. Such bandwidths are readily obtained with relatively simple and small interference filters, sufficient energy can be passed for available detectors, and good system stability may be maintained. Suitable water-vapor bands of good absorption are found at wavelengths of 1.37, 1.87, 2.7, 3.2, and 6.3 μ.

An experimental airborne hygrometer uses a 48-pass folded cell system to get an 84-foot path in one of the near-infrared water bands. Multiple dielectric interference filters are used in a 350-cycle vibrator-chopper to isolate a narrow water-absorption band (1.87 μ) and a corresponding reference band (2.16 μ) nearby. A variable-incidence interference filter is used to attenuate the reference band energy to an optical null match with that of the absorption band. The lead sulfide cell detector and servo of the absorption cell system drives a potentiometer whose resistance is tailored to represent the total amount of water in the cell. A bridge computer circuit including inputs of pressure, temperature, and sample compression into the cell, allows an output potentiometer to be servo-driven to an output counter reading of atmospheric humidity in dewpoint temperature, degrees centigrade.

The response delay of the instrument is under one second. The output scale reads from −85°C to 35°C dewpoint. Sensitivity is satisfactory down to the low end of the scale, although zero drift limits accuracy to 0.5°C down to −40° and 2° at −55°C dewpoint.

5.3.5 RADIOMETERS AND PYROMETERS[8]

REMOTE temperature measurement by means of infrared radiometry is possible because the radiation emitted by a body is a well-known function of its temperature. A radiometer, in the modern sense of the term, is an optical instrument which collects radiation from a narrow field of view and converts the received energy into an electrical signal. The amplitude of this electrical signal can be measured with great accuracy. Also, since the characteristics of radiation are well established by basic laws and relationships, it is possible to calibrate the electrical output in terms of temperature for a given source. Thus, a practical means has been established for measuring temperature without physical contact.

From the basic radiation laws, it is seen that the radiation emitted by objects is uniquely related to their temperature and that almost all of the energy is in the infrared portion of the spectrum. Most common objects have nearly constant emissivity in the infrared and, hence, have radiation distributions similar to black bodies of the same temperature. The temperature of objects can, hence, be determined through measurement of their infrared radiation emitted and computations using the radiation laws.

All radiation measurements involve comparison with a primary or secondary reference standard. Since absolute levels of infrared radiation are defined with respect to absolute zero, the level of the incoming radiation must be compared to some known reference level before an absolute level of temperature can be derived for the target. The reference level of radiation is usually contained within the radiometer.

The radiometer focuses the infrared radiation from the object (the "source" or "target") onto an infrared radiation detector. For measurement of total infrared radiation, the radiometer optical system must be equally efficient at all infrared wavelengths, and this generally requires the use of reflecting optics. The infrared detector must also have uniform electrical output proportional to incident radiation for all wavelengths of infrared energy incident on it. It must hence be a "black" or "thermal" type infrared detector.

The detector measures the radiation difference ΔW between the source radiation energy focused upon the detector and the radiant-energy reference level in the radiometer. This basic radiation measurement is expressed as:

$$\Delta W = W_S - W_R, \tag{1}$$

where W_S is the source energy focused upon the detector, and W_R is the radiant energy reference level.

The voltage output of the detector is proportional to ΔW in the following manner:

$$\Delta V = R\Delta W, \tag{2}$$

where ΔV is the voltage produced by ΔW, and R is the "responsivity" of the detector, which defines the voltage output of the detector for each watt of radiant energy focused upon it. The stability of W_R depends upon the basic design of the radiometer. Thus, it can be seen that the form of reference level employed determines the ultimate accuracy of the instrument.

[7] Prepared by R. H. Ostergren.
[8] Obtained from manufacturers' literature.

Industrial Radiometers and Pyrometers

Industrial radiometers and pyrometers are widely used for process control. Fig. 4 shows Barnes Engineering Company's OptiTherm radiometer; Fig. 5 is a pyrometer manufactured by the Servo Corporation of America. The two instruments are similar, containing components to perform two functions: The "head" or sensing unit collects infrared radiation and converts it into a proportionate electric current. The control circuit then receives this variable current, and amplifies it to sufficient strength for operating meters, indicators, recording or automatic control instruments.

In the sensing head, the infrared radiation from the "target" (the object, material, or process equipment under observation) enters through the infrared lens that functions much like any optical lens except that it transmits infrared wavelengths exclusively. Incoming infrared is focused on the detector cell, usually a bolometer, which is a section of material whose electrical conductivity varies sharply with its temperature. This is the conversion point, or "transducer," where infrared energy is converted into electric energy. The electric signal, or current, coming from the bolometer is always in direct relationship to the amount of infrared radiation coming in through the lens. This newly-formed electric signal is then handled through regular circuitry designed for the purpose.

The principal characteristics of three different types of modern infrared radiometers and the form of reference level which they employ are discussed below and outlined in the accompanying table.

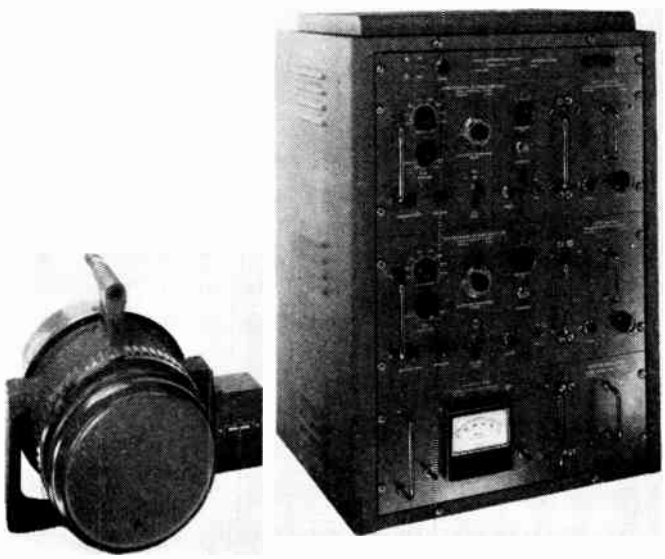

Fig. 4—OptiTherm radiometer.

Fig. 5—Servotherm pyrometer model 1372.

Principles of Operation of Different Radiometer Types

Type	Infrared Detector and Speed of Response	Reference Radiation Level $[W_R]$	Radiation Measurement $[\Delta W=(W_S-W_R)]$	Electrical Signal $[\Delta V=R\Delta W]$
dc Infrared Radiometer	Thermopile Detector Speed: 2 seconds System Speed: 2 seconds	Emissivity and temperature of thermopile	Difference of source radiation and thermopile radiation	Electromotive force from compensated dc thermopile
ac Blackened Chopper	Thermistor Detector Speed: 1 msec. System Speed: 25 msec	Emissivity and temperature of blackened chopper	Difference of source radiation and blackened chopper radiation	ac signal from compensated thermistor bolometer bridge
ac Mirror	Thermistor Detector Speed: 1 msec System Speed: Adjustable 16 msec to 1.6 seconds	Temperature of black body reference (emissivity = 1.0) which is temperature controlled or monitored within 0.2°C	Difference of source radiation and reference black-body radiation. Null method may be used with temperature controlled black body	ac signal from compensated thermistor bolometer bridge. Null detection method when using controlled black body

dc Infrared Radiometers

The dc radiometer employs no chopper. It is an industrial infrared radiometer of a type now used fairly extensively for remote temperature measurement of inaccessible objects having temperatures in excess of 250°C. The instrument measures a change in dc electrical properties of a thermoelectric or bolometric infrared-sensing element. Instruments with various lens and mirror optical systems are available, depending upon the temperature range to be measured.

The radiation difference, ΔW, is the difference between the source energy focused by the radiometer optics on the infrared detector and the radiant-energy level of the detector itself. The emissivity and temperature of the infrared detector determine the reference radiation level of this instrument and are, hence, of great importance.

Since the reference level of this type of instrument is determined by the emissivity and temperature of the detector, this reference level is subject to ambient drift. This ambient drift is of no major significance as long as the target temperature is considerably above ambient. However, if the target temperature approaches ambient, the drift in reference level may cause significant errors. Elaborate methods of compensating for this drift are available and these are extensively discussed in the literature on the subject.

ac Infrared Radiometers

Recent advances in high-speed infrared detectors have led to the development of a new type of radiometric instruments, called ac infrared radiometers, since they employ ac chopping techniques and since ac electrical signals are developed by the detectors. Because it is desirable to have the radiometer sensitive over the wavelength range from 1.8 to 40 μ, high-speed thermal detectors are used for total radiation measurement.

Alternating-current infrared radiometers can be classified into two groups: those employing a blackened radiation chopper, and those employing a mirror chopper and reference black-body source. In the blackened chopper system, the infrared detector alternately sees the image of the source and a blackened chopper. The radiation signal measured is the difference between the source and chopper radiation. The reference radiation level in this instrument is determined by the emissivity and temperature of the blackened chopper. The mirror chopper system alternately directs radiation from the source and from an internal black body onto the infrared detector. The temperature of the internal black body is either controlled and adjustable or it is precisely monitored. The reference radiation level in this instrument is that of the internal black body and, hence, is precisely known.

A few of the typical uses of industrial radiometers and pyrometers are:

Calcining drums: The infrared radiometer is particularly useful in finding "hots spots" in industrial equipment before they cause damage. For example, calcining operations are carried on in very large revolving steel drums. At times, the reacting material attaches itself to the inside of the drum, causes local overheating, and may result in burning a hole in the drum. A radiometer, scanning the drum, will detect the hot spot before it causes damage.

Transmission lines: A thermistor radiometer is now being used by a large utility company to check overhead electrical transmission lines. Here, faulty joints develop excessive resistance and heat up when the line is in use. The radiometer optically examines the transmission line joints and picks out the faulty ones while the line continues in operation.

Printing presses: In modern, high-speed printing presses, particularly in those using multiple-color processes, it is most important to dry the printing inks immediately after they are applied. This is done by heating the paper after it passes through the printing unit at rates of 500 to 1500 feet per minute. The paper is actually heated momentarily to the point where solvents are flashed out of the ink by burning. Ideally, the gas dryers should be adjusted to the point where the ink is dried rapidly but the paper is not damaged by overheating. Efforts have been made to measure the paper temperature using contact pyrometers, but these have proved unsatisfactory.

Primary metals industries: Pyrometers are used for the temperature measurement and control of: ferrous and nonferrous metals in sheet, bar, roll, or tubing form undergoing extrusion, moulding, casting, drawing, rolling, overheating, melting, die casting, induction heating, heat hardening, annealing and heat processing; as well as control of associated dies, rollers, jigs and other shaping tools.

Metal fabrication: The temperature measurement and control of metals undergoing induction hardening, machining, forging, brazing, cutting, boring, stamping, forming, welding, joining, drawing, heating, grinding, finishing, and enamel baking.

Stone, clay, and glass products: Temperature measurement and control of mineral processing, crystal growing, glass rolling, polishing and annealing.

Chemical products: Temperature measurement and control of rolling, moulding, die-pressing, extruding and curing of plastic in sheet, roll or tubing form. Control has also been achieved for critical change of state temperatures of plastics and synthetic fibers. Control by temperature measurement likewise has been attained in refinery processes, synthetic rubber processes and product testing, manufacture of asphalt shingles and coating procedures, and precision drying of photographic color and black-and-white film.

Web processes—paper and textile products: Temperature measurement, and control of drying, curing, gluing, dyeing, sizing and coating of paper, cotton, synthetics, etc.

Background-Discriminating Radiometers[9]

The Aerojet-General Corporation manufactures very highly sensitive radiometers which are able to measure the radiant power of a source against a radiant background. This is accomplished by means of a unique background-discriminating reticle. The output of the system is proportional to the net difference between the radiance of the source and the radiance of the background it obscures. Since the radiance of the background is usually considerably less than that of the source, the data obtained are very good. The head consists of a small radiometer of range from 1.8 to 2.7 μ, a larger radiometer of range from 3 to 5 μ, a tracking telescope, and a motion-picture camera.

The data are recorded on a recording oscillograph which is synchronized with the camera. By the use of multiple galvanometers in the oscillograph, dynamic range is achieved. The major advantage of this instrument is that measurements of airborne sources are readily obtained any time of the day without the necessity of special test setups or calibration techniques.

Gas Radiation Pyrometer[10]

An Infrared Gas Radiation (IRGAR) Pyrometer is being developed for the Propulsion Laboratory, Wright Air Development Center, to fulfill the requirement for a device to succeed the thermocouple probe in future operational engines utilizing the higher tmeperatures and new fuels which prohibit conventional measurement techniques. The principles employed in the IRGAR detector should find broad application in industrial applications where a sensor must operate under a severe physical ambient and yield a rapid, reliable and reproducible indication of temperature.

The sensor for the IRGAR pyrometer is shown diagrammatically in Fig. 6. Two identical cylindrical chambers are formed in a silver housing and filled with a partial pressure of CO_2 gas. One chamber is exposed to radiation from the combustion gas through an infrared-transmitting window of synthetic sapphire. Radiant energy is absorbed by the detector gas, which is thereby heated above the ambient temperature of the CO_2 in the reference chamber. The difference in temperature is measured by a thermopile.

The development of this detector has been deeply concerned with material and fabrication problems. Silver was selected because its high thermal conductivity assured isothermal wall surfaces for the detector chambers, and because of its high infrared reflecting characteristics when polished and its high resistance to corrosion and oxidation at elevated temperature. Sapphire is a good window material because of its excellent physical properties at high temperature and its ability to transmit infrared energy out to about 5 μ.

[9] Prepared by R. W. Powell.
[10] Prepared by E. L. Woodcock.

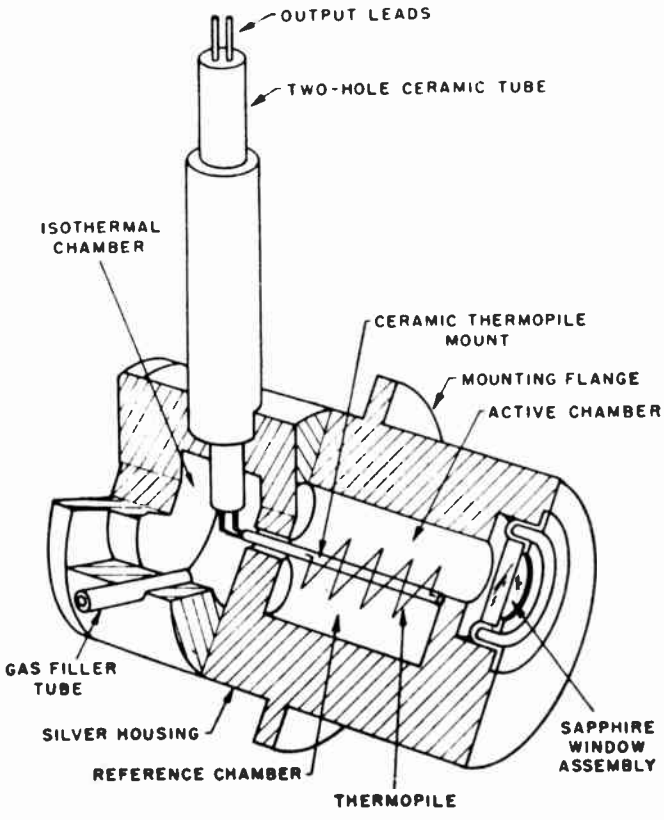

Fig. 6—Pyrometric detector body showing thermopile sensing element.

The thermopile is made physically small to restrict its thermal mass and to reduce its tendency to cool the gas in the receiver chamber by conduction.

This detector does not measure temperature directly. Its output is a function of the radiation from the combustion gas and, hence, a function of that gas temperature. It is also a function of the receiver ambient temperature, since it measures radiation heating with respect to that ambient. Calibration of the output to give a temperature indication will require some correction or compensation to account for the fluctuations in output resulting from ambient temperature changes.

Initial testing of models of the IRGAR pyrometer performed on a simulated ramjet burner at the National Bureau of Standards, a test turbojet combustor at Allison Division of General Motors, and on a J-47 afterburner at Wright Air Development Center have demonstrated the expected influence of disturbing factors on detector output. Some of them can be made negligibly small; for instance, the effect of black-body radiation from hot metal engine parts is minimized by operating the detector at the same temperature as the engine, resulting in a net zero radiant interchange between the two. Effects of detector ambient can be eliminated by thermocoupling the detector housing and adding a portion of this emf to the detector output. Corrections for other factors such as mass flow, fuel-to-air ratio, etc., can be added in a similar fashion.

The output from the detector is not linear, since the

radiation increases more rapidly than the temperature. This factor will be eliminated in the empirical calibration of the pyrometer system which is expected for each type of installation. The nonlinearity makes the IRGAR system potentially more precise at higher temperatures.

5.3.6 FIRE DETECTION[11]

Aircraft Fires

SPOTTING and extinguishing fires in aircraft has long been a perplexing problem. Today, the problem has become aggravated by the introduction in jet fighter designs of submerged rocket storage to reduce drag. The Electronics Corporation of America has developed a unique infrared device to solve this problem. An infrared detecting element immediately discovers the presence of fire by actually "seeing" the flame.

In the airplane whose engines are to be protected by the system, the detecting elements (detectors) are installed in each engine compartment zone. When a detector indicates a fire, the control unit flashes a light in the cockpit, warning the crew that a fire has started in a particular engine.

The cells accurately show, by very rapid resistance changes, the varying radiation emitted by a flame. They detect by responding to the flame flicker in the same way the human eye does when it sees a fire.

Similar devices are designed specifically to prevent explosion and fire on a combat airplane after an incendiary bullet makes a direct hit on a fuel tank. When the explosion detector sees infrared radiation—and such radiation is present in large quantities in all fires and explosions—its resistance changes with great rapidity. On a combat airplane, the detector is designed to react before an incendiary bullet, travelling at 3000 feet per second, is halfway through the wing. The reaction or change in resistance of the detector electronically triggers or sets off the detonator. The latter, in turn, spreads the extinguishing agent throughout the fuel tank of the plane at the rate of about 300 feet per second.

Extensive tests demonstrated that this sequence of events takes place with such speed as to adequately suppress explosions in the fuel cells. The effect of the extinguishing fluid on the fuel is negligible; most of the fluid goes into vapor and out the vent, but if it does not, it does not harm the fuel.

Quite apart from its military significance, the device also has important implications for industry. As an explosion suppressor or extinguisher, it opens up the entirely new field of "explosion prevention." The response of the system is in no way dependent on flame contact, pressure rise, or temperature rise.

The biggest present markets for the fire detector and the explosion suppressor are the Air Force and the Navy. However, now that it is released for commercial production it will be marketed on a broad scale. Applications already are being made by engineers in ground fuel-storage tanks, pumping stations, and similar areas where explosions are ever-present hazards.

Forest-Fire Protection

Infrared scanners can automatically survey large areas of state and national forests. The units can be mounted in established lookout stations to supplement the visual equipment. Small battery-operated infrared units can also be located in hidden canyons to give advanced warning of fires which otherwise could be detected only by large quantities of smoke. They could operate with only annual replacement of batteries.

When a fire is detected, infrared photographs of the area can determine the location and intensities of the "hot spots." The photographs can be used to outline the strategy of controlling the fire. In the case of arson, additional blazes can quickly be noted.

In the actual fighting of the fire, simple infrared seeker systems can direct water or chemical bombs onto the hottest points of the fire. These seeker systems can be simplified versions of infrared guidance heads currently used for military missiles.

Infrared Hot Box Detective

For many years, overheated journal boxes have presented a menace to the railroads. Overheated journals which develop into hot boxes have been the largest single cause of derailments, have chewed up one-half of the total expenditures for freight-car repair and maintenance, have cost millions in damaged equipment and delayed and destroyed goods, and have torn up rights-of-way and disorganized schedules. This situation was becoming progressively worse as faster, longer trains operated with fewer stops. Many solutions were tried to overcome the damaging costs of overheated journals. Out of this project emerged the SERVOSAFE, a Hot Box Detective, an infrared-electronic system manufactured by the Servo Corporation of America. It instantly detects and records overheated journals on freight trains passing at speeds up to seventy miles per hour. Operating equally well in cold or heat, day or night, the system works in rain, dust, fog, or smoke. Today, seventeen major lines have purchased or leased the Detective. Two major roads have already installed them strategically throughout their systems.

The Hot Box Detective is being used to inspect trains entering a terminal yard, so that abnormally hot journals can be "selectively serviced," even after the train has cooled off. Thus, a small crew can handle a great many cars more effectively, and the frequency of outgoing hot boxes is greatly reduced.

A typical Hot Box Detective system consists of detectors, wheel pickups, power supply signal amplifier, and Servograph Recorder. The detectors and pickups are permanently installed at trackside in rugged, weather-proof cases. For two-way systems, two detec-

[11] Obtained from manufacturers' literature.

tors are mounted in each detector housing, one for each direction of traffic.

In operation, the train's wheel flanges pass over the first pickup. The ensuing voltage pulse causes the cover of the detector's lens to open and activates the recorder. When the wheel flanges pass over the second pickup, the resulting voltage pulse deactivates the Recorder. In this way, only the heat radiated from the journal box is recorded, so that spurious indications from steam pipes or other heat sources are prevented.

5.3.7 THERMAL IMAGING DEVICES[12]

Scanning Cameras

INFRARED pictures can and have been made by using infrared-sensitive film and image-converter tubes. The disadvantage of these is that to date their infrared sensitivity extends only through the near-infrared region out to approximately 1.5 μ. Consequently, their use as detectors of thermal emission is limited to those objects at temperatures over 1000°F. While the presence of bodies at lower temperatures can be detected by illuminating them with infrared radiation in the region of from 1 to 1.5 μ, such detection reveals nothing concerning the thermal characteristics.

Many of the most important applications of thermal photography require measurements at temperatures from 300°F down to −170°F. The energy emitted by bodies at these lower temperatures is distributed almost entirely in the long-wavelength far-infrared region. Practical detectors for field work against these temperatures are thermistor bolometers, which have uniform spectral sensitivity from the ultraviolet through the far infrared. However, indium antimonide detectors are being used by Radiation Electronics Corporation. The Engineer Research and Development Laboratories of the Army are sponsoring infrared Vidicon development at the Radio Corporation of America. Westinghouse is developing a device known as the Thermocom. Also, General Electric is working on a TV-type infrared tube for incorporation in an infrared camera device.

While infrared radiometers are the most effective means for remote temperature and radiation measurements, their field of view is ordinarily restricted to small target areas ranging from $\frac{1}{8}$ inch$\times\frac{1}{8}$ inch square to 1 inch$\times$1 inch square at a distance of 10 feet. Many temperature and radiation measurements require knowledge of the thermal distribution over much larger areas. Although this information can be obtained by scanning a radiometer over the desired field of view, such a process is slow and is difficult to interpret. With an infrared scanning camera, a field of view as large as 20° wide by 10° high, containing 60,000 resolution elements, can be scanned quickly, and temperature differences as small as 0.1°C can be recorded.

Far-infrared scanning cameras followed closely the development of far-infrared reconnaissance equipment. The far-infrared cameras made by Barnes Engineering Company, Servo Corporation of America, and Radiation Electronics Corporation, Illinois, all bear some resemblance to the thermograph described previously.[13] These cameras are essentially scanning radiometers using thermistor bolometer detectors or indium antimonide cells. The detector output is an electrical signal which is proportional to the radiation level in the instantaneous field of view. After suitable amplification, the electrical output is used to modulate a light beam and generate a visible photograph.

The scanning-camera electronic system contains attenuator controls which permit the operator to adjust the system to cover a very narrow or a very wide temperature range. There is another type of control, known as electronic temperature offset, which permits the operator to shift his selected temperature range up or down the temperature scale.

The optical system of the Barnes Engineering Company's camera consists of an 8-inch radiometer and an imaging attachment. In the latter, an oscillating plane mirror mounted at 45° in front of the radiometer aperture is cam-driven to produce a horizontal scan of 20° with a quick return. During the return, the mirror tilts upward one line width, thus causing the elemental field of the radiometer to scan the object line by line, covering a maximum of 20°$\times$10°. The back of this same oscillating mirror scans a light spot from a Sylvania Type 1B59 glow modulator tube over a Polaroid Land or conventional photographic film. The spot is made proportional in size to the instantaneous radiometer field of view and the glow tube is intensity-modulated by the radiometer output signal. Since the mirror is simultaneously scanning both the target and the film, perfect synchronization automatically results and the imaging attachment forms a thermal picture of the object being scanned by the radiometer.

A quantitative, two-dimensional record of the total infrared emission in the object plane can be obtained from the density of the photographic picture. In order to facilitate this, a gray-scale generator has been incorporated in the device which places eight density steps on the photograph, ranging from black to white. These are produced by electrical signals which go through the glow-tube modulation-drive circuit exactly like the radiometer output signals. They therefore calibrate the film in terms of the radiometer signal and make the calibration of the photographic record independent of the glow tube or developing process.

The quantitative analysis of a record consists of interpreting the gray-scale steps in terms of object radiance. This is done by first finding the object radiance level which produces zero output signal, or black on the picture, and then computing and adding thereto the

[12] Obtained from manufacturers' literature.

[13] See Fig. 13 in R. S. Wiseman and M. W. Klein, "Infrared viewing systems," paper 5.1.6, this issue, p. 1617.

radiance differences corresponding to the gray-scale steps.

The far-infrared scanning cameras are used by the military to study the passive infrared radiation patterns of targets and backgrounds. They are also being used on industrial and laboratory problems for the study of temperature distribution in objects ranging from oil refineries to wind-tunnel models. The heating patterns in complicated electronic equipment, as well as jet engines, have been observed. Use in nondestructive testing to observe thermal patterns in metal honeycomb structures is being investigated.

The sensitivity of a thermograph can be extended so that it will indicate differences in ice surface temperature. A Barnes thermograph is now being employed in the Arctic regions to detect hidden ice crevasses by means of the minute temperature differences which exist on the surface. The equipment has a noise equivalent temperature of 0.006°C.

Some of the most interesting applications of thermography are the applications to medicine. It is a well-recognized fact that breast cancer provokes varying degrees of local inflammatory reactions associated with an increased blood and lymphatic supply. Subcutaneous veins over the chest are often noticeably dilated. Increased metabolism of accelerated cell division unquestionably causes a raised local heat production through chemical reactions. What is desired in human thermography is a quickly obtainable visual image of the heat patterns between 2 and 5 μ or between 10 and 15 μ, of adequate clarity and sensitivity of a large enough area of the body to supply normal reference points.

Dr. R. N. Lawson of the Department of Surgery, Royal Victoria Hospital, Montreal, and Department of Experimental Surgery of McGill University, has written illuminating articles on thermography.[14] He states:

> While research in chemo-therapy, wherein our main hope of cure lies, continues, current data indicates that improved surgical results can be obtained through the discovery and application of more efficient diagnostic methods. The only "early" sign of breast cancer is an anatomically small lump in the breast. It would seem that even this is not exactly always an early sign—it is apparent then that new diagnostic methods using other techniques than human tactile sensation must be explored, if we are to materially improve surgical results.
>
> An investigational approach as follows was commenced:
>
> Two advanced cases of metastatic breast cancer were given 1 ml heptaldehyde intramuscularly, and within five minutes, both reported pain in the visible tumor nodules. It was difficult to assess or interpret this pain, but some vascular disturbance within the neoplasm seemed a likely possibility. Accordingly, temperature readings were made.
>
> The first significant fact was the observation that the skin temperatures overlying the cancers were definitely higher than that of the surrounding areas.[15] The temperature increases were often 2 to 3 degrees F, and could be measured by direct contact with relatively insensitive instruments.
>
> The second observation was that the ipsilateral areolar temperature was also increased regardless of the location in the breast of the primary carcinoma. It was noted that these temperature elevations corresponded to those elevations found in acute mammary infections. Following heptaldehyde, a fairly prompt reduction in temperature occurred, both over the areola and lump, only if a malignant tumor was present. Heptaldehyde had no influence in the temperatures associated with benign or inflammatory lesions.[16]

Dr. Lawson then discusses the use of the Baird Evaporograph and the Barnes Thermograph, showing that localized areas of temperature changes can be identified and correlated with abnormal areas diagnosed as benign or malignant. More recently,[14] he has used the thermal imaging device produced by the Radiation Electronics Corporation of Skokie, Ill. This device, THERMOSCAN, has a resolution of 5 milliradians over a field of view of 20°×10°, with a frame time of 1 second. The detector is a photoconductive-type indium antimonide cell operated at −80°C. Fig. 7 shows a case of an abscessed right breast. The gray scale on the infrared photographs shows actual temperature variations over the surface of the skin. Electronic systems noises do not appear in the pictures.

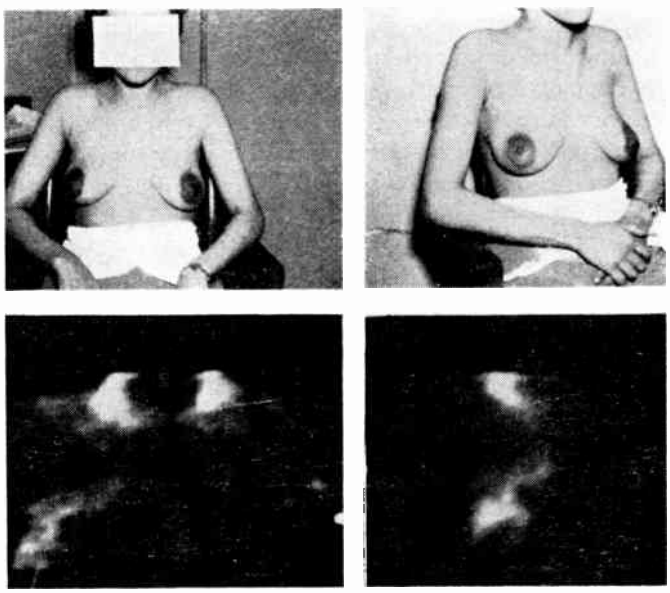

Fig. 7—Thermographs of breast tumor. Light areas indicate higher temperatures.

In summary, the objectives of Dr. Lawson's work are several. First, he is investigating whether or not infrared measurements will reveal the presence of near-surface abnormal growths such as tumors and cancers. Second, he wishes to determine whether diagnosis can be made of the malignancy of the abnormality. Third, he wishes to investigate the possible retardation of cancerous growths by the injection of specific chemical compounds. Obviously, if thermal imaging techniques can reveal the presence and extent of near-surface ab-

[14] R. N. Lawson, "Thermography—new tool in breast lesion investigation," *Canad. Services Med. J.*, vol. 13, pp. 517–524; September, 1957. Also, "A new infrared imaging device," *Canad. Services Med. J.*, vol. 79, pp. 402–403; September 1, 1958.

[15] R. N. Lawson, "Implications of surface temperatures in the diagnosis of breast cancer," *Canad. Med. Assoc. J.*, vol. 75, p. 309; 1956.

[16] R. N. Lawson, A. L. Saunders, and R. D. Cowen, "Breast cancer and heptaldehyde," *Canad. Med. Assoc. J.*, vol. 75, p. 486; 1956.

normalities, they should prove to be a valuable tool in the hands of a medical scientist who wishes to study diagnostic and retardation techniques.

The Evaporograph (Nonscanning Camera)

While the Evaporograph was originally intended for military applications, it now appears that its most profitable area of exploitation will be in the industrial and medical field. For instance, Fig. 8 shows the legs of a patient afflicted with phlebitis. It will be noted that the phlebitis is in the patient's right leg and that the picture of this leg is lighter in color than the picture of the normal left leg. This indicates that during this exposure, the afflicted right leg was at a higher temperature than the left leg. The original picture was in color; however, the black and white reproduction still shows the temperature difference. This work was done at Massachusetts General Hospital. Similar photographs have been taken of cancer patients and of various incisions made during operations.

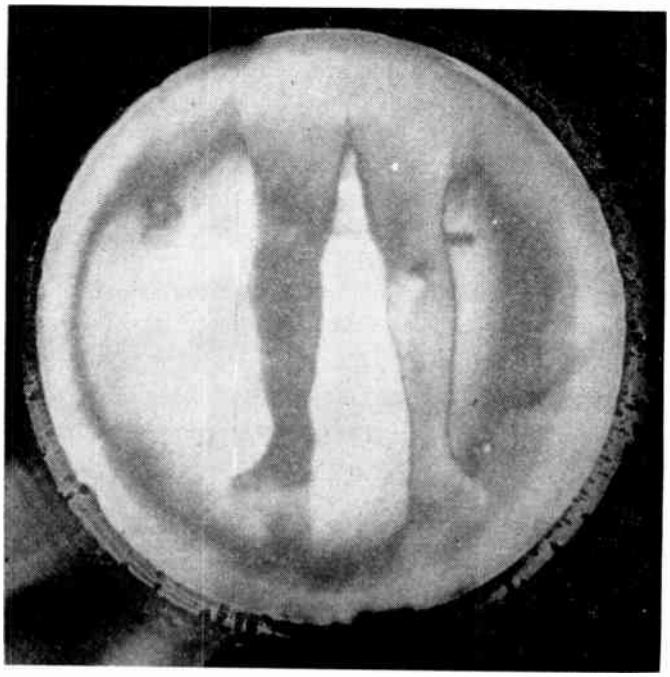

Fig. 8—Evaporograph picture of leg with phlebitus.

While it is not possible at this time to forecast accurately the ultimate applications of Thermal Scanning Cameras or the Evaporograph in the field of medicine, it would seem that such tools will augment the capabilities of medical research to locate and assess the extent and nature of afflicted near-surface body areas. On the other hand, it remains for medical research to interpret the significance of observable body surface temperature differences and to correlate this information with diagnosis based on other techniques.

The Evaporograph has been developed in this country under the sponsorship of the Armed Services. The work was first begun by Baird-Atomic, Inc., for the Aerial Reconnaissance Laboratory of Wright Air Development Center. Subsequently, the Signal Corps, the University of Michigan under Project Michigan, and the Engineer Research and Development Laboratories at Fort Belvoir have conducted further research and development on the Evaporograph.

The Evaporograph, illustrated in Fig. 9, has the advantage of requiring no moving parts. It gives a picture in color of the interference pattern formed by the oil film on the membrane. The wavelength coverage is determined by the nature of the optics and the quality of the gold black on the membrane. In other words, the Evaporograph sees the total radiation emitted by a target. The heart of the Evaporograph is a nitrocellulose membrane so thin that it reflects white light as a color, similar to the action of an oil film on water. This membrane is housed in an evacuated two-compartment cell between an optical system and a viewing system. The back part of this cell is heated slightly, and contains an oil which can be condensed at will upon the rear side of the membrane. The sequence of operation is as follows:

1) The optical system gathers infrared radiation from the field of view and forms an image of the field on the membrane.

2) The special coating on the front surface of the membrane absorbs this radiation and changes temperature from point to point in accordance with the amount of radiation received by each portion of the membrane. A heat "picture" is thus impressed on the membrane.

3) These point-to-point temperature variations alter the thickness of an oil film being condensed on the rear side of the membrane. Thus, temperature differences are resolved into differences in oil thickness.

4) These thickness variations cause white light to be reflected as different colors, giving a visible, colored, thermal image of the entire field of view. The colors have no relation to the visible colors of the objects, but are interference colors and refer only to temperatures.

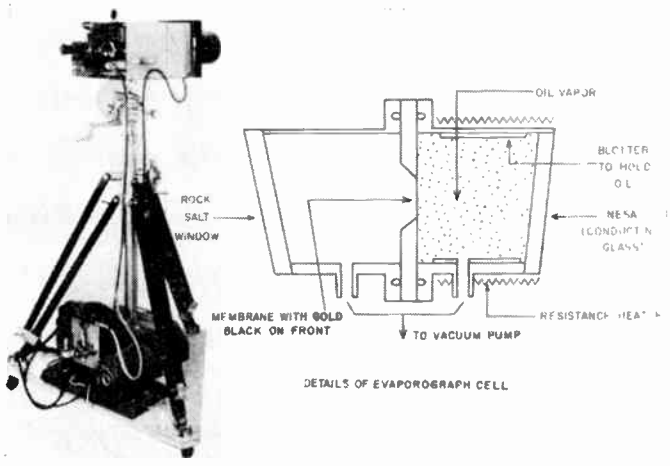

Fig. 9—The Baird Evaporograph.

5) From the rates of change in film thickness, temperatures of the entire field of view can be determined. A reference point in the field of view of known temperature and emissivity is usually employed as a basis of comparison.

Resolutions have been obtained up to 10 to 14 lines per millimeter at 10°C difference for high-emissivity material. In the laboratory, temperature differences ranging between a few tenths of a degree to several thousands of degrees have been measured. However, under field conditions the sensitivity would more likely be on the order of one-degree temperature difference. The exposure time will vary from a few seconds for hot targets to several minutes for very cool targets.

An interesting application is shown in Fig. 10, which is a nondestructive test by Evaporograph of a honeycomb aircraft structure. The light areas in the center indicate that voids exist in the panel.

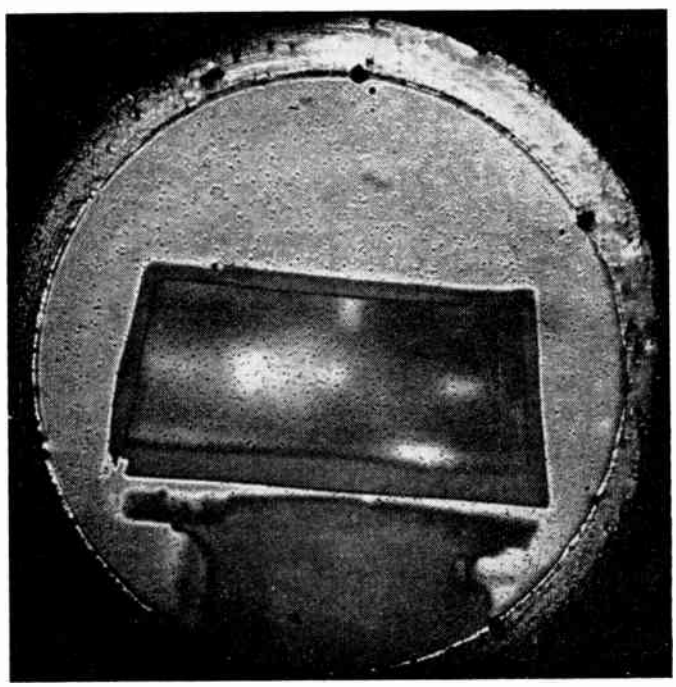

Fig. 10—Nondestructive Evaporograph test of honeycomb aircraft panel.

5.3.8 PROXIMITY WARNING INDICATORS

THE tremendous growth rate of commercial and military air transportation during the past several decades has resulted in a crowding of the airways, as exemplified by the increasing number of mid-air collisions.

Although a completely automatic Collision Avoidance System is the ultimate solution to the avoidance of mid-air collisions, as a first step the danger will be considerably reduced if the involved aircraft have a reliable indication of their proximity to each other in sufficient time for taking evasive action. It is entirely possible that this positional information of approaching aircraft can be reliably provided by infrared scanners. The infrared scanners with a display unit will, therefore, form a Proximity Warning Indicator (PWI) which provides proximity information to the existing "computer"—the pilot. In view of increasing air speeds, the addition of an electronic computer would provide the capability for automatic evasive action, thus creating an automatic Collision Avoidance System.

The design parameters of an infrared PWI scanner for commercial airlines is somewhat different from those for the infrared scanners discussed under military applications. One of the major differences is that infrared scanners designed for military purposes are usually required to achieve maximum range, while for the PWI considerations the pilot should be alerted to the presence and direction of an approaching aircraft only in sufficient time for effective action. But he should not be disturbed unless the danger of collision actually exists. When the minimum warning time permitting evasive action (20 seconds, for example) has been established, the necessary detection ranges can be determined by an analysis of the horizontal and vertical closing rates of approaching aircraft on a collision or near-collision course.

The infrared radiations from various types of aircraft operating at various altitudes and ranges and viewed from different aspects must be measured and compiled to determine the system capabilities which will provide maximum warning consistent with the minimum of unnecessary signals.

The use of an infrared PWI could provide the first major step toward a completely automatic Collision Avoidance System, and for a small sacrifice in weight and space, should greatly reduce the danger of mid-air collisions.

5.3.9 COMMUNICATION

THE applications of infrared communications[17] to civilian use cover a vast and intriguing multitude of possibilities.

Short-Range Uses

From the top to the bottom of a fireman's ladder—this was the first intended use of the original handy-talkie radio. It can be done with infrared with perhaps one-fourth the size of the handy-talkie, and with freedom of interference between systems. This means the fire chief on the ground could point in turn to men on several ladders and give each individual instructions without confusion.

Down and along mine shafts where wires cannot be laid and radios would interfere, infrared would seem very desirable.

Between surveyors.

Between members of a construction crew working on large buildings, bridges, and roads.

[17] See M. R. Krasno and W. R. Wilson, "Infrared communication," paper 5.1.8, this issue, p. 1621.

Long-Range Uses

Between engineers on any kind of field test that keeps the men on line of sight. Here privacy, quick contact, lack of interference with any home radio or television, and freedom to set up anywhere without requesting and awaiting FCC approval, are all desirable features.

Fixed installations between buildings, forestry fire towers, etc.

Between the control tower of an airport and planes both on the ground and about to land or take off. In fair weather, traffic is heaviest, and a method that can talk to each plane separately allows much tighter traffic control at the airport.

Between commercial or private aircraft. Without disturbing normal radio contacts, the ability to communicate directly with craft within sight, might conceivably aid in avoiding collisions by making each pilot's intentions known.

An infrared Identification Friend or Foe (IFF) system may be located on commercial aircraft to provide military defense systems with proper identification. This equipment could also be used to communicate.

Between ships at sea. Here the first use as an anti-collision aid, by direct bridge-to-bridge communication, might prevent disasters which occur in good visibility by making the skippers' plans known to each other. Even the delay now encountered in relaying messages to and from the radio room might be obviated. Under wartime conditions where lights could not be exposed and radio silence could not be broken, infrared intership communication would be useful. In fishing fleets, the further advantage of private discussion of the location of the catch might be valuable. Pleasure boats might engage in gossip and idle chatter without thereby cluttering up the air.

Ship-to-Shore. A cooperative infrared system could assist ships through narrow channels or warn the ships of shallow water and submerged objects. The IR beacons could be mounted in buoys, lighthouses, and other convenient locations. The same IR receivers used for communications could probably be used to detect the warning. The beacons could be modulated to distinguish the beacon source from surrounding heat sources. Privacy could be attained in ship-to-shore communications without scrambling circuits and without crowding the radio spectrum.

Finally, in any emergency area. Here, where power lines may be down and portable radio gear is engaged in long-range net traffic, precise noninterfering point-to-point infrared equipment might well aid in the directing of disaster operations.

Paper 5.4

What Is the Future of Infrared?*

PAUL J. OVREBO†

SCIENTISTS and engineers expect that out of all the research being done for the military will come know-how that can be put to use commercially. However, Dr. Van Zandt Williams, Executive Vice-President of the Perkin-Elmer Corporation, believes that for the next five years, military volume is sure to outstrip commercial volume.

One of the biggest potential industrial uses for infrared is in "running" chemical plants and glass plants automatically. Since these plants use manufacturing processes that depend on heat, it is conceivable, say engineers, that infrared instruments could control the manufacturing processes from start to finish by detecting the heat change in the various processes, then "telling" workers when to shut off valves and turn them on again.

"This technique might be only five or ten years off," claims Ray Wasson, a scientist with Corning Glass Works.[1]

Infrared is still a relatively new military science. As such, most of the engineers and scientists are absorbed in advancing the state-of-the-art. Already, infrared has broken the monopoly of radar and visual systems in a number of fields. With the reduction in the price of components and the simplification of techniques, commercial applications are increasing. The above discussions illustrate only a few of the many potential uses of infrared to improve American industry, travel, and home life. Significantly, this is a field of basic science which has blossomed and developed through a combination of university, industrial, and government research and development effort. Whereas a considerable segment of this effort was funded for military objectives, there have been and will continue to be significant "pay-offs" to, or side-effects in, technology as a whole.

* Original manuscript received by the IRE, July 13, 1959.
† Wright-Patterson Air Force Base, Dayton, Ohio.

[1] *Wall Street Journal*; February 16, 1959.

SECTION 6

A Selected Bibliography on Infrared Techniques and Applications*

WILLIAM L. WOLFE†

THE preparation of a bibliography on infrared techniques and applications is a challenge not because of lack of publications in the field, but because it is difficult to choose from the many which are available. For this reason, a certain degree of personal preference and experience necessarily enters into the selection of the entries. Nevertheless, the books and articles have been selected mainly because they are good reviews, or because they give a fairly comprehensive discussion of appropriate subjects. Items of a more specialized nature have been omitted because they can usually be found referenced in one of the bibliographical works. Only the archival literature of physics, chemistry, and engineering has been included, although progress reports and technical reports, which have been prepared in connection with government-sponsored research investigations, often describe significant advances. The latter type of information is often difficult to locate, but IRIA, the Infrared Information and Analysis Center of the Willow Run Laboratories of The University of Michigan, has been established to assist infrared scientists with this problem. The reader is therefore referred to the IRIA for information about this nonarchival, so-called borderline scientific literature.[1,2]

The bibliography is divided into a section entitled "Textbooks" and into several sections which are somewhat representative of the disciplines comprising infrared technology. The former contains references to many of the elementary physics and engineering texts which are particularly applicable to problems of radiative heat transfer, of optics, and of solid-state physics. The other sections generally include references to the monographs and articles which might be particularly useful in the specialized areas which are indicated.

The Library of Congress, under the sponsorship of the Office of Naval Research, has compiled several bibliographies on infrared. The work cited here [18] includes unclassified literature up to, and including, 1953. The articles of Sutherland and Lee [22], of Williams [24], and the book by Barnes, *et al.* [20], are oriented toward spectroscopic applications, but they also include good discussions of basic techniques. The last reference has an excellent bibliography (as of its publication date). Although Smakula's report [23] is devoted primarily to optical properties of materials, it also includes a bibliography on infrared-in-general. His list of references is characterized by a large number of foreign entries.

Many of the listed works in optics are widely known. Special mention should be made of the less familiar ones. Bouwers [26] describes the properties and the development of the various concentric systems, which now generally bear his name in conjunction with that of Maksutov, who independently devised some of the same systems. Born's book [25], emphasizing electromagnetic theory in optical problems, is being revised and translated for publication this year by Pergamon Press, Inc., as "Principles of Optics," by M. Born and E. Wolf; "Design of Fire Control Optics" [28] presents a number of different reflective and refractive systems and their basic parameters. "The Optical Industry Directory" [41], although not a technical publication, is a useful reference for the designer. It is occasionally revised to reflect the changes in optical instruments and suppliers. Herzberger's contributions to geometrical optics during the past fourteen years, which include a different aberration-classification system and ray-tracing problems applied to automatic computers, are described in considerable detail in his excellent, up-to-date work [34].

Spectroscopy is the oldest, and probably the largest, commercial application of infrared techniques; accordingly, much has been published on the topic. The reader is referred to the classic works of Herzberg [6], [7] and to Bellamy [49] for the theory. Spectroscopic instruments are emphasized, since the design techniques and components are particularly pertinent to military infrared and to process and control applications of infrared technology. The recent work of Lecomte [57] is an excellent review on the subject, and Brügel [51] made a comparable survey in 1954. Sawyer's text [62] is particularly helpful as a handbook for use in the spectroscopy laboratory, and one might compare the papers of Ballard [46] and Golay [53] for an indication of progress in the field of spectrometric and spectrophotometric instrumentation.

Several excellent discussions of general infrared interest appear in the section entitled "Other Instrumentation." Among these are the work of Sanderson [69], which is a discussion of infrared as applied to missile guidance, an excellent discussion of radiometry by Forsythe [65], the works of Walsh [71], Weber [72], and Wolfe [73], and of Wood and Cork [74] on photometry, radiometry, temperature measurement, and pyrometry.

* Original manuscript received by the IRE, July 6, 1959.
† Willow Run Labs., Univ. of Michigan, Ann Arbor, Mich.
[1] W. L. Wolfe, "Infrared information and analysis," Research Reviews, Office of Naval Research, pp. 20–24; January, 1959.
[2] W. L. Wolfe, "Some comments on the IRIA retrieval system," *American Documentation*, vol. 10, pp. 74–77; January, 1959.

respectively. It should be mentioned that the book edited by Wolfe [73] was an undertaking of the American Institute of Physics and can be considered as a companion volume to "Temperature—Its Measurement and Control in Science and Industry," the earlier work of the American Institute of Physics [64] on this subject.

The literature on optical materials is scattered. Ceramicists, crystallographers, glass-makers, and solid-state physicists, as well as optical design specialists, have been interested in the development of new materials for windows, lenses, prisms, cells, and the like. A compendium of the important properties of the various substances was prepared by Ballard, *et al.* in 1947, but this government report is now out of print and generally unavailable. The report of Smakula [23], can be obtained in microcard or photostat form from the Office of Technical Services, Department of Commerce, but the data are now somewhat obsolete. An extensive report on both semiconducting and "conventional" optical materials has recently been completed at The University of Michigan by Ballard, McCarthy, and Wolfe.[3] Most of the properties of materials of importance in infrared optical design, and a short bibliography of government reports dealing with optical materials are included.

An excellent list of reports and a review of the properties of lead salt photoconductors—lead sulfide, lead selenide, and lead telluride—written by T. S. Moss, appeared in the PROCEEDINGS OF THE IRE, Solid-State Electronics Issue [85]. "Photoconductivity Conference at Atlantic City," edited by Breckenridge, Russell, and Hahn [76], presents many of the basic data on other infrared photoconductive detectors, *e.g.*, germanium, silicon, and indium antimonide. The monograph by Smith, Jones, and Chasmar [12] should also be consulted for the theory of operation of both photoconductive and nonselective detectors.

Atmospheric transmission is very often the most unwieldy variable with which one must work. Astronomical and meteorological investigations are consulted in specific cases, but it is safe to say that most calculations are made on the basis of the data of Gebbie, *et al.* [91] or of Taylor and Yates [98]. In using and understanding these data, discussions of atmospheric models by Goody [92] and by Elsasser [90] are important. The ARDC Geophysics Handbook [101] also presents some useful data and includes the latest ARDC model atmosphere, which is particularly helpful in some applications.

BIBLIOGRAPHY

Textbooks

[1] J. M. Cork, "Heat," John Wiley and Sons, Inc., New York, N. Y., 2nd ed.; 1942.
[2] A. J. Dekker, "Solid-State Physics," Prentice-Hall, Inc., Englewood Cliffs, N. J.; 1958.
[3] R. W. Ditchburn, "Light," Interscience Publishers, Inc., New York, N. Y.; 1953.
[4] W. C. Dunlap, "An Introduction to Semiconductors," John Wiley and Sons, Inc., New York, N. Y.; 1957.
[5] A. C. Hardy and F. H. Perrin, "The Principles of Optics," McGraw-Hill Book Co., Inc., New York, N. Y.; 1932.
[6] G. Herzberg, "Spectra of Diatomic Molecules," D. Van Nostrand Co., Inc., Princeton, N. J., 2nd ed.; 1950.
[7] G. Herzberg, "Infrared and Raman Spectra of Polyatomic Molecules," D. Van Nostrand Co., Inc., Princeton, N. J., 2nd ed.; 1954.
[8] F. A. Jenkins and H. E. White, "Fundamentals of Optics," McGraw-Hill Book Co., Inc., New York, N. Y., 3rd ed.; 1957.
[9] C. Kittel, "Introduction to Solid-State Physics," John Wiley and Sons, Inc., New York, N. Y., 2nd ed.; 1956.
[10] F. K. Richtmyer and E. H. Kennard, "Introduction to Modern Physics," McGraw-Hill Book Co., Inc., New York, N. Y., 4th ed.; 1955.
[11] F. Seitz, "Modern Theory of Solids," McGraw-Hill Book Co., Inc., New York, N. Y.; 1940.
[12] R. A. Smith, F. E. Jones, and R. P. Chasmar, "The Detection and Measurement of Infrared Radiation," Oxford Press, London, Eng.; 1957.
[13] J. Strong, "Concepts of Classical Optics," W. H. Freeman and Co., San Francisco, Calif.; 1958.
[14] J. Strong, "Procedures in Experimental Physics," Prentice-Hall, Inc., New York, N. Y.; 1938.
[15] H. E. White, "Introduction to Atomic Spectra," McGraw-Hill Book Co., Inc., New York, N. Y.; 1934.
[16] R. W. Wood, "Physical Optics," The Macmillan Co., New York, N. Y., 3rd ed.; 1934.
[17] M. W. Zemansky, "Heat and Thermodynamics," McGraw-Hill Book Co., Inc., New York, N. Y., 4th ed.; 1957.

Bibliographies and General Review Articles

[18] C. R. Brown, M. W. Ayton, T. C. Goodwin, and T. J. Derby, "Infrared: A Bibliography," Library of Congress, Washington, D. C.; 1954.
[19] O. S. Duffendack, "Wartime developments in the detection and measurement of thermal radiation," *The Engineers' Digest (American)*, vol. 3, pp. 483, 529–530; 1946.
[20] R. B. Barnes, R. C. Gore, U. Liddel, and V. Z. Williams, "Infrared Spectroscopy—Industrial Applications and Bibliography," Reinhold Publishing Corp., New York, N. Y.; 1944.
[21] V. Krizek and V. Vand, "The development of infrared techniques in Germany," *Electronic Engrg.*, vol. 18, pp. 316–317, 322; 1946.
[22] G. B. B. M. Sutherland and E. Lee, "Development in the infrared region of spectrum," *Repts. Progr. Phys.*, (published by The Physical Society, London, Eng.) vol. 11, pp. 144–177; 1947.
[23] A. Smakula, "Physical Properties of Optical Crystals with Special Reference to Infrared," Office of Technical Services, U. S. Department of Commerce, Document No. 111053; October, 1952.
[24] V. Z. Williams, "Infrared instrumentation and techniques," *Res. Sci. Instr.*, vol. 19, pp. 135–178; 1948.

Special Topics in Optics

[25] M. Born, "Optik," Julius Springer, Berlin, Germany; 1933.
[26] A. Bouwers, "Achievements in Optics," Elsevier Publishing Co., New York, N. Y.; 1950.
[27] A. C. Candler, "Modern Interferometers," Hilger and Watts, Ltd., London, Eng.; 1951.
[28] "Design of Fire Control Optics," vols. 1 and 2, The Ordnance Corps.
[29] C. Deve, "Optical Workshop Principles," Hilger and Watts, Ltd., London, Eng., 2nd English ed.; 1954.
[30] R. W. Ditchburn, "Light," Interscience Publishers, Inc., New York, N. Y.; 1953.
[31] S. Flügge, Ed., "Handbuch der Physik," Julius Springer, Berlin, Ger., vol. 24; 1956.
[32] K. J. Habell, "Engineering Optics, Principles of Optical Methods in Engineering Measurements," Pittman Publishing Co., New York, N. Y.; 1953.
[33] O. S. Heavens, "Optical Properties of Thin Solid Films," Butterworth Scientific Publications, London, Eng.; 1955.
[34] M. Herzberger, "Modern Geometrical Optics," Interscience Publishers, Inc., New York, N. Y.; 1958.
[35] A. G. Ingalls, "Amateur telescope making," *Scientific American*, New York, N. Y., vols. 1–3; 1955.
[36] L. Jacobs, "An Introduction to Electron Optics," John Wiley and Sons, Inc., New York, N. Y.; 1951.
[37] Z. Kopal, Ed., "Astronomical Optics and Related Subjects,"

[3] W. L. Wolfe and S. S. Ballard, "Optical materials, films, and filters for infrared instrumentation," paper 4.2.3, this issue, p. 1540. See reference 1, S. S. Ballard, K. A. McCarthy, and W. L. Wolfe, "IRIA State-of-the-Art Report, Optical Materials for Infrared Instrumentation," Univ. of Michigan, Ann Arbor, Rept. No. 2389-11-S; January, 1959.

North Holland Publishing Co., Amsterdam, The Netherlands; 1956.
[38] L. C. Martin, "Technical Optics," Sir Isaac Pitman and Sons, Ltd., London, Eng., vols. 1 and 2; 1950.
[39] G. S. Monk and W. H. McGorkle, eds., "Optical Instrumentation," McGraw-Hill Book Co., Inc., New York, N. Y.; 1954.
[40] T. S. Moss, "Optical Properties of Semi-Conductors," Academic Press, Inc., New York, N. Y.; 1959.
[41] "The Optical Industry Directory," Optical Publishing Co., Huntington, N. Y.; 1956–1957.
[42] A. Sommerfeld, "Optics" (Lectures on Theoretical Physics, Vol. IV), Academic Press, Inc., New York, N. Y.; 1954.
[43] J. P. C. Southall, "Mirrors, Prisms and Lenses," The Macmillan Co., New York, N. Y., 3rd ed.; 1918.
[44] S. Tolansky, "Multiple Beam Interferometry of Surfaces and Films," Oxford Press, London, Eng.; 1948.
[45] F. Twyman, "Prism and Lens Making," Hilger and Watts, Ltd., London, Eng.; 1952.

Spectroscopy (Especially Spectroscopic Instruments)

[46] S. S. Ballard, "Spectrophotometry in the United States," in "Proceedings of the London Conference on Optical Instruments" 1950, John Wiley and Sons, Inc., New York, N. Y., pp. 133–150; 1952.
[47] E. C. C. Baly, "Spectroscopy," Longmans Green Publishing Co., New York, N. Y., vols. 1–3; 1924.
[48] A. Beer, Ed., "Vistas in Astronomy," Pergamon Press, Inc., New York, N. Y., vols. 1–2; 1955–1956.
[49] L. J. Bellamy, "Infrared Spectra of Complex Molecules," John Wiley and Sons, Inc., New York, N. Y.; 1954.
[50] W. R. Brode, "Chemical Spectroscopy," John Wiley and Sons, Inc., New York, N. Y., 2nd ed.; 1943.
[51] W. Brügel, "Einführung in die Ultrarotspektroscopie," Dietrich Steinkopf, Darmstadt, Ger.; 1954.
[52] T. A. Cutting, "Manual of Spectroscopy," Chemical Publishing Co., New York, N. Y.; 1949.
[53] M. J. E. Golay, "Comparison of various infrared spectrometric systems," *J. Opt. Soc. Am.*, vol. 46, pp. 422–427; 1956.
[54] C. Haeusler, "Instrumentation in the far infrared," *J. Phys. Rad.*, vol. 16, pp. 882–888; 1955.
[55] G. R. Harrison, R. C. Lord, and J. R. Loofbourow, "Practical Spectroscopy," Prentice-Hall, Inc., New York, N. Y.; 1948.
[56] J. Lecomte, "Infrared spectrometry and its recent progress," *Cahiers de Phys.*, vol. 38, pp. 26–54; 1954.
[57] J. Lecomte, "Spectroscopie dans l'infrarouge," in "Encyclopedia of Physics," Springer-Verlag, Berlin, Germany, vol. 26, pp. 244–936; 1958.
[58] J. Lecomte, P. Le Roux, R. Freyman, H. L. Tardy, and A. Boyle, "La Spectrometrie Infrarouge et ses Applications," *Editions de la Revue d'optique théorique et instrumentale*, Paris, France; 1934.
[59] E. Lippert, "Apparatus developments in infrared scectroscopy, I–II," *Z. angew. Physik*, vol. 4, pp. 390–397, 434–440; 1952.
[60] R. C. Lord and T. K. McCubbin, Jr., "Infrared spectroscopy, from 5 to 200 microns with a small grating spectrometer," *J. Opt. Soc. Am.*, vol. 47, pp. 689–697; 1957.
[61] C. Schaeffer and F. Matossi, "Das Ultrarote Spektrum," Julius Springer, Berlin, Ger.; 1930.
[62] R. A. Sawyer, "Experimental Spectroscopy," Prentice-Hall, Inc., New York, N. Y., 2nd ed.; 1951.
[63] V. Z. Williams, "Infrared instrumentation and techniques," *Rev. Sci. Instr.*, vol. 19, pp. 135–178; 1948.

Other Instrumentation

[64] American Institute of Physics, "Temperature—Its Measurement and Control in Science and Industry," Reinhold Publishing Corp., New York, N. Y., vol. 1; 1941.
[65] W. E. Forsythe, "Measurement of Radiant Energy," McGraw-Hill Book Co., Inc., New York, N. Y.; 1937.
[66] W. S. Huxford and J. R. Platt, "Survey of near infrared communication systems," *J. Opt. Soc. Am.*, vol. 38, pp. 253–268; 1948.
[67] "Le Rayonnement Infra-Rouge," Memorial de l'Artillérie Française; 1952, 2e fascicule Imprimérie Nationale, Paris, France; 1955.
[68] A. C. Menzies, "Recent developments in applied optics," *J. Sci. Instr.*, vol. 30, pp. 441–452; 1953.
[69] J. A. Sanderson, "Emission, transmission and detection of the infrared," in "Guidance," Arthur S. Locke, Ed., D. Van Nostrand Company, Inc., Princeton, N. J., ch 5; 1955.
[70] H. S. Snyder and J. R. Platt, "Principles of optical communication systems," *J. Opt. Soc. Am.*, vol. 38, pp. 269–278; 1948.
[71] J. W. Walsh. "Photometry," Constable and Co., Ltd., London, Eng.; 1953.
[72] R. L. Weber, "Heat and Temperature Measurement," Prentice-Hall, Inc., New York, N. Y.; 1950.
[73] H. C. Wolfe, Ed., "Temperature—Its Measurement and Control in Science and Industry," Reinhold Publishing Corp., New York, N. Y., vol. 2; 1955.
[74] W. P. Wood and J. M. Cork, "Pyrometry," McGraw-Hill Book Co., Inc., New York, N. Y., 2nd ed; 1941.

Optical Materials

[75] S. S. Ballard and K. A. McCarthy, "Optical materials for infrared instrumentation," *Nuovo Cimento*, suppl. no. 3 to vol. 2, ser. 10, pp. 648–652; 1955.

Detectors

[76] R. G. Breckenridge, B. R. Russell, and E. E. Hahn, Eds., "Photoconductivity Conference Held at Atlantic City," John Wiley and Sons, Inc., New York, N. Y.; 1956.
[77] M. Czerny and P. Mollet, "Quasi-photographic method of infrared detection," *Z. Phys.*, vol. 108, pp. 85–100; 1937.
[78] N. Fuson, "The infrared sensitivity of superconducting bolometers," *J. Opt. Soc. Am.*, vol. 38, pp. 845–853; 1948.
[79] M. J. E. Golay, "Theoretical considerations in heat and infrared detection, with particular reference to the pneumatic detector," *Rev. Sci. Instr.*, vol. 18, pp. 347–356; 1947.
[80] M. J. E. Golay, "Pneumatic infra-red detector," *Rev. Sci. Instr.*, vol. 18, pp. 357–362; 1947.
[81] D. F. Hornig and B. J. O'Keefe, "The design of fast thermopiles and the ultimate sensitivity of thermal detectors," *Rev. Sci. Instr.*, vol. 18, pp. 474–482; 1947.
[82] R. C. Jones, "Performance of Detectors for Visible and Infrared Radiation," in "Advances in Electronics," Academic Press, Inc., New York, N. Y., vol. 5, ch. 1; 1953.
[83] S. W. Kurnick and R. N. Zitter, "Photoconductive and photomagnetoelectric effects in InSb," *J. Appl. Phys.*, vol. 27, pp. 278–285; 1956.
[84] M. Lasser, P. Cholet, and E. C. Wurst, Jr., "High-sensitivity crystal infrared detectors," *J. Opt. Soc. Am.*, vol. 48, pp. 468–473; 1958.
[85] T. S. Moss, "Lead salt photoconductors," PROC. IRE, vol. 43, pp. 1869–1881; December, 1955.
[86] T. S. Moss, "Photoconductivity in the Elements," Academic Press, Inc., New York, N. Y.; 1952.
[87] T. S. Moss, "Optical Properties of Semiconductors," Academic Press, Inc., New York, N. Y.; 1959.
[88] E. M. Wormser, "Properties of thermistor detectors," *J. Opt. Soc. Am.*, vol. 43, pp. 15–21; 1953.

Properties of the Atmosphere

[89] T. Elder and J. Strong, "Infrared transmission of atmospheric windows," *J. Franklin Inst.*, vol. 255, pp. 189–208; 1953.
[90] W. M. Elsasser, "Heat Transfer by Infrared Radiation in the Atmosphere," Harvard Meteorological Studies, No. 6; 1942.
[91] H. A. Gebbie, W. R. Harding, C. Hilsum, A. W. Price, and V. Roberts, "Atmospheric transmission in the 1 to 14 μ region," *Proc. Roy. Soc. (London)*, vol. 206A, pp. 87–107; 1950.
[92] R. M. Goody, "Physics of the Stratosphere," Cambridge University Press, London, Eng.; 1954.
[93] J. N. Howard, D. E. Burch, and D. Williams, "Infrared transmission of synthetic atmospheres. II. Absorption by carbon dioxide," *J. Opt. Soc. Am.*, vol. 46, pp. 237–241; 1956.
[94] J. N. Howard, D. E. Burch, and D. Williams, "Infrared transmission of synthetic atmospheres. III. Absorption by water vapor," *J. Opt. Soc. Am.*, vol. 46, pp. 242–245; 1956.
[95] J. N. Howard, D. E. Burch, and D. Williams, "Infrared transmission of synthetic atmospheres. IV. Application of theoretical band models," *J. Opt. Soc. Am.*, vol. 46, pp. 334–338; 1956.
[96] W. E. K. Middleton, "Vision Through the Atmosphere," University of Toronto Press, Toronto, Can.; 1952.
[97] R. Sloan, J. H. Shaw, and D. Williams, "Infrared emission spectrum of the atmosphere," *J. Opt. Soc. Am.*, vol. 45, pp. 455–460; 1955.
[98] J. H. Taylor and H. W. Yates, "Atmospheric transmission in the infrared," *J. Opt. Soc. Am.*, vol. 47, pp. 223–226; 1957.
[99] H. C. Van de Hulst, "Light Scattering by Small Particles," John Wiley and Sons, Inc., New York, N. Y.; 1957.
[100] C. S. White, "Physics and Medicine of the Upper Atmosphere," University of New Mexico Press, Albuquerque, N. M.; 1952.
[101] "Handbook of Geophysics, for Air Force Designers," Geophysics Research Directorate, Air Force Cambridge Research Center, Air Research and Development Command, United States Air Force (with fifty-six contributors and an editorial staff of six); 1957.

Correspondence

A Technique for Processing Nickel Matrix (Molded) Thermionic Cathodes*

The ruggedness of moulded thermionic cathodes as well as their ability to operate under conditions of high emission density are properties that were originally indicated by MacNair,[1] *et al.* The characteristics as reported have been substantiated in this laboratory as well as others. This note concerns the processing of this type of cathode for use in small high perveance electron gun structures. The process is applicable to most gun structures with modifications.

The molded cathode consists of a compressed mixture containing nickel powder and barium and strontium carbonate powders. Spectrographic carbon may be added to this mixture to accelerate the reduction of the carbonates but experiments do not indicate that this is necessary. A cathode design which has been employed in high frequency retarding-field oscillators is sketched in Fig. 1. A relatively large pellet of the mixture is pressed to shape in a nickel shell and then processed as will be explained later. This model operated satisfactorily for short periods of time when employed in continuously pumped oscillators. Its use in sealed-off models was not found satisfactory due to release of large amounts of gas and slight shrinkage of the compressed pellet. It has been determined that by controlling the pellet thickness and processing, several important improvements are possible.

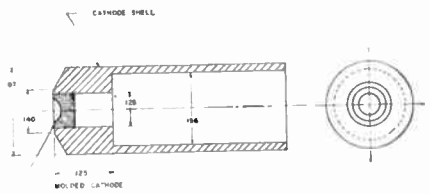

Fig. 1.—Large volume molded cathode.

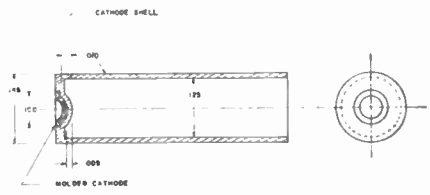

Fig. 2.—Small volume molded cathode.

Fig. 2 indicates a design which has been found to operate quite successfully. It will be noted that a thin pellet of the mixture is pressed to the desired shape. Actually this pellet is about 0.005 inch in thickness. The advantages of this construction over that of Fig. 1 are: 1) lower temperature operation is possible, 2) much less gas is evolved, 3) nickel evaporation is reduced, and 4) after several hundred hours of operation, the cathode maintains its shape and size.

To obtain the thin layer of cathode mixture shown in Fig. 2, the fabrication procedure is as follows. A nickel cathode shell, having a flat surface at the position of pellet formation, is undercut 0.005 inch on this flat surface with the diameter of this undercutting being approximately two times the actual cathode diameter. This larger diameter is necessary so as to obtain a sharp corner around the periphery of the spheroidal cathode surface. A mixture of Mond carbonyl nickel powder, 200 through 300 mesh, 70 per cent by weight, Radio Mixture No. 3, 29 per cent by weight, and spectrographic carbon, 1 per cent by weight, having been mixed with a glass stirring rod (do not roll) is spread into the undercut portion of the cathode shell. This is accomplished by placing some mixture on a hardened and ground steel block, pressing the shell against the mixture by hand until the shell has a fairly dense flat coating of the mixture. This is then pressed at 100,000 psi with a smooth flat punch and die to form a hard flat cathode surface. To obtain the desired spheroidal shape, a second pressing is necessary utilizing mating punch and die of the desired form. With a pressure of 160,000 psi both the pellet and shell are formed to the spheroidal shape.

A cleaning procedure is necessary and the following method has been found satisfactory even though it may seem somewhat elaborate. The pressed cathode is placed in a cold furnace with a dry hydrogen atmosphere and the temperature is raised to 600°C. At this temperature, the atmosphere is replaced by pure dry nitrogen and the temperature increased to 1000°C. The temperature is then reduced to 600°C, the atmosphere returned to dry hydrogen, and the temperature is finally lowered to that of the room. The gas curtain on the furnace is always extinguished before removing the cathode so as to minimize moisture absorption. The cathode should be installed and sealed-off as soon as possible or stored in a vacuum desiccator.

Activation of the cathode proceeds in the usual manner. The cathode temperature is maintained at 925°C for about the first eight hours after which it is lowered to 850°C. After a 24-hour bake-out and activation period, a short life test of this cathode has been made. It has operated with essentially no change in current for 700 hours at an average cathode loading of 1 amp/cm². This means that some portions of the cathode were actually operating with emission densities of 4 amp/cm² for the spheroidal high perveance gun under test. The test was discontinued at this point to investigate the cathode surface. It was found to have maintained its smooth surface and dimensions. The cathode temperature was 850°C during this test and no excessive nickel evaporation was noted.

It might be of interest to mention that the same processing and fabrication technique has been applied with a Kouar rather than nickel cathode shell. Essentially the same results were obtained as described above.

An interesting property of the nickel matrix cathode is the uniformity of emission[2] over the emitting surface. Emission patterns have been obtained by use of a thermionic electron emission microscope. Photographs of two emitting surfaces are given in Fig. 3 and Fig. 4. Emission patterns displayed upon

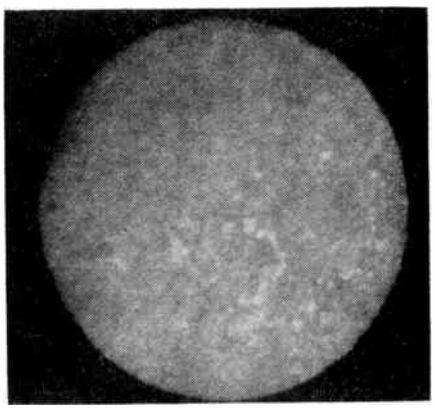

Fig. 3.—Fully active Ni matrix cathode. $T=950°C$, $V_A=17$ kv, ×200.

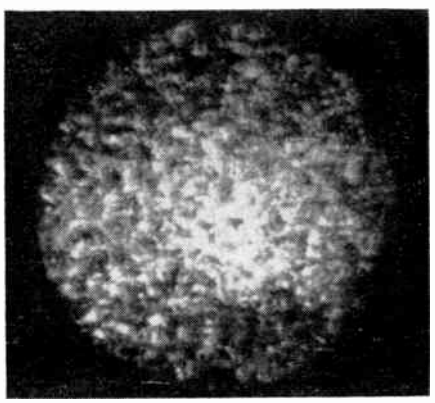

Fig. 4.—Oxide-coated cathode, fully active. $T=900°C$, $V_A=17$ kv, ×200.

the screen of the microscope are photographed, permitting comparisons of different types of emitting surfaces. Cathodes tested were all of emitting areas having diameters of about 0.050 inch or less. It will be noted that emission from the nickel matrix cathode appears considerably more uniform than the oxide coated cathode. Kahng[2] presents comparisons of other cathode types.

Electron guns used in microwave oscillator tubes also show improved operation

* Received by the IRE, February 24, 1959.

[1] D. MacNair, R. T. Lynch, and N. B. Hannay, "Moulded thermionic cathodes," *J. Appl. Phys.*, vol. 24, pp. 1335–1336; October, 1953.

[2] D. Kahng, Eng. Rept. No. 1, Wright Air Dev. Center Contract No. AF 33(616)-5073. WADC Tech. Rept. 58-282, ASTIA Document No. AD 202558, p. 59–67. E. M. Boone, W. H. Cornetet, Jr., D. Kahng, *et al.*

with the use of matrix cathodes. At approximately the same beam current and voltage, a retarding-field oscillator using a nickel matrix cathode produced an output power 1.5 to 1.6 times that obtained with the other types of cathode. The increased power is believed to result from improved uniformity of the electron beam, especially with respect to transit angle in the interaction region.

E. M. Boone
W. H. Cornetet, Jr.
D. Kahng
S. Taylor
The Ohio State University
Columbus, Ohio

Parametric and Pseudo-Parametric Amplifiers*

To the knowledge of the author, the simplest electronic parametric amplifier using the transverse oscillations of an electron beam in a time-varied potential-well transverse to the direction of flow has not been built. Such a tube would be made of an input and an output coupler separated by an interaction region. The input coupler impresses a transverse modulation on the beam. In the interaction region, the beam is affected by a transverse field of the type:

$$E = -y(E_0 + E_1 \cos(\omega_p t)) \qquad (1)$$

in which E is the transverse field, y the transverse direction, E_0, E_1 constants, t time and ω_p the radian frequency of the "pump." The transverse equation of motion is thus:

$$\frac{d^2y}{dt^2} + \eta y[E_0 + E_1 \cos(\omega_p t)] = 0 \qquad (2)$$

in which η is the electron charge to mass ratio. It is a Mathieu equation.

The Maxwellian solution nearest to (1) is given by the potential distribution:

$$\phi = \tfrac{1}{2}(x^2 - y^2)(E_0 + E_1 \cos \omega_p t) \qquad (3)$$

in which ϕ is the potential and x the transverse direction orthogonal to y.

Eq. (3) is the potential distribution of an axial cylinder which has a quadrupolar cross section, when opposite poles are kept at the same potential. Assuming E_0 positive, the poles in the y direction are at a lower average potential than the poles in the x direction. When E_1 remains smaller than E_0, the force on the electrons in the y direction is always a restoring force pointed toward the axis. This force, however, changes with time. As well known, the solutions of (2) are unstable (not purely periodic) when for example:

$$\omega_p = 2\sqrt{\eta E_0}. \qquad (4)$$

In such a case, the oscillations of a given electron in the interaction region are either enhanced or decreased depending on the phase of the pumping field when the electron entered that region. When the oscillations of the electron are enhanced, the pump provides energy to the beam. When the oscillations decrease, the beam provides energy to the pump. Because an electron cannot provide more energy to the pump than the transverse energy it has received in the input coupler, while an electron can receive an amount of energy from the pump only limited by the length of the interaction region, the exchange of energy is always favorable and power amplification occurs. This power is sucked out in the output coupler.

The equation of motion in the x direction of the quadrupolar field is also of interest. It is:

$$\frac{d^2x}{dt^2} - \eta X (E_0 + E_1 \cos \omega_p t) = 0. \qquad (5)$$

The solutions of (5) are in general unstable and would be unstable even for E_1 zero. The beam tends to spread rapidly in the x direction. One can, however, compensate the diverting force by the action of a magnetic field. The magnetic field must be in the y direction and follow (Gaussian units)

$$B = E_0 \left(\frac{c}{v_0}\right) x \qquad (6)$$

with B the magnetic field, c the velocity of light, and v_0 the axial velocity of the electrons.

Such a field can be approximated by a magnetic axial cylinder of quadrupolar cross section. The poles are placed grosso-modo on the bisectrices of the x,y axis. The poles on the first bisectrix are North, on the second bisectrix South.

The field can also be generated by passing currents through appropriate conductors, but the amount of current necessary is generally large.

It should be noted that an interaction region in which the transverse modulation impressed on a beam in the x direction is affected by the equation of motion:

$$\frac{d^2x}{dt^2} - \eta X E_0 = 0 \qquad (7)$$

also yields amplification provided E_0 is positive. There does not exist any reason, however, for naming such process parametric. In particular, (7) is linear in the time and the frequency domain, while (2) is linear only in the time domain.

It appears that the "low-noise electron-beam parametric amplifier"[1] does use an interaction region where an equation of the type (7) applies and for that reason should not be called parametric.

In this case, the electrons, when deflected in an input coupler, rotate at cyclotron frequency under the influence of an axial magnetic field while drifting through a drift space from input to output. In the drift space the electrons are continuously influenced by a radial diverting force.

Such a radial diverting force cannot be produced by a field of rotational symmetry without the introduction of a conductor on the axis of the drift space. One can, however, produce the necessary field in one radial direction without introducing an inner conductor. Suffice it now that the field rotates with the electrons so that the electrons always see the same field. The ac quadrupolar field used in the "simplest electronic parametric amplifier" discussed above can produce the necessary rotation of the field. Here, however, the electrons do not remain on the fixed axis y, on the contrary, they rotate with the field and keep in synchronism with the direction of maximum diverting force. The radial equation of motion simplifies into:

$$\frac{d^2r}{dt^2} - \eta r E_1 = 0 \quad (E_0 = 0, E_1 > 0) \qquad (8)$$

with r the radius of the trajectory. Centrifugal and Coriolis forces do not appear because they are compensated by the force due to the axial magnetic field.

P. A. Clavier
Westinghouse Electric Corp.
Electronic Tube Div.
Elmira, N. Y.

The Dependence of Combiner Diversity Gain on Signal Level Distribution*

The theoretical gain of combiner diversity over selector diversity depends on the observation, due to L. Kahn,[1] that by suitably weighting and adding signals received over two or more paths, one can obtain a composite signal having a signal-to-noise ratio better than that over any one path. Subsequently, a number of authors[2-4] have attempted to evaluate this gain, under fading conditions. It has been pointed out[5] that there is a discrepancy of some engineering importance between these various evalutions. For dual diversity, for example, in the small signal region 1½ db combiner improvement is predicted[2,3] compared with a 3-db prediction,[4] all the authors assuming Rayleigh-type fading. The error appears to be in Mack[4] and would seem to be due to use of numerical evaluation of integrals which, in the other references, are dealt with analytically.

In the case of two nearly equal signals (a condition that will usually be confined to non-fading periods) a 3 db improvement would, in fact, be expected. Bearing this in mind, it may be conjectured that reports of improvements of this order have perhaps been based on long-term averaged observa-

* Received by the IRE, March 16, 1959.

[1] R. Adler, G. Hrbek, G. Wade, "A low-noise electron-beam parametric amplifier," Proc. IRE, vol. 46, pp. 1756–1757; October, 1958.

* Received by the IRE, January 5, 1959.

[1] L. Kahn, "The ratio squarer," Proc. IRE, vol. 42, p. 1704; November, 1954.

[2] F. J. Altman and W. Sichak, "A simplified diversity communication system for beyond-the-horizon links," IRE Trans. on Communications Systems, vol. CS-4, pp. 50–55; March, 1956.

[3] H. Staras, "The statistics of combiner diversity," Proc. IRE, vol. 44, pp. 1057–1058; August, 1956.

[4] C. L. Mack, "Diversity reception in UHF long-range communications," Proc. IRE, vol. 43, pp. 1281–1289; October, 1955.

[5] L. P. Yeh, "Basic analysis on controlled carrier operation of tropospheric scatter communication systems," 1958 IRE National Convention Record, pt. 8, pp. 261–283.

tions. However, from the viewpoint of system performance, the comparatively infrequent periods of simultaneous facing on all paths are of primary importance, and it is in such periods that theory predicts the smaller improvement.

Fading, over both line-of-sight and scatter systems, is not necessarily of Rayleigh form. Fig. 1 shows probability distributions for Rayleigh, Gaussian, and two-, three-, and four-path fading, all of which are consistent with various reported conditions. It thus becomes of interest to consider the effect on combiner diversity gain of departure of the fading law from the Rayleigh form. Since one is primarily interested in low-probability conditions, it is adequate (as appears from Fig. 1) to consider a fading law of the form

$$P \propto V^k \tag{1}$$

where P is the probability that the received voltage will not exceed a level V, in one path, and k is a quantity depending on the type of fading. For Rayleigh fading $k=2$, while for Gaussian and two-path (equal signal) fading, $k=1$. It can readily be shown that with dual diversity the improvement of the combiner over the selector then becomes

$$\left\{\frac{4}{k}\,\frac{\Gamma(k)}{\left[\Gamma\left(\frac{k}{2}\right)\right]^2}\right\}^{1/2k} \text{(voltage ratio)} \tag{2}$$

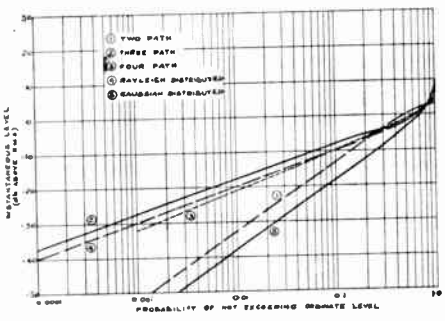

Fig. 1—Probability distributions for various fading mechanisms.

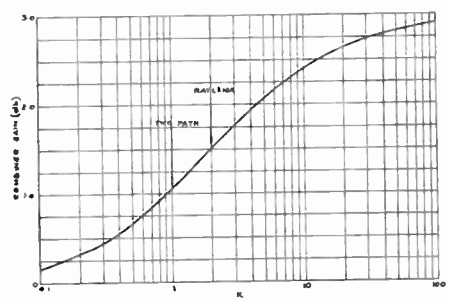

Fig. 2—Variation of gain of combiner (over selective switch) with slope of probability curve asymptote.

both diversity systems being compared at the same (low) probability level. Expression (2) is plotted in Fig. 2. It is seen that, in agreement with Altman and Sichak,[2] and Staras,[3] under Rayleigh conditions a gain of 1½ db results from the use of combiner instead of selector diversity. With Gaussian or two-path fading only 1 db is predicted. 3 db is approached only for very steep slopes of the probability fading curve.

In the above and other[2–5] treatments it is assumed that the major part of the noise is contributed by the receiver. Supposing that the fading is due to an addition of echoes,[6] intermodulation distortion will also appear, and there is some evidence[7] that in a deep fade this may be substantial. When only receiver noise is considered, the baseband signal-to-noise in a frequency-modulation system will follow the same probability law as that governing the carrier fading, for sufficiently high signal-to-noise ratios. For the present purpose, this law has been approximated by (1). It is to be expected that the appearance of intermodulation noise in deep fades will have the effect of reducing the k value appropriate to the baseband signal-to-noise. From Fig. 2, this will result in decreased combiner diversity gain relative to that of the selector system.

B. Easter
C. H. Maddock
R. G. Medhurst
Research Labs.
The General Elec. Co. Ltd.
Wembley, Eng.

[6] R. L. Kaylor, "A statistical study of selective fading of super-high frequency radio signals," *Bell Sys. Tech. J.*, vol. 32, pp. 1187–1202; September, 1953.
[7] R. G. Medhurst and M. Hodgkinson, "Intermodulation distortion due to fading in frequency-modulation frequency-division multiplex trunk radio systems," *Proc. IEE*, vol. 104, pt. C, pp. 475–480; September, 1957.

Derivatives and Integrals of the Laguerre Polynomials*[1,2]

Orthonormal series are of increasing importance in signal analysis[3] and approximate characterization of unknown transferences.[4] These operations involve differentiation and integration processes of the analyzed signals and consequently of the individual series terms. Relatively simple expressions can be derived for the ith derivative, or integral, of the nth series term as a function of a limited number of other polynomial terms. Some of these affinities, believed not to have been published before, are given below for the Laguerre polynomial series.

When the function $f(t)$, defined for $0<t<+\infty$, is to be approximated by the sum

$$S_k = \sum_{n=0}^{n=k} c_n L_n(t),$$

where $L_n(t)$ is an nth order polynomial in t, while the integral of the square of the approximation error weighted with the factor e^{-t}

$$\int_0^\infty [f(t) - S_k]^2 e^{-t}dt,$$

is to be minimized, one obtains the Laguerre polynomials by postulating finality for the coefficients c_n—

$$L_n(t) = \frac{1}{n!}\,e^t\,\frac{d^n}{dt^n}\,(t^n e^{-t}). \tag{1}$$

$$\int_0^\infty L_i(t)L_j(t)e^{-t}dt = \begin{cases}1, & i=j,\\ 0, & i\neq j.\end{cases} \tag{2}$$

The Laguerre spectrum c_n

$$c_n = \int_0^\infty f(t)L_n(t)e^{-t}dt$$

of the analyzed signal $f(t)$ is particularly advantageous as it lends itself to an easy realization on an analog computer.[5]

The Laguerre polynomials are generated by the function

$$\Psi(t,\tau,n) = \frac{1}{n!}\,\frac{e^{-t\tau/1-\tau}}{1-\tau}, \tag{3}$$

by the simple process of differentiation with respect to τ

$$\frac{\partial^n}{\partial\tau^n}\,\Psi(t,\tau,n)\bigg|_{\tau=0} = L_n(t). \tag{4}$$

Differentiating the generating function $\Psi(t,\tau,n)$ with respect to t,

$$-\frac{\partial}{\partial t}\,\Psi(t,\tau,n) = \frac{\tau}{1-\tau}\,\Psi(t,\tau,n), \tag{5}$$

leads to the recurrent equation

$$-L_n'(t) = L_{n-1}(t) - L'_{n-1}(t);\qquad n = 1, 2, 3\cdots \tag{6}$$

Starting with $n=1$ and considering successively increasing values for n, one obtains

$$-L'_n(t) = \sum_{k=0}^{n-1} L_k(t);\qquad n>1. \tag{7}$$

Differentiate the last equation—

$$-L_n''(t) = \sum_{k=0}^{n-1} L_k'(t). \tag{8}$$

Considering again, successively increasing values of n, we obtain

$$L''_n(t) = \sum_{k=0}^{n-2} (n-k-1)L_k(t). \tag{9}$$

Continued differentiation of (7) leads to

$$-L'''_n(t) = \sum_{k=0}^{n-3} \frac{1}{2!}\,(n-k-1)\cdot(n-k-2)L_k(t), \tag{10}$$

and, in general, to the ith derivative of $L_n(t)$

$$L_n^{(i)}(t) = (-1)^i \sum_{k=0}^{n-i} \frac{1}{(i-1)!}\,(n-k-1)(n-k-2)\cdots(n-k-i+1)L_k(t), \tag{11}$$

or

$$L_n^{(i)}(t) = (-1)^i \sum_{k=0}^{n-i} \frac{(n-k-1)!}{(n-k-i)!(i-1)!}\,L_k(t). \tag{12}$$

* Received by the IRE, February 24, 1959.
[1] "Oeuvres de E. N. Laguerre," vol. 1, pp. 104–107, 428–437, Paris, France; 1898.
[2] Courant and Hilbert, "Methods of Mathematical Physics," Interscience Publishers Inc., New York, N. Y., vol. 1, pp. 93–95; 1953.
[3] W. H. Huggins, "Representation and Analysis of Signals," Pt. 1, The Johns Hopkins University Rept. No. AFCRC Tr-57-357; September, 1957.
[4] L. Braun and E. Mishkin; "On the approximate identification of process dynamics in computer controlled adaptive systems," (to be published)
[5] S. E. Mishkin, "On the computer realization of an orthonormal spectrum of a given signal function," Proc. IRE, vol. 47, p. 1003; May, 1959.

Integrating (6) we obtain

$$\int_0^t L_n(\tau)d\tau = -L_{n+1}(t) + L_n(t). \quad (13)$$

Successive integrations of (6) lead to

$$\int_0^t \int_0^t L_n(\tau)d\tau = L_{n+2}(t) - 2L_{n+1}(t) + L_n(t) \quad (14)$$

$$\int_0^t \int_0^t \int_0^t L_n(\tau)d\tau = -L_{n+3}(t) + 3L_{n+2}(t) - 3L_{n+1}(t) + L_n \quad (15)$$

$$\vdots$$

$$L_n^{-(i)} = \sum_{k=0}^{k=i} (-1)^k \frac{i!}{(i-k)!k!} L_{n+k}(t), \quad (16)$$

where $L_n^{-(i)}$ is the ith definite integral of $L_n(\tau)$ taken from 0 to t.

E. Mishkin
Microwave Res. Inst.
Polytech. Inst. of Brooklyn
Brooklyn, N. Y.

Means for Counting "Effective" Numbers of Objects or Durations of Signals*

It is well known[1] that, if a signal has approximate duration T and approximate bandwidth W, it can be specified by approximately 2 TW numbers or coefficients. In dealing with signals of large time-bandwidth product, it is customary to speak of the "effective" number of degrees of freedom as the number of these coefficients that are "sufficiently" large. Except in the case of band limited signals, however, no means of computing the "effective" number of degrees of freedom has been suggested.

The following means of counting the effective number of objects of different size is proposed. Let N objects a_n all have the same size, a. Then we have

$$\sum |a_n| = N|a| \quad (1)$$

$$\sum |a_n|^2 = N|a|^2, \quad (2)$$

so that by squaring (1) and dividing by (2) we have

$$\frac{(\sum |a_n|)^2}{\sum |a_n|^2} = N. \quad (3)$$

In general, the sum of the magnitudes is difficult to handle analytically. When such is the case, we may use

$$\frac{(\sum |a_n|^2)^2}{\sum |a_n|^4} = N. \quad (4)$$

We may now take either (3) or (4) as the *definition* of the effective number of objects when the a_n differ in size. Generally, we choose (4), since (3) does not converge in the common case of an infinite sequence of objects, a_n, whose magnitudes decrease as $1/n$.

These definitions give greatest weight to the largest of the objects, so that a collection of one large object and a number of small ones is counted as not much more than one object. This is illustrated by the following groups, calculated from (4).

$$N(1, 1, 1, 1, 1) = 5$$
$$N(1, 1, 1, 1, 2) = 3.2$$
$$N(1, 1, 1, 1, 4) = 1.54. \quad (5)$$

The problem of defining the effective duration or bandwidth of a signal was considered by Gabor.[2] He identified rms duration of a waveform $y=y(x)$ with the radius of gyration of the area under the curve $|y(x)|^2$, about a y-axis passing through its centroid,

$$(\text{duration})^2 = 4\frac{\int |y|^2(x-x_0)^2dx}{\int |y|^2dx}, \quad (6)$$

where x_0 is so chosen that

$$\int (x-x_0)|y|^2dx = 0.$$

This definition has the advantage of leading to a minimum possible duration bandwidth product (TW product) for a signal.

Gabor's definition has three disadvantages. First, in order to obtain a meaningful calculation of bandwidth by formula (6), it is necessary to use single-sided spectra. Secondly, there are important applications (notably time-sharing schemes) in which a total waveform is broken into pieces which may be transmitted at different times. In this connection, an expression for the integrated duration of the dismembered waveform ought to be independent of the order and time intervals at which the individual pieces are transmitted. Gabor's definition causes the calculated duration to depend critically on both these factors. In the third place, if one wishes to fix the effective bandwidth or duration of a signal in a variational problem, he discovers that the constraint is satisfied in a trivial way by a pair of impulses separated by the given duration.

Instead of radius of gyration, formulas equivalent to the counting rules suggested above may be written. The formula for the duration, T, of a continous signal equivalent to (3) is

$$T = \frac{\left[\int |f(t)|\,dt\right]^2}{\int |f^2(t)|\,dt} = \frac{\left[\int |f(t)|\,dt\right]^2}{E}, \quad (7)$$

where E is the signal energy. As with Gabor's definition, (7) does not converge for signals of finite energy which decrease as $1/t$ for large t. From this point of view, and also from the point of view of analytic simplicity, the expression equivalent to (4) is suggested.

$$T = \frac{\left[\int |f(t)|^2\,dt\right]^2}{\int |f^4(t)|\,dt} = E^2 \Big/ \int |f^4(t)|\,dt. \quad (8)$$

The effective duration of a number of standard waveforms, according to (8), is tabulated below.

Type	Effective Length, T
triangle, base $2a$	$\frac{10a}{9}$
exponential, $e^{-t/a}$, $t>0$	a
normal error curve, $e^{-t^2/2a^2}$	$2\sqrt{\frac{\pi}{2}}\,a$
single pole magnitude $[1+(t/a)^2]^{-1/2}$	$2\pi a$

Formulations (7) and (8) for the effective duration of the signal are equally applicable to double- and single-sided spectra. They are especially useful where it is desired to count all the areas for which the waveform has substantial magnitude, but not the dead spaces in between. As constraints for fixed duration in a variational problem, they do not presuppose a knowledge of the maximum value of $f(t)$, nor can the constraint be satisfied by a pair of impulse functions separated in time by an amount T.

The use of definition (7) leads to a minimum possible duration-bandwidth product for a signal.[3] The use of (8) leads only to no minimum TW product other than zero. TW products for several waveform-spectrum pairs, according to (8) are tabulated below.

Type	TW product
rectangle, $\sin x/x$	3/2
damped exponential, single pole	1
Gaussian, Gaussian	.707
$f(t)=\|t\|^{-1/4}$, $\|t\|<1$ $=t^{-2}$, $\|t\|\geq 1$ and corresponding spectrum	0

Robert M. Lerner
Mass. Inst. Tech.
Lincoln Lab.
Lexington 73, Mass.

A Semiconductor Current Limiter*

The above article[1] contains two equations[2] which are derived in detail in my paper "A theory of the technetron" submitted to the IRE in June, 1958, and presented at the 1959 IRE Convention. Eq. (31), however, is doubly erroneous as it stands.

In my paper, the pinch-off voltage is expressed as

* Received by the IRE, February 26, 1959. The work reported here was performed at Lincoln Laboratory, a technical center operated by the Massachusetts Institute of Technology, with the joint support of the Army, Navy and Air Force.

[1] C. E. Shannon, "Communication in the presence of noise," Proc. IRE, vol. 37, pp. 10–21; January, 1949.

[2] D. Gabor, "Theory of information," *J. IEE*, pt. III, vol. 93, p. 429; 1946.

[3] Apparently the Gaussian signal, e^{-t^2}, leads to this minimum product, although no formal proof has been obtained.

* Received by the IRE, January 26, 1959.

[1] R. M. Warner, Jr., W. H. Jackson, E. I. Doucette, and H. A. Stone, Jr., Proc. IRE, vol. 4, pp. 44–56; January, 1959.

[2] *Op. cit.*, (30) and (31), p. 54.

$$V_p = \frac{\rho}{4\epsilon} b^2,$$

and it is shown that the pinch-off channel resistance is twice the cold resistance:

$$R_p = 2R_0 = \frac{2l}{\pi\sigma b^2}.$$

Hence the pinch-off current

$$I_p = \frac{V_p}{R_p} = \frac{\pi\rho\sigma b^4}{8\epsilon l}.$$

ρ: charge density
σ: conductivity
b: neck radius
l: neck length
ϵ: permittivity.

A. V. J. Martin
Dept. of Elec. Eng.
Carnegie Inst. Tech.
Pittsburgh 13, Pa.

Authors' Comments[2]

We appreciate your pointing out our typographical error; the factor N_n in (31) should instead be N_n^2. However, we believe that the numerical coefficient $\frac{1}{16}$ stated in (31) is correct. As of this writing your analysis is not available to us, and so a detailed comparison is not possible. Our derivation, which was suggested by the field-effect experiments with germanium filaments performed by H. E. Haring at Bell Telephone Laboratories several years ago, is presented in outline below. We will use Shockley's gradual approximation. The statement of Poisson's Equation applicable to the cylindrical diode is

$$\frac{1}{r}\frac{d}{dr}\left(r\frac{d\Psi}{dr}\right) = -\frac{qN_n}{\kappa\epsilon_0} \qquad (1)$$

where the symbols are defined in our paper. Integrating this equation twice and using as boundary conditions that radial electric field equals zero and potential equals v (the full voltage across the junction) at $r = r_D$ where r_D is the radius of the inner boundary of the depletion layer, we have

$$v = \frac{qN_n r_0^2}{2\kappa\epsilon_0}\left[\frac{1}{2} - \frac{1}{2}\left(\frac{r_D}{r_0}\right)^2 + \left(\frac{r_D}{r_0}\right)^2 \ln\left(\frac{r_D}{r_0}\right)\right]. \qquad (2)$$

Channel current can be introduced through Ohm's Law,

$$\frac{I}{\pi r_D^2} = \sigma\frac{dv}{dx}, \qquad (3)$$

where x is the axial coordinate and I is the current magnitude. Integrating from 0 to L on x and from r_0 to r_{DD} on r_D, where r_{DD} is the radius of the depletion layer boundary at $x = L$, we obtain this expression for channel current:

$$I = \frac{\pi q^2\mu N_n^2 r_0^4}{4\kappa\epsilon_0 L}\left[\left(\frac{r_{DD}}{r_0}\right)^4 \ln\frac{r_{DD}}{r_0} - \frac{1}{4}\left(\frac{r_{DD}}{r_0}\right)^4 + \frac{1}{4}\right]. \qquad (4)$$

[2] Received by the IRE, February 19, 1959.

When $(r_{DD}/r_0) \to 0$, the first two terms vanish, leaving

$$I_p = \frac{\pi q^2\mu N_n^2 r_0^4}{16\kappa\epsilon_0 L}. \qquad (5)$$

R. M. Warner, Jr.
W. H. Jackson
E. I. Doucette
H. A. Stone, Jr.
Bell Telephone Labs.
Murray Hill, N. J.

Gamma-Derived Capacitors*

In parallel plate variable capacitor, a monotonic capacity vs rotation law can be maintained over an angle $\alpha > \pi$ provided the rotor subtends an angle $\theta_R > \alpha$, and the stator an angle $\theta_S < 2\pi - \alpha$. Thus $\theta_R > \theta_S$ and, over part of the range at least, the capacity variation will depend on the *difference* between the rates at which area is occluded or exposed at the two stator edges. I recently had occasion to design a straight-line frequency (SLF) capacitor with extended rotation and while a reference was found for the design of the conventional type,[1] no analysis of the above differential type appears to have been published. For aesthetic reasons, it is given here.

We first assume that $\theta_R = 2\pi$. This means that the action will be differential over the entire range $\alpha \approx 2\pi - \theta_S$. Later we shall see how this restriction can be avoided if desired. Let

θ = angle between reference radius vector on rotor, and principal stator edge (OA in Fig. 1),
θ_S = angle subtended by stator ($\angle OB$),
$r(\theta)$ = rotor profile.
K = capacity per unit area (total, all gaps).

Then neglecting fringing, we have for the capacitor

$$\frac{dC}{d\theta} = K\left[\frac{r^2(\theta+\theta_s)}{2} - \frac{r^2(\theta)}{2}\right], \qquad (1)$$

while for the resonant circuit (Fig. 2):

$$\frac{dC}{d\theta} = \frac{d}{d\theta}\left[\frac{1}{\omega^2 L} - C_0\right] = -\frac{2}{L\omega^3}\frac{d\omega}{d\theta}.$$

For an SLF capacitor $d\omega/d\theta$ is constant. Let us represent it by σ. The reference line on the rotor from which θ is measured is arbitrary, but our equations will be simpler if we take it to be the radius vector which would coincide with OA if the rotor were turned to the (extrapolated) scale position corresponding to $\omega = 0$. Then $\omega = \sigma\theta$, and we have

$$\frac{dC}{d\theta} = -\frac{2}{L\sigma^2}\frac{1}{\theta^3}. \qquad (2)$$

Combining (1) and (2) yields the difference equation

* Received by the IRE, February 12, 1959.

[1] H. C. Forbes, "The straight line frequency variable condenser," Proc. IRE, vol. 13, pp. 507–509; August, 1925.

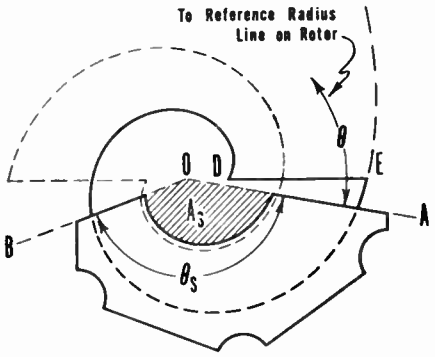

Fig. 1.

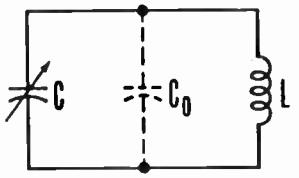

Fig. 2.

$$r^2(\theta) - r^2(\theta+\theta_s) = \frac{4}{KL\sigma^2}\frac{1}{\theta^3}. \qquad (3)$$

By substituting $\theta + \nu\theta_S$ for θ ($\nu = 0, 1, 2, 3, \cdots$) and adding the resulting equations, we find

$$r^2(\theta) - r^2(\infty) = \frac{4}{KL\sigma^2\theta_s^3}\sum_{\nu=0}^{\infty}\frac{1}{\left(\frac{\theta}{\theta_s}+\nu\right)^3} = \frac{4}{KL\sigma^2\theta^3}\sum_{\nu=1}^{\infty}\frac{1}{\left(\frac{\theta}{\theta_s}-1+\nu\right)^3}.$$

We now assume that $r^2(\infty) = 0$. This amounts to assuming $C_0 = 0$ since, in writing the above sum, we have tacitly assumed the SLF characteristic would hold for $\omega = \infty$, if only the same function were continued. We then obtain the primitive solution

$$r^2(\theta) = \frac{2C_s}{K\theta_s}\psi\left(\frac{\theta}{\theta_s} - 1\right), \qquad (4)$$

where C_s = capacity required to tune L to $\omega_s \equiv \sigma\theta_s$, and

$$\psi(x)^2 = \sum_{\nu=1}^{\infty}\frac{2}{(x+\nu)^3} = \frac{d^3}{dx^3}\ln(x!).$$

The primitive solution (4) forms the basis for a whole family of possible solutions. From (1) it is apparent that any periodic function $f(\theta)$ of period θ_s may be added without affecting $dC/d\theta$. Thus the general solution is

$$\left.\begin{aligned} r^2(\theta) &= \frac{2C_s}{K\theta_s}\psi\left(\frac{\theta}{\theta_s} - 1\right) + f(\theta) \\ &- \frac{2C_s}{K\theta_s}\psi\left(\frac{\theta}{\theta_s} - 1\right) \le f(\theta) = f(\theta+\theta_s) < \infty \end{aligned}\right\}. \qquad (5)$$

In certain cases, it may be desirable to use fully the freedom solution (5) offers. For example, $f(\theta)$ may be set equal to

[2] $\psi(x)$ is (the negative of) the so-called tetragamma function and is tabulated in the "Mathematical Tables of the British Association of Science," vol. I, pp. xxiii, 52–55.

$-(2C_s/K\theta_s)$ over the interval $\theta_{max}-\theta_s < \theta < \theta_{max}$. In this way, $r(\theta)$ may be made zero over this same interval and the subtended angle of the rotor reduced. This allows the plates to be staked onto the rotor shaft. In general, however, $f(\theta)$ will simply be set equal to a negative constant, the purpose of which is simultaneously 1) to reduce the rotor size for given values of the other parameters, 2) to make available capacity for C_0. Reducing $r(\theta)$ in this way improves the accuracy since the capacity error, ΔC, caused by a small profile error, Δr, existing over an angle ϕ is $\Delta C = Kr\,\Delta r\phi$, and is proportional to r.

From (5) we have

$$r^2(\theta) = A\psi\left(\frac{\theta}{\theta_s} - 1\right) + B,$$

where A and B are to be determined. Let:

r_a = maximum desired rotor radius (OE, Fig. 1)
r_b = minimum desired rotor radius (OD, Fig. 1)
θ_0 = value of θ corresponding to rotor radius OE ($\theta_0 + 2\pi$ is value corresponding to rotor radius OD)

$$\psi_a = \psi\left(\frac{\theta_0}{\theta_s} - 1\right)$$

$$\psi_b = \psi\left(\frac{\theta_0 + 2\pi}{\theta_s} - 1\right).$$

Then by substitution in (6) we find

$$A = \frac{r_a^2 - r_b^2}{\psi_a - \psi_b} \tag{6a}$$

$$B = \frac{\psi_b r_a^2 - \psi_a r_b^2}{\psi_a - \psi_b}. \tag{6b}$$

Of course the constant A has already been expressed in terms of the other parameters as $2/KL\sigma^2\theta_s^3$, so we have the constraint

$$KL\sigma^2\theta_s^3(r_a^2 - r_b^2) = 2(\psi_a - \psi_b).$$

If, for example, L, σ, θ_s, r_a, r_b, and θ_0 are already given, K is then fixed and the airgap and number of plates must be properly chosen to give this value.

The extra capacity from the fringing flux at the edge of a capacitor plate is equal to that which would be produced by an additional strip of width,[3]

$$d = \frac{2g}{\pi}\left[\ln 2 + \left(1 + \frac{t}{4g}\right)\ln\left(1 + \frac{t}{4g}\right)\right]$$

where

t = plate thickness
g = airgap between rotor and stator. (See Fig. 3.)

As a result the effects of fringing may be almost completely compensated by trimming a strip of width d off the rotor profile and also off the stator edges OA and OB (the latter will no longer intersect at O, but rather slightly below).

Having determined the final rotor profile, the shaded area A_s (see Fig. 2) which would always be well covered by the rotor may be cut from the stator plates. This reduces the minimum capacity to a value a much less than $1/\omega^2_{max}L$ and therefore leaves almost this full capacity available for C_0.

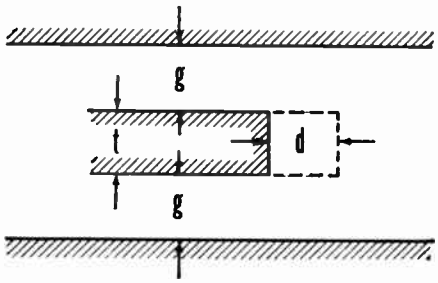

Fig. 3.

Capacitors designed in this fashion have been built to cover the frequency range of 100 kc to 150 kc in a beating oscillator application. The tracking curves obtained generally lie within ±50 cycles of the true SLF characteristic. The actual errors seem mainly due to lack of flatness in the plates.

For RC oscillators where $C = 1/\omega R$ and

$$\frac{dC}{d\theta} = -\frac{1}{R\omega^2}\frac{d\omega}{d\theta},$$

an exactly parallel analysis applies, the primitive solution being given by the trigamma function

$$\frac{d^2}{dx^2}\ln(x!) = \sum_{\nu=1}^{\infty}\frac{1}{(x+\nu)^2}.$$

Other members of this family of functions arise if the scale law is generalized to include any power law, not just the linear case. Thus if $\omega = S\theta^n$, an RC oscillator will require the function

$$\frac{d^{n+1}}{dx^{n+1}}\ln(x!),$$

and an LC oscillator will require the function

$$\frac{d^{2n+1}}{dx^{2n+1}}\ln(x!).$$

Finally, if the desired scale law is expressible as a polynomial or power series, each term will contribute a corresponding gamma derivative term to $r^2(\theta)$. It is rather remarkable to find this whole family of somewhat esoteric functions involved in such a homely problem.

Bernard M. Oliver
Hewlett-Packard Co.
Palo Alto, California

[3] W. R. Smythe, "Static and Dynamic Electricity," McGraw-Hill Book Co., Inc., New York, N.Y., 2nd ed., p. 205; 1950.

Peak Flyback Voltage in Transistorized TV Horizontal Deflection Circuits*

Introduction

The peak flyback voltage across an efficient switching device is derived. This is shown to be approximately ten times the supply voltage used for a near-ideal switch such as the transistor. Values are given for practical transistors.

On the further assumption that the "on" voltage of the switch is less than 10 per cent of the supply voltage, the ratio of peak to saturation voltage must be at least 100:1.

Flyback Voltage Factor

In the conventional horizontal deflection circuit, a tube or transistor is used to connect the deflection yoke coils across the supply battery.[1] Current builds up in the yoke circuit to a value determined by (1),

$$I_p = \frac{V}{L}t_{fs} \tag{1}$$

I_p = peak yoke current
V = yoke voltage during forward scan
L = yoke inductance
t_{fs} = time of forward scan,

assuming that the yoke time constant is much greater than t_{fs},

$$\frac{L}{R} \gg t_{fs} \tag{2}$$

where R is the total series resistance in the yoke-switch-supply circuit.

The yoke inductance is tuned by a capacitance to a frequency which has a half-period approximately that of the desired retrace time. This capacitance absorbs the energy stored in the yoke inductance when the switch is opened, thus suppressing the induced voltage to the minimum value consistent with the desired retrace time. The peak "flyback" voltage is therefore a function of the inductively stored energy and, inversely, of the value of capacitance used.

Assuming no losses (*i.e.*, an ideal switch having high "off" resistance and zero opening time) and a very high Q for the tuned circuit, we may equate the inductively-stored energy just prior to turn-off to the capacitively-stored energy after a quarter period or 90° of oscillation (*i.e.*, at peak flyback voltage).

$$W = \frac{LI_p^2}{2} = \frac{CV_m^2}{2} \tag{3}$$

when C = yoke timing capacitance and V_m = peak yoke voltage. The retrace time being one half cycle of oscillation or a half period,

$$t_r = \frac{P}{2} = \frac{2\pi\sqrt{LC}}{2}. \tag{4}$$

We obtain:

$$C = \frac{t_r^2}{\pi^2 L} \tag{5}$$

which is substituted in (3).

$$LI_p^2 = \frac{t_r^2 V_m^2}{\pi^2 L}. \tag{6}$$

Solving for V_m,

$$V_m = \frac{\pi L I_p}{t_r}, \tag{7}$$

substituting from (1)

[1] G. Schiess and W. Palmer, "Transistorized TV horizontal deflection and high voltage system," IRE Trans. on Broadcast and Television Receivers, pp. 19–35; June, 1958.

* Received by the IRE, February 11, 1959.

TABLE I

t_r (μs)	Flyback Factor		
	1) Eq. (10)	2) Eq. (8)	3) For alloy transistors
9.5	10.9	10 to 10.5	9 to 10 approximately
12.5	8.3	7.6 to 8.0	7 to 7.5 approximately
15.0	6.7	6.1 to 6.4	5.5 to 6.0 approximately

$$V_m = \frac{\pi V t_{fs}}{t_r}.$$

This is the voltage across the tank circuit as a result of transfer of energy from the yoke to the timing condenser. To this voltage we must, of course, add the supply voltage itself in order to obtain the peak voltage across the switch during flyback.

$$V_{cm} = \frac{\pi t_{fs}}{t_r} V + V_{cc} \tag{8}$$

where $V_{cm} = V_m + V_{cc}$ is the peak switch voltage, V_{cc} is the supply voltage. If the switch is efficient, we may take:

$$V \approx V_{cc} \tag{9}$$

(*i.e.*, if "on" voltage $\ll V_{cc}$ or $\approx 0.1\, V_{cc}$), then:

$$V_{cm} \approx \left(\frac{\pi t_{fs}}{t_r} + 1\right) V_{cc}. \tag{10}$$

We may define

$$\left(\frac{\pi t_{fs}}{t_r} + 1\right)$$

as the "flyback factor." For $t_r = 9.5$ and $t_{fs} = 30$ μs, $V_{cm} \approx 10.9\ V_{cc}$ assuming the "on" voltage is zero and there are negligible losses in the tuned circuit and the switch.

A more accurate solution using (8) and $V = 0.9$ to $0.95\, V_{cc}$ (for a practical transistor at 5 to 20 amperes of collector current) will yield figures of about 10 to 10.5.

This will also be reduced somewhat by turn-off losses in the transistor so that a factor of 10 is a useful one to remember if alloy transistors are to be used. In general, the tank circuit losses are such as to be negligible during the first quarter cycle or 90° of oscillation. Turn-off losses in the transistor will usually be in the 5 to 15 per cent range for alloy power types, but may be considerably lower for certain diffused-base types.

In the event that longer retrace times may be tolerated, a larger tuning capacitance may be used, and the flyback factor is reduced considerably, allowing greater yoke current to be controlled by a given transistor. For retrace times of 12.5 and 15 μs, the factors are about 8 and 6 respectively (assuming 28.5 and 27 μs respectively as forward scan times).

Table I summarizes this data, Column 1) giving flyback factor calculated according to (10), column 2) according to (8). Those of column 1) should be used for very fast-switching, low-saturation voltage transistors, while those of column 2) are conservative for present day alloy transistors (*e.g.*, $V_{c\,sat}$ of about 0.5 v and current fall times of over 3 μs). Column 3) gives approximate operating values for such transistors.

It should be noted that these figures are actual voltage flyback ratios and do not include any allowance for safety factors. The transistor must be adequately rated for the worst operating conditions to which it will be exposed.

Flyback to Saturation Voltage Ratio

As shown above, the flyback to supply voltage ratio may be as great as 10 or 11:1 (see Table I). Further, the assumption of (9) was that the supply to saturation voltage ratio should be $\geq 10{:}1$ for high efficiency.

Combining the two ratios suggests that the transistor to be used in these applications should have a maximum voltage rating of over 100 times its saturation voltage.

$$V_{cm} \geq 100 V_{c\,sat}.$$

W. F. Palmer
Sylvania Electric Products Inc.
Semiconductor Div.
Woburn, Mass.

Proposed Feasibility Study of Frequency Shift in Sealed Atomic Beam Frequency Standards*

In February, 1958, the U. S. Army Signal Research and Development Laboratory initiated a program of large scale intercomparison of atomic beam frequency standards both in the United States and in England.[1] Two automatic and sealed-off atomic beam frequency standards manufactured by National Co. under the trade name "Atomichron," were flown to the British National Physical Laboratory at Teddington, England, and were compared during the past 10 months with the British Cs Beam Frequency Standard built by Dr. L. Essen and coworkers and based on quite a different design.[2,3] The British model is not sealed and has no servo mechanism for automatic lock of the frequency translator to the atomic resonance line. The result of the comparison was an agreement of the U. S. and the United Kingdom Cs frequency standards within the measurement precision of about $1\text{p}{:}10^{10}$.[4]

A third Atomichron was made available to J. A. Pierce of Cruft Laboratory, Harvard University, to allow a precision measment[5] of standard radio signals transmitted by the British stations MSF (60 kc), GBZ (19.6 kc), and GBR (16 kc), by the U. S. stations WWV (5 mc) and KK2XEI (60 kc), by the German station DCF77 (77.5 kc) and the Swiss station HBB (96.04 kc). His measurements are not only interesting from the point of view of propagation studies, as discussed elsewhere,[6,7] but also because his Atomichron is the first device of this kind which is nearly continuously operating since March, 1958. It had accumulated by the end of January a total operational lifetime of more than 8200 hours, which is a remarkable record for a sealed Cs beam tube. After 4190 hours and again after some 8000 hours, the signal-to-noise of the beam detector became so low that a reflashing of the Ti getter in the attached miniaturized evapor-ion pump seemed to be necessary. After the reflashings, the equipment worked normally again as with a new beam tube.

Four weeks before the first reflashing was carried out, an unexpected drift of the output frequency at a nearly steady rate of $+8\text{p}{:}10^{11}$ per day[8] was observed which gave rise to a total accumulated error of $+2.2\text{p}{:}10^{9}$ at the day of the first reflashing. There are several explanations possible for this phenomenon:

1) By sheer coincidence, the electronic servo control could have slowly drifted out of adjustment due to aging of servo controls. The steadiness of the drift and the size of the total error, just before the first reflashing and complete readjustment of the electronic system, do not favor this explanation. On the other hand, it cannot be completely dismissed since the electronics adjustment could not be checked before the reflashing due to insufficient signal-to-noise of the beam tube resonance signal caused by the deteriorating vacuum in the Cs beam tube.

2) When the first Ti film approached its saturation, the vacuum in the beam tube deteriorated and this, in turn, caused a loss of signal-to-noise at the detector due to beam scattering. The decrease in signal-to-noise reduced steadily the over-all servo gain. If we assume now that the 5 mc quartz crystal flywheel oscillator at the lower end of the frequency translator had some unusual drift rate, it is obvious that the decreasing servo gain would have introduced an increasing gap between the line resonance frequency defined by the maximum of the resonance curve and the frequency to which the servo actually locked the translator. It was tried recently at USASRDL to measure the order of this effect by simulating the loss of signal-to-noise caused by poor vacuum by decreasing the Cs oven temperature from 70°C

* Received by the IRE, March 16, 1959.

[1] F. H. Reder, "Minutes of Coordination Conference on Comparison of U.S. and U.K. Cs Beam Standards," held at Frequency Control Div., USASRDL, Ft. Monmouth, N. J.; February 24, 1958.

[2] A. O. McCoubrey, "Results of the comparison: Atomichron—British Cs beam standard," *Proc. 12th Annual Symp. Frequency Control*, pp. 648–664; May 6–8, 1958.

[3] L. Essen, J. Parry, J. Holloway, W. Mainberger, F. Reder, and G. Winkler, "Comparison of Cesium frequency standards of different construction," *Nature*, vol. 182, pp. 41–42; July 5, 1958.

[4] L. Essen, J. Parry, J. Holloway, W. Ma nberger, F. Reder and G. Winkler, "Comparison and evaluation of Cs atomic beam frequency standards," final report to be submitted to Proc. IRE.

[5] J. A. Pierce, "Intercontinental Frequency Comparison by Very Low Frequency Radio Transmission," Cruft Lab., Harvard Univ., Cambridge, Mass., Tech. Rept. No. 220; February 15, 1957.

[6] L. Essen, J. Parry, and J. A. Pierce, "Comparison of Cs resonators by transatlantic radio transmission," *Nature*, vol. 180, pp. 526–528; September 14, 1957.

[7] J. A. Pierce, "Recent long-distance frequency comparisons," Cruft Lab., Harvard Univ., Cambridge, Mass., Tech. Rept. No. 270, September 10, 1958.

[8] J. A. Pierce, Weekly letter-type progress report to agencies participating in the comparison project; August 24, 1958

to 40°C, at which temperature the system fell out of lock. The maximum error was not larger than 1p:10^{10} despite the fact that the experiment was done a few hours after warm-up where the crystal oscillator drift is generally larger than one would expect in the case of Mr. Pierce's Atomichron, which was in continuous operation over several thousand hours. This fact sheds doubt also on this explanation.

3) The increasing deterioration of the vacuum might have caused a growing inherent frequency shift because of the perturbing influence of impurity molecules or of neighboring Cs atoms. Beaty's experiments with atomic gas cell frequency standards using buffer gases[9] revealed strong frequency changing effects of certain buffer gases. Since the ion pump is located near the detector, which is connected to the critical interaction region through a 3-ft long beam tube of very small cross section, it is not impossible that the pressure in the interaction region was growing to a value several orders of magnitude higher than the normal operating pressure of 10^{-8} mm Hg. Beaty and co-workers, for instance, give the frequency drift of a Cs-He gas cell with 1600 cps per mm Hg of He pressure, which amounts to a necessary He pressure of 12 μ to explain the observed total frequency shift of 2.2p:10^{9}. This is, of course, unrealistic but Helium is a "neutral" buffer gas. If we assume, however, the presence of non-neutral gases having magnetic dipole moments as, *e.g.*, oxygen, or if we assume the increase of the Cs vapor background pressure due to the deteriorating vacuum, it seems quite possible that the observed loss of signal intensity caused by beam scattering in poor vacuum is accompanied by the observed frequency shift which is caused by deforming collisions and magnetic field perturbations from neighbors of the atoms getting through to the detector.

In view of the trend to advocate sealed Cs beam frequency standards more and more for primary frequency and time control, it is proposed to start a careful investigation of this frequency shift phenomenon and to find out if such an inherent shift caused by a deteriorating vacuum is possible at all. The experiment could be carried out along two lines:

1) Scientific laboratories in possession of conventional beam type spectrometers could investigate the influence of poor vacuum on the resonance frequency of the observed atoms by admitting a controlled amount of impurities into the interaction region between the two Ramsey cavities and measuring beam intensity at the detector and maximum-position of the resonance pattern as a function of pressure in the interaction range.

2) Laboratories in possession of two Atomichrons could proceed as follows: As soon as the signal-to-noise of the beam tube output signal starts to decrease, which is indicated by the need of higher preamplifier and servo gain, this Atomichron should be used as a resonator, as shown in Fig. 1,[10] in order to eliminate possible perturbations introduced by its electronics and, in particular, by the servo control mechanism. This way, the dc resonance curves of the beam tube can be plotted point for point first with the ion pump still operating and from there

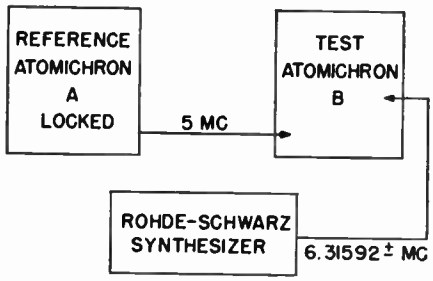

Fig. 1—Setup for measuring the dc resonance curve of B. 1) Disconnect cable from J2005 and connect with 5 mc output of A. 2) Disconnect 100 cps modulation cable from J6008 to prevent distortion of dc curve. 3) Break connection between pin 1 of XV6021 and TP6010 and inject a 1 v output signal from synthesizer at pin 1 of XV6021. 4) Change synthesizer frequency slowly around the center value of 6.31592 mc and plot ion current meter reading versus twice the synthesizer frequency. The center of the resonance pattern should then be at 12.631840 mc.

on with the pump disconnected to speed up the decay of the vacuum. A possible shift of the resonance frequency with increasing background pressure could thus be measured. After loss of the signal, the ion pump could be reconnected and the getter flashed to establish the proper vacuum for further use of the beam tube.

If inherent shifts are substantiated by experiments, one could prevent them in the future by reflashing the evapor-ion pump getter at the first indication of a growing saturation of the getter film.

FREDERICK H. REDER
U. S. Army Signal Res. and Dev. Lab.
Fort Monmouth, N. J.

[9] E. C. Beaty, P. Bender, and A Chi, "Narrow hyperfine absorption lines of Cs^{133} in various buffer gases," *Phys. Rev.*, vol. 112, pp. 450–452; October 15, 1958.

[10] G. M. Winkler used this method successfully at USASRDL for measuring the beam tube bandwidth.

Stabilities of Common Emitter and Emitter Follower Transistor Amplifiers*

Dion[1] has pointed out an equivalence between common emitter and emitter follower amplifiers. Recently, Purton[2] has commented on the power gain stabilities of these two configurations. These ideas may be extended further to provide design equations for transistor amplifier stability with respect to the common emitter current gain, α_{fe}.

Fig. 1 shows the common emitter configuration. Standard analysis yields for the voltage, current, and power gains, respectively.

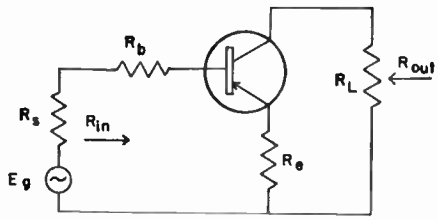

Fig. 1—Common emitter transistor amplifier.

$$G_v = \frac{-\alpha_{fe}R_L}{R_b + (1+\alpha_{fe})R_e} \tag{1a}$$

$$G_i = -\alpha_{fe} \tag{1b}$$

$$G_p = \frac{\alpha_{fe}^2 R_L}{R_b + (1+\alpha_{fe})R_e}, \tag{1c}$$

and for the input and output impedances,

$$R_{in} = R_b + (1+\alpha_{fe})R_e. \tag{1d}$$

$$R_{out} = R_L. \tag{1e}$$

Using standard differentiation techniques, we obtain from (1)

$$\delta G_v = \frac{1+w}{w+(1+\alpha_{fe})}\,\delta\alpha_{fe} \tag{2a}$$

$$\delta G_i = \delta\alpha_{fe} \tag{2b}$$

$$\delta G_p = \frac{1+2w+(1+\alpha_{fe})}{w+(1+\alpha_{fe})}\,\delta\alpha_{fe} \tag{2c}$$

$$\delta R_{in} = \frac{\alpha_{fe}}{w+(1+\alpha_{fe})}\,\delta\alpha_{fe} \tag{2d}$$

$$\delta R_{out} = 0 \tag{2e}$$

where w is defined by

$$w = \frac{R_b}{R_e} \tag{3}$$

and the notation δX represents the per cent change in the variable X. Solving (2) for w we find

$$w = \frac{(1+\alpha_{fe})\delta G_v - \delta\alpha_{fe}}{\delta\alpha_{fe} - \delta G_v} \tag{4a}$$

$$w = \frac{(1+\alpha_{fe})\delta G_p - (2+\alpha_{fe})\delta\alpha_{fe}}{2\delta\alpha_{fe} - \delta G_p} \tag{4b}$$

$$w = \left[\frac{\delta\alpha_{fe}}{\delta R_{in}} - 1\right]\alpha_{fe} - 1. \tag{4c}$$

To design for a given stability requirement in terms of a known or estimated variation, $\delta\alpha_{fe}$, the appropriate (4) is solved for w. The specification of R_{in} and w uniquely determines R_b and R_e. Should more than one stability requirement be specified, (4) is first solved in terms of one of the requirements, and the result introduced into (2). The solutions of (2) are then compared with the remaining stability requirements.

In addition to providing design data, (2) and (4) provide information on the best possible stabilities. Should (4) yield a negative value for w, or if, in the case of multiple stability requirements, (2) results in an unacceptable stability for a remaining requirement, then the specifications cannot be met with a single transistor stage.

For the emitter follower (Fig. 2), the corresponding equations are

$$G_v = \frac{(1+\alpha_{fe})R_e}{R_b + (1+\alpha_{fe})R_e} \tag{5a}$$

* Received by the IRE, February 20, 1959.

[1] D. F. Dion, "Common emitter transistor amplifiers," PROC. IRE, vol. 46, p. 920; May, 1958

[2] R. F. Purton, "Common emitter transistor amplifiers," PROC. IRE, vol. 46, p. 1961–1962; December, 1958.

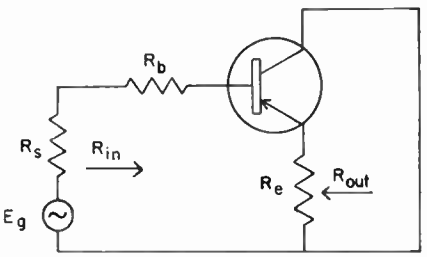

Fig. 2—Emitter follower transistor amplifier.

$$G_i = 1 + \alpha_{fe} \tag{5b}$$

$$G_p = \frac{(1+\alpha_{fe})^2 R_e}{R_b + (1+\alpha_{fe})R_e} \tag{5c}$$

$$R_{in} = R_b + (1+\alpha_{fe})R_e \tag{5d}$$

$$R_{out} = \frac{R_e(R_b + R_s)}{(1+\alpha_{fe})R_e + R_b + R_s} \tag{5e}$$

where R_s is the Thevenin equivalent resistance of the driving source. The corresponding stabilities are given by

$$\delta G_i = \frac{w}{w + (1+\alpha_{fe})} \cdot \frac{\alpha_{fe}}{1+\alpha_{fe}} \delta\alpha_{fe} \tag{6a}$$

$$\delta G_i = \frac{\alpha_{fe}}{1+\alpha_{fe}} \delta\alpha_{fe} \tag{6b}$$

$$\delta G_p = \frac{2w + (1+\alpha_{fe})}{w + (1+\alpha_{fe})} \delta\alpha_{fe} \tag{6c}$$

$$\delta R_{in} = \frac{\alpha_{fe}}{w + (1+\alpha_{fe})} \delta\alpha_{fe} \tag{6d}$$

$$\delta R_{out} = \frac{\alpha_{fe}}{w + (1+\alpha_{fe}) + \dfrac{R_s}{R_e}} \delta\alpha_{fe} \tag{6e}$$

and in terms of w

$$w = \frac{(1+\alpha_{fe})^2 \delta G_i}{\delta G_i - \alpha_{fe}(\delta\alpha_{fe} - \delta G_i)} \tag{7a}$$

$$w = \frac{[1+\alpha_{fe}][\alpha_{fe}\delta\alpha_{fe} - (1+\alpha_{fe})\delta G_p]}{(1+\alpha_{fe})\delta G_p - 2\alpha_{fe}\delta\alpha_{fe}} \tag{7b}$$

$$w = \alpha_{fe}\left[\frac{\delta\alpha_{fe}}{\delta R_{in}} - 1\right] - 1 \tag{7c}$$

$$w = \alpha_{fe}\left[\frac{\delta\alpha_{fe}}{\delta R_{out}} - 1\right] - \left[1 + \frac{R_s}{R_e}\right]. \tag{7d}$$

Eqs. (6) and (7) are thus the pertinent design equations for the stabilities of the emitter follower configuration, and are employed in the same manner as (2) and (4) for the common emitter case.

The reader will be quick to notice the similarities between (2) and (6). In the usual case, $\alpha_{fe} \gg 1$, they are nearly equivalent. This means that for the proper choice of w, the two configurations can be made to have nearly equivalent stabilities. There is, however, one other factor which should be considered. Let us form the ratios of the voltage and power gains for the two cases, assuming equal values for R_{in}:

$$\frac{G_{vce}}{G_{vef}} = \frac{-\alpha_{fe}R_L}{(1+\alpha_{fe})R_e} \tag{8a}$$

$$\frac{G_{pce}}{G_{pef}} = \frac{\alpha_{fe}^2 R_L}{(1+\alpha_{fe})^2 R_e}. \tag{8b}$$

If we now assume $\alpha_{fe} \gg 1$, we see that the common emitter voltage and power gains are greater than the respective emitter follower gains by a factor of R_L/R_e. The important fact is that with the emitter follower, one is forced to accept as the load impedance whatever value of R_e that is dictated by the stability requirements; whereas with the common emitter amplifier no such restriction exists. Thus, the common emitter amplifier affords more design freedom than the emitter follower. In practice, there will be a limitation on the size of R_L. However, it is not difficult to make $(R_L/R_e) \gg 1$, thereby obtaining with the common emitter amplifier more voltage and power gain without affecting the stability.

If the design equations presented here are to be used frequently, it may prove worthwhile to form graphical solutions of (2) and (6) with w as a parameter for several representative values of α_{fe}. The graphical technique has a decided advantage where multiple stability requirements are involved as graphical trial and error solutions converge very rapidly.

Bruce D. Wedlock
Dept. of Elec. Engrg.
Mass. Inst. Tech.
Cambridge 39, Mass.

Values of the Periodic and Radial Mathieu Functions and Their First Derivatives*

The periodic and radial Mathieu functions and their derivatives appear in a large variety of physical problems,[1-7] but in spite of this, there is a scarcity of published values for these quantities. Although some data are available for the lower orders of the periodic functions,[1,3,8,9] almost no data have been published for the radial functions or for the first derivatives of the periodic and radial functions. During the course of a recent investigation, it became necessary for the present authors to calculate a fairly large number of values of the functions and derivatives, and these have been assembled in two technical reports.[10,11] The contents of these reports are extensive enough so that they may prove to be of value to other investigators. Included in each report is a brief introduction which contains the infinite series representations for the several functions. The notations and normalization used are essentially the same as those given in the NBS tables[12] and are similar to those used by other authors.[1,2]

The reports contain values of the periodic Mathieu functions $Se_n(s, v)$ and $So_n(s, v)$ for v between 0 and 2π, of the radial functions $Je_n(s, u)$, $Jo_n(s, u)$, $Ne_n(s, u)$, $No_n(s, u)$, $He_n^{(1)}(s, u)$, and $Ho_n^{(1)}(s, u)$ for $0 \leq u \leq 2.0$, and of the first derivatives of these functions for the same ranges of v or u. (The parameter s is identical with that used in the NBS tables.[12] Results are given for orders 0, 1, and 2, and for the following values of s: ± 3, ± 6, ± 9, ± 15, and 25. Some data were also calculated for $s = 1, 2, 4, 5, 7, 8$, and 40. Tables of the first and second zeros of the radial functions $Je_n(s, u)$ and $Jo_n(s, u)$, and the first zeros of the first derivatives of these functions are also included. Nearly all of the tabulated quantities have also been plotted. About seventy pages of graphs, including more than 250 separate curves, are presented. The graphs are perhaps more valuable than the tables, since the curves show the stationary and zero points of the functions, give an indication of the effect of variation of the parameter s, and permit rough interpolation of the tabulated values.

The computations were performed at the Radiation Laboratory of the Johns Hopkins University, and were sponsored by Wright Air Development Center under contract number AF 33(616)-3374.

James C. Wiltse
Electronic Commun. Inc.
Timonium, Md.
Marcia J. King
Johns Hopkins Univ.
Rad. Lab.
Baltimore, Md.

* Received by the IRE, March 17, 1959.

[1] P. M. Morse and H. Feshbach, "Methods of Theoretical Physics," McGraw-Hill Book Company, Inc., New York, N.Y.; 1953.
[2] J. A. Stratton, P. M. Morse, L. J. Chu, and R. A. Hutner, "Elliptic Cylinder and Spheroidal Wave Functions," John Wiley and Sons, Inc., New York, N. Y.; 1941.
[3] N. W. McLachlan, "Theory and Application of Mathieu Functions," Oxford University Press, Eng.; 1951.
[4] L. J. Chu, "Electromagnetic waves in elliptic hollow pipes of metal," *J. Appl. Phys.*, vol. 9, pp. 583–591; September, 1938.
[5] J. Y. Wong, "On the theory of a coaxial transmission line consisting of elliptical conductors," *Can. J. Phys.*, vol. 34, pp. 354–361; 1956.
[6] G. Sinclair, "The patterns of antennas located near cylinders of elliptic cross section," Proc. IRE, vol. 39, pp. 660–668; June, 1951.
[7] L. Brillouin, "Wave Propagation in Periodic Structures," Dover Publications, Inc., New York, N Y., 2nd ed.; 1953.
[8] E. Jahnke and F. Emde, "Tables of Functions," Dover Publications, Inc., New York, N. Y.; 1945.
[9] R. Campbell, "Théorie Générale de l'Equation Mathieu," Masson et Cie, Paris, France; 1955.
[10] J. C. Wiltse and M. J. King, "Values of the Mathieu Functions," The Johns Hopkins University, Rad. Lab. Tech. Rept. AF-53; August, 1958.
[11] M. J. King and J. C. Wiltse, "Derivatives, Zeros, and Other Data Pertaining to Mathieu Functions," The Johns Hopkins University, Rad. Lab. Tech. Rept. AF-57; December, 1958.
[12] Natl. Bur. Stand. "Tables Relating to Mathieu Functions," Columbia University Press, New York, N. Y.; 1951.

Determination of the Orbit of an Artificial Satellite*

Recently, Carrara, Checcacci and Ronchi[1] described a 4-station Doppler satellite tracking system which purported to obtain 3 initial ranges and the frequency of the vehicle oscillator from a solution of several equations containing successive time-dependent observations by the fourth station. Having the initial conditions and instantaneous frequency, the instantaneous coordinates of the vehicle are then obtainable from a solution of 3 equations containing the simultaneous observations of 3 stations.

* Received by the IRE, March 16, 1959.

[1] N. Carrara, P. F. Checcacci, and L. Ronchi, "Determination of the orbit of an artificial satellite," Proc. IRE, vol. 47, p. 75; January, 1959.

The problem addressed by the authors is a venerable one, as engineering problems go, as the first publications appeared shortly after World War II.[2-6] Several 3 and 4 station Doppler tracking systems have been proposed, of which at least 3 generic types have been built; these are DOVAP, a 3-station system requiring an iterative solution, HYPERDOP, a 3-station system allowing closed solution but requiring initial ranges and the vehicle transmitter frequency, and DORAN, a 4-station system requiring iteration. In general, Doppler systems may be classed as open-solution or close-solution systems, depending upon whether or not they require iteration; the open systems obviously extrapolate to the initial ranges while the closed systems require this data be supplied by radar or some other range measuring device. In order for the polystation Doppler system to function, one has the choice, roughly, of an additional computer or additional radars.

Conventional passive Doppler systems, whether open or closed, will, in general, track only friendly satellites, that is, those having known oscillator frequencies. The problem of continuous tracking of satellites with unknown frequencies, an advantage the authors seem to claim, is considerably more difficult, primarily because the Doppler data itself is not obtainable without knowledge of the vehicle frequency. It is true that the frequency, as well as the initial ranges, may theoretically be obtained from the solution of a sufficient number of simultaneous, time-dependent equations; however, all such determinations require at least second-order differences of the data. These differences, for the usual frequencies employed, shrink to the order of magnitude of the errors inherent in the system, and increase with the number of data used in computation.

As an open solution, for friendly satellites, the authors' method has two shortcomings. First, the initial range of the fourth station is overlooked; thus, when the equation

$$v_i(t) = \frac{d}{dt} R_i(t) \qquad i = 1, \cdots, 4 \quad (1)$$

is integrated, we get R_4 as a function of its own initial range:

$$R_4 = R_4(t, f_0, R_{01}, R_{02}, R_{03}, R_{04}), \quad (2)$$

as well as the remaining variables (unless station S_4 is at the launch site). Hence, one is still left knowing nothing more than 4 velocity rates, with 5 unknowns; the necessity of an open solution is evident. Second, an open solution can be obtained with less stations, as is done by DOVAP-type systems, which also insure a known frequency by utilizing a ground-based transmitter and a transponder in the vehicle.

If the vehicle must be acquired in space, the conventional Doppler system must have an initial range estimate, obtained from an external measuring device. The precision of this initial estimate determines whether the subsequent solution of the coordinate equations shall be open or closed. If the estimate is poor, or a guess, an open, or iterative, solution by a high-speed computer is mandatory. If the estimate is precise to within 1 per cent, for instance, and the vehicle carries an oscillator, the 3-station passive system can be operated in the same manner as if the vehicle were acquired on the ground, and a closed solution, with a small computer or an accurate analog is feasible. The system is, nevertheless, subject to errors due to frequency drift, a quite serious matter because of the low Doppler frequency. In fact, since the carrier is modulated in both frequency and amplitude, by any time-varying interacting signal, the Doppler frequency is certain to contain errors due to vehicle angular motion and ionospheric modulation, particularly the Faraday rotation. While phaselock detectors may provide a signal unmodulated in amplitude, the Doppler frequency, nevertheless, contains error components corresponding to all the time-varying signals with which the carrier interacts. Furthermore, the use of an optimum filter guarantees only that the sum of the error squares is minimized; there is still no insurance that the sum will not be large enough to render the Doppler data unusable. Thus, Doppler accuracy is improved only by minimizing the *absolute* value of each error independently.

One of the earliest and most persistent difficulties has been that of maintaining phase coherence (in which we include the grosser problem of frequency drift) between vehicle and local oscillator. The conventional approach, for Doppler tracking, has been the use of a single ground-based oscillator with vehicle-borne beacon; this approach necessitates an open solution, which can be demonstrated as follows. The range increments, ΔR_i, measured by the Doppler data are:[2]

$$\Delta R_i = U + R_i - R_{0i} \quad i = 1, \cdots, n \quad (3)$$

where U is the transmitter-beacon path, R_i the beacon-receiver paths, and R_{0i} the transmitter-receiver paths. Since only R_{0i} and ΔR_i are known or constant, an exact solution of (3) requires $n+1$ independent equations, whereas only n are obtainable. The only possible solution of (3) thus requires iteration. These are the DOVAP equations. Eq. (3) is solvable with n equations, only if U is known, or constant, or vanishes. Whereas the first two possibilities are not feasible, the third is realized by placing the transmitter in the vehicle. The $n+1$ unknowns in (3) then reduce to n unknowns in:

$$\Delta R_i = R_i - R_{0i} \qquad i = 1, \cdots, n. \quad (4)$$

By equating the ΔR_i to the corresponding Doppler data, and writing the R_i as functions of x, y, z, and the station coordinates, (4) gives 3 equations in 3 unknowns, which are solvable exactly for the position coordinates, x, y, and z.

For the restricted problem of tracking friendly vehicles, a frequency-independent solution may exist for four observations. The necessary relations are:

$$(x - x_i)^2 + (y - y_i)^2 + z^2 = R_i^2 \qquad i = 1, 2, 3, 4 \quad (5)$$

where x_i and y_i are the station coordinates in the ground plane, relative to an origin at the launch site, and R_i is the slant range from the ith station. R_i is related to the Doppler data and the station geometry by

$$R_i = R_{0i} + \Delta R_i = R_{0i} - \lambda_0 Q_i + ct \qquad i = 1, \cdots, 4 \quad (6)$$

where R_{0i} is the initial range from the ith station to the launch site, and Q_i an integral Doppler cycle count defined by

$$\Delta R_i = \int_{t_{i1}}^{t_{i2}} \lambda_0 (f_0 - f_i) dt_i = -\lambda_0 (Q_i \pm \phi_i) + ct \qquad \phi_i < 2\pi. \quad (7)$$

Since the Q_i are measured, a solution of (6) necessitates primary knowledge of λ_0 and the R_{0i}. Clearly, a unique solution exists when the coordinate origin is taken at the launch site, which assumes an exact knowledge of the launching site position. A particular solution of (5) and (6) has been obtained for 4 stations arranged in a cross of diagonal $2R_0$ and launching site at the center. Eq. (5) becomes, for this geometry,

$$\begin{aligned} (x \pm R_0)^2 + y^2 + z^2 &= R_i^2 \quad i = 1, 2 \\ (y \pm R_0)^2 + x^2 + z^2 &= R_i^2 \quad i = 3, 4. \end{aligned} \quad (8)$$

Equating and solving for x, y, z and λ_0:

$$x = \tfrac{1}{4} R_0 [\lambda_0^2 (Q_3^2 - Q_1^2) - 2\lambda_0 (Q_3 - Q_1)(ct + R_0)] \quad (9)$$

$$y = \tfrac{1}{4} R_0 [\lambda_0^2 (Q_4^2 - Q_2^2) - 2\lambda_0 (Q_4 - Q_2)(ct + R_0)] \quad (10)$$

$$z = [ct + (R_0 - Q_4)^2 - x^2 - (y + R_0)^2]^{1/2} \quad (11)$$

$$\lambda_0 = 2(Q_4 - Q_3 + Q_2 - Q_1)(R_0 + ct) / (Q_4^2 - Q_3^2 + Q_2^2 - Q_1^2) \quad (12)$$

which gives the wavelength in terms of the second-order differences. It is obvious that (12) is not a continuous solution and, if the differences are either large or small, there exist nonlinearities in the λ_0 error function.

It is also possible to determine the required range increments by a straightforward measurement of propagation time: if the vehicle oscillator is turned on and off, or radiates time markers at precise, constant intervals, we have only to measure the differentials of the known and measured intervals to obtain the range increments

$$\Delta R_i = t_2 - t_1 - c(t_{i2} - t_{i1})$$

where $t_2 - t_1$ is the constant interval and t_{i1} and t_{i2} are the times of arrival of the first and second markers at the ith station. The vehicle coordinates are then expressible as functions of the initial ranges and the time differentials only. Such a system, of course, has little to do with the Doppler effect, depending entirely on measurements of propagation time; thus it is more akin to an inverse loran than to Doppler. However, it is frequency independent, where Doppler is not.

JULIAN T. ANDERSON
Philco Corporation
Western Development Labs.
Palo Alto, Calif.

[2] S. Kusaka, "Doppler Determination of Projectile Trajectory," Ballistic Research Laboratory, Rept. No. 609; 1946. (Declassified.)
[3] B. Garfinkel, "Doppler Determination of Position," Ballistic Research Laboratory, Rept. No. 638; 1947. (Declassified.)
[4] A. L. G. de Bey and E. D. Hofflitt, DOVAP, "Instrumentation and an Analysis of Operational Results," Ballistic Research Laboratory, Rept. 677; 1948. (Declassified.)
[5] B. Garfinkel, "Least Square Determination of Position from Radio Doppler Data," Ballistic Research Laboratory Rept. 707; 1949. (Declassified.)
[6] R. K. Weller, "An Alternative Least Squares Solution for Determination of Position from Radio Doppler Data," Ballistic Research Laboratory, Memo. No. 565; 1951. (Declassified.)

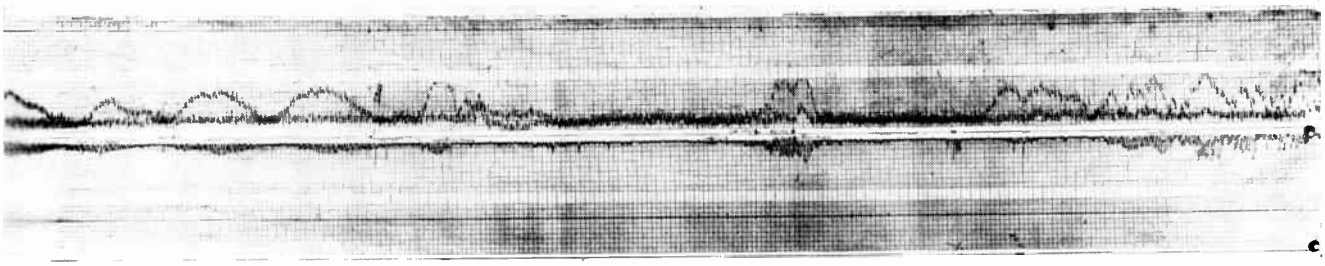

Fig. 1

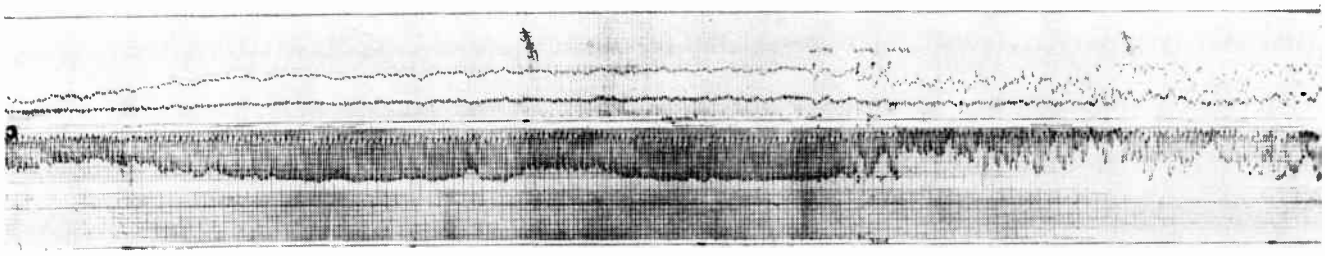

Fig. 2.

A New Method for Studying the Auroral Ionosphere Using Earth Satellites*

Among the problems of investigation of the auroral ionosphere is the nature of absorption associated with auroral displays. While visual auroral displays are well known for their patchy and complex forms, very little is known about the spatial distribution or the height of the associated radio absorbing regions. However, recent observations in College, Alaska,[1] and Ottawa, Canada,[2] indicate that the extent of the visual display is a poor index of the magnitude of absorption. The following describes a technique for studying this problem using the 20-mc transmission from Sputnik III.

Since the latitude of College is very nearly 65°, the satellite 1958 δ2 (Sputnik III) travels essentially from due west to due east during overhead passes. A signal strength recording of these passes indicates the absorption structure, and is effectively the same as measuring the absorption of cosmic noise by scanning with a "pencil beam" antenna. If the satellite signal path intersects an absorbing zone, a decrease in recorded signal strength results. By recording simultaneously in this manner at two stations, the height of the absorbing region is determined from simple geometric considerations. If H is the height of the satellite, h the height of the absorbing region, L the distance between stations, and v the velocity of the satellite, the east station records the absorption T seconds before the west station. The height h is determined from the relation

$$\frac{vT}{L} = \frac{H - h}{h}. \qquad (1)$$

Fig. 1, above, shows the absorption recorded at two stations 19 km apart on an east-west line. At this time the riometer equipment measuring cosmic noise showed an aurorally-associated absorption of 0.97 db at 27 mc.[3] Although the onset of the absorption is not well defined in both records, a hole in the middle of the fairly-broad absorbing zone allowed the signal to come through with a time difference of 38 ± 1 seconds between the stations. This corresponds to a height for the absorbing region of 104 km/3 km.

This same technique yields an answer to the question regarding the height of the regions which give rise to the scintillations and sometimes violent breakups in the signal strength. From an earlier study[4] it was concluded that the mechanism for this phenomenon was probably the same as that producing scintillations in the signals from radio stars. This mechanism depends on the presence of clouds of excess ionization at certain levels in the ionosphere. It was pointed out that these clouds are confined in clearly-bounded zones. Using the same two station techniques as before, four clearly-marked scintillation events have been identified during the few days of observations using high-speed Sanborn recorders. The satellite has been at apogee during these days. One of these is shown in Fig. 2, above. It was found from these observations that the irregularly-ionized zones producing the scintillations occur as high as 1000 km. It must be pointed out that the nature of diffraction through an irregular screen does not require a one-to-one correspondence of individual scintillations with large separation of the receivers. Nevertheless, Fig. 2 does permit the identification of the boundary of the scintillation zone within a second. Thus, the measured time difference of about half a second in the three runs (on June 3, 9, 11) combined with a possible error in measurement of one second indicates that it is possible to have irregularities in ionization at heights above 800 km and probably at 1000 km. Since the amplitudes of the individually-identified pulses do not behave in the same way at the two receivers, we rule out the possibility of the transmitter itself behaving erratically, and for the same reason a cloud of ionization surrounding the satellite itself is ruled out.

R. Parthasarathy
R. P. Basler
R. N. DeWitt
Geophysical Institute
College, Alaska

* Received by the IRE, June 17, 1959. This project was supported by the National Science Foundation under Grant No. NSF-32:42/268.

[1] S. Chapman and C. G. Little, *J. Atmos. Terres. Phys.*, vol. 10, p. 20, 1957.

[2] G. C. Reid, and C. Collins, *J. Atmos. Terres. Phys.*, vol. 14, p. 63, 1959.

[3] H. Leinbach (private communication).

[4] R. Parthasarathy and G. C. Reid, "Signal strength recordings of the satellite 1958 δ2 (Sputnik III) at College, Alaska," PROC. IRE, vol. 47, pp. 78–79; January, 1959.

Standard Frequency Transmissions*

Since October 9, 1957, the National Bureau of Standards radio stations WWV and WWVH have been maintained as constant as possible with respect to atomic frequency standards maintained and operated by the Boulder Laboratories, National Bureau of Standards. On October 9, 1957, the USA Frequency Standard was 1.4 parts in 10^9 high with respect to the frequency derived from the UT 2 second (provisional value) as determined by the U. S. Naval Observatory. The atomic frequency standards remain constant and are known to be constant to 1 part in 10^9 or better. The broadcast frequency can be further corrected with respect to the U.S.A. Frequency Standard, as indicated in the table; values are given as parts in 10^{10}. This correction is *not* with respect to the current value of frequency based on UT 2. A minus sign indicates that the broadcast frequency was low.

The WWV and WWVH time signals are

* Received by the IRE, July 22, 1959.

synchronized; however, they may gradually depart from UT 2 (mean solar time corrected for polar variation and annual fluctuation in the rotation of the earth). Corrections are determined and published by the U. S. Naval Observatory.

WWV and WWVH time signals are maintained in close agreement with UT 2 by making step adjustments in time of precisely plus or minus twenty milliseconds on Wednesdays at 1900 UT when necessary; no time adjustment was made during this month at WWV and WWVH.

National Bureau of Standards
Boulder, Colo.

WWV Frequency†

1959		#1	#2	#3
June	1	−34	−34	−30
	2	−33	−34	−30
	3	−32	−34	−30
	4	−32	−34	−31
	5	−32	−34	−30
	6	−32	−34	
	7	−32	−34	
	8	−32	−34	−31
	9	−32	−34	−31
	10	−33	−34	−31
	11	−33	−34	−31
	12	−33	−34	−31
	13	−33	−33	
	14	−32	−33	
	15	−32	−33	−30
	16	−32	−33	−30
	17	−32	−33	−30
	18	−31	−33	−30
	19	−32	−33	−30
	20	−32	−33	
	21	−32	−33	
	22	−32	−33	−30
	23	−31	−33	−30
	24	−31	−33	−30
	25	−31	−33	−30
	26	−32	−33	−30
	27	−32	−33	
	28	−31	−33	
	29	−31	−33	−29
	30	−32	−34	−30

† WWVH frequency is synchronized with that of WWV.
Column #1 Vs NBS‡ atomic standards, 30-day moving average seconds pulses at 15 mc.
Column #2 Vs atomichron at WWV, measuring time one hour at 2.5 mc.
Column #3 Vs atomichron at NRL, measuring time 56 minues at 2.5 mc.
‡ Method of averaging is such that an adjustment of frequency of the control oscillator appears on the day it is made. No adjustment was made during June.

System Loss in Radio-Wave Propagation*

It is the purpose here, to call to the attention of IRE members, a recommendation made by the Consultative Committee on International Radio (CCIR) at their recent meeting in Los Angeles, Calif. The definitions recommended by this group have been found to be most useful at the Central Radio Propagation Laboratory[1] in providing a vehicle suitable for the precise description of radio-wave propagation phenomena in a way which at the same time is useful directly to those engaged in the development of radio systems. The recommendation of the CCIR follows.

THE CONCEPT OF TRANSMISSION LOSS IN RADIO SYSTEMS STUDIES

(Question No. 81 and Study Programme No. 85)
Los Angeles, 1959.

The CCIR

CONSIDERING:

1) that the radio frequency signal power, p_a, available* at the terminals of a receiving antenna for a given power input, p_t, to the terminals of a transmitting antenna provides a measure which is useful in determining at the terminals of the receiving antenna the service from or the interference produced by a radio system involving a transmitting antenna, a receiving antenna, and the intervening propagation medium;

2) that the ratio, p_t/p_a, which will be called the system loss, is a convenient dimensionless form for expressing this measure of the combined radio propagation and the circuit loss characteristics of such a system;

3) that the available power at the terminals of the receiving antenna is sometimes a simpler and more directly useful concept than that of the effective field strength, especially where the effective field is the resultant of a large number of received field components corresponding to several modes of propagation arriving at the receiving antenna with different angles and possibly with different polarizations;

4) that the relationship between the system loss and the conditions in the neighborhood of the receiving antenna does not depend solely on the received field strength, because the impedance of the antenna is itself dependent upon the conditions in its neighborhood;

5) that the power P_t' radiated from the transmitting antenna† required for satisfactory reception in the presence of noise is precisely determined for a system with transmission loss L by the simple relation: $P_t' = L + P$; P is the minimum signal power available from an equivalent lossless receiving antenna that is required to provide satisfactory reception (as defined in Rept. No. 65);

6) that it is desirable to standardize on terminology and notation for describing system loss and its various components;

RECOMMENDS:

that the terminology and notation given in the Annex be adopted for use by the CCIR, in accordance with the further discussion of the use of these terms given in Rept. No. . . . (Doc. 193 rev.).

* The available power p_a is the power which would go to the load if it were matched to the antenna impedance.

† Throughout this recommendation, capital letters are used to denote the ratios, expressed in decibels, of the corresponding quantities designated with lower-case-type; *e.g.*, $P_t' = 10 \log_{10} p_t'$ is the power radiated from the transmitting antenna expressed in decibels above one watt.

ANNEX

System Loss (L_s)

The system loss of a radio circuit consisting of a transmitting antenna, receiving antenna, and the intervening propagation medium is defined as the ratio, p_t/p_a, where p_t is the radio-frequency power input to the terminals of the transmitting antenna and p_a is the resultant radio-frequency signal power available at the terminals of the receiving antenna. Both p_t and p_a are expressed in watts. The system loss is usually expressed in decibels:

$$L_s = 10 \log_{10} (p_t/p_a) = P_t - P_a.$$

Note that the system loss, as above defined, excludes any transmitting or receiving antenna transmission line losses since it is considered that such losses are readily measurable. On the other hand, the system loss includes all of the losses in the transmitting and receiving antenna circuits, including not only the transmission loss due to radiation from the transmitting antenna and reradiation from the receiving antenna, but also any ground losses, dielectric losses, antenna-loading coil losses, terminating resistor losses in rhombic antennas, etc. The inclusion of all of the antenna-circuit losses in the definition of system loss provides a quantity which can always be measured accurately and which is directly applicable to the solution of radio-system problems.

Transmission Loss (L)

The transmission loss of a radio circuit consisting of a transmitting antenna, receiving antenna, and the intervening propagation medium is defined as the dimensionless ratio, p_t'/p_a', where p_t' is the radio frequency power radiated from the transmitting antenna, and p_a' is the resultant radio-frequency signal power which would be available from the receiving antenna if there were no circuit losses other than those associated with its radiation resistance. The transmission loss is usually expressed in decibels:

$$L = 10 \log_{10} (p_t'/p_a') = L_s - L_{tc} - L_{rc}.$$

where L_{tc} and L_{rc} are the losses, expressed in decibels, in the transmitting and receiving antenna circuits, respectively, excluding the losses associated with the antennae radiation resistances; *i.e.*, the definitions of L_{tc} and L_{rc} are $10 \log_{10} (r'/r)$ where r' is the resistive component of the antenna circuit and r is the radiation resistance.

Basic Transmission Loss (L_b)

The basic transmission loss (sometimes called path loss) of a radio circuit is the transmission loss expected between ideal, loss-free, isotropic, transmitting and receiving antennae at the same locations as the actual transmitting and receiving antennae.

Path-Antenna Directivity Gain (G_p)

The path-antenna directivity gain is equal to the increase in the transmission loss when lossless, isotropic, antennae are used at the same locations as the actual antennae.

$$G_p = L_b - L.$$

Path-Antenna Power Gain (G_{pp})

The path-antenna power gain is equal to the increase in the system loss when lossless isotropic antennae are used at the same locations as the actual antennae.

$$G_{pp} = L_b - L_s = G_p - L_{tc} - L_{rc}.$$

Note that G_{pp} will be negative when the antenna circuit losses exceed the path-antenna directivity gain.

In some idealized situations the path-antenna power gain, G_{pp}, is simply the sum $(G_{tp} + G_{rp})$ of the free-space power gains, G_{tp} and G_{rp}, of the transmitting and receiving antennae relative to lossless isotropic antennae. However, in most practical situations G_{pp} is less than $(G_{tp} + G_{rp})$ because of the complex nature of the received field. The path-antenna power gain may be measured by determining the increase in the system loss when both the transmitting and receiving antennae are replaced *simultaneously* by simple standard antennae such as short electric or magnetic dipoles, and then adding the calculated path-antenna power gain corresponding to the use of the standard antennae. In the case of ionospheric or tropospheric scatter propagation, the path-antenna power gain is sometimes substantially smaller than the sum of the free-space power gains $(G_{tp} + G_{rp})$; in such cases the path-antenna power gain cannot be defined by the sum of the effective power gains of the transmitting and receiving antennae (as determined by replacing first one antenna and then the other successively by a standard antenna) since such effective power gains depend upon the gain of the antenna used at the other terminal.

In the case of ionospheric or tropospheric propagation, the transmission loss L, the basic transmission loss L_b, and the path antenna gain G_p, are all random variables with respect to time, and tend to be normally distributed about their expected values. Typically, L and G_p are negatively correlated with each other, and thus the variance of L_b is usually substantially less than the sum of the variances of L and of G_p; for this reason it will often be more practical simply to measure the system loss with the particular antennae intended for use rather than attempt to calculate the expected system loss and its variance with time in terms of the measured or calculated values of the basic transmission loss, the path-antenna gain, and the losses L_{tc} and L_{rc}. Note also that the path-antenna gain may actually be negative. For example, the path-antenna gain will usually be negative for ground-wave or tropospheric-wave propagation between a vertically-polarized and a horizontally-polarized antenna, and the concept of path-antenna gain should prove to be useful for expressing the results of such cross-polarization measurements.

Propagation Loss (L_p)

The propagation loss is the system loss expected if the antennae gains and circuit resistances were the same as if the antennae were located in free space:

$$L_p = L_s - L_t - L_r.$$

L_t and L_r are defined by $10 \log_{10} (r'/r_f)$ where r' is the actual antenna resistance and r_f is the resistance the antenna would have if it were in free space and there were no losses other than radiation losses.

Further information about the work of the CCIR is given in recent Proceedings papers by de Wolf[2] and Cross.[3] The other recommendations and reports of the CCIR IX Plenary Assembly at Los Angeles, Calif., will be published in the near future, and may be obtained by writing directly to the International Telecommunication Union at Geneva, Switzerland.

In a recent paper[1] a summary is presented of the ways in which the concept of system loss and the closely-related concepts

* Received by the IRE, June 8, 1959.

[1] K. A. Norton, "System loss in radio-wave propagation," *NBS J. of Res.*, Sec. D, Radio Propagation, vol. 63 D, pp. 53–73; July-August, 1959.

[2] F. C. de Wolf, "The 1959 international radio conference," Proc. IRE, vol. 45, pp. 1618–1621; December, 1957.

[3] J. S. Cross, "The international radio consultative committee," Proc. IRE, vol. 45, pp. 1622–1628; December, 1957.

of transmission loss, basic transmission loss, propagation loss, and path-antenna gain may be used for precise, yet simple, descriptions of some of the characteristics of radio-wave propagation which are important in the design of radio systems. Definitions of various terms associated with the concept of system loss are given which introduce a greater flexibility into its use without any loss in precision. It is shown that the use of these added terms and concepts makes feasible the extension of the use of this method of description to any portion of the radio spectrum.

A more general formula for the system loss is given which may be used for antennas with an arbitrarily small separation. Using this formula it is shown that the system loss between small electric or magnetic dipoles separated by a distance $d \ll \lambda$ can be made arbitrarily small even though the individual antennas have large circuit losses.

Formulas are developed for the percentage of time that a desired signal is free of interference, and these are used to demonstrate methods for the efficient use of the spectrum.

An analysis is made of the variance of the path-antenna gain in ionospheric scatter propagation.

Methods are given for the calculation of the transmission loss for the ground wave and tropospheric scatter modes of propagation through a turbulent model atmosphere with an exponential gradient. Examples of such calculations are given which cover a wide range of frequencies and antenna heights.

Finally, examples are given of the expected range of various tropospheric point-to-point scatter systems such as an FM multi-channel teletype system, a television relay or an FM broadcast relay.

KENNETH A. NORTON
National Bureau of Standards
Central Radio Propagation Lab.
Boulder, Colo.

Comparison of Coherent and Phase-Comparison Detection of a Four-Phase Digital Signal*

This note contains a further discussion of the error performance of the differentially-coherent digital phase modulation systems considered by Lawton in a previous correspondence.[1] In his letter, Lawton states correctly that a binary phase-reversal system in which demodulation is effected by phase comparison of successive pulses requires only slightly more power for a given error rate than one using ideal coherent detection of individual pulses. The ratio of the power required for the two systems approaches zero db for low error rates. However, this conclusion does not apply to a four-phase differentially-coherent system, such as Kineplex, despite the fact that a four-phase signal can be considered as the combination of two binary phase-reversal signals added in phase quadrature. As will be shown, the four-phase system suffers slightly less than a 3-db penalty when phase comparison detection is used instead of coherent detection.

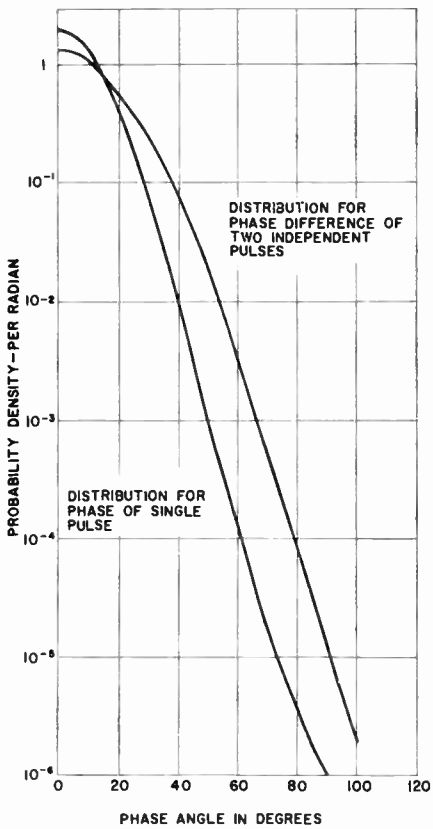

Fig. 1—Probability density functions of phase.

The reason for this difference between binary and four-phase systems is that the phase-comparison detection process for a four-phase system does not separate the received signal plus noise into two independent binary channels but provides an output in the form of characters chosen from a "four-level" alphabet. It may be seen that an error in the output character occurs if, and only if, the differential phase deviates by more than 45° from the undisturbed value, which may be taken as zero without loss of generality. This error may occur in either or both of the bits. Since the probability density of the phase of a single pulse is essentially Gaussian for small angular deviations, an approximate 3-db penalty is expected for the four-phase system due to use of phase comparison of successive noisy pulses. This conclusion is in accord with the original experimental results obtained for Kineplex.[2] Because the Gaussian approximation breaks down for large angular deviations, the smaller degradation previously mentioned is found for the binary phase-reversal case. An asymptotic evaluation of the degradation for a four-phase system has been obtained, the resulting value being 2.3 db in the limit as the probability of error approaches zero.

To verify the above conclusions, the probability density function for the phase difference between two noisy pulses was calculated for the case $E/N_0 = 6$ (or 7.8 db), where E is the energy per bit (energy per pulse $= 2E$) and N_0 is the noise power density. The probability density of the phase θ of a single pulse may be shown to be[3]

$$p(\theta) = \frac{1}{2\pi} e^{-2E/N_0}\left[1 + \sqrt{8\pi E/N_0}\cos\theta \cdot e^{(2E/N_0)\cos^2\theta}\Phi(\sqrt{4E/N_0}\cos\theta)\right] \quad (1)$$

where $\Phi(x)$ is the probability integral defined by

$$\Phi(x) = \frac{1}{\sqrt{2\pi}}\int_{-\infty}^{x} e^{-x^2/2}dx \quad (2)$$

Eq. (1) is plotted in Fig. 1, for the above value of E/N_0. The probability density of the phase difference between two noisy pulses may be found from (1) by numerical calculation of a convolution integral. The results are also shown in Fig. 1. The expected increased spread in the distribution for the phase difference of two pulses is evident. A numerical integration for the area under the latter curve for $|\theta| > 45°$ yields a probability of error $= 0.0083$.

Comparison with Lawton's curve shows that coherent detection achieves this error rate for $E/N_0 = 2.9$ (4.6 db). However, for a fair comparison, the value of E/N_0 should be determined which for coherent detection gives a probability of 0.0083 that the phase of a single pulse deviates by more than 45° from its true value. The result is $E/N_0 = 3.5$ (5.4 db), so that the indicated penalty is 2.4 db in good agreement with the predicted limiting degradation of 2.3 db and with the previously published experimental data.[2] In view of the above discussion, it must be concluded that the new experimental data presented by Lawton for Kineplex is valid for binary phase-reversal operation only and that four-phase Kineplex still may be expected to have an approximate 3-db penalty with respect to a coherent-detection system.

CHARLES R. CAHN
Communications Systems Dept.
Ramo-Wooldridge
Div. of Thompson-Ramo-Wooldridge, Inc.
Los Angeles 45, Calif.

Author's Comment[4]

I wish to thank Mr. Cahn for pointing out the error in applying the results of my analysis of differentially-coherent detection of binary phase-shift keyed signals to the four-state Kineplex system. It is to be noted that the experimental data[1] were taken with one channel of a Kineplex system operating as a binary differentially-coherent channel. The agreement between the experimental data and the results of analysis, therefore, is not affected by Mr. Cahn's communication.

JOHN G. LAWTON
Cornell Aeronautical Lab., Inc.
Buffalo 21, N. Y.

* Received by the IRE, February 26, 1959.

[1] J. G. Lawton, "Theoretical error rates of 'differentially-coherent' binary and 'Kineplex' data transmission systems," PROC. IRE, vol. 7, pp. 333–334; February, 1959.

[2] M. L. Doelz, E. T. Heald, and D. L. Martin, "Binary data transmission techniques for linear systems," PROC. IRE, vol. 45, pp. 656–661; May, 1957.

[3] C. R. Cahn, "Performance of digital phase modulation communication systems," IRE TRANS. ON COMMUNICATIONS SYSTEMS, vol. PGCS-7, pp. 3–6; May, 1959.

[4] Received by the IRE, March 26, 1959.

A Distributed Amplifier Employing Triodes*

The employment of triodes in conventional distributed amplifier arrangements causes circulating waves and multiple reflections due to electrostatic induction through the grid-to-anode capacitance. It has been observed,[1] however, that it is possible to eliminate circulating waves and insure only one traveling wave in either line by providing the proper amount of mutual inductive coupling between the lines to achieve directional coupling properties, and by suitably proportioning the impedance of the plate line at the tube points to obtain what may be called active matching.

As an example let us consider the circuit of Fig. 1 which represents an arrangement of a distributed pair. In a codirectional coupler consisting of two coupled lines the voltages and currents in the inducing line can be represented as the sum of two waves traveling in the same direction with two different velocities, and those in the induced line as the difference of the two waves.

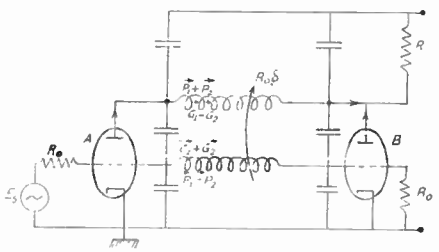

Fig. 1.

Thus when an input is applied to the grid line, two traveling waves are launched there, the sum of which is the first grid input voltage. The induced wave in the plate line is their difference $\vec{G_1}-\vec{G_2}$. The plate current of the first tube A causes a traveling wave $\vec{P_1}+\vec{P_2}$ to be launched in the plate line and an induced wave $\vec{P_1}-\vec{P_2}$ in the grid line. There will be no reflection at the load R if the voltage drop due to the incoming current wave from the plate line and the tube current of B flowing through R equals the incoming voltage wave in the plate line. This requires that

$$G_m = \frac{1}{R_0} = \frac{1}{2R}.$$

A current amplification factor of two is thus obtained. Furthermore, there are no reflections either in the plate line or in the grid line, and there is no circulating wave. It will be observed that the output is developed across a load $R=R_0/2$. The impedance can be transformed to that required for feeding the next stage by employing a nonuniform transmission line.

Experimental results with a distributed pair confirm these speculations.

N. B. Chakrabarti
J. K. Inst. of Appl. Phys.
University of Allahabad
India

* Received by the IRE, March 2, 1959.

[1] B. M. Oliver, "Directional electromagnetic couplers," Proc. IRE, vol. 42, pp. 1686–1692; November, 1954.

Combined AM and PM for a One-Sided Spectrum*

A simple means of obtaining a one-sided spectrum seems unreported in the literature. In this scheme the signal modulates the phase as well as the amplitude of the carrier, the signal being shifted by 90° before application to the phase modulator. The spectrum of such a modulated wave is completely one-sided. One important requirement, however, is that the modulation depths in AM and PM correspond.

For a sine wave signal at angular frequency w_0 the modulated wave can be written as

$$\begin{aligned}(1+m\cos\omega_s t)\sin(\omega_0 t+m\sin\omega_s t) &= (1+m\cos\omega_s t)[J_0(m)\sin\omega_0 t \\ &+ J_1(m)(\sin(\omega_0+\omega_s)t-\sin(\omega_0-\omega_s)t) \\ &+ \cdots]=J_0\sin\omega_0 t \\ &+\left[J_1+\frac{m}{2}\left(\frac{J_0}{2}+\frac{J_2}{2}\right)\right]\sin(\omega_0+\omega_s)t \\ &+\left[J_2+\frac{m}{2}(J_1+J_3)\right]\sin(\omega_0+2\omega_s)t \\ &+\cdots=J_0\sin\omega_0 t+2J_1\sin(\omega_0+\omega_s)t \\ &+3J_2\sin(\omega_0+2\omega_s)t+\cdots. \qquad (1)\end{aligned}$$

Eq. (1) shows that the spectrum is one-sided. It is also evident that the modulated wave can be received on an ordinary AM or FM receiver. Results on a test modulator indicate good agreement with the theory.

The system, however, has the following limitations: 1) in common with narrow-band PM, m has to be small in order that the higher modulation sidebands do not have substantial amplitude to offset the advantage gained by suppressing one side of the spectrum; 2) in common with AM, large carrier power is needed.

N. B. Chakrabarti
J. K. Inst. of Appl. Phys.
University of Allahabad
India

* Received by the IRE, March 2, 1959.

Measurement of Electric-Field Distributions in a Waveguide Containing a Dielectric Slab*

Some experimental work which gives additional information on the results published by Straus[1] is described.

Initially the experiments were to measure the variations of the electric field across the cross section of a transmission line consisting of a rectangular slab of distrene ($\epsilon_r=2.57$) placed between the plates of a parallel-plate transmission line. The relative electric field was measured by determining the setting of a calibrated waveguide attenuator required to keep the output constant for all positions of the probe. A typical result is shown in Fig. 1 and it is seen that the experimental and theoretical results agree apart from the abrupt change at the interface. This is clearly the same phenomenon as that reported by Straus. To obtain more information concerning this abrupt change, it was decided to carry out the corresponding measurements with the dielectric slab placed in a rectangular waveguide, which was, in fact, the same experimental arrangement as that of Straus. These measurements were made at S band (W.G. No. 10), since a device for measuring the transverse field pattern was already available in this size guide. This transverse-field plotter was very similar to that described by Straus, except that the probe unit was a tunable crystal-detector assembly from a conventional standing-wave indicator, and not a simple RF probe. The probe was set to zero penetration to avoid having to cut slots in the dielectric slab. The experimental results from this are shown in Fig. 2 and it is seen that although the abrupt change is different

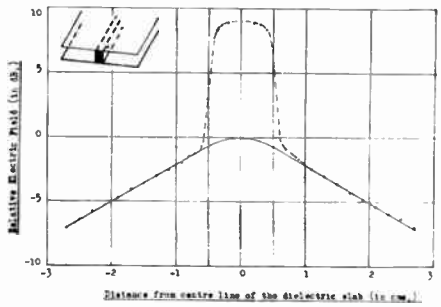

Fig. 1—The transverse electric-field distribution in a parallel-plate transmission line containing a longitudinal dielectric slab. Width of slab = 1.0 cm; free-space wavelength = 9.14 cm.
———— Theoretical distribution.
—·—·—·— Measured distribution.

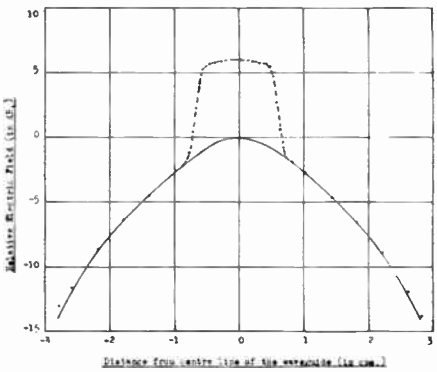

Fig. 2—The transverse electric-field distribution in rectangular waveguide containing a central longitudinal dielectric slab. Width of slab = 1.27 cm; free-space wavelength = 9.14 cm.
———— Theoretical distribution.
—·—·—·— Measured distribution.

in magnitude, the results are essentially the same as those of Straus.

The most important factor contributing to this abrupt change is easily explained. The output from the crystal detector is determined by the electric field in the vicinity of the probe, and when the probe is over the air region of the waveguide, this probe field is directly related to the electric field immediately beneath it. Similarly, when the probe is over the dielectric, the crystal detector output will again correspond to the field in the vicinity of the probe, *i.e.*, to the electric field immediately above the dielec-

* Received by the IRE, April 13, 1959.

[1] T. M. Straus, "Field displacement effects in dielectric and ferrite loaded waveguides," 1958 WESCON Convention Record, pt. 1, pp. 135–146.

tric. Now the boundary conditions require that the normal component of the electric flux must be continuous through the dielectric surface. It follows, therefore, that there must be a discontinuity in the normal component of the electric field, *i.e.*, the electric field immediately above the dielectric is ϵ_r times the electric field in the dielectric. Thus the abrupt increase in the apparent electric field shown in Fig. 2 should be 20 $\log_{10}$ 2.57, or 8.2 db, provided that the detector probe can be tuned to the same sensitivity when over the dielectric as it can be when over the air. The experimental value is 6½ db, and although lower than the predicted value, it is of the same order.

A straightforward way of testing this explanation would be to use such a probe that when making measurements in the air region, the probe could be surrounded by air, but when making measurements in the dielectric retion, the probe could be surrounded by the dielectric, thus avoiding any discontinuity at the top surface of the dielectric slab. The probe therefore was designed so that a dielectric sleeve could be fitted over the probe when required. Although the probe assembly had to be removed from the transverse-sliding carriage to remove or replace the dielectric sleeve around the probe, the probe assembly could then be replaced with the same probe penetration as before. When making measurements, the probe was set about 0.005 inch above the top of the dielectric slab. A series of four measurements was made, each involving the determination of the apparent relative electric field as a function of position across the guide.

Air probe:

a) Having tuned the probe for maximum output when in the air region, this tuning was then kept unaltered.
b) At each position the probe was returned where necessary.

Dielectric sleeved probe:

c) Having tuned the probe for maximum output when over the center of the dielectric slab, this tuning was then kept unaltered.
d) At each position the probe was then retuned where necessary.

The results are shown in Fig. 3. It had been expected that the air-region section of curve (b) and the dielectric-region section of curve (d) would form a smooth curve which would also agree with the theoretical curve. In fact, this is not so. However, the difference between the curves (b) and (d) corresponding to the air region is between 8¾ db and 9 db, and this is close to the predicted value of 8.2 db. Furthermore, almost the same difference (8½ db) occurs between the same two curves corresponding to the dielectric region. However, in each curve the abrupt change at the interface is only 6 db to 6½ db. This, in our opinion, is because the probe cannot be tuned to the same sensitivity in the air and over the dielectric with the existing simple tuning facilities. Indeed, it is significant that although a marked amount of tuning was necessary for the air probe as shown by curves (a) and (b), no retuning was necessary for the dielectric-sleeved probe. If one assumes that the abrupt change at the interface should be equal to the difference between the curves (b) and (d), *i.e.*, 9 db instead of 6½ db, then the relative electric-field values at all points in the dielectric region in curve (d) must be increased by 2½ db. If these modified points and those corresponding to the air-region section of curve (b) are then plotted together as in Fig. 4, it is seen that they lie very close to the theoretical distribution which is also shown in Fig. 4. The discrepancy between the expected 8.2 db and the observed 9.0 db is probably because the probe dielectric sleeve was made of perspex rod, whereas the slab was distrene. These materials have the same nominal relative permittivity but their precise values were not measured.

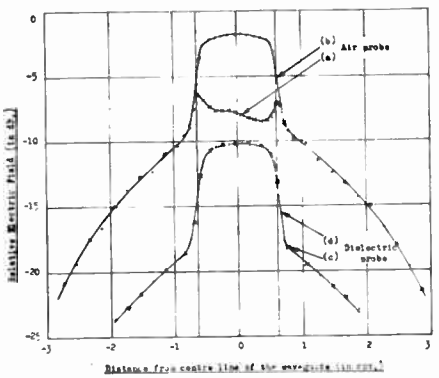

Fig. 3—The apparent transverse electric-field distribution in rectangular waveguide containing a central longitudinal dielectric slab, measured with different probes. Width of slab = 1.27 cm; free-space wavelength = 9.14 cm.
—x—x—x—x— Probe assembly with fixed tuning.
—·—·—·—·— Probe assembly with variable tuning.

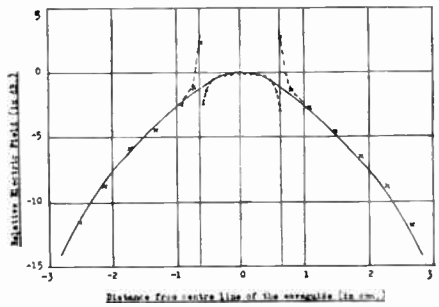

Fig. 4—The apparent transverse electric-field distribution in rectangular waveguide containing a central longitudinal dielectric slab, obtained by plotting curve (b) of Fig. 3, together with a modified form of curve (d) of Fig. 3. Width of slab = 1.27 cm; free-space wavelength = 9.14 cm.
—x—x—x—x— Curve (b) of Fig. 3.
—·—·—·—·— Modified form of curve (d) of Fig. 3.
———————— Theoretical distribution.

Let us deal particularly with one or two points in the paper by Straus. In the initial test experiment of the transverse-field plotter using the empty guide, it is probable that the reason for the nonagreement of the field distribution near the edges of the waveguide is that the proximity of the waveguide wall affected the tuning of the probe. (This can result in an unexpected peak near the wall.)

The abrupt and unexpected increase in the apparent relative electric-field strength observed at the interface of the dielectric is seen to be a phenomenon intimately associated with this technique of measurement. The measured value of the abrupt change is considerably influenced by the tuning of the probe assembly. It is expected that a probe of the form used in the experiments described in this note, *i.e.*, a probe which can be either air-spaced or dielectric-sleeved, with the further facility of being completely tunable would enable the true relative electric-field strength variations to be measured properly.

It is expected that a complete account of the experiments mentioned here will be published shortly.

K. W. H. Foulds
P. M. J. C. da S. Sampaio
Microwave Labs.
Dept. of Elec. Engrg.
City & Guilds College.
London, Eng.

An *X*-Band Parametric Amplifier*

A great deal of interest has been evidenced of late in parametric amplifiers for microwave frequencies due chiefly to the low-noise figures obtainable with these devices. This paper presents preliminary results for such an amplifier designed to operate in the degenerate mode about a center frequency of 11.55 kmc. It utilizes special point-contact Gallium Arsenide (GaAs) diodes assembled at our Holmdel laboratory.

The GaAs point contact rectifier diodes are mounted in a miniature case as shown in Fig. 1 and have been partially described in a recent paper.[1] The miniature mounting

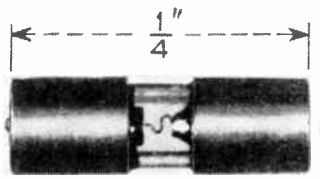

Fig. 1—Photograph of cartridge-type GaAs rectifier holder.

arrangement introduces a very small shunting capacitance (0.06 $\mu\mu$fds) in parallel with the "active" or variable capacitance characteristic of the diode proper. The design also minimizes the series inductance. The characteristics of the diodes depend on the doping of the GaAs material and the processing of the point-contact areas. A number of units suitable for parametric amplifiers and oscillators have been made. A typical bias voltage-capacity curve of such a diode measured at 100 kc is shown in Fig. 2. The low-frequency resistance of an average diode exceeds 0.25 megohm for bias voltages between −8.0 and +0.4 volts.

A sketch of the parametric amplifier is shown in Fig. 3. The pump energy at a frequency of 23.10 kmc enters from the *K*-band guide and is matched into the crystal by means of a *K*-band sliding piston. A coaxial connection is made between the *K*-band and *X*-band guides with the diode inserted in series with the center conductor. A second sliding piston and an adjustable iris with an associated tuning screw comprise the *X*-band signal circuit. The amplifier is thus a one-port device for the signal and is operated in conjunction with a circulator.

* Received by the IRE, May 4, 1959.
[1] W. M. Sharpless, "High frequency gallium arsenide point contact rectifiers," *Bell Sys. Tech. J.*, vol. 38, pp. 259–269; January, 1959.

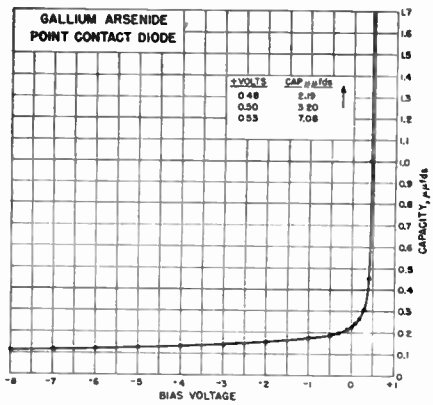

Fig. 2—Typical capacity-bias voltage characteristic of point-contact GaAs rectifiers.

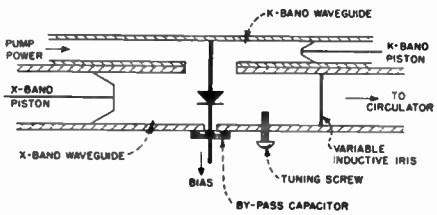

Fig. 3—Parametric amplifier.

The Q of the signal circuit can be controlled by the adjustable iris. By increasing the Q the gain may be increased, at the expense of bandwidth, and strong oscillations at half the pump frequency (11.55 kmc) are easily produced. The amplifier shown in Fig. 3 has produced a gain of 10 db with a 75-mc bandwidth with 100 mw of pump power. Oscillations at two frequencies symmetrically located about the half pump frequency, *i.e.*, such that $f_1+f_2=f_{\text{pump}}$ have also been observed and are not difficult to produce.

Noise figure measurements are in progress. Final performance figures will be reported later.

C. B. De Loach
W. M. Sharpless
Bell Telephone Labs.
Holmdel, N. J.

Bandwidth of Ferrite Phase Shifters for Phased Array and Direction-Finding Use*

For any beam steering application where a wide RF bandwidth is required the dependence of $\Delta\phi$, the relative phase shift, on λ, the RF wavelength is of primary importance. Fig. 1 shows the significant lengths involved in two elements of an array. The direction of the beam off normal is given by

$$\sin\theta = \frac{h}{S}, \tag{1}$$

where S is the fixed spacing between the elements. If the RF wavelength changes from λ_1 to λ_2, then the electrical phase β, represented by the distance h, changes from

$$\frac{2\pi h}{\lambda_1} \quad \text{to} \quad \frac{2\pi h}{\lambda_2},$$

* Received by the IRE, April 10, 1959. This research was supported by the AF Cambridge Research Center under contract number AF 19(604)-2407.

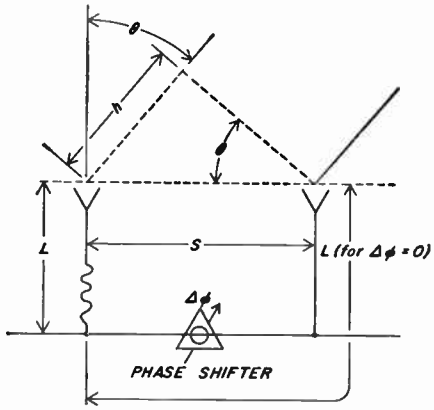

Fig. 1—Schematic diagram of array elements.

i.e.,

$$d\beta = \frac{-2\pi h}{\lambda_1\lambda_2}d\lambda = -\frac{\beta_1}{\lambda_2}d\lambda.$$

Since S remains constant and the distance from aperture to feed point (L) for the two elements is the same, this difference in phase must be compensated by the phase shifter, or

$$d\Delta\phi = -\frac{\Delta\phi_1}{\lambda_2}d\lambda. \tag{2}$$

For a ferrite phase shifter (in a nondispersive structure, *e.g.*, stripline or coax) the electrical length is given by

$$\phi = \frac{2\pi\sqrt{\epsilon\mu}\,l}{\lambda}, \tag{3}$$

where

ϵ = dielectric constant of ferrite.
μ = real part of effective permeability of the ferrite (a function of magnetic field and frequency).
l = length of ferrite.
λ = wavelength in air dielectric.

The interesting quantity is μ. For a stripline ferrite phase shifter operating on the high field side of resonance, a typical curve of μ vs H, the applied field, for two different wavelengths is given in Fig. 2.

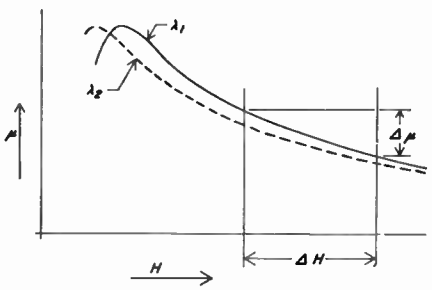

Fig. 2—Permeability vs applied field for ferrite operating on the high-field side of resonance.

From (3) the change in ϕ as a function of H, or the relative phase shift, is given by

$$\frac{\Delta\phi}{\Delta H} = \frac{\pi\sqrt{\epsilon}\,l}{\sqrt{\mu}\,\lambda}\frac{\Delta\mu}{\Delta H} \tag{4}$$

Now the change in relative phase shift as a function of λ (dropping ΔH's) is given by

$$\frac{d\Delta\phi}{d\lambda} = \pi\sqrt{\epsilon}\,l\left[\frac{1}{\sqrt{\mu}\,\lambda_0}\frac{d\Delta\mu}{d\lambda} - \frac{\Delta\mu}{2\mu^{3/2}\lambda}\frac{d\mu}{d\lambda} - \frac{\Delta\mu}{\sqrt{\mu}\,\lambda^2}\right] \tag{5}$$

Phase shifters are usually operated as far off resonance as possible, and in this region both

$$\frac{d\Delta\mu}{d\lambda} \quad \text{and} \quad \frac{d\mu}{d\lambda}$$

are quite small. In addition, the two variations are usually of opposite sign and tend to compensate. This being true it remains that

$$d\Delta\phi = -\frac{\pi\sqrt{\epsilon}}{\sqrt{\mu}}\frac{l}{\lambda}\frac{d\lambda}{\lambda} = -\Delta\phi\frac{d\lambda}{\lambda}, \tag{6}$$

which is the functional dependence desired. For large wavelength changes where true derivatives do not hold

$$d\Delta\phi = -\Delta\phi_1\frac{d\lambda}{\lambda_2}, \tag{7}$$

where $\Delta\phi_1$ is the phase shift at λ_1.

In summary then, a ferrite phase shifter device can operate over an extremely broad band if care is exercised in selecting its operating region so that

$$\frac{1}{\sqrt{\mu}\,\lambda_0}\frac{d\Delta\mu}{d\lambda} - \frac{\Delta\mu}{2\mu^{3/2}\lambda}\frac{d\mu}{d\lambda} \approx 0. \tag{8}$$

Measured phase shift curves at 400 and 500 mc are shown in Fig. 3 for a stripline

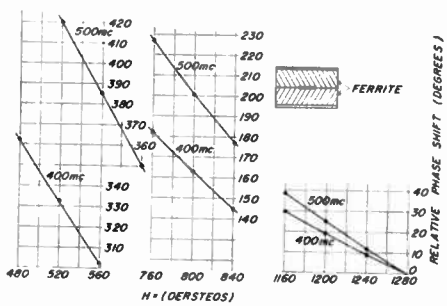

Fig. 3—Measured phase shift characteristics of a stripline ferrite phase shifter.

ferrite phase shifter operating in an axial magnetic field on the high-field side of resonance. These curves are normalized at 1280 oersteds. From this point down to $H=760$ oersteds, $\Delta\phi$ is 227.0° at 500 mc ($\lambda=60$ cm) and 182.0° at 400 mc ($\lambda=75$ cm). The difference between the two gives $d\Delta\phi=45°$. From (7)

$$d\Delta\phi = 227.0 \times 15/75 = 45.4°$$

or

$$d\Delta\phi = 182.0 \times 15/60 = 45.5°.$$

Thus, there is very close agreement between the measured characteristic and the simple ideal relation.

C. M. Johnson
Electronic Communications, Inc.
Timonium, Md.

Contributors

W. N. ARNQUIST

Warren N. Arnquist was born in New Richmond, Wis., on August 12, 1905. He received the B.S. degree in physics and mathematics from Whitman College, Walla Walla, Wash., in 1927 and the Ph.D. in physics in 1930 from the California Institute of Technology, Pasadena.

In 1930 he became assistant professor and later associate professor of physics at the Alabama Polytechnic Institute. During the years 1935–1941 he was a physicist at the Gulf Research and Development Company in Pittsburgh, Pa., and the World War II years were spent as research associate and later section supervisor at the California Institute of Technology in rocket development work under an OSRD contract. In 1945 he joined the newly established Naval Ordnance Test Station as assistant head, Experimental Operations Department, and in 1947 he transferred to the Office of Naval Research Branch Office, Pasadena, Calif. After a two-year tour of duty as Scientific Liaison Officer at the London Branch Office of ONR in 1953–1955 and a comparable period in the Western Regional Office of the Office of Ordnance Research, in 1958 he joined the Systems Development Corporation, where he is now Assistant Director for Research in the Engineering Directorate. Since 1958 he has been a consultant to the Research Projects Laboratory of the Army Ballistic Missile Agency; he has been a member of the teaching staff of the Mechanical Engineering Department, University of Southern California, Los Angeles, since 1956.

His major fields of research include atomic physics, electrical measurements, two-phase fluid flow, dielectric phenomena, rocket propulsion and exterior ballistics, ballistic range instrumentation and safety, upper atmosphere physics, semiconductors, and military infrared. During the years 1949–1953 he organized and conducted the series of conferences on military infrared problems which later became the Infrared Information Symposia (IRIS), and he was a member of Project Metcalf, which studied the Navy's research and development infrared program in 1951–1953. He was a member of the Executive Committee of IRIS from 1955 to 1958. He has attended a number of international scientific conferences including the meeting of the International Consultative Radio Committee in London, 1953, and the eleventh general assembly of URSI at The Hague, The Netherlands, in 1954, as a member of the U. S. delegation.

Dr. Arnquist is a fellow of the American Physical Society and of the American Association for the Advancement of Science, and a member of Phi Beta Kappa and Sigma Xi.

G. F. AROYAN

George F. Aroyan (S'55–M'57) was born in Poitiers, France, in June, 1923. He received the B.S. degree from the U. S. Naval Academy, Annapolis, Md., in 1945, the degree of Naval Engineer from the Massachusetts Institute of Technology, Cambridge, in 1951, and the M.S. degree in electrical engineering from the University of California at Berkeley in 1956. He served in the U. S. Navy as an officer from 1945 until 1954 in various shipboard and technical assignments.

From 1956 to the present, he has been employed as a member of the technical staff at Ramo-Wooldridge, where he has been engaged in project management, infrared system studies, and research in electro-optical filtering and signal modulation methods.

❖

S. S. BALLARD

Stanley S. Ballard was born in Los Angeles, Calif., on October 1, 1908. He received the A.B. degree from Pomona College, Claremont, Calif., in 1928 and the M.A. and Ph.D. degrees in physics from the University of California at Berkeley in 1932 and 1934, respectively. He has been in academic work for most of his professional life, first at the University of Hawaii, Honolulu, then at Tufts College, Medford, Mass., where he was Chairman of the Physics Department from 1946 to 1953, and then as a research physicist at the University of California's Scripps Institution of Oceanography, La Jolla. Since 1958, he has been Professor of Physics and Chairman of the Department of Physics of the University of Florida in Gainesville.

During World War II he served for over five years on active duty as a naval reserve officer in the ranks of lieutenant, lieutenant commander, and commander. His chief assignment was in the Bureau of Ordnance of the Navy Department, where he was in charge of research and development of optical and infrared instrumentation, with additional duty in guided missile research and development. At the Bikini atom bomb tests in the summer of 1946 he was chief of the radiometry section, with the assignment of measuring the total radiation and the spectra of the two explosions.

After the war, he continued his interest in infrared instrumentation, first as a consultant to Baird Associates (now Baird-Atomic, Inc.). His major infrared activities since 1952 have been as a consultant to The RAND Corporation, with a year of full-time employment in the Electronics Division of RAND, 1953–1954, most recently, he has pursued his interest in infrared optical materials at the Willow Run Laboratories of the University of Michigan, Ann Arbor.

Dr. Ballard is the author of many classified reports and of numerous scientific papers in pure and applied physics. He is co-author of "Physics Principles" (D. Van Nostrand Co., 1954), a college textbook of engineering physics. He is active in scientific societies both in this country and abroad. He is a fellow of the American Physical Society, the Physical Society of London, the Optical Society of America, and the American Association for the Advancement of Science, and is a member of several additional organizations, such as the German Society of Applied Optics, the Netherlands Physical Society, the Hawaiian Academy of Science, and the Florida Academy of Sciences. He is a member of Phi Beta Kappa and of Sigma Xi.

Dr. Ballard has served as an officer and member of the board of directors of the Optical Society of America since 1947, most recently as vice-president for meetings. He was vice-president of the International Commission of Optics from 1948 to 1956, and president from 1956 to 1959. He was chairman of the Western Spectroscopy Association, 1956–1957, and executive secretary of the Armed Forces-National Research Council's Committee on Vision, 1956–1959. He is national president of Sigma Pi Sigma, the collegiate physics honor society. He has been active in organized infrared activities, having been program chairman for 1953–1954 of the West Coast IRIS organization and subsequently a member of the national executive committee and an associate editor of *Proceedings of IRIS*.

❖

E. E. BELL

Ely E. Bell was born on December 26, 1915 in Trinidad, Colo. He received the B.A. and M.A. degrees in Physics from the University of Colorado, Boulder, and the Ph.D. degree from The Ohio State University, Columbus, in 1947.

He has worked chiefly with infrared problems, including the study of detectors, high-resolution molecular spectra, and far-infrared spectral measurements. He has measured the infrared radiance from flames and from sky and terrain. He worked on the infrared properties of impurities in silicon and germanium during the year 1952–1953 while at the Naval Research Laboratory. He has been a member of the Physics

Department at The Ohio State University since 1947, and is now an Associate Professor. He served during the summer of 1959 as a consultant to the Infrared Systems Department of Ramo-Wooldridge.

Dr. Bell is a member of the American Physical Society.

❖

R. J. Cashman was born in Wilmington, Ohio on September 27, 1906. He received the A.B. degree from Bethany College, W. Va., in 1928, and the M.A. and Ph.D. degrees in 1930 and 1935, respectively, both from Northwestern University, Evanston, Ill. He received an honorary Doctor of Science degree in 1953 from Bethany College.

R. J. Cashman

He has been associated with Northwestern University since 1928, successively as instructor in physics, 1930–1936, assistant professor, 1936–1941, associate professor, 1941–1947, and professor since 1947. He was on leave during 1941 doing infrared research work at the University of Michigan, Ann Arbor. After World War II, he received certificates for war research from the Army and Navy. His research has been concerned primarily with the study of photoelectric phenomena and associated electrical and optical properties of metal films and semiconductors. Some of these researches have resulted in several inventions in photoemissive and photoconductive devices which have applications in the detection and measurement of ultraviolet and infrared radiations, and in sound reproduction from optical sound tracks.

Dr. Cashman is a fellow of the American Physical Society, and a member of the Optical Society of America and Sigma Xi.

❖

William A. Craven, Jr. (S'49–A'51–M'56) was born on December 16, 1923 in East Orange, N. J. He received the B.S. and M.S. degrees in electrical engineering in 1947 and 1948, respectively, from Princeton University, Princeton, N. J. He served three years with the United States Air Force, during which time he attended the Radar School (Harvard-M.I.T.) and performed radar field testing. He was the recipient of the National Research Fellowship in Electronics for research on microwave transmission systems at Princeton University in 1949–1950, and also won a Sayre Fellowship at Princeton in 1943.

W. A. Craven, Jr.

Since 1950 he has been a member of the technical staff of Hughes Aircraft Company, with experience in microwave equipment, optical system design, and missile system guidance design and development.

Mr. Craven is a member of Sigma Xi and the Optical Society of America.

❖

Stanton H. Cushner was born in New Castle, Pa., in 1929. He received the B.S. degree in physics from the University of Pittsburgh, Pa., in 1951. From 1951 to 1952 he worked at the U. S. Naval Air Missile Test Center, Point Mugu, Calif. in the test program of an air-to-air missile system and assisted in the analog simulation of the system. From 1952 to 1953, he did graduate work in physics and mathematics at the University of California at Los Angeles.

S. H. Cushner

From 1953 to 1956 he worked at the infrared laboratory at Point Mugu, where he performed infrared measurements on military targets. In 1956 he joined Ramo-Wooldridge, where he has been working on infrared and millimeter-wave passive detection systems.

Mr. Cushner is a member of the Optical Society of America.

❖

Joseph I. Davis (S'48–A'49–M'55–SM'57) was born in Detroit, Mich. on January 2, 1925. He attended the University of Michigan, Ann Arbor, where he received the B.S. degree in 1945 and the M.S. degree in 1948, both in electrical engineering.

J. I. Davis

From 1948 to 1950, he was engaged in microwave antennas and circuit designs for the Sparrow II missile system at Bendix Aviation Research and Development Laboratories. From 1951 to 1955, while employed at Hycon Manufacturing Company, he was responsible for the design and development of the AN/DSM-2 microwave automatic go-no-go missile test set. Subsequently he was in charge of field engineering and data analysis associated with missile test set. From 1956 to 1957, he was chief engineer in charge of Titan ICBM ground instrumentation program at Associated Missile Products Corporation.

In 1957, he joined Hoffman Laboratories Division of Hoffman Electronics Corporation as manager of the Missile and Space Electronics Section. He is currently responsible for design and fabrication of communication ancillary equipment, automatic missile test equipment, digital data-handling systems, and solar power supplies for space vehicles.

Russell De Waard was born in Holland, Mich., on March 12, 1914. He received the B.S. degree in physics with honors from the Polytechnic Institute of Brooklyn, N. Y., in 1950.

R. De Waard

He was employed from 1939 to 1953 in the Physics Division of American Cyanamid Research Laboratory, where, as a research physicist, he was engaged in electro-optical and electromechanical instrumentation for studying physical properties of materials. He joined the Barnes Engineering Company in May, 1953, and is now head of the Detector Section of the Engineering Division, responsible for development and production of thermistor infrared detectors. His work with thermistors has resulted in the development of controlled-time-constant detectors, high-speed detectors, immersed detectors, printed detectors and printed detector arrays. Much of this work is described in NAVORD Report No. 5495, "Thermistor Infrared Detectors, Properties and Developments," which he co-authored with E. M. Wormser.

He has also published several papers on instrumentation for basic studies of physical properties, and holds numerous patents on the designs for electromechanical testing instruments.

Mr. De Waard is a member of the American Physical Society.

❖

Harvey A. Dubner was born in New York, N. Y., on July 14, 1928. He received the Bachelor's and Master's degrees in electrical engineering from the Polytechnic Institute of Brooklyn, N. Y., in 1949 and 1951, respectively.

H. A. Dubner

From 1949 to 1951 he was employed by ARMA Corporation in Brooklyn. Since 1951, he has been with Avion Division, ACF Industries Incorporated, Paramus, N. J.

At present he is manager of the Advanced Development Laboratory, where he is working in the fields of infrared, missile guidance and astronautics.

Mr. Dubner is a member of Eta Kappa Nu.

❖

Richard H. Genoud was born in Portland, Ore. on December 29, 1927. He received the B.E. degree in electrical engineering from Yale University, New Haven, Conn., in 1948 and the M.S. degree in electrical engineering from Stanford University, Stanford, Calif., in 1950.

That same year, he was employed by the

Hughes Aircraft Company as an engineer engaged in the development of infrared equipment. He spent a year with the infrared group in the Engineering Division of The RAND Corporation and in 1957 returned to Hughes Aircraft Company to continue his work in infrared applications.

R. H. Genoud

Mr. Genoud is a member of Tau Beta Pi and an associate member of Sigma Xi.

❖

J. G. Goodenough received the B.A. degree from Cambridge University, England. Following this, he served with the Royal Canadian Air Force, and was engaged in power plant development as a member of an Arctic experiment group. He was later employed as chief engineer and general manager of Dorman, Long and Company, England, and as general manager of Vard, Inc., manufacturers of precision aircraft components. He was also engaged in mechanical engineering at G. M. Giannini Corporation and the Stanford Research Institute at Menlo Park, Calif. He has been at the Santa Barbara (Calif.) Research Center since 1953, responsible for the design and development of balloon-borne instrumentation and the direct transfer method of cooling infrared detectors.

J. G. Goodenough

❖

Milburn B. Grier (SM'57) was born in San Antonio, Tex., on August 12, 1919. He attended Los Angeles City College, Calif., the Moore School of Electrical Engineering, University of Pennsylvania, Philadelphia, and the University of California at Los Angeles, from which he received the B.S. degree in applied physics in 1947. During World War II he was a member of the U. S. Army Signal Corps, specializing in AM and FM communications equipment. From 1947 to 1949 he was a consultant in optics and applied physics. During this period he conducted studies in optics and applied solid-state physics, particularly electro-optics.

M. B. Grier

After additional graduate study in physics at UCLA, he became, in 1951, staff physicist at Burton Manufacturing Company, Los Angeles, Calif. where he was concerned with problems of low-level visual photometry and optical navigation instruments. In 1953, as Assistant to the Research Director of the Ralph M. Parsons Company, Pasadena, Calif., he was concerned with administrative problems associated with electronic missile instrumentation.

Since 1954, he has been with the Northrop Corporation, where he is an engineering specialist in the Infrared Group of the Electronic Systems and Equipment Department, Nortronics Division. Here he has conducted studies in thin-film optics, microcircuitry, and thermoelectricity. He has also conducted studies in the field of optical information, particularly image definition, spectrophotometry, and spatial discrimination.

Mr. Grier is a member of the Optical Society of America, the AAAS, and the American Physical Society.

❖

Freeman F. Hall, Jr. was born in Kansas City, Mo., on September 29, 1928. He received the B.A. degree in physics from Occidental College, Los Angeles, in 1950 and the M.S. degree from the University of California at Los Angeles in 1957. From 1951 to 1953 he served with the First Guided Missile Battalion, U. S. Marine Corps.

F. F. Hall, Jr.

After a year as research assistant at the University of New Mexico, he joined Lockheed's Missile Systems Division at Van Nuys, Calif. in 1954. While there, he was concerned with missile instrumentation and solar furnace investigations of nose cone materials. Since 1957 he has been with ITT Laboratories in San Fernando, Calif. working principally on research and development of infrared systems and components, including image converters, and a large satellite tracking radiometer.

Mr. Hall is a member of the Optical Society of America, the American Meteorological Society, Phi Beta Kappa, and Sigma Pi Sigma.

❖

Marvin R. Holter was born on July 4, 1922, near Rochester, N. Y. He received the B.S. degree in physics in 1949, the M.S. degree in mathematics in 1951, and the M.S. degree in physics in 1958, all from the University of Michigan, Ann Arbor. During the period 1940–1946, he held positions as draftsman and designer with the St. Regis Paper Company in Oswego, N. Y.; The Ford Willow Run Bomber Plant in Ypsilanti, Mich.; The Mixing Equipment Company in Rochester, N. Y.; and The Palmer Bee Company in Hamtramck, Mich. During the period 1947–1956, he was research assistant and research engineer at what is now called the Willow Run Laboratories of the University of Michigan, working with radar, infrared, digital and analog computers, air-defense system design, and as supervisor of Project Wizard concerned with defense against ballistic missiles. In 1956–1957, he was associate professor of engineering mechanics at The University of Toledo, Ohio. Since 1957, he has been with the Willow Run Laboratories, first as a member of the Technical Operations and Long Range Planning Staffs and presently as head of the Sensory Devices Group of the Infrared Laboratory.

M. R. Holter

❖

John N. Howard was born in Philadelphia, Pa., on February 27, 1921. He received the B.S. degree from the University of Florida in 1943. He received the M.S. and Ph.D. degrees in physics in 1949 and 1953, respectively, both from The Ohio State University, Columbus.

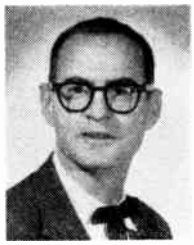

J. N. Howard

After spending a year in the Spectroscopy Laboratory of the University of Florida, he joined the Spectroscopy Laboratory of the National Advisory Committee for Aeronautics (now NASA) in Cleveland, Ohio, where he spent two years in ferrous and nonferrous spectrochemical analysis and had his first exposure to infrared. His two years of military service were served as a Special Agent in the Air Force Counter-Intelligence Corps, following which he returned to graduate school. Since 1954 he has been associated with the Geophysics Research Directorate of the Air Force, Bedford, Mass., where he is chief of the Infrared Techniques Branch.

Dr. Howard is a member of the American Physical Society, the Optical Society of America, the Society for Applied Spectroscopy, Phi Beta Kappa, and Sigma Xi. He is an Air Force Member of the Steering Committee of IRIA and of the Executive Committee of IRIS.

❖

Jerome E. Jacobs (S'48–A'52–M'57–SM'57) was born in Rochester, N. Y. on January 27, 1919. He received the B.S. and M.S. degrees in electrical engineering in 1950 and 1951, respectively, from the California Institute of Technology, Pasadena.

J. E. Jacobs

He joined Hughes Aircraft Company in 1950. His work has been in the fields of precision measurements, mechanical

design, circuit analysis, system reliability, electronic circuit design, and systems analysis. He is presently head of the Systems Planning Section of the Missile Systems Department, Systems Analysis Laboratories, Hughes Aircraft Company. Mr. Jacobs is a member of the American Association for the Advancement of Science and RESA.

❖

John A. Jamieson (S'55–M'57) was born in Barnet, England, on March 16, 1929. He received the B.S. degree in electrical engineering from University College, London, in 1953, and the M.S. and Ph.D. degrees from Stanford University, Calif., in 1955 and 1957, respectively.

J. A. Jamieson

He has been employed by the Aerojet-General Corporation of Azusa, Calif. since 1956. He has worked on information processing in infrared systems, especially the analysis of space filtering, and scanner analysis with particular regard to the detector configuration.

Dr. Jamieson is a graduate member of the IEE and a member of Sigma Xi.

❖

R. Clark Jones was born in Toledo, Ohio, on June 30, 1916. He received the A.B. degree in physics summa cum laude in 1938, and the A.M. and Ph.D. degrees in 1939 and 1941, respectively, both in theoretical physics; he received all these degrees from Harvard University, Cambridge, Mass., where he was a National Scholar.

R. C. Jones

In 1941 he became a member of the technical staff at Bell Telephone Laboratories, Murray Hill, N. J., where he worked on sirens of large output, and on acoustic torpedoes. In 1944, he joined the Polaroid Corporation in Cambridge, Mass., where he is now a senior physicist. At Polaroid he has worked in various aspects of the military application of infrared, on instrumentation for cancer research, on the properties of instruments that use polarized light, on detectors for visible and infrared radiation, and on the performance of photographic films.

He has published about sixty scientific papers, most of them in optics or acoustics. He is a member of the Optical Society of America, the Acoustical Society of America, the American Astronomical Society, the Society of Photographic Scientists and Engineers, and the Archaeological Institute of America. He is also a member of Phi Beta Kappa, Sigma Xi, and the American Academy of Arts and Sciences, and received the Adolph Lomb Medal of the Optical Society of America in 1944.

Dr. Jones is currently a member of the USA National Committee of the International Commission on Optics, is editorial vice-president of the Society of Photographic Scientists and Engineers, and is a consultant to the Defense Department.

❖

Myron W. Klein was born in Rochester, N. Y., on June 17, 1919. He received the A.B. degree in physics from the University of Rochester in 1943.

M. W. Klein

Entering the Armed Forces in June, 1943, he took basic training at Fort Riley, Kans., and studied at the University of Nebraska at Lincoln under the Army Student Training Program. Later, he taught mathematics in the Ordnance Automotive School at Fort Crook, Neb., then was assigned to the Engineer Board (now the U. S. Army Engineer Research and Development Laboratories), Fort Belvoir, Va., where he worked on the development of the first infrared Sniperscope and Metascope. He was awarded the Legion of Merit for his work in this field. Following his release from the Army in February, 1946, he remained at the Laboratories in a civilian capacity and is presently employed as chief of the Research Section of the Warfare Vision Branch.

Mr. Klein is a member of the Optical Society of America.

❖

Kenneth V. Knight was born in Carrollton, Ohio, on November 30, 1914. He received the B.A. degree in math-physics from Ohio Wesleyan University in 1936, the M.A. degree in mathematics from Syracuse University in 1936, and the M.S. degree in mathematics from the University of Illinois in 1940. He served American District Telegraph Company as a technical writer during 1940–1941, and American Optical Company as a mathematician-physicist from 1941 to 1944. He was an optical project officer in the U. S. Naval Reserve, and was assigned to the Navy Department Bureau of Ordnance from 1944 to 1946. For the next ten years he was a Navy Department physicist specializing in aircraft fire control, with emphasis on research and development of infrared and optical-electronic techniques.

K. V. Knight

In Space Technology Laboratories, Mr. Knight was inertial guidance project engineer and operations planner for one on the ICBM projects from 1956 to 1958. He then joined the Infrared Systems Department at Ramo-Wooldridge, where he is now chief project engineer.

He is a member of Pi Mu Epsilon, Sigma Pi Sigma, and Phi Beta Kappa.

❖

Maxwell R. Krasno was born in Berlin, Wis., on July 1, 1908. He received the B.A. degree in physics from the University of Wisconsin, Madison, in 1930. He taught in the physics department and did research in physics and electrophysiology at the University of Wisconsin, where he received the M.A. and Ph.D. degrees in physics in 1932 and 1935, respectively.

M. R. Krasno

He joined the Clough-Brengle Company in 1937, and designed laboratory instruments and radio test equipment. From 1940 to 1946 he was employed by Electronic Laboratories at Indianapolis and Toronto, where he designed and was in charge of design of vibrator converters and power supplies, high-intensity electrical flash equipment for IFF, emergency landing beacons, and infrared equipment. Since 1951 he has been with Raytheon Company at Santa Barbara. As manager of the Infrared Engineering Department, he has directed all of Raytheon's research, development, and design effort in infrared communications, reconnaissance, detection, and fire control systems.

Dr. Krasno is a member of the Optical Society of America, Sigma Xi, and the American Rocket Society.

❖

Edgar W. Kutzscher was born in Leipzig, Germany, on March 21, 1906. He received his professional education at the Universities of Leipzig, Goettingen, and Berlin. He received the Ph.D. degree in physics and chemistry from the University of Berlin, where he also was a research assistant. Later, he received the Doctor's degree in applied physics from the Institute of Technology in Berlin, where he became a member of the faculty and the head of the Infrared Department of the Institute. Parallel to this position, he was the head of the Ground-to-Air Detection Group of the Technical Development Division of the German Air Force Department. From 1937 until the end of World War II, he organized and was the head of the Infrared Research and Development Division of the Electroacustic Company in Kiel, Ger-

E. W. Kutzscher

many. In this capacity, he was responsible for many of the infrared component and system developments for the German Air Force and Navy Departments.

Shortly after the war, the United States Navy offered him a contract. He worked until 1951 as a specialist in the infrared field at the U. S. Naval Air Missile Test Center, Point Mugu, Calif., and then as the head of the solid-state physics department of the Santa Barbara Research Center for two and a half years. In 1954, he joined Lockheed Aircraft Corporation, California Division, and is presently the head of the Infrared Department.

❖

Lewis Larmore was born in Anderson, Ind. on July 29, 1915. He received the A.B. and M.A. degrees in physics from Indiana University, Bloomington, in 1937 and 1938, respectively. In 1939 he was granted the M.A. degree in astronomy from Indiana University following a one-year fellowship at Lowell Observatory, Flagstaff, Ariz. He received the Ph.D. degree in physics from the University of California at Los Angeles in 1952.

L. LARMORE

During 1943 and 1944, he served as instructor in physics at the University of Utah, Salt Lake City. From 1944 to 1946, he served in the U. S. Navy as an aerial navigator and as a special research investigator at the Harvard Observatory Station at Climax, Colo. Since the war, he has held the posts of head of Physics Division at Arizona State University, physicist at RAND Corporation, Head of Experimental Physics Department at Lockheed Missiles and Space Division, and head of Experimental Physics at Systems Laboratories Corporation. At present, he is the Corporate Research Advisor for the Lockheed Aircraft Corporation.

His primary interests in the infrared field are concerned with atmospheric transmission, infrared stellar emission, and infrared photography. He served for over three years as the program chairman for IRIS and has been an associate editor of the *Proceedings of IRIS* since the founding of the journal. He has published over 20 scientific papers, as well as a textbook on the basic scientific principles of photography.

Dr. Larmore is a member of the Optical Society of America, Sigma Xi, the American Astronomical Society, and the Institute of Navigation.

❖

Henry Levinstein was born in Themar, Germany, on December 4, 1919. He received the B.S. degree in 1942 and the Ph.D. degree in physics in 1947, both from the University of Michigan, Ann Arbor. He was a teaching fellow, a research assistant and lecturer at the University of Michigan from 1942 to 1947. Since 1947 he has been at Syracuse University, N. Y., where he is now professor of physics.

He has done research in electron microscopy and surface phenomena. His main interest has been the study of the physical properties of infrared detector materials. This has led to the development of several types of detectors. He has acted as consultant to several companies and government agencies in connection with that work.

H. LEVINSTEIN

Dr. Levinstein is a member of the American Physical Society, the American Association of Physics Teachers, and Sigma Xi.

❖

Richard K. McDonald was born in Paris, France, on December 16, 1927. He received the B.S. degree in physics in 1948, and the M.S. degree in physical chemistry in 1950, both from the University of Washington, Seattle.

R. K. MCDONALD

During the years 1950 to 1952 he worked as a research chemist for the Weyerhaeuser Timber Company and the Reichhold Chemical Company. Since then he has been employed by the Boeing Airplane Company in Renton, Wash. Here his work gradually shifted from analytical chemical instrumentation to infrared spectroscopy, to radiometric laboratory work, to military applications of infrared. Currently he is concerned with the application and design of infrared equipment for airborne weapons systems.

Mr. McDonald is a member of the Optical Society of America and the American Chemical Society.

❖

Raymond H. McFee was born in Somerville, Mass. on March 1, 1916. He received the B.S. and M.S. degrees in 1937 and 1938 respectively and the Ph.D. degree in physics in 1943, from the Massachusetts Institute of Technology, Cambridge, Mass.

R. H. MCFEE

Since then, he has been engaged in various phases of infrared research and development. He spent ten years with the Electronics Corporation of America, where he was Director of Research. He joined Aerojet-General Corporation in 1956, and is presently the Director of Research for the avionics division of that corporation. In this capacity, he supervises the company's research activities in infrared, which include systems analysis, preliminary design, radiation, measurements, and components research.

Dr. McFee is a member of the American Physical Society, the Optical Society of America, and the American Association of Physics Teachers, and is a fellow of the American Association for the Advancement of Sciences.

❖

Hans F. Meissinger (M'55–SM'59) was born in Villingen, Germany, on November 25, 1918. He received the Dipl.Ing. degree in mechanical engineering from Berlin Technical University, Germany, in 1942 and the M.S. degree in applied mathematics from New York University, N. Y., in 1949.

H. F. MEISSINGER

From 1942 to 1945, he did research on problems of aerodynamic stability and automatic control as a staff member of the German Aeronautical Research Laboratories (DVL), Berlin-Adlershof. In 1947 he joined the staff of Project Cyclone, Reeves Instrument Corporation, New York, N. Y. and became engaged in the development and application of electronic analog computers. His work primarily involved guided missile simulations and control systems analyses which were performed under contract with the Office of Naval Research and the U. S. Navy Bureau of Aeronautics. Since 1955, he has been with the Hughes Systems Development Laboratories at Culver City, Calif. where he is in charge of the Dynamic Analysis and Simulation Section of the Missile Systems Department.

Mr. Meissinger is the author of numerous technical articles on analog computation and guided missile simulation.

❖

Thomas P. Merritt was born in Chicago, Ill., on June 21, 1914. He received the A.B. degree from North Central College, Naperville, Ill., in 1937, the M.S. degree from Northwestern University, Evanston, Ill., in 1939, and the Ph.D. degree from Boston University, Mass., in 1949.

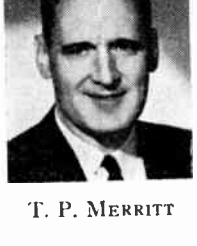

T. P. MERRITT

Between 1940 and 1946 he was employed, successively, as Special Agent and Physicist for the F.B.I., Research Associate at the Harvard University Underwater Sound Laboratory, and Physicist for Polaroid Corporation. He taught physics at Simmons College in Boston, and was for the six years between 1949 and 1955 head of the Department of Mathematics and Physics at Albright College, Reading, Pa.

Since 1955, he has held the position of Optics Group Engineer at Lockheed Aircraft Engineering Research Laboratory in Burbank, Calif. and has been senior member of the technical staffs at Systems Laboratories Corporation and ITT Laboratories. He is presently employed as senior scientific adviser in the Development Planning Department of Lockheed Aircraft Corporation. His fields of concentration have been physical optics and solid-state physics, with recent emphasis in the area of infrared technology.

Dr. Merritt is a member of the American Physical Society, the American Association of Physics Teachers, Sigma Xi, and Sigma Pi Sigma.

❖

George A. Morton (A'39–SM'46–F'51) was born in New Hartford, N. Y., on March 24, 1903. He received the B.S. degree in electrical engineering in 1926, the M.S. degree in electrical engineering in 1928, and the Ph.D. degree in physics in 1932, all from the Massachusetts Institute of Technology, Cambridge.

G. A. Morton

From 1933 to 1941 he was a research engineer at the RCA Manufacturing Company in Camden, N. J., and from 1942 to 1946 he was a member of the technical staff of RCA Laboratories in Princeton, N. J. In 1946, on leave from RCA, he was employed as a nuclear physicist at the U. S. Atomic Energy Commission in Oak Ridge, Tenn. In 1947 he returned to RCA Laboratories at Princeton as a member of the technical staff, and from 1955 to the present time he has been Associate Director of the Physical and Chemical Research Laboratory.

He has contributed in the fields of infrared, scintillation counting, television, and electronics and has many publications in these fields. He is also co-author of several volumes on television and electron optics. During World War II and after, he served as a member of the National Defense Research Committee, AAF Scientific Advisory Board, and the Infrared Panel of the Research and Development Board.

Dr. Morton is a Fellow of the American Physical Society and a member of Sigma Xi, American Association for the Advancement of Science, and AIEE.

❖

Lloyd G. Mundie was born in Udney, Ont., Canada, on December 15, 1916. He obtained the B.S. and M.S. degrees in physics at the University of Saskatchewan, Saskatoon, Sask., in 1935 and 1937, respectively. In 1943 he was awarded the Ph.D. degree in physics by Purdue University, Lafayette, Ind., for his research in interference spectroscopy, in which he used the atomic beam in emission for hyperfine structure studies.

He continued working in this field until 1947, when he joined the Naval Ordnance Laboratory, Silver Spring, Md., as an infrared physicist; here, he was concerned primarily with detector testing techniques. In 1951 he joined the National Bureau of Standards, and was transferred to the Corona, Calif., Laboratories. In 1953, these laboratories were incorporated into the Defense Department as the Naval Ordnance Laboratory, Corona.

L. G. Mundie

In 1954 Dr. Mundie took charge of the Infrared Laboratory of the Willow Run Laboratories, University of Michigan, Ann Arbor, where he directed research and development in many areas of military infrared, including detector research, thermal maging, airborne scanner development and background studies. He was also instrumental in establishing the Infrared Information and Analysis (IRIA) facility. He transferred to the Systems Division of the Bendix Aviation Corporation, Ann Arbor, Mich. in 1957, where he is head of the Surveillance and Detection Department

He is a member of Sigma Xi, Sigma Pi Sigma, and Optical Society of America.

❖

L. W. Nichols was born in Phoenix, Arizon February 10, 1919. He received the B.S. degree from the University of Arizona, Tucson, in 1941.

L. W. Nichols

In the period 1941–1946, he worked for several companies in the field of precision optical instruments. Since 1946, he has been employed by the Naval Ordnance Test Station, China Lake, Calif. where he has done research and development work on projects involving military infrared equipment. He is now head of the Research Division of the Aviation Ordnance Department at the Naval Ordnance Test Station.

❖

Paul J. Ovrebo was born in Summit, S. Dak., in 1901. He received the B.A. degree from St. Olaf College, Northfield, Minn., in 1923, and the Ph.D. degree in physics from the University of Chicago, Ill., in 1928. He was assistant professor of physics at West Virginia University, Morgantown, from 1928–1930, and then professor of physics at Susquehanna University, Selinsgrove, Pa.

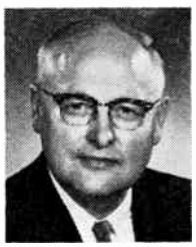

P. J. Ovrebo

In 1943, he became a project engineer in the Special Projects Laboratory at Wright-Patterson Air Force Base, Dayton, Ohio, where he directed and participated in the development of radio-frequency power measurement equipments for use with RF countermeasure transmitters. He obtained six patents covering phases of this work; he also participated in making measurements on the altitude dependence of cosmic ray air showers. In 1945 he became unit chief of the Infrared Section. Later he became section chief of the Applied Physics Section of the Aerial Reconnaissance Laboratory. He participated in the first night-time air-to-air infrared detection and tracking of an aircraft. Following this, he directed and participated in a program for making ground-level measurements of the infrared patterns of U. S. aircraft. Concurrently, he directed and participated in a program of night-time, air-to-air detection and tracking of aircraft which was to lay the basis for much of the Air Force program of development that was to follow. Following the successful air-to-ground night-time detection of a blacked-out power plant and later of tanks and trucks, a program of measurements against ground targets was begun. This led to a program of development of infrared reconnaissance equipments.

He has served on various Air Force and Department of Defense ad hoc groups, as well as on the old NAN Committee and the Infrared Panel of the Electronics Committee of the Research and Development Board. He is responsible for several infrared equipment and systems concepts which are presently being developed.

In 1957, Dr. Ovrebo received the honorary degree of Doctor of Science from St. Olaf College for his activities in infrared and military science. He is a member of the American Physical Society, the Optical Society of America, Sigma Xi, and Sigma Pi Sigma. He has held several amateur radio licenses, the first being issued in 1916 with the call letters 9AHS.

❖

Sidney Passman was born in New York, N. Y., on August 5, 1927. He was graduated from Columbia College, N. Y., in 1948 with honors, special distinction in physics. He did his graduate work at Columbia University, N. Y., receiving the A.M. degree in 1949 and the Ph.D. in physics in 1952. While a graduate student, he served as a research assistant in nuclear physics at the Columbia Cyclotron Laboratories. During the period 1945–1946, he served in the U. S. Navy as a radar technician.

S. Passman

In 1952, upon joining the Hughes Research and Development Laboratories, he began working in the infrared detection field in connection with the early design, systems analysis, and flight testing of the IR-guided Falcon air-to-air missile. In addition to IR scanning system analysis and IR atmos-

pheric transmission studies, Dr. Passman was an early worker in the field of infrared countermeasures. At the time he left Hughes to join The RAND Corporation, in 1955, he was project engineer responsible for an all-infrared weapon system project involving IR fire control as well as missile considerations. At The RAND Corporation, he took over the infrared group activities begun by his predecessors and co-editors of this issue, Drs. S. S. Ballard and L. Larmore, with whom he joined in writing RAND Report R-297, "Fundamentals of Infrared for Military Applications."

In the last four years, his principal activities in infrared have been concerned with air warfare and ballistic missile defense systems applications. He has also been active in the affairs of the IRIS organization, having served as Program Officer and member of the National Executive Committee for the past two years. He is active in scientific committee work for various parts of the Department of Defense, and has served as a consultant to the Advanced Research Projects Agency and the Air Force Scientific Advisory Board.

Dr. Passman is a member of the Optical Society of America, the American Physical Society, Sigma Xi, and Phi Beta Kappa.

❖

Richard L. Petritz (A'54) was born on October 24, 1922, in Rockford, Ill. He received the B.S. degree in 1944, the B.S.E.E. degree in 1946, the M.S.E.E. degree in 1947, and the Ph.D. degree in theoretical physics in 1950, all from Northwestern University, Evanston, Ill. In the interim, 1944–1946, he served as radar officer aboard a destroyer which received the Presidential Unit Citation. While completing his graduate studies at Northwestern University, where he was a Walter P. Murphy Fellow, he held various part-time positions including: instructor, Department of Electrical Engineering; and electronics engineer at Aerial Measurements Laboratory. During the summer of 1949, he was a research assistant in the Theoretical Division at Los Alamos Scientific Laboratory.

R. L. PETRITZ

In 1950 he joined the faculty of the Department of Physics of the Catholic University of America, Washington, D. C.; he also worked part-time with the Semiconductor Branch at the Naval Ordnance Laboratory, White Oak, Md. In 1954, he joined the Naval Ordnance Laboratory on a full-time basis as chief of the Semiconductor Research Branch. During the period of 1954–1958, Dr. Petritz continued his association with the academic profession by lecturing at the University of Maryland, College Park, and sponsoring graduate student research for the University of Maryland, Catholic University, and M.I.T. In July, 1958 he joined the Central Research Laboratory of Texas Instruments Incorporated as Director of the Device Research Department.

He has published over twenty research papers pertaining to the field of semiconductor physics and devices, theory of noise, surface physics, information theory, and photoconductivity.

The IRE, in March, 1954 awarded him the Browder J. Thompson Memorial Prize, and in December, 1954, the U. S. Navy honored him with the Meritorious Civilian Service Award.

Dr. Petritz is a member of the American Physical Society, Eta Kappa Nu, Tau Beta Pi, Sigma Xi, and the Washington Philosophical Society.

❖

Gilbert N. Plass was born in Toronto, Ont., Canada on March 22, 1920. He received the B.S. degree in physics from Harvard University, Cambridge, Mass., in 1941 and the Ph.D. degree in physics from Princeton University, Princeton, N. J., in 1947. From 1941 to 1945, he was associated with some of the early work on nuclear reactors at the Metallurgical Laboratory in Chicago. He was a member of the faculty of The Johns Hopkins University, Baltimore, Md., from 1946 to 1955, most recently as an associate professor of physics. During this period he was also a visiting associate professor of physics at Northwestern University, Evanston, Ill., and at Michigan State University, East Lansing. From 1955 to 1956, he was a research associate for the Lockheed Aircraft Company.

G. N. PLASS

Since then, he has been a member of the senior staff, Office of Advanced Research, of Aeronutronic Systems, Inc.

He has done research in such fields as infrared physics, high-temperature emissivities, properties of planetary atmospheres, classical equations of motion with radiative reaction, action-at-a-distance theories of electromagnetism and gravitation, electrostatic electron optics, theory of nuclear reactors, and theories of climatic change.

Dr. Plass is a fellow of the American Physical Society and the Royal Meteorological Society, and a member of the Optical Society of America and the American Meteorological Society.

❖

Roy F. Potter received the B.S. degree in physics from the University of Washington, Seattle, in 1947, and the M.S. degree in physics from the University of Maryland, College Park, in 1951.

He joined the staff of the National Bureau of Standards in 1948 and was a member of the Solid-State Physics Section until he joined the staff of the Naval Ordnance Laboratory at Corona, Calif. in 1957, where he is presently head of the Infrared Division. Some of his publications have been on the following subjects: charge transfer phenomena and other gas-ion physics, elastic constants and internal friction measurements in indium antimonide, and piezoresistivity in InSb.

R. F. POTTER

Mr. Potter is a member of the American Physical Society.

❖

Richard W. Powell was born in Powell, Wyo. in 1918, and attended the University of Wyoming, Laramie, from 1935 to 1937. He received the B.S. degree in electrical engineering in 1940 and the M.S. degree in electrical engineering in 1947, both from the California Institute of Technology, Pasadena.

R. W. POWELL

From 1940 to 1948, he was affiliated with Lockheed Aircraft Corporation, where he was in charge of research instrumentation and electrical-component evaluation. During 1948–1950 he was associated with G. M. Giannini and Company, Inc., as Chief Development Engineer, instrument and autopilot research and development.

Since 1950 he has been employed by the Aerojet-General Corporation in various capacities. As chief engineer in the Avionics Division he exercised supervision of research, development, and pilot production of infrared systems and subassemblies. He has been assistant manager of the Avionics Division since 1957.

Mr. Powell is a registered Electrical Engineer of California. He is a member of the Aircraft Industries Association, Electronic Equipment Technical Committee, and the Research Society of America. A member of the Executive Committee of the Infrared Information Symposia, he also serves as the national treasurer of IRIS.

❖

Foster F. Rieke was born in Barrington, Ill. on December 15, 1905. He received the B.S. degree in physics, mathematics, and astronomy from Northwestern University, Evanston, Ill., in 1928. He received the M.A. degree in physics in 1930, and the Ph.D. degree in physics in 1933 from Harvard University, Cambridge, Mass.

F. F. RIEKE

During the time that he was at Harvard, he carried out

research work on the spectroscopic study of the intermolecular transfers of rotational energy, and together with Professor O. Oldenburg, he investigated OH radicals as formed in water vapor by thermal dissociation and by gas discharges. He went to The Johns Hopkins University, Baltimore, Md., in 1936 to take part in research on the mechanism of photosynthesis in green plants, and this work was continued at the University of Chicago, Ill., from 1938 to 1942. Early in 1942 he joined the Radiation Laboratory at the Massachusetts Institute of Technology, Cambridge. There he conducted an extended program of research on microwave magnetrons which had a widespread influence on magnetron development and application; he received the Presidential Certificate of Merit for this work, which is largely summarized in four chapters of Vol. 6 of the Radiation Laboratory Technical Series. In 1946 he went to Purdue University, Lafayette, Ind., as associate professor of physics where he had charge of the design and construction of a linear electron accelerator and associated gear, and also supervised research in gas discharges and in microwaves.

Since 1952, he has been director of the Physics and Chemistry Division of Chicago Midway Laboratories, The University of Chicago, supervising research in semiconductors, infrared detectors, and physical electronics.

Dr. Rieke is a member of the American Physical Society, American Association for the Advancement of Science, Phi Beta Kappa, and Sigma Xi.

❖

David Z. Robinson was born in Montreal, Canada in September, 1927. He received the A.B. degree in chemistry and physics (magna cum laude) in 1946, the A.M. degree in chemistry in 1947, and the Ph.D. degree in chemical physics in 1950, all from Harvard University, Cambridge, Mass.

D. Z. Robinson

In the summer of 1948, he worked as an infrared spectroscopist with Canadian Industries Limited, McMasterville, Quebec. In 1949, he joined Baird Associates Inc. (now Baird-Atomic, Inc.), as a physicist, and in 1952 was made Assistant Director of Research. In 1959 he joined the Office of Naval Research, London Branch, where he is a Scientific Liaison Officer. He has worked on problems in theoretical chemistry; absolute intensities of infrared absorption bands; the Evaporograph, a heat-imaging device; and the application of communication theory to optics.

Dr. Robinson is a member of the Optical Society of America, the Coblentz Society, the Faraday Society, the Infrared Discussion Group, the Photoelectric Spectrometry Group, the Applied Spectroscopy Group of the Institute of Physics, and the Physical Society Optical Group. He is also a member of Phi Beta Kappa and Sigma Xi.

Raymond R. Sawyer was born in Reading, Mass., on April 7, 1926. He received the B.S. degree from St. Anselm's College, Manchester, N. H., and the M.S. degree at the State University of Iowa, Iowa City.

R. R. Sawyer

Following this, he was employed as a spectroscopist in the Tonawanda, N. Y., Research Laboratories of the Linde Division of the Union Carbide Corporation. He is presently head of the molecular spectroscopy group of the Application Engineering Department of the Perkin-Elmer Instrument Division, Perkin-Elmer Corporation, Norwalk, Conn.

❖

Lawrence W. Schmidt (A'56) was born in Carlinville, Ill. on June 22, 1920. He attended the College of Engineering of West Coast University, Los Angeles, Calif., receiving the B.S. degree in electronics in 1950 and the M.S. degree in applied physics in 1952. In 1951 and 1952 he was a Teaching Fellow at West Coast University, teaching basic physics and mathematics. From 1953 to 1956, he was with Hydro-Aire, Inc., Burbank, Calif. doing controls analysis for gas turbines and later manufacturing transistors and transistor circuit design. In 1956, he joined the technical staff of Hoffman Laboratories Division of Hoffman Electronics Corporation, where he has since been concerned with the design and application of silicon solar cells for solar electric power supplies for emergency communication systems and space vehicles.

L. W. Schmidt

❖

Roderic M. Scott was born on April 9, 1916 in Sandusky, Ohio. In 1938 he received the B.S. degree in physics from the Case School of Applied Science, Cleveland, Ohio, and the M.A. degree and, in 1945, the Ph.D. degree in astronomy, both from Harvard University, Cambridge, Mass.

R. M. Scott

He taught physics and astronomy at Vanderbilt University, Nashville, Tenn. in 1941 and 1942.

During World War II he was asked to join a group at Harvard to aid in research on submarine warfare, mainly in the field of underwater sound detection. He was research assistant at Harvard from 1942 to 1945, an editor for the Summary Technical Report of NDRC Division 6 (Underwater Sound), and has been a member of the Commission on Underwater Sound. In 1945, he was employed by the Sharples Corporation in Philadelphia, Pa., as a research physicist, where he acquired several patents on powdered metals. He joined the Perkin-Elmer Corporation in 1948 as Assistant Director of Research, becoming Director of Engineering, and in 1956, Vice-President and General Manager of the Electro-Optical Division. During these periods, he has administered a large number of programs involving the design, development, and production of optical instruments. In January, 1958, he was appointed Consulting Scientist for the Corporation and at the present time directs the recently organized Reconnaissance Branch. His special fields include spectroscopy, infrared, electronics, servomechanisms, supersonics, spherical and aspherical optics.

Dr. Scott is a member of the American Astronomical Society, American Ordnance Association, American Physical Society, American Society of Photogrammetry, Optical Society of America, and the Society of Photographic Scientists and Engineers.

❖

Werner K. Weihe (A'50–SM'54) was born in Magdeburg, Germany, in 1903. He attended the Universities of Halle and Jena, Germany, and received from the latter the degree of Dr.phil.nat. in 1928.

W. K. Weihe

From 1928 to 1930, he was a member of the Research Institute of the Allgemeine Elektrizitaets-Gesellschaft, Berlin, Germany. In 1930 he joined the Carl Zeiss Company, Jena, Germany, and became, in 1935, chief of its Electrotechnical Laboratory in charge of research and development of optical-electrotechnical devices. In 1945 he came to the U. S. and joined the U. S. Army Engineer Research and Development Laboratories, Fort Belvoir, Va., where he is now chief of the Far-Infrared Branch.

Dr. Weihe is a member of the Optical Society of America, the USAERDL Branch of the Scientific Research Society of America, and the National Executive Committee of IRIS.

❖

Robert S. Wiseman was born in Robinson, Ill., on February 27, 1924. He received the B.S., M.S., and Ph.D. degrees in electrical engineering in 1948, 1950, and 1954, respectively, all from the University of Illinois, Urbana. He joined the Army Air Corps in 1942 and served until 1946, during which time he studied pre-meteorology at the University of Chicago, Ill., and communications and

R. S. Wiseman

electronics at Yale University, New Haven, Conn., and Boca Raton, Florida. He was a communications and electronics officer for the 4th Emergency Rescue Squadron on Iwo Jima, Saipan, and Guam. He established and taught the Illuminating Engineering Option of electrical engineering at Mississippi State College from September, 1948 to June, 1951.

Since 1954, he has been with the U. S. Army Engineer Research and Development Laboratories in a civilian capacity; he served as chief of the Research and Photometric Section and is at present chief of the Warfare Vision Branch, which performs research and develops viewing equipment which enables the soldier to fight, move, observe, and work at night.

Dr. Wiseman is a member of the Illuminating Engineering Society, the AIEE, the Optical Society of America, the American Society for Engineering Education, Sigma Xi, Tau Beta Pi, Sigma Tau, Eta Kappa Nu, Pi Mu Epsilon, and RESA. He is a registered professional engineer in the State of Mississippi.

❖

W. L. Wolfe

William L. Wolfe was born in Yonkers, N. Y. on April 5, 1931. He received the B.S. degree in physics from Bucknell Universtiy, Lewisburg, Pa., in 1953, and the M.S. degree in physics in 1956 from the University of Michigan, Ann Arbor.

He worked on the measurement of thermal conductivity and specific heat of the Johns-Manville Research Laboratory, Manville, N. J., and on waveguide-component design on Microwave spectroscopy at the Sperry Gyroscope Company, Great Neck, N. Y. He then joined the Willow Run Laboratories of The University of Michigan. Since 1956, he has been in charge of the Infrared Information and Analysis Center.

Mr. Wolfe is a member of Phi Eta Sigma, Pi Mu Epsilon, Sigma Pi Sigma, Omicron Delta Kappa, and Phi Beta Kappa; he is also a member of the Optical Society of America and the American Association for the Advancement of Science.

❖

E. M. Wormser

Eric M. Wormser was born in Germany in 1921. He received his secondary education in England.

After coming to this country in 1939, he attended the Massachusetts Institute of Technology, Cambridge, and received the Bachelor of Science degree in mechanical engineering in 1942. He did graduate work in physics and mathematics at New York University, N. Y.

For a period of two years he was a development engineer in the field of optical fire-control instruments for Universal Camera Corporation. In the military service during 1945 and 1946, he was connected with development activities and technical intelligence on United States and German guided missiles. From 1946 to 1949 he engaged in the development of infrared detection and guidance systems for Hillyer Instrument Company. He headed the Infrared Physics Group at Servo Corporation of America from 1949 to 1952, supervising the development of many of the early military infrared systems. He joined Barnes Engineering Company at its inception in 1952 as Chief Engineer of the Infrared Division. He is now Vice-President for Engineering and supervises all of the technical activities of the Company. His engineering specialties are in the physics of infrared detectors and in the design of optical-mechanical systems. He is the author of several published papers and of numerous classified reports.

Mr. Wormser is a member of the Instrument Society of America, the Optical Society of America, and the American Rocket Society. He is presently serving on the Executive Committee of the Infrared Information Symposia (IRIS) and the Department of Defense Inter-Service Group on Infrared Backgrounds.

Scanning the Transactions

Instrument Approach and Landing is the timely subject of an unusual special issue published by the PGANE. Thirteen articles prepared by leading experts trace the history, outline the current status, and predict the future progress of the development of automatic aircraft landing systems. CAA records show that last year the number of routine instrument *approaches* was about one million, but the number of routine instrument *landings* was zero. This is not to say that instrument landings have never been made. Indeed, the first full instrument landing was made by General Doolittle as long ago as 1929. In 1947 came an historic automatic "push-button" flight in which a plane made a fully automatic "hands off" flight across the Atlantic from takeoff through landing. During the past three years over 2000 automatic landings have been made in tests conducted by Bell Aircraft Corp. However, it is one thing to perform instrument landings under closely controlled conditions at carefully chosen sites using selected aircraft. It is quite another to be able to do this at any and all airfields with any and all planes under any and all conditions. The papers in this issue make at least two points clear. First, many improvements to the existing instrument approach system are possible which will insure its use for many years to come. Secondly, a true instrument landing system is now within the state of the art, but it will be a considerable amount of time before a suitable system can be chosen, developed, and put to full-scale use. (Instrument Approach and Landing Issue, IRE TRANS. ON AERONAUTICAL AND NAVIGATIONAL ELECTRONICS, June, 1959.)

A tubeless record player has been discovered. An IRE member in Memphis reports that a school boy rushed home all excited because his teacher had a new kind of portable record player without tubes or plug-in—just a crank. ("The Editor's corner," IRE TRANS. ON AUDIO, May–June, 1959.)

How to attract the attention of management to material in laboratory reports brings to mind the technique employed by the farmer who sold a mule to his neighbor with the promise that if he spoke to the mule with kindness, the mule would obey his every command. The next day the neighbor was back with the mule, complaining that he would not obey. The farmer promptly picked up a 2 by 4, hit the mule squarely between the eyes, and then spoke gently to him. The mule obeyed with alacrity. "But you said to speak to him with kindness," protested the neighbor. "Perfectly true," replied the farmer," but you have to get his attention first!" In writing reports for management it would be wiser to use kindness first, and the 2 by 4 only as a last resort. Kindness means recognizing the fact that your report must compete for management attention with reports from other major parts of the company—sales, public relations, legal, etc., many of whom are professionals in the art of communication and persuasion. Kindness also means writing the report in a way that will be most useful to management. What does management want in a laboratory report? The following survey[1] made by the Scientific Apparatus Makers Association tells the story.

40% want a better conclusion
32% want more stress on long-term implications
32% want more stress on what findings mean in dollars
22% want them shorter
21% want more graphic material
13% want them less scientific
11% want more stress on new product implications.

(I. Goldman, "Administering information input and output in research laboratories," IRE TRANS. ON ENGINEERING MANAGEMENT, June, 1959.)

Redundancy as a technique for improving the reliability of electronic equipment has received an increasing amount of attention in the last several years. As a result we have heard much about redundant circuits. But now the experts are going a sizable step further and are talking about redundant machines. While the idea may sound a bit drastic, it has some attractive advantages in the computer field. Redundancy of complete machines allows for the use of already existing machines to obtain a very reliable system. On the other hand, redundancy of small units within the machine involves a special design for each system application, extensive use of switching elements to choose between good or failed units, and a serious maintenance problem in finding and replacing failed components of redundant units. For these reasons, it appears that redundancy of complete machines may be more practical in applications where a failure would be very costly. One such application that looks promising is in the automation of large fabrication industries. Analog machines used in process-control industries do not have the precision required to control a manufacturing plant, and to date there has been a reluctance to use digital machines because of the reliability problem. The use of redundant digital machines may provide a practical answer. (D. E. Rosenheim and R. B. Ash, "Increasing reliability by the use of redundant machines," IRE TRANS. ON ELECTRONIC COMPUTERS, June, 1959.)

How to become a more intelligent reader: Not long ago, this was a problem that could have applied only to people. Today, we find that machines are rapidly taking on the same characteristics and functions as humans. Perhaps it is only fair, then, that machines should suffer some of our problems, too. In any event, the matter of intelligent readers is now of concern not only in the field of education but also in the field of pattern-recognition systems. Various character-reading systems for automatic processing of printed documents have been proposed in the past few years. In considering such systems the emphasis in the past has been on the electronics and mechanical aspects of the pattern-scanning mechanism, or on the judicious coding of the read-in material. In virtually all these systems the reading mechanism has been designed to scan each pattern completely, redundancies and all, leaving it up to the coder to remove the redundancies. However, now attention is being turned to the problem of designing a more intelligent reader—one that will not scan the entire pattern area, but only a judiciously chosen portion of it. This would not only make the coder's job easier but would speed up the operation and simplify some of the equipment. Initial studies of the problem have given encouraging results, especially in dealing with standardized patterns such as alpha-numerical characters. (A. Gill, "Minimum-scan pattern recognition," IRE TRANS. ON INFORMATION THEORY, June, 1959.)

A classical study of musical instruments has been published by the Audio Group. A 29-page article presents the most comprehensive study of amplitudes and frequency spectra of orchestral and instrumental music ever published. Interestingly enough, the work was carried out at Bell Laboratories 30 years ago. In fact the paper was first presented before the Acoustical Society of America in 1929 and published in their Journal in 1931. During the intervening years, however, the results have been subject to some misinterpretation because they were presented in a form which, although reasonable at the time, turned out to be somewhat outside the vocabulary of later-day acousticians and audio engineers. One of the authors recently undertook the formidable task of revising the original data in accordance with present-day usage. The result is a document which makes more useful than ever a body of information that has served as a fundamental basis for designing music recording systems for three decades. (L. J. Sivian, H. K. Dunn, and S. D. White, "Absolute amplitudes and spectra of certain musical instruments and orchestras," IRE TRANS. ON AUDIO, May–June, 1959.)

[1] From *Chemical and Engineering News*, p. 38; January 20, 1958.

Books

Principles of Circuit Synthesis, by Ernest S. Kuh and Donald O. Pederson

Published (1959) by the McGraw-Hill Book Co., 330 W. 42 St., N. Y. 36, N. Y. 222 pages+4 index pages+2 bibliography pages+10 appendix pages +xiii pages. Illus. 6×9¼. $8.50.

This book is unique in that it is the first undergraduate textbook on the subject. In order to understand the reason for the proposed changes in undergraduate teaching, we review the general problem of technical education.

As knowledge advances, there is an inevitable cyclic process in education. For a decade or two, contemporary new material is included by adding more and more courses at the advanced graduate level, while keeping undergraduate course material almost static. But this expansion phase cannot continue indefinitely; eventually one finds that there are many men past 30 years old still in graduate schools, learning material that they could have learned just as easily, if not more easily, at the age of 20. Then a contraction phase sets in; much of what has been considered "advanced" material seems less so as one becomes more familiar with it. It can be passed down to undergraduate courses, *provided* that the rest of the curriculum is revised to accommodate it. This means, of course, an increasing emphasis on fundamentals rather than specialized applications, in undergraduate teaching.

This trend toward teaching fundamentals is sometimes criticized as a trend to abstractions, away from practical matters. But, however one may feel about the relative merits of the abstract and the practical, it is a stubborn fact that teaching fundamentals is the only possible way of ensuring that our students will be able to handle the practical matters of their later professional life.

This is a lesson which electrical engineers have learned particularly well from their experiences in the 1940's. Before World War II, electrical engineers were taught to think almost exclusively in terms of circuit concepts, spent a great deal of time on specialized topics such as AC motors, and were scarcely aware of the existence of Maxwell's equations. The result is still fresh in our minds; wartime development of microwave techniques had to rely largely on physicists. Engineering schools moved quickly to correct this situation, and today an electrical engineering student will find that Maxwell's equations and their use are as familiar to him as the back of his hand. Anyone with this background of fundamentals can quickly learn the practical aspects of AC motors, *if* that turns out to be his job. His advantage is that he can just as quickly learn the practical aspects of any one of a hundred other devices; and no one can foretell what specific things he will be working on twenty years from now. This is well recognized by the more enlightened industrial concerns; no one expects that an engineer fresh out of school will have sound practical judgment. The practical part of his education will take place largely in the first few years on the job.

The book under review is a text for a second-semester senior course in communication circuits given at the University of California in Berkeley, having as a prerequisite a one-semester course in linear circuit and systems analysis. Chapter 1 is a short but excellent nonmathematical discussion of two widely different systems (transoceanic cable with repeaters, and microwave pulse system) in which accurate circuit synthesis in, respectively, the frequency and time domains is required.

The mathematical development starting in Chapter 2 may appear to begin rather abruptly, as the first equation given is the full set of integrodifferential equations of an n node-pair network, introduced without any explanatory illustration or definition of "node." However, one must remember that this text is building on the foundations laid in the prerequisite circuit analysis course, and for the full story one must have the textbooks of both courses. The complex frequency variable $p=\sigma+j\omega$ is introduced immediately, and in the next five pages we are given the partial fraction expansion of the free response, the time-domain form by inverse Laplace transformation, the definition and polynomial form of the network function, and the condition for stability in terms of its complex poles and zeroes. All this before the bottom of page 11! This gives a good idea of the pace of the book, and the excellence of the preceding analysis course. As if to emphasize its completely modern outlook, the first numerical example concerns a common-emitter transistor amplifier stage, whose response function has two poles on the negative real axis.

Chapter 3, on transmission criteria, introduces the magnitude and delay functions, and gives the theory of finding response functions by the maximally flat and equal-ripple criteria. It is impressive, to one who remembers how profound the equal-ripple (Tchebycheff polynomial) theory seemed only a few years ago, to see it now disposed of in three pages of an undergraduate textbook. Chapters 4 and 5 return to more "old-fashioned" material, giving a fairly standard discussion of general relations in 2-port networks, along the lines of Guillemin's classical treatment.

Chapter 6 takes up 1-port lossless networks, and the only real criticism this reviewer has to make about the book concerns the discussion of tests for physical realizability. It seems poorly organized, with properties emphasized without being used, and does not lead to the formulation of any definite procedure for testing, which always works. By the time I finished reading this part, I was in a state of fairly complete confusion. However, the authors again prove their merits in the latter part of the chapter, by giving a beautifully clear derivation, via simple physical arguments, of the canonical Foster and Cauer syntheses.

Chapters 7, 8, and 9 cover the realization and synthesis of lossless 2-ports, while Chapters 10 and 11 give the analogous theory for RC networks. Chapters 12 and 13 are concerned with synthesis of cascaded 2-ports on a constant-R and image-matched basis respectively.

In the concluding Chapter 14, we are again treated to some relatively new material, the general theory of the scattering matrix and its use in evaluating mismatch distortion. Although the treatment is always very concise, there are plenty of numerical examples and well-thought-out problems throughout the book.

It is less than five years since the chief engineer of one of our largest manufacturers of radio and TV sets told me, with obvious pride, that the engineers of his company had just adopted the very latest "highbrow" methods of circuit design. The first step is to decide on the over-all response characteristic of the receiver, and to locate all its complex poles. Then the best apportionment of these poles among the various stages is found from practical considerations. The process was so well organized that it was only a slight exaggeration to say that engineer E_a is concerned exclusively with the proper care and feeding of pole P_a, and its wanderings in the face of component and tube drifts. Now it is possible to teach the principles underlying this in a routine undergraduate course!

This is real progress, coming at a very opportune time. One can express the hope that all engineering schools will be quick to follow the lead of the University of California in this upgrading of educational standards. However, it must be emphasized again that improvement in the teaching of one subject is feasible only in conjunction with similar improvements in other parts of the program. What we need is a dozen new textbooks like this one.

In concluding, I cannot resist the temptation to look into the future and speculate on further improvements which we might hope to accomplish in another ten or fifteen years. The material presently included under the topic "Circuit Synthesis" still bears the stamp of its historical beginnings in the concentration on certain specialized problems which are by no means the only ones encountered in practice. Even at low frequencies, there is less and less need to confine attention to lumped-constant circuits; in many applications the use of electrical and electromechanical delay lines is entirely feasible. The basic principles are readily formulated in a way which remains valid here, and the same remark applies to the use of nonreciprocal passive elements. Often, the basic design requirements have little to do with power transfer or distortion; the signal/noise ratio may be the only thing that really matters. Thus the Wiener theory of prediction and smoothing, as simplified by Bode and Shannon, ought to be considered as belonging to this field. Chapter 2 of the present book either develops or presupposes all the mathematical equipment, including the fundamental factorization problem, needed in this theory. The theory of optimal antenna design is very similar, both in concepts and mathematical detail, to certain problems of circuit synthesis. Indeed, an an-

tenna is just a particular kind of filter, operating in space instead of in time, and because of this the gain function $G(\theta)$ of an antenna is free from the physical realizability requirements which complicate much of time-domain filter theory. Thus one can visualize a more general field, "Linear System Synthesis" in which a single fundamental viewpoint applies to, and unifies, several fields now considered distinct. I believe that, if we can maintain the present rate of improvement, it will soon become possible to present all of this in a single undergraduate course. The B.A. of 1970 may have a far better technical background than did the Ph.D. of 1950.

E. T. JAYNES
Microwave Lab.
Stanford Univ.
Stanford, Calif.

Electronic Circuit Theory: Devices, Models, and Circuits, by H. J. Zimmermann and S. J. Mason

Published (1959) by John Wiley and Sons, Inc., 440 Fourth Ave., N. Y. 16, N. Y. 537 pages+6 index pages+20 appendix pages+xvii pages. Illus. 6×9. $10.75.

As implied by the title, this valuable text presents unifying concepts essential to a basic understanding of electronic circuit theory. It is the latest book to originate from M.I.T. and adds significantly to the evolution of a modern undergraduate curriculum in electrical engineering. The approach is most comprehensive and provides interesting procedures for analyzing the complete spectrum of circuits involving diodes, triodes, transistors, pentodes, and thyratrons. The exposition relies upon piecewise-linear circuit models to bridge the gap between the nonlinear and linear circuit phenomena.

In Chapter One, fundamental building blocks are described. The plan of presentation is outlined starting with conduction processes, deducing terminal behaviors, contriving circuit models, and utilizing these models to understand the operation of basic electronic circuits. This is one of the more valuable chapters, since it delves into philosophical concepts which are none too common. In Chapter Two, a succinct description is given of the important aspects of conduction processes in metals, semiconductors, and gases and includes methods of releasing electrons and properties of vacuum diodes, gas diodes, and photo tubes.

Graphical analysis of resistive networks is treated in Chapter Three and extended to nonlinear circuits. The topics involve piecewise-linear models for vacuum diodes, semiconductor devices, gas-filled diodes, and for an arbitrary nonlinear resistance. Among the many developments, stepwise and parabolic approximations are also considered.

Chapter Four begins with the basic rectifier circuit, introduces capacitor smoothing, and extends the discussion to rectifier circuits with dc and ac input voltages. It also concerns itself with the clamping circuit, the voltage doubler, the electronic frequency meter, the full-wave rectifier, ripple filters, detectors, and balanced modulator circuits. Transistor models are explained in Chapter Five and the approach is applied to vacuum triodes in Chapter Six. Some of the fundamental properties of control valves are discussed in Chapter Seven and three specific devices—the vacuum pentode, the cryotron, and the thyratron—are considered as examples.

In Chapter Eight, basic ideas associated with wave-shaping and amplification are disclosed. The exposition touches upon the RC circuit response generated by step, pulse, ramp, and square wave excitations. Methods for determining waveforms and locus of operation for a triode circuit are elaborated upon and applied to pentode and transistor circuits.

Chapter Nine is devoted to a complete discussion of waveform generation utilizing transistor and triode circuits and derives operating characteristics of the relaxation oscillator, the multivibrator, the plate-coupled bistable circuit, and the blocking oscillator. Oscillations in RLC circuits is the principal topic of Chapter Ten. Concepts employing symmetry are included in Chapter Eleven and illustrated by the vacuum-tube voltmeter, the power amplifier, and the transformer-coupled push-pull amplifier.

This book achieves a very broad coverage of subject matter in a limited space by confining formal developments to the main points. Each chapter is very well documented and contains exceptional problems. It is indeed a most useful book for senior undergraduate students and for design engineers desirous of a thorough understanding of broad electronic principles and relevant devices.

ANTHONY B. GIODANO
Polytechnic Inst. of Brooklyn
Brooklyn, N. Y.

Molecular Science and Molecular Engineering, edited by Arthur von Hippel

Published (1959) by The Technology Press of M.I.T., Cambridge, Mass. and John Wiley and Sons, Inc., 440 Fourth Ave., N. Y. 16, N. Y. 430 pages +12 index pages+xv pages. Illus. 8½×11. $18.50.

In the preface, Professor von Hippel distinguishes three fundamental fields of science: *macroscience*, concerned with the classical laws of our daily experience and their extrapolation into the realms of the universe; *nuclear science*, concerned with the structure of nuclei and the basic reasons for the existence of particles and fields; and spanning these extremes, what von Hippel chooses to call *molecular science*, the broad realm of electrons, atoms, and molecules, and their interaction in gases, liquids, and solids under the domination of electrical and magnetic forces. Thus defined, molecular science encompasses many branches of physics, chemistry, and metallurgy.

In an era of increasing specialization, it is refreshing to welcome a book which is dedicated to demonstrating the essential unity of superficially different scientific disciplines, both pure and applied. In addition to laying stress on the underlying unity of its diverse subject matter, the book seeks to show, largely by well-chosen example, that the task of analyzing the properties of matter in aggregate has progressed far enough to allow a successful beginning of rational synthesis, according to which the properties of materials can be tailored to order by combining the proper atoms and molecules into specified arrangements. While it will be some time before we can dispense with empirical and heuristic methods in materials research, it is becoming increasingly clear that such research can be accelerated considerably by broadening the base of our scientific knowledge.

The present volume is actually the final part of a trilogy on modern materials research. The first part, "Dielectrics and Waves," is an introductory textbook on the electrical and magnetic properties of nonmetallic crystals authored by Professor von Hippel, Director of the Laboratory for Insulation Research at the Massachusetts Institute of Technology. The second part, "Dielectric Materials and Applications," which, together with the first part, appeared in 1954, includes some background material and reference data, as well as a number of survey articles on measurement techniques and the properties and present limitations of materials in equipment and device applications. The second part is an outgrowth of a summer session held in 1952 at the Laboratory for Insulation Research, just as the third (and present) part is an outgrowth of a similar session held in 1956. The third part also contains background material and a collection of survey articles. The contributors to parts two and three were drawn from among the participants at these apparently very fruitful summer sessions. All of them are recognized authorities in their fields.

Included in the present volume are modest summaries of atomic and molecular physics, electromagnetic theory, and crystallography, all contributed by von Hippel, as well as one on thermodynamics and statistical mechanics by O. K. Mawardi and von Hippel.

In addition, there are review articles on: conduction and breakdown in gases (von Hippel); atmospheric physics (J. P. Kuettner); microwave breakdown of gases (S. C. Brown); gas discharges as technical devices (E. O. Johnson); explosions in gaseous systems (B. Lewis); reaction mechanisms in liquid systems (C. G. Swain); molecular synthesis of polymers (W. H. Stockmeyer); ion-exchange resins (C. D. Coryell and Y. Marcus); and polyelectrolytes (R. M. Fuoss).

Further, there are review articles on: crystal growth and perfection (A. Smakula); irradiation effects (R. Smoluchowski); plasticity (E. Orowan); ferroelectricity and ferromagnetism (A. von Hippel); ferro- and antiferromagnetic materials (P. W. Forsbergh, Jr.); piezo- and ferroelectric devices (W. P. Mason); ferromagnetic materials and molecular engineering (D. J. Epstein); and ferromagnetic devices (R. A. Ramey, Jr. and B. W. Lovell).

Finally: parametric amplifiers, masers, and film memories (J. W. Meyer and D. O. Smith); mobilization of charge carriers in liquids and solids (A. von Hippel); rectifiers and transistors (R. B. Adler); and molecular engineering and the air vehicles of the future (K. Martinez).

This book should prove useful to anyone who wishes to be introduced to the broad subject of molecular science and engineering, and to gain a nodding acquaintance with its objectives, methods, and aspirations. Bearing in mind the fact that most of the book consists of review articles on diverse sub-

jects, it cannot be recommended as a textbook on solid-state physics, though it can be heartily recommended as a supplementary reader for such a course.

The review articles are uniformly well-written, and virtually all of them contain adequate reference lists for further study. The background material contributed by Professor von Hippel is outstanding for its clarity and organization. In addition to having an excellent subject index (but surprisingly no author index), the book is beautifully printed and illustrated.

FRANK HERMAN
RCA Labs.
Princeton, N. J.

Analysis of Straight-Line Data, by Forman S. Action

Published (1959) by John Wiley and Sons, Inc.' 440 Fourth Ave., N. Y. 16, N. Y. 231 pages+5 index pages+8 bibliography pages+xiii pages. 6×9¼. $9.00.

Engineers as well as many others often fit experimental data with straight lines or even more complicated curves. Most of us feel dissatisfied at times with our understanding of how well we have supported our conclusions and what meaning we can ascribe to the size of the departures from our fitted law. The present book takes the reader through the maze of statistical theories bearing on the subject and gives an honest appraisal of what we can accomplish in real cases.

A short first chapter describes the different models which we consciously or unconsciously may adopt. These models form most of the subject matter of the remaining chapters. A rather long second chapter considers the most common elementary case in which values of the independent variable are assumed to be selected without error and the dependent measured variable is assumed to have uniform variance throughout the range of the data. A complete summary is first given of the classical least-square-error method with a tabulation of formulas for various assumptions concerning prior knowledge, if any, of specific parameters. Then the quantitative measure of confidence in the results is explored. The reader is quickly made aware of a considerable body of statistical lore of which practically only the end results are stated and used.

In the very first problem on confidence limits, that of determining an interval of slope values which with specified high probability includes the true value when the errors are normally distributed, casual reference is made to Student's and the Chi-Square distributions. The innocent phrase "it can be shown that," without inclusion of how or where, was ultimately tracked down by the reviewer to three pages in Wilks' "Mathematical Statistics," not counting the necessary preliminary proof of Cochran's theorem. Now this is really an elementary problem compared to the ones treated in the remainder of the book. Its treatment illustrates the pattern of the exposition, namely —quantitative results and some qualitative support are given, but the reader who wants to verify for himself should have at hand a battery of other references not spelled out in the text.

Chapter 2 includes a number of alternate methods aimed at avoiding least squares calculations and normal law dependence. The first objective seems strange in these days of prevalent giant computers. Would many settle for less than the best just because squaring numbers is more laborious than adding them? Well, one should not lose sight of the fact that even the most rigorous classical procedures are based on original assumptions which might be questioned. The more heretical processes suffer from lack of demonstrated knowledge as to how good they are even under specified conditions, but many of them can be applied to non-normal distributions for which the classical methods are not well documented either.

In Chapters 3–6 inclusive the author works his way into the most general straight-line fitting condition considered, that in which both the independent and dependent variables are measured with errors which may be correlated and have inhomogeneous variance. Maximum likelihood estimates and two-parameter confidence regions are discussed mainly for bivariate normal populations. Chapters 7 and 8 deal with fitting of curves by polynomials and with what can be done by change of variable. Chapters 9 and 10 deal with the delicate problem of discarding data we do not like.

The book is intended more for self-education than classroom instruction. In conjunction with other statistical books it should meet its aim very well.

W. R. BENNETT
Bell Telephone Labs.
Murray Hill, N. J.

Linear Network Analysis, by S. Seshu and N. Balabanian

Published (1959) by John Wiley and Sons, Inc., 440 Fourth Ave., N. Y. 16, N. Y., 504 pages+7 index pages+4 bibliography pages+56 appendix pages. Illus. 6×9¼. $11.75.

This book was prepared for use in graduate work on network analysis at Syracuse University. Familiarity with complex variables and Laplace transforms is assumed, but the use of these mathematical tools is not so extensive as to make its use otherwise impossible, particularly since a 55 page appendix, "Theory of Functions of a Complex Variable and Laplace Transforms," is included. The subject matter is developed along classical lines using loop and nodal analysis with the aid of matrix algebra. Current and voltage designations are simplified by using arrows and polarity symbols uniformly throughout the book. Network topology is introduced and kept in proper balance. An effort has been made to emphasize the complete solution including both the transient response and the steady-state response by use of the Laplace transform. However, the results are generally left in the transform domain so it is doubtful whether the student will get a good insight to the transient behavior. The authors analyze active and passive networks simultaneously; this approach is commendable. Distributed parameters including transmission lines have been intentionally excluded.

The authors indicate in the preface the importance of the concept of energy, but essentially nothing is developed in terms of network power transfer and matching characteristics. Feedback and related topics are treated in 46 pages, which includes signal-flow graphs. Feedback analysis is largely restricted to unidirectional return as extensively employed in servomechanism using summing point analysis.

Generally, the authors have a tendency to "hammer away" at formal mathematical analysis without developing fully the engineering ideas behind the math. The result is that rather simple concepts are covered over by symbolism. No doubt, undergraduate courses, class discussions, and laboratory work are employed to supplement the analysis, but in the absence of these the student will have difficulties in following the analysis. Extensive problems following each chapter will be helpful.

Those responsible for academic courses in network analysis will want to consider the use of this book in their classrooms.

L. J. GIACOLETTO
Scientific Lab.
Ford Motor Co.
Dearborn, Mich.

Physics of Electricity and Magnetism, by William Taussig Scott

Published (1959) by John Wiley and Sons, Inc., 440 Fourth Ave., N. Y. 16, N. Y. 544 pages+31 index pages+60 appendix pages+xvi pages. Illus. 6×9. $8.75.

This is a senior or first-year-graduate text in electricity and magnetism, with the special feature of including substantial discussion of the physics behind the macroscopic electromagnetic properties of matter. In addition to the usual topics of electricity and magnetism, the book discusses conduction in metals and insulators, work function and contact potential, dielectric materials and properties, semiconductor effects, thermoelectric and electrochemical effects, and magnetic materials and properties, all in some detail. The book makes extensive use of differential and vector calculus, without, however, sacrificing physical intuition and reasoning. The student is encouraged to develop physical reasoning in terms of mathematical concepts rather than as a substitute for them.

The first 45 per cent of the book covers electrostatics taken broadly, including the topics in electrical physics mentioned above, and a chapter on dc circuits. The coverage is complete and extensive, and all the usual topics and classical problems are included. In addition, care is taken to lay a foundation for the later discussion of time-varying fields. Another 30 per cent of the book is devoted to magnetostatics, magnetic materials, and magnetic properties, with similar comments being applicable.

The remaining quarter of the book is equally divided between a chapter on ac lumped-constant circuit theory using the phasor method, with a very brief resume of Fourier and Laplace methods and a chapter on time-varying fields and electromagnetic radiation, with sections on transmission lines, wave propagation, energy and momentum, radiation, physical optics, waveguides and cavities, and special relativity. The electrical engineer will find this latter chapter extremely brief for his purposes.

In this reviewer's opinion, the book's chief defect is an attempt to cover advanced physics material in too brief a space. For example, the quantum theory of electrical

conduction, band theory, the Fermi distribution and Fermi level, and the electrochemical potential are all introduced in just four pages. This coverage is too sketchy to be meaningful to someone meeting the material for the first time, and would require extensive supplementing to provide understanding.

However, the book does provide a good and extensive text in classical electricity and magnetism, and with some outside assistance would also give a good understanding of the electrical properties of matter.

A. E. SIEGMAN
Stanford Univ.
Stanford, Calif.

Electronic Fundamentals and Applications, 2nd Edition, by John D. Ryder

Published (1959) by Prentice-Hall, 70 Fifth Ave., N. Y. 11, N. Y. 704 pages+7 index pages+10 appendix pages+xii pages. Illus. 6×9. $13.35.

This second edition of a previously successful text has been updated to include material on solid-state devices. The most significant additions are concerned with the analysis of circuits which employ transistors as driving elements. Dean Ryder has made every effort to accord the transistor the place in electronics that it deserves, and parallel analyses are included to show the performance of circuits when transistor driven and when vacuum tube driven. There has also been an addition of some material on direct-coupled and operational amplifiers. With the rearrangement of the material in the book, a good balance has been effected.

This book, as its predecessor, is primarily a textbook, and is not a manual for tube or equipment designers. It includes a broad sweep of the field of electronics. It provides an introduction to physical electronics, to electronic circuits, and to a selected area of industrial electronics, although the author does not specifically divide the book in this way. The chapters are titled: The Fundamental Particles; Electron Ballistics; The Cathode Ray Tube; Charge Behavior in Materials, Emission of Electrons; Semiconductor and Vacuum Diodes; Power Supplies and Filters; Four Terminal Networks; Control Devices, the Vacuum Tube; Control Devices, the Transistor; Small Signal Amplifiers; Feedback, Direct-Coupled Amplifiers; The Audio Frequency Amplifier with Large Signals; The Radio Frequency Amplifier with Large Signals; Oscillators; Modulation; Demodulation; Wave-shaping Circuits; Gaseous Conduction; Power Rectification; Gaseous Control Tubes and Circuits; and Photoelectric Devices. Each chapter is provided with a number of problems for student solution to illustrate the text material. Actually, a tremendous amount of detail has been packed within the present 721 pages. That all topics are not accorded full or equal treatment is inevitable. On the whole, however, the balance is good. It is expected that this book will continue to enjoy the acceptance accorded to the first edition.

SAMUEL SEELY
Case Inst. of Tech.
Cleveland 6, Ohio

Dictionary of Guided Missiles and Space Flight, edited by Grayson Merrill

Published (1959) by Van Nostrand Co., Inc., Princeton, N. J. 688 pages+vi pages. Illus. 7½×10. $17.50.

The "Dictionary of Guided Missiles and Space Flight" is a dictionary of terms in which the definitions vary in length from one to 500 words. A typical definition is made in approximately 50 words. Both conventional meanings and the esoteric meanings of words used by rocket engineers and scientists are covered. It is remarkably complete in the fields of physics, mechanics, aerodynamics, electronics, propulsion, control and military missiles and emphasizes the newer terms, particularly those not defined elsewhere. The best insight to the contents may be obtained from a few sample definitions which follow:

cislunar—(1) Pertaining to the moon. (2) Pertaining to the region of the earth-side of the moon. The term is frequently applied to solar-powered craft which require exposure to the sun for operation. They are thus said to be restricted to cislunar space.

jerk—In kinematics, the third derivative of displacement; rate of change of acceleration. Jerk is useful in defining the nature of shock loads.

Saros—The fact that eclipses occur in periodic intervals was known to the ancient Chaldeans, and probably even in prehistoric times. This period of 18 years, 11⅓ days (10⅓ days if there happen to be 5 leap years in the interval), is known as the Saros. If an eclipse should occur on January 1st, 1967, at noon, another similar eclipse would occur on January 12th, 1985, at eight o'clock in the evening. The eclipse would not occur at the same point on the earth but would be about 8 hours farther west in longitude. During the course of a Saros there are about 29 lunar and 41 solar eclipses, each repeated during the next Saros, but not at the same portion of the earth.

The dictionary is useful to both scientists and laymen who have needs to understand or use the terms of modern space technology. It establishes a common basis for understanding and for the written and spoken transmission of information and is a valuable asset to any space age library.

CONRAD H. HOEPPNER
Radiation, Inc.
Melbourne, Fla.

RECENT BOOKS

Band, William, *Introduction to Mathematical Physics*. D. Van Nostrand Co., Inc., Princeton, N. J. $7.25. An over-all survey from a unified and up-to-date philosophical viewpoint, focusing sharply on twentieth-century physics and mathematics.

Bowker, Albert H. and Gerald J. Lieberman, *Engineering Statistics*. Prentice-Hall, Inc., Englewood Cliffs, N. J. $11.00. How to apply modern statistical theory to the everyday problems of the engineer and the physical scientist.

Chernoff, Herman and Lincoln E. Moses, *Elementary Decision Theory*. John Wiley and Sons, Inc., 440 Fourth Ave., N. Y. 16, N. Y. $7.50. Demonstrates the use of decision theory as a means of clarifying basic principles of statistics.

Condoyannis, George E., *Scientific Russian*. John Wiley and Sons, Inc., 440 Fourth Ave., N. Y. 16, N. Y. $3.50. A concise description of the structural elements of scientific and technical Russian.

Dennis, Jack Bonnell, *Mathematical Programming and Electrical Networks*. The Technology Press, M.I.T. and John Wiley and Sons, Inc., 440 Fourth Ave., N. Y. 16, N. Y. $4.50. A research monograph which offers a new approach to mathematical programming based on an analogy with electrical networks.

Dodge, Harold F. and Harry G. Romig, *Sampling Inspection Tables: Single and Double Sampling*, 2nd edition. John Wiley and Sons, Inc., 440 Fourth Ave., N. Y. 16, N. Y. $8.00. Contains sampling inspection tables for guaranteeing outgoing quality and plans for economy of inspection within a manufacturing plant.

Jordon, R. O. and J. Cunningham, *The Sound of High Fidelity*. The Windsor Press, 200 E. Ontario St., Chicago 11, Ill. $3.95. A guide and text on the subject of high-fidelity sound reproduction—a primer for the novice and a guide for the buyer.

Pressman, Abraham I., *Design of Transistorized Circuits for Digital Computers*. J. F. Ryder, Inc., 116 W. 14 St., N. Y. 11, N. Y. $9.95. Using "worst-case" design, this book explains how switching time and drive capabilities and requirements of all the essential digital computer building blocks may be calculated, and how these blocks may be assembled to perform computer-type logical operations.

Pumphrey, Fred H., *Fundamentals of Electrical Engineering*, 2nd edition. Prentice-Hall, Inc., Englewood Cliffs, N. J. $8.50. An up-to-date coverage of the basic principles and factors in electrical engineering.

Schenck, Hilbert, Jr., *Heat Transfer Engineering*. Prentice-Hall, Inc., Englewood Cliffs, N. J. $9.25. On the modes of heat transfer, including basic conduction theory; free convection; forced convection, including transfer in compact surfaces, and to and from liquid metals; radiation theory and its applications; and transient conduction in one, two, and three dimensional systems.

Smith, Charles V. L., *Electronic Digital Computers*. McGraw-Hill Book Co., 330 W. 42 St., N. Y. 36, N. Y. $12.00. Discusses basic principles of computers in use today.

Turkevich, John and Ludmilla B. Turkevich, *Russian for the Scientist*. D. Van Nostrand Co., Inc., Princeton, N. J. $5.95. A handbook organized and designed for scientists and engineers as a tool for the use of Russian scientific literature.

Wagner, T. C. Gordon, *Analytical Transients*. John Wiley and Sons, Inc., 440 Fourth Ave., N. Y. 16, N. Y. $8.75.

Abstracts of IRE Transactions

The following issues of TRANSACTIONS have been recently published, and are now available from The Institute of Radio Engineers, Inc., 1 East 79th Street, New York 21, N. Y., at the prices indicated. The contents of each issue and, where available, abstracts of technical papers, are given herewith.

Sponsoring Group	Publication	Group Members	IRE Members	Non-Members*
Aeronautical & Navigational Electronics	ANE-6, No. 2	$2.25	$3.35	$5.75
Audio	AU-7, No. 3	0.45	0.65	1.35
Electronic Computers	EC-8, No. 2	2.15	3.20	6.45
Engineering Management	EM-6, No. 2	0.55	0.80	1.65
Engineering Writing & Speech	EWS-2, No. 2	1.00	1.50	3.00
Information Theory	IT-5, No. 2	1.85	2.80	5.35
Nuclear Science	NS-6, No. 2	1.50	2.25	4.50
Production Techniques	PT-4	0.80	1.20	2.40
Space Electronics & Telemetry	SET-5, No. 2	1.00	1.50	3.00

* Libraries and colleges may purchase copies at IRE Member rates.

Aeronautical and Navigational Electronics

VOL. ANE-6, NO. 2, JUNE, 1959

1959 Pioneer Awards (p. 50)

Instrument Approach and Landing

Introduction—The Editor (p. 57)
Foreword—F. B. Brady (p. 57)
Frontispiece: F. B. Brady (p. 58)
Editorial—F. B. Brady (p. 59)

Early Development

Instrument Landing at the National Bureau of Standards—F. G. Kear (p. 61)

In 1928 commercial aviation in the United States had developed to the point that the urgent need for additional facilities which would permit all-weather flight was evident to everyone. In anticipation of this need, the aircraft industry had undertaken the development of new and more precise aircraft instruments, including the sensitive altimeter, the artificial horizon, and the directional gyro. The aural radio range was beginning to be installed along the lighted airways and the National Bureau of Standards had completed initial development of the visual type range beacon. The aircraft radio group at the National Bureau of Standards, headed by Harry Diamond under the supervision of Dr. John H. Dellinger, undertook to coordinate these new facilities in an effort to solve the problem of flight during poor visibility.

With General (then Lieutenant) James Doolittle as pilot, an installation at Mitchel Field in 1929 of the low-power visual range beacon and low-frequency marker beacon, together with the new flight instruments permitted Doolittle to effect hooded landings. It was evident that additional information was necessary. This was achieved by the development of the landing beam or glide path. Operating on a frequency of about 100 mc, it provided a signal which informed the pilot as to his location with reference to a predetermined descent path. Combined with the radio range beacon, instrument landings now became possible. Furthermore, by combining the indications of the range beacon and the landing beam into a single cross-pointer instrument, the pilot was able to coordinate his flying with the radio indication. Over 100 hooded landings were made at College Park Airport by Pilot M. S. Boggs and others. This encouraged the National Bureau of Standards to make a complete installation at Newark Airport. The improved facilities offered by this field permitted Pilot James L. Kinney to make repeated hooded landings and to demonstrate to pilots and other members of the aeronautic industry the practicability of instrument landing of a commercial aircraft by means of a combination of visual range beacon, landing beam and marker beacons, associated with an adequate complement of aircraft flight instruments.

With the exception of the change in shape of the glide path from parabolic to a straight line, the basic principles employed at Newark in 1933 are the same as those presently in use in the ILS system.

Operational Flight Testing of Early Instrument Landing Systems—E. A. Cuttrell (p. 67)

The development of successful instrument approach and landing involved the solution of not only technical problems, but operational problems as well. A review of methods used to overcome operational problems is made, covering the period from the earliest successful instrument landing to the introduction of instrument approach into routine scheduled operation. Flight techniques are described, using early systems such as compass locator, constant intensity glide slope, and later, equisignal glide-slope facilities. Recognition of a requirement for visual aids to supplement electronic approach aids is outlined.

Ground-Controlled Approach—Its Development and Early Operational Use—C. Porterfield (p. 71)

Ground-Controlled Approach (GCA) was developed to meet military requirements for a "universal" blind-landing system, needing no additional airborne equipment or pilot indoctrination beyond short-range voice radio and basic instrument training. The talk-down principle, previously discredited in favor of beam-approach systems, was proved feasible when accurate information was available.

The requirements of rapid radar scanning, at low angles to the horizon, with a high degree of accuracy at short range, were met by linear dipole arrays at 3-cm wavelength, with mechanical variation of waveguide width varying the angle of radiated power to the array. Half-power beamwidth for the elevation antenna was 0.1°; for the azimuth antenna, 0.8°.

To translate range/angle data into a linear relationship of range vs deviation in feet from a selected approach path, a new type of indication was developed, *i.e.*, Expanded Partial PPI Indicator (EPI). This permitted direct interpretation and immediate transmission of the data to the pilot by the controller.

GCA's wartime service record, beginning late in 1944, proved its effectiveness under all conditions and led to further modifications and simplification for postwar commercial as well as military use.

All-Weather Landing—J. L. Anasti (p. 75)

The development of all-weather landing is reviewed, particularly with regard to automatic control aspects. Flare-out schemes are described as well as experience with various systems. Problems of cross wind and techniques for eliminating their effects are included, along the "weather cock" technique. Crab-angle elimination and castering cross-wind landing gear methods are touched upon.

Current Progress

A Survey of Instrument Approach Systems in the United States—H. I. Metz (p. 78)

A brief history and technical description of instrument landing system (ILS) and precision approach radar (PAR) is given. Improvements in ILS localizer and glide-slope designs are mentioned which reduce adverse site effects and hasten the day when fully automatic approaches may be authorized. Localizer improvements include a highly directional slotted-waveguide antenna. The waveguide system is essentially "added to" the conventional localizer and no change is required in the existing airborne receivers. This system is now operational (a version of the system is also in military use). For the glide slope, a runway-flush antenna has been developed and demonstrated. There are now 170 civil and about 50 military ILS installations in the United States with more under way.

PAR (known in military service as GCA) has only limited civilian use but rather general use by the military. In this system, the controllers on the ground "see" the aircraft and its deviation from the desired approach. Corrections in heading and rate of descent are transmitted to the pilot in voice with advice also on distance to touchdown.

Based on present trend and international acceptance of ILS, it is concluded that the number of ILS installations will be expanded to cover all aviation hubs and that automatic approaches will be authorized to further increase schedule efficiency and safety. PAR will probably not be further implemented for civil use. Distance measuring equipment (DME) compatible with the distance function of en route VORTAC facilities will be added to each ILS to give continuous indication of distance to touchdown. Other approach systems, involving ground computers, etc., have been demonstrated for specific military applications and may ultimately be applied to civil and common system operations.

Improvements on the Instrument Landing System—W. E. Jackson (p. 85)

The present paper deals primarily with CAA contribution to the art of instrument landing systems and is confined to the localizer and glide-path portions of the system. It describes briefly the present standard 8-loop localizer used at most sites as well as some modifications made in the basic localizer concept in order to adapt it to locations where siting problems exist. It also describes the standard glide slope as well as a new type of glide slope for use at extremely poor locations.

Electronic Aids for Carrier Aircraft—A. Brodzinsky (p. 95)

With no comparable change in landing areas, the landing speed of carrier aircraft has approximately doubled over the past 15 years. For this and other reasons the carrier landing procedure has become a very difficult task for which the aid of automatic electronic devices is sorely needed. Such systems would also greatly improve the continuity of flight operations through periods of poor visibility. A brief background of the problem is presented. The most recently developed fully automatic landing system consists of a three-coordinate tracking radar which provides closed-loop control through a ground-based computer, a ground-to-air data link and an autopilot in the aircraft. Recent successful sea trials indicate that the characteristics of this system are sufficiently accurate to provide a practical solution for the carrier landing problem.

Glide-Slope Antenna Arrays for Use Under Adverse Siting Conditions—F. W. Eden (p. 100)

The problems of generation of an adequate glide-slope signal on a practical airport site are examined, with particular attention to the path shape degradation introduced by inadequate smooth surface in the primary reflecting area, and hills and similar mirror obstructions under the approach line. Quality factors are derived to establish comparison standards to evaluate the relative performance to be expected in application of various of the available arrays to any particular site. Two antenna arrays are described, which have been found in an extensive program of flight testing to provide substantial improvement in certain of these defective sites.

Future Plans

The FAA Philosophy and Program of Instrument Approach and Landing System Development—L. C. Wright and D. J. Sheftel (p. 112)

An all-weather instrument landing system is urgently required by both civil and military users of the airspace. To this end the Government has pursued several developmental approaches which have contributed significantly to our knowledge and understanding of what steps must now be taken. This article describes much of what has been learned from previous efforts and describes the approach presently being taken by the Federal Aviation Agency to improve the present system, to achieve an interim landing system capability, and to provide a future system that will serve all users of the airspace.

A Look at the Future of Automatic Landing Systems—G. B. Litchford, A. Tatz, and F. H. Battle, Jr. (p. 118)

Current systems of instrument approach guidance, even with recent and forthcoming improvements, are shown to be inadequate for future operational needs. The potential weaknesses of current techniques include restrictions on flight-control maneuverability, limited landing rates, special terrain and siting requirements, and deterioration of service in the critical low-altitude region near touchdown.

A broad look at future requirements, especially those posed by jet operations, leads to a specific set of desirable system characteristics. An approach system that is suitable to replace the interim improvements now being implemented must provide a wide enough selection of flight paths to allow versatility in flight-control techniques; it must guide aircraft to actual landings; it must be fail-safe; and it must impose minimum burdens in terms of airborne equipment and of real estate.

A review of possible data sources and devices for use in an ultimate system reveals only a few promising contenders. A proposed multi-angular system of minimum complexity is described.

An Automatic Landing System—F. D. Powell (p. 128)

The concept, theory, implementation, and test results of the Bell Aircraft Automatic Landing System are presented. The system, which requires no additional airborne electronics equipment in land-based aircraft carrying an ILAS receiver and coupler, employs a precise ground-based radar and command computer. The major source of error of this closed-loop system is turbulence, while performance is limited chiefly by aircraft and autopilot properties. Flight test results covering over 2000 automatic touchdowns and a variety of propeller and jet aircraft are presented for vertical and lateral degrees of freedom.

REGAL—An Advanced Approach and Landing System—B. Cutler and L. Sanders (p. 135)

The FAA is developing an advanced approach and landing system called REGAL. Ground-based scanning beams set up a broad reference grid in space from which aircraft may determine their position and optimumly determine the landing maneuver. A breadboard system was designed and tested in 1957 and 1958, and the FAA experimental elevation system will be tested in 1959. Theory of the radar ground reflection problem is discussed and empirical data are presented to validate conclusions.

The AN/MSN-3: An Automatic Ground-Controlled Approach System—H. Goldstein and B. Cutler (p. 142)

A system is described whereby information gathered by a standard ground controlled approach (GCA) radar is utilized to compute automatically all GCA approach control commands; these commands are then transmitted simultaneously to a maximum of six aircraft via the USAF frequency division digital data link for automatic control of the aircraft approach. The system is designed to enable continuous human monitoring of the AGCA traffic-control operation and to include visual and aural warning signals in the monitoring system for added safety. Problems relating to optimum system response and gain parameters are discussed and control equations are defined. Results of extensive testing demonstrate a system capable of providing smooth control during the aircraft final approach under high-density traffic conditions. System accuracy is well within specified limits of ±50 feet in azimuth and ±30 feet in elevation at a minimum release point 100 feet above the runway.

PGANE News (p. 149)

Contributors (p. 150)

Audio

Vol. AU-7, No. 3, May–June, 1959

A Message from the New Chairman—A. B Bereskin (p. 41)

Newly Elected National Officers, 1959–1960 (p. 42)

Awards, 1958 (p. 43)

Chapter News—J. R. Macdonald (p. 45)

The Editor's Corner—M. Camras (p. 46)

Absolute Amplitudes and Spectra of Certain Musical Instruments and Orchestras—L. J. Sivan, H. K. Dunn, and S. D. White (p. 47)

Measurements made on instruments and orchestras, during the playing of selections, include average amplitudes in long intervals (15 seconds) and distribution of peaks in very short intervals (one-eighth second). Octave and half-octave bands are measured, as well as unfiltered music. The instruments tested were selected as possibly contributing extreme frequencies and amplitudes. Calculations of peak acoustic powers range as high as 27 watts.

Although different techniques would be applied today, such as the use of a recorded tape to insure exact duplication of a selection as different frequency bands are explored, and the measurement of rms rather than average amplitudes, it is nevertheless felt that the measurements were reasonably accurate. The type of presentation, however, left something to be desired. Both kinds of curves will be found here in new forms. For the peaks, the plan used later in presenting similar data on speech has been adopted. The average amplitudes are reduced to a per-cycle basis in a different manner. Both types are plotted in absolute rather than relative units, and are reduced to a common distance. The table of peak powers is recalculated, using the same assumptions as before, but making the estimate for the 1 per cent level of intervals, in all cases. All new reductions and calculations are made from the original measured data.

Some changes in the text are necessary to describe the revisions of the figures, and a few comments have been added. The term "bar" which was in current use in 1931 for "dyne per square centimeter," is changed here to "microbar." The "Historical Note," which appeared at the end of the original paper, has been shortened somewhat and made a part of the introduction.

Magnetic Tape Recording with Longitudinal or Transverse Oxide Orientation—R. F. Dubbe (p. 76)

A comparison is made of the performance of magnetic tape when the recording field is in the same direction as, or perpendicular to, the oxide particles as encountered in magnetic disc or video recording.

On the Response and Approximation of Gaussian Filters—J. Klapper and C. M. Harris (p. 80)

This paper discusses a filter whose amplitude response characteristic is $e^{-k\gamma^2}$ where γ is a function of frequency and k is a constant related to the filter bandwidth. The amplitude response curve of this filter has the shape of the Gaussian probability function and it is shown that the phase response curve may be assumed to be linear. Previous investigations have shown that such a filter has excellent transient characteristics and that, in some sense, it is the optimum filter for transient signals. The responses to impulse and step functions are discussed in this paper. A method for designing an approximate Gaussian filter is given, and the measured responses of such an approximate Gaussian filter are presented.

Contributors (p. 88)

Electronic Computers

Vol. EC-8, No. 2, June, 1959

Richard O. Endres, Chairman, 1959–60 (p. 89)

The Chairman's Column—W. H. Ware (p. 90)

Four papers from the 1959 Solid-State Circuits Conference

Thin-Film Memories—E. E. Bittmann (p. 92)

A small random-access memory using deposited magnetic thin films as storage elements, and with a cycle time of one microsecond, is described. Information is read from or written into the memory by linear or word selection techniques. The addressing, driving and sensing circuits are transistorized. The deposited thin films are 2000 Å thick, switch in 0.1 μsec and generate a 5-mv output signal in the sense winding. A sense signal is obtained of opposite polarity from a selected element when a "1" or a "0" is read out. A memory-plane wiring configuration has been selected which is least susceptible to noise.

Integrated Devices Using Direct-Coupled Unipolar Transistor Logic—J. T. Wallmark and S. M. Marcus (p. 98)

This article presents material that is new in three areas. First, a new logic system using directly-coupled unipolar transistors is analyzed. It is shown that unipolar transistors have important advantages over bipolar transistors in speed, tolerance of stray signals and noise, and device miniaturization. Second, devices of

extreme miniaturization built by an integrated device design and using this logic system are described. Third, how the passive components of the system, in this case resistors, have been integrated into the semiconductor devices is described.

P-N-π-N Triode Switching Applications—V. H. Grinich and I. Haas (p. 108)

The characteristics and switching applications of a developmental diffused silicon p-n-π-n triode are discussed. Although this unit is at present in a two-watt package, it is capable of handling short pulses of current of the order of 100 amperes. The electrical characteristics which consist of a low and high conductivity region (over 500 megohms and less than 1 ohm respectively), with an intermediate negative resistance region, are controllable by the base lead, and hence make it a flexible device for applications in the computer and communications fields. The theoretical and practical limitations are discussed. Experimental data covering current handling capabilities, frequency limitations and switching times are presented in conjunction with representative circuits. Two particular circuits discussed are an 80-ampere 500-mμsec pulse generator with rise and fall times in the order of 150 mμsec and 300 mμsec, respectively, that can operate up to a kilocycle repetition rate, and a 4-ampere 60-mμsec pulse generator with a PRF of 100 kc. Other examples described include monostable, bistable, and astable circuits, as well as types of communication circuitry for a wide range of currents.

An Electro-Optical Shift Register—T. E. Bray (p. 113)

An electro-optical shift register composed only of electroluminescent (EL) and photoconductive (PC) cells was designed and successfully operated. While its measured operating speed probably does not make this shift register currently competitive in high-speed applications, it is amenable to construction in an extremely small volume, and has certain other unique characteristics.

Processing Data in Bits and Pieces—F. P. Brooks, Jr., G. A. Blaauw, and W. Buchholz (p. 118)

A data-handling unit is described which permits binary or decimal arithmetic to be performed on data fields of any length from one to sixty-four bits. Within the field, character structure can be further specified: these processing entities, called bytes, may be from one to eight bits long. Fields may be stored with or without algebraic sign. On all operations, the relative offset or shift between the operand from memory and that from the accumulator can be specified.

Besides the arithmetic operations, three new logical instructions allow any of the sixteen logical connectives of two variables to operate upon each pair of bits in the memory and accumulator operands. The variable field length, variable byte-size features, extend the use of connective operations to a surprisingly wide variety of logical, housekeeping, and editing tasks.

These arithmetic and connective instructions are general and powerful programming fools which greatly simplify complex manipulations. Programming of typical tasks, with both the new instructions and with the instruction set of a conventionally-organized computer, has shown that the new set requires substantially fewer instructions to be written, stored, and executed. Furthermore, the new instruction set has considerably fewer distinct operations than the more conventional set. This is possible because the general-purpose instructions of the new set replace many *ad hoc* instructions which deal with pieces of instructions or data words, or which perform shifting, packing, or editing functions.

The initial application of the variable field length data-processing unit is in the IBM Stretch computer.

Increasing Reliability by the Use of Redundant Machines—D. E. Rosenheim and R. B. Ash (p. 125)

The improvement of reliability and availability through redundancy of entire machines rather than of components is investigated. An attempt is made to break down the cost of operating a digital computer, and to determine the relationship between cost and system failure. Three specific cases are discussed.

Case 1: Where n machines are operated independently, processing the same input data. The output is taken from a single one of them; if this machine fails, the output is promptly switched to a machine which is operating properly. As soon as repairs can be completed the machine which had failed is returned to operation. System failure occurs only when all n machines are in the failed condition at the same time. A penalty cost is assessed for system failure, this cost being proportional to the system down-time.

Case 2: Where n machines are operated as in Case 1, except that any machines which fail are not returned to operation until the beginning of the next operating period. Penalty cost for system failure is assessed in the same way as in Case 1.

Case 3: Where n machines are operated as in Case 2, but where the penalty cost for system failure is a fixed amount and is independent of the resulting down-time.

Boolean Matrix Equations in Digital Circuit Design—R. S. Ledley (p. 131)

A systematic digital computational method is given that involves the use of Boolean matrix equations for solving certain types of functional circuit design problems. Specifically, all sets of Boolean functions $f_1(A_1, \cdots, A_I), \cdots, f_J(A_1, \cdots, A_I)$ are found such that if circuits with these outputs are connected to a circuit that generates the known Boolean function $F(f_1, \cdots, f_J, X_1, \cdots, X_K)$, then the output will produce a given desired function $E(A_1, \cdots, A_I, X_1, \cdots, X_K)$. Illustrative examples of the method are presented.

The Residue Number System—H. L. Garner (p. 140)

A novel number system called the residue number system is developed from the linear congruence viewpoint. The residue number system is of particular interest because the arithmetic operations of addition, subtraction and multiplication may be executed in the same period of time without the need for carry. The main difficulties of the residue code pertain to the determination of the relative magnitude of two residue representations, and to the division process. A discussion of the arithmetic operations and the conversion process required to convert from a residue code to a weighted code is given. It is concluded that in its present state the residue code is probably not suitable for general purpose computation but is suitable for a special class of control problems. Further research in both components and arithmetic is required if a residue code suitable for general purpose computation is to be obtained.

Bibliography of Digital Magnetic Circuits and Materials—W. L. Morgan (p. 148)

A list of about 400 references relating to magnetic memory and logic circuits has been made. The bibliography is divided into 19 sections. Several sections are devoted to the physical, magnetic, and switching parameters of magnetic materials. Other parts cover the circuit and logical aspects of using magnetic cores, plates, "twistors," thin films, and transfluxors. Attention is given to the use of special memory techniques such as domain wall viscosity readout, cross-field effects, and circuits operated with RF carriers. The use of magnetic cores as half adders, gates, and shift registers is recognized in a separate section. A listing of sources of further information (conference proceedings, books, and other bibliographies) is included.

The Recording and Reproduction of Signals on Magnetic Medium Using Saturation Type Recording—J. J. Miyata and R. R. Hartel (p. 159)

This paper discusses the factors affecting the resolution in saturation magnetic recording. The effect on the recording process of the B-H characteristics of the coating, coating thickness, record-head gap width, head-to-coating separation, self-demagnetization, and record-head residual magnetization are discussed. Equations are derived for the playback process relating the signal amplitude and pulse width to the coating thickness, head-coating separation, and effective gap width of the playback head. It is shown that greatest improvement in resolution can be obtained by development of an extremely thin coating with high ratio of coercivity to remanence and having a rectangular B-H loop. The extremely thin coating will reduce the shortcomings of the record-head field pattern, the self-demagnetization effect, and the loss of resolution in playback process.

Magnetic Core Logic in a High-Speed Card-to-Tape Converter—E. Bloch and R. C. Paulsen (p. 169)

This report describes a static magnetic shift circuit and the logical connectives derived from it. The prime advantages of magnetic circuits are their low cost, high reliability, and ease of maintenance. The application of these circuits to the design of a card-to-tape converter is discussed.

The Use of a Repetitive Differential Analyzer for Finding Roots of Polynomial Equations—P. Madich, J. Petrich, and N. Parezanovich (p. 182)

The paper describes a procedure for obtaining real and complex roots of algebraic equations with real or complex coefficients by the use of a repetitive differential analyzer. The procedure requires only operational amplifiers and ganged linear potentiometers. Differential analyzers are very suitable for solving algebraic equations since they permit visual checking of the procedure and make it possible to investigate how the roots of the polynomial are affected by variation of its coefficients. The procedure is not iterative.

A High-Speed Analog-Digital Computer for Simulation—R. C. Lee and F. B. Cox (p. 186)

This paper describes the principles of operation and logical design of an analog-digital computer capable of simulating complex physical systems in real time. Information in the machine is represented by an analog voltage pulse and a digital number. Arithmetic operations are performed in time-shared analog computing components and conventional digital logical elements. A novel floating-point arithmetic feature is provided to extend the dynamic range of the machine variables.

Instructions and constants are stored on a magnetic drum before computation begins. The instructions determine the sequence of computer operations, and both the instructions and constants are arranged so that random access to the drum is not needed.

The programming techniques developed for the computer are described. The inherent simplicity of these techniques should permit engineers directly concerned with simulation to program their own problems for computer solution.

Six papers from the 1958 National Simulation Conference

Distributed Parameter Vibration with Structural Damping and Noise Excitation—R. V. Powell (p. 197)

A method is described for the electronic analog computer that will permit the determination of the vibration amplitude responses of a distributed system with structural damping to a random-noise excitation such as might be experienced by a missile structure accelerated by a jet propulsion system. There is general agreement among the investigators in the literature that structural damping is both frequency independent and amplitude depend-

ent. Simulation of the structure by a method of normal modes permits the introduction of a discrete equivalent viscous-damping coefficient for each mode frequency, thereby effecting the frequency-independent characteristic of structural damping.

Optimization by Random Search on the Analog Computer—J. K. Munson and A. I. Rubin (p. 200)

One method of searching a system for optimum operating conditions is to evaluate system performance for many randomly-chosen combinations of the independent parameters. This paper explains the use of standard electronic analog computer equipment to accomplish such a search of a mathematical model quickly and economically. Gaussian noise sources generate values of the independent parameters and sample-hold circuits hold those values which give the best value of the optimization criterion. An application of the method to a production allocation problem is mentioned.

Linear System Approximation by Differential Analyzer Simulation of Orthonormal Approximation Functions—E. G. Gilbert (p. 204)

Various analytic procedures have been proposed for minimum integral-square-error approximation of prescribed linear systems; however, they often involve computational difficulties. In the procedure developed in this paper, a group of N linear approximating systems with orthonormal impulse responses $\phi_n(t)$ are realized by operational amplifier circuits. When $h(-t)$ forces the systems ($h(t)$ is the impulse response of the prescribed system) it is found that their outputs at $t=0$ are a_n, the coefficients in

$$h^*(t) = \sum_{n=1}^{N} a_n \phi_n(t),$$

the approximate impulse response. The following points relative to the approximation procedure are developed: constrained and weighted integral-square-error approximations, derivation and realization of orthonormal functions, physical realization of $h^*(t)$, evaluation of error $h(t)-h^*(t)$, and analysis of computer errors. Several approximation examples are given.

Generalized Integration on the Analog Computer—G. A. Bekey (p. 210)

One of the major limitations of the electronic analog computer is its inability to perform directly an integration with respect to a dependent variable. This paper reviews the usual methods of overcoming this limitation, describes the results on an attempt to use Padé time-delay units in generalized integration, and presents the development of a new analog integrator based on a simple numerical integration formula. The integrator can be instrumented using standard analog computer components. The performance of the device is illustrated with several examples.

A Perturbation Technique for Analog Computers—L. Bush and P. Orlando (p. 218)

A study of the motion of a fin-stabilized rocket was undertaken to determine the effect of perturbing forces on the trajectory. The mechanization of a complete problem for an analog computer to include small disturbing forces would result in trajectories which are essentially indistinguishable from the "nominal" or "unperturbed" case because of analog computer accuracy limitations. Instead, the equations of motion for the "nominal" case and the "perturbed" case, derived by first order ballistic perturbation theory, were solved simultaneously with the nominal solution providing inputs to the perturbed solution. The analog computer solution provided both the nominal trajectory and perturbations from this trajectory.

To illustrate the method, the technique is applied to the two-dimensional motion of a rocket in the vertical plane and includes perturbations due to uncertainties in winds, atmospheric density, thrust malalignments, and stability margin.

A Four Quadrant Multiplier Using Triangular Waves, Diodes, Resistors, and Operational Amplifiers—R. E. Pfeiffer (p. 221)

A simple scheme of switching triangular waves and measuring the average current through resistors into a low impedance summing point makes possible four-quadrant multiplication with four diodes, precisely adjusted resistors, and a means of measuring the current. A practical circuit utilizes one operational amplifier to obtain $-(X+Y)/2$ and a second such unit to measure the summing point current. Addition of four auxiliary diodes reduces circuit interactions and makes less stringent requirements on the diodes. A simple operational adjustment procedure is described. Also, a simple means for obtaining the precise resistance balance is outlined. Calibration does not depend upon triangular wave frequency or symmetry. The amplifiers are not required to handle the triangular wave frequencies.

Engineering Management

Vol. EM-6, No. 2, June, 1959

Engineering Department Organization and Control in a Small Company—J. S. Brown (p. 41)

Organization of an engineering department in a small company is described. The four basic functions of the department are discussed; namely, custom engineering, sales assistance, production assistance, and new product design. The role of committees in carrying out interdepartment liaison is presented and the specific working committees and their functions are described. Comments are presented on Management's problems in the areas of 1) providing necessary technical skills, 2) budgetary control of manpower, as required for custom engineering on fixed price contracts and new product development, and 3) intradepartment organization versus integration of the department into the over-all company organization.

Measurement and Control of Economic Activities from the Standpoint of Profitability—J. C. Fisher (p. 46)

It is possible to go a long way toward optimizing the profitability of a complex enterprise by: 1) getting each local management team to commit itself in advance regarding the activities it believes to be marginal, then measuring the profitability of the marginal activities; 2) comparing the performance of company components with that of outside independent agencies; and 3) designing compensation schemes that properly reward efforts aimed at achieving long- and short-term goals.

An Analysis of Personnel Turnover and Replacement—L. A. Kenna (p. 49)

Personnel turnover is a problem facing practically all managerial staffs. It has become a serious problem for some. The same holds true for replacement of personnel.

This paper presents a method for analyzing personnel turnover. The method is relatively simple and yet systematic. Since evaluation techniques would involve too many variables, they are not discussed. Various techniques require specific examples as they do not apply in general. The analysis will apply, in general, to any turnover situation.

In addition the replacement of personnel is discussed. The results from the analysis, and subsequent evaluation, will determine the personnel policy for the hiring of new personnel.

Administering Information Input and Output in Research Laboratories—I. Goldman (p. 55)

Research and development laboratories use information as a raw material in the course of carrying out their assigned function. They, in turn, generate new information.

The input of information referred to is of several varieties—theory, data, applications, economic factors, etc. The information generated is likewise of several kinds—theory, data, devices, processes, etc., which are of importance to the company in maintaining and extending its competitive position and its prestige.

Input information is defined as all of the information that can be gleaned from all sources that will be useful as background in carrying out this project. Similarly, *output information* will be the results of the project when written up as company reports, scientific papers, general articles *plus* the ideas, devices, data, etc., *carried to* the manufacturing operation.

The handling of input information to the research project is a communication process which involves collection, evaluation and dissemination. In analogous fashion, these processes are operative in handling the information output of the laboratory. An analysis of the nature of input and output information components permits a more detailed study of specific requirements and leads to improved procedures for increasing the effectiveness of the communication process.

Recognizing the fact that technical information must compete for top management attention with reports from other major parts of the company—sales, public relations, legal, etc., the importance of the attention-getting power of research reports and communications becomes clearly evident. Some suggestions are given that may be helpful in attaining this objective.

Engineering Writing and Speech

Vol. EWS-2, No. 2, June, 1959

Working With Electrical Engineers in Seminar—A. M. Fountain (p. 46)

Universities are giving increased recognition to the fact that engineers are in dire need of more instruction in good writing. Here is one approach to a solution of this problem.

What are the reasons for publishing in Industry? What are some of the means to this end? This article gives one man's broad view of this rapidly expanding segment of the electronics industry.

While this article describes the uses that may be made of library facilities in one area, its content is equally applicable to similar institutions in other areas. Here, then, is a close look at a few of our sources of information.

By planning illustrations first and putting as much information as possible into them, you can produce a more interesting report with less effort than if you write the text first.

Information Theory

Vol. IT-5, No. 2, June, 1959

The main body of this paper reports on experimental results in sequential detection. In particular, it is shown that the Wald Theory of Sequential Analysis agrees well with experiment for the important case of Bernoulli Detection even when the excess over the boundaries at the termination of an experiment is neglected. The design of the experiments, as well as the experimental apparatus, are also discussed. Experimental curves of the Operating Characteristic (OC) and Average Sample Number (ASN) Functions for several sets of parameters are given.

A publication relative to the main body of this paper is summarized. The results of this publication are used in the Addendum, to study the resonant properties of the exponential class of sequential detectors. The practical use of these detectors for parameter estimation is discussed.

Minimum Scan Pattern Recognition—A. Gill (p. 52)

Speedier and simpler pattern-recognition systems can be realized when provided with a minimum-scan reading device. For the idealized case, where the input set of patterns is finite, binary and errorless, a theorem is proved which enables the designer to predict the efficiency range of the contemplated reading device. A constructive method, which can be readily programmed for computer processing, is proposed for finding the shortest scanning path realizable for any given set. In the case of noise, scanning paths are sought which maintain a prescribed minimal "distance" between the patterns, and hence yield a prescribed level of error-detecting capability The theorem previously proved is extended for this case, and a constructive method is proposed for finding the shortest path consistent with any specified minimal distance, for any given set of patterns.

On the Mean-Square Noise Power of an Optimum Linear Digital Filter for Correlated Noise Input—M. Blum (p. 58)

An asymptotic solution for the mean-square output noise power of an optimum digital filter is obtained. It is assumed that the input consists of a polynomial plus correlated noise. The asymptotic solution is found by fixing the interval between samples and allowing the number of samples to approach infinity. The solution obtained for the minimum variance filter is compared with the solution as obtained for the "least-squares filter," and it is shown that the latter filter is asymptotically efficient as compared to the former. It is shown for each of the above filters that the mean-square output noise power is proportional to the spectral density function of the correlated noise, evaluated at zero frequency, and that the factor of proportionality is the same.

Single-Error-Correcting Codes for Asymmetric Binary Channels—W. H. Kim and C. Freiman (p. 62)

In a highly-asymmetric binary channel it may be necessary to correct only those errors which result from incorrect transmission of one of the two code elements. Minimum weight-distance relationships and rules for generating single-error correcting codes in such situations are given. More code characters are generally obtained for a given character length than are obtained with codes designed for single-error correction in symmetric channels. Examples are given, including one which specifies the code which results in the highest average probability of correct transmission of equiprobable messages through a highly-asymmetric channel.

Optimal Filtering of Periodic Pulse-Modulated Time Series—W. A. Janos (p. 67)

The present study concerns the optimal filtering of a class of input time series in which the amplitude is modulated by uniformly-pulsed periodic functions. A uniform sampling of the output at a period equal to the pulsing period displays the property of time invariance. The consequent usage of bilateral Fourier-Laplace transformations and the separability of terms implicit in the time-invariant nature of the processing effectively inverts the Wiener-Hopf equation and solves the problem. The weighting function is shown to be the sum of the Wiener-Zadeh-Ragazzini solution for the unmodulated case and set of appropriately-weighted delta-function-derivative terms occurring at each end point of the pulsing intervals.

The Second-Order Distribution of Integrated Shot Noise—J. Keilson and N. D. Mermin (p. 75)

A Theorem on Cross Correlation Between Noisy Channels—J. Keilson, N. M. Mermin, and P. Bello (p. 77)

Signal-to-Noise Ratios in Smooth Limiters—J. Galejs (p. 79)

A Note on the Estimation of Signal Waveform—D. Middleton (p. 86)

The problem of estimating signal waveform from received data that is corrupted by noise is briefly considered from the viewpoint of decision theory, in extension of some earlier work. The noise is assumed to be a Gauss process, which may or may not be stationary. Here, however, nothing is known about the signal process except that it may be deterministic, entirely random, or a mixed process. Two new features in the present application are the representation of the signal process as a linear expansion (M. S.) in complete orthonormal sets, and suitable choices of these sets. Examples involving discrete and continuous sampling on a finite interval, with various choices of *a priori* distributions of signal parameters are described, including calculations of Bayes and Minimax risks.

Nuclear Science

VOL. NS-6, NO. 2, JUNE, 1959

Solid-State Issue

From the Editor—R. F. Shea (p. 4)

Transistorized Reactor Instrumentation and Protective Circuits—R. R. Hoge and D. J. Niehaus (p. 42)

Nuclear reactor instrumentation and protection circuits which cover a range of six and one-half decades of reactor power are described. The circuits have been designed to provide maximum protection for the reactor while maintaining the ability to prevent unscheduled shutdowns. To accomplish these features, solid state components and fail-safe designs have been employed wherever feasible.

Radiation Effects in Silicon Solar Cells—F. A. Junga and G. M. Enslow (p. 49)

Calculations have been performed to estimate the number of atoms displaced from normal sites by Compton Electrons from Co^{60} gamma rays and by slow and fast neutrons. The resultant change in carrier lifetimes and mobilities are used to predict the performance of a silicon solar cell under gamma and neutron irradiation. The effect of annealing of defects is considered, and from these computations an estimate is made to show the minimum flux necessary to produce noticeable damage. Data are presented showing the effects of Co^{60} gamma rays on 10 silicon solar cells and comparison is made with the theory.

Transistorized Log-Period Amplifier—E. J. Wade and D. S. Davidson (p. 53)

A log-period amplifier is described which is combined with power supply on a rack mounted chassis with a 7-inch panel. The circuits are transistorized except for electrometer tubes and log diodes. Input power is 25 watts. Noise reducing and calibrating circuits are built in as well as a catching circuit to keep the log diode in its logarithmic range.

Transistorized Linear Pulse Amplifiers—S. C. Baker (p. 57)

The basic investigation of transistor feedback amplifiers have proven mathematically simple and of great practical value. The behavior of single-stage common-emitter amplifiers is described and provides a building block with which cascaded feedback amplifiers can be analyzed and designed.

The problem of designing these amplifiers is complex, and what are felt to be the most important phases of the problem are discussed.

Beam-Profile Indicator—H. G. Jackson, D. A. Mack, and C. Wiegand (p. 64)

This paper describes an instrument for displaying intensity profiles of charged-particle beams that emerge from high-energy accelerators. The intensity vs position on a strip of 21 scintillation counters each 1 by 1 cm appears as a histogram on an oscilloscope. The display is accomplished by employing transistor circuits to amplify and integrate the outputs of the multiplier phototubes. The accumulated charge associated with each counter elements is then read out in sequence by means of a blocking-oscillator commutator. The output signal is further amplified logarithmically for oscilloscope deflection.

The Transistor Switch—A Solid-State Power Relay—P. F. Pittman (p. 69)

The Trinistor switch is a new semiconductor device which can be used to provide control of large amounts of load power. The characteristics of the Trinistor swtich are similar to those of a thyratron because the Trinistor will either absorb a high voltage and prevent the flow of load current or break over to a low voltage and allow load current to flow. A third terminal can be used for the application of a control current which initiates this breakover action.

The switching efficiency of the Trinistor is quite high because the device can block a voltage of several hundred volts at a few milliamperes leakage or conduct 50 amperes of current at a voltage drop of about 1.0 volt.

A power control device such as the Trinistor switch can be used to control either ac or dc power with a minimum of associated circuitry. This device can be used in place of relays or other switching devices to provide contactless switching in circuits which have a minimum of weight and require a minimum of space.

A Simplified Logarithmic Integrator Circuit—H. E. DeBolt (p. 74)

This article describes a simplified logarithmic integrator circuit as well as a synthesis technique for designing this circuit for a specific application. Comparisons are drawn between the circuit proposed herein and the Cooke-Yarborough log integrator circuit and Lichtenstein log integrator circuit.

Production Techniques

VOL. PT-4, JUNE, 1959

Design by Algorithm: A Mathematical Method of Designing Standard Assemblies for Minimum Manufacturing Cost—D. H. Evans (p. 4)

It is pointed out that in order to reduce manufacturing costs, it is often advantageous to make use of standard assemblies despite the waste incurred due to the non-use of parts of these standard assemblies in meeting specific requirements. A special prototype problem is considered based on that premise; it arose in practice, in the design for production of logic circuits. A problem is outlined which requires that 55 basic elements, with one to seven diode outputs each, be assembled into a number of standard assemblies, and with a minimum of waste of diode outputs.

The problem considered is: Given the number required for each size for basic elements of sizes n, $n-1, \ldots, 1$. Further, for $k=1$,

2, . . . , n, a basic element of size k may be used instead of a basic element of size k or $k-1$ . . . , or 1 but consequently incurring a waste proportional to 0, or 1, . . . , or $k-1$, respectively. Then the problem is to define a standard assembly in terms of the number and sizes of basic elements and the number of such standard assemblies necessary to fulfill the requirements, under the condition that the waste be a minimum. A simple algorithm is given for finding the make-up of the standard assembly.

The Appendix gives a more rigorous mathematical generalization for the solution of uniqueness and minimality, and its proof; linear programming is used in this treatment.

Design Improvement of an Airborne System Through Mathematical Prediction of its Vibrations and Dynamics—D. Ehrenpreis (p. 11)

An outline is presented of the analysis, engineering study, and theoretical investigation of the steady-state vibrations and the sudden-impulse-shock dynamic characteristics of a new military airborne gimbaled system.

A mathematical model is described which consists of three mathematical regimes—each defining the distribution of dynamic masses and motions for one plane of excitation. Comprehensive recursion tables for the three regimes were filled out by the high-speed No. 704 Digital Computer. Dynamic-equation matrix coefficients were determined for each frequency. Where the error function was zero, the recursion tables were filled out to determine true mode shapes and distributions. Additional programming determined forcing-function responses and, through the use of open parameters, determined the effects of modifying masses and other elements of the system. Aerodynamic loads for extreme flight conditions were rigorously investigated, and margins-of-safety were determined.

It is reported that this mathematical method led to recommendations for wieght savings, as well as improvement in the dynamic characteristics of the system.

An Approach to Airborne Digital Computer Equipment Construction—P. E. Boron and E. N. King (p. 18)

One method of building airborne digital equipment is discussed, which makes use of the modularized etched-wiring plug-in philosophy, and which utilizes an all-etched-wiring harness to accomplish the entire complex of connections between plug-in units. Of a possible 364 external connections, 183 are actually brought to a possible 1716 connector contacts. These contacts, and their associated printed wiring, tie together 32 flip-flop modules and 17 diode-gating etched-pattern matrix arrays, without the use of a single piece of conventional wiring. Points of emphasis are miniaturization, reliability, small weight, accessibility, and manufacturability of the equipment.

Increased Reliability and Better Quality Control Through Mechanized Assembly and Test—L. K. Lee and J. W. Buffington (p. 22)

It is pointed out that the electronics industry long a heavy contributor to automation in other industries, has until recently been in the role, one might say, of the cobbler's son who goes barefoot. Past and future expansion of the electronics industry is charted, as it is estimated that an all-out national emergency would demand an output of 10 times our present production rate. Automation is posed as a solution to this dilemma; as well as an aid to uniformity, miniaturization, conservation, quality, and reliability.

Changing production requirements are cited. It is also emphasized that the product, the process, or both must be completely changed in order to make automatic production feasible. Two automation approaches are discussed: that of the component-parts manufacturer, and that of the equipment assembler. Three machines are described: a simple bench-type individual-insertion machine, a fully-automatic in-line insertion machine, and an automatic forced-area dip-soldering machine. Assembly efficiency of the in-line machine is charted in detail (for early 1956 operation). A 7½% rework rate is quoted without insertion inspection, and a 0.07% rate with insertion inspection.

The need for greater reliability is stressed, and attainment of this greater reliability through automatic assembly and automatic test is treated at some length. In conclusion, the author admits that the present state of the art leaves much to be desired, as we build new machines and modify our products for mass-production suitability. Yet high hopes are expressed that much simpler quality-control procedures and much more uniform products will give considerably more reliable equipment in the field—and this, in the not too distant future.

Ultrasonics Applied to Metal Fusion-Joining Processes—E. E. Weismantel and J. G. Thomas (p. 28) (*Abstract only.*)

An Investigation of Production Problems Relating to the Power-Carrying Capacity of a K-Band Microwave Component—D. E. Davis and G. A. Moglia (p. 29)

Findings are presented on the effect of various mechanical parameters, performance criteria, environmental conditions, and production techniques. Discussion centers about a K-band microwave duplexer, with particular emphasis on the hybrid ring, in an attempt to reduce breakdown rejections. Of humidity, temperature and pressure, only the latter had a noticable effect on the breakdown measurements. Performance experiments covered pulse width, phasing, rise time and duty cycle with relation to both duplexer breakdown and magnetron life; and with rise time affecting breakdown. The mechanical aspects of dimensions, tolerances, imperfections and finish were investigated; and the latter two found to be the most important. The production techniques contributing to the determined causes were thoroughly investigated. Cleaning processes were proved to be of considerable importance. Corrective measures and effective rework procedures are described.

Space Electronics and Telemetry

Vol. SET-5, No. 2, June, 1959

Electromechanical Energy Conversions in a Cylindrical Pinch Process—J. L. Neuringer (p. 55)

The series circuit associated with the high current discharge (pinch effect) through a cylindrical tube filled with gas is analyzed from an energy viewpoint. The electromagnetic and mechanical energies, and their interconversions during the compression of the gas, are explicitly displayed and identified. As a consequence of the above analysis, the exact nonlinear circuit equation and appropriate initial conditions are then formulated. This equation, when coupled with the equation for the radial motion of the pinched gas, will yield an exact solution for the electromechanical interaction.

Problems of Ground Simulation of Long-Range Space Flight Environmental Conditions—T. C. Helvey (p. 57)

Consideration of RF Parameters for PCM Telemetry Systems—D. D. McRae (p. 61)

Considerable differences of opinion have existed concerning the requirements for transmission of PCM information. Quite often, PCM has been accepted as a system inherently requiring wide RF bandwidths and correspondingly poor noise performance. This paper considers selections of RF parameters for PCM telemetry systems. It points out that if these parameters are correctly chosen, the bandwidths and sensitivity of a PCM system may be made comparable with those of other existing telemetry systems.

A Digital Computer System for Terminal-Area Air Traffic Control—E. L. Braun and A. S. Gianoplus (p. 66)

The terminal-area air traffic control (ATC) operation is defined and a classification provided of its prob em areas which demonstrates that the use of both general purpose computation and special-purpose data processing are indicated. The characteristics of the digital-computing equipment for the functions of tracking, scheduling, and guidance are described. The over-all capabilities of the system are presented, including a description of the facilities for entry, sensing, communication, and display of pertinent data.

Glossary of Astronautics Terminology—D. C. Madrid (p. 73)

An intelligent comprehension of the rapidly expanding field of astronautics demands availability of ready reference sources of the latest terms which have a particular application in this field.

The 9898th Air Reserve Squadron (R&D) of Eau Gallie, Fla., which has many active participants in the daily activities of the Air Force Missile Test Center at Patrick Air Force Base, Fla., and the Atlantic Missile Range, has been especially concerned both with the problems of understanding the expanding field of astronautics, and with its responsibility of passing on information on terms which its members are now using in their daily livelihood.

The problem of developing a suitable glossary of astronautic terms was made a group project, and when the squadron members examined this problem, and completed their research and discussion, their decisions were submitted to designated leaders. Then the terms were analyzed with respect to peculiarity, and presence in lists of astronautic terms already available. The final list of terms presented here is regarded to be of sufficient interest to anyone having either presented or future astronautic activities.

A Super-Fast, Carrier Quieted Telemetry System for Missile Impact Instrumentation—J. L. Wright and J. C. Ruscus (p. 76)

A fast-rising, carrier quieted telemetry system has been developed which measures, to one microsecond, the time between events during the sled test destruction of an impacting missile. Because of the short transmission range expected during sled tests, reliable carrier quieting of the receiver is obtained with transmitters of power outputs under 100 mw. High speed of response is obtainable by the use of rapid on-off keying of the carrier and the use of receivers and pulse amplifiers of sufficient bandwidth.

The timing information from the missile is read from a digital chronograph instead of being obtained by analyzing taped information.

Short-Distance Telemetering of Physiological Information—H. G. Beenken and F. L. Dunn (p. 82)

A completely transistorized radio transmitter and a receiving system are described operating at 104 mc. The weight of the transmitter is under two pounds without the use of miniature parts. Design is for transmission of up to ten channels with bandwidths of 250 and 1000 cps. The channel reported has a carrier frequency of 2100 cps and was tested for EKG recording. Satisfactory calibrated records were obtained while walking and while on treadmill.

Operational Characteristics of the TLM-18 Automatic Tracking Telemetry Antenna—F. S. Coxe (p. 87)

A brief description of the TLM-18 antenna, including a block diagram, is followed by operational examples of its use in tracking missiles to the limits of radio line of sight. Present abilities of the antenna are discussed, and points are cited to show where these abilities exceed, in some aspects, requirements for missile tracking. It is shown that the location of the antenna and the type modulation of the missile can have adverse effects upon smooth operation.

Abstracts and References

Compiled by the Radio Research Organization of the Department of Scientific and Industrial Research, London, England, and Published by Arrangement with that Department and the *Electronic and Radio Engineer*, incorporating *Wireless Engineer*, London, England

NOTE: The Institute of Radio Engineers does not have available copies of the publications mentioned in these pages, nor does it have reprints of the articles abstracted. Correspondence regarding these articles and requests for their procurement should be addressed to the individual publications, not to the IRE.

The number in heavy type at the upper left of each Abstract is its Universal Decimal Classification number. The number in heavy type at the top right is the serial number of the Abstract. DC numbers marked with a dagger (†) must be regarded as provisional.

The Index to the Abstracts and References published in the PROC. IRE from February, 1958 through January, 1959 is published by the PROC. IRE, May, 1959, Part II. It is also published by *Electronic and Radio Engineer*, incorporating *Wireless Engineer*, and included in the March, 1959 issue of that journal. Included with the Index is a selected list of journals scanned for abstracting with publishers' addresses.

ACOUSTICS AND AUDIO FREQUENCIES

534.213:539.2 2444
Theory of Ultrasonic Absorption in Metals: the Collision-Drag Effect—T. Holstein. (*Phys. Rev.*, vol. 113, pp. 479–496; January 15, 1959.)

534.232:534.88 2445
High-Fidelity Underwater Sound Transducers—C. C. Sims. (PROC. IRE, vol. 47, pp. 866–871; May, 1959.) "The problems involved in designing an underwater sound transducer for the AF range are discussed, and a new transducer for the range from about 40 cps to about 20 kc is described."

534.232:537.228.1:546.431.824–31 2446
Description of the Resonances of Short Solid Barium Titanate Cylinders—J. S. Arnold and J. G. Martner. (*J. Acoust. Soc. Amer.*, vol. 31, pp. 217–226; February, 1959.) The distributions of axial and radial vibration on the plane surfaces of $BaTiO_3$ disks have been determined for a number of modes.

534.61 2447
Detecting Sound Fields—C. B. Sacerdote. (*J. Acoust. Soc. Amer.*, vol. 31, pp. 133–136; February, 1959.) A feedback system is described in which the sound pressure at any one point is automatically maintained constant. A controlling signal, derived from a microphone with uniform frequency response corrects for nonuniformity in the loudspeaker response. The method is applied to the calibration of microphones and in the study of diffraction and reflection effects.

534.61–8:621.395.616 2448
Condenser Microphones with Plastic Diaphragms for Airborne Ultrasonics: Part 1—K. Matsuzawa. (*J. Phys. Soc. Japan*, vol. 13, pp. 1533–1543; December, 1958.) Report of an investigation of microphones of the type described by Kuhl, *et al.* (985 of 1955), dealing in particular with the required roughness of the back plate and the prestraining of the diaphragm.

534.614–8:621.3.018.75 2449
Modifications to Standard Pulse Techniques for Ultrasonic Velocity Measurements—A. Myers, L. Mackinnon and F. E. Hoare. (*J. Acoust. Soc. Amer.*, vol. 31, pp. 161–162; February, 1959.) Modifications to the circuit proposed by Cedrone and Curran (1234 of 1955) allow measurements to be made on short solid specimens having low attenuation.

534.782 2450
Electronics and the Phonetician—H. J. F. Crabbe. (*Wireless World*, vol. 65, pp. 289–294; June, 1959.) Description of electronic equipment for speech analysis and synthesis.

534.782 2451
The Design and Operation of the Mechanical Speech Recognizer at University College London—P. Denes. (*J. Brit. IRE*, vol. 19, pp. 219–229; April, 1959. Discussion, pp. 230–234.) Description of a device which converts the sound waves produced by a speaker into a series of type-written digits.

534.782 2452
Theoretical Aspects of Mechanical Speech Recognition—D. B. Fry. (*J. Brit. IRE*, vol. 19, pp. 211–218; April, 1959. Discussion, pp. 230–234.)

534.839 2453
Noise Measurement—E. Lübcke. (*Frequenz*, vol. 12, pp. 209–213; July, 1958.) Various methods of objective noise measurement are discussed with particular emphasis on the need for taking account of the increase in annoyance with increasing frequency. A suitable noise meter with analyzer is described.

534.851:389.6 2454
The International Standardization of Disk Recording—P. H. Werner. (*Tech. Mitt. PTT*, vol. 36, pp. 355–360; September 1, 1958. In French and German.) Summary of the recommendations adopted by the International Electrotechnical Commission for the standardization of commercial and professional disk recordings, including the standards proposed for stereophonic recordings. For magnetic tape standards see 1010 of 1958.

621.395.61 2455
Acoustic-Front Damping in Dynamic Microphones—W. T. Fiala. (*Audio*, vol. 43, pp. 28–86; March, 1959.) Acoustic resistance is provided by a narrow circular slot formed between the pole plate and a solid cap. With this construction the controlling resistance improves the high-frequency response and forms a sound entrance which needs no further protection.

621.395.623.7 2456
Acoustic Interaction in Vented Loudspeaker Enclosures—E. de Boer. (*J. Acoust. Soc. Amer.*, vol. 31, pp. 246–247; February, 1959.) An expression for sound pressure at a distance is derived from the combined sound fields of diaphragm and aperture. Near-field interaction can be represented in the conventional electrical analog circuit by a mutual inductance. Applications are discussed. See also 3384 of 1957 (Lyon).

ANTENNAS AND TRANSMISSION LINES

621.315.212.001.4 2457
Capabilities of Coaxial Cable: Parts 1 and 2—E. T. Pfund, Jr., W. F. Croft, B. Suverkrop and P. S. Klasky. (*Electronic Ind.*, vol. 17, pp. 55–57 and 75–77; November and December, 1958.) The results are given of tests on six different 50-Ω solid-sheathed coaxial cables. Each cable was subjected to extremes of temperature, to vibration tests and to high-altitude corona discharge. Measurements were made of attenuation, capacitance and dielectric strength.

621.372.2 2458
General Considerations on the Theory of Multiple Lines—W. Oehl, G. Seeger and H. G. Stäblein. (*Arch. elekt. Übertragung*, vol. 12, pp. 245–250; June, 1958.) By orthogonal transformation a set of n coupled transmission lines is converted into n equivalent lines so that the equations of the two-wire transmission line become applicable.

621.372.2 2459
Theory of the Helical Line of Finite Wire Thickness with reference to the Rotation of the Plane of Polarization of Waveguide Waves—G. Piefke. (*Arch. elekt. Übertragung*, vol. 12, pp. 309–316; July, 1958.) A general equation is obtained for calculating the propagation constants of all possible modes on a helical line with finite wire thickness and any outer medium. Propagation of linearly polarized waves inside a metal tube with an internal helical groove is investigated to show that a rotation of the plane of polarization occurs.

621.372.2:621.372.51.012.11 2460
A New Circle Diagram for Transformations in Transmission-Line Technique—G. W. Epprecht. (*Arch. elekt. Übertragung*, vol. 12, pp. 289–293; June, 1958.) Quadripole imped-

ance transformation using a modified Carter diagram is described.

621.372.8 2461
The Application of the Asymptotic Integration of the Wave Equation to the Solution of some Waveguide and Resonator Problems—A. Gutman. (*Dokl. Ak. Nauk SSSR*, vol. 125, pp. 1252–1255; April 21, 1959.) Three types of waveguides are considered: (*a*) an infinite waveguide with consecutively increasing and decreasing circular cross section; (*b*) a semi-infinite waveguide with flared end; (*c*) a system of two helical waveguides.

621.372.8:621.372.413 2462
Resonant Properties of Nonreciprocal Ring Circuits—F. J. Tischer. (TRANS. IRE, vol. MTT-6, pp. 66–71; January, 1958. Abstract, PROC. IRE, vol. 46, p. 804; April, 1958.)

621.372.8.029.65 2463
Rectangular and Circular Millimetre Waveguides—P. D. Coleman and R. C. Becker. (*Electronics*, vol. 32, pp. 50–51; May 1, 1959.) Tables of the dimensions and electrical characteristics of waveguides for use in the frequency range 26–350 kmc.

621.372.829 2464
Space Resonance in a Helical Waveguide Located in a Magnetic-Dielectric Medium—V. P. Shestopalov and B. V. Kondratiev. (*Dokl. Ak. Nauk SSSR*, vol. 125, pp. 794–797; April 1, 1959.) A brief mathematical analysis. The retardation of waves by a helix and a dielectric is shown graphically. Examination of the curves indicates that the magnetic-dielectric medium not only increases the retardation but narrows the band within which only fast-moving waves can be propagated.

621.372.832.6 2465
Microwave Multiplexing Circuits—R. E. Stone. (*Electronic Ind.*, vol. 17, pp. 62–65; November, 1958.) A theoretical and practical discussion of the hybrid ring as a multiple coupling unit.

621.372.852.1:621.318.134 2466
A Microwave Ferrite Frequency Separator—H. Rapaport. (TRANS. IRE, vol. MTT-6, pp. 53–58; January, 1958. Abstract, PROC. IRE, vol. 46, p. 804; April, 1958.)

621.372.852.15:621.318.134 2467
Ferrite-Loaded, Circularly Polarized Microwave Cavity Filters—W. L. Whirry and C. E. Nelson. (TRANS. IRE, vol. MTT-6, pp. 59–65; January, 1958. Abstract, PROC. IRE, vol. 46, p. 804; April, 1958.)

621.372.852.32 2468
A Medium-Power Ferrimagnetic Microwave Limiter—E. N. Skomal and M. A. Medina. (PROC. IRE, vol. 47, pp. 1000–1001; May, 1959.) The limiter can be adjusted to attenuate an input of 30–1000 w peak to an output of 100 mw at frequencies near 9360 mc.

621.396.67:623.827 2469
Submarine Communication Antenna Systems—R. W. Turner. (PROC. IRE, vol. 47, pp. 735–739; May, 1959.) The special problems involved in the design of antennas for submarines are described.

621.396.677.3 2470
A Simple Graphical Method of Preparing Power Distribution Diagrams for Horizontal Dipole Arrays—P. J. Joglekar. (*J. Inst. Telecommun. Engrs., India*, vol. 5, pp. 49–54; December, 1958.) The horizontal-directivity factors are plotted for arrays one, two and four dipoles wide.

621.396.677.3:523.164 2471
Design of "Optimum" Arrays for Direction-Finding—N. F. Barber. (*Electronic Radio Eng.*, vol. 36, pp. 222–232; June, 1959.) A survey of the principles underlying the design of antennas for use in radio astronomy. See 3338 of 1958.

621.396.677.7:621.318.134 2472
Nonmechanical Beam Steering by Scattering from Ferrites—M. S. Wheeler. (TRANS. IRE, vol. MTT-6, pp. 38–42; January, 1958. Abstract, PROC. IRE, vol. 46, p. 804; April, 1958.)

621.396.677.7:621.318.134 2473
An Electronic Scan using a Ferrite Aperture Luneberg Lens System—D. B. Medved. (TRANS. IRE, vol. MTT-6, pp. 101–103; January, 1958. Abstract, PROC. IRE, vol. 46, p. 805; April, 1958.)

621.396.677.833.029.64 2474
Directivity Pattern of 3-cm Parabolic Reflector, Feed of which is Displaced from the Focus—S. Swarup and G. P. Srivastava. (*J. Inst. Telecommun. Engrs., India*, vol. 5, pp. 44–48; December, 1958.)

621.396.677.859 2475
Rigid Radome Design Considerations—P. Davis and A. Cohen. (*Electronics*, vol. 32, pp. 66–69; April 17, 1959.) Data are given on thin-shell and space-frame methods of construction.

AUTOMATIC COMPUTERS

681.142 2476
Random Number Generator using Subharmonic Oscillators—F. Sterzer. (*Rev. Sci. Instr.*, vol. 30, pp. 241–243; April, 1959.) The outputs of two 2-kmc oscillators driven from a common 4-kmc source are combined in a hybrid ring. The generator can produce random binary digits at a maximum rate of 3×10^7 digits per second.

681.142 2477
Pulsed Analogue Computer for Simulation of Aircraft—A. W. Herzog. (PROC. IRE, vol. 47, pp. 847–851; May, 1959.) A description is given of the logical design of a computer for solving the nonlinear differential equations encountered in the simulation of aircraft performance under various flight conditions.

681.142:061.3 2478
Summarized Proceedings of a Conference on Solid-State Memory and Switching Devices—London, September, 1958. (*Brit. J. Appl. Phys.*, vol. 10, pp. 153–158; April, 1959.) Some of the newer techniques are discussed with reference to ferrite, ferroelectric and superconducting devices, and magnetic thin films.

681.142:[621.314.7+621.318.042 2479
Transistors and Cores in Counting Circuits—F. Rozner and P. Pengelly. (*Electronic Engrg.*, vol. 31, pp. 272–274; May, 1959.) It is shown how square-loop magnetic cores and transistors can be combined to form noncritical reliable counting circuits capable of handling input frequencies up to 750 kc.

621.142:621.316.8 2480
Unifying Design Principle for the Resistance Network Analogue—F. C. Gair. (*Brit. J. Appl. Phys.*, vol. 10, pp. 166–172; April, 1959.) A "cell principle" technique due to Macneal (1331 of 1954) is extended and generalized. As an illustration, Poisson's equation is integrated over the volume of a representative small cell, in which form it is easier to appreciate the analogy with the resistance network and to arrive at the relevant design parameters.

681.142:621.316.8 2481
Use of an Electronic Analogue Computer with Resistance Network Analogues—J. P. Korthals Altes. (*Brit. J. Appl. Phys.*, vol. 10, pp. 176–180; April, 1959.) A method for solving partial differential equations of the elliptical type is described. The method is iterative and adjustments are made automatically by means of electronic storage elements and a switching mechanism. Some results are given.

681.142:621.318.134 2482
Magnetic Matrix Stores—W. A. Cole. (*Wireless World*, vol. 65, pp. 279–283; June, 1959.) Review of computer storage systems based on ferrites with rectangular hysteresis loops.

681.142:681.42.002.2 2483
Lens Designing by Electronic Digital Computer: Part 1—C. G. Wynne. (*Proc. Phys. Soc.*, vol. 73, pp. 777–787; May 1, 1959.) Different methods of designing optical lenses by digital computer are considered in the light of existing aberration theory.

CIRCUITS AND CIRCUIT ELEMENTS

621.3.049.7 2484
The D.O.F.L. Microelectronics Program—T. A. Prugh, J. R. Nall and N. J. Doctor. (PROC. IRE, vol. 47, pp. 882–894; May, 1959.) Some of the microminiaturization techniques used at the Diamond Ordnance Fuze Laboratories are described.

621.3.049.7 2485
The Micro-module: a Logical Approach to Microminiaturization—S. F. Danko, W. L. Doxey and J. P. McNaull. (PROC. IRE, vol. 47, pp. 894–903; May, 1959.) A review is given of the progress of miniaturization; the advantages of the micro-module system, the assembly of microelement components into units with a specified electronic function, are outlined.

621.3.049.7 2486
Micro-module Design Progress—P. G. Jacobs. (*Elec. Mfg.*, vol. 63, pp. 78–85; March, 1959.) Details are given of the application of a modular technique in the construction of a complete prototype communication receiver and certain digital circuits for multiplex equipment.

621.3.049.75 2487
Test Patterns for Printed-Circuit Materials—T. D. Schlabach and E. E. Wright. (*Bell Lab. Rec.*, vol. 37, pp. 93–95; March, 1959.)

621.3.049.75:621.396.65 2488
Printed Circuits Applied to Broad-Band Microwave Links—R. Rowland. (*Electronic Engrg.*, vol. 31, pp. 256–261; May, 1959.) Detailed review of the characteristics and advantages of typical printed circuits.

621.316.825 2489
Thermistors for Linear Temperature Readings—A. B. Soble. (*Electronic Ind.*, vol. 17, pp. 66–67; November, 1958.) Two circuits are described for deriving an error voltage which varies linearly with the difference between actual and desired temperature.

621.316.86 2490
The Performance of Pyrolytic Carbon Resistors—R. H. W. Burkett. (*Brit. Commun. Electronics*, vol. 6, pp. 264–268; April, 1959.) The major factors affecting performance are carbon film thickness, moisture permeability and thickness of protective coating, operating temperature, and the quality of the ceramic substrate. The effect of these factors is small if the carbon film has a thickness of at least 100 Å.

621.316.86.019.3 2491
Realistic Temperature-Power Derating Requirements for Carbon Composition Resistors—J. L. Easterday and H. Braner. (*Elec. Mfg.*, vol. 63, pp. 141–145, 182; March, 1959.) Two derating methods are described, based on statistical analyses of load/life data.

621.318.57:621.318.042 2492
Rectangular-Hysteresis-Loop Magnetic Cores as Switching Elements—J. F. Kaposi. (*Electronic Engrg.*, vol. 31, pp. 278–283; May, 1959.) Theoretical bases and experimental results are given for core switching with voltage and current pulses.

621.319.4.012 2493
Dielectric Losses with Periodic Rectangular Voltage Pulses—B. Gross. (*Frequenz*, vol. 12, pp. 230–231; July, 1958.) Application of a different method to the solution of a capacitor loss problem dealt with by Eisenlohr (1352 of 1957).

621.372.01 2494
Elements of Electronic Circuits: Part 3—Amplitude Limiting—J. M. Peters. (*Wireless World*, vol. 65, pp. 276–278; June, 1959.) Part 2: 2138 of July.

621.372.5 2495
A General Network Theorem—G. Wunsch. (*Nachrichtentech. Z.*, vol. 8, pp. 205–208; May, 1958.) The realization of the transmission factor of a four-terminal network with lumped circuit elements by a passive symmetrical quadripole and a transformer is discussed.

621.372.5 2496
Network Characteristics—J. T. Allanson. (*Electronic Radio Engr.*, vol. 36, pp. 233–237; June, 1959.) The "common network transformation" theorem of Griffiths and Mole (see 705 of 1957) is shown to lack generality.

621.372.5:512.831 2497
Matrix Analysis of Vacuum-Tube Circuits—M. N. Srikantaswamy and K. K. Nair. (*J. Inst. Telecommun. Engrs., India*, vol. 5, pp. 23–32; December, 1958.) The equivalent four-terminal network for a feedback amplifier is derived and the criterion for oscillation is deduced.

621.372.54 2498
Tchebycheff Approximation for Loss-Free Image-Parameter Filters according to Cauer—H. Zemanek and K. Walk. (*Nachrichtentech. Z.*, vol. 11, pp. 307–314; June, 1958.)

621.373 2499
Passage of a Nonlinear Oscillatory System through Resonance—B. V. Chirikov. (*Dokl. Ak. Nauk SSSR*, vol. 125, pp. 1015–1018; April 11, 1959.) A mathematical analysis of a nonlinear oscillator with one degree of freedom which can be described by a Hamiltonian.

621.373.1.018.756 2500
Improved Low-Repetition-Rate Millimicrosecond Pulse Generator—C. A. Burrus. (*Rev. Sci. Instr.*, vol. 30, pp. 295–296; April, 1959.) A discharge-line device using a vibrating reed type of mercury switch in a suitable coaxial mounting provides pulse repetition rates of up to 500 cps.

621.373.43 2501
Half-Cycle Resonant Delay Circuit—B. Howland. (PROC. IRE, vol. 47, pp. 993–994; May, 1959.) A new circuit generating a rectangular pulse of duration equal to the natural half cycle of an LC circuit. The principles are applicable to the generation of mμsec pulses.

621.373.431.1 2502
Series Diode Increases Multivibrator Sensitivity—M. M. Vojinovic. (*Electronics*, vol. 32, pp. 90–91; April 24, 1959.) "Triggering sensitivity of monostable multivibrators may be greatly increased by using a semiconductor diode as a series nonlinear element in the feedback loop. Good stability can be achieved."

621.373.431.1:621.314.7 2503
Multivibrator Circuit using p-n-p and n-p-n Junction Transistors—D. T. Jovanovic. (*Electronic Engrg.*, vol. 31, p. 301; May, 1959.) Details of an improved circuit giving low output impedance and small power consumption.

621.373.431.2:621.314.7 2504
Analysis and Design of a Transistor Blocking Oscillator including Inherent Nonlinearities—J. A. Narud and M. R. Aaron. (*Bell Sys. Tech. J.*, vol. 38, pp. 785–852; May, 1959.) The nonlinear differential equations governing circuit performance are derived. Analog and digital computer solutions yield pulse responses in agreement with experimental results.

621.374.3 2505
Ten-Mc/s Pulse-Amplitude Discriminator—J. Mey. (*Rev. Sci. Instr.*, vol. 30, pp. 282–284; April, 1959.) "A pulse-height discriminator has been developed which is capable of operating at repetition rates up to 10 mc. It accepts positive input pulses with a threshold adjustable from 1 to 11 v. The output signal is of constant shape and amplitude. The circuit is described and test results are given."

621.374.32 2506
A New Type of Ring Counter—P. J. Westoby. (*Electronic Engrg.*, vol. 31, pp. 295–298; May, 1959.) A system is described using separate Eccles-Jordan circuits, in which any number of stages may be employed. Advantages over other systems are indicated.

621.374.32:621.318.57 2507
How Ring Counters Work—E. Bukstein. (*Radio and Telev. News*, vol. 61, pp. 44–45, 160; March, 1959.) Basic thyratron and thermionic tube circuits are described and reference is made to the use of the circuit as an electronic rotary switch.

621.374.4 2508
Dividing Wide Frequency Bands—E. L. Laine. (*Electronic Ind.*, vol. 17, pp. 62–63; December, 1958.) A regenerative circuit is described which will divide a sinusoidal input frequency by two over a wide frequency range.

621.374.43:517.5 2509
Some Properties of Mathieu and Related Functions exemplified by the Regenerative Modulation Process—H. Jungfer. (*Frequenz*, vol. 12, pp. 169–178 and 223–227; June and July, 1958.) A frequency divider using regenerative modulation can be used as an analog method for the solution of Mathieu and Meissner differential equations. An experimental frequency divider is described and a number of waveforms obtained with it are reproduced.

621.374.5:531.76:534.22-8 2510
The Measurement of the Time Delay of Ultrasonic Delay Lines—Sears. (See 2698.)

621.374.5:621.372.412:621.396.96 2511
Quartz Delay Lines for Radar Systems—A. F. J. Swift. (*Brit. Commun. Electronics*, vol. 6, pp. 116–119; February, 1959.) Two lines are briefly discussed, the electromechanical type in which a silica or quartz bar is used in conjunction with one or two quartz crystal transducers, and the rectangular or polygon plate type, applicable to ultrasonic frequencies. Delay times from 2 μs to 3 ms are obtainable at low power levels.

621.375.1 2512
Band-Pass Amplifiers, their Synthesis and Gain-Bandwidth Factor—F. S. Atiya. (*Arch. elekt. Übertragung*, vol. 12, pp. 251–264 and 317–325; June and July, 1958. In English.) Seven types of band-pass amplifiers are investigated and compared, and their design formulas are given.

621.375.126(083.57) 2513
Using Cascading Charts—H. Urkowitz. (*Electronic Ind.*, vol. 17, pp. 80–81; November, 1958.) Charts are given for determining the required number of transitionally coupled double-tuned amplifier stages needed to provide a required gain and bandwidth. Two cases are considered: (*a*) equal damping of primary and secondary windings; (*b*) one-sided damping.

621.375.2.029.3 2514
Audio Amplifier Design cuts Plate Dissipation—R. B. Dome. (*Electronics*, vol. 32, pp. 72–74; April 10, 1959.) An auxiliary signal at ultrasonic frequency applied to the grid reduces plate dissipation at low signal levels.

621.375.223.029.33:621.397.62 2515
Overloading Effects with Cathode Compensation—(*Electronic Radio Eng.*, vol. 36, pp. 208–210; June, 1959.) Further details on cathode compensation of a video stage with RC anode load [see 1814 of June (Kitchin)] including compensation for an RC load in the anode of the preceding stage.

621.375.3 2516
Application of Magnetic Amplifiers to Engineering Problems—A. D. Cawdery and H. T. Carden. (*Brit. Commun. Electronics*, vol. 6, pp. 180–184; March, 1959.) The various types of magnetic-amplifier connection are discussed and a typical application of each is presented.

621.375.4 2517
Design of an Emitter-Current-Controlled Common Emitter Transistor I.F. Amplifier Stage—M. V. Joshi. (*J. Inst. Telecommun. Engrs., India*, vol. 5, pp. 17–22; December, 1958.) Input and output impedances, and their influence on the bandpass characteristics are studied. The stage is suitable for broadcast receivers.

621.375.4.018.75 2518
Transistorized Pulse Amplifier—J. N. Barry and D. M. Leakey. (*Electronic Radio Eng.*, vol. 36, pp. 200–207; June, 1959.) Instead of pulse transformers, drift transistors with high cutoff frequencies (10–30 mc) are used in diode logic circuits. With 10-v 0.6-μs input pulses the total rise and fall times are less than 0.05 μs, the delay between input and output pulses varying from 0.03 to 0.075 μs according to load conditions.

621.375.4.024:681.142 2519
D.C. Operational Amplifier with Transistor Chopper—W. Hochwald and F. H. Gerhard. (*Electronics*, vol. 32, pp. 94–96; April 24, 1959.) Description of a drift-compensated dc amplifier with which an accuracy of 0.005 per cent can be achieved in airborne analog computers. See Proc. NEC (Chicago), vol. 14, pp. 798–810; 1958.

621.375.9:538.569.4 2520
Weak-Field Nuclear-Magnetic-Resonance Naser—Benoit, Grivet and Ottavi. (See 2548.)

621.375.9:538.569.4 2521
Study of a Weak-Field Maser-Type Self-Oscillator—H. Benoit, P. Grivet and H. Ottavi. (*C.R. Acad. Sci., Paris*, vol. 248, pp. 220–223; January 12, 1959.) Characteristics of the maser described in 2548 below are discussed.

621.375.9:538.569.4.029.6 2522
Proposal for a "Staircase" Maser—A. E. Siegman and R. J. Morris. (*Phys. Rev. Lett.*, vol. 2, pp. 302–303; April 1, 1959.) A proposal for obtaining amplification at approximately twice the pump frequency, in which adiabatic fast passage is used to invert successively the 1–2 and 2–3 levels of a three-level system.

621.375.9:538.569.4.029.63 2523
Tunable L-Band Ruby Maser—F. R. Arams and S. Okwit. (PROC. IRE, vol. 57, pp. 992–993; May, 1959.) The product of voltage-gain and bandwidth was measured over the frequency range 850–2000 mc in a maser at temperatures of 1.5 and 4.2°K.

621.375.9.029.55:621.3.011.23 2524
Low-Frequency Prototype Travelling-Wave Reactance Amplifier—P. P. Lombardo and E. W. Sard. (PROC. IRE, vol. 47, pp. 995–996; May, 1959.) The circuit of an amplifier with special junction-diode nonlinear capacitors in a semidistributed transmission line is described. Performance data at a signal frequency of 4.5 mc show midband gains of 6.1–8.4 db with over-all effective input noise temperatures of about 120°K.

621.376.23:621.385.2.029.6 2525
Vacuum-Diode Microwave Detection—Dye, Hessler, Jr., Knight, Miesch and Papp. (See 2794.)

621.376.332:621.372.2 2526
A New Wide-Band Discriminator—N. B. Chakraborti. (*Indian J. Phys.*, vol. 32, pp. 537–546; December, 1958.) A transmission-line arrangement for frequency discrimination is described. Output is linear for frequency deviations up to 50 per cent. Two practical circuits are given, with center frequency 400 kc and 6.4 mc respectively.

GENERAL PHYSICS

537.222.2 2527
Surface Charges produced on Insulators by Short- and Long-Time Ionization—S. I. Reynolds. (*Nature, London*, vol. 183, pp. 671–672; March 7, 1959.)

537.311.33:539.2 2528
Note on the Motion of Electrons and Holes in Perturbed Lattices—R. R. Haering. (*Can. J. Phys.*, vol. 37, pp. 47–52; January, 1959.) "A new set of orthogonal, localized functions is discussed. The functions bear the same relation to the functions of Luttinger and Kohn [2316 of 1955] as the Wannier functions bear to the Bloch functions. The new functions are used to give an alternative derivation of the effective mass equation."

537.32 2529
Thermoelectricity at Very Low Temperatures—D. K. C. MacDonald. (*Science*, vol. 129, pp. 943–949; April 10, 1959.) Review of theory and discussion of recent experimental work at temperatures below 20°K.

537.52 2530
A Possible Mechanism of the Potential Variation of the Joshi Effect—M. Venugopalan. (*J. Phys. Soc. Japan*, vol. 13, pp. 1544–1546; December, 1958.)

537.52:621.374.3 2531
A Method of Studying the Electrical Recovery of a Gas after a Pulse Discharge—R. J. Armstrong. (*J. Electronics Control*, vol. 6, pp. 162–164; February, 1959.) A method devised for a triggered three-electrode discharge, *e.g.*, a thyratron.

537.56 2532
On the Temperature of Electrons in a Variable Electric Field—A. V. Gurevich. (*Zh. Eksp. Teor. Fiz.*, vol. 35, pp. 392–400; August, 1958.) The investigation shows that the electron gas can exist in two stable states with different temperatures; transition from one state to another occurs at certain critical values of the field and is followed by a considerable change in the electron temperature. A particular type of hysteresis is noted in the dependence of the electron temperature on the field amplitude and frequency. Expressions for the complex conductivity of the plasma are also derived.

537.56 2533
Measurement of the Attachment of Slow Electrons in Oxygen—L. M. Chanin, A. V. Phelps and M. A. Biondi. (*Phys. Rev. Lett.*, vol. 2, pp. 344–346; April 15, 1959.) Drift tube measurements are extended into the thermal energy range; a three-body attachment process is indicated.

537.56:538.56 2534
Theory of Excited Plasma Waves—M. Sumi. (*J. Phys. Soc. Japan*, vol. 13, pp. 1476–1485; December, 1958.) The excitation of oscillations in a uniform plasma by an injected electron beam is considered, and the frequency, phase velocity and time rate of growth of the excited waves are derived as functions of the wave number.

537.56:538.56 2535
Nonlinear Electron Oscillations in a Cold Plasma—J. M. Dawson. (*Phys. Rev.*, vol. 113, pp. 383–387; January 15, 1959.)

537.56:538.63 2536
Production of Two Temperatures in an Ionized Gas in a Magnetic Field—E. Larish and I. Shekhtman. (*Zh. Eksp. Teor. Fiz.*, vol. 35, pp. 514–515; August, 1958.) If the electrons radiate a considerable part of their energy in a time that is short compared to the relaxation time of the gas, the electronic temperature will differ considerably from the ionic temperature.

538.3:537.122 2537
A Consistency Condition for Electron Wave Functions—C. J. Eliezer. (*Proc. Camb. Phil. Soc.*, vol. 54, pp. 247–250; April, 1958.)

538.566:535.42]+534.26 2538
Geometrical Theory of Diffraction in Inhomogeneous Media—B. D. Seckler and J. B. Keller. (*J. Acoust. Soc. Amer.*, vol. 31, pp. 192–205; February, 1959.) The theory developed by an extension of Fermat's principle and considering smooth convex bodies, is applied to the calculation of the field of diffracted rays.

538.566:535.42]+534.26 2539
Asymptotic Theory of Diffraction in Inhomogeneous Media—B. D. Seckler and J. B. Keller. (*J. Acoust. Soc. Amer.*, vol. 31, pp. 206–216; February, 1959.) Problems discussed in 2538 above are treated here as boundary-value problems. They are solved exactly and the solutions are expanded asymptotically for high frequencies.

538.566:535.43 2540
A Note on the Scattering of a Plane Electromagnetic Wave by a Small, Thin-Walled, Cylindrical Dielectric Tube—J. Y. Wong. (*Can. J. Phys.*, vol. 37, pp. 77–78; January, 1959.)

538.566:537.56 2541
Nonreciprocal Electromagnetic Wave Propagation in Ionized Gaseous Media—L. Goldstein. (TRANS. IRE, vol. MTT-6, pp. 19–29; January, 1958. Abstract, PROC. IRE, vol. 46, p. 804; April, 1958.)

538.569.4 2542
Investigation of Relaxation in Magnetic Resonance by the Method of "Forced Transient Precession"—I. Solomon. (*C.R. Acad. Sci., Paris*, vol. 248, pp. 92–94; January 5, 1959.) A method is described for measuring directly the relaxation time in liquids.

538.569.4 2543
Radiation Damping in Nuclear Magnetic Resonance—A Szoke and S. Meiboom. (*Phys. Rev.*, vol. 113, pp. 585–586; January 15, 1959.) Observations on a nuclear two-level maser have demonstrated the effect of radiation damping obtained by "flipping" the magnetization through about 180°.

538.569.4:535.33 2544
Wide-R.F.-Level R.F. Unit for an NMR Spectrometer—K. N. Kapur and J. W. McGrath. (*Rev. Sci. Instr.*, vol. 30, pp. 272–274; April, 1959.) This unit makes use of a crystal-controlled oscillator for frequency stability and positive feedback to increase the effective Q of the sample RF coil. The circuit is well suited to saturation studies and relaxation-time measurements in nuclear-magnetic-resonance investigations.

538.569.4:538.221 2545
Effective Ferrimagnetic Resonance Parameters with Gilbert-Type Relaxation Terms—R. K. Wangsness. (*Phys. Rev.*, vol. 113, pp. 771–772; February 1, 1959.)

538.569.4:538.222 2546
Observation of the Overhauser Effect in a Gas in the Presence of a Solid Paramagnetic Material—J. P. Borel and P. Cornaz. (*C.R. Acad. Sci., Paris*, vol. 247, pp. 1988–1990; December 1, 1958.) Note of nuclear-magnetic-resonance measurements made on propane gas in diphenyl pioryl hydrazyl.

538.569.4:538.61:538.222 2547
The Influence of the Saturation of Paramagnetic Resonance Absorption on the Faraday Effect—H. Wesemeyer and J. M. Daniels. (*Z. Phys.*, vol. 152, pp. 591–598; October 16, 1958.) Experimental investigations on a crystal of Nd $(C_2H_5SO_4)_3 \cdot 9H_2O$ and discussion of results.

538.569.4:621.375.9 2548
Weak-Field Nuclear-Magnetic-Resonance Maser—H. Benoit, D. Grivet and H. Ottavi. (*C.R. Acad. Sci. Paris.*, vol. 247, pp. 1985–1988; December 1, 1958.) Description of an instrument for nuclear-magnetic-resonance investigations based on proton spin resonance in circulating benzene.

539.2:538.222 2549
Method of Treating Zeeman Splittings of Paramagnetic Ions in Crystalline Fields—G. F. Koster and H. Statz. (*Phys. Rev.*, vol. 113, pp. 445–454; January 15, 1959.)

GEOPHYSICAL AND EXTRATERRESTRIAL PHENOMENA

522.1 2550
The Royal Greenwich Observatory—R.v.d. R. Woolley. (*Nature, London*, vol. 183, pp. 640–643; March 7, 1959.) Reference is made to the national time service, associated equipment and land-line links with other standards.

523.16 2551
Low-Energy Corpuscular Radiation at High Latitudes—K. D. Cole. (*Nature, London*, vol. 183, p. 738; March 14, 1959.) An explanation based on an acceleration mechanism.

523.16:550.389.2:629.19 2552
Origin of the Radiation near the Earth Discovered by means of Satellites—T. Gold.

(*Nature, London*, vol. 183, pp. 355–358; February 7, 1959.) See also 2217 of July (Kellogg).

523.16:550.389.2:629.19 2553
Radiation around the Earth to a Radial Distance of 107400 km—J. A. Van Allen and L. A. Frank. (*Nature, London*, vol. 183, pp. 430–434; February 14, 1959.) Radiation measurements made during the flight of Pioneer III on December 6, 1958, are discussed, and a brief description is given of the two Geiger-Müller detector tubes used and the associated telemetry equipment. See also 2217 of July (Kellogg).

523.164.3 2554
Anomalous Night-Time Reception of a Major Solar Radio Burst—A. G. Smith, T. D. Carr and W. H. Perkins. (*Nature, London*, vol. 183, pp. 597–598; February 28, 1959.) A report of a noise burst received on five different arrays operating on frequencies between 18 and 27.6 mc at 0235 U.T. on March 8, 1958, in Florida. Possible modes of propagation are discussed.

523.164.32 2555
Time Relationship of Metre-Wave and 3-cm-Wave Bursts—M. R. Kundu. (*Nature, London*, vol. 183, pp. 1047–1048; April 11, 1959.) Meter-wave bursts have an average delay of 3 minutes, the delay being less for bursts of small apparent diameter.

523.42:621.396.96 2556
Radar Echoes from Venus—R. Price, P. E. Green, Jr., T. J. Goblick, Jr., R. H. Kingston, L. G. Kraft, Jr., G. H. Pettengill, R. Silver and W. B. Smith. (*Science*, vol. 129, pp. 751–753; March 20, 1959.) Report on tests made on February 10 and 12, 1958, using specially coded pulse trains at 440 mc and a maser-type amplifier for reception.

523.75:523.165 2557
Cosmic-Ray Increases associated with Solar Flares—L. C. Towle and J. A. Lockwood. (*Phys. Rev.*, vol. 113, pp. 641–647; January 15, 1959.) Data from a neutron monitor for the years 1956–1957 have been studied.

523.75:550.385.4 2558
Characteristics of Solar Outbursts to Excite Geomagnetic Storms—K. Sinno. (*J. Radio Res. Labs., Japan*, vol. 6, pp. 17–20; January, 1959.) For major outbursts a pronounced "first part" before the time of maximum flare is related to short-wave fade-out, while a large "second part" will cause a geomagnetic storm. It is concluded that the second part of the outburst provides evidence of a corpuscular cloud which will cause a storm.

523.78:551.524 2559
Fluctuations of Temperature accompanying the Solar Eclipse—K. Hirao, K. Akita and I. Shiro. (*J. Radio Res. Labs., Japan*, vol. 6, pp. 47–55; January, 1959.) During the eclipse there was a depression of the rms value of the fluctuations which was accompanied by a temperature inversion with a steep gradient as the eclipse passed the maximum blackout period. The rms value of the temperature fluctuations between two points vertically separated was found to increase with diminishing inversion and to continue to increase as the gradients changed from positive to negative values.

550.385:523.75 2560
Some Remarks on the Interaction of Solar Plasma and the Geomagnetic Field—J. W. Warwick. (*J. Geophys. Res.*, vol. 64, pp. 389–396; April, 1959.) An explanation of the small scale of magnetic disturbances on the earth's surface is that currents flow in plasma sheets and move along the curved magnetic lines of force. These sheets are less than one earth's radius away from the surface and would produce perturbation fields consistent with the size and direction necessary to explain storm-time geomagnetic variations.

550.385:523.78 2561
Preliminary Report on the Effect of the Solar Eclipse on April 19, 1958 on the Geomagnetic Field—T. Rikitake, S. Uyeda, T. Yukutake, I. Tanaoka and E. Nakagawa. (*Rep. Ionosphere Res. Japan*, vol. 12, pp. 174–181; June, 1958.) The changes in the *D* and *H* components are consistent with the decrease in E-layer conductivity but the *Z*-component changes are influenced by earth currents.

550.385:523.78 2562
Effect of the Solar Eclipse, 19th April, 1958 on the Geomagnetic Field and Earth Currents—Y. Yamaguchi, N. Banno, H. Ōshima and T. Araki. (*Rep. Ionosphere Res. Japan*, vol. 12, pp. 182–187; June, 1958.)

550.389.2:629.19 2563
The Sun's Artificial Planet—(*Brit. Commun. Electronics*, vol. 6, pp. 200–203; March, 1959.) General scientific information, based on a Russian report of the space rocket launched January 2, 1959.

550.389.2:629.19 2564
Two Atmospheric Effects in the Orbital Acceleration of Artificial Satellites—L. G. Jacchia. (*Nature, London*, vol. 183, pp. 526–527; February 21, 1959.) A discussion of oscillations in orbital acceleration and the variations of orbital acceleration with angular distance ψ of the perigee from the sub-solar point.

550.389.2:629.19 2565
Atmospheric Tides and Earth Satellite Observations—D. G. Parkyn and G. V. Groves. (*Nature, London*, vol. 183, pp. 1045–1047; April 11, 1959.) Harmonic tidal waves are suggested as the cause of the major anomalies in orbital observations; this explanation differs from that of Groves (1543 of May), who comments in reply.

550.389.2:629.19 2566
The I.G.Y. Optical Satellite Tracking Program as a Source of Geodetic Information—F. L. Whipple and J. A. Hynek. (*Ann. Géophys.*, vol. 14, pp. 326–328; July/September, 1958. In English.) A note on the visual and photographic tracking program and the subsequent computations.

550.389.2:629.19 2567
A New Value for the Earth's Flattening, derived from Measurements of Satellite Orbits—D. G. King-Hele and R. H. Merson. (*Nature, London*, vol. 183, pp. 881–882; March 28, 1959.) Data obtained from observations of 1957 β and 1958 $\beta 2$ have been combined, and give a value for the earth's flattening of $1/(298.20 \pm 0.3)$. See also 792 of March (Merson and King-Hele).

550.389.2:629.19 2568
Determination of Satellite Orbits from Radio Tracking Data—I. Harris, R. Jastrow and W. F. Cahill. (PROC. IRE, vol. 47, pp. 851–854; May, 1959.) "A computer program has been developed which permits an approximate determination of a satellite orbit from a minimal amount of tracking data."

550.389.2:629.19 2569
Observations of Sputnik III—P. F. Checcacci and C. Carreri. (*Ricerca Sci.*, vol. 29, pp. 72–73; January, 1959.) Radio observations of satellite 1958 $\delta 2$ for the period May 19–July 19, 1958 are tabulated. See also 1192 of April.

550.389.2:629.19 2570
Recordings of Transmissions from the Satellite 1958 $\Delta 2$ at the Antenna Laboratory, The Ohio State University—T. G. Hame and E. M. Kennaugh. (PROC. IRE, vol. 47, pp. 991–992; May, 1959.) Irregularities in 20-mc signals are attributed to polarization effects caused by variations in magnetic field near the observing point. Some periodic fading may be caused by a defect in the satellite antenna.

550.389.2:629.19:551.510.53 2571
Irregularities in the Density of the Upper Atmosphere: Results from Satellites—D. G. King-Hele and D. M. C. Walker. (*Nature, London*, vol. 183, pp. 527–529; February 21, 1959.) Results of observations of earth satellite orbits indicate that irregularities in air density, especially at heights between 180 and 225 km, tend to recur at intervals of about 28 days.

550.389.2:629.19:551.510.535 2572
Deduction of Ionospheric Electron Content from the Faraday Fading of Signals from Artificial Earth Satellites—W. T. Blackband, B. Burgess, I. L. Jones and G. J. Lawson. (*Nature, London*, vol. 183, pp. 1172–1174; April 25, 1959.) A method is described for determining horizontal variations in the ionosphere both above and below maximum ionization. Results are compared with values of electron content deduced from ionograms.

550.389.2:629.19:621.396.81.087.4 2573
Recording Radio Signals from Earth Satellites—G. H. Munro and L. H. Heisler. (*Nature, London*, vol. 183, pp. 809–810; March 21, 1959.) A method is described for presenting simultaneously on moving film the information necessary for Doppler frequency-shift measurements, for frequency sampling, and for the study of signal intensity variations.

551.510.52:621.396.11 2574
Models of the Atmospheric Radio Refractive Index—Bean and Thayer. (See 2725.)

551.510.53 2575
Geophysical Effects associated with High-Altitude Explosions—P. J. Kellogg, E. P. Ney and J. R. Winckler. (*Nature, London*, vol. 183, pp. 358–361; February 7, 1959.) Effects likely to be associated with high-altitude explosions are discussed and related to observations of a nuclear and a chemical explosion.

551.510.53:523.75 2576
Observations of Intense Ionization of Long Duration below 50 km Altitude after some Strong Solar Flares—B. Hultqvist and J. M. Ortner. (*Nature, London*, vol. 183, pp. 1179–1180; April 25, 1959.)

551.510.535 2577
Turbulence in the Upper Atmosphere—N. Matuura and T. Nagata. (*Rep. Ionosphere Res. Japan*, vol. 12, pp. 147–159; June, 1958.) Ionospheric irregularities are studied in terms of turbulence theory. The calculated scales of the irregularities and their random velocities are compared with experimental observations.

551.510.535 2578
Sporadic E and the F_2 Layer—T. W. Bennington. (*Wireless World*, vol. 65, pp. 262–263; June, 1959.) A comparison of curves of E_s percentage time with curves giving seasonal fluctuations of F_2-layer ionization for four stations in both hemispheres indicates that sporadic E may be caused by a downward drift of F_2 ionization.

551.510.535 2579
A Theoretical Consideration of the Electron and Ion Density Distributions in the Lower Portion of the F Region—T. Yonezawa, H. Takahashi and Y. Arima. (*J. Radio Res. Labs., Japan*, vol. 6, pp. 21–46; January, 1959.) Assuming that the photoionization processes in

the ionosphere are: $O^+ + O_2 \rightarrow O + O_2^+$; $O_2^+ + e \rightarrow O' + O''$, and $O^+ + N_2 \rightarrow N + NO^+$; $NO^+ + e \rightarrow N' + O'$, the physics of the lower F region can be explained fairly well. The appearance and disappearance of the F_1 layer with solar zenith and solar activity can be understood. No values of reaction coefficients can be found which are consistent with both the ion density distribution in the ionosphere and laboratory estimates of the coefficients.

551.510.535 2580
Occurrence of Giant Travelling Ionospheric Disturbances at Night—L. H. Heisler. (*Nature, London*, vol. 183, pp. 383–384; February 7, 1959.) Disturbances previously thought to be confined to winter daylight hours (3453 of 1958) have been observed on night ionosonde records. Characteristics of the phenomenon are discussed.

551.510.535 2581
Structure and Movement of Large Inhomogeneities in the Ionospheric F_2 Layer—V. D. Gusev, L. A. Drachev, S. F. Mirkotan, Y. V. Berezin, M. P. Kiyanovskil, M. B. Vinogradova and T. A. Gailit. (*Dokl. Ak. Nauk SSSR*, vol. 123, pp. 817–820; December 11, 1958.) Simultaneous measurements have been made, using three receivers 30–40 km apart, of the phase and angle of arrival of waves reflected from the F_2 layer. The size and shape of inhomogeneities and drift velocities have been calculated.

551.510.535:523.16 2582
A New Ionospheric Phenomenon—H. J. A. Chivers and H. W. Wells. (*Nature, London*, vol. 183, p. 1178; April 25, 1959.) Report of an isolated event recorded at Jodrell Bank at about 1400 U.T. on March 25, 1959, by five separate receivers, each monitoring various sectors of the sky on slightly different frequencies near 80 mc. A large increase of the noise level was recorded by three receivers, a small increase by another and a decrease by another.

551.510.535:[523.3+523.755 2583
Radio Reflexions from the Moon and Solar Corona—O. Burkhard. (*Nature, London*, vol. 183, p. 1180; April 25, 1959.) The formula for the rotation of the plane of polarization given by Daniels & Bauer (3455 of 1958) is revised for the case when, with low solar activity, the electron density in the ionosphere has decreased and the electrons in the space around the earth cannot be neglected.

551.510.535:550.38 2584
A Study of Noon F_2 Ionization in relation to Geomagnetic Co-ordinates—J. N. Bhar and P. Dhar Bhowmik. (*Indian J. Phys.*, vol. 33, pp. 1–17; January, 1959.) Earlier work of Bhar (2129 of 1957) has been extended to cover data collected between 1952 and 1955, an analysis of which indicates that for constant χ, the noon F_2 ionization varies with magnetic dip and geomagnetic latitude. The shape of the curve is related to the sunspot cycle and shows two maxima spaced asymmetrically on each side of the geomagnetic equator.

551.510.535:550.385 2585
Ionospheric Heating by Hydromagnetic Waves—A. J. Dessler. (*J. Geophys. Res.*, vol. 64, pp. 397–401; April, 1959.) The dissipation of hydromagnetic waves in the ionosphere causes heating; this heating is greatest between heights of 150 and 200 km. It appears that the heating only becomes important during magnetic storms; it may explain the lifting of the F region and the decrease in critical frequency during these periods. Hydromagnetic heating cannot, however, explain the variations in the horizontal component of the earth's field during the main phase of magnetic storms.

551.510.535:550.385 2586
Effect of Magnetic Activity on Drifts of the F_2 Region—B. R. Rao, E. B. Rao and V. V. R. Murty. (*Nature, London*, vol. 183, pp. 667–668; March 7, 1959.) An analysis of observations made at Waltair shows an approximately linear decrease of mean drift speed with increase of magnetic activity (K) in the range 0–6.

551.510.535:621.396.11 2587
Sporadic E at V.H.F. in the U.S.A.—R. M. Davis, Jr., E. K. Smith and C. D. Ellyett. (Proc. IRE, vol. 47, pp. 762–769; May, 1959.) The occurrence of sporadic-E propagation in the years 1952–1955 on the Cedar Rapids-Sterling path (1240 km) at frequencies near 28 and 50 mc has been analyzed. The dependence of the received power on time of day, season of year, sunspot cycle and frequency has been studied. A relation between oblique-signal intensity and vertical-incidence data has been found.

551.510.535:621.396.11 2588
On the S.W.F. Phenomenon (Dellinger Effect) and f_{min} in the World-Wide Distribution—I. Kasuya, Y. Hakura and H. Hojo. (*J. Radio Res. Labs., Japan*, vol. 6, pp. 1–15, January, 1959.) Assuming a Chapman distribution of ionization for the D region it is shown that f_{min} is a function of solar zenith angle and magnetic latitude while the increase of f_{min} during a sudden ionospheric disturbance depends on solar zenith angle only. Observational results are analyzed and the effective factor by which solar radiation is increased during a sid is estimated.

551.510.535:621.396.11:551.594.6 2589
Ionospheric Reflection Coefficients at V.L.F. from Sferics Measurements—A. G. Jean, Jr., L. J. Lange and J. R. Wait. (*Geofis. Pura Appl.*, vol. 38, pp. 147–153; September-December, 1957. In English.) The magnitude of the ionospheric reflection coefficient as a function of frequency is calculated from individual spectral analysis of the ground wave and the once-reflected sky wave. Results are compared with those obtained using an ionospheric model. The success of the method depends upon the accurate location of the source and the correct selection of strokes which contain only appreciable vertical currents in the discharge column.

551.510.535:621.396.11.029.45 2590
Diurnal Change of Ionospheric Heights Deduced from Phase Velocity Measurements at V.L.F.—Wait. (See 2735.)

551.510.535:621.396.11.029.62 2591
IGY Observations of F-Layer Scatter in the Far East—Bateman, Finney, Smith, Tveten and Watts. (See 2733.)

551.594.5 2592
Auroral Activity at Low Latitudes—D. Barbier. (*Ann. Géophys.*, vol. 14, pp. 334–355; July/September, 1958.) Spectroscopic observations made in southern France and at Tamanrasset during 1956–1957 are described.

551.594.5:550.385 2593
Movement of Auroral Echoes and the Magnetic-Disturbance Current System—R. S. Unwin. (*Nature, London*, vol. 183, pp. 1044–1045; April 11, 1959.) A brief review of the findings of other investigators and a report of observations made at Invercargill, New Zealand, on 55 mc. A preliminary analysis indicates that the ionization giving rise to VHF radar echoes occurs in the most intense portion of the disturbance current system, and that the observed movements of electrons can account for the magnitude of the disturbance vector.

551.594.6:621.396.11:551.510.535 2594
"Whistler Mode" Echoes Remote from the Conjugate Point—Dowden and Goldstone. (See 2731.)

550.389.2:629.19 2595
Scientific Uses of Earth Satellites (Book Review)—J. A. Van Allen (Ed.). Publishers: University of Michigan Press, Michigan, and Chapman and Hall, London, 1958, 316 pp., 75s. (*Nature, London*, vol. 183, p. 963; April 4, 1959.)

LOCATION AND AIDS TO NAVIGATION

534.88 2596
A Theory of Active Sonar Detection—J. L. Stewart and E. C. Westerfield. (Proc. IRE, vol. 47, pp. 872–881; May, 1959.) An investigation is carried out to determine the type of signal waveform or coding that will give the best echo/noise and echo/reverberation ratios.

534.88:621.398 2597
Survey of Underwater Missile Tracking Instrumentation—D. T. Barry and J. M. Formwalt. (Proc. IRE, vol. 47, pp. 970–977; May, 1959.)

621.396.93:621.396.11.029.45 2598
V.L.F. Propagation Measurements for the Radux-Omega Navigation System—Casselman, Heritage and Tibbals. (See 2736.)

621.396.933 2599
A Lightweight and Self-Contained Airborne Navigational System—R. K. Brown, N. F. Moody, P. M. Thompson, R. J. Bibby, C. A. Franklin, J. H. Garton and J. Mitchell. (Proc. IRE, vol. 47, pp. 778–807; May, 1959.) Automatic computing techniques are used to give steering and positional information from input data obtained from an inertial north indicator, a Doppler navigational radar and an airspeed indicator.

621.396.933.2 2600
Direction Finder with Automatic Read-Out—J. F. Hatch and D. W. G. Byatt. (*Electronics*, vol. 32, pp. 52–54; April 17, 1959.) The accuracy of an hf direction-finder can be improved by averaging bearings; circuits are described which give automatic read-out and averaging.

621.396.934 2601
Miss-Distance Indicator scores Missile Accuracy—J. A. Adams. (*Electronics*, vol. 32, pp. 42–45; April 17, 1959.) Transponder and antenna systems in missile and target form a space-coupled oscillatory system. The oscillation is modulated at a frequency which depends on their separation distance.

621.396.96 2602
Problems connected with Echo Filtering in Radar—V. Tiberio. (*Ricerca Sci.*, vol. 28, pp. 2464–2481; December, 1958.) Various systems of filtering combined with carrier stabilization are described and the resulting increase in range, even in the presence of jamming, is discussed. For comment by U. Pizzarelli, with details of calculations relating bandwidth and sweep velocity, see *ibid.*, pp. 2585–2590.

621.396.96:551.5 2603
Meteorological "Angel" Echoes—D. Atlas. (*J. Met.*, vol. 16, pp. 6–11, February, 1959.) An analysis of meteorological conditions associated with radar echoes suggests four sources of reflection: thermal columns below cumulus clouds; cumulus cloud boundaries; layers associated with sharp vertical gradients or minima moisture; and, under conditions of anomalous propagation, boundary surfaces between differentially moistened surface air over adjacent cold and warm water.

621.396.96:551.5 2604
Study of Mesosystems associated with Stationary Radar Echoes—T. Fujita. (*J. Met.*, vol. 16, pp. 38–52; February, 1959.)

621.396.96:621.397.24 2605
Scan Converter aids Phone-Line Radar Relay—H. W. Gates and A. G. Gatfield. (*Electronics*, vol. 32, pp. 48–51; April 17, 1959.) A scan-converter storage tube is substituted for the radar tube; its reading gun scans its screen at a slow rate and the output is used to modulate a carrier which can be transmitted over a telephone line.

621.396.962.3(083.57) 2606
Predicting Accurate Radar Ranges—L. Young. (*Electronic Ind.*, vol. 17, pp. 58–61; November, 1958.) Formulas and a chart are given for determining the maximum range of a pulse radar equipment scanning in azimuth.

621.396.962.33 2607
Frequency Stability Requirements on Coherent Radar Oscillators—M. M. Brady. (PROC. IRE, vol. 47, pp. 1001–1002; May, 1959.) A discussion of stability criteria for Doppler radar systems.

621.396.962.33 2608
The Performance of Doppler Navigation Systems—T. G. Thorne and J. A. Billings. (*Brit. Commun. Electronics*, vol. 6, pp. 176–179; March, 1959.) A review is given of the performance of military Doppler equipment under various conditions and reference is made to the important design features that control the accuracy and reliability of Doppler systems.

621.396.968 2609
Phenomena of Scintillation Noise in Radar Tracking Systems—J. H. Dunn, D. D. Howard and A. M. King. (PROC. IRE, vol. 47, pp. 855–863; May, 1959.) The effects of different components of target noise on the performance of tracking systems have been studied theoretically and experimentally; suggestions are made for minimizing these effects.

621.396.969.11 2610
The C.A.A. Doppler Omnirange—S. R. Anderson and R. B. Flint. (PROC. IRE, vol. 47, pp. 808–821; May, 1959.) Theoretical and experimental investigations show that the Doppler VOR is compatible with the VHF omnirange and gives a 7:1 improvement in siting errors. See also 1897 of June (Hansel).

621.396.969.11:621.396.822 2611
Noise-Modulated Distance Measuring Systems—B. M. Horton. (PROC. IRE, vol. 47, pp. 821–828; May, 1959.) An analysis is carried out of distance-measuring systems involving correlation between the random noise modulation on the transmitted and reflected signals. Such systems are not subject to the ambiguities present in periodically modulated signals, nor to the "fixed error," and are suitable for measuring distances down to a few feet.

621.396.969.13 2612
Precision Radar Height Finder—(*Engineering, London*, vol. 186, p. 560; October 31, 1958.) Description of the Marconi Type-S 244 height finder and ancillary equipment. The vertical angle of the antenna is measured relative to the ground, and the absolute height accuracy obtainable is better than ±1700 feet at 150 miles.

MATERIALS AND SUBSIDIARY TECHNIQUES

533.583:621.385.032.14 2613
Barium Getter Films—J. J. B. Fransen and H. J. R. Perdijk. (*Philips Tech. Rev.*, vol. 19, pp. 290–300; April 30, 1958.) Experiments to investigate the action and properties of getter films are described.

535.215:537.311.33 2614
A Lateral Photovoltaic Effect in *p-n* Junctions—P. Gosar. (*Compt. rend. Acad. Sci., Paris*, vol. 247, pp. 1975–1977; December 1, 1958.) A theoretical study of a one-dimensional model in which nonuniformity of illumination is due to shadows formed by soldered contacts of unequal size. See also 2639 of 1957 (Wallmark).

535.215:546.817.221:539.23 2615
Measurement of the Reflection Factor, the Optical Absorption and the Spectral Response of Photoconductive Layers. Case of Oxidized Lead Sulphide—V. Schwetzoff. (*Compt. rend. Acad. Sci., Paris*, vol. 247, pp. 2117–2119; December 10, 1958.)

535.215:[546.482.21+546.482.31 2616
Dependence of Induced Conductivity on Electron Energy in Thin Films of Cadmium Sulphide and Cadmium Selenide Bombarded by Slow Electrons—Li-Chzhi-Tsyzan'. (*Fiz. Tverdogo Tela*, vol. 1, pp. 77–81; January, 1959.) The method and apparatus are described. Measurements have been made on films of thickness $\sim 10^{-4}$ cm under bombardment by electrons of energy 0–15 ev. An irregular step-like function is observed in the variation of the induced conductivity with the energy of bombarding electrons. The energy distance between two consecutive steps is 2.5 ev for CdS and 1.8 ev for CdSe. See also *ibid.*, pp. 82–88.

535.215:546.482.21 2617
On the Irradiation of Photoconductive Single Crystals of Cadmium Sulphide by Protons at 1.4 MeV—R. Barjon, C. Brachet, M. Lambert, M. Martineau and J. Schmouker. (*Compt. rend. Acad. Sci., Paris*, vol. 248, pp. 83–86; January 5, 1959.) Four phenomena are noted: green luminescence, induced conductivity, a permanent modification of the photoconductivity and modification of the spectral response. See also 1994 of May (Martineau).

535.215:546.482.21 2618
Research on Fluorescent Emission Lines and on Luminous Absorption Lines in Pure Cadmium Sulphide, Cooled to 4.2°K—M. Bancie-Grillot, E. F. Gross, E. Grillot and B. S. Razbirine. (*Compt. rend. Acad. Sci., Paris*, vol. 248, pp. 86–89; January 5, 1959.)

535.215:546.87:539.23 2619
The Temperature Dependence of the Spectral Photoelectric Electron Emission of Semiconducting Bismuth Films—R. Suhrmann, G. Wedler and E. A. Dierk. (*Z. Phys.*, vol. 153, pp. 96–105; October 27, 1958.)

535.342-15:546.87 2620
De Haas-vanAlphen-Type Oscillations in the Infrared Transmission of Bismuth—W. S. Boyle and K. F. Rodgers. (*Phys. Rev. Lett.*, vol. 2, pp. 338–339; April 15, 1959.)

535.37:546.482.21 2621
Some Properties of Green and Red-Green Luminescing CdS.—Y. T. Sihvonen, D. R. Boyd and C. D. Woelke. (*Phys. Rev.*, vol. 113, pp. 965–968; February 15, 1959.)

535.37:546.482.21:538.6 2622
Influence of a Magnetic Field on the Lines of Blue Fluorescence or Luminous Absorption of Certain Crystals of Pure Cadmium Sulphide Cooled to 4.2°K—E. F. Gross, E. Grillot, B. P. Zakhartchenia and M. Bancie-Grillot. (*Compt. rend. Acad. Sci., Paris*, vol. 248, pp. 213–216; January 12, 1959.) A Zeeman splitting has been observed on three lines. There was no diamagnetic displacement.

535.376 2623
Phosphor with Fluorescence Larger than the Energy Gap—S. P. Keller and G. D. Pettit. (*Phys. Rev.*, vol. 113, pp. 785–786; February 1, 1959.) An emission which is energetically greater than the energy gap is observed at 770°K with a Pr^{+3}-activated SrS phosphor.

535.376 2624
On Cathodothermoluminescence—A. Bril, H. A. Klasens and T. J. Westerhof. (*Physica*, vol. 24, pp. 821–827; October, 1958.) When phosphors are heated from −180°C to 20°C in a demountable tube, strong maxima and minima of the light output are observed. If sealed and thoroughly degassed tubes are used, the effect disappears. Gas adsorption on the phosphors is a probable explanation of the effect.

535.376:546.472.21 2625
Preparation of Zinc Sulphide Single Crystals—T. Matsumura, H. Fujisaki and Y. Tanabe. (*Sci. Rep. Res. Inst. Tohoku Univ., Ser. A.*, vol. 10, pp. 459–471; December, 1958.) Details of preparation by gas reaction and sublimation methods.

537.226 2626
Dielectric Properties of some Polycrystalline Stannates and Cerates—B. Piercy. (*Trans. Faraday Soc.*, vol. 55, pp. 39–51; January, 1959.) The substances have a perovskite structure but do not exhibit ferroelectric or antiferroelectric properties. A negative temperature coefficient of capacitance was observed in $BaSnO_3$ below room temperature.

537.226:546.431.824-31 2627
Temperature Dependence of the Breakdown Field of Barium Titanate—P. H. Fang and W. S. Brower. (*Phys. Rev.*, vol. 113, pp. 456–458; January, 15, 1959.) The breakdown field in general decreases with increasing temperature but shows minima of the critical temperatures of the phase transformations.

537.266:546.431.824-31 2628
Thermal Conductivity of $BaTiO_3$ Ceramics—I. Yoshida, S. Nomura and S. Sawada. (*J. Phys. Soc. Japan*, vol. 13, pp. 1550–1551; December, 1958.)

537.226:546.431.824-31:536.2.082.74 2629
Coefficient of Thermal Expansion of Barium Titanate—J. R. G. Keyston, J. D. Macpherson and E. W. Guptill. (*Rev. Sci. Instr.*, vol. 30, pp. 246–248; April, 1959.) The coefficient of expansion can be found by measurement of the resonance frequency, over a temperature range of −200 to 100°C, of one or more modes of a microwave cavity constructed of $BaTiO_3$.

537.227/.228 2630
Charge Release of Several Ceramic Ferroelectrics under Various Temperature and Stress Conditions—L. W. Doremus. (PROC. IRE, vol. 47, pp. 921–924; May, 1959.) The results are given of measurements on the polarization change, piezoelectric coefficient and pyroelectric charge release for several polycrystalline compounds.

537.227 2631
On the Effect of Polarization on the $Pb_3NiNb_2O_9$-$Pb_3MgNb_2O_9$ Solid Solutions—G. A. Smolenskii, A. I. Agranovskaya, and S. N. Popov. (*Fiz. Tverdogo Tela*, vol. 1, pp. 167–168; January, 1959.) The dependence of permittivity and loss angle on temperature in the range −200 to +250°C is shown graphically.

537.227 2632
New Ferroelectric with Composition of the Type A_2^{2+} $(B_I^{3+}B_{II}^{5+})O_6$: Part 1—G. A. Smolenskiĭ, V. A. Isupov & A. I. Agranovskaya.—(*Fiz. Tverdogo Tela*, vol. 1, pp. 170–171; January, 1959.) The temperature dependence of the dielectric constant and loss angle for $Pb_2Sc\ Nb\ O_6$ and $Pb_2\ Sc\ Ta\ O_6$ from −150 to +200°C is shown graphically.

537.227:538.569.4 2633
Electron Paramagnetic Resonance of Manganese IV in $SrTiO_3$—K. A. Müller. (*Phys. Rev. Lett.*, vol. 2, pp. 341–343; April 15, 1959.)

537.227:546.431.824–31 2634
Direct Observation of Antiparallel Domains during Polarization Reversal in Single-Crystal Barium Titanate—R. C. Miller and A. Savage. (*Phys. Rev. Lett.*, vol. 2, pp. 294–296; April 1, 1959.) The domains have been observed by looking along the ferroelectric axis through the electrodes (either transparent aqueous lithium chloride or semitransparent metal films). The sample was mounted between crossed polaroids, and white light was used.

537.227:546.431.824–31:621.318.57 2635
A Possible Model for the Switching of Barium Titanate Crystals—J. C. Burfoot. (*Proc. Phys. Soc.*, vol. 73, pp. 641–649; April,1, 1959.) "It is suggested that an adequate explanation of the switching current in barium titanate single crystals can be given by a domain model which includes an effective wall mass and a 'viscous' opposition, but no depolarizing field and no specific representation of impurities or lattice imperfections."

537.228.1:534.133:538.566.029.64 2636
Attenuation of Hypersonic Waves in Quartz—H. E. Bömmel and K. Dransfeld. (*Phys. Rev. Lett.*, vol. 2, pp. 298–299; April 1, 1959.) Report of measurements of the acoustic absorption in crystalline quartz at frequencies between 1 and 4 kmc from room temperature to 4.2°K.

537.311.33 2637
Characteristics of Stationary Electronic Processes in Semiconductors—G. M. Guro. (*Fiz. Tverdogo Tela*, vol. 1, pp. 3–12; January, 1959.) Examination of the bipolar diffusion in which the diffused length does not depend on the concentration of traps. It is shown that the equilibrium charge density produced by nonuniform generation is determined not only by electron and hole mobility but also by the capture of minority carriers by traps and recombination centers. The charge density can be of either sign, and is zero for a particular fractional occupancy of the trap. See 2443 of 1958.

537.311.33 2638
The Application of the Thermodynamics of Irreversible Processes to Conduction Phenomena in Semiconductors—W. Czaja. (*Helv. Phys. Acta.*, vol. 32, pp. 1–23; March 10, 1959.) (In German.) Isothermal and non-isothermal effects are investigated and general equations for the behavior of an isothermal *p-n* junction are derived. The thermal conductivity of a homogeneous semiconductor under various conditions is calculated. See also 2693 of 1958 (van Vliet).

537.311.33 2639
Theory of the Field Effect—I. V. Boiko. (*Fiz. Tverdogo Tela*, vol. 1, pp. 13–15; January, 1959.) Mathematical analysis based on the results of the general theory of the field effect for the limiting case when the mean free path of the carriers tends to zero.

537.311.33 2640
Field Effect at High Frequency—F. Berz. (*J. Electronics Control*, vol. 6, pp. 97–112; February, 1959.) Theory is developed using the same basic assumptions as Garrett (153 of 1958) with more complete conditions at the back surface. Results are illustrated by a numerical example.

537.311.33 2641
The Behaviour of some Impurities in III–V Compounds—J. T. Edmond. (*Proc. Phys. Soc.*, vol. 73, pp. 622–627; April 1, 1959.) Investigation of the behavior, as acceptors or donors, of Mg, Zn, Cd, Si, Ge, Sn, Pb, S, Se and Te in InSb, InAs, GaSb and GaAs.

537.311.33 2642
Theoretical Transport Coefficients for Polar Semiconductors—R. T. Delves. (*Proc. Phys. Soc.*, vol. 73, pp. 572–576; April 1, 1959.) Calculation of mobility, thermoelectric power and Hall coefficient for carriers scattered by optical-mode lattice vibrations.

537.311.33:535.215 2643
Influence of Surface Recombination on Photoconductivity of Semiconductors—G. L. Bir. (*Fiz. Tverdogo Tela*, vol. 1, pp. 67–76; January, 1959.) Results of an investigation show that the magnitude of photoconductivity can be determined from the amount of surface recombination and also from the properties of the surface barrier. This explains the great sensitivity of photoconductive cells to surface treatment. In the case of an anisotropic layer the electric field decreases the surface recombination velocity and increases the photoconductivity.

537.311.33:538.214 2644
Theory of Impurity Paramagnetism in Semiconductors at Low Temperature—J. Seiden. (*Compt. rend. Acad. Sci., Paris*, vol. 247, pp. 2313–2315; December, 22, 1958.) Interaction between nonionized impurities as a function of concentration is discussed and the susceptibility is calculated approximately.

537.311.33:538.22 2645
Magnetic Properties of A^{III} B^{V} Compounds—G. A. Busch and R. Kern. (*Helv. Phys. Acta*, vol. 32, pp. 24–57; March 10, 1959. In German.) The magnetic susceptibility of Si, GaP, GaAs, GaSb, InP, $InP_{0.2}As_{0.8}$, InAs and InSb was measured in the temperature range from 60°K to below the respective melting point. A model is proposed to account approximately for the abnormal characteristics obtained for InSb, but quantitative agreement with experimental results is not achieved.

537.311.33+538.221]:539.2 2646
Behaviour of Semiconductor and Magnetic Materials in Radiation Environment—A. Boltax. (*Elec. Mfg.*, vol. 63, pp. 90–95; March, 1959.) Results of irradiation tests on Ge, Si, Cu_2O, and seven typical magnetic-core materials are summarized in graphs and charts. Techniques for minimizing radiation effects are noted.

537.311.33:539.2 2647
Cyclotron Resonance in Semiconductors with Complex Equipotential Surfaces—Yu. A. Firsov. (*Fiz. Tverdogo Tela*, vol. 1, pp. 44–61; January, 1959.)

537.311.33:546.23 2648
Investigation of Influence of Annealing Time on the Thermoelectric Power of Polycrystalline Selenium—D. Vidal and G. Blet. (*Compt. rend., Acad. Sci., Paris*, vol. 247, pp. 2109–2110; December 10, 1958.)

537.311.33:[546.28+546.289 2649
Influence of Deformation on the Energy Spectrum and Electrical Properties of *p*-Type Germanium and *p*-Type Silicon—G. E. Pikus and G. L. Bir. (*Fiz. Tverdogo Tela*, vol. 1, pp. 154–156; January, 1959.) An expression is derived for the energy spectrum of a deformed crystal.

537.311.33:546.28 2650
Stabilization of Silicon Surfaces by Thermally Grown Oxides—M. M. Atalla, E. Tannenbaum and E. J. Scheibner. (*Bell Sys. Tech. J.*, vol. 38, pp. 749–783; May, 1959.) A detailed study has been made of the stable surfaces obtained with the system $Si\text{-}SiO_2$. Information is given on the thermal oxidation process and properties of the oxide, the electronic properties of the resulting interface, the practical application of the process and resulting device characteristics.

537.311.33:546.28 2651
Diffusion of Phosphorus into Silicon under Conditions of Controlled Vapour Pressure—M. J. Coupland. (*Proc. Phys. Soc.*, vol. 73, pp. 577–584; April 1, 1959.) Detailed report of an experimental study of the relation between surface concentration and ambient vapor pressure. See 3518 of 1958.

537.311.33:546.28 2652
Breakdown in Silicon *p-n* Junctions—J. Shields. (*J. Electronics Control*, vol. 6, pp. 130–148; February, 1959.) Some useful empirical relations for the variation of effective ionization coefficients associated with the avalanche breakdown phenomena in *p-n* junctions are derived from measurements on Si alloy junctions.

537.311.33:546.289 2653
Large-Scale Preparation of Ultra-pure Germanium—J. M. Wilson. (*Research, London*, vol. 12, pp. 47–53; February, 1959.) Chemical and physical purification processes are described.

537.311.33:546.289 2654
Plastic Creep of Germanium Single Crystals—H. G. Van Bueren. (*Physica*, vol. 24, pp. 831–837; October, 1958.)

537.311.33:546.289 2655
Deformation Potential in Germanium from Optical Absorption Lines for Exciton Formation—W. H. Kleiner and L. M. Roth. (*Phys. Rev. Lett.*, vol. 2, pp. 334–336; April 15, 1959.) A second absorption peak observed by Zwerdling *et al.* (*Phys. Rev.*, to be published) is explained by the presence of strain.

537.311.33:546.289 2656
Two Electrical Phenomena on Liquid Germanium Surfaces—A. I. Bennett. (*Phys. Rev.*, vol. 113, pp. 773–774; February 1, 1959.) The separate phenomena described are (*a*) repulsion of surface scum by electric discharge from the molten surface to a solid Ge electrode; (*b*) induction of nucleation by an electric field applied to the surface of supercooled Ge.

537.311.33:546.289 2657
Conductivity of Grain Boundaries in Grown Germanium Bicrystals—B. Reed, O. A. Weinreich and H. F. Mataré. (*Phys. Rev.*, vol. 113, pp. 454–456; January 15, 1959.) Grain-boundary conduction has been studied as a function of doping. Resistivities of about 3000–11,000 Ω/square were found for various samples and the behavior shows only a small temperature dependence from 2°K to 300°K. This suggests that grain-boundary behavior is not due to the segregation of impurities at the boundary.

537.311.33:546.289 2658
Effect of Minority Impurities on Impurity Conduction in *p*-Type Germanium—H. Fritzsche and K. Lark-Horovitz. (*Phys. Rev.*, vol. 113, pp. 999–1001; February 15, 1959.) Two

different processes for impurity conduction at low and high impurity concentrations could be distinguished by observing the change of resistivity resulting in a change in the degree of compensation in the temperature range of impurity conduction (as for *n*-type Ge).

537.311.33:546.289 2659
Optical Constants of Germanium in the Region 1 to 10 eV—H. R. Philipp and E. A. Taft. (*Phys. Rev.*, vol. 113, pp. 1002–1005; February 15, 1959.)

537.311.33:546.289:535.215:538.63 2660
The Influence of Fast Holes on the Photoelectromagnetic Effect in Germanium—A. K. Walton and T. S. Moss. (*Proc. Phys. Soc.*, vol. 73, pp. 692–694; April 1, 1959.) Results of measurements of the short-circuit photoelectromagnetic current are consistent with the existence of 2 per cent of fast holes which have six times the normal mobility.

537.311.33:546.289:538.569.4 2661
Electron Spin Resonance in Nickel-Doped Germanium—G. W. Ludwig and H. H. Woodbury. (*Phys. Rev.*, vol. 113, pp. 1014–1018; February 15, 1959.) Electron spin resonance absorption, proportional in intensity to the Ni-concentration, has been detected at 14 kmc.

537.311.33:546.289:538.63 2662
Analysis of Phonon-Drag Thermomagnetic Effects in *n*-Type Germanium: Part 2—C. Herring, T. H. Geballe and J. E. Kunzler. (*Bell Sys. Tech. J.*, vol. 38, pp. 657–747; May, 1959.) Observations reported in Part 1 (3885 of 1958) have been accounted for quantitatively by theory, and yield information on phonon-phonon scattering, transport and deformation-potential theories and surface effects.

537.311.33:546.289:538.632 2663
Measurement of Dependence of the Hall Effect in *n*-Type Ge on Pressure up to 10,000 kg/cm²—A. I. Likhter and T. S. D'yakonova. (*Fiz. Tverdogo Tela*, vol. 1, pp. 95–103; January, 1959.)

537.311.33:546.289:539.16 2664
Energy Levels in Irradiated Germanium—E. I. Blount. (*Phys. Rev.*, vol. 113, pp. 995–998; February 15, 1959.)

537.311.33:546.289:621.314.7 2665
A Self-Limiting Electrolytic Etching Method for the Manufacture of Thin Base Layers of *n*-type Germanium—E. Fröschle. (*Telefunken-Röhre*, vol. 35, pp. 63–76; September, 1958.) In the method described a negatively biased rectifying contact is placed on the rear of the wafer to be etched, and etching will cease when the barrier layer has been reached. Mirror-like surfaces of diameter 50–250 μ and thickness 2.5–25 μ have been obtained.

537.311.33:546.682.19 2666
Some Effects of Copper as an Impurity in Indium Arsenide—C. Hilsum. (*Proc. Phys. Soc.*, vol. 73, pp. 685–686; April 1, 1959.) Room-temperature annealing, and doping with Cu, are found to give similar effects on heat-treated InAs.

537.311.33:546.73.86 2667
Alloying of the Semiconductor Compound $CoSb_3$—L. D. Dudkin and N. Kh. Abrikosov. (*Fiz. Tverdogo Tela*, vol. 1, pp. 142–151; January, 1959.) The effect of 13 different elements on the thermoelectric and thermal properties of $CoSb_3$ is investigated. Impurity atoms of Ni and Te act as donors, Sn as an acceptor; Fe lowers the thermal conductivity of the lattice.

537.311.33:546.786–31 2668
Electrical Conduction in Crystals and Ceramics of WO_3—S. Sawada and G. C. Danielson. (*Phys. Rev.*, vol. 113, pp. 803–805; February 1, 1959.) Experimental measurements of resistivity up to 1000°K are described and discussed. Hall measurements near room temperature gave reasonable results for carrier density and mobility.

537.311.33:[546.812.231+546.289.231 2669
Anomalous Behaviour in the Hall Coefficients of the Semiconducting Compounds SnSe & Gense—S. Asanabo and A. Okazaki. (*Proc. Phys. Soc.*, vol. 73, pp. 824–827; May 1, 1959.) During thermal cycles, anomalous variations were observed in the resistivity and Hall coefficient but not in their ratio. Possible explanations are suggested.

537.311.33:546.873.241 2670
Some Adiabatic and Isothermal Effects in Bismuth Telluride—W. Williams. (*Proc. Phys. Soc.*, vol. 73, pp. 739–744; May 1, 1959.) Isothermal and quasi-adiabatic Hall and Nernst coefficients were measured on *n*- and *p*-type Bi_2Te_3 at temperatures from 100°K to 450°K. With the magnetic field in two orthogonal directions, the difference between the two Hall coefficients showed the expected temperature variation, but the Nernst coefficients did not.

537.311.33:621.317.3 2671
Determination of the Surface Conductivity of Semiconducting Crystals by the "Wedge" Method—R. N. Rubinshtein and V. I. Fistul'. (*Dokl. Ak. Nauk SSSR*, vol. 125, pp. 542–545; March 21, 1959.) The specific resistance of the crystal is measured by two probes which are moved along the surface of a Ge sample cut in the shape of a wedge of an angle $\leq 7°$. By measuring the gradient of the potential along the specimen, the surface and volume conductivity are calculated by means of formulas derived. Experimental results are given for inhomogeneous and homogeneous Ge samples before and after etching with H_2O_2.

537.312:537.531 2672
Conductivity induced by Radiation in Polycrystalline Cadmium Sulphide and Polyethylene—C. G. Clayton, B. C. Haywood and J. F. Fowler. (*Nature, London*, vol. 183, pp. 1112–1113; April 18, 1959.)

538.22 2673
Low-Temperature Electrical and Magnetic Behaviour of Dilute Alloys: Mn in Cu and Co in Cu—I. S. Jacobs and R. W. Schmitt. (*Phys. Rev.*, vol. 113, pp. 459–463; January 15, 1959.)

538.22:538.569.4 2674
Magnetic Absorption in the Spin System of some Paramagnetic Salts at about 1325 Mc/s—H. Hadders, P. R. Locher and C. J. Gorter. (*Physica*, vol. 24, pp. 839–847; October, 1958.) A description primarily of the apparatus and resonant cavity method of measurement of absorption and dispersion, and of relating absorption with susceptibility. Results are given of measurements made at 20.4°K of absorption as a function of a parallel and of a perpendicular static magnetic field. It is suggested that in parallel fields the absorption connected with the nondiagonal elements of the magnetic moment plays a dominating role. See also 1834 of 1957 (Smits *et al.*).

538.22:538.632 2675
Change of Sign of the Hall Constant when Atoms in an Alloy assume an Ordered Arrangement—A. P. Komar, N. V. Wolkenstein and G. V. Fedorov. (*Dokl. Ak. Nauk SSSR*, vol. 125, pp. 530–531; March 21, 1959.) Brief investigation of the variation of the Hall coefficient in Ni_3Mn alloy in the temperature range 296°–4.2°K.

538.221 2676
Measurement of the Boundary Layer Width between Domains in Ferromagnetics—L. V. Kirenskii and V. V. Veter. (*Dokl. Ak. Nauk SSSR*, vol. 125, pp. 526–529; March 21, 1959.) A description of a method for the measurement of boundary layers of ferromagnetics containing 3 per cent Si. The results show that the width of the layer in single crystals is not fixed. Values of 0.89 μ and 0.64 μ were obtained on two different samples.

538.221 2677
On the Influence of the Demagnetizing Field on Domain Structure—J. Kociński. (*Acta Phys. Polon.*, vol. 17, pp. 283–294; 1958.) A discrepancy between experimental results and Néel's theory of domain structure for a crystal rod of Fe can be partly explained by the influence of the demagnetizing field acting near the end of the rod.

538.221 2678
Temperature Dependence of Spontaneous Magnetization in Small Ferromagnetic Particles—E. Kneller. (*Z. Phys.*, vol. 152, pp. 574–585; October 16, 1958.) An investigation of the spontaneous magnetization of a superparamagnetic alloy with ferromagnetic particles of average diameter 23 Å, in the temperature range 0.38–0.93 θ, where θ is the Curie point. Results are discussed with reference to previous measurements.

538.221 2679
On the Ferromagnetic Phase in Manganese-Aluminium System—H. Kōno. (*J. Phys. Soc. Japan*, vol. 13, pp. 1444–1451; December, 1958.) A metallographical investigation of the Mn-Al system in the composition range 47 per cent–60 per cent Mn is described. The conditions necessary for formation, structure and stability, and the thermal and magnetic properties of a metastable tetragonal ferromagnetic phase are discussed.

538.221:538.632 2680
On the Hall Effect at the Curie Point—N. S. Akulov and A. V. Cheremushkina. (*Zh. Eksp. Teor. Fiz.*, vol. 35, pp. 518–519; August, 1958.) Brief description of an investigation carried out on Fe-Al alloys between −200 and +500°C. Results are shown graphically.

538.221:538.632 2681
Anomalously High Hall Effect in the Chromium-Tellurium Ferromagnetic Alloy—I. K. Kikoin, E. M. Buryak and Yu. A. Muromkin. (*Dokl. Ak. Nauk SSSR*, vol. 125, pp. 1011–1014; April 11, 1959.) Examination of galvanomagnetic effects in ferromagnetic alloys with nonferromagnetic constituents. A 50 per cent Cr-Te alloy showed a very large Hall coefficient.

538.221:539.23 2682
Thin Magnetic Films—R. S. Webley. (*Nature, London*, vol. 183, pp. 999–1000; April 4, 1959.) A description of apparatus for monitoring the low-frequency hysteresis loop both during deposition of the film and afterwards. Experiments indicate that the variation in coercivity during formation is influenced very strongly by secondary effects such as the nature of the substratum.

538.221:539.23 2683
Dependence of Geometric Magnetic Anisotropy in Thin Iron Films—T. G. Knorr and R. W. Hoffman. (*Phys. Rev.*, vol. 113, pp. 1039–1046; February 15, 1959.) Results indicate that the magnetic anisotropy results from a fiber axis structure which develops during deposition.

538.221:621.317.411.029.63 2684
Internal Ferromagnetic Resonance in Nickel—J. C. Anderson and B. Donovan. (*Proc. Phys. Soc.*, vol. 73, pp. 593–599; April 1, 1959.) The internal resonance revealed by

measurements of the complex permeability of polycrystalline and colloidal Ni has been investigated over the temperature range 5°–100°C.

538.221:621.318.124 2685
An Anomaly in the Characteristics of the Magnetic Properties of Ba Ferrite as a Function of Final Sintering Temperature—G. Heimke. (*Naturwiss.* vol. 45, pp. 260–261; June, 1958.) Anomalies in the density, magnetic saturation and remananence were observed in specimens containing CaO. SiO_2 sintered at 1150° and 1180°C.

538.221:621.318.134 2686
Reversing Ferrite Temperature Coefficients—A. B. Przedpelski. (*Electronic Ind.*, vol. 17, pp. 74–76; November, 1958.) The results are given of an investigation of the influence of a dc magnetic field on the temperature coefficient of permeability of ferrite and yttrium garnet materials. As flux density is increased, the temperature coefficient in each case is found to change polarity and increase negatively until saturation of the material is approached.

538.221:621.318.134 2687
Crystal-Oriented Ferroxplana—A. L. Stuijts and H. P. J. Wijn. (*Philips Tech. Rev.*, vol. 19, pp. 209–217; February 10, 1958.) Methods for aligning crystals are described and the subsequent magnetic properties are discussed. The permeability of some specimens is increased by a factor of 2.5–3 and the limiting frequency is about 0.8 times that of unaligned specimens. See also 1202 of 1958 (Jonker *et al.*) and 1802 of 1958 (Braun).

538.221:621.318.134 2688
On the Solubility of MgO in Magnesium Ferrite—L. C. F. Blackman. (*Trans. Faraday Soc.*, vol. 55, pp. 391–398; March, 1959.)

538.221:621.318.134 2689
Resonance Measurements on Nickel-Cobalt Ferrites as a Function of Temperature and on Nickel Ferrite-Aluminates—J. E. Pippin and C. L. Hogan. (TRANS. IRE, vol. MTT-6, pp. 77–82; January, 1958. Abstract, PROC. IRE, vol. 46, p. 804; April, 1958.)

538.221:621.318.134 2690
Ferrimagnetic Resonance in Some Polycrystalline Rare-Earth Garnets—G. P. Rodrique, J. E. Pippin, W. P. Wolf and C. L. Hogan. (TRANS. IRE, vol. MTT-6, pp. 83–91; January, 1958. Abstract, PROC. IRE, vol. 46, pp. 804–805; April, 1958.)

538.222:538.569.4 2691
Millimetre-Wave Paramagnetic Resonance Spectrum of ^{6}S-State Impurity (Fe^{+++}) in $MgWO_4$—M. Peter. (*Phys. Rev.*, vol. 113, pp. 801–803; February 1, 1959.) Experimental determination of the spectrum and its description by a spin Hamiltonian containing only second-order terms.

538.632 2692
Hall-Effect Devices—W. J. Grubbs. (*Bell Sys. Tech. J.*, vol. 38, pp. 853–876; May. 1959.) A general survey of operation of 18 devices.

539.23:546.86 2693
Electrical and Magnetic Properties of Thin Films of Antimony—A. Colombani, C. Vautier and P. Huet. (*Compt. rend. Acad. Sci., Paris*, vol. 247, pp. 1838–1841; November 24, 1958.) Results are given of resistivity, Hall effect and magnetoresistance measurements on vapor-deposited films of thickness 100–2500 Å.

621.315.61:678.84 2694
Selection Guide for Silicone Dielectrics—C. G. Currin. (*Electronics*, vol. 32, pp. 64–65; April 10, 1959.) Dielectric and mechanical properties and the average life of silicone insulating materials are tabulated.

MATHEMATICS

517.63:517.522 2695
The Application of the Laplace Transformation for the Summation of Weakly Convergent Series—O. Heymann. (*Arch. elekt. Übertragung*, vol. 12, pp. 326–330; July, 1958.)

517.94:621.372.8 2696
Asymptotic Behaviour of the Characteristic Functions of the Equation $\Delta\mu+K^2\mu+0$ with Boundary Conditions along Equidistant Curves and the Scattering of Electromagnetic Waves in a Waveguide—V. P. Maslov. (*Dokl. Ak. Nauk SSSR*, vol. 123, pp. 631–633; December 1, 1958.)

517.5:621.374.43 2697
Some Properties of Mathieu and Related Functions exemplified by the Regenerative Modulation Process—Jungfer. (See 2509.)

MEASUREMENTS AND TEST GEAR

531.76:534.22-8:621.374.5 2698
The Measurement of the Time Delay of Ultrasonic Delay Lines—J. Sears. (*J. Brit. IRE*, vol. 19, pp. 237–244; April, 1959.) "A method of determining the delay of wide-band ultrasonic delay lines to an accuracy of better than 0.1 microsecond is described. Alternative methods are discussed."

621.3.011.4(083.74) 2699
Determination of the Unit of Capacitance—A. F. Dunn. (*Can. J. Phys.*, vol. 37, pp. 35–46; January, 1959.) The absolute unit of capacitance has been determined to an accuracy within ±0.0025 per cent using laboratory-maintained frequency and resistance units and a modified Wien-bridge measuring circuit.

621.3.018.41(083.74) 2700
Canadian Standard of Frequency—S. N. Kalra, C. F. Pattenson and M. M. Thomson. (*Can. J. Phys.*, vol. 37, pp. 10–18; January, 1959.) Three laboratories each with 100-kc Essen ring type crystal oscillators jointly compose the standard of frequency, intercomparison being made over telephone lines. Results indicate a frequency stability within about 2 parts in 10^{10} over short and long periods.

621.3.018.41(083.74) 2701
Canadian Caesium-Beam Standard of Frequency—S. N. Kalra, R. Bailey and H. Daams, (*Nature, London*, vol. 183, pp. 575–576; vol. 183, pp. 575–576; February 28, 1959.) The equipment is similar in principle to that described by Essen and Parry (204 of 1958) but differs in the methods of synthesis and measurement of frequency and in the detailed design of the atomic-beam apparatus.

621.317.34:621.372.2 2702
The Evaluation of Quadripole and Material Measurements with the Logarithmic Transmission-Line Chart—K. Jost and G. Schiefer. (*Arch. elekt. Übertragung*, vol. 12, pp. 295–300; July, 1958.) The method described facilitates the numerical evaluation of the permeability and dielectric constants of materials from hf measurements using a slotted coaxial line. Logarithmic charts are given with curves of constant voltage SWR and constant node displacement.

621.317.34.029.64:621.317.755 2703
A Microwave Reflectometer Display System—G. M. Clarke and R. D. Rookes: J. C. Dix and M. Sherry. (*Electronic Engrg.*, vol. 31, pp. 300–301; May, 1959.) Comment on 1308 of April and authors' reply.

621.317.4:621.385.833 2704
Method of Measurement of the Induction and its Derivatives on the Axis of Magnetic Electron Lenses—P. Durandeau, B. Fagot and M. Laudet. (*Compt. rend. Acad. Sci., Paris*, vol. 247, pp. 2316–2318; December 22, 1958.) Application of a method proposed by Laudet (1560 of 1957). Accuracy depends on the precision of measurement of the flux, whatever the diameter of the search coil.

621.317.7:621.314.7 2705
Accurate Measurement of Transistor Cut-Off Frequency—Y. Tarui. (*Electronic Engrg.*, vol. 31, pp. 284–287; May, 1959.) Equipment is described for measurement of current gain, α, of transistors in the frequency range 1–20 mc. The absolute value and phase of α can be measured to within 1.5 per cent. A rapid determination of α cutoff frequency is possible.

621.317.7:621.373.43 2706
Calibrated Source of Millimicrosecond Pulses—E. J. Martin, Jr. (*Electronics*, vol. 32, pp. 56–57; April 17, 1959.) A simple generator using a coaxial discharge line.

621.317.715:621.373.13 2707
Galvanometer Feedback Systems—J. A. Sirs. (*J. Sci. Instr.*, vol. 36, pp. 223–237; May, 1959.) "The principles of applying feedback to a galvanometer, after optical and electronic amplification, are discussed. In particular, the galvanometer performance is examined when proportional, differential, compound and selective feedback systems are used. The latter method is compared with mechanical and series-capacitor tuning of the galvanometer response."

621.317.729.1:621.3.032.269.1 2708
Investigation of Planar Electron Guns with a Rheographic Tank by the Method of Current Injection—J. Bonnerot. (*Compt. rend. Acad. Sci., Paris*, vol. 247, pp. 1824–1826; November 24, 1958.) A note on the method of simulating space-charge effects by means of current-injecting probes in an electrolyte tank.

621.317.737 2709
An Instrument for the Measurement of the *Q*-Factor of Inductances by the Method of Complex Compensation—W. Wisch. (*Nachrichtentech. Z.*, vol. 8, pp. 214–220; May, 1958.) The equipment described covers the frequency range 100 cps–40 kc for inductances from about 1 mh to 10 h with a resistive component between 0.1 Ω and 5 kΩ.

621.317.74:621.373.43 2710
Pulse and Square-Wave Generators—(*Electronic Radio Eng.*, vol. 36, pp. 211–219; June, 1959.) A review of circuits, special features, and performance limits of commercial instruments.

621.317.742.029.64 2711
An Automatic Standing-Wave Indicator for the 3-cm Waveband—E. Laverick and J. Welsh. (*J. Brit. IRE*, vol. 19, pp. 253–262; April, 1959.) The instrument is based on the rotary type of indicator, the mechanical rotation of the detector being replaced by a ferrite polarization-rotating section and a fixed detector. Voltage SWR or reflection coefficient is indicated directly on a meter. The errors of the instrument and its applications are discussed.

621.317.75 2712
Frequency Analyser uses Two Reference Signals—T. B. Fryer. (*Electronics*, vol. 32, pp. 56–57; May 1, 1959.) Circuit details are given of an instrument which can be used from sub-audio up to radio frequencies. A wide range of filter bandwidths is available.

621.317.755 2713
Low-Voltage Oscilloscope Tubes—F. de

Boer and W. F. Nienhuis. (*Philips Tech. Rev.*, vol. 19, pp. 159–164; November 30, 1957.) An account of the development of two tubes requiring an anode voltage of 400 v.

621.317.794 2714
Radiation Measurements at Radio Frequencies: a Survey of Current Techniques—W. A. Cumming. (PROC. IRE, vol. 47, pp. 705–735; May, 1959.) A general survey of measuring techniques in diffraction, scattering, transmission and reflection, current distribution, aperture fields, radiation patterns and gain. One hundred and twenty-nine references.

OTHER APPLICATIONS OF RADIO AND ELECTRONICS

551.508.8:621.19:629.398 2715
Tracking Earth's Weather with Cloud-Cover Satellites—R. Hanel, R. A. Stampfl, J. Cressey, J. Licht, and E. Rich, Jr. (*Electronics*, vol. 32, pp. 44–49; May 1, 1959.) A description of the instrumentation of a satellite which scans the cloud cover and transmits pictures to the ground. See *Convention Rec. IRE*, vol. 6, Part 5, pp. 136–141; 1958. (Hanel and Stampfl).

621.365.5:621.387 2716
A Method of Producing Eddy-Current Heating—R. J. Armstrong. (*J. Sci. Instr.*, vol. 36, pp. 246–247; May, 1959.) A circuit is described which uses two gas-filled triodes to generate trains of damped oscillations. In the particular case considered about 1 kw is generated at about 1 mc and there are fifteen oscillations in each train.

621.38/.39:656.2 2717
Electronics in the Railway Industry—B. K. Cooper. (*Elec. Rev., London*, vol. 164, pp. 335–339; February 20, 1959.) Signaling and traffic control applications of radar, television and automatic computers are discussed.

621.384.613 2718
On the Electron Capture Mechanism and Limiting Current in Betatrons—A. N. Matveev. (*Zh. Eksp. Teor. Fiz.*, vol. 35, pp. 372–380; August, 1958.) In this investigation, account is taken of the Coulomb interaction of electrons in the beam and of the electron losses on the walls of the vacuum chamber. A formula is derived for the limiting current which is also applicable to relativistic electron energies.

621.384.622.2 2719
22-MeV Electron Linear Accelerator—N. A. Austin and S. C. Fultz. (*Rev. Sci. Instr.*, vol. 30, pp. 284–289; April, 1959.) An accelerator of the traveling-wave type with a wide range of pulse lengths, repetition rates and beam energies.

621.384.8:537.4 2720
Strong-Focusing Ion Source for Mass Spectrometers—C. F. Giese. (*Rev. Sci. Instr.*, vol. 30, pp. 260–261; April, 1959.) Starting with an ion beam 0.375 inch square, the lens produces a line focus 0.60 inch long and 0.025 inch wide with a half angle of divergence beyond the crossover of 0.034 radian.

621.385.833 2721
Ion Focusing Properties of a Quadrupole Lens Pair—H. A. Enge. (*Rev. Sci. Instr.*, vol. 30, pp. 248–251; April, 1959.) The focusing properties of quadrupole lens pair have been studied, and the results of thick-lens calculations are presented in the form of graphs showing the field-strength parameters and magnifications as functions of object and image distances.

621.398:621.396.934:621.317.7 2722
Canaveral Test Range: Timing-Signal Transmission—R. P. Wells. (*Bell Lab. Rec.*, vol. 37, pp. 96–99; March, 1959.) The methods used to send range-timing signals over a single channel of the Canaveral-Puerto Rico cable system are described.

PROPAGATION OF WAVES

621.396.11 2723
Wave Propagation over an Irregular Terrain: Part 3—K. Furutsu. (*J. Radio Res. Labs., Japan*, vol. 6, pp. 71–102; January, 1959.) General formulas for field strength, obtained earlier, are used for estimating ridge and precipice effects on ground waves. The results are displayed in diagrams for practical use. Part 2: 1845 of 1958.

621.396.11 2724
Radio Echoes Observed on Sea Swell at the Casablanca Ionospheric Sounding Station—A. Haubert. (*Ann. Géophys.*, vol. 14, pp. 368–372; July/September, 1958.) At ranges up to 100 km, echoes are observed which have a regular period that is inversely proportional to the RF. Quantitative checks show that these echoes probably originate from sea waves; the beat frequency is consistent with a Doppler shift in the frequency of the reflected wave. See also 1237 of 1958 (Okamoto *et al.*).

621.396.11:551.510.52 2725
Models of the Atmospheric Radio Refractive Index—B. R. Bean and G. D. Thayer. (PROC. IRE, vol. 47, pp. 740–755; May, 1959.) Improved prediction of refraction effects, particularly over long distances and at great heights in the atmosphere, is given from the value of refractive index at the transmitting point by the two models described.

621.396.11:551.510.52 2726
Airborne Radiometeorological Research—W. S. Ament. (PROC. IRE, vol. 47, pp. 756–761; May, 1959.) A summary of the work of the Naval Research Laboratory in radar and propagation investigations.

621.396.11:551.510.535 2727
Investigations of Great-Circle Propagation between Eastern Australia and Western Europe—H. J. Albrecht. (*Geofis. Pura Appl.*, vol. 38, pp. 169–180; September/December, 1957. In English.) Observations made during sunspot minimum in the frequency range 3–30 mc are analyzed and discussed with reference to ionospheric predictions.

621.396.11:551.510.535 2728
On the Reflection of Electromagnetic Waves in the Ionosphere with Vertical Sounding—P. Szulkin. (*Bull. Acad. Polon. Sci., Sér. Sci. Tech.*, vol. 7, no. 1, pp. 65–68; 1959. In English.) When the gradient of refractive index exceeds a certain value, a wave will undergo partial reflection at a height below the height of total reflection. For a typical case, it is shown that partial reflections will occur only at heights less than 2 km from the height of total reflection. This is confirmed by experimental observations.

621.396.11:551.510.535(98) 2729
The Development of Radio Traffic Frequency Prediction Techniques for Use at High Latitudes—O. A. Sandoz, E. E. Stevens and E. S. Warren. (PROC. IRE, vol. 47, pp. 681–688; May, 1959.) Some prediction techniques are described with particular attention to the problem in Northern Canada. The use of backscatter and oblique-incidence sounding is discussed. Fifty references.

621.396.11:551.510.535:523.78 2730
Propagation Mechanism of High-Frequency Waves related to the Annular Eclipse of 19th April, 1958—S. Kanaya and K. Ueno. (*Rep. Ionosphere Res. Japan*, vol. 12, pp. 188–195; June, 1958.) The propagation mechanism for distances up to 3000 km can be studied by ionospheric sounding at the path midpoint and the measurement of angle of elevation at the receiving point.

621.396.11:551.510.535:551.594.6 2731
"Whistler Mode" Echoes Remote from the Conjugate Point—R. L. Dowden and G. T. Goldstone. (*Nature, London*, vol. 183, pp. 385–386; February 7, 1959.) Echoes of pulsed signals from Tokyo on a frequency of 17.44 kc, with delays of about 0.2 s, have been detected at Hobart, Tasmania, 3500 km from the geomagnetic conjugate point to Tokyo.

621.396.11:551.510.535:621.396.812 2732
Determination of an Absorption Index of the Ionosphere from an Automatic-Statistical Analysis of Field-Strength Recordings—H. Schwentek. (*Arch. elekt. Übertragung*, vol. 12, pp. 301–308; July, 1958.) Description of a method of determining nondeviative ionospheric absorption using field-strength measurements of CW transmissions at oblique incidence. The main transmission paths are separated by a statistical analyzer.

621.396.11.029.62:551.510.535 2733
IGY Observations of F-Layer Scatter in the Far East—R. Bateman, J. W. Finney, E. K. Smith, L. H. Tveten and J. M. Watts. (*J. Geophys. Res.*, vol. 64, pp. 403–405; April, 1959.) Peculiar signal enhancements observed during transmissions at 36 to 50 mc between the Philippines and Okinawa appear to represent F-layer scatter. These signals are observed nightly for periods of several hours during the months of September and October. Pulse tests indicate F-layer heights for these signals. Considerable pulse broadening is observed and the signals generally arrive from somewhat off the great circle path.

621.396.11.029.64 2734
Microwave Propagation over the Sea Beyond the Line of Sight—K. Nishikori, A. Takahira and H. Irie. (*J. Radio Res. Labs., Japan*, vol. 6, pp. 57–70; January, 1959.) Measurements were taken for 3 years of the meteorological conditions over a 200-km path and from them refractive indexes were calculated. These measurements were used to produce duct-shaped distributions. Using ray tracing methods and Fresnel expressions for reflection and penetration of ducts, quantitative values of attenuation and fading of microwave propagation over the same path were calculated; these agreed with the actual measured values.

621.396.11.029.45:551.510.535 2735
Diurnal Change of Ionospheric Heights Deduced from Phase Velocity Measurements at V.L.F.—J. R. Wait. (PROC. IRE, vol. 47, p. 998; May, 1959.) The phase stability of 16-kc waves propagated over long distances [see *e.g.*, 2524 of 1958 (Crombie *et al.*)] is deduced from waveguide-mode theory.

621.396.11.029.45:621.396.93 2736
V.L.F. Propagation Measurements for the Radux-Omega Navigation System—C. J. Casselman, D. P. Heritage and M. L. Tibbals. (PROC. IRE, vol. 47, pp. 829–839; May, 1959.) Measurements of the phase stability of 10–18-kc transmissions over a 4200-km path are reported.

621.396.81.029.62 2737
Some Characteristics of Persistent V.H.F. Radio-Wave Field Strengths Far Beyond the Radio Horizon—L. A. Ames, E. J. Martin and T. F. Rogers. (PROC. IRE, vol. 47, pp. 769–777; May, 1959.) Ground and air measurements have been made at 220 mc up to distances 700 miles beyond the horizon and at alti-

tudes up to 40,000 feet. Dependence on "angular distance" and the effect of tropospheric layers are discussed and prediction curves are presented. Weak fields measured beyond 800 miles are believed to be caused by ionospheric propagation. Airborne measurements on ionospheric scattering at 50 mc up to 1700 miles are also reported.

621.396.11.029.63 2738
Phase Front Fluctuations of Ten-Centimetre Radio Waves Propagated over a Sea Surface—A. V. Men', S. Ya Brande and V. I. Gorbach. (*Dokl. Ak. Nauk SSSR*, vol. 125, pp. 1019–1022; April 11, 1959.) A description of an experimental investigation of the propagation of vertically polarized waves over a range of 33 km. The phase fluctuations were measured in the range 0.01–100 cps during the periods July–September (summer–autumn) and October–December (autumn–winter). Results indicate that with a few rare exceptions the fluctuations obeyed a normal distribution law.

621.396.8.029.62:551.510.535:523.78 2739
Signal Intensity of Ionospheric Forward Scatter at V.H.F. during the Annular Eclipse of 19th April 1958—(*Rep. Ionosphere Res. Japan*, vol. 12, pp. 196–197; June, 1958.) No significant variation either in continuous wave signal strength or in the pattern of received pulses could be associated with the solar eclipse.

621.396.812.029.62 2740
A Year's Field-Strength Measurements in the V.H.F. Band at Kolkberg near Berlin—U. Kühn. (*Geofis. Pura Appl.*, vol. 38, pp. 157–168; September/December, 1957. In German with English summary.) The results of measurements made in the frequency range 88–100 mc are correlated with temperature, air pressure and air mass, and with the length of the propagation path. On the average the lowest field strengths were observed in June and December.

RECEPTION

621.396.621:621.396.666 2741
Investigations on Diversity Reception by the Aerial Selection Method—R. Heidester and K. Vogt. (*Nachrichtentech. Z.*, vol. 11, pp. 315–319; June, 1958.) Receiver switching methods are compared with an antenna switching method. Equipment for antenna diversity reception using transistors is described and operational results obtained with it are discussed.

621.396.666:621.396.62:621.314.7 2742
A Diode Circuit for Automatic Volume Control in Transistor Receivers—R. Cantz. (*Telefunken-Röhre*, no. 35, pp. 31–42; September, 1958.) Difficulties experienced in AVC for transistor receivers can be overcome by using a crystal diode in parallel with the transistor input stage. To reduce the dc consumption a transistor can be used in place of the diode.

621.396.822 2743
Measurement of Atmospheric Noise—B. B. Ghosh and S. N. Mitra. (*J. Inst. Telecommun. Engrs., India*, vol. 5, pp. 2–16; December, 1958.) Measurements were made in India at four frequencies in the hf range by both objective and subjective methods. Data are given for more than two years. Comparison between the two methods indicates that a protection of 40 db against noise is required for satisfactory broadcast reception 90 per cent of the time.

STATIONS AND COMMUNICATION SYSTEMS

621.39:358.236 2744
Progress and Problems in U. S. Army Communications—R. E. Lacy. (Proc. IRE, vol. 47, pp. 650–660: May, 1959.) Radio equipment, transmission, multiplexing, switching and data processing are discussed.

621.391 2745
Probability of Error for Optimal Codes in a Gaussian Channel—C. E. Shannon. (*Bell Sys. Tech. J.*, vol. 38, pp. 611–656; May, 1959.) "A study is made of coding and decoding systems for a continuous channel with an additive Gaussian noise and subject to an average power limitation at the transmitter. Upper and lower bounds are found for the error probability in decoding with optimal codes and decoding systems. These bounds are close together for signaling rates near channel capacity and also for signaling rates near zero, but diverge between. Curves exhibiting these bounds are given."

621.391 2746
The Reliability of Binary Transmissions for Various Types of Modulation—H. J. Held. (*Nachrichtentech. Z.*, vol. 11, pp. 286–292; June, 1958.) The error probability is calculated for the more important binary keying systems, and an approximation formula of general applicability is given. A comparison is made with experimental results.

621.391 2747
Note on Binary Decoding—M. J. E. Golay. (Proc. IRE, vol. 47, pp. 996–997; May, 1959.) The logical basis of decoding techniques is discussed in relation to time taken and equipment required.

621.395.44:621.315.1.052.63 2748
High-Frequency Transmission on High-Voltage Lines—A. de Quervain. (*Tech. Mitt. PTT*, vol. 36, pp. 349–354; September 1, 1958.) The suitability of power lines for multichannel carrier telephony is discussed, with particular reference to the causes of interference and to the means of overcoming major difficulties inherent in such systems.

621.396/.397(047.1) 2749
Sound and Television Broadcasting—E. Schwartz. (*VDI Z.*, vol. 101, pp. 189–191; February 11, 1959.) A progress review for 1958 with 85 references, mainly to German literature.

621.396.1.029.51 2750
The Engineering of Communication Systems for Low Radio Frequencies—J. S. Belrose, W. L. Hatton, C. A. McKerrow and R. S. Thain. (Proc. IRE, vol. 47, pp. 661–680; May, 1959.) The factors affecting design of systems in the frequency range 80–200 kc are reviewed, with particular emphasis on propagation, antenna design and modulation system. Practical examples relating to arctic regions are given.

621.396.4:552.510.52 2751
Tropospheric Scatter System using Angle Diversity—J. H. Vogelman, J. L. Ryerson, and M. H. Bickelhaupt. (Proc. IRE, vol. 47, pp. 688–696; May, 1959.) A microwave system is proposed using multiple primary feeds to each parabolic reflector with one transmitter or receiver for each feed. The results of a simple experiment show that the wave-angle diversity obtained should reduce the "medium to aperture" coupling loss. The method also allows higher total transmitter power to be used at microwave frequencies.

621.396.4:621.376.2 2752
A Critical Analysis of some Communication Systems Derived from Amplitude Modulation—W. D. Nupp. (Proc. IRE, vol. 47, pp. 697–704; May, 1959.) A comparison is made between SSB suppressed-carrier operation and a system of DSB suppressed-carrier operation, as applied to aeronautical mobile services.

621.396.5 2753
"Frena," a System of Speech Transmission at High Noise Levels—F. de Jager and J. A. Greefkes. (*Philips Tech. Rev.*, vol. 19, pp. 73–83; October 9, 1957.) A nonlinear system in which the frequency and amplitude components are transmitted in two separate channels. If the amplitude component is transmitted as an FM signal, the necessary minimum signal/noise ratio is 6 db. This can be reduced to 4 db using the "Frenac" system in which the amplitude component is coded.

621.396.5:534.76 2754
Tunable F.M. Multiplex Adapter for Stereo—W. B. Bernard. (*Electronics*, vol. 32, pp. 66–67; April 10, 1959.) Fifty kc bandwidth is obtained at 455 kc, and a heterodyne system eliminates the need for filters. Muting is also provided.

621.396.5:534.78 2755
The Effect of Restricted Frequency Characteristics on Intelligibility of Speech in Radio Telephone Channels—A. R. Ravi Varma and H. D. Krishna Prasad. (*J. Inst. Telecommun. Engrs., India*, vol. 5, pp. 38–43; December, 1958.)

621.396.65 2756
Swedish Norwegian S.H.F. Link—(*Overseas Eng.*, vol. 32, p. 255; March, 1959.) The multichannel radio link being installed between Oslo and Karlstad (Sweden) operates in the frequency band 3.8–4.2 kmc and provides 600 telephone channels or one high-definition television channel. Two two-way paths and one reversible one-way path are to be constructed.

SUBSIDIARY APPARATUS

621.311.69 2757
The American Miniature Nuclear Generator, Snap III—W. S. Eastwood, L. B. Mullett and J. L. Putman. (*Nature, London*, vol. 183, pp. 643–644; March 7, 1959.) A note on a power supply system for telemetry apparatus in a space rocket. The decay energy of a radioactive Po capsule is converted directly to electrical energy by means of thermocouples, giving an output of 5 w with efficiency 8–10 per cent.

621.316.721.078.3:621.318.381:621.314.7 2758
A Transistor Stabilized Supply to Feed an Electromagnet used for Nuclear Resonance Studies—M. Sauzade. (*Compt. rend. Acad. Sci., Paris*, vol. 248, pp. 205–207; January 12, 1959.) A circuit is described for a 70 v 15 a supply, with current stabilized to 3 parts in 10^5.

621.316.722.1:621.314.63 2759
Zener Diodes Stabilize Tube Heater Voltages—P. L. Toback. (*Electronic Ind.*, vol. 11, pp. 64–66; December, 1958.) Typical applications of zener power diodes to the regulation of ac and dc heater supplies are described.

621.352.7.001.4 2760
Internal Resistance of Dry Cells—(*Tech. Bull. Nat. Bur. Stand.*, vol. 43, pp. 23–25; February, 1959.) A description of a simple nondestructive pulse technique for investigating the effect of a momentary or continuous discharge on internal resistance. For a more detailed account see *J. Electrochem. Soc.*, vol. 106, pp. 471–475; June, 1959.

TELEVISION AND PHOTOTELEGRAPHY

621.397.5 2761
Television Study Centre—M. Boella. (*Ricerca Sci.*, vol. 29, pp. 25–39; January, 1959.) Report on the research work carried out between 1953 and 1957 at the National Research Council center in Turin.

621.397.61:535.623 2762
An N.T.S.C. Colour Modulator for the

C.C.I.R. Standard—F. Jaeschke. (*Arch. elekt. Übertragung*, vol. 12, pp. 271–288; June, 1958.) Design problems of the equipment are considered, particularly that of the conversion of the three monochrome signals supplied by the camera tube into the luminance and chrominance components. Measurement and control accessories are also discussed.

621.397.61.004.5 2763
Television Monitoring Installations—O. Macek. (*Frequenz*, vol. 12, pp. 214–223; July, 1958.) A survey of modern equipment and monitoring methods, mainly as used in Germany. Sixty references.

621.397.62 2764
A Luminous Frame around the Television Screen—J. J. Balder. (*Philips Tech. Rev.*, vol. 19, pp. 156–158; November 30, 1957.) The results of subjective tests are given.

621.397.62 2765
Contrast Filters for Television Sets—R. Suhrmann. (*Elektron. Rundschau*, vol. 12, pp. 227–232; July, 1958.) Measurements of filter transparency combined with subjective tests on television receivers indicate little difference in effectiveness between grey filters and selective filters placed in front of tube screens.

621.397.62:621.385.3 2766
The Pin Triode in the Frequency Range of the Television Bands IV and V—Maurer. (See 2796.)

TUBES AND THERMIONICS

621.314.63 2767
The Time-Lag of Germanium Diodes and its Effect in Simple Rectifier and Limiter Circuits—W. Heinlein. (*Frequenz*, vol. 12, pp. 159–163 and 191–198; May and June, 1958.) The delay effects for diodes operating with sinusoidal voltages are investigated, and related to the results obtained for pulse operation (see 2907 of 1958).

621.314.7 2768
The H.F. Transistor and its Complex Characteristics in the Frequency Range 0–2 Mc/s—G. Ledig. (*Frequenz*, vol. 12, pp. 137–148 and 178–190; May and June, 1958.) Detailed theoretical treatment of n-pole networks by matrix methods. The transistor is considered as a three-pole network and its parameters and characteristics are calculated with particular regard to its practical application in receivers at 470 kc. Procedure and equipment for measuring the complex characteristics are described and equivalent circuits of the transistor are derived.

621.314.7 2769
Power Transistors—D. S. Grant, R. O. Jones and T. Scott. (*Research, London*, vol. 12, pp. 21–25; January, 1959.) Techniques for increasing emitter efficiency and heat dissipation are summarized.

621.314.7 2770
The Limits of Validity and the Model-Based Deviation of the Equivalent Circuit of Junction Transistors—M. A. Nicolet. (*Helv. Phys. Acta*, vol. 32, pp. 58–77; March 10, 1959. In German.) Parameters of the hybrid-π equivalent circuit of junction transistors were accurately measured for several types of transistor. The results can be interpreted by reference to the model of Webster (2798 of 1954) and Rittner (3390 of 1954) if account is taken of three additional effects. A modified equivalent circuit is proposed which has an extended range of application.

621.314.7 2771
Experimental Investigations on the Influence and Creation of Lattice Defects in Junction Transistors—E. Baldinger, H. Bilger, and M. A. Nicolet. (*Helv. Phys. Acta*, vol. 32, pp. 78–88; March 10, 1959. In German.) Measurements have been made to determine the influence of lattice defects in Si and Ge transistors. Results are interpreted with reference to the theory of Sah *et al.* (3899 of 1957). The influence of fast and thermal neutron radiation on differential parameters and noise of Ge transistors is also investigated. Low-frequency noise appears to be mainly due to surface effects.

621.314.7 2772
Avalanche Transistors—R. C. V. Macario. (*Electronic Engrg.*, vol. 31, pp. 262–267; May, 1959.) Review of characteristics, equivalent circuits and applications.

621.314.7 2773
The Charge Storage in a Junction Transistor during Turn-Off in the Active Region—R. S. C. Cobbold. (*Electronic Engrg.*, vol. 31, pp. 275–277; May, 1959.) "Through the solution of the one-dimensional diffusion equation for a junction transistor, equations are derived for the emitter and collector currents that exist under conditions of minimum turn-off time. These equations are shown to be in fairly good agreement with the practical results."

621.314.7 2774
Calculation of Transients in Transistors—A. A. Grinberg. (*Fiz. Tverdogo Tela*, vol. 1, pp. 31–43; January, 1959.) Calculation of the transient conductivity of a transistor with consideration of the limiting value of the internal resistance, the collector capacitance and the load resistance.

621.314.7:517.7 2775
Jacobians—a New Computational Tool—T. R. Nisbet and W. W. Happ. (*Electronic Ind.*, vol. 17, pp. 69–71; November, 1958.) Tables are given for converting transistor parameters for each of the three circuit configurations.

621.314.7:621.317.7 2776
Accurate Measurement of Transistor Cut-Off Frequency—Tarui. (See 2705.)

621.314.7:621.318.57 2777
A Storing and Switching Transistor—W. v. Münch and H. Salow. (*Nachrichtentech. Z.*, vol. 11, pp. 293–299; June, 1958.) Insertion of a tungsten point into the collector of a p-n-p-type transistor during the alloying process produces a switching transistor with thyratron-like input characteristics. The transistor has a differential input impedance of 1 mΩ in the blocked state, and $<10\Omega$ in the conducting state. See also 3244 of 1956 (Salow and v. Münch).

621.314.7:621.318.57 2778
Transistors for Electronic Switching—T. R. Robillard and R. W. Westberg. (*Bell Lab. Rec.*, vol. 37, pp. 88–92; March, 1959.) A description of design problems in the development of transistors for the new electronic telephone switching system.

621.314.7:621.385.4 2779
Field-Effect Tetrode—(*Electronic Radio Eng.*, vol. 36, p. 210; June, 1959.) A new four-terminal semiconductor developed by Bell Telephone Laboratories which can function as a transformer, gyrator, isolator, nondistorting modulator, or short-circuit-stable negative resistance.

621.314.7.004.15:629.19 2780
An Estimate of Transistor Life in Satellite Applications—A. J. Heeger, T. R. Nisbet and W. W. Happ. (PROC. IRE, vol. 47, p. 991; May, 1959.) Transistors used in satellite instruments will be affected by the radiation bands in the outer atmosphere. Their expected life is of the order of 10^4 hours.

621.314.7.012.8 2781
The Junction Transistor as a Network Element at Low Frequencies: Part 2—Equivalent Circuits and Dependence of the h Parameters on Operating Point—J. P. Beijersbergen, M. Beun and J. te Winkel. (*Philips Tech. Rev.*, vol. 19, pp. 98–105; October 9, 1957.) Part 1: 1719 of May.

621.314.7.029.3 2782
Low Frequencies Vary T-Parameters—G. N. Kambouris. (*Electronic Ind.*, vol. 17, pp. 69–71; December, 1958.) An examination of certain AF transistors indicates that, due to feedback, their characteristic impedances are not constant above 50 cps. Measurements of equivalent T-parameters should therefore be made at frequencies at which the feedback impedance can be neglected.

621.383.2:535.371.07 2783
Image Converters and Image Intensifiers for Military and Scientific Use—M. W. Klein. (PROC. IRE, vol. 47, pp. 904–909; May, 1959.)

621.385.029.6 2784
Microwave Power Tubes—a Survey—(*Electronic Ind.*, vol. 17, pp. 103–131; November, 1958.) The survey includes characteristics of different types of tubes, listed under the manufacturer's name, and a glossary of microwave terms and abbreviations.

621.385.029.6 2785
The Multigap Klystron, a Generator of Short Electromagnetic Waves—R. Hechtel. (*Telefunken-Röhre*, pp. 5–30; September, 1958.) Theoretical investigation of the characteristics of a new type of klystron in which the drift tube has a number of cylindrical gaps. A comparison with the reflex klystron shows the advantages of this tube with regard to bandwidth and efficiency.

621.385.029.6 2786
Surface Waves in Electron Beams in the Presence of a Magnetic Field—G. Mourier. (*Compt. rend. Acad. Sci., Paris*, vol. 247, pp. 1978–1980; December 1, 1956.) A study of electron velocities in a beam of finite thickness, using a dynamic model.

621.385.029.6 2787
An Experimental C.W. Power Travelling-Wave Tube—M. O. Bryant, J. F. Gittins and F. Wray. (*J. Electronics Control*, vol. 6, pp. 113–129; February, 1959.) Design, performance and constructional methods are detailed. Power output is about 1 kw at X-band frequencies with gain up to 22 db. Bandwidth at fixed beam voltage is about 1.5 per cent. With varying beam voltage a 6 per cent range of frequencies is covered. The slow-wave structure is of the clover-leaf type. Ferrite isolators in the feed waveguides ensure stability.

621.385.029.6:061.3 2788
International Convention on Microwave Valves. (*Proc. IEE*, part B, vol. 105, supplement no. 10, pp. 401–608; 1958.) The text is given of the following papers which were among those read at the IEE Convention held in London, May 19–23, 1958.

Traveling-Wave Tubes—I:

(*a*) **Design of a 100-mW Helix Traveling-Wave Amplifier at 50 Gc/s**—W. E. Danielson, H. L. McDowell and E. D. Reed (pp. 405–408).

(*b*) **Experimental Medium-Power High-Gain Travelling-Wave Tubes of Very Short Structure, with Permanent-Magnet Focusing, for the 4- and 6-Gc/s Bands**—W. Klein and H. Neufischer (pp. 408–411).

(*c*) **An Application of the Spatial-Harmonic Wave on a Large-Diameter Helix**—J. Koyama (pp. 412–414).

Discussion (pp. 415–418).

Magnetrons:

(*d*) **A New Design of High-Power *S*-Band Magnetron**—H. A. H. Boot, H. Foster and S. A. Self (pp. 419–425).

(*e*) **A 200-kW 80-Watt *Q*-Band Magnetron**—R. Zwobada (pp. 426–428).

(*f*) **An Investigation into the Factors Affecting the Life of Magnetrons**—F. C. Thompson (pp. 429–430).

(*g*) **The Theory of Circular Magnetrons with Uniformly Rotating Space Charge**—R. Dunsmuir (pp. 431–439).

(*h*) **A 3.8-mm-Wavelength Pulsed Magnetron**—A. J. Monk (pp. 440–442).

Discussion (pp. 443–445).

Travelling-Wave Tubes—II:

(*i*) **Theory of Travelling-Wave Tubes using Paralleled Electron Streams**—C. K. Birdsall (p. 445).

(*j*) **Power Limitations in Helix Travelling-Wave Tubes and the Application of Fluid Cooling**—G. M. Clarke (pp. 446–454).

(*k*) **An *M*-Type Pulsed Amplifier**—O. Doehler, A. Dubois and D. Maillart (pp. 454–457).

(*l*) **A 20-kW Pulsed Travelling-Wave Tube**—J. D. Pearson and H. S. Cockroft (pp. 458–463).

(*m*) **Constructional and Design Difficulties of Wide-Band High-Power Pulsed Travelling-Wave Tubes in the 10-Gc/s Region**—C. H. Dix and R. G. Robertshaw (pp. 464–467).

(*n*) **Some Transient Phenomena in Microwave Tubes**—A. V. Brown (pp. 468–474).

(*o*) **A 4-Gc/s Travelling-Wave Tube for Microwave Radio Links**—P. F. C. Burke (pp. 475–479).

(*p*) **A Package-Type Travelling-Wave Amplifier with a New Magnetic Focusing System**—M. Kenmoku and S. Yasuda (pp. 480–484).

Gas-Discharge Valves and Plasma: (See 2800 below).

Backward-Wave Oscillators—I (Devices):

(*q*) **Frequency Pushing in Crossed-Field Oscillators**—R. I. Buick, A. Reddish and I. J. Zucker (pp. 525–529).

(*r*) **Operation Characteristics of the Carmatron Tube**—O. Doehler, B. Epsztein and J. Arnaud (pp. 529–533).

(*s*) **Results Obtained on Cross-Field Carcinotrons under Pulsed Operation**—M. Favre (pp. 533–537).

(*t*) **Anomalous Behaviour in the *M*-Type Carcinotron**—J. Nalot and R. Visocekas (pp. 538–542).

Discussion (pp. 452–543).

Grid Control Tubes:

(*u*) **Electrode Spacing in Disc-Seal Triodes**—M. R. Gavin, W. Fulop and L. J. Herbst (pp. 544–549).

(*v*) **Advances in the Techniques and Applications of Very-High-Power Grid-Controlled Tubes**—M. V. Hoover (pp. 550–558).

(*w*) **Magnetic Coupling by Parallel-Wire Grids and Soldered Cross-Lateral Grids in Disc-Seal Triodes**—J. Kellerer (pp. 559–562).

(*x*) **Measurement of the Active Admittances of a Triode at 4 Gc/s**—M. T. Vlaardingerbroek (pp. 563–566).

(*y*) **A New Method of Making Accurate Fine-Wire Grids for Use in Radio Valves**—A. E. Widdowson, D. C. Gore and C. H. Butcher (pp. 567–576).

(*z*) **Microwave Triodes**—H. Groendijk (pp. 577–582).

(*aa*) **A New Method of Measuring the Input Admittance of Ultra-High-Frequency Triodes**—K. Takashima and T. Misugi (pp. 583–585).

Discussion (pp. 585–587).

Backward-Wave Oscillators—II (Theory):

(*bb*) **The Magnitude of the Locking-Signal for Backward-Wave Oscillators**—E. A. Ash (pp. 588–593).

(*cc*) **Interaction of Electromagnetic Waves and Electron Beams in Systems with Centrifugal-Electrostatic Focusing**—Z. S. Chernov (pp. 594–596).

(*dd*) **A New Crossed-Field Travelling-Wave Tube, the M-J**—C. C. Johnson and C. K. Birdsall (p. 597).

(*ee*) **An Experimental Study of Large-Signal Behaviour in *M*-Type Valves in the Presence of Space Charge by the Use of an Analogue Method**—B. Epsztein (pp. 598–604).

(*ff*) **Aspects of *M*-Type Interaction with Particular Reference to the Backward-Wave Magnetron Amplifier**—J. W. Kliiver (pp. 605–608).

621.385.029.6:537.533:621.396.822 2789

Investigations of the Anomalous Noise in Magnetically Focused Electron Beams—H. P. Louis. (*Tech. Mitt. PTT*, vol. 36, pp. 333–348; September 1, 1958.) The excess noise produced by scalloped beam amplification in Brillouin-focused beams is investigated experimentally.

621.385.029.65 2790

BWO uses Ridge-Loaded Ladder Circuit—J. A. Noland and L. D. Cohen. (*Electronics*, vol. 32, pp. 66–69; May 1, 1959.) The backward-wave oscillator described operates in the frequency range 60–75 kmc and uses the ladder circuit described by Karp (1212 of 1955 and 2647 of 1957). It was found to be reliable and suitable for use with permanent-magnet focusing.

621.385.032.213.13 2791

Dispenser Cathodes—(*Philips Tech. Rev.*, vol. 19, pp. 177–190; December 23, 1957.)

Part 1: **Introduction**—A. Venema (pp. 177–179).

Part 2: **The Pressed Cathode**—R. C. Hughes and P. P. Coppola (pp. 179–185).

Part 3: **The Impregnated Cathode**—R. Levi (pp. 186–190).

Two types of cathode are described using the same principle as, and having similar characteristics to, the *L* cathode [see *e.g.* 773 of 1951 (Lemmens *et al.*)] but having the advantage that they can be more readily manufactured.

621.385.032.213.13 2792

Evaporation of Barium from Cathodes Impregnated with Barium-Calcium-Aluminate—I. Brodie, R. O. Jenkins and W. G. Trodden. (*J. Electronics Control*, vol. 6, pp. 149–161; February, 1959.) The rate of barium formation during the life of impregnated cathodes has been shown to decay in a manner dependent on the thickness and porosity of the tungsten.

621.385.1.002 2793

Modern Trends of Construction in the Development of Valves—H. Katz. (*Nachrichtentech. Z.*, vol. 11, pp. 281–285; June, 1958.) Review of structural design and electrode and envelope materials suitable for operation at high temperatures and high frequencies, and capable of meeting exacting performance specifications.

621.385.2.029.6:621.376.23 2794

Vacuum-Diode Microwave Detection—N. E. Dye, J. Hessler, Jr., A. J. Knight, R. A. Miesch and G. Papp. (*Electronics*, vol. 32, p. 110; April 24, 1959.) Tests with specially constructed coaxial diodes indicate that noise figures do not compare favorably with crystal performance.

621.385.3:621.365.5 2795

The Use of Oscillator Triodes in High-Frequency Generators with Variable Load—E. G. Dorgelo. (*Elektron. Rundschau*, vol. 12, pp. 241–247; July, 1958.) The performance of triodes specially designed for use in RF heating equipment is discussed.

621.385.3:621.397.62 2796

The Pin Triode in the Frequency Range of the Television Bands IV and V—R. Maurer. (*Telefunken-Röhne*, no. 35, pp. 43–62; September, 1958.) The limitations imposed by lead inductances on the use of pin triodes for frequencies in the range 470–800 mc are discussed. Equations are derived and evaluated for the triode Type PC86, which has been designed for operation in this range.

621.385.3.029.63 2797

A Transmitting Triode for Frequencies up to 900 Mc/s—P. J. Papenhuijzen. (*Philips Tech. Rev.*, vol. 19, pp. 118–128; October 16, 1957.) Detailed description of the construction and characteristics of an air-cooled disk-seal triode Type TBL 2/300 which delivers as an oscillator a power of 405 w at 470 mc and 155 w at 900 mc.

621.385.3.029.64 2798

A 4000-Mc/s Wide-Band Amplifier using a Disc-Seal Triode—J. P. M. Gieles. (*Philips Tech. Rev.*, vol. 19, pp. 145–156; November 30, 1957.) Description of an amplifier based on a valve Type EC56 or EC57 with which an output power of 0.5 or 1.5 w respectively can be obtained, with a gain of 8 db.

621.385.832.032.9 2799

Automatic Electrical Welding of Cathode-Ray Tubes—(*Engineering, London*, vol. 186, pp. 554–555; October 24, 1958.) Description of a new mass-production glass sealing plant incorporating many automatic processes which include electrical welding to make pressure-tight joints between the main glass sections of the bulb.

621.387+537.56]:061.3 2800

International Convention on Microwave Valves—(*Proc. IEE*, part B, vol. 105, supplement no. 10, pp. 485–524; 1958.) The text is given of the following papers which were among those read at the IEE Convention held in London, May 19–23, 1958. For titles of other papers included in supplement no. 10 see 2788 above.

Gas-Discharge Valves and Plasma:

(*a*) **A New Form of *X*-Band Pre-T.R. Cell**—A. B. Parker (pp. 488–491).

(*b*) **A Microwave Pulsed Attenuator using an R.F.-Excited Discharge**—P. D. Lomer and R. M. O'Brien (pp. 500–504).

(*c*) **Active Microwave Duplexing Systems**—P. O. Hawkins (pp. 505–507).

(*d*) **Passive Protection Cells**—P. D. Lomer (pp. 508–509).

(*e*) **A Wide-Band Multi-Way Electronic Switch for Use at Microwave Frequencies**—S. M. Hamberger (pp. 510–515).

(*f*) **Electromechanical Modes in Plasma Waveguides**—R. W. Gould and A. W. Trivelpiece (pp. 516–519).

(*g*) **One-Dimensional Non-Stationary Flow in a Plasma**—G. Kalman (p. 520).

Discussion (pp. 521–524).

MISCELLANEOUS

061.3:621.3 2801

Highlights of '59 IRE Show—J. M. Carroll, W. E. Bushor and S. Weber. (*Electronics*, vol. 32, pp. 39–43; May 1, 1959.) Description of some of the developments reported in papers read at the IRE National Convention, New York, 1959, including guidance of land vehicles by radar, microwave computers, plans for tracking space ships, inertial navigation, and microwave measurements on semiconductors. For the Convention program and summaries of papers, see PROC. IRE, vol. 47, pp. 456–489; March, 1959.

061.4:621.396.6 2802

Radio Components Show—(*Wireless World*,

vol. 65, pp. 211–218; May, 1959.) Detailed review of components and accessories at the R.E.C.M.F. Exhibition held in London, April 6–9, 1959.

621.3:623.8 2803

Some Representative Electronic Subsystem Development Problems in Naval Ordnance—E. H. Beach, M. J. Parker, P. Yaffee and R. B. Knowles. (PROC. IRE, vol. 47, pp. 929–945; May, 1959.) Design problems are discussed for equipment required for underwater and missile-carried ordnance, for field-system evaluation and test sets.

621.38.004.15 2804

Numerical Approach to Electronic Reliability—J. J. Naresky. (PROC. IRE, vol. 47, pp. 946–956; May, 1959.) A description of progress made at Rome Air Development Center, N. Y., in obtaining maximum reliability in electronic equipment.

621.38.004.15:061.3 2805

American Electronics Reliability Symposium—R. Brewer. (*Brit. Commun. Electronics*, vol. 6, pp. 197; March, 1959.) A brief report of the Fifth National Symposium on Reliability and Quality Control in Electronics held in Philadelphia, Pa., January, 1959.

621.38.004.6 2806

Predicting the Reliability of Complex Electronic Equipment—A. G. Field. (*Trans. Soc. Instrum. Technol.*, vol. 11, pp. 18–23; March, 1959.) The reliability is calculated on the basis of a constant component failure rate. The effects of ambient conditions on failure rate are discussed.

629.19:621.396 2807

The Challenge of Space—H. A. Manoogian. (*Electronics*, vol. 32, pp. 65–80; April 24, 1959.) Includes a short description of possible systems of communication, navigation and guidance for interplanetary flight.